WOODHEAD PUBLISHING SERIES IN TEXTILES

Fibrous and composite materials for civil engineering applications

Edited by R. Fangueiro

The Textile Institute

WP
WOODHEAD PUBLISHING

Fibrous and composite materials
for civil engineering applications

Related titles:

Textiles, polymers and composites for buildings
(ISBN 978-1-84569-397-8)
Textiles, polymers and composites are increasingly being utilised within the building industry. This pioneering text provides a concise and representative overview of the opportunities available for textile, polymer and composite fibres to be used in construction and architecture. Initial chapters examine the main types and properties of textiles, polymers and composites used in buildings. The second part of the book presents a selection of applications within the building industry. Chapters range from the use of textiles in tensile structures, sustainable building concepts with textile materials and innovative composite-fibre applications for architecture, to smart textile and polymer fibres for structural health monitoring.

Blast protection of civil infrastructures and vehicles using composites
(ISBN 978-1-84569-399-2)
This title provides a thorough understanding of the science and application of blast protection and containment using composites. Composites provide an ideal material for blast protection as they can be engineered to give different levels of protection by varying the reinforcements and matrices. The book covers blast simulation and modelling and the response of composites to blast loadings. It also includes the retrofitting of composite blast mitigation materials to existing structures, design of blast absorbing materials, protection of buildings, protection of vehicles and composite blast walls.

Strengthening and rehabilitation of civil infrastructures using fibre-reinforced polymer (FRP) composites
(ISBN 978-1-84569-448-7)
The book discusses the mechanical and in-service properties, the relevant manufacturing techniques and other aspects related to externally bonded FRP composites to strengthen/rehabilitate/retrofit civil engineering structural materials. It focuses on: mechanical properties of the FRP materials used; analysis and design of strengthening/rehabilitating/retrofitting beams and columns manufactured from reinforced concrete (RC), metallic and masonry materials; failure modes of strengthening systems; site preparation of the two adhered materials; durability issues; quality control, maintenance and repair of structural systems; case studies.

Details of these and other Woodhead Publishing materials books can be obtained by:

- visiting our web site at www.woodheadpublishing.com
- contacting Customer Services (e-mail: sales@woodheadpublishing.com; fax: +44 (0) 1223 832819; tel.: +44 (0) 1223 499140 ext. 130; address: Woodhead Publishing Limited, 80 High Street, Sawston, Cambridge CB22 3HJ, UK)

If you would like to receive information on forthcoming titles, please send your address details to: Francis Dodds (address, tel. and fax as above; e-mail: francis.dodds@woodheadpublishing.com). Please confirm which subject areas you are interested in.

Woodhead Publishing Series in Textiles: Number 104

Fibrous and composite materials for civil engineering applications

Edited by
R. Fangueiro

Oxford Cambridge Philadelphia New Delhi

Published by Woodhead Publishing Limited,
80 High Street, Sawston, Cambridge CB22 3HJ, UK
www.woodheadpublishing.com

Woodhead Publishing, 1518 Walnut Street, Suite 1100, Philadelphia, PA 19102–3406, USA

Woodhead Publishing India Private Limited, G-2, Vardaan House, 7/28 Ansari Road,
Daryaganj, New Delhi – 110002, India
www.woodheadpublishingindia.com

First published 2011, Woodhead Publishing Limited

British Library Cataloguing in Publication Data
A catalogue record for this book is available from the British Library.

ISBN 978-1-84569-558-3 (print)
ISBN 978-0-85709-252-6 (online)
ISBN 2042-0803 Woodhead Publishing Series in Textiles (print)
ISBN 2042-0811 Woodhead Publishing Series in Textiles (online)

The publisher's policy is to use permanent paper from mills that operate a sustainable forestry policy, and which has been manufactured from pulp which is processed using acid-free and elemental chlorine-free practices. Furthermore, the publisher ensures that the text paper and cover board used have met acceptable environmental accreditation standards.

Typeset by RefineCatch Ltd, Bungay, Suffolk
Printed by TJI Digital, Padstow, Cornwall, UK

Contents

Contributor contact details

(* = main contact)

Editor

R. Fangueiro*
Department of Textile Engineering
University of Minho
Azurém Campus
4800–058 Guimarães
Portugal
e-mail: rfang@det.uminho.pt

Chapter 1

M. de Araújo
School of Engineering
University of Minho
Azurém Campus
4800–058 Guimarães
Portugal
e-mail: mario.araujo@det.uminho.pt

Chapter 2

R. Alagirusamy* and A. Das
Department of Textile Technology
Indian Institute of Technology – Delhi
Hauz Khas
New Delhi – 110016
India
e-mail: alajiru@gmail.com; apurba@textile.iitd.ernet.in; apurba65@gmail.com

Chapter 3

R. Fangueiro*
Department of Textile Engineering
University of Minho
Azurém Campus
4800–058 Guimarães
Portugal
e-mail: rfang@det.uminho.pt

F. Soutinho
Fibrous Materials Research Group
University of Minho
Azurém Campus
4800–058 Guimarães
Portugal
e-mail: filipesoutinho@det.uminho.pt

Chapter 4

J. A. O. Barros
Institute for Sustainability and Innovation in Structural Engineering (ISISE)
Department of Civil Engineering
University of Minho
Portugal
e-mail: barros@civil.uminho.pt

Chapter 5

F. Pacheco Torgal*
Sustainable Construction Group
C-TAC Reasearch Unit
University of Minho
Azurém Campus
4800–058 Guimarães
Portugal
e-mail: f.pachecotorgal@gmail.com

Professor S. Jalali
Department of Civil Engineering
University of Minho
Azurém Campus
4800–058 Guimarães
Portugal
e-mail: said@uminho.pt

Chapter 6

K. Raoufi*
Materials Sensing Laboratory
School of Civil Engineering
Purdue University
550 Stadium Mall Drive
West Lafayette
Indiana
USA
e-mail: kraouif@purdue.edu

J. Weiss
Pankow Materials Laboratory
School of Civil Engineering
Purdue University
550 Stadium Mall Drive
West Lafayette
Indiana
USA
e-mail: wjweiss@ecn.purdue.edu

Chapter 7

A. T. Marques
Department of Mechanical Engineering
Faculty of Engineering
University of Porto
Portugal
e-mail: marques@fe.up.pt

Chapter 8

R. Fangueiro*
Department of Textile Engineering
University of Minho
Azurém Campus
4800–058 Guimarães
Portugal
e-mail: rfang@det.uminho.pt

C. Gonilho Pereira
Fibrous Materials Research Group
Portugal
The Polytechnic Institute of Setubal Setubal
email: christina.pereira@estabarreiro.ips.pt

Chapter 9

A. Guemes*
Department of Aeronautics
Polytechnic University of Madrid
28040 Madrid
Spain
e-mail: alfredo.guemes@upm.es

J. R. Casas
School of Civil Engineering
Technical University of Catalonia
08034 Barcelona
Spain
e-mail: joan.ramon.casas@upc.edu

Chapter 10

X. Lu* and M. Viljanen
Department of Civil and Environmental Engineering
School of Science and Technology
Aalto University
P.O. Box 12100
FI-00076 Aalto
Finland
e-mail: xiaoshu@cc.hut.fi; martti.viljanen@hut.fi

Chapter 11

J. António
Department of Civil Engineering
University of Coimbra
Rua Luís Reis Santos – Pólo II da Universidade
3030–788 Coimbra
Portugal
e-mail: julieta@dec.uc.pt

Chapter 12

J. Monjo-Carrió*
Department of Construction and Technology in Architecture
Polytechnic University of Madrid
Avda. Juan de Herrera, 4
28040 Madrid
Spain
e-mail: juan.monjo@upm.es

J. Tejera
BAT, Buró Arquitectura Textil
Calle de San Andrés, 25
28004 Madrid
Spain
e-mail: tejera@batspain.com

Woodhead Publishing Series in Textiles

1 **Watson's textile design and colour Seventh edition**
Edited by Z. Grosicki
2 **Watson's advanced textile design**
Edited by Z. Grosicki
3 **Weaving Second edition**
P. R. Lord and M. H. Mohamed
4 **Handbook of textile fibres Vol 1: Natural fibres**
J. Gordon Cook
5 **Handbook of textile fibres Vol 2: Man-made fibres**
J. Gordon Cook
6 **Recycling textile and plastic waste**
Edited by A. R. Horrocks
7 **New fibers Second edition**
T. Hongu and G. O. Phillips
8 **Atlas of fibre fracture and damage to textiles Second edition**
J. W. S. Hearle, B. Lomas and W. D. Cooke
9 **Ecotextile '98**
Edited by A. R. Horrocks
10 **Physical testing of textiles**
B. P. Saville
11 **Geometric symmetry in patterns and tilings**
C. E. Horne
12 **Handbook of technical textiles**
Edited by A. R. Horrocks and S. C. Anand
13 **Textiles in automotive engineering**
W. Fung and J. M. Hardcastle
14 **Handbook of textile design**
J. Wilson
15 **High-performance fibres**
Edited by J. W. S. Hearle
16 **Knitting technology Third edition**
D. J. Spencer
17 **Medical textiles**
Edited by S. C. Anand

18 **Regenerated cellulose fibres**
Edited by C. Woodings
19 **Silk, mohair, cashmere and other luxury fibres**
Edited by R. R. Franck
20 **Smart fibres, fabrics and clothing**
Edited by X. M. Tao
21 **Yarn texturing technology**
J. W. S. Hearle, L. Hollick and D. K. Wilson
22 **Encyclopedia of textile finishing**
H-K. Rouette
23 **Coated and laminated textiles**
W. Fung
24 **Fancy yarns**
R. H. Gong and R. M. Wright
25 **Wool: Science and technology**
Edited by W. S. Simpson and G. Crawshaw
26 **Dictionary of textile finishing**
H-K. Rouette
27 **Environmental impact of textiles**
K. Slater
28 **Handbook of yarn production**
P. R. Lord
29 **Textile processing with enzymes**
Edited by A. Cavaco-Paulo and G. Gübitz
30 **The China and Hong Kong denim industry**
Y. Li, L. Yao and K. W. Yeung
31 **The World Trade Organization and international denim trading**
Y. Li, Y. Shen, L. Yao and E. Newton
32 **Chemical finishing of textiles**
W. D. Schindler and P. J. Hauser
33 **Clothing appearance and fit**
J. Fan, W. Yu and L. Hunter
34 **Handbook of fibre rope technology**
H. A. McKenna, J. W. S. Hearle and N. O'Hear
35 **Structure and mechanics of woven fabrics**
J. Hu
36 **Synthetic fibres: nylon, polyester, acrylic, polyolefin**
Edited by J. E. McIntyre
37 **Woollen and worsted woven fabric design**
E. G. Gilligan
38 **Analytical electrochemistry in textiles**
P. Westbroek, G. Priniotakis and P. Kiekens
39 **Bast and other plant fibres**
R. R. Franck
40 **Chemical testing of textiles**
Edited by Q. Fan
41 **Design and manufacture of textile composites**
Edited by A. C. Long

42 **Effect of mechanical and physical properties on fabric hand**
Edited by Hassan M. Behery
43 **New millennium fibers**
T. Hongu, M. Takigami and G. O. Phillips
44 **Textiles for protection**
Edited by R. A. Scott
45 **Textiles in sport**
Edited by R. Shishoo
46 **Wearable electronics and photonics**
Edited by X. M. Tao
47 **Biodegradable and sustainable fibres**
Edited by R. S. Blackburn
48 **Medical textiles and biomaterials for healthcare**
Edited by S. C. Anand, M. Miraftab, S. Rajendran and J. F. Kennedy
49 **Total colour management in textiles**
Edited by J. Xin
50 **Recycling in textiles**
Edited by Y. Wang
51 **Clothing biosensory engineering**
Y. Li and A. S. W. Wong
52 **Biomechanical engineering of textiles and clothing**
Edited by Y. Li and D. X-Q. Dai
53 **Digital printing of textiles**
Edited by H. Ujiie
54 **Intelligent textiles and clothing**
Edited by H. R. Mattila
55 **Innovation and technology of women's intimate apparel**
W. Yu, J. Fan, S. C. Harlock and S. P. Ng
56 **Thermal and moisture transport in fibrous materials**
Edited by N. Pan and P. Gibson
57 **Geosynthetics in civil engineering**
Edited by R. W. Sarsby
58 **Handbook of nonwovens**
Edited by S. Russell
59 **Cotton: Science and technology**
Edited by S. Gordon and Y-L. Hsieh
60 **Ecotextiles**
Edited by M. Miraftab and A. R. Horrocks
61 **Composite forming technologies**
Edited by A. C. Long
62 **Plasma technology for textiles**
Edited by R. Shishoo
63 **Smart textiles for medicine and healthcare**
Edited by L. Van Langenhove
64 **Sizing in clothing**
Edited by S. Ashdown
65 **Shape memory polymers and textiles**
J. Hu

66 **Environmental aspects of textile dyeing**
Edited by R. Christie
67 **Nanofibers and nanotechnology in textiles**
Edited by P. Brown and K. Stevens
68 **Physical properties of textile fibres Fourth edition**
W. E. Morton and J. W. S. Hearle
69 **Advances in apparel production**
Edited by C. Fairhurst
70 **Advances in fire retardant materials**
Edited by A. R. Horrocks and D. Price
71 **Polyesters and polyamides**
Edited by B. L. Deopura, R. Alagirusamy, M. Joshi and B. S. Gupta
72 **Advances in wool technology**
Edited by N. A. G. Johnson and I. Russell
73 **Military textiles**
Edited by E. Wilusz
74 **3D fibrous assemblies: Properties, applications and modelling of three-dimensional textile structures**
J. Hu
75 **Medical and healthcare textiles**
Edited by S. C. Anand, J. F. Kennedy, M. Miraftab and S. Rajendran
76 **Fabric testing**
Edited by J. Hu
77 **Biologically inspired textiles**
Edited by A. Abbott and M. Ellison
78 **Friction in textile materials**
Edited by B. S. Gupta
79 **Textile advances in the automotive industry**
Edited by R. Shishoo
80 **Structure and mechanics of textile fibre assemblies**
Edited by P. Schwartz
81 **Engineering textiles: Integrating the design and manufacture of textile products**
Edited by Y. E. El-Mogahzy
82 **Polyolefin fibres: Industrial and medical applications**
Edited by S. C. O. Ugbolue
83 **Smart clothes and wearable technology**
Edited by J. McCann and D. Bryson
84 **Identification of textile fibres**
Edited by M. Houck
85 **Advanced textiles for wound care**
Edited by S. Rajendran
86 **Fatigue failure of textile fibres**
Edited by M. Miraftab
87 **Advances in carpet technology**
Edited by K. Goswami
88 **Handbook of textile fibre structure Volume 1 and Volume 2**
Edited by S. J. Eichhorn, J. W. S. Hearle, M. Jaffe and T. Kikutani
89 **Advances in knitting technology**
Edited by K-F. Au

90 **Smart textile coatings and laminates**
Edited by W. C. Smith
91 **Handbook of tensile properties of textile and technical fibres**
Edited by A. R. Bunsell
92 **Interior textiles: Design and developments**
Edited by T. Rowe
93 **Textiles for cold weather apparel**
Edited by J. T. Williams
94 **Modelling and predicting textile behaviour**
Edited by X. Chen
95 **Textiles, polymers and composites for buildings**
Edited by G. Pohl
96 **Engineering apparel fabrics and garments**
J. Fan and L. Hunter
97 **Surface modification of textiles**
Edited by Q. Wei
98 **Sustainable textiles**
Edited by R. S. Blackburn
99 **Advances in yarn spinning technology**
Edited by C. A. Lawrence
100 **Handbook of medical textiles**
Edited by V. T. Bartels
101 **Technical textile yarns**
Edited by R. Alagirusamy and A. Das
102 **Applications of nonwovens in technical textiles**
Edited by R. A. Chapman
103 **Colour measurement: Principles, advances and industrial applications**
Edited by M. L. Gulrajani
104 **Fibrous and composite materials for civil engineering applications**
Edited by R. Fangueiro
105 **New product development in textiles**
Edited by B. Mills
106 **Improving comfort in clothing**
Edited by G. Song
107 **Advances in textile biotechnology**
Edited by V. A. Nierstrasz and A. Cavaco-Paulo
108 **Textiles for hygiene and infection control**
Edited by B. McCarthy
109 **Nanofunctional textiles**
Edited by Y. Li
110 **Joining textiles: principles and applications**
Edited by I. Jones and G. Stylios
111 **Soft computing in textile engineering**
Edited by A. Majumdar
112 **Textile design**
Edited by A. Briggs-Goode and K. Townsend
113 **Biotextiles as medical implants**
Edited by M. King and B. Gupta

114 **Textile thermal bioengineering**
Edited by Y. Li
115 **Woven textile structure**
B. K. Behera and P. K. Hari
116 **Handbook of textile and industrial dyeing. Volume 1: principles processes and types of dyes**
Edited by M. Clark
117 **Handbook of textile and industrial dyeing. Volume 2: Applications of dyes**
Edited by M. Clark
118 **Handbook of natural fibres. Volume 1: Types, properties and factors affecting breeding and cultivation**
Edited by R. Kozlowski
119 **Handbook of natural fibres. Volume 2: Processing and applications**
Edited by R. Kozlowski
120 **Functional textiles for improved performance, protection and health**
Edited by N. Pan and G. Sun
121 **Computer technology for textiles and apparel**
Edited by Jinlian Hu
122 **Advances in military textiles and personal equipment**
Edited by E. Sparks
123 **Specialist yarn, woven and fabric structure: Developments and applications**
Edited by R. H. Gong
124 **Handbook of sustainable textile production**
M. Tobler-Rohr

1

Natural and man-made fibres: Physical and mechanical properties

M. DE ARAÚJO, University of Minho, Portugal

Abstract: A *fibre* is a unit of matter characterized by flexibility, fineness and a high ratio of length to thickness. Because fibres have a high surface to volume ratio, they can be extremely strong materials. According to their origin, textile fibres may be classified as *natural fibres*, when they occur in nature in fibre form, and *man-made fibres*, when they do not occur in nature in fibre form. This chapter addresses the relationship between their structure and properties, and their use in civil engineering applications, such as road construction, bridges, non-structural gratings and claddings, structural systems for industrial supports, buildings, long-span roof structures, tanks, thermal insulators, etc.

Key words: fibres, modulus, strength, density, civil engineering.

1.1 Introduction

A *fibre* is a unit of matter characterized by flexibility, fineness and a high ratio of length to thickness (Fig. 1.1).[1] As fibres have a high surface to volume ratio, they can be extremely strong materials.

Fibres are normally constituted by long and chain-like molecules known as macromolecules or polymers, which may be of organic or inorganic nature. These molecules are able to pack together closely to each other resulting in regions of

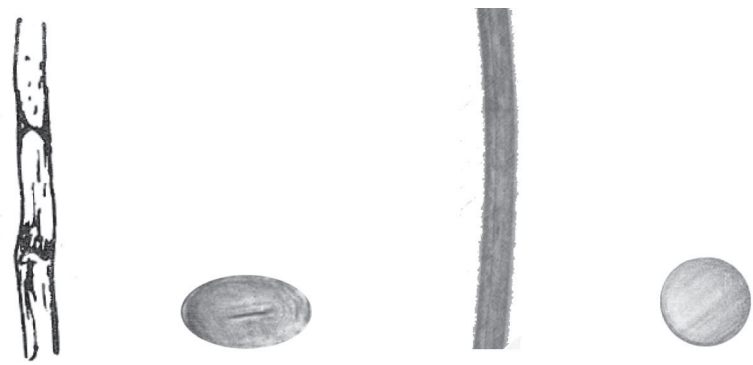

1.1 Typical textile fibres: (a) flax, longitudinal view; (b) flax, cross-sectional view; (c) polyester, longitudinal view; (d) nylon 6.6, cross-sectional view.

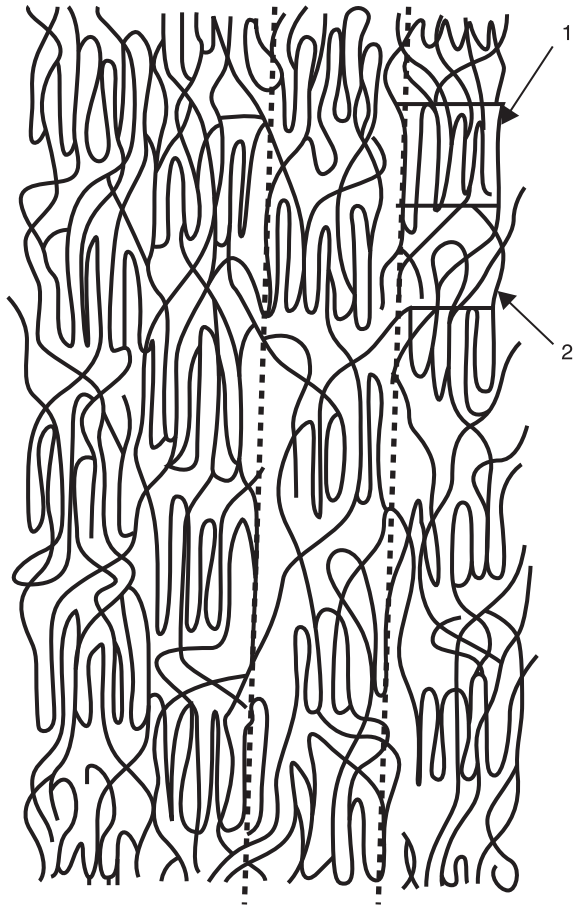

1.2 Model of molecular arrangement in nylon fibre:[12] (1) crystalline region; (2) amorphous region.

crystallinity (Fig.1.2(1)). The degree of orientation of these regions is an important factor in determining the usefulness of a fibre for a particular application. There are other regions, however, where the molecules do not hold together and form random arrangements or amorphous regions (Fig. 1.2(2)). The *crystalline regions* provide strength and rigidity to the fibres, while the *amorphous regions* are responsible for flexibility and reactivity. The ratio of crystalline to amorphous material has an important influence on the properties of the fibres.

According to their origin, textile fibres may be classified as *natural fibres*, when they occur in nature in that form, and *man-made fibres*, when they do not occur in nature in fibre form. Within the latter, some are made of a natural polymer that has been spun into *natural polymer fibres*, and others are made of a synthetic polymer that has been spun into *synthetic fibres*.

High-performance fibres are mostly synthetic fibres that are engineered for specific applications that require very high performance in terms of strength, stiffness, heat resistance or chemical resistance. These fibres have generally higher tenacity and higher modulus than standard fibres.

There are also some inorganic *man-made non-polymeric fibres* such as metal threads.

Fibres are used in many civil engineering applications including road construction, bridges, non-structural gratings and claddings, structural systems for industrial supports, buildings, long-span roof structures, tanks, thermal insulators and so on.

1.2 Natural fibres

Traditional natural fibres, such as cotton, wool and silk, have tenacities in the order of 0.1–0.4 N/tex and initial moduli ranging from 2–5 N/tex. However, fibres such as flax, hemp, jute and ramie may have higher strength and stiffness. With the exception of silk, which was used in more demanding applications such as protective and parachute fabrics, they are all short fibres, and this hinders the conversion efficiency of the fibre's strength into yarns and fabrics.

The usefulness of natural fibres in civil engineering applications (Fig. 1.3) is limited by their moderate mechanical properties. However, there may be

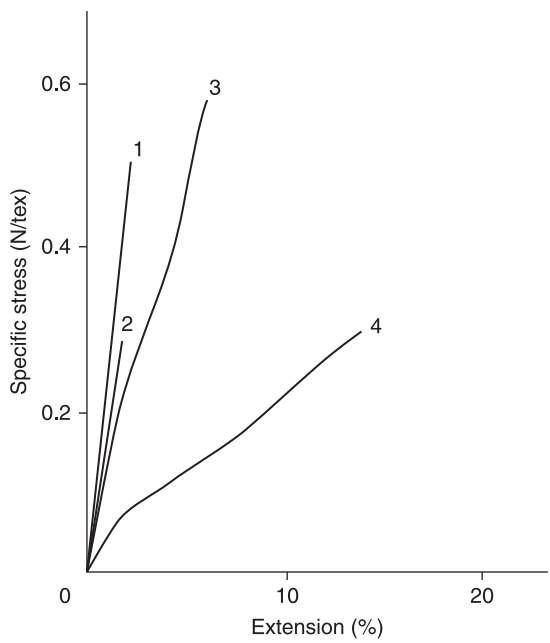

1.3 Typical stress–strain curves of cellulosic fibres: (1) flax; (2) jute; (3) fortisan; (4) tenasco.

advantages from using some of these fibres for the reinforcement of composites used as building materials. The low specific gravity of fibres like jute results in a higher specific strength and stiffness than glass fibres and this may be a benefit, especially in parts designed for bending stiffness. The tensile strength and modulus of jute are lower than those of glass fibres; however, the specific modulus of the jute fibre is higher than that of glass and, on a modulus-per-cost basis, jute can also be superior. The specific strength per unit cost of jute, too, approaches that of glass. The advantage of using jute fibres as a substitute for glass fibres, partly or in total, in the reinforcement of composite materials arises from its lower specific gravity (1.50) and higher specific modulus (11.46 N/tex) when compared with glass (2.58 and 10.85 N/tex respectively). Furthermore, the lower cost and the renewable nature of jute, requiring less energy for its production (approximately 2% of that of glass), make it an attractive reinforcing fibre in composites for some civil engineering applications.[2]

1.3 Man-made fibres

1.3.1 Natural polymer fibres

Viscose rayon and acetate, which were amongst the first regenerated cellulose fibres, exhibited tenacities below 0.2 N/tex. The need to improve the strength of cellulosic fibres led to the development of continuous-filament rayon yarns (*Tenasco*), with a tenacity of 0.4 N/tex, which were used for tyre cords. Further improvements led to strengths of the order of 0.6 N/tex, with an extension to break in the region of 13%. Other developments led to fibres with higher stiffness, such as *Fortisan,* which was developed from highly stretching acetate yams which were subsequently converted into cellulose. This increased the tenacity to 0.6 N/tex and the modulus to 16 N/tex. Another example is *Bocell*, which is a cellulose fibre spun from a liquid-crystal solution in phosphoric acid and has tenacities and moduli of the order of 1.1 N/tex and 30 N/tex, respectively.[3]

It should be noted that the extension to break of regenerated fibres is generally high, ranging from around 6–27%. The low to moderate mechanical properties of these fibres render their usefulness quite limited in civil engineering applications at the present time.

1.3.2 Synthetic fibres

The first synthetic fibre was a polyamide, generally known as nylon, which started to be marketed in 1938 and found applications in wartime technical uses. Its tenacity was in the region of 0.5 N/tex and the modulus 2.5 N/tex. Another synthetic fibre that followed was the polyester fibre (polyethylene terephthalate), which had a similar tenacity but a higher modulus of around 10 N/tex. Varieties of these fibres developed for industrial applications, such as ropes and tyre cords,

exhibit tenacities over 0.8 N/tex for both nylon and polyester and moduli of 9 N/tex for nylon and 12 N/tex for polyester.

Another fibre of increasing interest in technical applications is polypropylene. Its tenacity is in the region of 0.65 N/tex with a modulus of 7.1 N/tex and a specific gravity of 0.91.

Nylons, but especially polypropylene and polyester, are widely used in geosynthetics, and polyester is very much used for tensile surface structures, particularly in Europe. Other applications of polypropylene include anti-crack building products for wall surfaces.

High-performance fibres were developed in the latter part of the twentieth century and inhibit a step change in strength and stiffness, compared to previous ones.

Advances in the 1960s led DuPont scientists in the USA to spin para-aramid fibres from liquid-crystal solutions. These highly oriented fibres achieved tenacities in excess of 2 N/tex and moduli reaching 80 N/tex. More-recent developments enabled some polymer fibres to attain tenacities above 3.5 N/tex and moduli exceeding 150 N/tex.

Other interesting characteristics of para-aramids include flame resistance (self-extinguishing), low electrical conductivity, high chemical resistance, excellent dimensional stability, low thermal shrinkage, high toughness (work of rupture) and high cut resistance. Apart from their use in the reinforcement of composite materials, para-aramids are also of interest for ropes and cables and as a replacement for asbestos materials.

The first high-strength carbon fibres were developed at the Royal Aircraft Establishment in the UK, and were produced by high-temperature processing of acrylic fibres under tension. This resulted in tenacities of up to 3 N/tex and moduli of over 400 N/tex.

Carbon fibre is engineered for strength and stiffness, but variations differ in electrical conductivity, thermal, and chemical properties. The primary factors governing the physical properties are the degree of carbonization, the orientation of the layered carbon planes, and the degree of crystallization. They have lower thermal expansion coefficients than both the glass and aramid fibres, and the material has a very high fatigue and creep resistance.

Much research is also now being done using carbon fibre-reinforced plastic (CFRP) as internal reinforcement in concrete structures, such as beams and bridge decks. The material has many advantages over conventional steel, especially in that it is much stiffer and corrosion resistant. CFRP has become of prominent importance in structural engineering, due to its cost-effectiveness in the repair of old bridges, many of which were designed to tolerate far lower service loads than they are subject to today. Reinforcing with CFRP is a much cheaper alternative when compared with the cost of replacing the bridge. Due to the very high stiffness of CFRP, it can be used underneath spans to help prevent excessive deflections, or wrapped around beams to limit shear stresses.

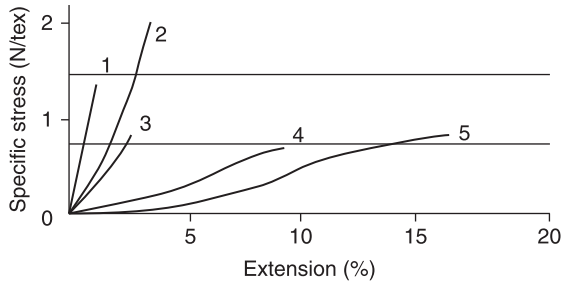

1.4 Typical stress–strain curves of synthetic fibres: (1) carbon; (2) aramid; (3) glass; (4) polyester; (5) nylon.

Glass fibres are used widely as reinforcements in order to increase the stiffness of composite materials. The tenacity of glass fibres may reach 1.6 N/tex and their moduli 35 N/tex, which are lower than those of aramids (on a weight basis). The development of ceramic fibres is primarily related to their high-temperature performance in metal and ceramic matrix composites to use in engines. However, because of their structure they exhibit high moduli, which may reach 100 N/tex, with tenacities of up to 1 N/tex, which may not be considered particularly high (on a weight basis).

Glass fibres are divided into three classes, i.e. E-glass, S-glass and C-glass. The E-glass is designated for electrical use, and the S-glass for high strength. The C-glass is for high corrosion resistance, and it is not of common use in civil engineering applications. Of the three fibres, the E-glass is the most common reinforcement material used in civil engineering structures.

Glass fibres are also used for fire-protective walls, floors and ceiling panels, as well as fireproof curtains and partitions for indoors and outdoors. They are used for heat insulation in heating systems, power generation and incinerators.[2]

Basalt fibres have similar applications to carbon and glass fibres in the reinforcement of composite materials, having better physical-mechanical properties than glass and being much cheaper than carbon fibre (Fig. 1.4). Basalt fibre products include: chemically resistant chopped strands for concrete reinforcement; high-strength rovings for pultruded load-bearing parts and concrete reinforcing bars; basalt woven fabrics for heat, sound insulation, and fire protection; geogrids for road and land reinforcement; and stucco nets for wall reinforcing and renovation.

1.4 Textile fibres for use in civil engineering applications: an overview

Most of the fibres used in civil engineering applications are synthetic fibres. In fibre properties evaluation for particular applications, four aspects are of interest,

Table 1.1 Specific properties of some high-performance fibres in comparison with steel

Specific properties	Carbon HM	Para-aramid HM	E-glass	Basalt CBF	Steel
Specific modulus: E/ρ (N.m/kg)	256	80	28	32	27
Specific strength: σ/ρ (N.m/kg)*	1.2	2	0.775	0.75	0.25

ρ = density
σ = tensile strength
E = Young's modulus
*Also known as strength-to-weight ratio

namely: fibre geometry and dimension, mechanical properties, physical properties, and chemical durability (Table 1.1).

A synthetic fibre can be described as a flexible, macroscopically homogeneous body, with a high length-to-thickness ratio (aspect ratio) and a small cross-section. All fibres have one particular structural feature in common: a preferential orientation of their elemental units with respect to the fibre axis.

Synthetic fibres are available in many different geometries and dimensions, such as monofilaments, rovings (tows) and fibrillated polymers.

Monofilaments are single straight fibres usually made by drawing molten polymers. Such fibres are usually round in cross-section, ranging in diameter from 50 μm to 0.5 mm, being usually strong.[4] However, the smooth surface may result in a low interfacial bond strength, which limits the reinforcing capability of the fibre. Bond strength is primarily determined by the nature of the polymer. If bond strength at the interface between the fibre and the matrix is too high, the fibre ruptures after the first crack initiates. On the other hand, the fibre is easily pulled out if the bond strength is too low. Bond strength may dominate the mechanical properties of fibre-reinforced concrete in this way and the combination of fibre and matrix needs to be selected prudently to get efficient bond strength.

Rovings of polyaramid present the highest bond strength, slightly higher than polyacrylic monofilaments. Polyamide and polyester monofilaments present one of the lowest bond strengths.

Many polymers are spun in the form of filaments (fibrils) whose diameters vary from 5–15 μm. Several thousand fibrils are spun simultaneously, by drawing them from a single die and bundling together. Rovings are cut into short lengths when adding them to concrete. In the concrete, the yarn separates into individual fibrils that need to be dispersed efficiently during mixing. Dispersed rovings act as individual monofilaments within the cement matrix. The high surface-to-volume ratio should increase the effective interfacial bonding.

The geometry of a fibrillated fibre can be described in terms of a film thickness (generally 15–100 μm) and the width of each fibril (100–600 μm). During mixing, the bundles are opened up by the aggregate to act as individual fibrils, each one

1.5 Typical continuous fibre-mat, high-performance, fibre-reinforced cement composite.[2]

contributing to the reinforcing action. The fibres are easy to handle and to disperse uniformly within a concrete mix (Fig. 1.5).

Fibre-reinforced composites are gaining popularity within the civil construction sector. Applications like fibre-reinforced concrete, concrete retrofitting, concrete jacketing and internal and external reinforcement of composite concrete structures are, among others, applications where fibres and fibrous structures play an important role. In these emerging applications, fibres such as glass, carbon and aramid are of paramount importance because of their high strength, high modulus, and the possibility of competing with the conventional, structural construction materials.

In applications related to the geotechnical and geoenvironmental applications, where properties beside mechanical ones are of paramount importance, fibres and textile structures are already commonly used materials. Examples such as embankments and retaining walls, road construction and road overlaying, erosion control of steepened slopes, shore protection, construction of waste landfills, architectural membranes and offshore applications, among others, show that fibres and fibrous structures are the core construction materials. In these applications, polyamide fibres, and especially polypropylene and polyester fibres, are used in an indiscriminate way.[4]

The use of natural fibres in civil engineering applications is constrained by their moderate mechanical properties. However, their low specific gravity and their

renewable nature make some of these fibres, more specifically the bast fibres, attractive as the reinforcing elements in composites used for some civil engineering applications.

The bast or stem fibres are cellulosic fibres that form the fibrous bundles in the inner bark of the stems of dicotyledenous plants, i.e. plants that form two seed leaves. These fibres are constructed of long thick-walled cells that overlap one another. They are cemented together by non-cellulosic materials to form continuous strands that may run the entire length of the plant stem. The strands of bast fibres are normally released from the cellular and woody tissue of the stem by a process called retting. Often the strands are used commercially without separating the individual fibres one from another. Some examples of bast fibres are flax, hemp, jute and ramie (Table 1.2).

Table 1.2 Tensile properties and density of typical textile fibres used for technical applications in comparison with metals

Fibre	Tenacity (N/tex)	Tensile strength (GPa)	Extension to break (%)	Young's modulus (N/tex)	Young's modulus (GPa)	Density (g/cm^3)
Natural						
Flax	0.54	0.831	3	18	27.72	1.54
Hemp	0.47	0.705	2.2	21.7	32.55	1.50
Jute	0.31	0.465	1.8	17.2	25.8	1.50
Ramie	0.59	0.885	3.7	14.6	21.9	1.50
Natural polymer						
Tenasco	0.27	0.405	16.9	6	9	1.50
Fortisan	0.59	0.885	6.4	16.1	24.15	1.50
Synthetic						
Nylon 6.6 HT	0.66	0.752	16	4.4	5	1.14
Polyester HT	0.56	0.778	7	13.2	18.35	1.39
Polypropylene	0.65	0.591	17	7.1	6.46	0.91
Para-aramid HM	2	2.88	2.4	80	115.2	1.44
Carbon HM	1.20	2.196	0.7–1.7	256	468.48	1.83
E-glass	0.78	2	4	28	72.24	2.58
Basalt CBF	0.7–0.9	1.8–2.5	3.1	30–35	80–93	2.65
PVA fibres	0.7–1.23	0.91–1.60	7	6.5–17	8.45–22	1.3
SWNTs	10–41	13–53	16	770–3846	1–5 × 10^3	1.3–1.4
Metals						
Stainless steel fibres	0.22–0.28	1.7–2.21	1.5–11	25.19	199	7.9
Steel	–	0.34–2.1	–	–	210	7.8
Aluminium	–	0.14–0.62	–	–	70	2.7

HT: high tenacity
HM: high modulus
CBF: continuous basalt fibre
PVA: polyvinyl alcohol
SWNTs: Single-Walled carbon NanoTubes
Tex is the mass in g of 1 km of fibre or yarn

1.5 Natural textile fibres for use in civil engineering applications

1.5.1 Flax

Flax is a bast fibre and it comes from the stem of the *Linum usitatissimum* plant, which is an annual plant that grows in various temperate and sub-tropical regions around the world. The erect plant grows to about 1.2 m. The plant is also known as flax and the textiles made of it are called linen and are mainly used in apparel and home textiles.

The highest quality flaxes come from Belgium, Northern France and Holland. Russian flaxes are normally weaker but give very fine fibres.

Structure and properties

Flax is a unicellular fibre and its length may vary from 45–60 cm with a mean diameter of 0.02 mm. Under the microscope the cells look like long and transparent cylindrical tubes. The fibre cell has a narrow lumen running through the centre and the cell walls are thick and polygonal in cross-section.

Flax has an average tenacity of around 0.57 N/tex and an extension at break of around 1.8% (dry fibre) or 2.2% (wet fibre). It has a specific gravity of 1.54 and a regain of about 12%. It resists heat decomposition up to 120°C, when it begins to discolour. It is a good heat conductor. Under normal environmental circumstances flax has a high resistance to rotting. However, in a damp, warm and contaminated condition it may be attacked by mildews.[5]

1.5.2 Hemp

Hemp is a bast fibre and it comes from a plant known as *Cannabis sativa*, which is an annual plant cultivated in many countries around the world, the major producers being Canada, France and China. The plant may grow to a height of 3 m or even taller, and it is used mainly to make string, cord, rope, sacks and canvas.

Structure and properties

Hemp is dark in colour and the individual cells are cylindrical and thicker than flax with an average length of around 13–26 mm, presenting many irregularities on the surface. The cells of the hemp fibres have a thick wall and are polygonal in cross-section, and the central lumen is wider than that of flax. Hemp is stiffer than flax as it is more lignified. It has an average tenacity of around 0.47 N/tex and an extension at break of around 2.2%, with a specific gravity of 1.50.[5]

1.5.3 Jute

Jute is a bast fibre and it comes from the inner bark of an annual herbaceous plant known as *Corchorus*, which grows in the hot and damp regions of Asia, mainly in India and Bangladesh. The plant may grow to a height of 5 m with a stalk diameter of around 20 mm. It is used for sacks and packaging materials, particularly for the storage and transport of agricultural products.

Structure and properties

Jute's colour may vary from dirty grey to yellow and brown, and it has a silky luster. It consists of bundles of individual fibres that may reach 2 m in length. The individual cells of jute have an average length of 2–6 mm. The cell surface is generally smooth presenting some nodes and cross-markings, and the fibres are covered with a layer of woody material. The cross-section of the cells is polygonal with thick walls and a broad lumen of oval cross-section and irregular along the length. Due to the irregular thickness of the cell walls, jute is not as strong or durable as flax or hemp, with an average tenacity of around 0.31 N/tex and an extension at break of around 1.8%. It has a specific gravity of 1.50 and it is a very hygroscopic fibre with a regain of about 13.75%, absorbing up to 23% of water in humid conditions. Due to the protective effect of lignin it is quite resistant to rot.[5]

1.5.4 Ramie

Ramie is a bast fibre and it comes from a perennial plant known as *Boehmeria nivea*, which is grown mainly in China, South America, The Philippines, Korea, Japan and Indonesia. The plant sends up many stalks that may reach a height of 1.2–2 m. As a result of its high molecular crystallinity, ramie is stiff and brittle and breaks if flexed repeatedly in the same place. It lacks resiliency and is low in elasticity and elongation potential. Its main application is in heavy industrial fabrics, mainly canvas and packing materials.

Structure and properties

Ramie fibres are lustrous and white. The fibre is durable and stiff and it absorbs water quite readily. The individual cells are up to 45 cm in length and are smooth and cylindrical with thick walls. The surface of the cell has markings and the lumen disappears towards the ends of the cell, which tapers to a round point. The fibres are strong with an average tenacity of around 0.59 N/tex and an extension at break at around 3.7%, with a specific gravity of 1.50.[5]

1.6 Synthetic textile fibres for use in civil engineering applications

1.6.1 Nylon

Nylon is a generic name, given to a group of synthetic polymers known as polyamides, which was first produced in 1935 by Carothers at DuPont. Nylon was the first truly synthetic fibre to be commercialized (1939). It is a polyamide fibre, derived from a diamine and a dicarboxylic acid and, because a variety of diamines and dicarboxylic acids can be produced, there are a very large number of polyamide materials available to produce nylon fibres. The two most common versions are nylon 6/6 (polyhexamethylene adiamide) and nylon 6 (polycaprolactam, a cyclic nylon intermediate). Raw materials for these are variable and sources used commercially are benzene (from coke production or oil refining), furfural (from oat hulls or corn cobs) or 1,4-butadiene (from oil refining). There are other commercial nylon products, such as nylon 11, 12, 6/10, 6/12, and so on. These others are mainly used in tubing extrusion, injection moulding, and coatings of metal objects.[6] Because nylons offer good mechanical and thermal properties, they are also a very important engineering thermoplastic. For example, 35% of total nylon produced is used in the automobile industry.[7] Nylon's outstanding characteristic in the textile industry is its versatility. It can be made strong enough to stand up under the punishment tyre cords must endure, fine enough for sheer, high-fashion hosiery, and light enough for parachute cloth and backpackers' tents.[8] Nylon is used both alone and in blends with other fibres, where its chief contributions are strength and abrasion resistance. Nylon washes easily, dries quickly, needs little pressing, and holds its shape well since it neither shrinks nor stretches. It is produced by melt spinning and is available in staple, tow, monofilament, and multi-filament form. The fibre has outstanding durability and excellent physical properties.

Structure and properties

Nylons are semi-crystalline polymers. The amide group – (–CO–NH–) – provides hydrogen bonding between polyamide chains, giving nylon high strength at high temperatures and toughness at low temperatures, combined with its other properties, such as stiffness, wear and abrasion resistance, low friction coefficient and good chemical resistance. These properties have made nylons one of the strongest man-made fibres in common use. Two-step melt spinning, comprised of spinning and drawing, is considered to be the conventional method to manufacture nylon filaments. After melting, filtering, and de-aerating, the molten polymer is extruded through a spinneret into a chamber where the melt solidifies into a filament form. These filaments must be drawn subsequently to increase molecular orientation and crystallinity, and therefore improved properties such as initial modulus, tenacity, elongation-at-break, density equilibrium and moisture sorption.

Rather than two-step spinning (extrusion) and drawing, a one-step, high-speed spinning process is being used increasingly.

Nylon 6/6 has a melting point of 263°C, high for a synthetic fibre, though not a match for aramids. This fact makes it the most resistant to heat and friction and enables it to withstand heat setting for twist retention. Nylon 6 has a much lower melting point than nylon 6/6.[8]

Nylon 6/6 has the following properties:

- tenacity (N/tex): around 0.66
- extension at break (%): in the region of 16
- elastic recovery at 8% extension (%): 100
- specific gravity: 1.14
- melting point: 263°C
- thermal conductivity (mW m^{-1} K^{-1}): 250
- extremely chemically stable
- no mildew or bacterial effects
- moisture regain (%): 4–4.5
- degraded by light as natural fibres
- permanent set by heat and steam
- abrasion resistant
- resilient.

1.6.2 Polyester

Polyesters are a type of polymer obtained by a condensation reaction between small molecules which link to form ester groups. There is a variety of polyesters, however, the most common one is polyethylene terephthalate (PET) which is obtained by the condensation of terephthalic acid or a derivative (e.g. dimethyl terephthalate) with ethylene glycol.

Polyesters can be made into fibres. The fibre-forming substance is any long-chain synthetic polymer composed of at least 85% by weight of an ester of a substituted aromatic carboxylic acid, including but not restricted to substituted terephthalic units, $p(–R–O–CO–C_6H_4–CO–O–)_x$ and parasubstituted hydroxy-benzoate units, $p(–R–O–CO–C_6H_4–O–)_x$.

Polyesters may also be produced in numerous other forms such as sheets and three-dimensional shapes. While combustible at high temperatures, polyesters tend to shrink away from flames and self-extinguish upon ignition. Polyester fibres have high tenacity and E-modulus as well as low water absorption and minimal shrinkage in comparison with other fibres.

Structure and properties

The properties of polyester fibres are strongly affected by the fibre structure. The fibre structure depends considerably on the process parameters of fibre

formation, such as spinning speed, hot drawing, stress relaxation and heat-setting speed.

Any stretching of the fibre, whether obtained during fibre spinning or hot drawing, extends the PET molecules, resulting in better uniformity, lower elongation and higher strength, greater orientation, and high crystallinity. Relaxation consists of relieving the stresses and strains of the extended molecules, which results in a reduced shrinkage of the fibres. Heat setting is a treatment used to stabilize the molecular structure, enabling the fibres to resist dimensional changes. The degree of crystalline orientation and the percentage of crystallinity may be adjusted in response to process parameters and this strongly affects fibre properties.

The glass transition is usually around 75°C and crystallization and melting are around 130°C and 260°C, respectively.

Polyester fibres display good resistance to sunlight, but long-term degradation appears to be initiated by UV radiation. Although PET is flammable, the fabric usually melts and drops away instead of spreading the flame. Polyester fibres are resistant to mildew, aging and abrasion.[9]

The properties of PET may be summarized as:

- strong
- resistant to stretching and shrinking
- resistant to most chemicals
- quick drying
- crisp and resilient when wet or dry
- wrinkle resistant
- mildew resistant
- abrasion resistant
- thermal conductivity (mW m^{-1} K^{-1}): 140
- specific gravity: 1.38
- moisture regain (%): 0.4
- melting temperature (°C): 258–263.

In addition, polyester high-tenacity filament yarn has the following properties:

- tenacity (N/tex): 0.62–0.85
- extension at break (%): 10–20
- elastic recovery at 5% extension (%): 90
- initial modulus (N/tex): 10.2–10.6.

1.6.3 Polypropylene

Polypropylene (PP) is extremely versatile as a fibre-forming material. It is a thermoplastic polymer that may be used in a range of applications, including fibres, packaging, stationery, automotive components, and so on. Since its introduction into the textile industry in the 1950s, the list of successful products and markets for polypropylene fibre has increased exponentially.

Polypropylene may be recycled and its recycling ID code is 5. Melt processing of polypropylene may be achieved through extrusion and moulding, and the extrusion methods normally used include melt-blown and spun-bond fibres to be used in products such as face masks, filters, nappies and so on.

Structure and properties

Polypropylene fibres are composed of crystalline and non-crystalline regions. Fibre spinning and drawing causes the orientation of both crystalline and amorphous regions, and may lead to the formation of highly anisotropic microfibrillar structures, which in turn may result in anisotropic fibre properties.[10]

Polypropylene fibres have the following properties:

- very lightweight
- specific gravity: 0.91 (very low)
- high strength (wet or dry)
- tenacity (N/tex): 0.65
- extension at break (%): 17
- initial modulus (N/tex): 7.1
- thermal conductivity (mW m^{-1} K^{-1}): 120
- resistant to deterioration from chemicals, mildew, insects, perspiration, rot and weather
- abrasion resistant
- low moisture absorption
- stain and soil resistant
- lowest static component of any man-made fibre
- sunlight resistant
- good washability, quick drying, unique wicking
- resilient, mouldable, very comfortable
- thermally bondable.

1.6.4 Aramid

Aramid fibres are highly oriented aromatic polyamides that are heat resistant and very strong. The US Federal Trade Commission describes aramid fibre as 'a manufactured fibre in which the fibre-forming substance is a long-chain synthetic polyamide in which at least 85% of the amide linkages, (–CO–NH–), are attached directly to two aromatic rings'. The first meta-aramid fibre was introduced by DuPont (USA) in the early 1960s under the tradename of Nomex. Various other meta-aramids are: Teijinconex produced by Teijin (Japan), Kermel by Kermel (France) and New Star by Yantai (China). These have excellent heat resistance and they do not melt or ignite under normal levels of oxygen. These fibres are used in fire-fighting apparel and other items that require heat resistance, amongst which are special gloves and racing car drivers' suits.

Another group of aramid fibres is the para-aramids such as Kevlar, which was first introduced by DuPont (USA) in 1973. Other para-aramids were introduced at a later stage, such as Twaron by Akzo (Netherlands) and Technora by Teijin (Japan). These fibres have a much higher modulus of elasticity and tensile strength and a lower elongation at break than the meta-aramid fibres. They are used in applications that require energy absorption, such as bullet-proof apparel and armor and the reinforcement of composite materials amongst others.

Structure and properties

Rebouillat 11 presented a review of the relationship between structure and properties of aramid fibres.[11]

Kevlar fibres are made up of long chains of molecules produced from PPTA (poly-paraphenylene terephthalamide), and inter-chain hydrogen bonds make these fibres extremely strong (Fig. 1.6).

The molecules that form the structure of Kevlar are relatively rigid, which is typical of planar sheet-like structures.

Aramid fibres have the following properties:

- high degree of orientation (which dominates their properties)
- good resistance to abrasion
- good resistance to organic solvents
- non-conductive
- no melting point, degradation starts from 500°C
- low flammability
- good fabric integrity at elevated temperatures
- sensitive to acids and salts
- sensitive to ultraviolet radiation
- prone to static build-up unless finished.

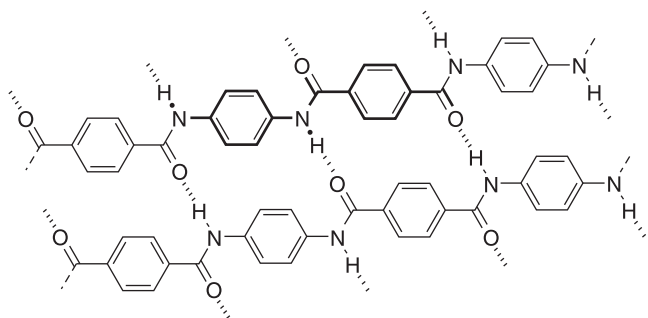

1.6 Molecular structure of Kevlar:[20] bold – monomer unit; dashed – hydrogen bonds.

In addition, para-aramids (such as Kevlar and Twaron) have the following properties:

- outstanding strength-to-weight properties
- tenacity (N/tex): 2 (high)
- extension at break (%): 2.4
- initial modulus (N/tex): 80 (high)
- low creep
- specific gravity: 1.44.

1.6.5 Carbon

Carbon fibres are mainly composed of carbon atoms that are bonded together to form microscopic crystals orientated along the fibre axis. These fibres are extremely fine with a diameter range of 0.005–0.010 mm. The fine filaments may be assembled into yarns and these may be woven into fabrics for the reinforcement of composite materials with a high strength-to-weight ratio, which is ideal for applications in aerospace, civil engineering, military, motor-sports and other competition sports.[12]

Rayon-based carbon fibres are only of historical interest. Most commercial production of carbon fibres is based on polyacrylonitrile (PAN) technologies. Pitch-based fibres are used for niche applications while vapor-gown fibres are at a starting stage.

Structure and properties

The physical properties of carbon fibres have been reviewed extensively by Dresselhaus *et al*.[13]

The characterization of carbon fibre microstructure has been mainly performed by X-ray scattering and electron microscopy techniques. In contrast to graphite, the structure of carbon fibre lacks any three-dimensional order. In PAN-based fibres, the linear chain structure is transformed to a planar structure during oxidative stabilization and subsequent carbonization. Basal planes oriented along the fibre axis are formed during the carbonization stage.

In general, it is seen that the higher the tensile strength of the precursor the higher is the tenacity of the carbon fibre. Tensile strength and modulus are significantly improved by carbonization under strain when moderate stabilization is used. X-ray and electron diffraction studies have shown that in high modulus type fibres, the crystallites are arranged around the longitudinal axis of the fibre, with layer planes highly oriented parallel to the axis. Overall, the strength of a carbon fibre depends on the type of precursor, the processing conditions, heat treatment temperature and the presence of flaws and defects. Carbon fibres are very brittle because the layers in the fibres are formed by strong covalent bonds.

The sheet-like aggregations allow easy crack propagation and, on bending, the fibre fails at very low strain.[14]

Carbon HM fibres have the following properties:

- specific gravity: 1.83
- tenacity (N/tex): 1.2 (high)
- extension at break (%): 0.7–1.7
- initial modulus (N/tex): 256 (high).

1.6.6 Glass

Fibreglass is made up of very fine fibres of glass. It has a number of applications mainly for insulation, filtration media, reinforcement, and as optical fibres. It is quite an ancient technology but the great push was given by Russell Games Slayter of Owens-Corning in 1938. The basis of textile-grade glass fibres is silica (SiO_2) and in its pure form it exists as a polymer $(SiO_2)_n$.

Structure and properties

Fibreglass or glass fibre, as it is also known, has no true melting point. However, it softens at 2000°C, where it starts to degrade. At 1713°C most of the molecules can move about freely, and if the glass is then cooled quickly they will be unable to form an ordered structure.[15] In the polymer, it forms SiO_4 groups that are configured as a tetrahedron with the silicon atom at the centre and four oxygen atoms at the corners. These atoms then form a network bonded at the corners by sharing the oxygen atoms. Glass fibre is formed when thin strands of silica-based, or other formulation glass, are extruded into many fibres with small diameters suitable for textile processing. Glass, even as a fibre, has little crystalline structure. The properties of the structure of glass in its softened stage are very much like its properties when spun into fibre. One definition of glass is 'an inorganic substance in a condition which is continuous with, and analogous to, the liquid state of that substance, but which, as a result of a reversible change in viscosity during cooling, has attained so high a degree of viscosity as to be, for all practical purposes, rigid'.[16]

By trapping air within them, blocks of glass fibre make good thermal insulation, with a thermal conductivity in the order of 0.05 W/mK. Because glass has an amorphous structure, its properties are the same along the fibre and across the fibre. Humidity is an important factor in the tensile strength.

E-Glass fibres have the following properties:

- specific gravity: 2.58
- tenacity (N/tex): 0.78
- extension at break (%): 4
- initial modulus (N/tex): 28
- specific heat (J $g^{-1}K^{-1}$): 0.8.

1.6.7 Basalt

The basalt fibre is made up of very fine fibres of basalt, and its composition consists of the minerals plagioclase, pyroxene and olivine. It has many of the applications of carbon and glass fibre. It is used as a textile for fireproofing in aerospace and automotive applications, and it can also be used as a composite reinforcement, including concrete reinforcement, in the construction of buildings, roads and runways.

Structure and properties

Basalt is a common extrusive volcanic rock, which is usually grey to black and fine-grained due to rapid cooling of lava at the surface of a planet. It may be porphyritic, containing larger crystals in a fine matrix, or vesicular, or frothy scoria. Unweathered basalt is black or grey. The manufacture of basalt fibre requires the melting of the quarried basalt rock to about 1400°C, this is then extruded through small nozzles to produce continuous filaments of basalt fibre. There are three main manufacturing techniques, which are centrifugal-blowing, centrifugal-multiroll and die-blowing. The fibres typically have a filament diameter of 9–13 µm, which is far enough above the respiratory limit of 5 µm to make basalt fibre a suitable replacement for asbestos. They also have a high elastic modulus, resulting in an excellent specific tenacity that is three times that of steel. The continuous basalt fibres derived from basalt rock have proven technical characteristics and performance specifications.

Basalt fibres have the following properties:[17,18]

- fibre diameter (µm): 9
- specific gravity: 2.65
- high thermal resistance (thermostability) and low flammability
- low-strength degradation at temperatures as low as −200 to 250°C and as high as +700 to 900°C., and of high humidity
- operative temperature (°C): −200 to +900
- high thermal and acoustic insulation properties
- sound proofing for 400–1800 Hz: 80–95%
- excellent adhesion to polymer resins and rubbers
- relatively high mechanical strength, abrasion resistance and elasticity
- tenacity (N/tex): 0.67–0.93
- extension at break (%): 3.1
- initial modulus (N/tex): 30–35
- high dielectric properties
- moisture regain (%): 1
- low water absorption
- high chemical resistance (especially to concentrated acids-based materials)
- ecologically clean and non-toxic.

1.6.8 Polyvinyl alcohol (PVA) fibres

PVA fibres are essentially composed of polyvinyl alcohol and produced by wet spinning, and also by a special process that combines dry and melt spinning. There are various types of PVA fibres. However, in this section only the high-strength and high-modulus PVA fibres will be considered. They are high strength, high modulus, acid-proof, alkali-proof, abrasion resistant and sunlight resistant, and these properties render them excellent for use as fabric in textiles, as a reinforcing material in building construction applications, as a packaging material, and in ropes and meshes. PVA fibres are high-performance fibres for use in cement, concrete and mortar, and they can be used together with steel reinforcement, where PVA fibres' micro-crack control helps to prevent water penetration and improves toughness and stiffness. They can also be used on their own as a truly structural fibre. Like steel, carbon, aramid and fibreglass, these PVA fibres have higher tensile strength and a greater modulus of elasticity than regular concrete. Unlike steel and other structural fibres, PVA is hydrophilic, causing it to form a molecular bond with the cement matrix during hydration and curing. This unique combination of bond strength, tensile strength and high modulus of elasticity gives PVA-reinforced concrete substantial tensile and flexural strength. In an engineered matrix, PVA fibres may be able to absorb as much as 500 times more energy than typical fibre-reinforced concrete in tension and bending. PVA fibres are produced in a variety of diameters including the range from 0.027 to 0.7 mm, and in a variety of cut lengths including the range from 6 to 30 mm, both depending on the application envisaged.

In PVA-engineered cementitious composites (PVA-ECC) a small percentage (around 1%) of PVA fibres are effective in controlling:

- plastic shrinkage cracking
- drying shrinkage cracking
- autogenous cracking
- fatigue cracking
- spalling.[19]

Structure and properties

The PVA molecule contains a great number of hydroxyl groups and polyvinyl alcohol itself is soluble in water, and so the initially developed fibres were limited to specialized water-soluble fibre applications. Efforts were made in Japan to produce water-resistant PVA fibres that succeeded and resulted in the high-strength/high-modulus PVA fibres used in civil engineering applications. The latter fibres are heat treated or acetalized to render them insoluble in water.

Fibres are smooth on the surface, and white with silk-like lustre. The cross-section is generally U-shaped like a flattened tube. There is a pronounced skin layer, which is more crystalline than the core. The mean value of crystallinity is around 50%.[20]

PVA fibres have the following properties:

- specific gravity: 1.3
- tenacity (N/tex): 0.7–1.23
- extension at break (%): 7%
- initial modulus (N/tex): 6.5–17.

1.6.9 Metallic fibres

The ductility of metals makes possible their conversion into wire by drawing the metal through dies that become successively smaller. They are quite rigid materials and this rigidity imposes mechanical difficulties in textile processing. However, the flexibility of materials is a function of the cross-sectional area. As the diameter of a rod is reduced by one-half, its flexibility is increased by a factor of four. The problem of producing metal fibres of adequate flexibility resolves itself, therefore, into that of producing filaments of the necessary fineness. In the case of a metal such as stainless steel, a filament of approximately 12 μm has a flexibility equivalent to that of a nylon filament of 3.3 dtex. During the 1960s, methods of producing metal filaments of the required fineness were developed essentially for military and aerospace applications because of the high cost and low production quantities.

Stainless steel fibre is a grey filament of near-round cross-section with diameters that can vary from 4 to 50 μm.[20]

Subsequent developments enabled metal fibres to be produced in large quantities and at a lower cost, making them competitive for application in other areas.

The most important metallic fibre for civil engineering applications is steel and so this section will be dedicated to this type of metal fibre.

Concrete reinforced with steel fibre as compared to hand-tied rebar is less expensive and still increases the tensile strength quite considerably. The shape and dimensions of the fibre are important aspects to consider. For shotcrete a standard size fibre would be about 1 mm in diameter and 45 mm in length, but for steel fibres other lengths may be used (30 to 80 mm) and shapes (i.e. end-hooks). Steel fibres should only be used on surfaces that are corrosion and rust-stains free. Some steel fibre surfaces may be covered by special materials (Fig. 1.7).

1.7 Different types of steel fibres used for concrete reinforcement.

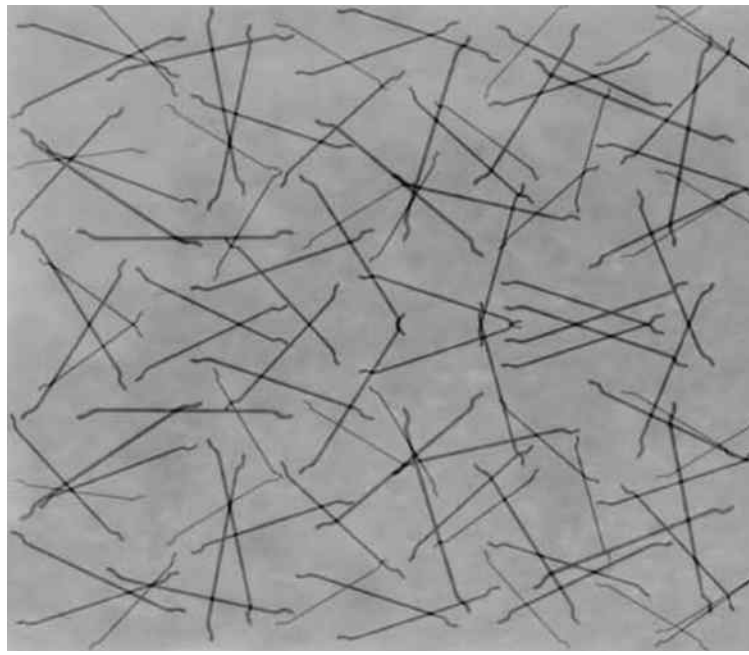

1.8 Steel fibre-reinforced concrete.[13]

Steel fibre-reinforcement offers constructors an efficient and cost-effective alternative for mesh or rebar reinforcement (Fig. 1.8). Working with fibre reinforcement not only means using less steel, but it also takes less man hours to put in place. Steel fibre reinforcement also offers ultimate flexibility. Even complex shapes and structures are possible. Steel fibres have the ability to make concrete more ductile, and steel fibres, having hooked ends, enable the best anchorage and controlled pull-out.[21]

Structure and properties

The properties of a metal fibre are essentially those of the metal itself.

The molecular architecture of metals imposes a characteristic behaviour under stress that differs from that of a typical organic textile fibre. The stress–strain curve of a metal fibre shows a completely elastic behaviour up to the yield point. It is devoid of viscous components such as are found in organic high polymers, and which are identified as primary creep. The absence of a significant viscous behaviour characteristic of metal fibres ensures dimensional stability of structures.

A typical cold-drawn steel wire fibre with hooked ends used for concrete reinforcement may have a diameter of 0.8 mm, a length of 60 mm and a tensile strength of 1000 N/mm^2.

Stainless steel fibres (type 304) have the following properties:

- specific gravity: 7.9
- tenacity (cN/tex): 22.1–28.3
- extension at break (%): 1.5 (hard)–11 (annealed)
- modulus of elasticity (N/tex): 25.19.

1.6.10 Nanofibres

Polymeric nanofibres may range in diameter from 50 to 500 nanometers, since a polyester crystallite has dimensions in the order of 40 nanometers. Polymeric nanofibres may be produced by several methods, including electrospinning, melt blowing a fibre with a modular die, and spinning bicomponent fibres that split or dissolve (e.g. islands-in-the-sea (INS) fibres using a standard spin/draw process).[22]

Carbon nanotubes are an ordered array of carbon atoms which can have tensile strength up to 15 times that of steel. These tubes or fibres are often called graphite or carbon nanofibres as well as nanotubes. The technology for manufacturing carbon nanotubes is very different from common fibre-production techniques. Shorter nanotubes (0.05–3 μm range) may be produced by a variety of techniques including arc-discharge, laser oven, high-pressure CO conversion (HiPco) and fluidized bed chemical vapor deposition (CVD). Longer nanotubes (from 100 μm up to the cm scale) may be produced by substrate growth CVD and catalytic gas flow CVD.

Fibres containing only carbon nanotubes (CNTs) will yield great advances in high-tech applications if they can attain a significant portion of the extraordinary mechanical and electrical properties of individual CNTs. Doing so will require that the CNTs in the fibre are sufficiently long, highly aligned and packed in an arrangement that is nearly free of defects.

The method of CNT production strongly influences the type (multi-walled CNT vs. single-walled CNT), length (submicron to millimetre), chirality and processability, which in turn determine the properties of the final CNT-based macroscopic product.[23]

An important advantage of nanofibres is the very high increase in surface area to volume ratio leading to a higher specific surface area. This may lead to a considerable enhancement of all sorts of fibre properties. In relation to strength, it was recognized by Griffiths that the strength of any material was determined by the presence of flaws of critical dimension. He demonstrated for glass that increasing the surface-to-volume ratio would lead to increased strength by reducing the number of flaws of critical dimension. Thus, high-strength materials will be filamentary of fine diameter. In this context the strength of nanofibres should be extremely high.[24]

Thanks to their extraordinary properties, some of the nanofibres described, especially CNTs, may be of great interest in civil engineering applications in the future.

Structure and properties

Carbon nanotubes have attracted a lot of attention in recent years for their extraordinary properties. They are cylindrical nanostructures of allotropes of carbon, and some of the most recently developed nanotubes may have a length-to-diameter ratio of up to 132 000 000:1.

Because of their properties, they find applications in a variety of fields including nanotechnology, electronics, optics and potentially in architectural fields. They are extremely strong, have very interesting electrical properties and are excellent thermal conductors.

Nanotubes belong to the fullerene structural family. Nanotube chemical bonding may be described by orbital hybridization, which is a field of applied quantum chemistry, and it is composed entirely of sp^2 bonds, which are identical to those of graphite. Another interesting characteristic of carbon nanotubes is that they self-align, forming 'ropes' held together by Van der Waals forces.

Single-walled CNTs have the following properties:

- specific gravity: 1.3–1.4
- tenacity (N/tex): 10–41
- extension at break (%): 16
- modulus of elasticity (N/tex): 770–3846.

1.7 Fibre–matrix adhesion

It is very important that there is good adhesion between the reinforcing fibres and the concrete or cement matrix, otherwise debonding may take place. Because fibres and cement are different materials, poor adhesion at the interface is a problem that often occurs. To improve adhesion, various approaches may be used, including the increase of the specific surface area of the fibre by changing the fibre cross-section from circular to irregular (e.g. serrated), coating the fibre with a material that promotes adhesion, using chemical agents to improve bonding, and so on.

The addition of latex to CFRC (carbon fibre-reinforced cement), and hot water curing of CFRC, dramatically increases fibre–matrix adhesion. Both latex (with an anti-foam agent) and hot water curing may increase the flexural strength by 40% over normal CFRC, and latex increases toughness 100%. Alteration of fibre–matrix adhesion changes the failure mode from fibre pull-out to fibre rupture. Optimum strength and toughness of CFRC result from an intermediate level of fibre–matrix adhesion.[25]

1.8 Sources of further information and advice

The present chapter has the objective of presenting in an integrated and concise form the main fibres that are of use for civil engineering applications. For further

information the reader should consult more specialized literature, like those suggested below:

- Boron Fibre and SCS Silicon Carbide Fibre: http://www.specmaterials.com
- Composites in Civil Engineering: http://www.tifac.org.in/news/civil.htm
- Cook, J.C. (1984) *Handbook of Textile Fibres: Man-made Fibres*. Darlington: Merrow Pub. Co. Ltd.
- Cook, J.C. (1984) *Handbook of Textile Fibres: Natural Fibres*. Darlington: Merrow Pub. Co. Ltd.
- Deopura, B.L., Alagirusamy, R., Joshi, M. and Gupta, B. (eds) (2007) *Polyesters and Polyamides*. Cambridge: Woodhead Publishing Ltd.
- Hearle, J.W.S. (ed.) (2001) *High-Performance Fibres*. Cambridge: Woodhead Publishing Ltd.
- Hearle, J.W.S. and Morton, W.E. (1993) *Physical Properties of Textile Fibres*. Manchester: The Textile Institute.
- International Jute Study Group: http://www.jute.org/home2.htm
- Large Volume, High Performance Application of Fibres in Civil Engineering: http://www.engineeredcomposites.com/publications/li_APS02.pdf
- Netcomposites: http://www.netcomposites.com
- Publications on Natural Fibre Composites: http://www.agrofibrecomposites.com/publications.htm#26
- The National Academies Press: http://www.nap.edu/books/0309096146/html

1.9 References

1. Denton, M.J. and Daniels, P.N. (1963) *Textile Terms and Definitions*. Manchester: The Textile Institute, 63.
2. Gopalakrishnan, D. *High Performance Applications of Textile Fibres in Civil Engineering*. Sardar Vallabhbhai Patel Institute of Textile Management, Coimbatore, India.
3. Hearle, J.W.S. (2001) 'Introduction' in J.W.S. Hearle (ed.) *High-Performance Fibres*. Cambridge: Woodhead Publishing Ltd., 1–22.
4. Fangueiro, R. Pereira, C.G. and de Araújo, M. (2007) 'Applications of polyesters and polyamides in civil engineering' in B.L. Deopura, R. Alagirusamy, M. Joshi and B. Gupta (eds) (2007) *Polyesters and Polyamides*. Cambridge: Woodhead Publishing Ltd., 542–593.
5. Cook, J.C. (1984) *Handbook of Textile Fibres: Natural Fibres*. Darlington: Merrow Pub. Co. Ltd.
6. Meplestor, P. (1997) *Modern Plastics* 74: 66 (Jan.).
7. Dasgupta, S., Hammond, W.B. and Goddard III, W.A. (1996) *J. Am. Chem. Soc*. 118: 12291–12301.
8. Hegde, R.R., Atul Dahiya, A., Kamath, M.G., Kannadaguli, M. and Kotra, R. (2004) *Nylon Fibres* (April): http://www.engr.utk.edu/mse/pages/Textiles/Nylon%20fibres.htm
9. Hegde, R.R., Atul Dahiya, A., Kamath, M.G., Kannadaguli, M. and Gao, X. (2004) *Polyester Fibres* (April): http://www.engr.utk.edu/mse/pages/Textiles/Polyester%20fibre.htm

10. Hegde, R.R., Atul Dahiya, A., Kamath, M.G., Rong, H. and Kannadaguli, M. (2004) *Olefin Fibre* (April): http://www.engr.utk.edu/mse/pages/Textiles/Olefin%20fibres.htm
11. Rebouillat, S. (2001) in J.W.S. Hearle (ed.) *High-Performance Fibres*. Cambridge: Woodhead Publishing Ltd., 23–61
12. *Harper International Carbon Fibre Lines*: http://www.harperintl.com/carbon-fibre-lines.htm?gclid=CMervMu566MCFciWzAodfD3T2g
13. Dresselhaus, M.S., Dresselhaus, G., Sigihara, K., Spain, I.L. and Goldberg H.A. (1988) *Graphite Fibres and Filaments*. Berlin: Springer-Verlag.
14. Hegde, R.R., Atul Dahiya, A., Kamath, M.G., Kannadaguli, M. and Rong, H. (2004) *Carbon Fibres* (April): http://www.engr.utk.edu/mse/pages/Textiles/Carbon%20fibres.htm
15. Gupta, V.B. and Kothari, V.K. (1997) *Manufactured Fibre Technology*. London: Chapman and Hall, 544–546.
16. Loewenstein, K.L. (1973) *The Manufacturing Technology of Continuous Glass Fibres*. New York: Elsevier Scientific, 2–94
17. *Basalt Fibre and Composite Materials Technology Development*: http://www.basaltfm.com
18. Ziv, M. *The Main Principles and Device for Continuous Basalt Fibres Production*. Basalt Tech: http://www.dse-energy.com/basalt/public1temp.htm
19. Kuraray PVA fibres, http://www.kuraray-am.com/pvaf/index.php
20. Cook, J.C. (1984) *Handbook of Textile Fibres: Man-made Fibres*. Darlington: Merrow Pub. Co. Ltd.
21. Bekaert steel fibres: http://www.bekaert.com
22. Hills Inc.: http://www.hillsinc.net/Polymeric.shtml
23. Behabtu, N., Green, M.J. and Pasquali, M. (2008) 'Carbon Nanotube-Based Neat Fibres', *Nanotoday* 3(5–6): 24–34 (Oct–Dec) Elsevier (ISSN: 1748 0132).
24. Griffith, A.A. (1921) 'The phenomena of rupture and flow in solids', *Philosophical Transactions of the Royal Society of London*, Series A, Vol. 221. London: The Royal Society, March, pp. 180–183.
25. Larson, B.K., Drzal, L.T. and Sorousia, P. 'Carbon fibre-cement adhesion in carbon fibre-reinforced cement composites', *Construction and Building Materials* 5(2): 83–92 (June), Elsevier.

2

Yarns: Production, processability and properties

R. ALAGIRUSAMY and A. DAS, Indian Institute of Technology, Delhi, India

Abstract: Textile materials in the form of fibres, yarns and fabrics are used in various civil engineering applications. Textile reinforcements improve the tensile and flexural performances of the resulting cement composite. Fabric reinforced cement composites exhibit strain-hardening behavior even when the reinforcing yarns have a low modulus of elasticity. Various fibres, yarn and fabrics used in different civil engineering applications, like geotextiles and reinforced concrete are discussed. Manufacturing techniques used for making yarns from natural fibres as well as synthetic polymers are considered in detail. Special emphasis is provided for production of composite yarns, which are used in cement reinforcements. The relationships between the textile structures and the properties of reinforced concrete are also explained.

Key words: composite yarns, synthetic yarns, natural fibre yarns, carbon yarns, tapes, geotextiles, cement reinforcement.

2.1 Introduction

Technical yarns are produced for the manufacture of technical textiles to be used in civil engineering applications. They have to meet the specific functional requirements of the intended end-use. This may be achieved through special yarn production techniques or through the selection of special fibre blends, or a combination of both.

Reinforcement by textiles improves the tensile and flexural performances of the cement composite. Several researchers reported that fabrics could significantly improve the mechanical behaviour of cement composites.[1,2,3] In addition to the improved strength, these fabric-reinforced cement composites exhibited strain-hardening behaviour even when the reinforcing yarns had low modulus of elasticity. This was explained by the enhancement in bonding due to the mechanical anchoring provided by the non-linear geometry of the individual yarns within the fabric as induced by fabric structure.[4,5,6]

Therefore, matrix penetrability into the fabric, especially between the filaments, depends heavily on the nature of the fabric junctions and the resultant tightening effects, the structure of the fabric, the number of filaments in the bundle, and the production process of the composite. The process of preparing cement composites with textile fabrics must ensure good penetrability of the cement particles between the spaces within both the fabric and the bundle filaments that compose the fabric.

Pultrusion, a composite production technique that promotes high cement matrix penetrability, generates composite elements with mechanical properties superior to those achieved with ordinary casting.[7,8]

Geotextiles can be formed of synthetic fibres, natural fibres, or a combination of the two. Specifications, processes for the selection, production and utilization of synthetic geotextiles are well established worldwide. In many ground-engineering situations, for example temporary haul roads, basal reinforcement, consolidation drains, and so on, geotextiles are only required to function for a limited time period, whereas suitable synthetic materials often have a long life. In these applications, natural fibres have an important role to play. Although, there are numerous animal and mineral natural fibres available, they lack the required properties essential for geotextiles, particularly when the emphasis of use is on reinforcing geotextiles. Vegetable fibres such as jute, sisal and coir have mechanical properties that are very much comparable to synthetic fibres that find use in geotextile applications. Although natural fibres have always been available, no one visualized their potential as a form of geotextile, until synthetic fibres enabled diverse use and applications of geotextiles to emerge. Manufacturers are now attempting to produce synthetic fibres that will mimic the properties of natural fibres, but at a greater expense. Depending upon the fibres, technical yarns applied for geotextiles and civil engineering can be classified mainly into two classes: synthetic filament yarns and natural fibre-based yarns. Apart from these classes, there are some special yarn structures like core-spun yarns for specific applications.

2.2 Synthetic filament yarns

A filament yarn is made from one or more continuous strands called filaments where each component filament runs the whole length of the yarn. Those yarns composed of one filament are called monofilament yarns, and those containing more filaments are known as multifilament yarns. According to the shape of the filaments in the yarn, filament yarns are classified into two types: flat and bulk. The filaments in a flat yarn lie straight and neat, and are parallel to the yarn axis. Thus, flat filament yarns are usually closely packed and have a smooth surface. The bulked yarns, in which the filaments are either crimped or entangled with each other, have a greater volume than the flat yarns of the same linear density.

Texturing or crimping is the main method used to produce the bulked filament yarns. A textured yarn is made by introducing durable crimps, coils, and loops along the length of the filaments. As textured yarns have an increased volume, the air and vapour permeabilities of fabrics made from them are greater than those from flat yarns. Studies have shown that the crimps in the yarns, used for cement reinforcement, enhance the properties.[9] There have been many types of filament yarns developed for technical applications in civil engineering, such as cement reinforcing, geotextiles and earthquake protection. The reinforcing technical yarns have high modulus, high strength, or both. Yarns for protecting applications can be

resistant to safety hazards such as heat and fire, chemical and mechanical damage. Synthetic filament yarns used in civil engineering applications are discussed.

2.2.1 Glass filament yarns

Glass is an incombustible textile fibre presenting high tenacity. It has been used for fire-retardant applications and is also commonly used in insulation of buildings. Because of its properties and low cost, glass fibre is widely used in the manufacture of reinforcement for composites. There are different types of glass fibres, such as E-glass, C-glass and S-glass. E-glass has very high resistance to attack by moisture and has high electrical and heat resistance. It is commonly used in glass-reinforced plastics in the form of woven fabrics. C-glass is known for its chemical resistance to both acids and alkalis, and is widely used for applications where this type of resistance is required, such as in chemical filtration. The S-glass is a high-strength glass fibre and is used in composite manufacturing. Glass filament yarns are brittle compared to conventional textile yarns. It has been shown that the specific flexural rigidity of glass fibre is 0.89 mNmm, about 4.5 times more rigid than wool. As a result, glass yarns are easy to break in textile processing. Therefore, it is important to apply a suitable size to the glass yarn to minimize the interfibre friction and to hold the individual fibres together in the strand. Dextrinized starch gum, gelatine, polyvinyl alcohol, hydrogenated vegetable oils and non-ionic detergents are commonly used sizes. When handling glass fibres, protective clothing and a mask should be worn to prevent skin irritation and inhalation of glass fibres.

Glass fibre reinforced plastic (GFRP) rebars are usually composed of glass fibres bound together with a thermosetting resin, and manufactured using a pultrusion process. The specific gravity of GFRP rebars is approximately one-quarter of steel rebars. This will facilitate transportation and easy handling. The mechanical properties of GFRPs vary significantly from one product to another. Factors such as volume and type of fibre and resin, fibre orientation, quality control during the manufacturing process, play a major role in the characteristics of the product. GFRP rebars are strongly anisotropic with the longitudinal axis being the strongest.[10] Generally, GFRP rebars have a higher tensile strength than steel rebars. The compressive strength of GFRP rebars is much lower than its tensile strength, approximately *40 to 60%* of tensile strength. GFRP rebars are weaker in compression than in tension. They also behave linearly elastically until failure. The tensile modulus of elasticity of GFRP rebars is much lower than steel, approximately 25% of that of steel. The compressive modulus of elasticity of GFRP rebars is lower than that of the tensile modulus of elasticity, approximately 83–89%. Glass fibres have excellent resistance to creep; however, this is not true for most resins. Therefore, the volume and orientation of fibres have great influence on the creep behaviour of GFRP rebars.

The flexural behaviour of concrete beams reinforced with GFRP bars was first experimentally investigated by Nawy and Neuwerth.[11] The tests showed that at ultimate load, the deflection of GFRP-reinforced beams was approximately three

times greater than that of the corresponding steel-reinforced beams. There were more cracks in GFRP-reinforced beams than in steel-reinforced beams. The large number of distributed cracks in the GFRP-reinforced beams indicated a good mechanical bond between the GFRP and concrete.

2.2.2 Aramid filament yarns

Aramid fibre is a chemical fibre in which the fibre-forming substance is a long-chain synthetic polyamide where at least 85% of the amide linkages are attached directly to two aromatic rings. Nomex® and Kevlar® are two well-known trade names of aramid fibre, owned by Du Pont. Aramid fibres have high tenacity and high resistance to stretch, most chemicals and high temperature.

Kevlar® fibres, being polymeric in nature with close packing of aromatic polymer chains, exhibit high strength, toughness, and stiffness with a high melting temperature. These enhanced properties provide better structural performance and work better than steel, but with a fraction of its weight. Kevlar® combines high strength (five times stronger than steel) with low weight, and comfort with protection. Kevlar® is also made at low temperatures. Kevlar® is used as a reinforcement of cement concrete in the form of chopped fibres, both for ordinary and autoclave cure types. Kevlar® can also be used with other materials as a protective coating.

Aramid yarns are more flexible than their other high-performance counterparts, such as glass and carbon, and thus are easier to use in subsequent fabric-making processes, be it weaving, knitting, or braiding. Care should be taken, though, because aramid yarns are much stronger and much more extensible than the conventional textile yarns, which could make the fabric formation process more difficult.

Twaron® and Technora® filament yarns are increasingly finding their way into the civil engineering markets. Thanks to their excellent mechanical properties, easy handling and resistance to corrosion, these high-performance fibres provide solutions in a wide range of areas where safe and durable structures are essential. Twaron® is a very strong, light para-aramid fibre (poly-paraphenylene terephthalamide), is also available in filament form, and is five times stronger than steel. Technora® is a very strong para-aramid fibre. This aromatic copolyamid (co-poly-(paraphenylene/3,4′-oxydiphenylene terephthalamide)) is ideal for dynamic performance applications involving significant motion. It is eight times stronger than steel and three times stronger than fibreglass, polyester or nylon yarns. Both of them have high tensile strength, high modulus, low creep and are thermally stable, and highly impact and chemical resistant.

These fibres are used for concrete reinforcement and masonry reinforcement. In masonry reinforcement, Twaron® meshes are used as an alternative to a steel mesh. In addition to its mechanical properties, a Twaron® mesh offers advantages over steel due to its easy installation, resistance to corrosion, and superior lifetime. It can be used to reinforce composite blast panels, for instance, to reduce or mitigate fragments caused by a bomb blast in an interior structure. Twaron®

fabrics are suitable as geotextiles, because of their high strength, high modulus and good dimensional stability (low creep). Twaron® offers solutions in the geotextile market in situations where traditional materials such as polyester and propylene do not meet the requirements.

2.2.3 Carbon filament yarns

Carbon fibres are commonly made from precursor fibres such as rayon and acrylic. When converting acrylic fibre to carbon, a three-stage heating process is used. The initial stage is oxidative stabilization, which heats the acrylic fibre at 200–300°C under oxidizing conditions. This is followed by the carbonization stage, when the oxidized fibre is heated in an inert atmosphere to temperatures around 1000°C. Consequently, hydrogen and nitrogen atoms are expelled from the oxidized fibre, leaving the carbon atoms in the form of hexagonal rings that are arranged in oriented fibrils. The final stage of the process is graphitization, when the carbonized filaments are heated to a temperature up to 3000°C, again in an inert atmosphere. Graphitization increases the orderly arrangement of the carbon atoms, which are organized into a crystalline structure of layers. These layers are well oriented in the direction of the fibre axis, which is an important factor in producing high modulus fibres.

Like the glass yarns, most carbon fibres are brittle. Sizes are used to adhere the filaments together to improve the processability. In addition to protecting operatives against skin irritation and short-fibre inhalation, protecting the processing machinery and auxiliary electric and electronic devices needs to be considered too, as carbon fibre is conductive.

Carbon fibre reinforced Polymer (CFRP) is composed of very thin carbon fibres with a diameter of 5–10 µm, embedded in polyester resin. The commercial carbon fibres have the tensile strength of 3500–7000 MPa, an elastic modulus of 230–650 GPa and an elongation at failure ranging from 0.6–2.4%. CFRP was first used to strengthen the Ibach Bridge near Lucerne in Switzerland in 1991.[12] Laminated bands, size 150 mm × 1.75 mm or 150 mm × 2.00 mm and 5000 mm long, glued to the reinforced zones were used. The T3000 fibres that form 55% of the laminated content, have a tensile strength of 1900 MPa and a longitudinal elastic modulus of 129 GPa. Today this technique of the strengthening of building structures is increasingly used.

In 1996 in Winterthur, Switzerland, the Storchenbrucke,[13] a cable-stayed single pylon bridge of 124 m length, was built. Here the CFRP stay cables were applied experimentally for the first time. Each of the stay cables, consisting of 241 wires with a diameter of 5 mm, interacts with conventional steel stay cables. The appointment of this small bridge for applying CFRP for the first time was optimal as this material has practically zero thermal-expansion coefficient. At a length of about 35 m, it does not cause any problems when used in co-operation with cables composed of different materials. The technical characteristics of the CFRP wires used in the stay

cables mentioned above are as follows: T700 S fibres, material density in the wires 1.56 g/m^2, fibres content in the wires 68%, tensile strength 3300 MPa, longitudinal elastic modulus 165 GPa, thermal expansion coefficient 0.2×10^{-6} K^{-1}.

2.2.4 High-density polyethylene (HDPE) filament yarns

HDPE refers to high-density polyethylene. Although the basic theory for making super-strong polyethylene fibres was available in the 1930s, commercial high-performance polyethylene fibre was not manufactured until recently. Spectra®, Dyneema®, and Tekmilon® are among the most well-known HDPE fibres. The gel-spinning process is used to produce the HDPE fibres. Polyethylene with an extra-high molecular weight is used as the starting material. In the gel-spinning process, the molecules are dissolved in a solvent and spun through a spinneret. In solution, the molecules that form clusters in the solid state become disentangled and remain in this state after the solution is cooled to give filaments. The drawing process after spinning results in a very high level of macromolecular orientation in the filaments, leading to a fibre with very high tenacity and modulus. Dyneema®, for example, is characterized by a parallel orientation of greater than 95% and a high level of crystallinity of up to 85%. This gives unique properties to the HDPE fibres. The most attractive properties of this type of fibre are: (1) very high tensile strength (1400–3090 MPa), (2) very high specific modulus (120 N/tex), (3) low elongation (2.7–4.5%) and (4) low fibre density (960–990 kg/m^3) that is lighter than water.

HDPE fibres are made into different grades for different applications. Dyneema®, for example, is made into SK60, SK65 and SK66. Dyneema® SK60 is the multipurpose grade and it is used, for example, for ropes and cordage, for protective clothing and for reinforcement of impact-resistant composites. Dyneema® SK65 has a higher tenacity and modulus than SK60, and this fibre is used where high performance is needed and maximum weight savings are to be attained. Dyneema® SK66 is specially designed for ballistic protection, and provides the highest energy absorption at ultrasonic speeds.

High-strength Spectra® fibre, commonly used in bullet-resistant body armour, is a key component in novel curtains that can protect windows and doors during hurricanes in civil engineering constructions. Brittle failure is an inherent property of cementitious materials, and one way to overcome this problem is by using reinforcing fibres. In a study by Parviz Soroushian *et al.*,[14] high-modulus polyethylene fibre and fibrillated polyethylene pulp were used to reduce the brittle failure of cement. In this investigation, high-modulus polyethylene fibre had a tensile strength of 375 ksi (2588 MPa), a Young's modulus of 17 000 ksi (117 300 MPa), an elongation at break ranging from 5–8%, a specific gravity of 0.97, a filament diameter of 0.0015 in (38 micrometres), and a length of 0.25–0.5 in (7–13 mm). The fibrillated polyethylene pulp used had a specific gravity of 0.91 to 0.97 and a diameter of 0.43×10^{-3} to 8.5×10^{-3} in (1 to 20 μm). Both polyethylene pulp

and fibre increased the impact resistance of cementitious materials and their interaction is also important at the 95% level of confidence. Combined use of the two fibres leads to higher impact test results, where the interaction of the two fibres actually pronounces each other's effectiveness in increasing the impact resistance. Both polyethylene fibre and pulp have important effects on flexural strength and toughness at the 95% level of confidence. In general, the combined use of the two fibres leads to improved flexural performance characteristics; however, excessive amounts of the fibres have negative effects on flexural performance. While fibres generally have negative effects on the compressive strength of cement-based matrices, the presence of one fibre type was observed to reduce or eliminate the negative effects of the other one on compressive strength.

In another study,[15] staple (discontinuous) fibres of Kevlar 49, Technora, Spectra 900 and Herculon PP were used in FRC. For Spectra FRC, the tensile strength is not significantly different from that for FRC with Herculon PP fibres. However, the post-peak stress of Spectra FRC decreases with crack opening less rapidly than does that of aramid FRC. Significant amounts of Spectra fibres in these composites were observed to be uniformly distributed in the matrix. Here the major mechanism contributing to the post-cracking resistance was fibre pull-out. As a result, the fracture energy of Spectra FRC is higher than that of most of the aramid FRC mixes. When Spectra 900 and Technora fibres are blended together as reinforcement, the performance of such hybrid FRC is improved over the FRC using only one species of fibres, with both relatively high strength and high fracture energy.

2.2.5 Polyester yarn

Polyester yarn is made from post-consumer waste such as bottles, fabrics, etc., in the composition of polyester ethylene terephthalate (PET), and because of its superior strength and elasticity it is applicable to a number of geotechnical applications: roadbed reinforcement of road and railway, crack prevention, increase of roadbed strength; reinforcement and stabilization of riverside, embankment and side slope, dyke reinforcement on soft ground for stress evenness, sedimentation adjustment, increase of stability and loading capacity of fundus, and reinforcement of the surface of roads and bridges.

In a study by T. Ochi *et al*.,[16] pellets produced from PET bottles were melted and drawn to produce monofilaments; during this process, caution was taken to ensure that sufficient strength would be installed in the monofilaments. Subsequently, indents were marked on the monofilaments and they were cut to produce PET fibre. Temperature control of the monofilaments was found to be crucial for accurate indentation. The specifications of the PET fibre produced: specific gravity 1.34 ± 0.02, diameter (mm) 0.7, length (mm) 30 ± 1 or 40 ± 2, mass (mg) $15.2 \pm 15\%$ (30 mm length), and tensile strength above 450 MPa. The authors obtained desirable results for the wetting tension, alkali resistance, and combustion gases of

the produced PET fibre. The mixability of the PET fibre was examined by hand mixing; the PET fibre was found to mix very easily with concrete. The machine-mixing ability of the PET fibre with concrete was also found to be good.

2.2.6 Polypropylene yarn

Polypropylene is a famous alternative for geogrids or geomatrices, as it is strong and chemically static. Polypropylene is poor in long-term creep behaviour but is economical and light in weight. Woven geotextile erosion control using polypropylene as the material has the merits of low weight, high reinforcement, low elongation, easy installation, low price, etc.; moreover, it can be fixed with one side or two sides of needle-punched geotextile to form reinforcement geotextile.

Besides, many other types of materials may be applied to make geotextiles, according to their applications. Geotextiles are more and more applied in civil engineering works and so their production has new openings to the textile industries. New and various types of geotextiles are made worldwide and are applied in a variety of applications. The majority of geofabrics are made from synthetic materials, but there are few uses that require biodegradable natural materials such as coir or jute. Unlike synthetics, they can absorb and store moisture, their natural flexibility permits them to match directly to soil profile and their bulk provides great productive cover/weight ratio. As natural material, these are well-matched with surrounding vegetation and are easily available with an economical rate. Yarns based on natural fibres used in civil engineering applications are discussed in a later section.

2.3 Natural fibre yarns

The general properties of man-made fibres compared to natural fibres still tend to fall into distinct categories. Natural fibres possess high strength, modulus and moisture uptake and low elongation and elasticity. Regenerated cellulose fibres have low strength and modulus, high elongation and moisture uptake and poor elasticity. Man-made fibres have high strength, modulus and elongation with a reasonable amount of elasticity and relatively low moisture uptake. Natural fibres can be of vegetable, animal or mineral origin. Vegetable fibres have the greatest potential for use in geotextiles because of their superior engineering properties. Animal fibres have a lower strength and modulus and higher elongation than vegetable fibres. Mineral fibres are very expensive, brittle and lack strength and flexibility. The use of natural fibres and yarns in civil engineering area is an ancient issue. Two of the earliest surviving examples of material strengthening by natural fibres are the Ziggurat in the ancient city of Dur-Kurigatzu (now known as Agar-Quf) and the Great Wall of China.

Natural geofibre (fibres used for geotechnical applications) composites are composite materials that are reinforced with geofibres from natural or renewable

resources, in contrast to, for example, carbon fibres that have to be synthesized (with crude oil as origin). Natural geofibres may come from plants, animals or minerals. However, in the following discussion only cellulose-based fibres from plants will be considered. The use of natural geofibres and natural geofibre composites are certainly not new to mankind. Bricks made from clay reinforced with straws have been used for thousands of years as building material. Textiles and ropes made from flax and hemp have been around for a very long time and are still used today. Paper and cotton sheets impregnated with phenol- or melamine-formaldehyde resin were introduced in the early 1900s for electronic purposes. Natural geofibres in composites offer some interesting properties. Geofibres such as flax have relatively good specific properties, similar to those of glass fibres. Natural geofibres are environmental friendly, and together with a thermoplastic matrix they are also recyclable. Economical aspects are of course important, and the ever-rising oil price has led to an increased interest in the use of natural geofibres over recent years. Drawbacks of natural fibres are sensitivity to moisture, low compatibility to non-polar polymers used as matrix, and lack of well-defined mechanical properties. The latter is because many parameters (geographic location, climate, soil condition, etc.) affect the growth of plants and consequently their properties (they may even vary a lot from different locations within the plant).

2.3.1 Coconut (coir) rope

Coconut (coir) rope is mainly used for binding and also to produce matting. Used or recycled coconut fibres can also be used. Coconut matting provides an effective and sustainable solution to the problems of soil erosion and land-slides on man-made slopes such as motorway and railway embankments. Figure 2.1 shows typical constructions of coconut coir grid and knotted coir grid.

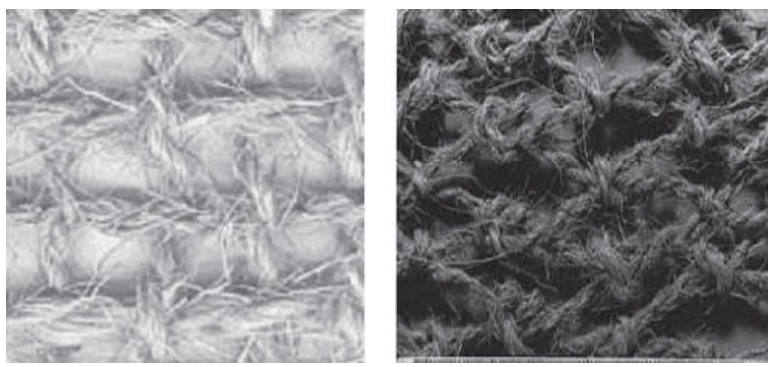

(a) (b)

2.1 Coir grids: (a) coconut coir grid;[17] (b) knotted coir grid.[18]

A coconut consists of water and copra contained in a hard shell that is covered with a fibrous husk protecting it from damage. The fibre is mechanically extracted from the coconut husk and used to make several products with a variety of applications. One such product is two-ply yarn made of coir fibre, which is used in rope making, matting, mat making and geotextiles. The yarn also has applications in agriculture, construction and packaging in geotextiles, for example to prevent soil erosion on embankments. It can be produced by hand spinning, using motorized ratts, or by automatic spinning. New products such as geotextiles require considerable quantities of coir yarn, and as such there is scope for the production of coir yarn using an automatic spinning machine to produce yarn of a superior variety. Before spinning, the fibre is put through a willowing machine, which loosens it and makes it more flexible. It is then fed to the spinning heads of an automatic spinning machine, in which it is automatically twined and spun into two-ply yarn. Finally, the yarn is wound on a bobbin within the machine.

2.3.2 Jute yarn

Jute is natural multifilament fibre, durable and simple to both produce and dispose of. Biodegradable jute yarns are accessible in a number of weave densities, initially anticipated as a geotextile to avoid land-sliding consequent to deforestation. Jute is available in large quantities at a cheaper price, and jute geotextiles can perform a vital function in the control of soil erosion by revegetation; it has many uses, which are cheaper as well as easy to accomplish. It has many benefits as a geotextile, because of its high water-absorption capability, flexibility and drapeability. The growth of jute-based geotextiles is huge due to its various applications in infrastructure development. The possible market for jute geotextiles is bigger, though it is not yet being completely utilized.

Functionally, Jute geotextile is very similar to man-made geotextiles – commonly known as synthetic geotextiles – made of artificial fibres with various petrochemical derivatives as their source. It provides separation, filtration, drainage and initial reinforcement. The biodegradability of jute means that it coalesces with the soil, increasing its permeability and creating a microclimate that is conducive to vegetative growth. In fact, jute geotextile is the best available biotechnical solution to vulnerable exposed soil. These geotextiles act as catalysts in the process of improving the engineering properties of soil. Two years has been found to be sufficient for natural consolidation of soil, known as ‘filter cake’ formation, from extensive laboratory tests by leading academics and field trials. The methods of yarn production and construction are discussed in Section 2.5.

2.3.3 Flax yarn

Flax fibres are twisted to produce yarns and woven matting, which can then be set in lofts or put into wall cavities as insulation materials. Fabrics made from flax

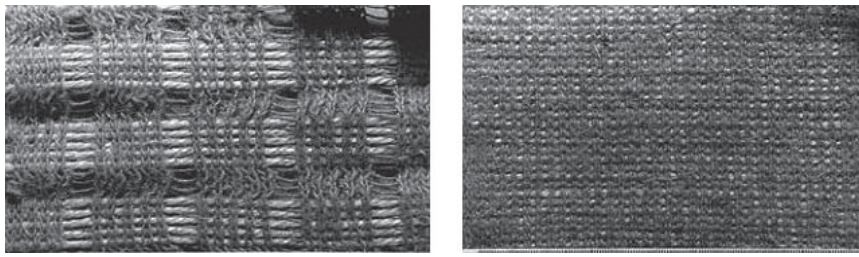

(a) (b)

2.2 Knitted flax/sisal grids: (a) knitted flax/sisal grid;[18] (b) knitted flax/sisal inlay grid.[18]

yarns are also used as geotextiles and applied in areas of erosion control, soil conservation, and other civil and bioengineering applications. They also have the appropriate strength and toughness to protect the slopes from erosion while permitting vegetation to flourish, because they can dissolve the energy of flowing water and absorb the extra solar radiation (Fig. 2.2).

2.4 Synthetic yarn manufacture

2.4.1 Extrusion of filaments, tapes and films

In the extrusion, or melt-spinning process, granules are melted in a screw extruder to the exclusion of oxygen and moisture. The polymer is then fed to the spinning pumps that meter the required amount of polymer and press it through a filter and a spinneret provided with a large number of holes. The spun threads, that is the filaments, are then cooled with air or water. A very similar process is used for extruding tapes and films, but in this case the polymer is pressed through slits. The slit can have various forms, for example a rectangular or circular shape, when a flat or profiled sheet is required.

Tapes can be cut from films or can be produced directly by means of a die containing several slits. In both processes the extruders are provided directly by means of a die containing several slits. In both processes, the extruders are provided with granules or are fed directly from a continuous polymerization unit (mainly polyester and polyamide 6.6, and 6 being less used since it is necessary to remove monomers).

After the spinning and extrusion process, tapes and filaments are subjected, often in more than one step, to drawing and thermosetting processes in which two or more different heat treatments are given. The drawing and setting can be carried out separately from the extrusion and spinning, or can be integrated into these processes. Film and tape extrusion processes always include a drawing process as shown in

Fig. 2.3. These treatments are necessary in order to give the material required tensile strength, modulus, breaking strain, shrinkage or creep. In this process, the molecular chains are oriented further along the lengthwise direction, resulting in improved tensile properties in the axial direction. The complete process is shown in Fig. 2.4.

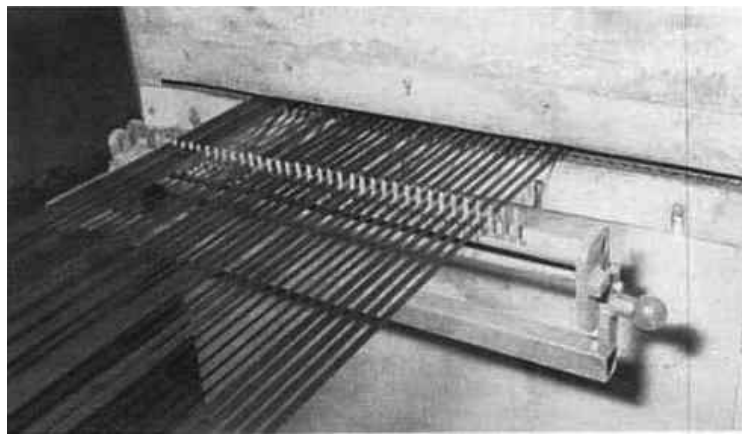

2.3 Production of stretched tapes.[23]

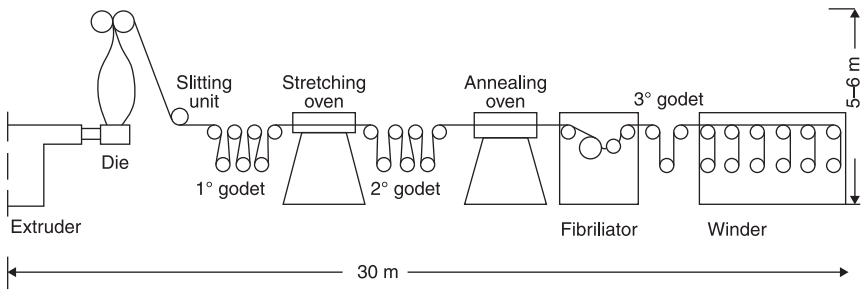

2.4 Schematic drawing of complete film fibre line (by blowing).[23]

Monofilament yarns

Monofilaments are single, generally circular, cross-sectioned threads with a diameter ranging from 0.1 mm up to a few millimetres, which are extruded together, cooled, heat drawn and thermally post-treated. The production process is carried out on extrusion drawing machines that are often horizontal. These machines are also used for producing tapes and films as shown in Fig. 2.5.

2.5 Extrusion die for producing monofilament.[23]

Multifilament yarns

A multifilament yarn is composed of a bundle of very thin, infinitely long threads. The threads are generally referred to as filaments. These yarns are generally spun on vertical machines with filaments extruded out of the spinnerets and air-cooled before getting wound onto spools. After this, the thin filaments (maximum about 280) are stretched to the required draw ratio in a more or less continuous drawing process. Multifilament yarns contain a multitude of fine, continuous filaments (often 5 to 100 individual filaments) usually with some twist in the yarn to facilitate handling. Sizes range from 5–10 denier up to a few hundred denier. Individual filaments in a multifilament yarn are usually about 1–5 denier. Because of their large effective surface area, multifilaments can be heat-treated more homogenously during drawing. Therefore, they can be drawn more effectively than monofilaments, and as a result they have a greater specific strength and a higher modulus. Because of the very small diameters of the filaments in multifilament yarns, their bending stiffness is much lower than that of monofilaments. This leads to much more flexible end-products. Furthermore, using multifilament yarns, denser fabrics can be obtained yielding smaller pores.

Tapes

Tapes are flat, infinitely long plastic strips between 1 mm and 15 mm wide with a thickness of 20 to 80 μm, and they can be wound up as a single tape or together.

Tapes are produced by extrusion through a die that has many slots; or they can be cut from a film, after which they are subjected to an integrated drawing process.

Tapes can be given a profiled surface; they can also be mechanically fibrillated after the stretching process. This is achieved by slitting the film to produce a net (Fig. 2.6). Sometimes the material is twisted, in which case it is referred to as tape yarn.

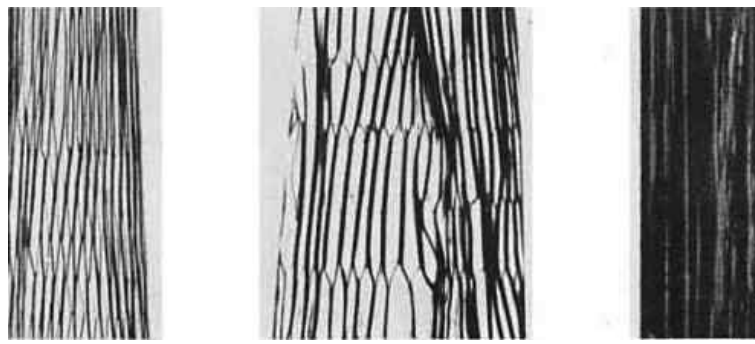

2.6 Fibrillated tapes.[19]

A weaving film is sometimes used for the warp 'threads'. In this case the wide film is not cut into tapes in the integrated extrusion process, but is stretched as a whole, post-heat treated and rolled up. Several of these rolls are then placed in front of the loom as a form of warp beam. The weaving film is then cut into warp tapes on the loom.

Yarns prepared from films

Yarns are also obtained from strips cut from wide films. Two kinds of yarns can be produced: film yarns and split-film yarns. A split-film yarn is a film yarn with a fibrous quality obtained by mechanical fibrillation. The width of the strips can vary from a few millimetres to several centimeters, and the thickness from 20 to 80 μm. The strips can have a profiled surface, and for geotextile applications the material is usually mechanically fibrillated. The yarns are always rolled individually. Twisting is a separate process and the amount of twist depends strongly on the required end-characteristics of the yarn and the fabric.

Additives

The surface of yarns and monofilaments can be provided with additives to facilitate further processing. Surface additives, referred to as finishes, are usually made from three types of components:

- A mixture of lubricants which brings the friction between the yarn and machine parts to the required level (about 50%);
- One or more surface-active materials which act as anti-static and/or as emulsifier (about 50%);
- Anti-corrosion, anti-oxidation additives and biocides (0–5%).

Composite yarns

The development of a grid is critical in civil, geotechnical, environmental and structural engineering applications. Composite yarns spun from multifilament and staple fibres have undergone much research and development, to produce favourable yarn characteristics and to increase the yield of the yarn.[20] The complex covered yarn is a kind of composite yarn, and it is manufactured using an innovative technology for weaving a grid. The selection of core yarns and covering materials is a key factor to manufacturing qualified geogrids. The characteristics of the core yarn, including strength, elongation, Young's modulus, creep, thermal shrinkage and others, should be considered.

High-tenacity polyester filaments are generally used in geogrids. In some particular applications, high-tenacity vinylon and glass fibres are used. The use of a geogrid depends on the characteristics of the covering materials, including ultraviolet resistance, base resistance, acid resistance, biodegradation resistance, toxicity, treatment temperature, adherence, strength and others. Polyvinyl chloride and other materials such as latex, acrylic and bitumen have been applied in civil engineering.[21,22] Polyethylene terephthalate (PET) is a thermoplastic material commonly used in the form of fibres and films, whose stability in environmental applications is of substantial interest.[23] It must be protected to prevent its degradation by the environment.

The polypropylene/polyester composite-covered yarn was spun using a rotor twister and the geogrids were woven with the spun yarn to improve the performance of the geogrids by Yehia E. El Mogahzy *et al*.[24] This work used polypropylene (PP) to wrap the PET and thus protect the core yarn. Numerous woven geogrids were tested and discussed to investigate the effects of process parameters on their mechanical properties and evaluate the optimal conditions.

As presented in Fig. 2.7, the high-tenacity polyester filaments were put under tension with a tensioner, and were wrapped in polypropylene filaments installed on a rotor to spin the composite-covered yarn. A tension meter (SHIMPO Limit 1000 gf) was used to measure the tension of the polyester filaments during twisting. In this experiment, the tension of the polyester filaments and the take-up speed were held constant; composite-covered yarns were spun by changing the rotational rate of rotor.

Figure 2.8 shows the grids developed in these experiments by Yehia E. El Mogahzy *et al*. It can be noted that the completely melted PP material covered the core polyester yarns. Geogrids must exhibit high strength and low elongation, so

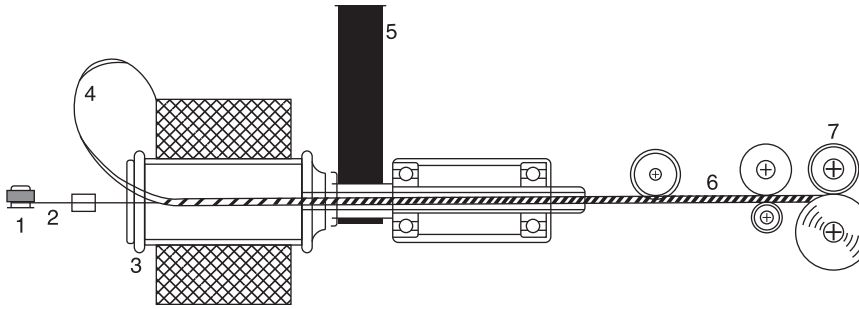

2.7 Profile of a rotor twister:[24] 1. a tension device; 2. polyester filaments; 3. rotor, 4. polypropylene filaments; 5. belt; 6. complex covered yarn; 7. take-up roller.

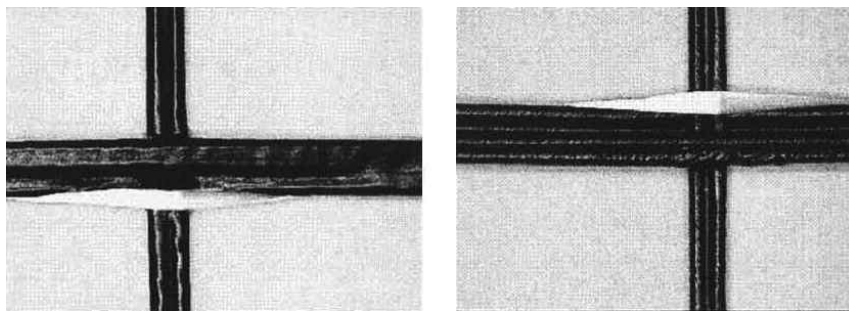

2.8 Grids with completely melted covering material.[24]

PET and PP were selected as the materials herein, because of the economic and mechanical considerations. The PP/PET composite-covered yarn produced by the rotor twister had several advantages, as shown in the following. First, the covered yarn was of desirable strength. Second, the 30/70 (PP/PET) covered yarns were relatively cheap to manufacture and produced lighter geogrids, which could be more conveniently transported and constructed. Finally, unlike polyvinyl chloride, PP is not toxic and so does not pollute the environment. The findings reveal that a twist multiple of 8.3 and a heating time of 4 minutes were optimal for spinning composite-covered yarn. The longitudinal and transverse tension resistances of this composite-covered yarn were 46.4 kN/m and 23.2 kN/m; the junction strength reached 6.2 kN/m, and the longitudinal elongation was 11.4%. The experimental results indicate that the geogrids with the covered yarns under the specified conditions were more effective than the usual woven geogrids because they had a lighter unit weight.

2.5 Natural fibre yarn manufacture

Among natural fibres, cotton is rarely found in technical applications of civil engineering like flax, jute and other bast fibres that are commonly used in geotextile applications. Hence, only the manufacturing methods followed for these bast fibres are discussed.

The flax fibre, a bast fibre, grows in bundles embedded in the layer of pectinous gums that lie between the woody core and the outer bark of the flax plant stem.[25,26] The plant achieves a height of up to 1.5 m and each fibre is composed of a large number of ultimates that have a mean length of about 30 mm and a mean diameter of about 20 μm; the ultimates are cemented together by the same pectinous gums that permeate the whole fibre layer. Jute fibre, also a bast fibre, grows in concentric layers of bundles around the central woody core of the plant stem which may grow up to about 5 m tall and up to 20 mm thick. The ultimates of jute are much shorter than those in flax, having a mean length of about 2.5 mm; the mean diameter is similar to that of flax, being about 18–20 μm. The conversion processes of these fibres into yarns are completely different to those of the conventional cotton-spinning process. Flow charts of the flax- and jute-processing sequences, i.e. conversion of fibres to yarns, are given in Fig. 2.9(a) and Fig. 2.9(b), respectively.

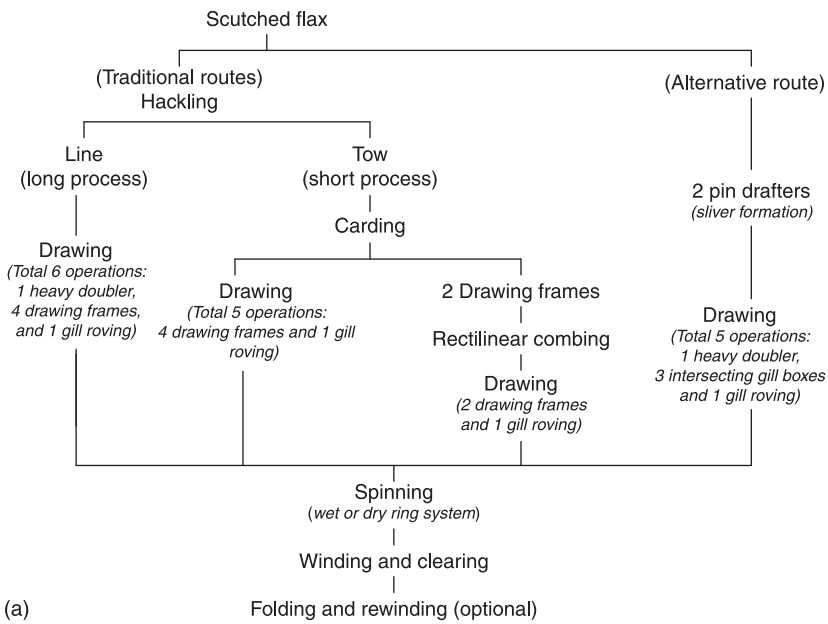

2.9 (a) Flow chart of the flax yarn manufacturing process.

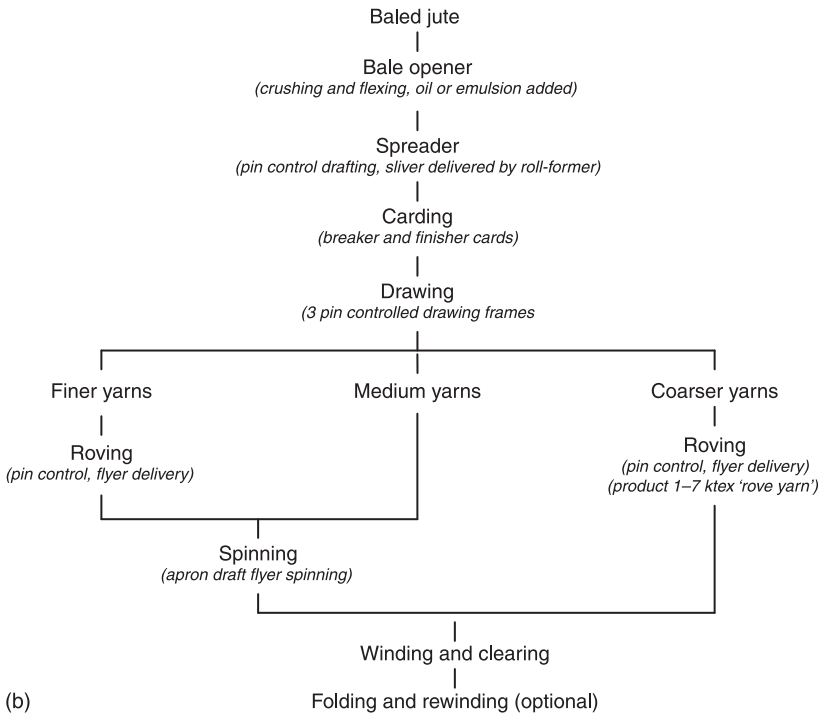

2.9 (b) Flow chart of the jute yarn manufacturing process.

2.5.1 Fibre extraction and preparation

Flax fibre

The bulk of the flax fibre bundles are interconnected and form a network from root to tip, but the majority of forks are in the form of an upright 'Y' when the plant is standing. For this reason, a short section of the root end is processed first in both hackling and scutching, allowing the remaining length to be processed towards the tip, thereby minimizing the breakage of the bundles.[26] About one third of the stem is fibre, and the rest is made up of the woody core and the outer bark. The seeds are usually mechanically removed from the head of the plant before retting.

Retting

Retting consists of a fermentation process that decomposes the pectins that hold the fibre bundles, and it also rots the woody part of the stem so that it will break up and aid its removal.

Drying

Drying is used to terminate retting before undue damage occurs to the fibre bundles themselves, and to enable the dried straw to be stored for a few weeks if necessary before further processing.

Breaking and scutching

Breaking consists of passing the straw root-end first between six to twelve pairs of intermeshing fluted rollers, which do not contact each other, in order to crush and break the brittle parts of the straw prior to scutching. The objective of scutching is to remove the crushed wood and cortex from the fibre bundles with a minimum of fibre breakage.

Hackling

Hackling is intended to produce the finest and longest fibres possible by disentangling and straightening the fibres; by separating the fibre bundles and splitting each bundle up; by removing the remaining impurities after scutching; and by removing short fibres, known as hackling tow.

Jute fibre

After harvesting, the stems are stripped of the leaves, etc., and are retted prior to stripping of the fibre bundles from the stem before being dried and baled. At this stage the jute is in the form of a long mesh of interconnected fibres ranging from 1 to 4.5 m long. The jute is subjected to flexing and crushing actions with oil or emulsion added, prior to carding which breaks the jute into separate branched 'fibres'. It is restricted to coarse yarns, in which appearance is usually of minor importance, for use in products such as sacking, carpet backing and some wall coverings.[25]

2.5.2 Carding

Flax carding

Flax tow from processes such as scutching and hackling are passed through a worker and stripper-type carding process.[27] The tow is finer and shorter from each succeeding process prior to carding. The tows, which form during the extraction and preparation process, may consist of a combination of single ultimates and some fine bundles which have been stripped from the line fibres – fibre strands torn from the line more-or-less intact, plus dirt, and neps.

In addition to the general objectives of carding, the flax-carding process aims to split the fibre bundles to form fine structures that can then be treated as fibres. The

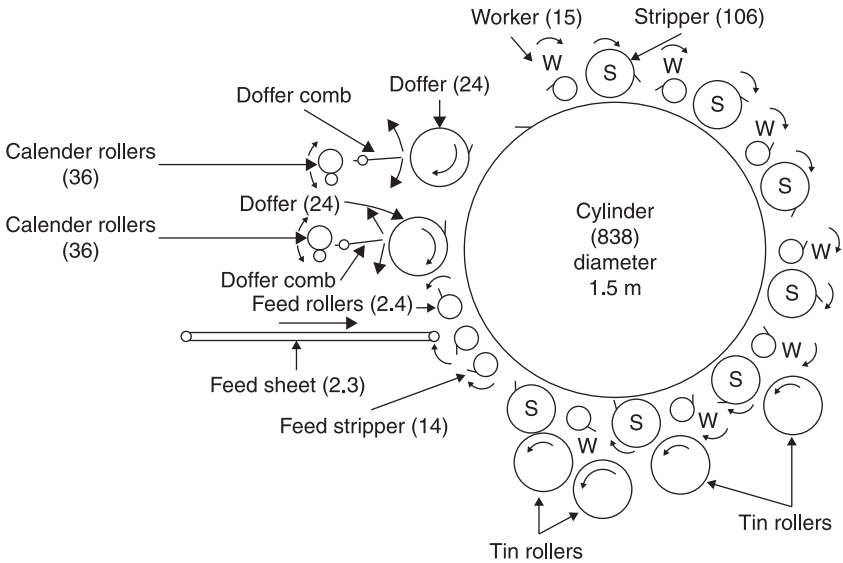

2.10 Roller arrangement on a flax breaker-finisher card (figures in brackets represent surface speed in m/min).[27]

roller arrangement of a flax breaker-finisher card is shown in Fig. 2.10. This particular machine arrangement is described as a down-striking, seven pair, full-circular card with double doffers. The fibres, after feeding, are carded by a series of pairs of pinned rollers called workers and strippers.

Jute carding

The jute-carding process is intended to break the jute reeds into separate fibres, which may be composed of single, branched, or intermeshed structures. The fibre length of a carded jute sliver is very variable, with a small number of long fibres and a large number of short fibres. The basic operations of jute carding are similar to that of flax carding. Jute fibres, in general, contain higher quantity of trash materials, so a two-stage carding process is recommended, i.e. a breaker card at first stage, which mainly removes dust and trash particles, followed by a finisher card for final carding action.[27] The general roller arrangements of jute breaker and finisher cards are shown in Fig. 2.11 and Fig. 2.12 respectively. The breaker card is mainly for harsh action whereas the finisher card is for relatively gentle action.

Breaker cards are usually down-striking and half circular because bits of bark, stick, and small fibres fall down from the point of feed. The delivered sliver is usually about 60–90 ktex. Finisher cards are usually down-striking and full-circular, and deliver a sliver of about 90 ktex.

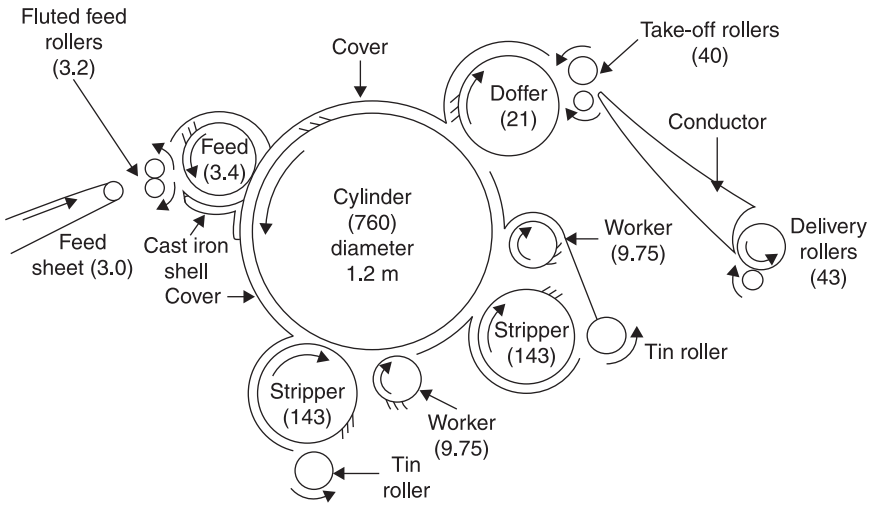

2.11 Roller arrangement on a jute breaker card (figures in brackets represent surface speed in m/min).[27]

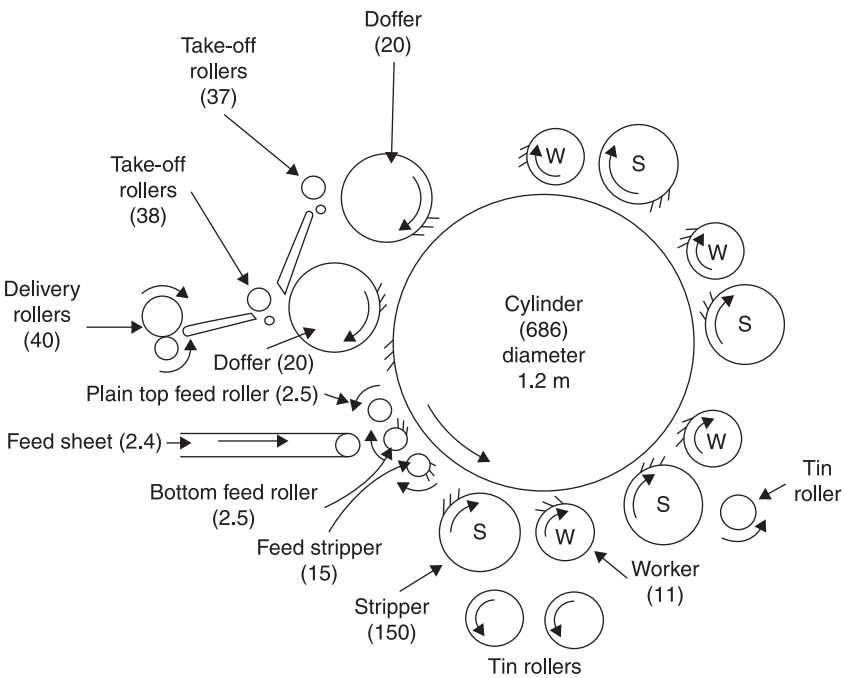

2.12 Roller arrangement on a jute finisher card (figures in brackets represent surface speed in m/min).[27]

2.5.3 Drawing

The traditional drawing machines used in flax drawing provide fibre control in drafting by using upward-pointing faller pins in the drafting zone.[26] It is usual for the fallers to have a higher surface speed than the back rollers; this is known as 'lead' or 'back draft'. Back draft is necessary to ensure adequate pin penetration, but it is normally kept as low as possible. However, double-pin control drawing has been widely used in the processing of relatively long fibres such as jute, flax, spun silk, and worsted. A side elevation of the main working parts of a double-faller (intersecting gill box) drawing system is shown in Fig. 2.13.

To help to minimize the drafting irregularities generated during the faller movement, a front doubling plate is fitted to combine the slivers from each drafting head into a single composite delivered sliver: this arrangement is represented in Fig. 2.14. By using this method, the load in the pins at each head is reduced (a single sliver is fed in to each drafting zone) and yet a thick enough composite sliver is produced to provide adequate cohesion for can delivery. At the same time, by using a 'good' front draft between the fallers and the front rollers of the drafting zone, the faller-bar marks from each head can be displaced longitudinally relative to each other to reduce their effect in the composite delivered sliver.

In jute drawing, the sliver from the finisher card is passed through a drawing set usually consisting of three drawing frames which are similar to those used in flax processing with pin control during drafting, and on the first two operations a front doubling-plate arrangement at the delivery.[25] A jute card sliver contains a large number of short fibres, about 60% of the fibres may be shorter than the front ratch, which is usually about 50 mm. Consequently the front doubling plate, as in the case of flax drawing, and a good front draft are essential features in jute drawing.

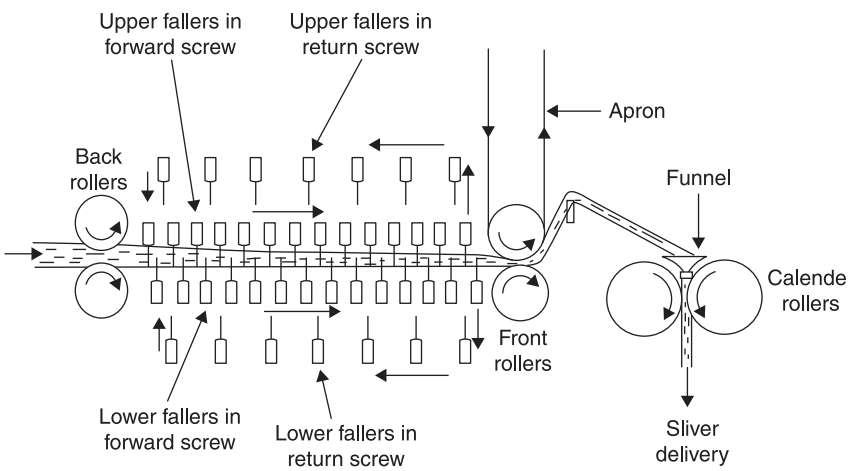

2.13 Intersecting gillbox: side view of main working parts.[26]

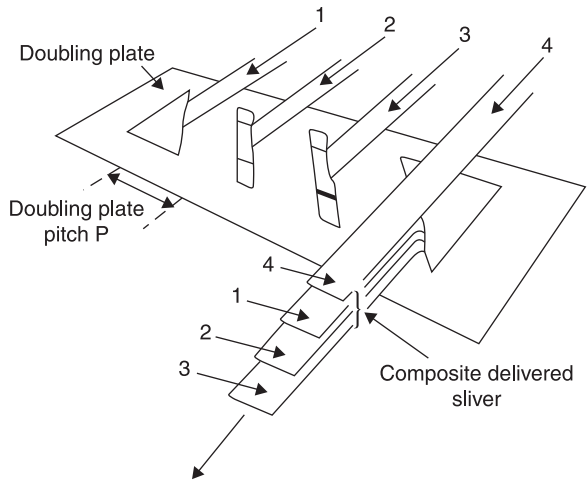

2.14 Flax or jute drawing front doubling plate.[26]

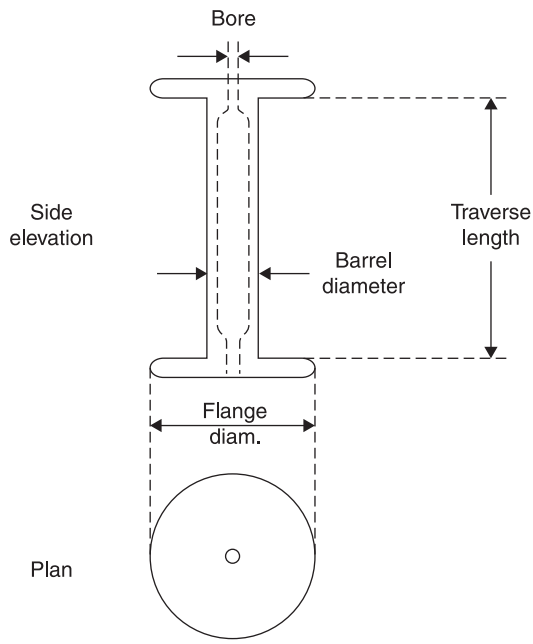

2.15 Flyer lead delivery double-flanged bobbin.[25]

A back draft of about 1.05 helps to ensure suitable pin penetration of the single set of upward-pointing faller pins.

2.5.4 Spinning

This is the final process of yarn manufacturing. The spinning process basically consists of three important stages. (a) Reduction of strand thickness from the supply roving (or sliver) to the required yarn count. This is usually done by roller drafting with some means of fibre control such as double apron, but a different arrangement is used in open-end spinning and in mule spinning. It is important that the correct yarn count is produced, because there is no subsequent opportunity for correcting any mistakes in this respect. (b) The prevention of further fibre slippage – usually by twist insertion, although there are other methods. (c) Winding on to a package which is convenient for handling and which protects the yarn. There are different types of spinning machines for jute/flax fibres, e.g. flyer spinning, ring spinning and cap spinning.[25,26] Of the conventional frame-spinning machines, ring spinning has proved to be the most amenable to improvements in speed and

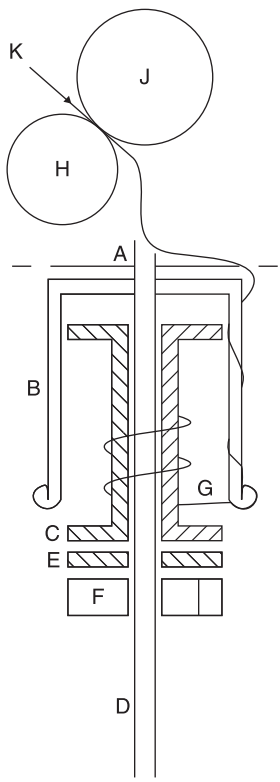

2.16 Flyer lead delivery side elevation.[25]

package size. The flyer-spinning method uses the yarn to pull the bobbin round; it is only suitable for thick counts and, because of relatively lower spindle speed, flyer spinning has been replaced by ring spinning where possible. It is also used for spinning flax, hemp, and jute yarns thicker than about 240 tex at spindle speeds up to about 5000 rev/min with a bobbin capacity of about 500–600 g. This method is used where twist insertion is required as well as package formation; the type of package used is a double-flanged bobbin (Fig. 2.15). The method is only suitable for relatively long and strong fibrous materials such as jute and flax, because the slubbing produced must be strong enough to pull the bobbin round during winding on. There is no drive to the bobbin and it rotates by flyer with the help of yarn pull. The twisting take place by flyer rotation, whereas the winding is carried out due to a difference in motion of the flyer and the bobbin.

The spindle arrangement in the flyer-spinning method is shown in Fig. 2.16. (a) hollow spindle top; (b) flyer leg; (c) bobbin; (d) spindle (driven from bottom); (e) felt drag washer; (f) lifter rail (vertical traverse); (g) slubbing (pulling bobbin round); (h) drafting zone bottom front roller; (j) drafting zone top front roller; (k) drafted fibres.

2.6 Yarn parameters on cement reinforcement

2.6.1 Fibre type and yarn bundle size

Textile fabric reinforcements can be in knitted, woven, non-woven, glued, or plaited structures, which differ by the manufacturing process and several other parameters such as yarn density, the fineness and the number of filaments in the bundle that construct the fabric. These characteristics can influence the stability and the mechanical properties of the whole fabric, ultimately affecting the penetrability of the particulate cement matrix. For example, a fabric comprising multifilament yarns (bundles) reduces the potential penetrability of the cement particles between the bundle spaces since the junction points of the fabric induce tightening effects that hold the bundle filaments firmly in place and prevent them from opening.[6,28]

Alva Peled *et al*.[29] used different types of yarns, namely HDPE, aramid, AR-glass and PP to produce weft insertion, warp-knitted fabrics as shown in Fig. 2.17. Straight yarns in the warp direction (lengthwise) were inserted into stitches (loops) and assembled together with straight yarns in the weft direction (crosswise). The stitches were tightly connected with the two sets of perpendicular yarns, which were very difficult to separate, thereby producing a single, strong unit of fabric. All yarns, warp and weft, were in a multifilament non-twisted form. The stitches in all the fabrics were arranged at a density of 2.5 stitches per cm and were made from 16.7 tex PP (tex being a measurement of yarn or bundle weight per length ratio, in grams per 1000 m of yarn). The weft yarns were inserted into every second loop (stitch), giving the fabric a 'one loop in one loop out' structure, so that between every two weft yarns was an empty loop. This design gave a

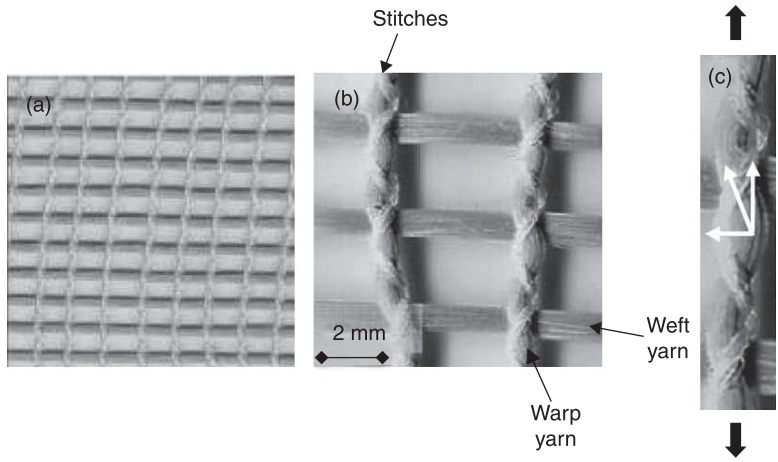

2.17 Weft insertion warp-knitted fabrics for cement reinforcement. (a) Over structure of the weft insertion warp knitted fabric; (b) Details of the stitches; (c) Components of forces acting in the loop.[29]

relatively open net structure that enhanced cement penetrability (Fig. 2.17(b)). The weft yarns in all the fabrics were composed from aramid with 167 tex yarns. Oriented in the warp direction, the reinforcing yarns comprised different raw materials: HDPE, aramid, AR-glass and PP.

In this work, it was found that the geometry of warp-knitted fabric strongly influenced the performance of cement-based composites and, therefore, fabric geometry must be carefully considered when fabric is used to reinforce such composites. Two main parameters were studied: the size of the loops composing the knitted fabric, and the linear density of the reinforcing yarns in the fabrics (bundles, their tex number). Increasing loop size and reducing bundle size improve composite performance. The influence of loop size was more pronounced with larger bundle sizes, due to their improved cement penetrability between the reinforcing filaments. Composites made from aramid and HDPE fabric exhibited the best tensile performance in terms of strength and toughness. Glass fabric composites showed improved performance at low strain values but with brittle behaviour.

The PP fabric did not bond strongly with the cement matrix, resulting in relatively low composite performance. The aramid–PP yarn combination in a hybrid fabric should be considered as reinforcement for cement composites. It exhibited behaviour similar to that of the single-aramid composite, when half of the aramid yarns were replaced with the inferior, low-cost PP yarns. Although its volume content (Vf) of reinforcement, 2.6%, was much lower, the hybrid composite also performed much better than the single PP fabric composite, which had a Vf of 6.2%.

2.6.2 Yarn crimp

In general, the use of high-strength, high-modulus fibre, such as glass, carbon, aramid and high-density polyethylene (HDPE), usually increases the strength and toughness of the cement composite, providing strain-hardening behaviour. Low-modulus fibre, such as polypropylene (PP) and polyethylene (PE), enhances mainly the ductility of the cement composite, but not its strength, resulting in a strain-softening or elastic–plastic behaviour.

Several researchers studied the influence of the modulus elasticity of the fibre on the bond between the fibre and the cement matrix.[6,30] It was reported that increasing the modulus of elasticity of the fibre enhances the bond strength. Low modulus fibres such as PE and PP develop low bond with the cement matrix, whereas high modulus fibres such as aramid, carbon or HDPE provide a strong bond with a cement matrix. This is due to higher clamping stresses which develop around the fibres due to matrix autogenously shrinkage.[30] Also, in the low modulus yarns, there is a detrimental effect on bond strength induced by Poisson effect.[31] Such differences in bonding affect the mechanical behaviour of the cement composite. Despite the hydrophobic characteristics of PP and PE fibres and their poor bond with the cement matrix, these fibres are considered as attractive for the reinforcement of cement matrices because of their high resistance to the alkaline environment of the cement matrix (about 12.5 pH) and their low cost. In view of this, there is an interest to improve the bond of the low-modulus fibres with the cement matrix, which can lead to a strain-hardening behaviour of the low-modulus fibre composites. Several studies were carried out employing various methods to alter the surface of fibres by changing the geometry of the fibres, as well as treating the fibre surface by physical and chemical means.[32,33,34] Also, modifications of the cement matrix with PP fibres by addition of polymers were studied to improve bond.[35] The biggest improvement was achieved with fibres having special geometry such as crimped, twisted, fibrillated or mesh form. These special geometries can provide a mechanical anchoring of the fibre to the cement matrix, resulting in a strong bonding. In a mesh form, for example, the mechanical anchoring is developed by the penetration of the cement matrix in between the openings of the mesh.

Three different fabric structures were studied by Paled *et al.*:[9] weft insertion warp-knitted fabric (Fig. 2.18(a)), short weft warp-knitted fabrics (Fig. 2.18(b)), and woven fabric (plain weave (Fig. 2.18(c)) [weft and warp are the terms used for the yarns in the different orientations of the fabrics]. The fabric structures differ by the way the yarns are combined together: (a) In the weft-insertion knitted fabric the reinforcing yarns are straight (this fabric is similar to the fabrics used in plastic composites); (b) In the short weft-knitted fabric the reinforcing yarns are in a relatively complicated geometry; (c) In the woven fabric the reinforcing yarns are in a crimped shape.

The geometry of the fabric showed a marked effect on the flexural properties of cement composites, demonstrating opposing influences: improved performance

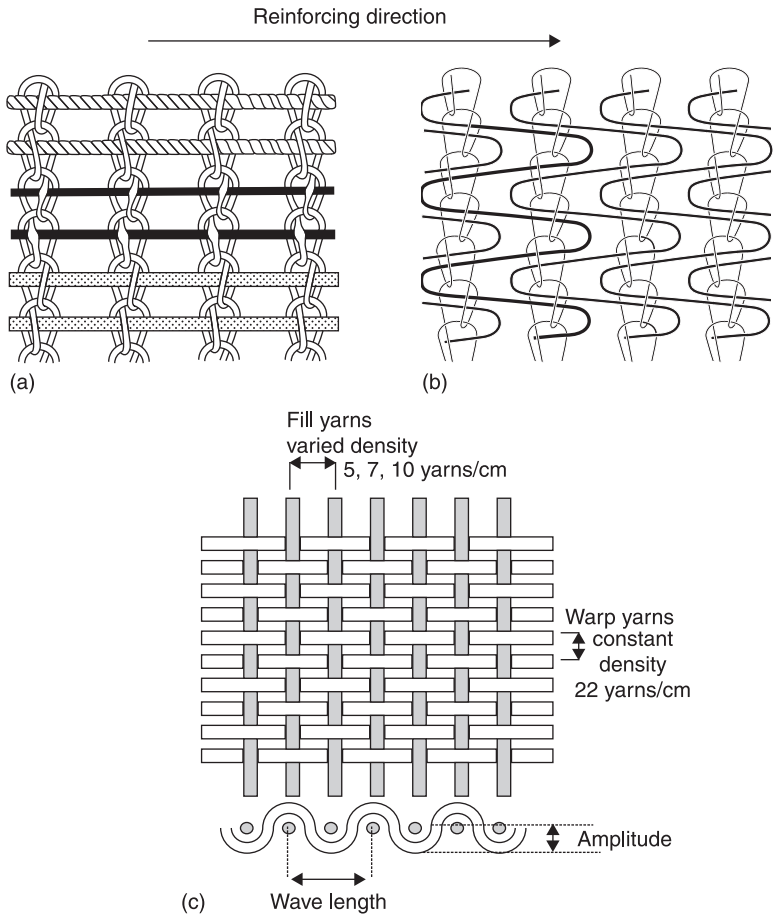

2.18 The different fabric structures: (a) weft insertion knitted fabric; (b) short weft-knitted fabric; (c) woven fabric (plain weave).[9]

of woven and short weft-knitted fabrics (compared to the straight yarn), and reducing drastically the performance of weft-insertion knitted fabric (compared to the straight yarn). It should be kept in mind that the shape and nature of the individual yarn in the different fabrics are rather different: in the weft-insertion knitted fabrics, the yarns are in a bundled form and a straight geometry, whereas in the woven and short weft-knitted fabrics they are monofilament and do not maintain straight geometry (they are in crimp geometry in woven fabrics and in a relatively complex geometry, 'zigzag' in the short weft-knitted fabric). Such differences in yarn geometry and nature may affect the bond and as a result the overall flexural performance.

It was shown that the woven fabric structure significantly improves the bonding with cement matrix, compared to its straight yarn that is not in a fabric form. The

crimped geometry of the individual yarn within the woven fabric was found to have the major contribution to its bonding, due to a strong anchoring effect. This improved bonding by the crimped geometry may explain the increased flexural performance with a strain-hardening response of the composites with the woven fabrics. The improved flexural strength induced by the crimp geometry of the individual yarn is seen in Fig. 2.19, in which comparison is made with the flexural behaviour of a woven fabric, individual crimped yarns untied from this fabric and individual straight yarns from the same material. Both composites, with woven fabric and untied crimped yarns, performed much better than the composite reinforced with straight yarns; whereas the crimped yarn composite is the best. Moreover, the efficiency values in flexural strength are also higher for the crimped yarn (untied from the fabric) compared to the woven fabric (Fig. 2.20). It can be concluded that the improved mechanical performance of the woven fabric can be accounted for by the crimped geometry of its individual yarns, which is associated with improved bonding.

In the short weft-knitted fabric, the shape of the reinforcing yarns is more complex than the crimping geometry of the yarn in the woven fabric. Moreover, these reinforcing yarns are held tightly by the fabric structure, which apparently induces extremely strong anchoring effects. This enhanced bonding can result in the improved performance of the composite with the short weft-knitted fabric, leading to a strain-hardening behaviour and an extremely high efficiency factor in flexural strength. The situation is quite different for the weft-insertion knitted fabric, where the fabric structure is associated with a marked reduction in flexural properties. In this case, the values of the efficiency factors are lower than the

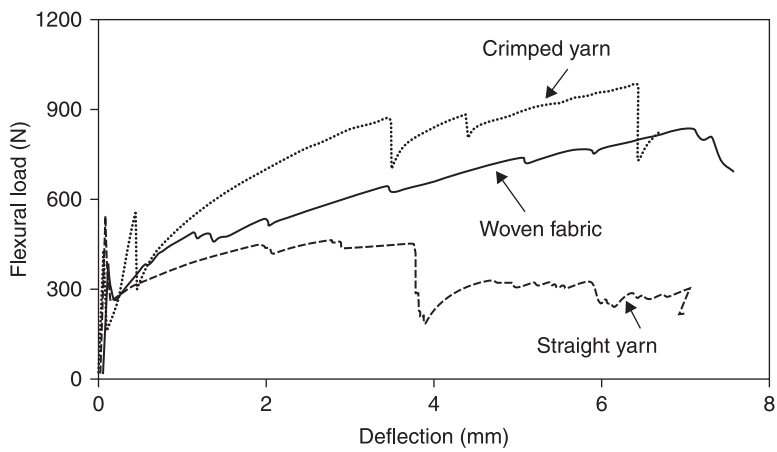

2.19 Flexural behaviour of cement composites with woven fabric, untied crimped yarns and straight yarns, all from PE (fabric and yarns are with a density of 7 fills/crimps per cm, Vf 5.7%).[9]

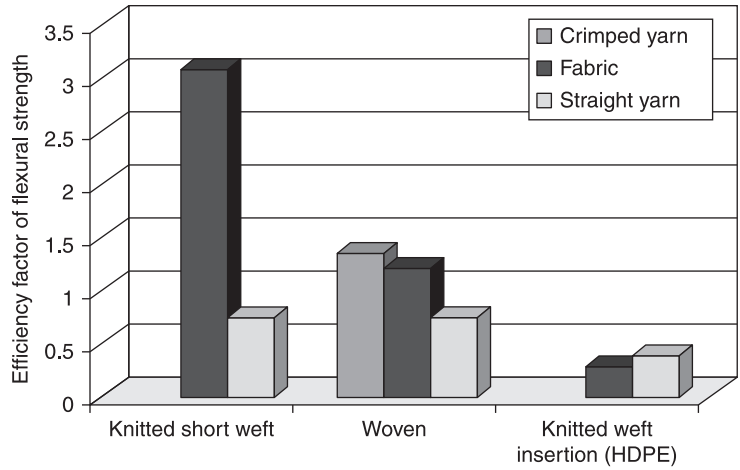

2.20 Efficiency factors of flexural strength for the different fabrics, untied crimped yarns and straight yarns.[9]

values of the straight yarns for both HDPE and PP composites. This correlates with the poor bond of these knitted fabrics. In the weft insertion knitted fabrics the yarns are bundled and straight, as well as being connected at the joint points by stitches. The efficiency of bundles as reinforcement for the cement composite was found to be quite low, due to poor penetration of the matrix between the filaments.[36,37] When these bundles are kept in a straight form, but as part of a knitted fabric structure, the penetrability of the matrix is even lower, due to the presence of the bulky stitches themselves, as well as the tightening effect of the stitches, which strongly hold the filaments in the bundle and prevent spaces from being opened between them. Therefore, the bigger decrease in bonding occurred in the bundled yarns with the larger number of filaments, i.e. with the HDPE having 900 filaments. This HDPE knitted fabric shows a poor performance relative to the superior properties of its yarn (it is no better than the low modulus PE fabrics). A similar trend is also observed for the PP composites.

2.6.3 Geometrical characteristics of yarn

Alva Peled *et al*. studied the effect of geometrical characteristics of the individual nylon yarns on the bond strength in concrete.[6] In the case of bundled yarns, twisting is often employed. Figure 2.21 compares the external interfacial bonding of bundles (made from nylon) with various geometries: straight, twisted, double-twisted (×2) and double-twisted (×2) with latex coating.

The latex coating, which is hydrophilic in nature, was applied with the intention of increasing the bonding with the cement matrix. It is quite clear that twisting of the bundle improved the bonding considerably. This bond improvement was

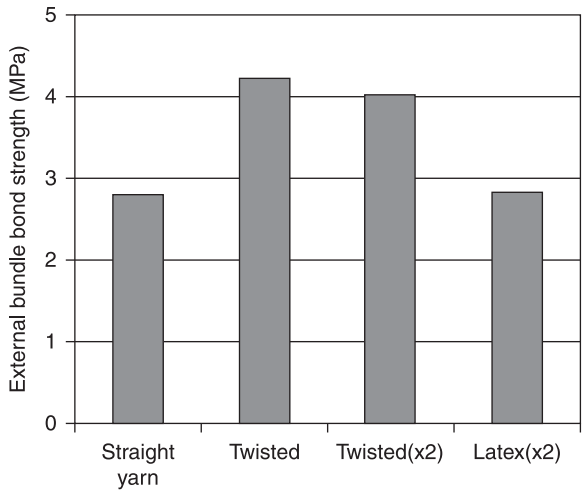

2.21 External bond properties of nylon bundle with various geometries.[6]

supported by microstructural characterization using SEM. The twisted fibrils remained in the groove after the pull-out, which is indicative of an intimate bonding and, perhaps, some anchoring effect. With the straight yarns, the fibrils separated completely from the groove and none were seen to remain there. Twisting together of two separate twisted yarns did not enhance the bonding significantly compared to a single twisted yarn (Fig. 2.21). The latex coating decreases the bond properties (Fig. 2.21), and this reduction may be due to the smooth surface created on the bundle by the latex coating, which perhaps acts as a bond breaker rather than a sizing for bond improvement.

The yarn in the fabric does not always maintain a simple straight geometry. This is the case for the yarn in the woven fabric, which is forced to undulate above and below the perpendicular yarns that it crosses. The extent of crimping (i.e. crimp density) is a function of the fabric density. The influences of individual yarn geometry on the bond showed a marked improvement in the bond of deformed yarns over that of a straight yarn. This can be attributed to the irregular shape of these yarns, which leads to mechanical anchoring to the cement matrix. The improvement in bond is larger in the crimped yarns (increase by a factor of 3.5–4) and is smaller in twisted yarn (increase by a factor of about 1.5).

2.7 Conclusions

Textile materials in various forms are used in civil engineering construction towards attaining various functions such as reinforcement, insulation, filtration, drainage, etc. In this chapter, different types of yarns of both natural and synthetic

origins that are used in these applications are discussed. Yarns made out of high-tenacity polyester filaments, high-tenacity nylon and glass fibres are used in geogrids. Composite yarns spun from multifilament and staple fibres have undergone much research and development, to produce favourable yarn characteristics and to increase the yield of the yarn. The complex covered yarn manufactured using an innovative technology for weaving a grid is explained in detail. Methods of manufacturing of yarns used in civil engineering for both synthetic and natural fibres are provided. The influence of yarn structure, the crimp, bundle size and other geometrical features are discussed in detail.

2.8 References

1. Reinhardt HW, Kruger M and Grosse U (2003) Concrete prestressed with textile fabric. *J Adv Concrete Technol* 1(3):231–239.
2. Bentur A, Peled A and Yankelevsky D (1997) Enhanced bonding of low modulus polymer fibres-cement matrix by means of crimped geometry. *J Cement Concrete Res* 27(7):1099–1111.
3. Jesse F and Curbach M (2003) Strength of continuous AR-glass fibre reinforcement of cementitious composites, in *Fourth International Workshop on High Performance Fibre Reinforced Cement Composites* (*HPFRCC 4*). Bagneux, FR: RILEM Publications, pp. 337–348.
4. Peled A, Bentur A and Yankelevsky D (1998) Effects of woven fabrics geometry on the bonding performance of cementitious composites: mechanical performance. *J Adv Cement Based Mater* 7(1):20–27.
5. Peled A, Bentur A and Yankelevsky D (1999) Flexural performance of cementitious composites reinforced by woven fabrics. *J Mater Civil Eng (ASCE)* 11(4):325–30.
6. Peled A and Bentur A (2000) Geometrical characteristics and efficiency of textile fabrics for reinforcing composites. *J Cement Concrete Res* 30:781–790.
7. Peled A and Mobasher B (2000) Pultruded fabric–cement composites. *ACI Mater J* 102(1):15–23.
8. Peled A, Sueki S and Mobasher B (2006) Bonding in fabric–cement systems: effects of fabrication methods. *J Cement Concrete Res* 36(9):1661–1671.
9. Peled A. and Bentur A (2003) Fabric structure and its reinforcing efficiency in textile reinforced cement composites, in *Composites: Part A 34*, pp. 107–118.
10. Benmoktane B, Chaallalt O, and Masmoudi R (1995) Glass fibre reinforced plastic (GFRP) rebars for concrete structures. *Construction and Building Materials* 9(6): 353–364.
11. Nawy EG and Neuwerth GE (1971) Behaviour of fibre glass reinforced concrete beams. *J Struct Civil Eng (ASCE)* September: 2203–2215.
12. Meier U (1992) Carbon fibre-reinforced polymers: modern materials in bridge engineering. *Struct Eng Int* 1.
13. Meier U and Meier H (1996) CFRP finds use in cable support for bridge. *Mod Plastics* 4.
14. Soroushian P, Atef T, Alhozaimy A and Khan A (1993) Development and characterization of hybrid polyethylene-fibre-reinforced cement composites. *Construction and Building Materials* 7(4):221.
15. Youjiang Wang, Victor C Li and Backer S (1990) Tensile Properties of Synthetic Fibre Reinforced Mortar. *Cement & Concrete Composites* 12:29–40.

16. Ochi T, Okubo S and Fukui K (2007) Development of recycled PET fibre and its application as concrete-reinforcing fibre. *Cement & Concrete Composites* 29:448–455.
17. El Mogahzy Y (2008) *Engineering Textiles: Integrating the Design and Manufacture of Textile Products*. Cambridge: Woodhead Publishing Ltd.
18. Horrocks AR and Anand SC (eds) (2000) *Handbook of Technical Textiles*. Cambridge: Woodhead Publishing Ltd, pp. 43–60 and 358–405.
19. Van Santvoort GPTM (1994) *Geotextiles and Geomembranes in Civil Engineering*. London: Taylor & Francis, pp. 45–67.
20. Ching-Iuan Su, Ching-Shyang Leu, (1998) Cross-Sectional Structure of Composite Yarns. *Textile Res. J*. 68(10):715–718.
21. GRI Test Method GG2, Standard Test Method for 'Individual Geogrid Junction Strength'. Drexel: Geosynthetics Research Institute.
22. Jeon HY, Kim SH, and Yoo HK (2002) Assessment of long-term performances of polyester geogrids by accelerated creep test. *Polymer Testing* 21:489–495.
23. Mohammadian M, Allen NS and Edge M (1991) Environmental Degradation of Polyethylene Terephthalate. *Textile Res. J*. 61(11):690–696
24. El Mogahzy YE, Gowayed Y and Elton D (1994) Theory of Soil/Geotextile Interaction. *Textile Res J* 64(12):744–755.
25. Atkinson RR (1964) *Jute – Fibre to Yarn*. Mesa, AZ: Heywood.
26. Pringle A V, The theory of flax spinning, H. R. Carter, Belfast (1949).
27. Mather JN (1969) *Carding – Jute and Similar Fibres*. Cambridge: Iliffe.
28. Jesse F, Ortlepp R and Curbach M (2002) Tensile. Stress–strain behavior of textile reinforced concrete, in *Proc. IABSE Symposium*, Melbourne (September).
29. Peled A, Cohen, Pasder Y, Roye A and Gries T (2008) Influences of textile characteristics on the tensile properties of warp knitted cement based composites. *Cement & Concrete Composites* 30:174–183.
30. Stang H (1996) Significance of shrinkage-induced clamping pressure in fibre–matrix bonding in cementitious composite materials. *Adv Cem Bas Mater* 4:106–115.
31. Bentur A and Mindess S (1990) *Fibre-Reinforced Cementitious Composites*. Amsterdam: Elsevier.
32. Peled A, Guttman H and Bentur A (1992) Treatments of polypropylene fibres to optimize their reinforcing efficiency in cement composites. *Cem Concr Compos* 14:227–285.
33. Li VC, Wang W and Backer S (1990) Effect of inclining angle, bundling and surface treatment on synthetic fibre pull-out from cement matrix. *Composites* 21:132–140.
34. Hannanh DJ, Zonsveld JJ and Hughes DC (1978) Polypropylene film in cement based materials. *Composites* 9:83–88.
35. Chu TJ, Robertson RE, Najm H and Naaman AE (1994) Effect of polyvinyl alcohol on fibre cement interfaces. Part II. Microstructure. *Adv Cem Bas Mater* (3):122–130.
36. Balaguru PN and Shah SP (1992) *Fibre-Reinforced Cement Composites*. New York: McGraw-Hill.
37. Bartos PJM and Zhu S (1997) Assessment of interfacial microstructure and bond properties in aged GRC using a novel micro-indentation method. *Cem Concr Res* 27:1701–1712.

3

Textile structures

R. FANGUEIRO and F. SOUTINHO,
University of Minho, Portugal

Abstract: This chapter presents an overview of the textile structures used in civil engineering, including planar, three-dimensional, directionally oriented and hybrid fibrous structures. The techniques to produce these fibrous structures, ie, weaving, knitting, braiding and nonwoven, are described and discussed. Several examples of applications of textile structures in civil engineering are presented illustrating the large range of possibilities provided by fibrous materials for this purpose. Moreover, the required guidelines for fibrous structure selection according to the requirements of a particular application are presented.

Key words: textile structures, 3D fabrics, woven fabrics, nonwoven fabrics, braided fabrics, warp-knitted fabrics, DOS structures and hybrid structures.

3.1 Introduction

Textile structures, in the form of woven, knitted, braided or nonwoven fabrics, are used in civil engineering in many applications due to their excellent properties provided by the type, orientation and architecture of the fibers used. Textile techniques, including weaving, braiding, knitting and nonwoven, are just used to place these fibers according to the requirements of a particular application. The characteristics and properties of each textile structure determine its suitability for a particular application. For instance, due to the air content of the structure, a nonwoven fabric is more suitable for acoustic insulation than a woven fabric. On the other hand, a woven fabric, with fibers oriented at 0° and 90°, is much more suitable for structural reinforcing purposes, like concrete reinforcement, than a knitted or a nonwoven fabric. Textile techniques provide a wide range of fiber orientation and architecture possibilities from planar to very complex three-dimensional (3D) fibrous structures with fibers oriented in the third dimension.

Textile techniques may provide high strength and high modulus textile fabrics to the construction industry as a potential replacement for more traditional building materials such as wood, concrete, masonry, and steel (Isley, 2002).

One of the most promising and interesting application fields of textile structures is concrete reinforcement. Concrete structures are constantly subjected to loads as well as to aggressive and degrading agents. These drawbacks lead to a poor mechanical performance, a limited service life and to a high rehabilitation-maintenance cost. Recently, a new approach to concrete reinforcement has been developed in order to overcome steel-reinforced-concrete deterioration problems, and improve the service life and durability. Textile reinforced concrete (TRC) is

an innovative material where fibrous structures are used as reinforcement material for concrete elements. TRC, benefiting from corrosion resistance and light weight, has proven to be attractive in many applications and presents many opportunities to be used as an alternative material to replace conventional materials such as timber, steel and aluminium in buildings. Besides, TRC can provide an important contribution to the safe and economical use of resources (Isley, 2002).

The use of fibrous structures as reinforcement of cementitious composites is potentially quite attractive. Fibrous structures – for example, knitted, woven and braided fabrics – have been recognized as very attractive composite reinforcement materials thanks to the possibility of producing preforms, and allowing fiber orientation according to the application needs, conformability and handling (Marques, 2008).

Regarding production processes, there are only a few that can be used to manufacture fibrous structures for concrete reinforcement. Each manufacturing process allows the production of a wide range of reinforcements with the required mechanical properties. The most important factor in these structures is the possibility of creating an open grid-like structure, with high stability, not only giving good permeability/adhesion with concrete, but also ensuring a reasonable handling of the structure – one the yarns/filaments cannot displace (Scardino, 2009; Brameshuber, 2006).

The main textile technologies to produce fibrous structures for composites are weaving, knitting, braiding and nonwoven production techniques. Each of these technologies can produce products from conventional to innovative structures. The selection of the appropriate structure depends on the financial nature and also on the main restrictions imposed by the application itself.

Textile structures can be used for concrete reinforcement in different applications, including (Weiland, 2007):

- strengthening, rehabilitation and retrofitting (slabs, beams, columns, shear, torsion);
- semifinished products (integrated formworks, formwork elements);
- new structural members/buildings (facades, slabs, structural elements);
- industrial products/consumer goods (design, concrete furniture, engineering);
- artwork (sculptures, repair, etc.).

3.1.1 Classification of textile structures

There are various ways of classifying textile structures considering the different factors. The most commonly used classification considers the technique used to produce each structure, grouping textile structures into woven, knitted, braided or nonwoven fabrics if, respectively, weaving, knitting, braiding and nonwoven techniques are used. This classification is commonly used in conventional textiles where the performance of the fabric itself is, most of the time, less important than

the aesthetics provided. However, for technical uses, the most suitable classification takes into consideration the orientation of the fibers in the structure, no matter what technique is used to produce it. In this way, textile structures can be classified as:

- planar or conventional structures (2D)
- three-dimensional structures (3D)
- directionally oriented structures (DOS)
- hybrid structures.

Two-dimensional (2D) planar structures

Figure 3.1 shows different 2D planar structures produced by the textile techniques mentioned previously. In a 2D planar structure, fibers are in-plane oriented and their production does not require any special adaptation of the existing textile technologies for the textile structures mostly used in conventional applications, such as clothing and household textiles. However, this type of structure, although produced by conventional processes, can also find many technical applications, depending on the type of fibers used.

2D nonwoven fabrics are produced directly from fibers that are randomly oriented in the structure in a discontinuous way; woven fabrics are produced by the orthogonal interlacement of two set of yarns, warp and weft, placed continuously at 0° and 90°; braided fabrics present fibers oriented continuously in the bias direction; knitted fabrics are formed by loops with segments of yarns/fibers oriented in different directions.

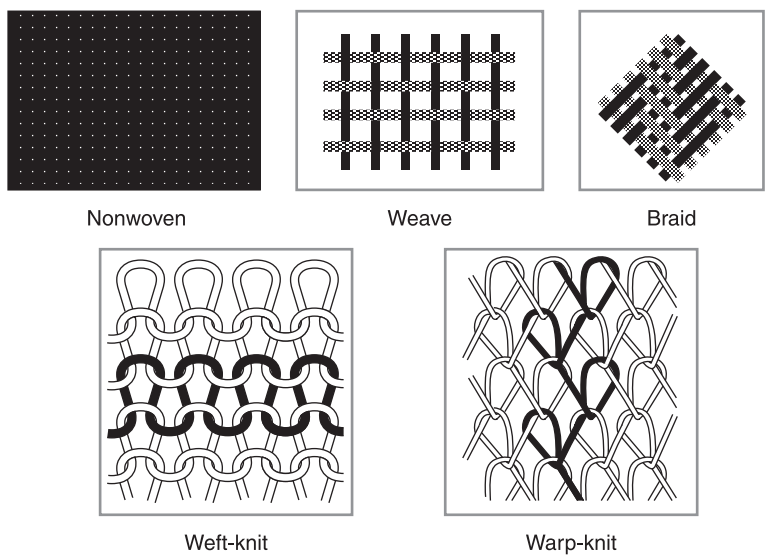

3.1 2D planar structures.

Three-dimensional (3D) structures

Three-dimensional (3D) structures are an organized and integrated set of fibers with multiaxial orientation, and the development of 3D structures first occurred in the nineteenth century. However, the large-scale application of these structures was initiated at the end of the 60s, answering the aerospace industry's needs to manufacture materials able to withstand multidirectional loads under extreme thermal conditions. The first composite materials were applied at the beginning of the 60s, being reinforced with planar 2D structure. Only later was it found what was required to solve the problem of the weak interlaminar resistance of the 2D structures. Since then, a great number of 3D textile structures have been developed, being able to meet the most demanding conditions of each end-use.

When compared to 2D fibrous structures, 3D structures provide high mechanical properties in x, y and z directions. These structures can be produced on special equipment which was already developed. Nowadays, there is a wide range of 3D structures that can be produced (Goran, 2005 and Krenkel, 2008).

There is no simple method to classify 3D textile structures. In general, any classification of these structures has to consider the macrogeometry (form and dimension); the structure formation method (construction) and the microgeometry of the resultant structure (that it includes the reinforcement directions); the linearity of the reinforcement in each direction; the continuity of the reinforcement; the density of the fibers; the size of the fiber beam in each direction and the geometric characteristic of the fiber beams – that is, linear or curvilinear, the degree of bending, etc.

Normally, 3D fibrous structures may be grouped as 3D solid structures with fibers oriented in the third dimension, and as 3D near-net-shape structures wherein fibers are forced, during the production process, to get a shaped architecture like a helmet, an elbow or a tube.

Figure 3.2 shows a representation of a 3D structure with fibers oriented in x, y and z directions.

Each production technique can form numerous 3D structures, including multilayer, sandwich or spacer and near-net-shape.

Directionally-oriented structures (DOS)

In order to improve the mechanical properties of the structures in predefined directions it is possible to in-lay reinforcing yarns, oriented according to the main directions of the forces applied to the material. These types of structures are 2D in nature, but due to the in-plane reinforcement provided by the in-laid yarns they are normally called directionally oriented structures (DOS). In this way, a wide range of reinforced fibrous structures can be designed according to the specifications of the envisaged application. DOS can be classified into mono-, bi-, tri- and multiaxial according to the number of directions of the reinforcing yarns, as can be seen in Table 3.1.

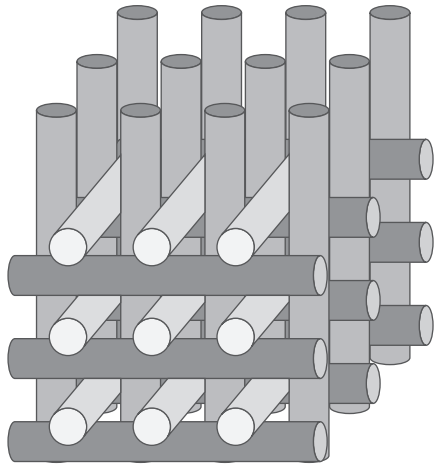

3.2 Representation of a 3D fibrous structure.

Table 3.1 Classification of directionally oriented structures

Monoaxial structure	Biaxial structure	Triaxial structure	Multiaxial structure
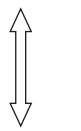	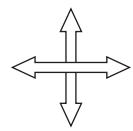		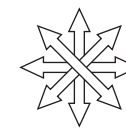
Warp reinforced	Warp and weft reinforced	Warp and diagonal directions reinforced	Warp, weft and diagonal directions reinforced
		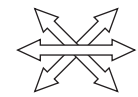	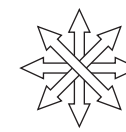
Weft reinforced	Diagonal directions reinforced	Weft and diagonal directions reinforced	Warp, weft and diagonal directions reinforced

Warp-knitting technology is particularly suitable to produce DOS allowing the introduction of reinforcing yarns in four different directions. Warp-knitted multiaxial fabrics are being used to advantage in polymeric matrix reinforcements, while biaxial structures are used in textile membranes for architecture purposes and in house wall construction in order to prevent small cracks.

Hybrid structures

Hybrid structures are mainly produced by sewing and warp-knitting technologies. The basis of manufacturing these structures is the combination of the properties of two independent structures manufactured under the form of a composite in a single operation. In this way, a synergetic effect of properties is achieved, where each structure contributes its properties to the behaviour of a structure with better properties than those of each component.

Combinations of biaxial warp-knitted fabrics and needle-punched nonwoven fabrics are being used with advantage in geotextiles. The warp-knitted fabric provides the required mechanical properties while the nonwoven fabric provides the porosity and the soil layers separation.

3.2 Planar (2D) textile structures

3.2.1 Woven fabrics

Woven fabrics are produced by interlacing two sets of yarns: one called warp, whose yarns are along the length of the fabric, while the other is the weft, whose yarns run along the width of the fabric. Both sets of yarns are mutually positioned under the angle of 90° (warp at 0° and weft at 90°). The warp and weft yarns can be interlaced in various ways, presenting a regular pattern called the weave structure. The most common woven structures used in technical applications are plain weave, twill weave and satin weave (Fig. 3.3) (Araújo, 2000).

Woven fabrics are usually dimensionally stable, although they possess lower extensibility and porosity than other structures. The mechanical properties of woven fabrics are very important for composites and they depend on different factors, namely raw materials, warp and weft linear mass, yarn density and weave structure. The strength of the fabric is usually higher in warp and weft directions, while the diagonal directions present lower mechanical properties, higher elasticity and lower shear resistance (Goran, 2005).

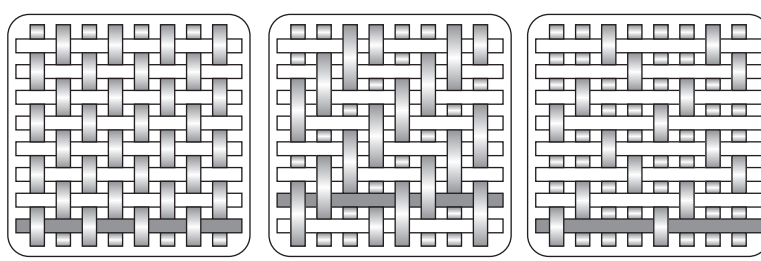

3.3 Main weave structures: (a) plain weave; (b) twill weave; (c) satin weave (Araújo, 2000).

Some disadvantages related to the fabrics which can be difficult in some composite designs are: their tendency to unravel at edges when cut, anisotropy, limited conformability, reduction on tensile efforts transference from the yarn to the fabric due to crimp, and the handling difficulty of open structures. However, some of these drawbacks can be overcome by using special fibrous structures, for instance triaxial wovens. This type of structure is produced by the interlacing three yarn systems at 60° angles providing an enhanced isotropy, higher in-plane rigidity, more uniform conformability, and fewer problems in the handling of very open structures. Nevertheless, none of the woven fabric structures offers sufficient extensibility (Scardino, 2009; Araújo, 2009).

Fangueiro *et al*. (Marques, 2008) studied the mechanical performance of 30 × 15 cm concrete slabs reinforced by glass fiber-woven fabrics. Within this research work, several fabrics (DOFS), in a grid-like structure, have been used with a different number of rovings in each direction, as can be seen in Table 3.2 and Fig. 3.4.

Concrete slabs have been produced according to the steps shown in Fig. 3.5.

The results obtained in the bending tests performed on the slabs produced with self-casting concrete (SCC) are shown in Fig. 3.6

The results show that the higher the roving linear mass, the better the performance of the slabs reinforced by woven fabrics, approaching the mechanical behaviour of welded wire steel-reinforced concrete. The roving linear mass, or roving density, has been shown to have a significant influence on DOFS reinforced concrete load-bearing capacity.

Woven fabrics usually used in concrete reinforcement are composed of rovings of continuous filaments yarns with the same linear mass, or different, in the warp and weft (Araújo, 2009). The reinforcement can be provided by 2D and multi-layer woven fabrics. 2D structures are usually used to avoid crack propagation in plaster mortar but they can also be used in the reinforcement of foam, gypsum and wood elements, and in acoustic and heating insulation sandwich panels.

Table 3.2 DOFS characterization

Longitudinal reinforcement			Transversal reinforcement	
DOFS	Roving linear mass (Tex)	Rovings density (no. of rovings/30 cm)	Roving linear mass (Tex)	Rovings density (no. of rovings/15 cm)
1	1 rov* × 2130 Tex	4	1 rov × 2140 Tex	6
2	1 rov × 2130 Tex	8	1 rov × 2140 Tex	6
3	2 rov × 2130 Tex	4	1 rov × 2140 Tex	6
4	4 rov × 2130 Tex	4	1 rov × 2140 Tex	6
5	2 rov × 2130 Tex	4	1 rov × 2140 Tex	3
6	1 rov × 2130 Tex	8	1 rov × 2140 Tex	3

* Roving

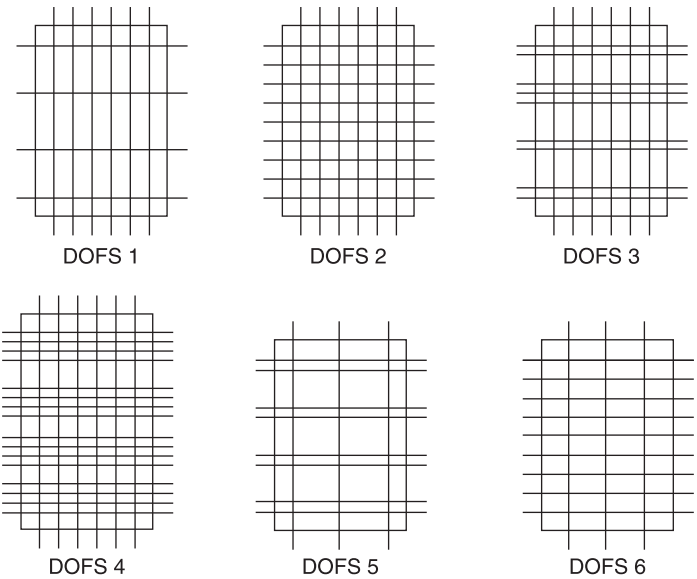

3.4 Woven structures.

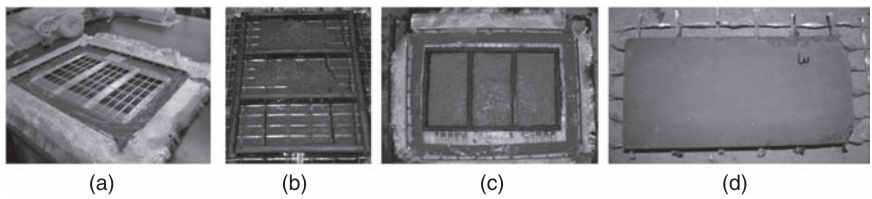

3.5 (a)–(d) Process to produce concrete slabs reinforced by woven fabrics.

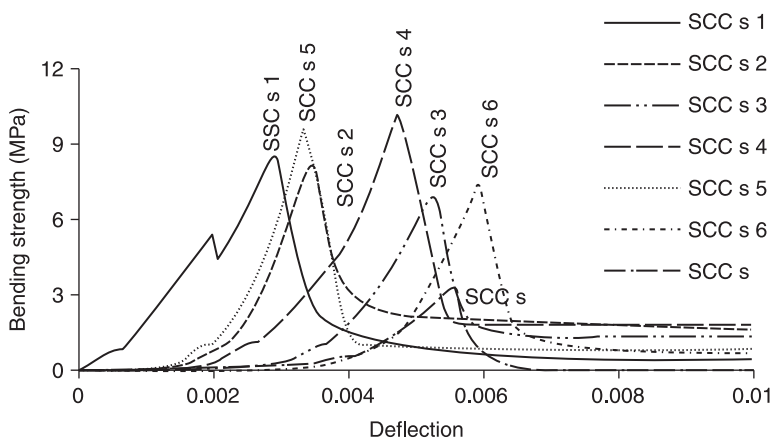

3.6 Bending tests results.

An open structure with yarns stabilized in the cross direction is an important requirement for using a woven structure in concrete reinforcement (Brameshuber, 2006).

3.2.2 Nonwoven fabrics

Defining nonwovens is not a very easy task due to the wide range of products that are available and also because they are different from conventional textile fabrics. The most common definitions used nowadays are those provided by the Association of the Nonwovens Fabrics Industry (INDA) and the European Disposables and Nonwovens Association (EDANA). Recently the following definition for nonwovens has been proposed to the International Standardization Organization by EDANA and INDA:

> nonwoven is a sheet of fibers, continuous filaments, or chopped yarns of any nature or origin, that have been formed into a web by any means, and bonded together by any means with the exception of weaving or knitting; felts obtained by wet milling are not nonwovens; wetlaid webs are nonwovens provided they contain a minimum of 50% of man-made fibers or other fibers of non vegetable origin with a length-to-diameter ratio equal or greater than 300, or a minimum of 30% of man-made fibers with a length-to-diameter ratio equal or greater than 600, and a maximum apparent density of 0.40 g/cm^3. Composite structures are considered nonwovens provided their mass is constituted of at least 50% of nonwoven as per the above definitions, or if the nonwoven component plays a prevalent role.

Nonwovens production is divided into web formation and bonding. The web formation is further differentiated into four processes: hydrodynamic, aerodynamic, mechanical and spunlaid web formation. Regarding the bond process, this is done mechanically, thermally and/or chemically.

Nonwovens are engineered fabrics that may have a limited life, such as single-use fabrics or very durable fabrics. Nonwoven fabrics provide specific functions such as absorbency, liquid repellency, resilience, stretch, softness, strength, flame retardancy, washability, cushioning, filtering, bacterial barrier and sterility. These properties are often combined to create fabrics suited for specific jobs, while achieving a good balance between product use-life and cost. They can mimic the appearance, texture and strength of a woven fabric and can be as bulky as the thickest paddings. In combination with other materials they provide a spectrum of products with diverse properties, and are used alone or as components of clothing, home furnishings, health care, engineering, industrial and consumer goods.

The deformation mechanism of nonwoven fabrics differs from the one shown by woven fabrics in the fact that, in woven fabrics, the initial effect of loading results in slippage and rearrangement of the yarns in the fabric, while in the nonwoven fabrics the rearrangement is fully dependent on the type of the binding or bonding in the mechanically bound fabrics, on the type and density of the fiber

or yarn interlacing, in adhesive-bonded fabrics on the elongation of the fibers and bonds as well as on the bonding density, and on the density and arrangement on the bonding points.

Nonwovens that are more appropriate to be used in advanced composites are fiber mats, nonwovens stitch-bonded, adhesively bonded, and the xyz nonwovens (3D) (Scardino, 2009; Araújo, 2009).

Waste fiber nonwoven mats have been used by Lundhal *et al*. (2010) to produce eco-composite panels for acoustic insulation. Layers of waste fiber nonwoven mats have been combined with polypropylene films in different configurations using compression moulding techniques. Moreover, similar research work has been undertaken by Torres (2010) using nonwoven mats composed of waste and polypropylene fibers to produce 3D-shaped eco-composite panels by compression moulding techniques.

Nonwovens find numerous applications. Some of the important areas where nonwovens are treated as the primary alternative for traditional textiles include geotextiles, materials for building, thermal and sound insulating materials, hygienic and health care textiles, and the automotive industries. In civil engineering, specific applications of nonwovens include:

- roofing and tile underlay
- underslating
- thermal and noise insulation
- house wrap
- facings for plaster board
- pipe wrap
- concrete moulding layers
- foundations and ground stabilization
- vertical drainage.

3.2.3 Knitted fabrics

Knitted fabrics are fibrous structures characterized by a basic structure called loop, and are produced by the interlooping of one or more yarns. They can be produced using warp-knitting technology, and also by weft-knitting technology, producing fabrics with different characteristics and properties. In weft-knitted fabrics, loops are produced in courses from at least one yarn, while in warp-knitted fabrics loops are produced in wales using a number of yarns identical to the number of wales to be formed. In both structures, by varying the type of loops produced, the loop length, the yarn linear density, the cover factor and the density of wales and courses, a wide range of structural combinations can be achieved.

The tensile behaviour of knitted fabrics is strongly restricted by its loop formation. During the application of a tensile load, the loops change their shape in

order to accommodate the applied load. In this part of the deformation small loads lead to large displacements, which is the typical behaviour of low-stiffness materials. When this type of structure is used as reinforcement, the mechanical properties of the composite material may be considerably hindered, as the resin may bear the initial load and fail before the load is transferred to the reinforcing fibers (Bruer, 2005).

The lack of stiffness of these structures at the initial stage of loading may be overcome by the introduction of straight yarns in various directions, or by pre-stressing the structure in a particular direction in order to attain jamming conditions and immediate transfer of the applied loads to the load-bearing yarns. Very important contributions to this subject have been made by Araújo *et al*. (2009) in a research work undertaken to improve the stiffness in the coursewise direction of weft-knitted fleece glass-fiber fabrics to be used in 3D tubular or 2D flat preforms for technical applications. In this work, the effects of fiber orientation were analyzed by comparing the tensile testing results obtained for different types of fleece structures. The fleece structure was chosen for this work for its relative advantages and it may be manufactured in 3D complex shapes in electronic flat-knitting machines. For some applications, the knitting or ground yarns work as a scaffold to hold the laid-in or the pile yarns, which are the reinforcing yarns, in the proper position for increasing the stiffness in the coursewise direction (Araújo, 2007).

Other disadvantages of these structures for specific applications are their low thickness and high consumption of yarn in relation to the covering degree. A potential limitation of knitted fabrics is their high porosity which, unlike woven fabrics, cannot be reduced below a certain value determined by the construction. As a result, applications requiring very low porosity usually incorporate woven materials (Scardino, 2009).

Warp-knitted fabrics have a larger potential for use in civil engineering applications due to the ability to design the properties of the fabric in each direction according to the application needs. However, weft-knitting is the most suitable textile technology to produce 3D complex-shaped fabrics that could be explored for some particular applications in civil construction.

In a warp-knitted fabric (Fig. 3.7), loops are formed from a separate yarn, called warp, mainly introduced in the longitudinal fabric direction. In this structure, neighbouring loops of one course are not being created from the same yarn. These structures show mechanical properties very similar to those of woven fabrics; however, they are very flexible and, depending on the construction, they can be elastic or inelastic.

Some special warp-knitted structures, named weft-inserted warp knits, can be produced with maximum stability due to the laid-in yarn systems in biaxial directions. Usually they are used for manufacturing composites, and this is of huge interest as these structures preserve the yarn properties and, due to their flexibility, fulfil design performance requirements from complete dimensional

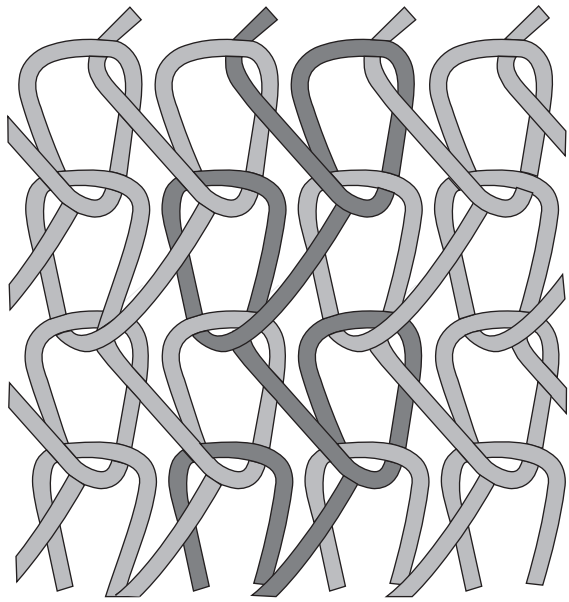

3.7 Warp-knitted fabric.

stability to directional elongation. In addition, they provide higher yarn-to-fabric tensile translation efficiencies, greater in-plane shear resistance, and better handling in open structures when compared to wovens.

Thus, for reinforcement it is possible to use weft-inserted warp-knitted fabrics characterized by an insertion of yarns in the weft direction and multibar weft-inserted warp-knit at the same time where yarns are inserted in both warp and weft directions. The reinforcing yarns are introduced in the structure without crimp, allowing the optimization of mechanical properties (Scardino, 2009; Goram, 2005; Araújo, 2009).

The equipment used for the production of warp-knitted fabrics are Tricot and Raschel looms. The first, Tricot, is not able to produce complex structures, is finer in gauge and is more rapid, while the Raschel produces more complex structures but is slower in production (Gries, 2005).

The warp-knitted structure is extremely versatile, and can be engineered with a variety of mechanical properties similar to those of woven fabrics (Goran, 2005).

3.2.4 Braided fabrics

Generally, braided textile structures are produced by interlacing different yarn systems in a tubular form. There are three main types of braided structures: diamond, regular and hercules (Fig. 3.8).

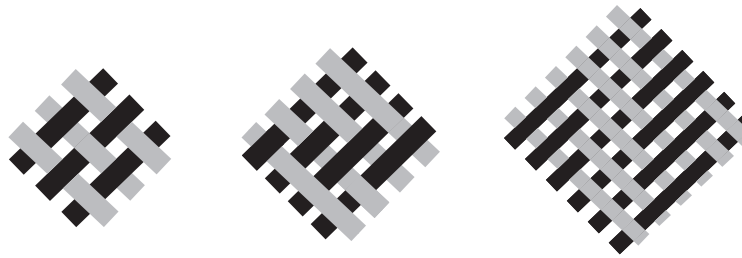

3.8 Braided conventional structures: (a) diamond; (b) regular; (c) hercules.

Diamond structure is obtained when yarns cross alternatively over and under the yarns in opposite directions and, in this case, the rotation is one by one. This rotation may be modified to two by two and three by three to obtain the other two structures. Diamond is the most stable structure while hercules is the one presenting the lower stability (Gries, 2004).

Braids are produced in a tubular form of biaxial yarns; however, if yarns (middle-end-yarn) oriented longitudinally are inserted into the structure, a triaxial braid is obtained. Also it is possible to insert into the middle of the tubular form fiber bundles to obtain a triaxial structure with axial fibers (Goran, 2005).

Braided diameter is controlled by some parameters, namely number of yarns, braiding angle, number of fiber intersections per unit length of the yarns, and fiber linear density (tex) (Araújo, 2009). The braiding angle can vary between 10–80° and it is the main feature of a braided structure being influenced by few factors, such as yarn fineness, the type of structure (biaxial or triaxial), cover factor and the longitudinal yarns volume ratio (Goran, 2005).

Depending on the yarns' orientation and on their number per transversal section (thickness direction), braids can be classified into 2D or 3D. The first technology has been used especially in the production of hollow pieces, with or without core, and for coatings (electrical cables) and they consist of two or three yarn diameters oriented and that cross in x and y directions. 2D braids can be planar or circular. 3D braids present three or more yarn diameters per transversal section in thickness direction and their applications are very specific, solving situations where the relation between weight and strength are extremely important (Gries, 2004). The 3D braiding technology is a very suitable technology to manufacture complex textile preforms (Gries, 2004).

Braid is a flexible product and can be manufactured in various shapes, using a mandrel which can shape the braid in several ways during the manufacturing stage. Their limitations are related to the equipment, presenting restricted width, diameter, thickness and shape selection. Braided structures present weak axial

stability and compression in yarn direction, and are conceived to have multidirectional conformability (Araújo 2009). Regarding 3D braids, their major limitations are productivity and fabric length (Scardino, 2009).

3.3 Three-dimensional (3D) textile structures

3.3.1 3D woven fabrics

3D fibrous structures can be produced using a weaving technique. 3D weaving is a variation of conventional weaving (2D) placing yarns in the third direction (thickness). Several 3D woven structures can be accomplished using special equipment. The simplest is when the warp is crossed by two sets of wefts (Fig. 3.9a). It is also possible to produce a 3D structure where multilayer warps cross the material providing an angle of 45° in x and y directions, and weft yarns cross between the warp providing the z direction (Fig. 3.9b) (Goran, 2005).

One important advantage of this technique is that preforms for a composite component with a complex geometry can be made to the near-net-shape, leading to a great reduction in the component cost and waste material, the need for machining and joining, and the amount of material handled during lay-up. Also, preforms can be made on standard industrial weaving looms used for producing 2D fabrics by making minor modifications to the equipment, which minimizes the cost and expensive custom-built looms are not required to produce 3D woven preforms.

Another advantage of 3D weaving is that wovens with a wide variety of fiber architectures can be produced with controlled amounts of binder yarns for through-thickness reinforcement (Mohamed, 2008).

Important developments in this domain have been provided by research works developed by Mohamed (2008), Kohkar (2008) and Busgen and Kastner (2003) aimed at the production of solid and shaped 3D woven fabrics.

The building industry has used 3D woven-glass composites in a couple of niche applications. One example is the I-beams made with a 3D woven composite

3.9 (a) 3D weave, the simplest structure; (b) multilayer 3D weave with x/y warp direction and z weft direction.

used in the roof of a ski chair-lift building in Germany. The main reason for its use is related to the difficulty in transporting and lifting heavy steel beams at the building site. Therefore, lighter 3D woven composite beams were used which demonstrated cost savings and improved performance over steel and conventional composite beams. Another civil infrastructure application for 3D woven composites has been for manhole covers in some petrol station forecourts (Mohamed, 2008).

3.3.2 3D nonwoven fabrics

For many technical applications, 3D nonwoven structures are required and are currently constructed from flat webs. In addition to the high cost of the conversion processes, irregularity is inevitably introduced into the final product because of the joints. There have been several attempts to produce 3D nonwoven fibrous structures directly.

Many nonwoven fabrics can be considered as 3D structures, although the fiber-orientation distribution in such fabrics is often assumed to be 2D because this simplifies theoretical analysis and experimental measurements.

In practice, fibers in 3D nonwoven fabrics may be aligned in all spatial directions. However, it is noticeable that in some specific nonwoven fabrics, such as needle-punched and spun-laced fabrics, many of the fibers that are not aligned in the fabric plane are aligned approximately perpendicular to it. Fibers that are not aligned in the fabric plane are assumed to be oriented in the direction of the fabric thickness (i.e. perpendicular to the fabric plane in the z direction).

Nowadays, 3D textiles made from yarns are widely applied in the field of technical textiles, including civil engineering. Needle-punched nonwovens-based 3D structures produced without any yarn are a novel development. Three groups of 3D nonwoven production processes can be identified:

- carding and vertical lapping: Struto and Wavemaker;
- stitch-bonding processes: Kunit, Multiknit, Malivlies;
- 3D Weblinker, NAPCO® technology for 3D structures.

3D nonwovens or nonwoven spacer fabrics such as Kunit and Multiknit, perpendicular-laid nonwovens (Santex Wavemaker, Struto and Napco) are an advance, and not only for economic reasons. However, they are a relatively recent development, and there is only a small amount of published information on their production process, mechanical properties and potential applications (Vasile, 2006; Hearle, 2008; Mohamed, 2008; Mecit, 2008) (Figs 3.10 and 3.11).

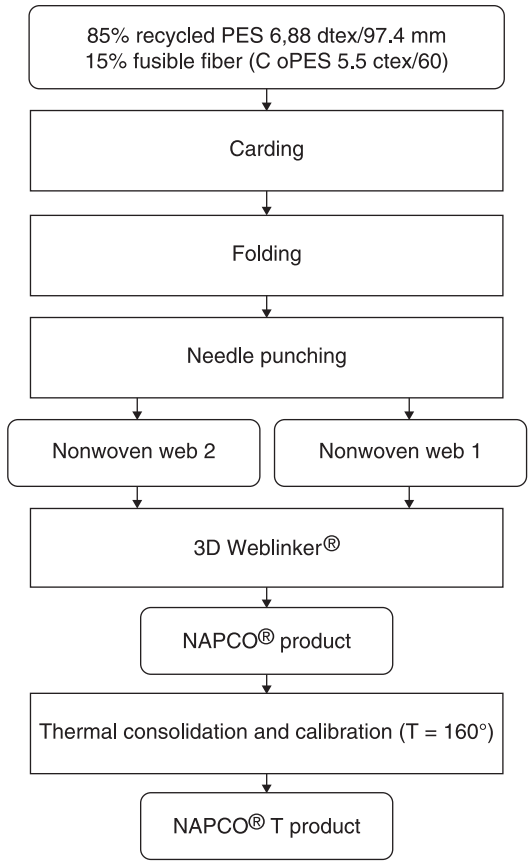

3.10 Processing technology of NAPCO® and NAPCO® T (Vasile, 2006).

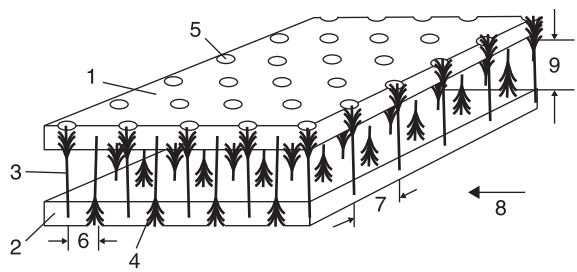

1, 2 Nonwovens
3 Bundle of fiber
4, 5 Formation of funnels
6 Feed space
7 Space between rows of needles
8 Direction of process
9 Space between nonwovens

3.11 NAPCO® spacer nonwoven fabric (Vasile, 2006).

3.3.3 3D knitted fabrics

3D weft-knitted fabrics

According to Fangueiro (2002) weft-knitting technology is the most versatile textile technology for the production of shaped preforms. The advantages of knitting technology when used for the production of preforms can be summarised as follows:

- very flexible – electronic needle selection and CAD contribute greatly to the design capability as well as to the quick set-up of knitting machines;
- no additional yarn preparation is required;
- due to the structural nature of knitted fabrics, properties such as axial strength (in various directions) may be achieved by introducing straight, in-laid yarns, or by other novel techniques;
- knitting to shape enables the formation of shaped fabrics in 2D and 3D.

Figure 3.12 shows different examples of complex-shaped preforms produced using a weft-knitting technique.

Weft-knitting technology may also be used to produce complex shaped sandwich preforms for composites. A knitted sandwich fabric is made of two separate outer fabrics, connected by yarns or by layers. Compared with other textile technologies, weft knitting allows the production of sandwich fabrics with almost unlimited thickness, thanks to the use of connection layers with a variable distance between the two outer layers and with different configurations of the outer layers. These possibilities enable the production of shaped sandwich fabrics (Fig. 3.13), which may be very interesting for composites reinforcement.

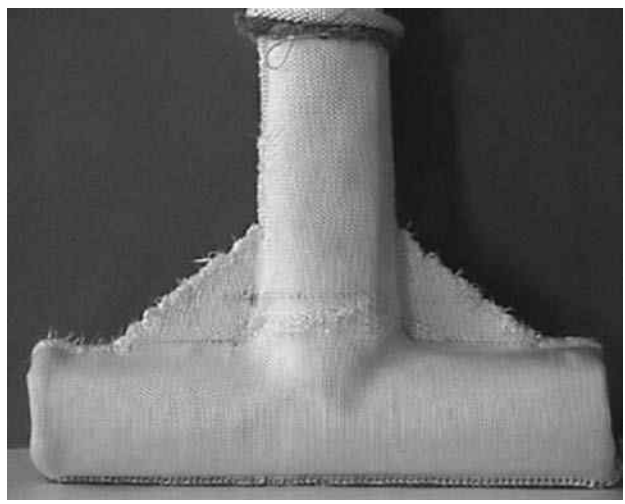

3.12 3D-shaped preform using a weft-knitting technique (Fangueiro, 2002).

3.13 Shaped sandwich fabrics (Fangueiro, 2002).

3D warp-knitted fabrics

Warp-knitted spacer or sandwich structures are one of the most interesting developments in textile structures over the last few decades. Composed of two separate fabric layers, top and bottom and interconnected by yarns oriented in the third dimension, a warp-knitted spacer fabric is a real 3D fibrous structure. Figure 3.14 illustrates some examples of warp-knitted spacer fabrics. Both fabric layers can be produced using different types of materials and have completely different structures. Usually the top and bottom fabric layers are connected to each other mostly by monofilaments that can either fix both directly or space them apart. This type of configuration allows heat and moisture transfer, makes the structure lighter, and confers good acoustic and insulating properties. Typically, spacer fabrics can be 1–15 mm thick, with faces 0.4–1 mm thick. The major single feature of warp-knitted spacer fabrics is that virtually any thickness can be obtained, depending upon the type of machinery used and the type of yarns and structures used (Anand, 2008; Hearle, 2008; Fortes, 2003; Roye 2007).

The most important characteristics of these fibrous structures are: lightness, flexibility, high stiffness and bending, excellent acoustic and insulating properties, and the possibility of having different thickness and compression values. However, the main drawback is their weak delamination resistance, and an impact in the

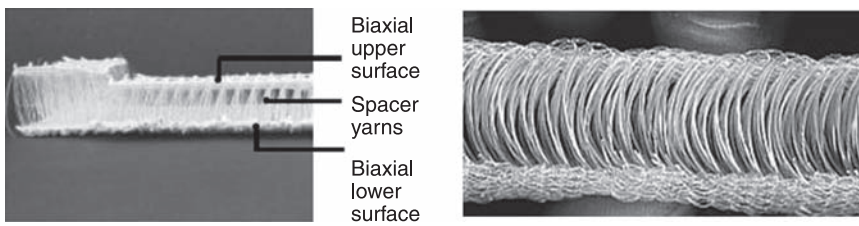

3.14 Three-dimensional spacer warp-knitted fabrics.

structure can cause separation between the top and bottom layers and the interconnecting layer. A solution to this problem consists of the use of double-face structures using double-bed Raschel knitting equipment (Roye, 2004; 2007).

Spacer fibrous preforms (Fig. 3.14) are produced on double-bed Raschel machines by knitting the top and bottom skins simultaneously on each needle bed (Anand, 2008).

Warp-knitted spacer structures are used in a wide range of applications. In civil engineering they are being used in geotextiles and as reinforcement for composite structures. An emerging area is in the production of thin sheet-cement components, which includes, for example, wall panels, claddings and exterior siding.

Recently, the application of warp-knitted spacer fabrics for the reinforcement of concrete has been researched (Roye, 2007). For this application, the spacer provides reinforcement in the third direction, which has the advantage of providing an armour system that can be easily placed into a mould and impregnated to its full thickness by a matrix in a single step, and at a defined positioning of the two outer layers. According to Mecit (2008), the third direction reinforcement provides shear resistance. When the reinforcement used in cement applications has a combined high strength and high elastic modulus, failure of the composite is often controlled by shear or interlaminar shear (between the layers of reinforcements) instead of bending, so reinforcement in the third direction is needed. In addition, due to the easier construction of spacer structures it is possible to reduce the cost of production. In order to produce warp-knitted spacer structures for concrete reinforcement applications, Aachen University, in Germany, modified a Raschel machine enabling the insertion of in-plane weft and warp reinforcements in a warp-knitted spacer fabric. This equipment has been used by Roye and Gries (Roye, 2007) to produce warp cement-based panels reinforced by this structure. In this study, it was concluded that it is relatively easy to produce wide structures with the desired properties for cement and concrete applications, and that the structure width and thickness can be adapted easily to the exact size of the concrete application, which is advantageous in technological and economical terms.

The production of sandwich elements leads to enormous possibilities in the field of lightweight construction. In aeronautic applications, as well as in civil engineering applications, the use of sandwich elements is becoming more and more common.

3.3.4 3D braided fabrics

Braiding technique can be successfully used to produce 3D fibrous structures. The basic 3D braiding principle consists of mutual yarns intertwining. Generally, braids are produced in a tubular form of biaxial yarns direction. Through the introduction of longitudinal-oriented yarns into the structure, a 3D axial braid is obtained. Moreover, in the centre of the tubular braid, additional fibers, called axial fibers, can be inserted (Goran, 2005). 3D braided structures present several

advantages such as higher levels of conformability, drapeability, torsion stability, and structural integrity, which make it possible to produce composite structures with geometries to the near-net-shape. This feature can reduce manufacturing costs considerably once the amount of fabric handling and waste material is reduced. 3D braided composites also have higher delamination resistance and better impact damage tolerance (Mohamed, 2008).

Despite the above advantages, the applications for 3D braided composites have been limited for several reasons. One major limitation is related to the maximum preform size, which is determined by the braiding machine size, and most industrial machines are only able to braid preforms with a small cross-section (under 100 mm in width).

Another problem is that many 3D braiding machines are still in the research and development stage, and only a few machines are presently able to commercially manufacture 3D preforms. 3D braiding machines are also slow and, as a result, 3D braids cannot presently compete with 2D braids and laminates on a cost-saving basis (Mohamed, 2008).

The current developments on the 3D braiding equipment are limited and therefore their costs are extremely high when, for example, compared to 3D weaving. 3D braided structures will remain limited until the issues mentioned above are solved.

Despite these problems, in the building industry a variety of components have been made that clearly illustrate the versatility of this textile process. 3D braiding has been used in C-, J-, I- and T-sections, I-beams, bifurcated beams and connecting rods.

Braided reinforced composite rods for concrete reinforcement (Fig. 3.15) were developed at the University of Minho. Advantages such as excellent corrosive resistance, mechanical properties similar to steel, high strength-to-weight (10 times higher than steel), excellent fatigue resistance, nonmagnetic properties, and low thermal expansion make them an alternative building construction material to steel (Pereira, 2006; 2008; Fangueiro, 2006).

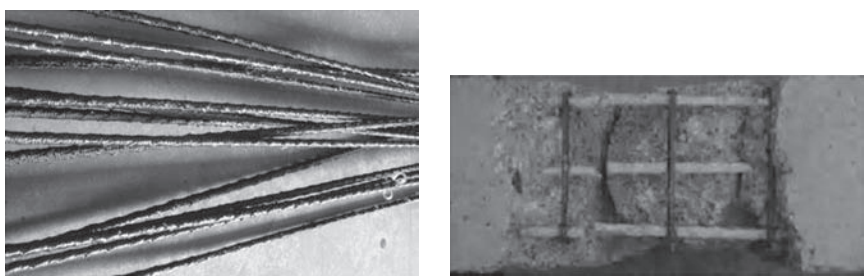

(a) (b)

3.15 Braided composite rods (a) and beam (b) produced with braided reinforced composite rods after testing.

3.4 Directionally oriented structures (DOS)

Directionally oriented structures are 2D structures with the peculiarity of possessing in-plane reinforcing yarns. Thus, it is possible to design a wide range of DOS reinforced in the desired direction, according to the envisaged application, using different textile technologies.

DOS can be classified according to the number of reinforced directions in: monoaxial, biaxial, triaxial and multiaxial structures. Figure 3.16 presents examples of DOS.

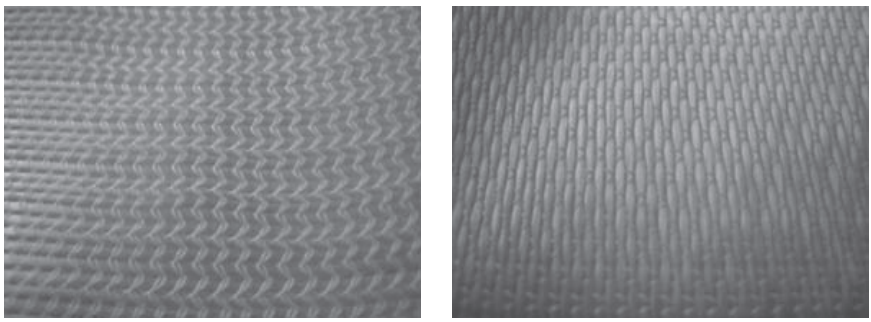

(a) (b)

3.16 Monoaxial (a) and triaxial (b) structures.

3.4.1 Monoaxial or unidirectional structures

Monoaxial structures present a high number of parallel fibers oriented in a preferred direction. Usually fibers are oriented at 0° along the warp direction or at 90° along the weft direction (Araújo, 2009). The great advantages of this structure are the straight and uncrimped fibers in the amount required. However, handling is a drawback. There are various methods to keep primary fibers in position in a monoaxial fabric including weaving, stitching, and bonding (Araújo, 2000). Figure 3.17 shows two examples of this type of structure.

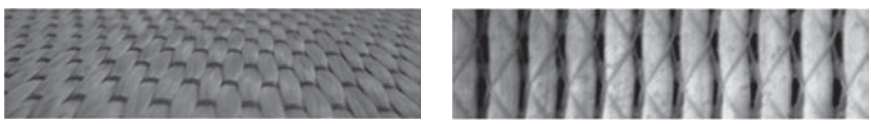

(a) (b)

3.17 Monoaxial structures: (a) woven tape; (b) stitched woven.

Warp- or weft-knitting technologies may also be used to produce monoaxial fabrics. Figure 3.18 shows some examples (Araújo, 2000).

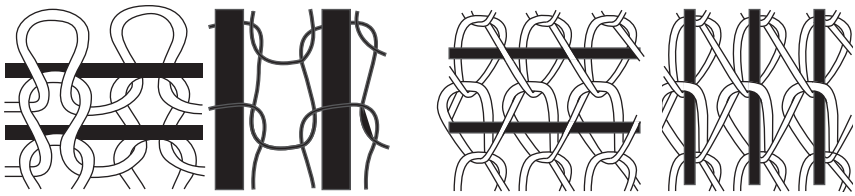

3.18 Monoaxial weft-knitted (a) and warp-knitted (b) structures.

Monoaxial weft-knitted structures may be produced based on fleece fabrics, as shown in Fig. 3.19 (Araújo, 2009).

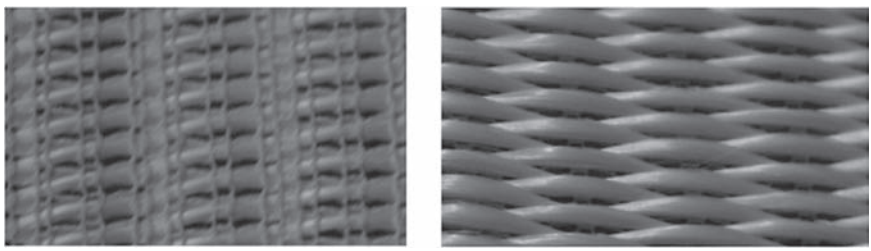

3.19 Monoaxial weft-knitted fleece structure (Araújo, 2009): (a) technical face; (b) technical back.

3.4.2 Biaxial structures

Biaxial DOS are usually reinforced in warp and weft directions in different ways. The characteristic crimp of yarns is removed, and the yarns are straight and settled in layers placed at 90° and attached by one linking yarn that represents 10% of the total. Some criteria for choosing the right fabric include easy handling and placing in site, mass per unit area (g/m^2) and thickness regularity, continuity of the reinforcement, and ease of impregnation (Araújo, 2009).

Biaxial structures are commonly used in building construction and in composites made of high-performance fiber-based yarns – namely glass, carbon, and aramid – for the manufacture of lightweight components. Leno biaxial structures, produced by a weaving technology known as woven mesh, are extensively used in wall reinforcement. Another application of this type of structure is the reinforcement of membranes in combination with PVC or silicone for textile architecture.

Figure 3.20 illustrates biaxial warp-knitted structures reinforced at 0/90° (Fig. 3.20(a)) and at 45°/90° directions (Fig. 3.20(b)).

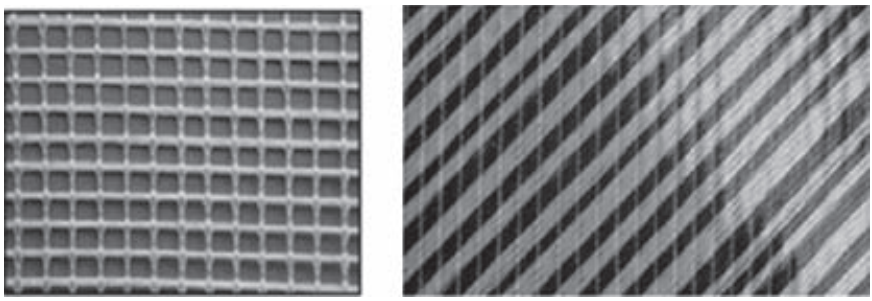

3.20 Woven biaxial structure in different directions: (a) 0–90°; (b) 90–+45°.

3.4.3 Triaxial structures

Triaxial fibrous structures are normally reinforced in bias directions at ±60° and in the weft direction at 0°. The main objective of the reinforcement is to make the ground fabric able to withstand applied efforts in those directions (Araújo, 2009).

Due to their specific arrangement, these structures cannot reach higher yarn densities. Triaxial structures have exceptional mechanical properties in several directions, and high shear resistance as the interlacing points are fixed into the fabric (Goran, 2005).

3.4.4 Multiaxial structures

In recent years, multiaxial structures have found a place in the construction of composite components. The conventional structures used usually for that purpose provide biaxial reinforcement (warp (90°) and weft (0°)). However, those structures present several drawbacks when load is applied in bias directions due to the material anisotropy. One way to overcome this problem consists in laying reinforcing yarns at +45° and −45° leading to multiaxial structures that provide four reinforcing directions giving an higher isotropic behaviour to the material. The main advantage of these structures is the complete use of yarn mechanical properties, although the same feature could be a disadvantage when loads are applied outside the plane causing delamination. Considering this drawback, other multiaxial structures were developed using warp-knitting technology in order to interlace reinforcing yarns (Roye, 2007). Two examples of multiaxial structures are shown in Fig. 3.21.

Figure 3.22 illustrates the scheme of a multiaxial warp-knitted structure. This structure is defined by a warp-knitted structure whose straight non-crimp yarns are introduced in a fabric structure in four directions, warp (90°), weft (0°) and bias directions (±45°). In order to produce this fibrous structure, one set of

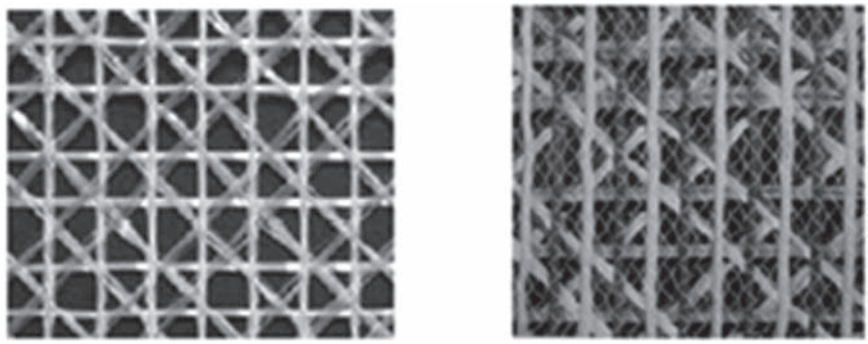

(a) (b)

3.21 Multiaxial structures: (a) stitch-bonded multiaxial structure; (b) multiaxial warp-knitted structure (Hausding, 2006).

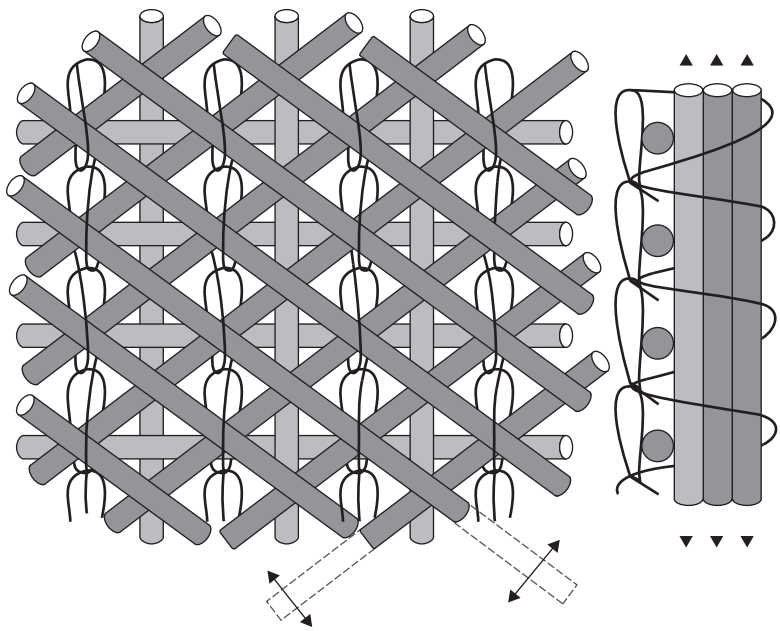

(a) (b)

3.22 Multiaxial warp-knitted fabric with oriented yarns in four directions: (a) top view; (b) cross section (Goran, 2005).

machine operations lays down sheets of reinforcing yarns, and then these are passed into the knitting zone where they are held together by the stitches of knitting yarns. If the aim is to reinforce the composite to withstand forces in all directions, this structure is particularly suitable.

Karl Mayer has developed a multiaxial high-performance machine, with high speed up to 1600 rpm for up to seven layers. Figure 3.23 shows the multiaxial structure obtained with the machine.

Several efforts to produce multiaxial interlaced fabrics have been made in the past. A number of European patents have described the tetraxial (Kazumasa, 1987; Dini, 1994; 2003) and multiaxial (Mood, 1992; Araújo, 2004) structures and machines for their production. Those patents propose different solutions for the problem of bias yarns feeding and criss-crossing, but none has proved to be sufficiently good for the construction of a reliable, commercial multidirectional weaving machine. A new multiaxial woven structure called Multiweave (Fig. 3.24), and the respective manufacturing process (Fig. 3.25) has been developed by Lima *et al*. at the University of Minho (Lima, 2009). This kind of

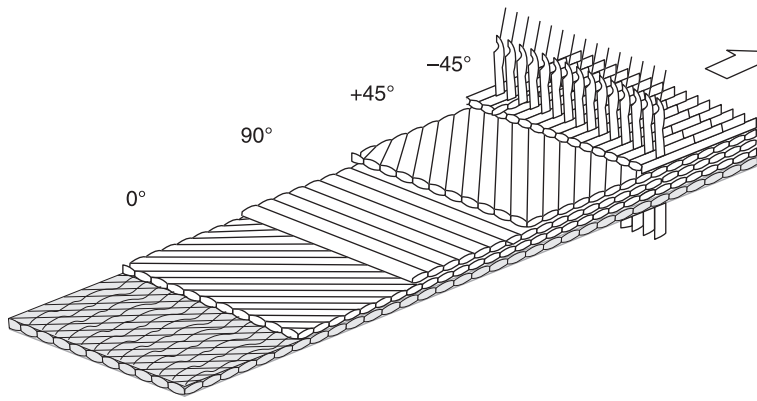

3.23 Karl Mayer multiaxial machine.

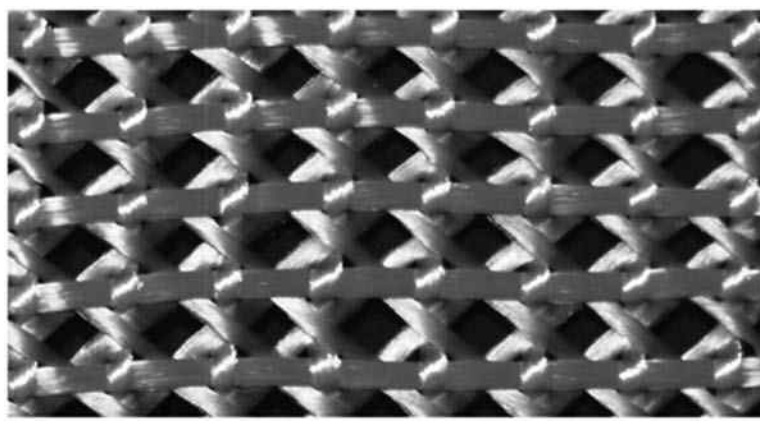

3.24 Multiweave fabric (Lima, 2009).

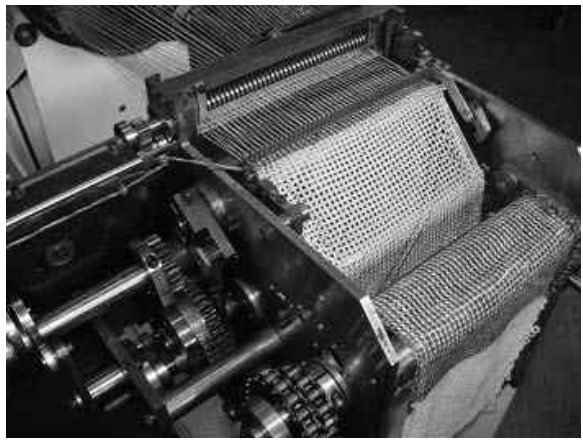

3.25 Multiweave prototype showing the fabric formation area (Lima, 2009).

fabric is designed to boost the reinforcement in bias directions by the insertion of interlaced yarns between the weft and the warp.

The design of a newly-developed multidirectional weaving system is concerned with the characteristics of the fabric structure, where there is criss-crossing between all sets of yarns, which increases the capability for supporting more severe mechanical loads without failure, namely without delaminating. Simultaneously, the strength–weight ratio is expected to increase, which can be very advantageous for applications such as in the aircraft and car industries, and in civil engineering. Fabrics produced with the prototype developed present a structure which is not very dense, mainly due to the limitations imposed by the relatively high bias pitch, hence more research and development is required to find out the appropriate solutions (Lima, 2009).

3.5 Hybrid structures

Hybrid structures are the result of a combination of different kinds of structures with the main purpose of balancing some characteristics or weakness of individual materials being used in specific applications. From the synergy of both structure properties, a fibrous structure with improved properties results (Araújo, 2009). Usually this type of structure is produced through warp-knitting technologies combining the properties of two structure-manufacturing processes in one. A warp-knitting technique may be used, for example, to bind nonwovens with directionally oriented warp-knitted fabrics in a unique operation (Fig. 3.26). The connection is given exclusively in the loop-crossing points, which allows the maintenance of the work amplitude of the knitted fabric preserving the nonwoven characteristics.

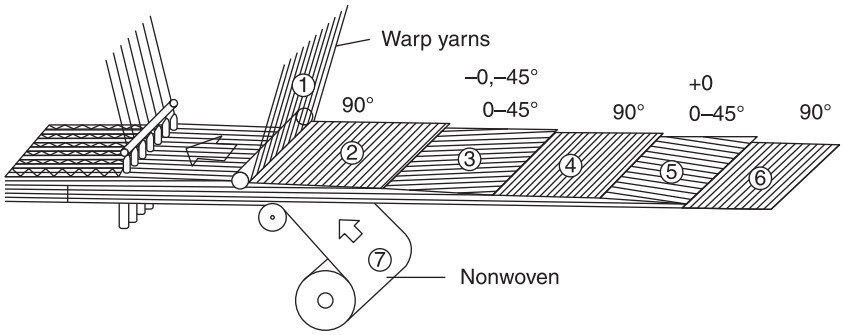

3.26 Production of a hybrid structure (warp knitted fabric + nonwoven fabric) (Libra Technology).

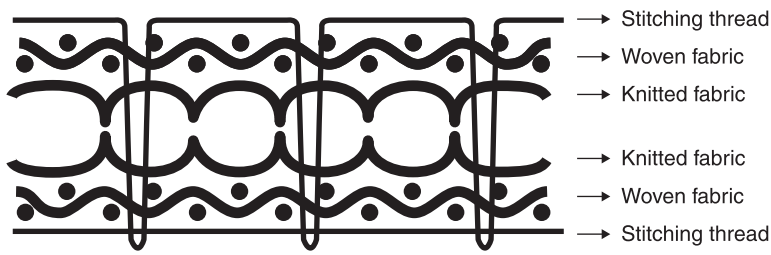

3.27 Representation of the stitched woven-knitted fibrous structure (Hong, 2010).

Hong *et al*. (2010) developed a very interesting research work on a stitched woven-knitted fibrous structure. The innovative hybrid fibrous structure (Fig. 3.27) used consists of two outer layers of a plain-woven fabric combined with two inner layers of weft-knitted fabrics.

The weft-knitted fabrics selected for the study were varied plain knit, 1×1 rib, milano rib, and interlock. The fabric layers, all produced with basalt fiber, were stitched together with Kevlar yarns. The hybrid structures were used as reinforcement of a polymeric matrix using a resin transfer moulding process. A very interesting approach has been followed by the authors to design the current hybrid structure, combining different planar fibrous structures with different fiber orientations. According to the authors, when subjected to impact loads the whole structure acts as follows:

(a) In the front and back layers, the impact stress waves should be quickly transmitted along the panel direction (fabric plane direction) due to straighter orientation of the yarns in the woven fabric.
(b) In the inner layers, the knitted fabrics should absorb the transmitted impact stress waves in the thickness direction (perpendicular to the fabric plane direction); due to the loop structure of the knitted fabrics, larger deformations

will take place when the impact load is applied and therefore a larger amount of energy can be absorbed.

(c) The stitching yarns play an important role in keeping all the fabric layers together, avoiding delamination.

This example shows that the combination of different fibrous structures allows the optimization of fiber-based materials for a particular application by placing the right fiber type, in the right amount, with the most appropriate orientation.

3.6 Sources of further information and advice

This chapter presents in a concise form the main textile structures used in civil engineering applications. For further information the reader may also consult the following literature:

- Adanur, S. (1995) *Wellington Sears Handbook of Industrial Textiles*. Basel, Switzerland: Technomic Publishing.
- Deopura, B. L., Alagirusamy, R., Joshi, M. and Gupta, B. (eds) (2007) *Polyesters and Polyamides*. Cambridge: Woodhead Publishing Ltd.
- Horrocks, A. and Anand, S. (2006) *Handbook of Technical Textiles*. London: Taylor & Francis Ltd (ISBN 978–0–8493–1047–8).
- Hu, J. (2008) *3D Fibrous Assemblies Properties, Applications and Modelling of Three-Dimensional Textile Structures*. Parkway, FL: CRC Press (ISBN 978–1–4200–7986–9.
- Proceedings of the First World Conference on 3D Fabrics and Their Applications, Manchester, UK, 10–11 April 2008.
- Proceedings of the Second World Conference on 3D Fabrics and Their Applications, Greenville, USA, 6–7 April 2009.

3.7 References

Anand, S. C. (2008) *Three-dimensional Knitted Structures for Technical Applications*. The 1st World Conference on 3D Fabric and Their Applications, 10–11 April, Manchester Conference Centre, University of Manchester, UK.

Araújo, M. D., Fangueiro, R. and Hong, H. (2000) *Technical Textiles: Materials for the New Millennium – Vol. II: Applications, Technologies and Testing*. Braga, Portugal: Edição Williams/DGI.

Araújo, M. D., Fangueiro, R. and Soutinho, F. (2009) Improving the stiffness of unidirectionally oriented weft-knitted structures for polymer matrix composite reinforcement, *Journal of the Textile Institute*, 100(8): 71.

Araújo, M. D., Lima, M. and Costa, N. (2004) *Multi-axial fabric and weaving loom for its production*. Eur Pat WO/2004/0059054 A1, TECMINHO, Guimarães, Portugal.

Araújo, M. D., Soutinho, F. and Fangueiro, R. (2007) Improving the Mechanical Properties of Directionally Oriented Weft-knitted Structures for Advanced FRP. AUTEX 2007 Conference, Tampere, Finland, 26–28 June.

Brameshuber, W. (2006) State-of-Art Report of Rilem Technical Committee 201, *TRC – Textile Reinforced Concrete: Report 36*, 3rd trimester.

Bruer, S. M., Powell, N. and Smith, G. (2005) Three-dimensionally knit spacer fabrics: a review of production techniques and applications, *Journal of Textile and Apparel Technology and Management*, 4(4): 1–31 (Summer). North Carolina State University.

Busgen, A. and Kastner, Y. (2003) *Three-dimensionally woven hollow bodies for material reinforcement*. Techtextil Symposium 2003. Frankfurt, 7–10 April. Available online: http://www.nonwoven.co.uk/reports

Cripps, D. *SP Guide to Composites*. Available online: http://www.netcomposites.com/education.asp?sequence=2

Dini, M. (1994), *Tetraxial fabric and weaving machine for its manufacture*. US Patent 5351722, D.I.M.A. Ricerche Technologiche S.R.L, (Drezzo, IT).

Dini, M. (2003), *Tetraxial fabric and machine for its manufacture*. WIPO Pat Application WO/2003/012184, TETRAXIAL S.r.l. (Milan, IT) A2 (2003).

Fangueiro, R. (2002) *Optimisation of Weft-knitted Preforms Development for Composite Materials*. PhD Thesis, The University of Minho, Portugal.

Fangueiro, R., Sousa, G., Araújo, M. D. and Gonilho Pereira, C. (2006) *Core Reinforced Composite Armour as a Substitute to Steel in Concrete Reinforcement*. International Symposium Polymers in Concrete, April 2006, Guimarães, Portugal.

Fortes, M. A. and Ferreira, P. J. (2003) *Materiais-2000: Capítulo 3*. Polímeros: IST Press (ISBN 972–8469–23–3).

Goran D. and Bogovea, G. (2005) Textile structures for the technical textiles – Part II: types and features of textiles assemblies, *Bulletin of the Chemists and Technologists of Macedonia*, 24(1): 77–86.

Gries, T., Roye, A., Kolkmann, A., Barlé, M., Hanisch, V., Henkel, F. and Laourine, jan Stüve, E. (2004) *New Developments on Manufacturing Fibers and Textile Structures for Technical Textiles*. International Textile Congress, Terrassa, Germany.

Hausding, J., Engler, T., Franzke, G., Köckritz, U. and Cherif, C. (2006) Plain stitched-bonded multiplies for textile reinforced concrete, *Autex Journal*, 6(2): 81–90.

Hearle, J. W. S. (2008) *Innovation for 3D Fabrics*. The 1st World Conference on 3D Fabrics and Their Applications, 10–11 April, Manchester Conference Centre, University of Manchester, UK.

Hong, H., Mingxing, Z., Fangueiro, R. and Araújo, M. (2010) Mechanical properties of composite materials made of 3D stitched woven-knitted preforms, *Journal of Composite Materials*, 14 January.

Isley, F. (2002) The use of high performance textiles in construction projects. *Journal of Industrial Textiles*, 31(3): 205–217.

Kazumasa, O., Reijiro, T. and Michihiro, O. (1987) *Tetraxial Woven Fabrics AND Tetraxial Weaving Machine Thereof*, European Patent 0263392 A2, Meidai Chemical Co., Ltd.

Khokar, N. (2008) *Second-Generation Woven Profiled 3D Fabrics from 3D Weaving*, 3D Fabrics Conference, Manchester, UK, 10–11 April.

Krenkel, W. (2008) *Ceramic Matrix: Composites – Fiber-Reinforced Ceramics and Their Applications*. Chichester: Wiley-VCH (ISBN 3527313613, 9783527313617).

Lundhal, A., Fangueiro, R., Soutinho, F. and Duarte, F. (2010) Waste fiber reinforced ecocomposites, *Materials Science Forum*, 636–637: 1414–1420.

Lima, M., Fangueiro, R., Costa, A., Rosiepen, C. and Rocha, V. (2009) Multiweave: a prototype weaving machine for multiaxial technical fabrics, *Indian Journal of Fiber & Textile Research*, 34: 59–63 (March).

Mayer, K. Textile *Machinery; Technical Textiles – Biaxial Structure*. Available Online: http://www.karlmayer.com/internet/en/textilmaschinen/963.jsp

Mecit, H. D. (2008) *Development and Defining of a Characterization Method for 3D Spacer Fabrics Considering Concrete Applications*, Master Thesis, Institut für Textiltechnik der RWTH Aachen, Matr. – Nr.: 262894.

Mohamed, M. (2008) *Recent Advances in 3D Weaving*. The 1st World Conference on 3D Fabric and Their Applications, 10–11 April, Manchester Conference Centre, University of Manchester, UK.

Mood, G. I. and Mahboubian-Jones, M. G. B. (1992) *Multiaxial Weaving*. European Patent EP0571461 B1, Short Brothers PLC, Northern Ireland, GB.

Pereira, C. G., Fangueiro, F., Jalali, S. and Araújo, M. (2006) *Mechanical Properties of Braided Reinforced Composites*. Feira Internacional De Aplicaciones Técnicas De Los Materiales Textiles 6, Valência.

Pereira, C. G., Fangueiro, F., Jalali, S. and Araújo, M. (2006); *The Mechanical Properties of Braided Reinforced Composites for Application in Concrete Structures*. 37th International Symposium on Novelties in Textiles, 15–17 June 2006, Ljubljana, Slovenia.

Pereira, C. G., Fangueiro, R., Jalali, S., Araújo, M. and Marques, P. (2008) Braided reinforced composite rods for concrete internal reinforcement, *Mechanics of Composite Materials*, 44(3): 221–230. Available online: http://www.selcom-srl.com

Pina Marques, P., Fangueiro, R. and Gonilho Pereira, C. (2008) *Concrete Slabs Reinforced by Directionally Oriented Fibrous Structures*, CCC2008 – Challenges For Civil Construction Proceedings, 16–18 April, FEUP, Porto, Portugal.

Roye, A. and Gries, T. (2007) 3D Textiles for advanced cement based matrix reinforcement, *Journal of Industrial Textiles*, 37: 163. Available online: http://www.allertex.com/wavemaker.html

Roye, A., Gries, T. and Peled, A. (2004) *Spacer Fabrics for Thin Walled Concrete Elements*, 6th RILEM Symposium on Fiber-Reinforced Concrete (FRC), BEFIB, Varenna, Italy, pp. 1505–1514.

Scardino, F. L. (1989) Introduction to textiles structures and their behaviour, in Tsu-Wei and Frank Ko (eds) *Textile Structural Composites*. New York: Elsevier.

Torres, D. (2010) *Development of Shaped Ecocomposites Based on Waste Fibers*, Master Thesis, University of Minho, Portugal.

Vasile, S. and Langenhove, L. V. (2006) Effect of production process parameters on different properties of a nonwoven spacer produced on a 3D web linker®, *Fibers & Textiles in Eastern Europe*, 14(4): 58.

Weiland, S., Ortlepp, R., Curbach, M., Köckritz, U., Hauptenbuchner, B., Schmidt, F. and Hankers, Ch. (2007) *First Application: Textile Reinforced Concrete for Rehabilitation and Strengthening of a Hypar Concrete Shell in Schweinfurt/Germain. Techtextil Symposium*. Frankfurt, 11–12 June.

4

Steel fibre reinforced concrete: Material properties and structural applications

J. A. O. BARROS, University of Minho, Portugal

Abstract: Short and randomly distributed steel fibres are often used for concrete reinforcement since they offer resistance to crack initiation and, mainly, to crack propagation. In steel fibre reinforced concrete (SFRC) of low fibre volume content, the fibre reinforcement effectiveness is only significant after matrix cracking, since fibres crossing the crack guarantee a certain level of stress transfer between the faces of the crack, providing to the concrete a residual strength, the magnitude of which depends on the fibre, matrix and fibre-matrix properties. The mechanical performance of SFRC is also highly influenced by the fibre dispersion, since the effectiveness of fibre reinforcement depends on the orientation and arrangement of the fibres within the cement matrix.

Key words: steel fibre reinforced concrete, steel fibre reinforced self-compacting concrete, tensile behaviour, flexural behaviour, shear and punching behaviour, façade panels, inverse analysis, finite element method.

4.1 Introduction

The use of discrete steel fibres as a reinforcement system for cement-based materials is now a current practice for several applications (di Prisco *et al*. 2004). The resulting material is designated steel fibre reinforced concrete (SFRC). The post cracking residual strength can be much higher in SFRC than in the homologous (same strength class) plain concrete (PC), due to fibre reinforcement mechanisms provided by fibres bridging the cracks (Barros *et al*. 2005b). In consequence, SFRC allows high level of stress redistribution, providing a significant deformation capacity of a structure between crack initiation and its failure, which increases the structural safety. This is especially relevant in structures of redundant number of supports (Barros and Figueiras 1998). The level of the post-cracking residual strength depends on several factors, such as: fibre geometric characteristics, fibre material properties, concrete properties, and method of SFRC application. When well conceived, fibre reinforcement can replace totally, or partially, conventional steel reinforcement for the flexural and shear resistance of concrete elements (Casanova 1995; Casanova *et al*. 2000; Roshani 1996). The percentage of this replacement depends on the type of element, support and loading conditions.

4.2 The fundamentals of fibre reinforcement effectiveness

In this chapter, relevant aspects of fibre reinforcement for the compression, tension, bending and shear behaviour of cement-based materials are considered. Structural applications of SFRC are explored, by using experimental and numerical strategies. The content of this chapter is fundamentally based on the research carried out in research programs related to steel fibre reinforced concrete coordinated by the author.

The benefits provided by fibre addition to cement-based materials come from the reinforcing mechanisms that develop during the fibre pullout process after crack initiation, since a considerable energy is dissipated in this process. The peak pullout force and the energy dissipated during the fibre pullout process depend on several parameters, such as: mechanical properties and geometric characteristics of the fibres, fibre inclination, fibre embedment length and concrete properties. Figure 4.1 and Fig. 4.2 show that, in general, fibre peak pullout force and energy dissipation increase with fibre inclination (up to of about 30°); the existence of bond, adhesive and anchorage mechanisms for the fibres (mechanical and chemical treatments); fibre embedment length; strength of the microstructure of the material surrounding the fibre.

However, if the fibre rupture occurs during the fibre pullout process, the benefits that fibre addition can provide to cement-based materials can be marginal, indicating that fibre type should be selected taking into account the concrete properties. The influence of the fibre orientation on the fibre pullout performance reveals that in order to assess the effectiveness of the fibre reinforcement from experimental tests it is mandatory that the casting, geometry and loading conditions of the specimens are representative of the real structural application, as much as possible.

During the loading process of a FRC structure, fibres offer resistance to the crack opening in consequence of fibre pullout mechanisms, promoting the development of diffuse crack patterns. As a result, the load-carrying capacity of a structure can significantly exceed its cracking load, due to the stress redistribution occurring during the process of formation of diffuse crack patterns. Another important aspect of the development of diffuse crack patterns is related to the durability of the concrete structures, since they correspond to cracks of smaller width for load levels at serviceability limit states.

The difference between the maximum load (F_u) and the cracking load (F_{cr}) of a structure increases with the support redundancy of this structure. In statically determinate FRC structures, $F_{cr,i}$ and $F_{u,i}$ are identical in the case of inadequate fibre orientation (Fig. 4.3(a)1), or $F_{u,i}$ can be significantly higher than $F_{cr,i}$ in the case of a proper fibre orientation (Fig. 4.3(a)2). The subscript i is used to associate the entity to statically determinate structures. In structures with high support redundancy (the subscript h is used to associate the entity to this type of structure),

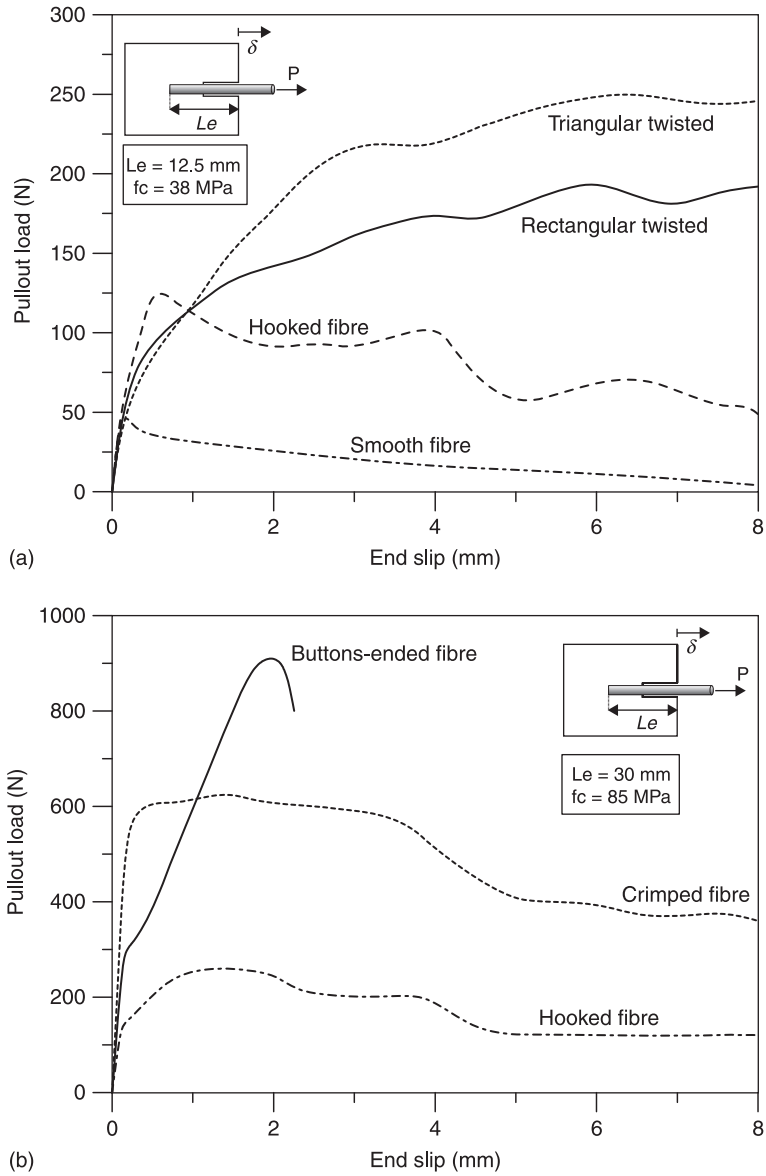

4.1 Comparison of typical pullout response of different steel fibres: (a) adapted from Naaman (2030); (b) adapted from Banthia and Trottier (1994).

such is the case with slabs supported on soil, piles or columns (see Fig. 4.3(b)), the difference between $F_{u,h}$ and $F_{cr,h}$ (ΔF_h) is, in general, much higher than the ΔF_i observed in statically determinate structures (Barros and Figueiras 1998; Falkner and Teutsch 1993).

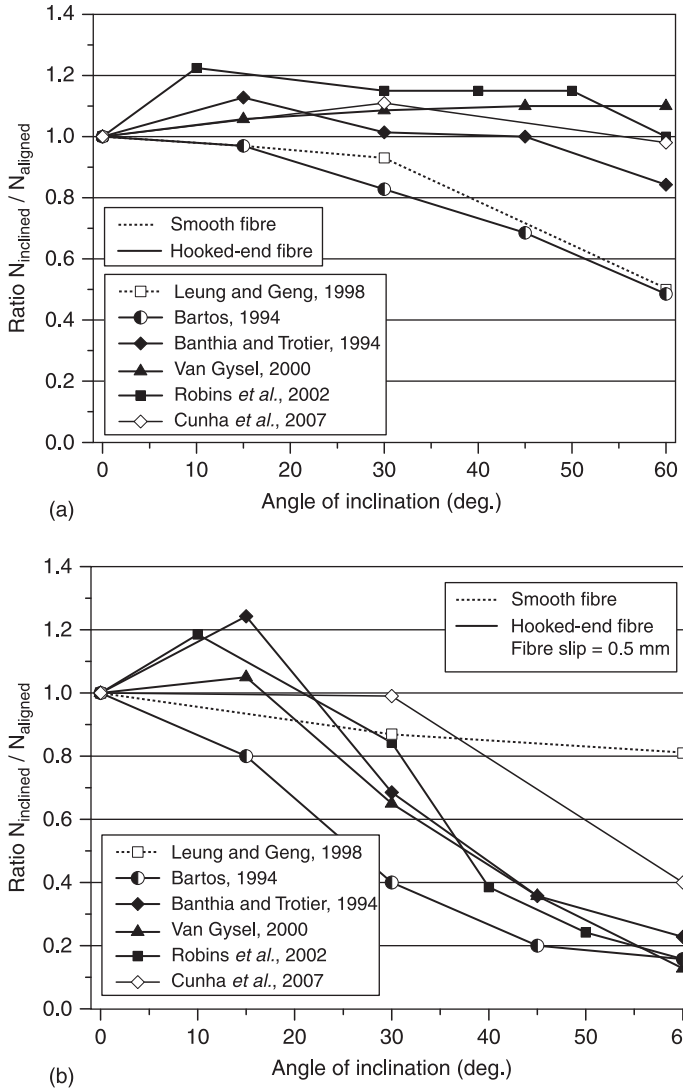

4.2 Relationship between normalized pullout force of an inclined fibre and the angle of fibre inclination: (a) for fibre slips at which the maximum pullout was achieved; (b) at a constant fibre slip of 0.5 mm (N is the fibre peak pullout force).

Combining fibres with conventional steel reinforcement is used mainly to increase the load-carrying capacity at serviceability limit states and to assure crack patterns of smaller crack width, in an attempt to design structures of higher durability. Figure 4.4(a) represents the tensile stress–strain diagrams of FRC under the influence of steel bars (tension-stiffening), and of FRC not affected

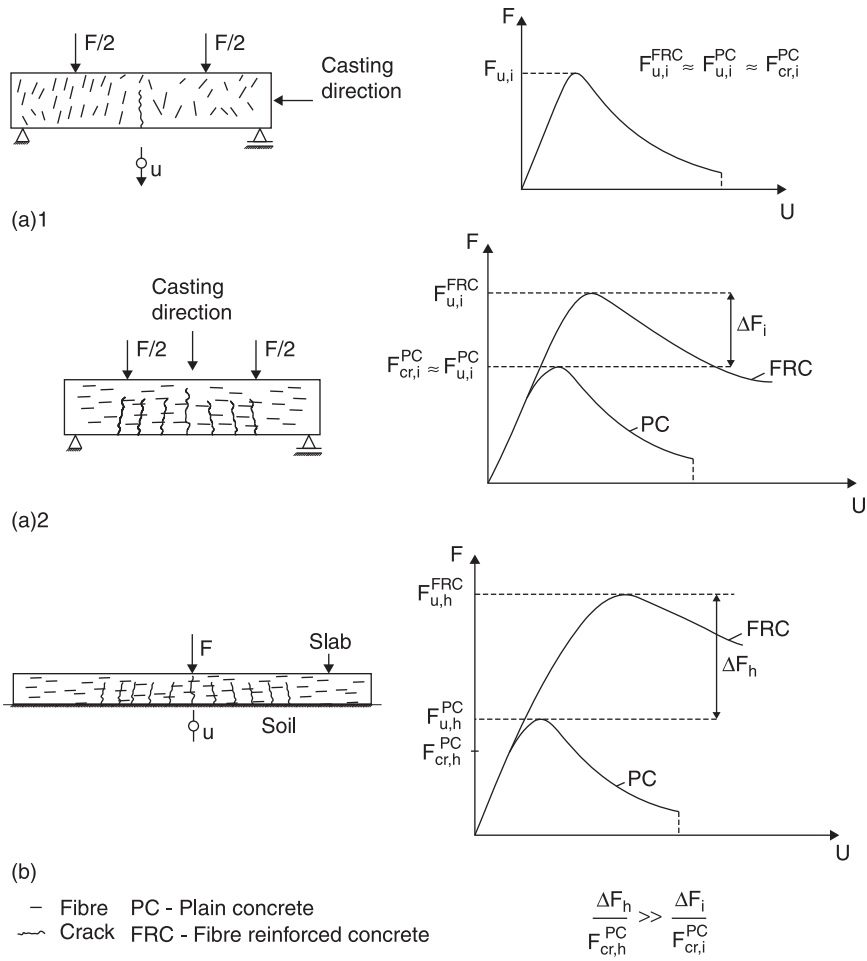

4.3 Fibre reinforcement contribution in: (a) statically determinate structures, where load and casting have (a)1 orthogonal and (a)2 parallel directions; (b) statically indeterminate structures.

by the mechanisms provided by steel bars. The highest residual tensile strength of FRC ($\Delta\sigma_t$) leads to an increase of the resistant bending moment of the cross-section (ΔM), for curvatures higher than the curvature at crack initiation (χ_{cr}), when M-χ of RC cross-section without fibres is taken for basis of comparison (Fig. 4.4(b)).

The ΔM provided by fibre reinforcement can be used to design structures of much more ductile and ultimate load carrying capacity. For instance, the maximum load-carrying capacity (p_{max}^{PC}) of the RC frame represented in Fig. 4.5 can coincide with the formation of the beam failure mechanism, due to the occurrence of the two 1 and 2 plastic hinges. However, well-designed FRC beams can lead to the

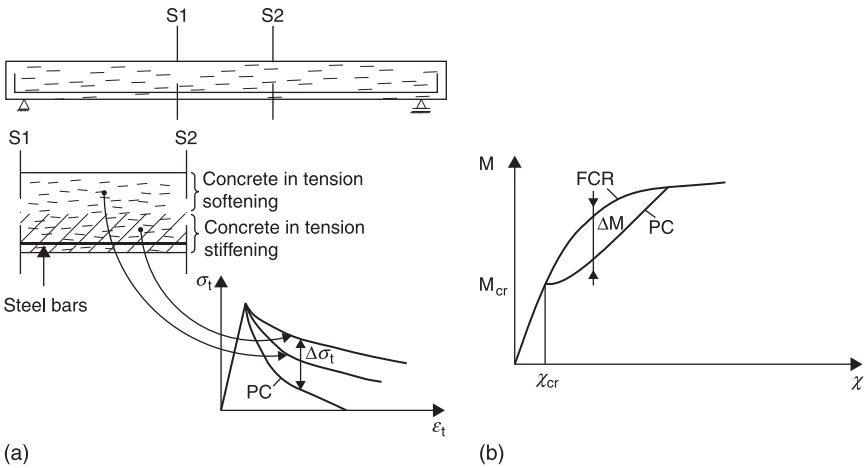

4.4 (a) Post-cracking residual tensile strength of PC and FRC; (b) moment-curvature of PC-RC and FRC-RC cross sections.

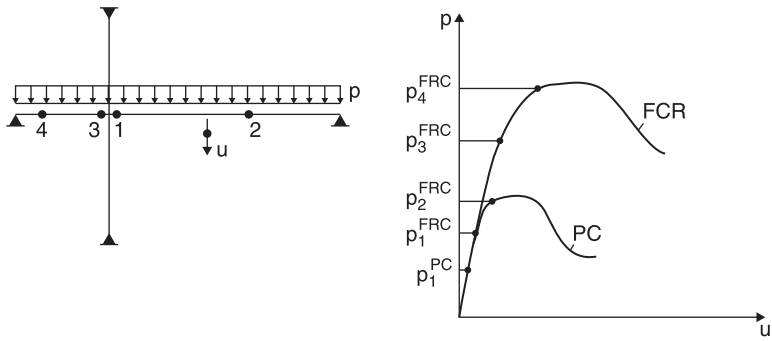

p_i - live load at the formation of the i^{th} plastic hinge

4.5 The FRC higher residual tensile strength contributes to RC structures of higher density and load-carrying capacity.

formation of two beam mechanisms, in consequence of an increment of $\Delta\sigma_t$ for the material (that results in an increment of ΔM for the cross-section), resulting in a structure with much higher ductility and load-carrying capacity.

The enhancement of the fracture toughness (post-cracking energy dissipation capacity) of concrete can be achieved either by adding other energy-dissipating elements to concrete or by changing the existing toughening mechanisms, in order to increase their energy-consuming ability. The addition of fibres to concrete belongs to the first alternative. The increase of the fracture toughness in FRC is the consequence of the great amount of energy dissipation through toughening mechanisms like fibre crack bridging, fibre bending, and fibre pullout or

debonding. The influence of the fibres may be approached in two different levels of observation that are at the meso- and at the macro-level (see Fig. 4.6). At the meso-level, during fracture and with the formation of the randomly distributed microcracks, fibres contribute to delay the damage and strain localization phenomena, enhancing resistance and ductility by means of the increase of energy dissipation in the above-mentioned toughening mechanisms. At the macro-level, when microcracks start to localise in macrocracks that propagate at a structure-scale size, fibres bridge the opposite crack faces and transfer tensile forces between them, improving bearing capacity and ductility of the structure. The optimisation of the fibres geometry takes into consideration the different requirements in attending these two functionalities. If the optimisation of the material behaviour (at a meso-level) is intended, fibres must act at the microcracks level and therefore have to be numerous, with small diameter, and short enough so that workability and placeability are not seriously compromised. If the intention is to provide more strength and ductility from a structural behaviour point of view (at a macro-level), macrocracks must be bridged with longer fibres, so that a sufficient anchorage length is assured. A too-large aspect ratio of the fibres negatively affects the workability and placeability of concrete.

Steel fibre reinforced self-compacting concrete (SFRSCC) can be defined as a steel fibre reinforced concrete that is able to flow in the interior of the formwork, filling it in a natural manner. SFRSCC has also the capability of passing through the obstacles, flowing and consolidating under the action of its own weight. Due to the relatively high content of fine particles applied in the manufacture of SFRSCC, a stiff and strong fibre-matrix interface can be achieved, which is a favourable medium to mobilize the fibre reinforcement mechanisms, resulting in a material of high post-cracking resistance and ductility, provided that the fibre rupture is avoided. However, the addition of steel fibres to granular

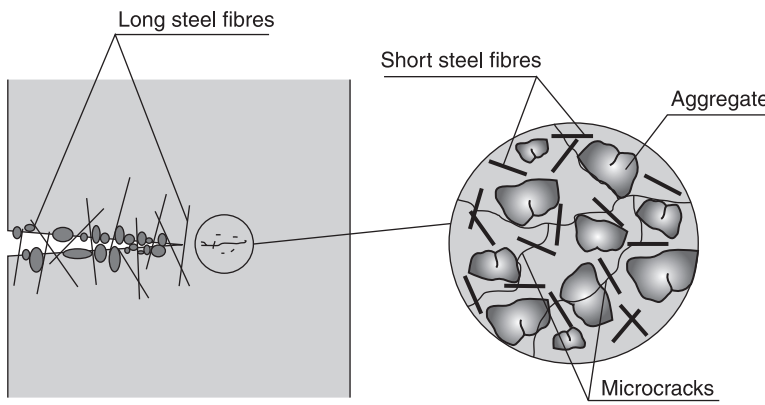

4.6 Meso- and microlevel approaches: steel fibres stitching macro- and microcracks (Pereira 2006).

cement-based materials perturbs the flowing ability of fresh concrete, which requires special mix methodologies to assure SCC characteristics (Gomes 2002, Pereira 2006).

SFRSCC is especially appropriate for the precasting industry, since high quality control over the material's constituents can be assured, as well as over the mixing, casting and curing procedures. Due to the inherent reinforcement provided by fibre addition, several structural elements, especially those involving difficulties in assuring good casting conditions when using conventional concrete, can be manufactured with SFRSCC with technical, economic and aesthetics benefits.

4.3 Mix design and steel fibre reinforced self-compacting concrete (SFRSCC) compositions

In general, the materials used for the development of SFRSCC, within the scope of the experimental programs of the present chapter, are cement (C) CEM I 42.5R (rapid hardening and high strength cement, according to EN197–1:2000), limestone filler (LF), a third generation superplasticizer (SP) based on polycarboxilates, water (W), three types of aggregates (fine river sand (FS), coarse river sand (CS), and crushed granite 5–12 mm (CG)) and hooked-end steel fibres. This fibre has a length (l_f) of 60 mm, a diameter (d_f) of 0.75 mm, an aspect ratio (l_f/d_f) of 80 and a yield stress of 1100 MPa. The methodology followed to formulate SFRSCC compositions is mainly based on the three following steps:

(i) the proportions of the constituent materials of the binder paste are defined;
(ii) the proportions of each aggregate on the final granular skeleton are determined;
(iii) binder paste and granular skeleton are mixed in distinct proportions until self-compacting requirements in terms of spreadability, correct flow velocity, filling ability, blockage and segregation resistance are met, allowing the determination of the optimum paste content in concrete.

A detailed description of the method can be found elsewhere (Pereira 2006). Table 4.1 includes the developed SFRSCC compositions (the amount of water

Table 4.1 SFRSCC compositions per m^3 of concrete

Comp. no.	C (kg/m^3)	LF (kg/m^3)	W (kg/m^3)	SP (kg/m^3)	FS (kg/m^3)	CS (kg/m^3)	CG (kg/m^3)	Fibres (kg/m^3)	SCC requirements		
									s (mm)	T_{50} (sec)	H_2/H_1
1	359.4	308.1	97.0	7.1	172.2	859.2	698.4	30	720	3.5	–
2	359.4	312.2	96.9	6.9	108.2	709.4	665.2	30	700	–	–
3	401.7	344.3	108.4	7.6	101.7	666.4	624.8	45	700	–	–
4	401.7	344.3	117.3	7.7	178.3	668.1	600.0	45	730	7	0.89

referred does not include the aggregate's saturation water). The first composition is used to assess the influence of the age on both the compressive strength and Young's modulus of the SFRSCC. This SFRSCC is also used to evaluate the punching and the flexural resistance of representative modules of façade panels. The second composition is used in the fibre pullout tests to determine the influence of fibre embedment length, fibre orientation and fibre anchorage characteristics on the fibre force–slip relationship. This and the third composition are used in an experimental program dedicated to the evaluation of analytical expressions able to simulate the compressive behaviour, according to the format of CEB-FIP Model code MC90 (1993). The fourth composition is used to appraise the performance of a cyclic analytical model for the simulation of the SFRSCC compressive behaviour when subjected to cyclic compressive loading. In all compositions the total spread, *s*, was measured, while in the first and fourth compositions the time to reach a spread diameter of 500 mm, T_{50}, was also determined (EFNARC 2002). In the fourth composition the H_2/H_1 parameter of the L Box test was also measured (EFNARC 2002). For the developed compositions, no visual sign of segregation was detected and the mixtures showed good homogeneity and cohesion, even while flowing through the smaller orifice of the Abrams cone (while testing, the Abrams cone was always used in the inverted position).

4.4 Fibre pullout

4.4.1 Introduction

The effectiveness of a given fibre as a medium of crack-opening arrest for cement-based materials is often assessed using a single fibre pullout test, where fibre slip is monitored as a function of the applied load on the fibre (Naaman and Najm 1991; Banthia and Trottier 1994; Li and Chan 1994; Groth 2000). The present section focuses on relevant results of a research project dedicated to the evaluation of the pullout behaviour of the hooked-end steel fibres indicated in Section 4.2, when embedded into a SCC medium. The details can be consulted in Cunha *et al*. (2007).

4.4.2 Test series and properties of the materials

The pullout tests of the experimental program can be divided in two main groups according to the type of used fibres: hooked ends and smooth. The influence of the various mechanisms of bond can, therefore, be assessed separately. Within these two main groups, the influence of the fibre embedded length and fibre orientation on the fibre pullout response is assessed. Smooth fibres were obtained cutting the hooked-end steel fibres with pliers. Code names for the series of tests consist of alphanumeric characters separated by underscore. The first character indicates the fibre type (S – smooth; H – hooked), the second string indicates the embedded

length in mm (for instance, lb10 represents a fibre embedded length of 10 mm), and the last numeral indicates the fibre inclination angle, in degrees, with the fibre pullout load orientation. The complete overview of all the performed fibre pullout tests, with reference to the type, aspect ratio, embedded length (lb) and inclination angle of the fibre, is given in Table 4.2. The second SCC composition of Table 4.1 was used in this experimental program. The concrete compressive strength was assessed by three cubic specimens with an edge length of 150 mm. The average value of the concrete compressive strength during the fibre pullout tests was 83.4 MPa with a coefficient of variation of 0.9%. Moreover, six single fibres were tested under direct tension in order to assess the fibre tensile strength. A fibre tensile strength of 1141 MPa was obtained, with a coefficient of variation of 2.0%.

4.4.3 Test setup

The pullout tests were performed in a servo-hydraulic Lloyd LR30K machine with a capacity of 30 kN. To record force values with high accuracy, a HBM S9 load cell with a capacity of 5 kN, and accuracy class 0.05 was attached to the machine test frame. The single-sided specimen was mounted in a steel specimen supporting system, see Fig. 4.7(a) and Fig. 4.7(b). This frame incorporates a steel system composed by a plate monolithically connected to a cylinder that is fixed to the testing machine frame. The cylinder/machine connection allows free rotations of the entire steel frame. A steel ring is coupled to the aforementioned

Table 4.2 Overview of the performed pullout tests

Series	Fibre type	Lb (mm)	Angle (°)	N. specimens
S_lb10_0	Smooth	10	0	–
S_lb10_30	Smooth	10	30	–
S_lb10_60	Smooth	10	60	3
S_lb20_0	Smooth	20	0	3
S_lb20_30	Smooth	20	30	3
S_lb20_60	Smooth	20	60	3
S_lb30_0	Smooth	30	0	3
S_lb30_30	Smooth	30	30	3
S_lb30_60	Smooth	30	60	3
H_lb10_0	Hooked	10	0	6
H_lb10_30	Hooked	10	30	6
H_lb10_60	Hooked	10	60	6
H_lb20_0	Hooked	20	0	6
H_lb20_30	Hooked	20	30	6
H_lb20_60	Hooked	20	60	6
H_lb30_0	Hooked	30	0	6
H_lb30_30	Hooked	30	30	6
H_lb30_60	Hooked	30	60	6

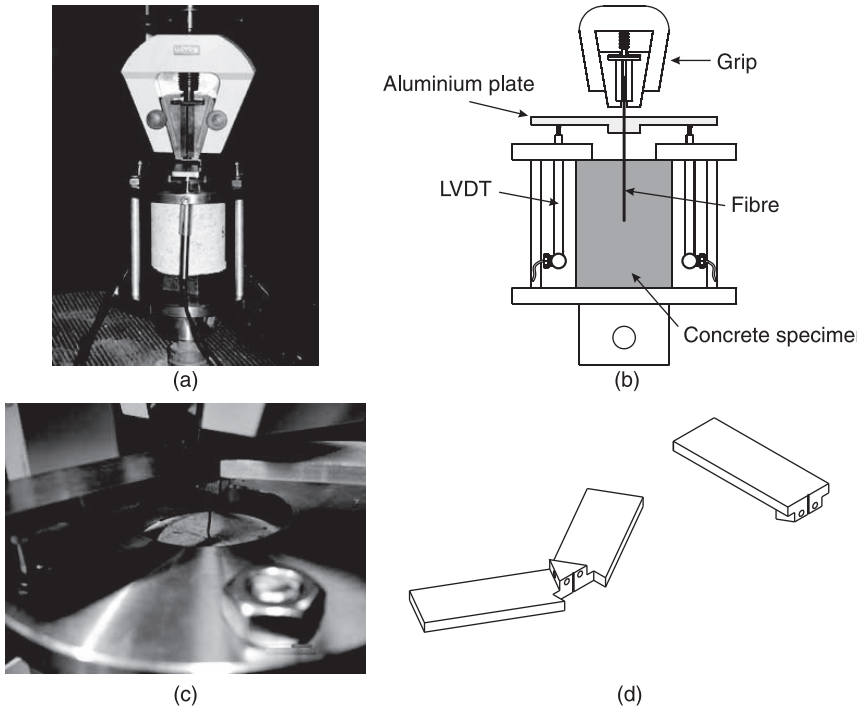

4.7 Configuration of the single fibre pullout test: (a) and (b) general view; (c) and (d) detailed view of the aluminium plate fixed to the fibre (Cunha *et al*. 2007).

steel system by three steel screws. The protruding end of the steel fibre is fastened to a standard 'Lloyd' grip, which allows a secure hold of the fibre. However, due to the small fibre diameter, special attention was given in fastening the fibre, since deforming the fibre end could induce that the fibre would break at the grip. For the measurement of the fibre pullout slip, three linear variable differential transformers (LVDT) (linear stroke ±5 mm) were used. To exclude measuring deformations of the testing rig and fibre slip at the grip, the LVDTs were fixed at the upper steel ring and touching the bottom surface of an aluminium plate fixed to the fibre. The plate was fixed to the fibre with two fine screws and was used as a support for this LVDT configuration (detail in Fig. 4.7(c) and Fig. 4.7(d)).

Since the three LVDTs were disposed around test specimen forming an angle of 120 degrees between consecutive LVDTs, the actual pullout slip of the fibre is the average of the three LVDT readouts. The closed-loop displacement control was performed by the testing machine internal displacement transducer, at the displacement rate of 10 μm/s.

4.4.4 Relevant results

The average pullout load–slip curves for the tested series are depicted in Fig. 4.8. In general, for both analyzed hooked and smooth aligned fibres, the configuration of the pullout load-slip curve was similar regardless of the fibre embedded length but, as expected, the peak load and the dissipated energy increased with it (see Fig. 4.8(a) and Fig. 4.8(b)). The vertical offset distance between curves can be regarded as the contribution of the embedded bond length increment or decrement between curves. In the case of hooked fibres with a 30° inclination angle, two failure modes occurred, resulting in two distinct types of pullout-slip curves. In Fig. 4.8(c), the average curve is represented up to the slip at which the fibre rupture took place.

The pre-peak branch of these curves is similar to the one observed for aligned hooked fibres. The nonlinear part is, however, more pronounced than for aligned fibres, due to the cracking and spalling of the matrix at the fibre bending point, as a consequence of the additional stress concentration at this zone for inclined fibres. Whenever, for a 30° inclination angle, the hooked fibre did not break, and therefore the fibre was fully pulled out, the post-peak behaviour was assessed. The post-peak curve of the latter specimens was similar to that observed for the aligned hooked fibres; however, an increment of the residual force was perceived up to a slip of 4 mm. Such difference is ascribed to the frictional resistance increase due to the force component perpendicular to the fibre axis. Afterwards, at slip of about 4.5 mm (corresponding approximately to the straightened hook length), a significant load decay was observed.

On the other hand, smooth fibres with an inclination angle of 30° revealed two distinct pre-peak behaviours. Regarding the series with an embedded length of 20 mm, the pre-peak behaviour was identical to the one observed for the aligned smooth fibres, with the exception that a higher peak load was attained as a consequence of the bending mechanism associated to fibre inclination angle. For a larger embedded length (30 mm), before reaching the peak load a decline in stiffness is observed, subordinated to several load decays corresponding to the cracking or spalling of the concrete matrix (see Fig. 4.8(d)). With respect to the post-peak behaviour, the load decreases with the increase of slip. Compared to the aligned smooth fibres, the load decay is less abrupt, since the influence of the frictional resistance is more significant for inclined fibres.

A completely distinct behaviour was observed for the series with an inclination angle of 60° (Fig. 4.8(e) and Fig. 4.8(f)). The hooked series with the latter inclination angle failed by fibre rupture, with the exception of one specimen, whereas in the smooth series, fibres were fully pulled out. With the increase of the inclination angle, the stress concentration at the fibre exit point from the matrix increases, and therefore the concrete matrix is more prone to cracking and spalling. In terms of pre-peak behaviour, this is reflected in a significant loss of stiffness. Comparing, respectively, Fig. 4.8(c), Fig. 4.8(d), and Fig. 4.8(e), Fig.4.8(f), it can be perceived

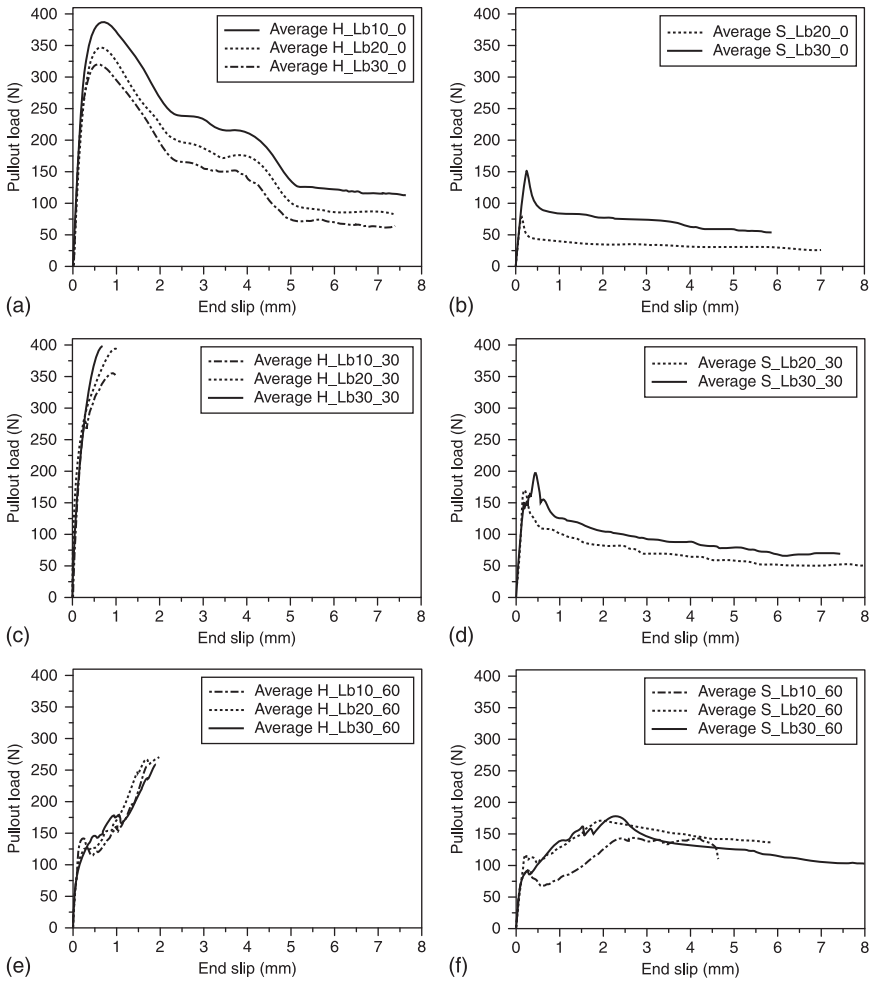

4.8 Average pullout load-slip curves for a fibre inclination angle: (a) and (b) 0 degrees; (c) and (d) 30 degrees; (e) and (f) 60 degrees (Cunha *et al*. 2007).

that for the series with a 60° angle, cracking and spalling start for a lower load level. Moreover, as a larger portion of concrete is pushed or pulled out, a greater fibre length can be more easily bent, which promotes the stiffness decrease up to the peak load. Regarding the post-peak phase in the 60° angled smooth fibres, a gradual load decay was observed, as opposed to smooth fibres both aligned and with a 30° angle, since for a 60° inclination angle the frictional resistance due to the force component perpendicular to the fibre axis is much higher.

4.5 Characterization of the mechanical properties

4.5.1 Introduction

This section discusses how FRC material properties can be measured. Special attention is given to the evaluation of the effect of age on the properties that characterize the SFRSCC compression and flexural behaviour.

4.5.2 Tensile behaviour

Tensile testing is the most suitable to assess the influence of fibre reinforcement in cement-based materials. From these tests, the values of the parameters of the constitutive models used to simulate the crack initiation and crack propagation, under the framework of the fracture mechanics, can be determined. Fracture mechanics has begun to assume its importance as the theoretical basis for the majority of simulation models implemented into finite element method (FEM)-based computer programs (Bazant and Oh 1983, de Borst 1986, Rots 1988, Barros and Figueiras 2001) and the physical comprehension of fracture processes in concrete (Hillerborg *et al.* 1976).

There are a few parameters that seem to have the most influence in the fracture behaviour of concrete, and are common to many theoretical models. In the fictitious crack model (FCM), one of the most important models in the progress of understanding tensile fracture in concrete, introduced by Hillerborg *et al.* (1976), the material parameters are the tensile strength f_{ct}, the Young's modulus, E_c, the shape of the descending branch of the stress–crack opening diagram, and the fracture energy G_f, which is defined as the area under the stress–crack opening diagram. The stress–crack opening relationship can be obtained from a direct tensile test, as schematized in Fig. 4.9.

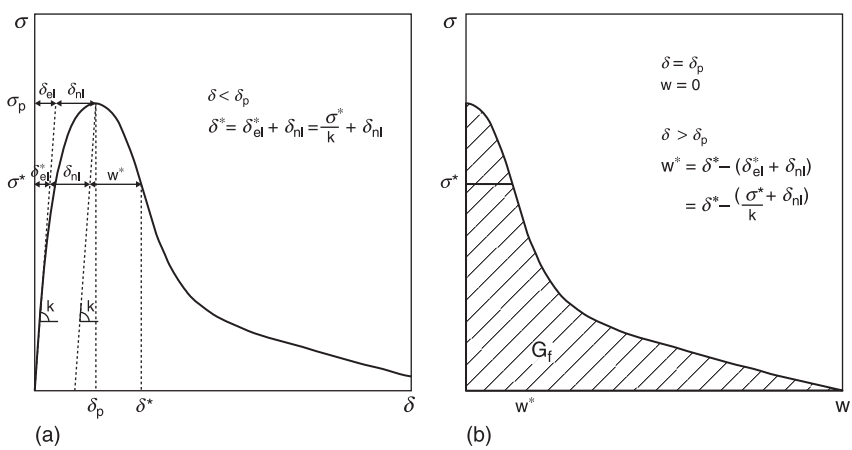

4.9 Stress–crack opening relationship (b) derived from the stress–deformation response in a direct tensile test (a).

The test equipment is absolutely essential when stable softening behaviour is required. In fact, the tests must be carried out in closed-loop control of very stiff testing rigs, like the one shown in Fig. 4.10 (Barros *et al*. 1994). It is well known that the shape of the softening branch depends on the boundary conditions of the testing specimen, which influences the fracture energy values derived from the tests, see Fig. 4.11. In case of pin-ended boundary conditions, the specimens are

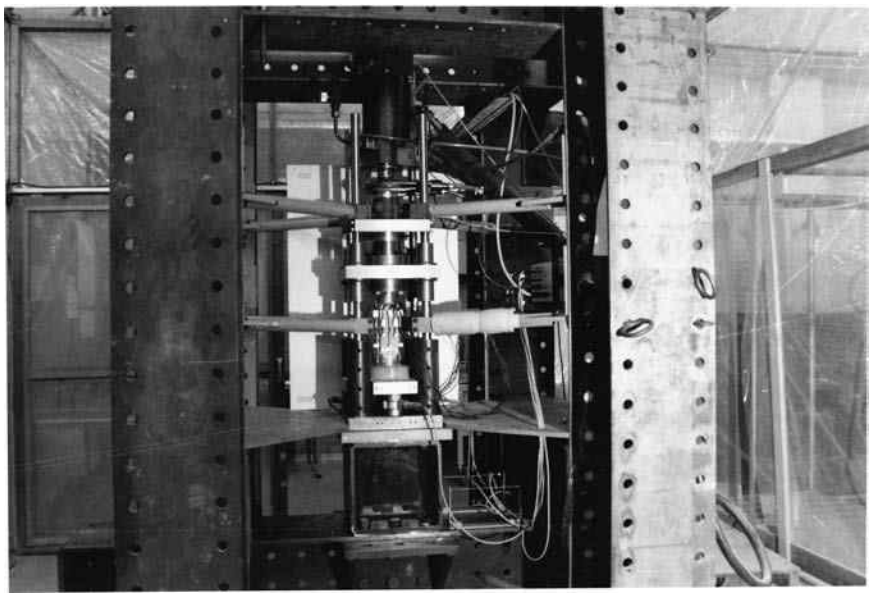

4.10 Photo of a testing rig used in tensile tests (Barros *et al.* 1994).

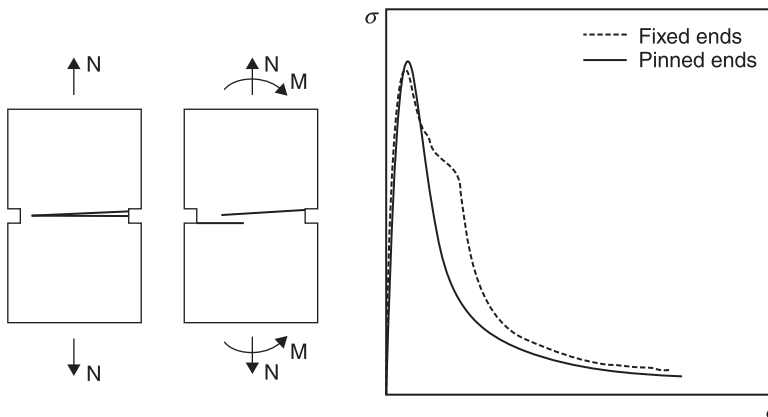

4.11 Influence of boundary conditions on the softening shape: pin-ended vs. clamped boundary (van Vliet 2000).

free to rotate when the onset of the macrocrack takes place and no additional restraint is introduced. In case of fixed-end platens, the eccentricity originated by the crack opening has to be balanced by the introduction of bending moments that contributes to the generation of multiple cracks. This behaviour influences, to certain extent, the softening behaviour, where a horizontal plateau can occur when a second macrocrack opens. The higher cracking density found in fixed boundary conditions leads generally to larger values of fracture energy relative to the ones achieved in uniaxial tensile tests conducted using pin-ended platens (van Vliet 2000; van Mier *et al*. 1996).

To assure tensile stable tests under the assumption that a three-dimensional (3D) non-uniform crack opening process can occur in the critical crack, the control signal of a servo testing unit should result from the average signal of the LVDTs placed in the corners of prismatic specimens, near the notched controlled fracture surface, see Fig. 4.12 (Hordijk 1991, Barros *et al*. 1994). In cylindrical specimens, three LVDTs should be placed around the specimen, forming 120 degrees between consecutive LVDTs (Barragan 2002) (Fig. 4.12).

The FCM assumes a linear stress–strain law for the pre-peak stage and a stress–crack opening diagram for the post-peak stage, agreeing with the idea that the deformation localization phenomenon invalidates the use of the concept of strain as a state variable. This approach is the basis of the discrete crack models for modelling crack initiation and crack propagation under the framework of finite element analysis (Rots 1998; Sena 2004). If cracks can be diffusively distributed into concrete, as in highly reinforced concrete and concrete reinforced with high

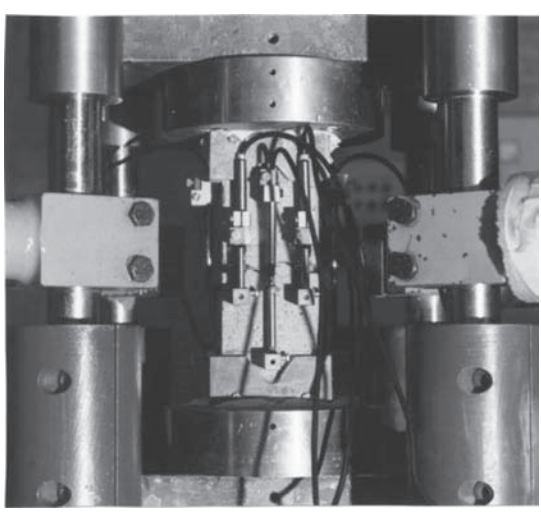

4.12 Arrangement of the measuring devices to assure tensile stable tests.

content of fibres, smeared crack models can be used for modelling the concrete post-crack behaviour. In this case, the crack strain is the crack opening divided by the crack bandwidth, which is a parameter depending on the characteristics of the finite element (Rots 1988; Oliver 1990).

The characteristic length, L_{ch}, physically related to the concept of the width of the damage zone, may be derived from the fracture parameters:

$$L_{ch} = \frac{E_c\, G_f}{f_{ct}^2} \qquad [4.1]$$

Many other expressions for computing the characteristic length are suggested by other authors, in the context of different assumptions and models, but it seems fair to assume that the characteristic length measures the brittleness of the material and is intimately related with factors like the size of the aggregates present in the concrete structural skeleton, the presence of another toughening mechanisms (like the addition of fibres), the properties of the cementitious matrix, and the behaviour of the interfacial transition zones (Taha and Shrive 2002).

When a concrete specimen is tested under uniaxial tension, the stress–deformation diagram obtained typically assumes the shape shown in Fig. 4.13. The example shows a typical strain softening behaviour after peak, but also strain hardening may be found for higher fibre contents. The measurement of the deformation depends on the positioning chosen for the measuring devices, since after reaching the peak load, deformations rapidly concentrate in the failure zone, and a strong discontinuity appears in the strain field. As shown in Fig. 4.13, distinct load–deformation curves

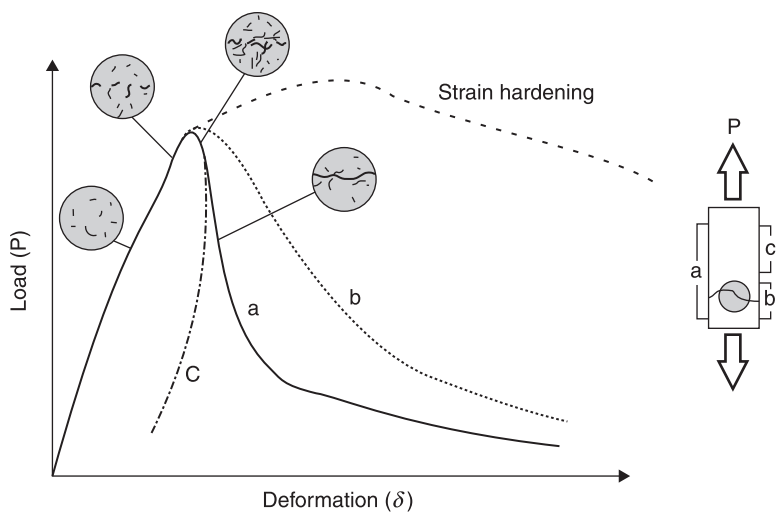

4.13 Behaviour of concrete under tension; strain localization (Pereira 2006).

may be obtained, depending on the localization of the deformation measuring device. After the peak load is reached, unloading (curve c), slow softening (curve b) or rapid softening (curve a) behaviours may be simultaneously found at the same specimen. The failure process of concrete in tension is clearly a localized phenomenon. The cracked material, where energy is dissipated during failure, is limited by a band of a certain width. The width of the damaged zone depends on the structure of concrete, with coarser grained concretes showing a wider damage zone than the finer grained ones. This is physically explained by bridging and branching mechanisms that become more important in coarse-grained materials. Also, fibre reinforcement contributes positively to increase the fracture energy, acting as additional bridging mechanisms and spreading cracking over a wider volume of the concrete specimen. When the crack opening reaches significant values and aggregates bridging at the crack surface fails, stress transfer over the crack is possible through the fibres crossing it. The maximum bridging stress that can be reached depends on the shape and deformability of the fibres, the number and inclination of the fibres with respect to the crack faces, and the pull-out behaviour (related to interfacial properties and matrix structure of concrete). It is reasonable to accept that small microcracks are present in concrete matrix before any mechanical tensile loading has been applied. These microcracks will extend under loading since the very beginning of loading procedure, and the load–deformation curve will tend to diverge, although very slightly at the beginning, from the ideal linear elastic behaviour, at a tangent to the initial part of the curve. Propagation of microcracks will be very dependent on the interaction of microcracks with each other, or between microcracks and aggregates, and the confining effect given by the presence of fibres.

A nonlinear branch before peak load can occur in fibrous specimens, being the amplitude of this branch as larger as higher is the content of fibres. Figure 4.14 shows a stress–deformation curve recorded in a tensile test with a prismatic specimen (Fig. 4.12) of concrete reinforced with 5%, in weight, of AR-glass fibres (Barros *et al*. 1994).

4.5.3 Compressive behaviour

The role of the fibre reinforcement

Concrete can be regarded as a three-phase heterogeneous material: the cementitious paste; the interface between aggregates and the bulk cement paste (interface transition zone (ITZ)); and the aggregates. The presence of the weak interfacial zones allows gradual and successive crack propagation almost from the beginning of the loading state, resulting in its highly nonlinear behaviour. Figure 4.15 identifies the four distinct consecutive stages of damage that can be identified in concrete under uniaxial load, based on initiation and propagation of cracks (Shah *et al*. 1995):

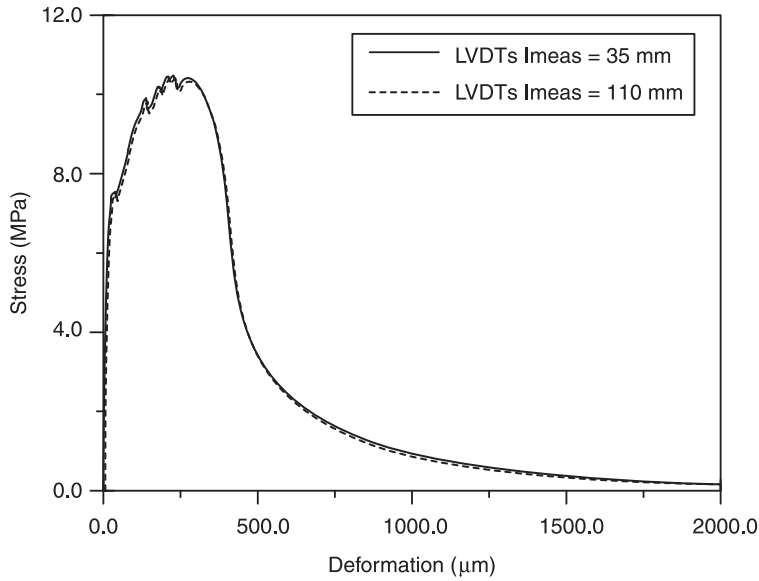

4.14 Stress-deformation curve for a GFRC spray-up specimen.

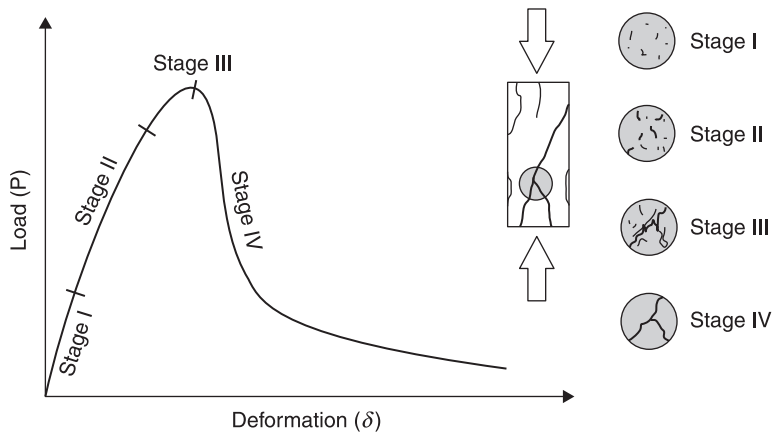

4.15 Strain localization in concrete behaviour under compression (Pereira 2006).

- Stage I – below 30% of the peak stress. The initiation of internal cracks is insignificant, and the stress–strain relationship may be considered as linear.
- Stage II – between 30% and 80% of the peak stress. First, the initial cracking at the ITZ starts to propagate and new microcracks develop. At approximately 60% of the peak stress, cracks at the cementitious matrix start to develop too. However, all these cracks are isolated and randomly distributed over the material volume.

- Stage III – between 80% and 100% of the peak stress. At this stage, all the small internal cracks become unstable and start to localize into major cracks. The crack growth is stable until peak is reached, which means that cracks only propagate if the load is increased. This phenomenon is referred to as damage localization or strain localization.
- Stage IV – after the peak load is reached. The major cracks continuously propagate, even though the load is decreasing. Unloading (snap-back) may occur in the material outside the damage zone, while the deformation at the localized damage band keeps increasing.

In fibrous concrete, the amplitude of Stages II and III is larger than that of the corresponding plain concrete. This amplitude depends, mainly, on the fibre type and content. However, the main influence of the fibre reinforcement mechanisms is especially visible in Stage IV where, depending on the fibre characteristics and concrete properties, a significant increase on the material energy absorption capacity can be obtained.

Age influence

Scarce research is available on the evaluation and modelling of the influence of SFRSCC age on its compressive behaviour. A good knowledge of the stress–strain relationship at early ages plays an important role in the determination of the time for the removal of shoring. This is the main concern in the precasting industry, since demolding the elements as soon as possible is an important requirement in terms of production profitability. To assure a safe demolding process, the influence of the SFRSCC age on its compressive behaviour should be known. For this purpose, uniaxial compression tests were carried out. The details of the test set-up and test procedures are described elsewhere (Cunha *et al*. 2008). The compositions numbered 2 and 3 in Table 4.1 were used in this experimental program, having received the designation of *Cf30* and *Cf45*, the first one reinforced with 30 kg/m^3 of fibres and the second one with 45 kg/m^3. Stress–strain laws are proposed to model the behaviour of the SFRSCC at all age values (in the hardened state). Additionally, equations derived from fitting the experimentally obtained results are proposed to predict the principal mechanical properties of SFRSCC in uniaxial compression.

Material properties

The average stress–strain curves, σ_c–ε_c, for the *Cf30* and *Cf45* series are represented in Fig. 4.16(a) and Fig. 4.16(b), respectively. Table 4.3 includes the average values of the compressive strength, f_{cm}, and the corresponding coefficients of variation, CoV. As expected, for both series, the f_{cm} increased with the age. Up to 24 hours the compressive strength of *Cf45* was higher than that of *Cf30*.

Table 4.3 Average values of the compressive strength and elasticity modulus

Age	*Cf30*				*Cf45*			
	f_{cm} (MPa)	CoV (%)	E_{ci} (GPa)	CoV (%)	f_{cm} (MPa)	CoV (%)	E_{ci} (GPa)	CoV (%)
12 hours	12.3	9.95	13.6	17.86	17.6	1.63	18.8	7.10
24 hours	24.7	8.38	25.3	4.96	25.3	1.24	22.4	5.83
3 days	52.3	1.90	37.1	4.31	47.9	1.10	31.4	2.04
7 days	58.1	4.32	40.4	0.78	51.0	2.61	31.9	2.14
28 days	69.7	1.73	41.5	2.31	56.2	2.15	34.5	4.33

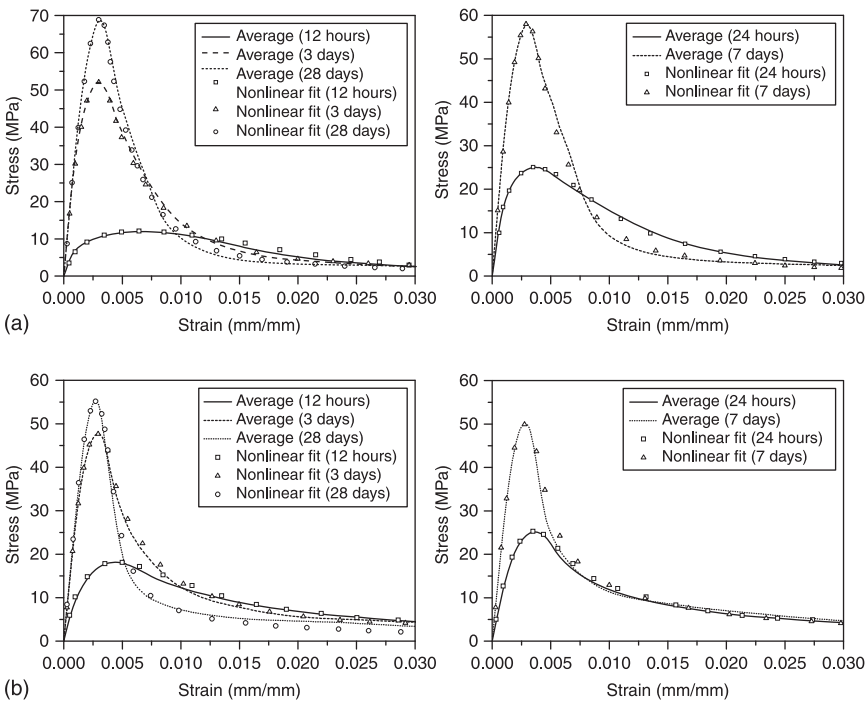

4.16 Experimental and analytical relationships for: (a) *Cf30* series; (b) *Cf45* series (Cunha *et al.* 2008).

However, after this age the f_{cm} of *Cf30* had a strengthening much more pronounced with time than the one measured in *Cf45*. The justification for this behaviour can be found elsewhere (Cunha *et al.* 2008).

The average values of the elasticity modulus, E_{ci}, and the correspondent CoV are also indicated in Table 4.3. The E_{ci} increased with age for both series and had a similar variation with age as f_{cm}. However, for *Cf30* the f_{cm} value increased significantly between 7 and 28 days, while the E_{ci} of *Cf30* had a marginal increment in this period. After the age of three days, the E_{ci} of *Cf45* had an increment of only

3 GPa. These results point out that the stiffness of both SFRSCCs at the age of 3 days is approximately 90% of the stiffness at 28 days, due to the high matrix compactness of these concretes. The difference between the values of elasticity modulus of *Cf30* and *Cf45* series may be due to the influence of the curing temperature and the content of limestone filler, as is justified elsewhere (Cunha *et al*. 2008). The influence of SFRSCC age on its compressive toughness was also evaluated (Cunha *et al*. 2008).

Modelling the compressive behaviour according to the EC2 format

To estimate the compressive strength and the Young's modulus of plain concrete (PC) at various ages, $f_{cm}(t)$ and $E_{ci}(t)$, respectively, the CEB-FIP Model code MC90 (1993) suggests the followings equations:

$$f_{cm}(t) = f_{cm}(28) \cdot \exp\left\{a\left[1 - \left(\frac{28}{t}\right)^{b}\right]\right\} \quad [4.2]$$

$$E_{ci}(t) = E_{ci}(28) \cdot \left\{\exp\left[a\left(1 - \left(\frac{28}{t}\right)^{b}\right)\right]\right\}^{c} \quad [4.3]$$

$$E_{ci} = E_{c0} \cdot \left(\frac{f_{cm}}{f_{cm0}}\right)^{a} \quad [4.4]$$

$f_{cm}(28)$ and $E_{ci}(28)$ being the average compressive strength and Young's modulus at 28 days, respectively. The MC90 proposes values for a, b, c, E_{c0} and f_{cm0} for PC. For the developed SFRSCC, new values for these parameters, indicated in Fig. 4.17 – 4.19, were obtained applying the nonlinear fitting method (Cunha *et al*. 2006).

To simulate the stress–strain behaviour of the developed SFRSCC, the equation proposed by the MC90 was also used for PC, which is schematically represented in Fig. 4.20. The branch represented by a full line is simulated by the following function:

$$\sigma_c(\varepsilon_c) = \frac{\frac{E_{ci}}{E_{c1}} \cdot \frac{\varepsilon_c}{\varepsilon_{c1}} - \left(\frac{\varepsilon_c}{\varepsilon_{c1}}\right)^2}{1 + \left(\frac{E_{ci}}{E_{c1}} - 2\right) \cdot \frac{\varepsilon_c}{\varepsilon_{c1}}} \cdot f_{cm} \qquad \text{for} \qquad \varepsilon_c \le \varepsilon_{c,\lim} \quad [4.5]$$

where E_{ci} and E_{c1} are, respectively, the tangent modulus and the secant modulus from the origin to the compressive strength, $E_{c1} = f_{cm}/E_{c1}$; σ_c, ε_c and ε_{c1} are the compressive stress, the compressive strain and the strain at the compressive strength, respectively. The strain $\varepsilon_{c,\lim}$ limits the applicability of Eq. 4.5, see

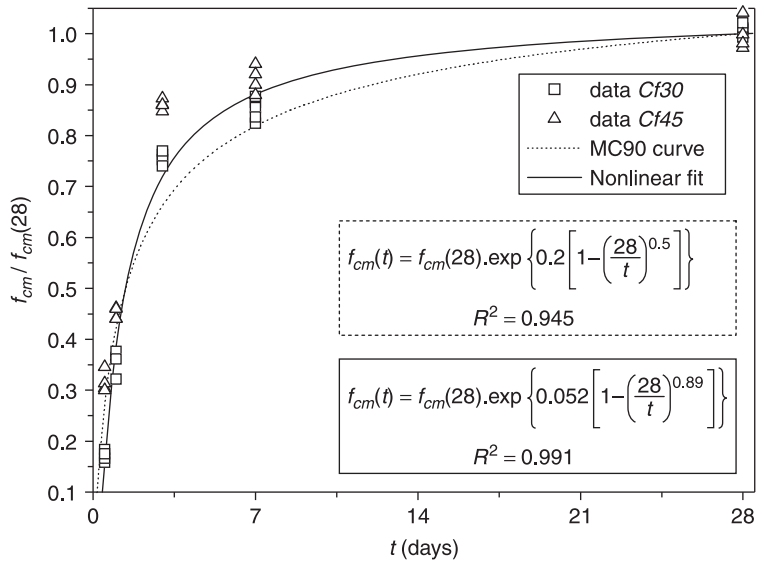

4.17 Simulation of the age influence on the concrete compressive strength (Cunha *et al.* 2008).

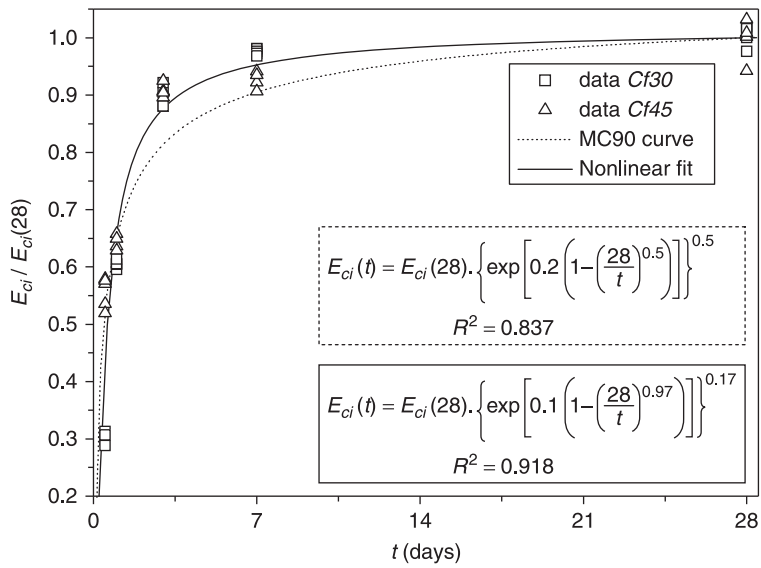

4.18 Simulation of the age influence on the concrete elasticity modulus (Cunha *et al.* 2008).

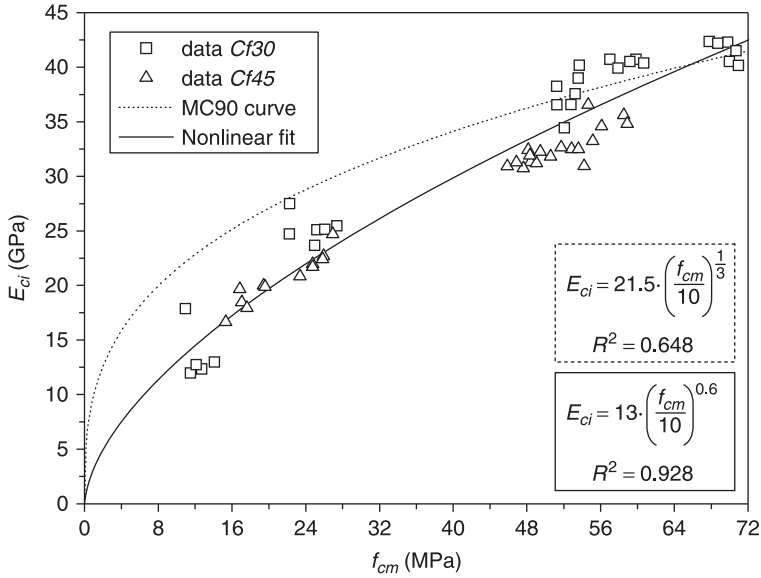

4.19 Relationship between the concrete elasticity modulus and the compressive strength (Cunha *et al.* 2008).

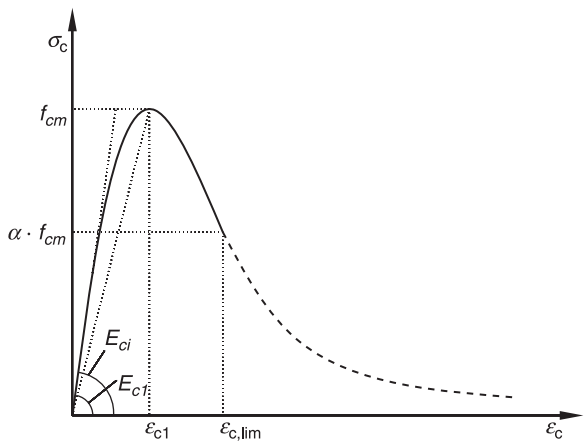

4.20 Stress–strain diagram for uniaxial compression.

Fig. 4.20. For the descending part of the stress–strain diagram, Eq. 4.5 is only valid for strain values up to $\varepsilon_{c,\lim}$. The strain $\varepsilon_{c,\lim}$ at $\sigma_{c,\lim}$ $(=\alpha . f_{cm})$ is computed from the following equation (Cunha *et al*. 2006):

$$\varepsilon_{c,\lim} = \left[\frac{1}{2}\left[(1-\alpha)\cdot\frac{E_{ci}}{E_{c1}} + 2\alpha\right] + \left[\frac{1}{4}\left[(1-\alpha).\frac{E_{ci}}{E_{c1}} + 2\alpha\right]^2 - \alpha\right]^{0.5}\right]\varepsilon_{c1} \qquad [4.6]$$

For $\varepsilon_c > \varepsilon_{c,\lim}$ the descending branch of the σ_c–ε_c, diagram (dashed line in Fig. 4.20) is defined using an equation of the type:

$$\sigma(\varepsilon_c) = \left[a\left(\frac{\varepsilon_c}{\varepsilon_{c1}}\right)^2 + b\frac{\varepsilon_c}{\varepsilon_{c1}} \right]^{-1} \cdot f_{cm} \qquad \text{for} \qquad \varepsilon_c > \varepsilon_{c,\lim} \qquad [4.7]$$

being the values of parameters a and b determined in order to assure the continuity of the function at $\varepsilon_c = \varepsilon_{c,\lim}$. Since the following conditions should be assured:

$$\underbrace{\sigma_c\left(\varepsilon_{c,\lim}\right)}_{\text{equation 4.5}} = \underbrace{\sigma_c\left(\varepsilon_{c,\lim}\right)}_{\text{equation 4.7}} \quad \wedge \quad \underbrace{\left.\frac{\partial \sigma_c}{\partial \varepsilon_c}\right|_{\varepsilon_{c,\lim}}}_{\text{equation 4.5}} = \underbrace{\left.\frac{\partial \sigma_c}{\partial \varepsilon_c}\right|_{\varepsilon_{c,\lim}}}_{\text{equation 4.7}} \qquad [4.8]$$

equation 4.7 is converted into the following:

$$\sigma(\varepsilon_c) = \left[\left[\frac{1}{\frac{\varepsilon_{c,\lim}}{\varepsilon_{c1}}} \xi \cdot \left(\frac{1}{2\alpha}\right)^2 - \frac{1}{\left(\frac{\varepsilon_{c,\lim}}{\varepsilon_{c1}}\right)^2} \cdot \frac{1}{\alpha} \right] \left(\frac{\varepsilon_c}{\varepsilon_{c1}}\right)^2 + \left[\frac{1}{\frac{\varepsilon_{c,\lim}}{\varepsilon_{c1}}} \cdot \frac{2}{\alpha} - \xi\left(\frac{1}{2\alpha}\right)^2 \right] \frac{\varepsilon_c}{\varepsilon_{c1}} \right]^{-1} \cdot f_{cm} \qquad [4.9]$$

with

$$\xi = \frac{4\left[\left(\frac{\varepsilon_{c,\lim}}{\varepsilon_{c1}}\right)^2 \cdot \left(\frac{E_{ci}}{E_{c1}} - 2\right) + 2\frac{\varepsilon_c}{\varepsilon_{c1}} - \frac{E_{ci}}{E_{c1}} \right]}{\left[\frac{\varepsilon_{c,\lim}}{\varepsilon_{c1}} \left(\frac{E_{ci}}{E_{c1}} - 2\right) + 1 \right]^2} \qquad [4.10]$$

The analytical stress–strain curves obtained from the best-fit procedure and the experimental average stress–strain curves are depicted in Fig. 4.16. The accuracy of the proposed equation toward the experimental data is quite high. Figure 4.21 presents an exponential function used to estimate the evolution of the parameter α with the age. The value suggested by MC90 for PC is also represented.

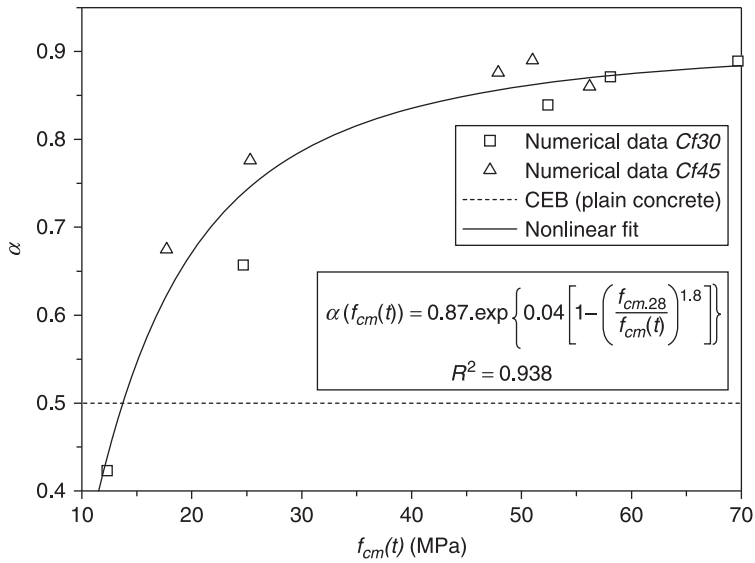

4.21 Relationship between parameter α and compressive strength (Cunha *et al*. 2008).

Cyclic behaviour

To evaluate the compression cyclic behaviour of SFRSCC, another experimental program was carried out with the specimens molded from composition number 4 (Table 4.1). The results derived from this experimental program were used to appraise a constitutive model to simulate the cyclic compressive behaviour of the developed SFRSCC. This experimental program is composed of nine cylinder specimens (150 mm diameter, 300 mm height). Six of them were tested with cyclic compressive loading, while the remaining three specimens were tested with monotonic loading, at the age of 14 days. At this age, the developed SFRSCC presented an average value for the Young's modulus, and compressive strength of 36 GPa and 55 MPa, respectively. Figure 4.22 shows typical cyclic and monotonic stress–strain curves obtained in this experimental program. It is evident that the monotonic curve corresponds to the envelope of the cyclic curve. All the results can be found elsewhere (Gonçalves and Barros 2007).

The model adopted to simulate the compression hysteretic behaviour of SFRSCC is schematically represented in Fig. 4.23. A general hysteretic scheme is simulated by the paths $\overline{BC}$, $\overline{CD}$, $\overline{DE}$, $\overline{EF}$, and $\overline{FG}$. These paths are modelled by the following equations (a negative signal was assumed for compression in this model):

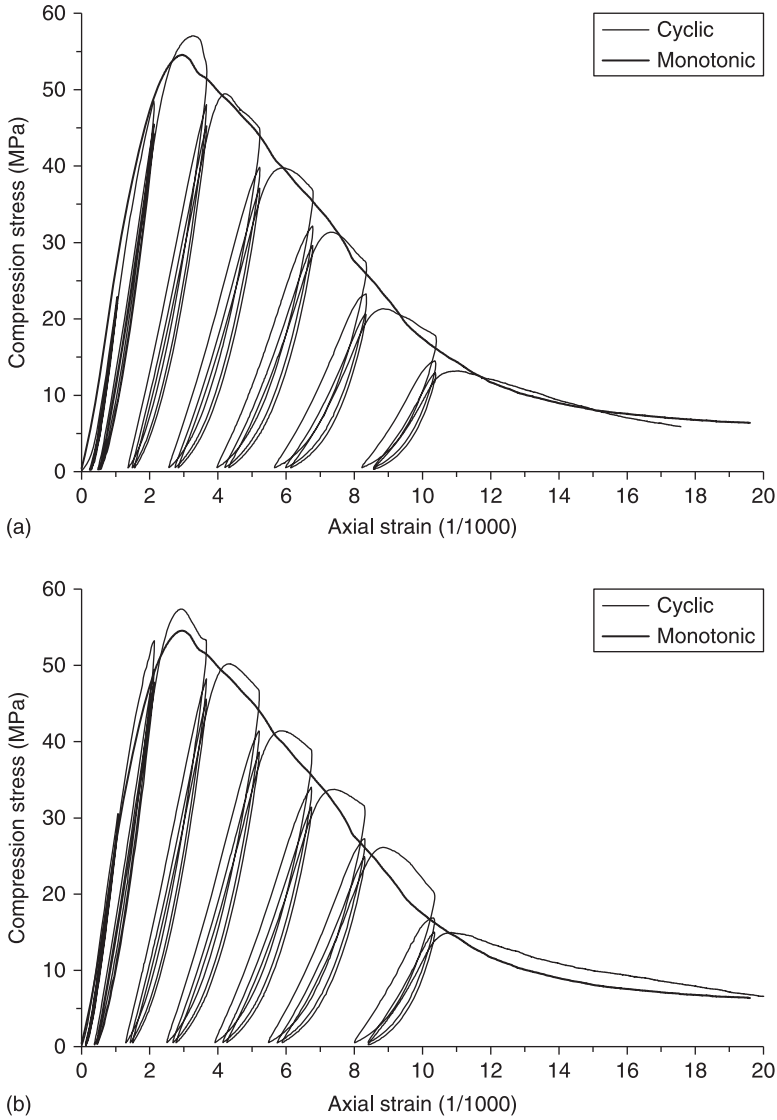

4.22 Typical cyclic versus monotonic stress–strain relationship obtained in experimental program: (a) Cyl19; (b) Cyl110 specimens.

$$\sigma_c = \bar{\sigma}_c^{\min}\left(\frac{\varepsilon_c - \varepsilon_c^{pl}}{\bar{\varepsilon}_c^{\min} - \varepsilon_c^{pl}}\right)^a \quad if \begin{cases} \varepsilon_{cu} < \varepsilon_c^{\min} \le 0 \\ \varepsilon_c^{\min} < \varepsilon_c \le \varepsilon_c^{pl} \quad (\overline{BC} \text{ and } \overline{DE}) \\ \Delta\varepsilon_c > 0 \end{cases} \qquad [4.11]$$

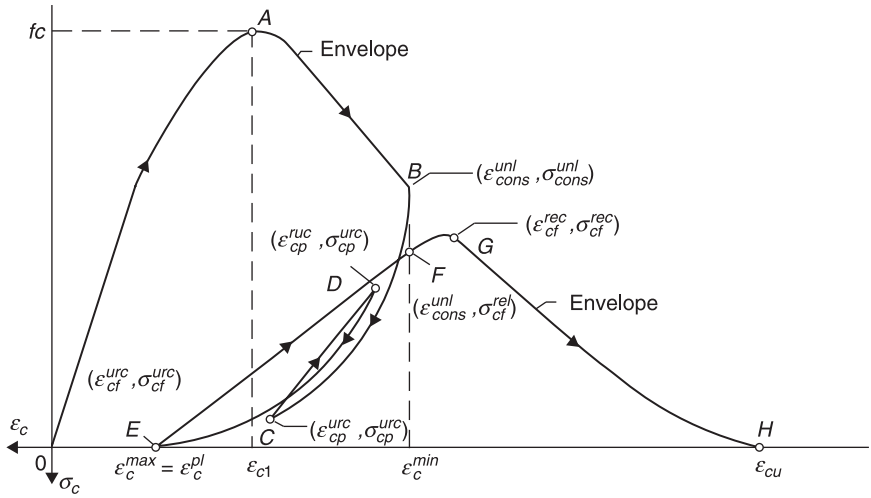

4.23 Cyclic hysteretic model for SFRCC.

$$\sigma_c = \sigma_{c(pf)}^{urc} + \left(\bar{\sigma}_c^{\min} - \sigma_{c(pf)}^{urc}\right)\left(\frac{\varepsilon_c - \varepsilon_{c(pf)}^{urc}}{\bar{\varepsilon}_c^{\min} - \varepsilon_{c(pf)}^{urc}}\right) \quad if \begin{cases} \varepsilon_{cu} < \varepsilon_c^{\min} \le 0 \\ \varepsilon_c^{\min} < \varepsilon_c \le \varepsilon_c^{pl} \quad (\overline{CD} \text{ and } \overline{EF}) \\ \Delta\varepsilon_c \le 0 \end{cases} \quad [4.12]$$

$$\sigma_c = \sigma_{cf}^{rec} + E_{c,env}^{rec}\left(\varepsilon_c - \varepsilon_{cf}^{rec}\right) + b\left(\varepsilon_c - \varepsilon_{cf}^{rec}\right)^2 \quad if \begin{cases} \varepsilon_{cu} < \varepsilon_c^{\min} \le 0 \\ \varepsilon_{cf}^{rec} < \varepsilon_c \le \varepsilon_c^{\min} \quad (\overline{FG}) \\ \Delta\varepsilon_c \le 0 \end{cases} \quad [4.13]$$

The monotonic branches $\overline{OB}$ and $\overline{GH}$ are simulated by the monotonic stress–strain relationship (Barros and Figueiras 1999). Equation 4.11 simulates the paths $\overline{BC}$ and $\overline{DE}$, i.e. both the partial and full unloading branches. In case of $\overline{BC}$, $\bar{\varepsilon}_c^{\min} = \varepsilon_{cons}^{unl}$ is the strain at point B, at the onset of unloading, and $\bar{\sigma}_c^{\min} = \sigma_{cons}^{unl}$ its corresponding stress, while in the case of $\overline{DE}$, $\bar{\varepsilon}_c^{\min} = \varepsilon_{cp}^{ruc}$ and $\bar{\sigma}_c^{\min} = \sigma_{cp}^{ruc}$, which is evaluated from the following equation:

$$\sigma_{cp}^{ruc} = \sigma_{cp}^{urc} + \left(\frac{\sigma_{cf}^{rel} - \sigma_{cp}^{urc}}{\varepsilon_c^{\min} - \varepsilon_{cp}^{urc}}\right)\left(\varepsilon_{cp}^{ruc} - \varepsilon_{cp}^{urc}\right) \quad [4.14]$$

where

$$\sigma_{cf}^{rel} = 0.92\,\sigma_{cons}^{unl} + 0.08\,\sigma_{cp}^{urc} \quad [4.15]$$

which is responsible for modelling the degradation in the compressive reloading stiffness. In Eq. 4.11 ε_c^{pl} is the compressive plastic strain that, according to Okamura and Maekawa (1991), can be evaluated from the following equation:

$$\varepsilon_c^{pl} = \varepsilon_c^{\min} - \frac{20}{7}\left[1 - \exp\left(-0.35\,\frac{\varepsilon_c^{\min}}{\varepsilon_{c1}}\right)\right]\varepsilon_{c1} \qquad [4.16]$$

The a shape factor of Eq. 4.11 can be determined from the equation proposed by Wang *et al*. (1981):

$$a = 1.0 + 0.7\left(\frac{\varepsilon_c^{\min}}{\varepsilon_{c1}}\right) \qquad [4.17]$$

Equation 4.12 simulates the paths $\overline{CD}$ and $\overline{EF}$, i.e., the partial reloading and the reloading up to the experienced minimum compressive strain (ε_{cons}^{unl}). For the partial reloading, branch $\overline{CD}$, $\varepsilon_{c(pf)}^{urc} = \varepsilon_{cp}^{urc}$ and $\sigma_{c(pf)}^{urc} = \sigma_{cp}^{urc}$ are the strain and the stress at point C. For this branch, $\overline{\varepsilon}_c^{\min} = \varepsilon_{cons}^{unl}$ and $\overline{\sigma}_c^{\min} = \sigma_{cp}^{ruc}$, where σ_{cp}^{ruc} is calculated from Eq. 4.14 and 4.15. In the case of the branch $\overline{EF}$, $\varepsilon_{c(pf)}^{urc} = \varepsilon_{cf}^{urc} = \varepsilon_c^{pl}$, $\sigma_{c(pf)}^{urc} = \sigma_{cf}^{urc} = 0$, $\overline{\varepsilon}_c^{\min} = \varepsilon_{cp}^{ruc}$ and $\overline{\sigma}_c^{\min} = \sigma_{cp}^{ruc}$, with σ_{cp}^{ruc} calculated from Eq. 4.14 and Eq. 4.15.

The strain of the returning point G on the compressive envelope curve can be obtained from the following equation:

$$\varepsilon_{cf}^{rec} = \varepsilon_{cons}^{unl} + \frac{4}{3}\left(\frac{\sigma_{cons}^{unl} - \sigma_{cf}^{rel}}{\sigma_{cf}^{rel}}\right)\left(\varepsilon_{cons}^{unl} - \varepsilon_c^{pl}\right) \qquad [4.18]$$

and the corresponding stress, σ_{cf}^{rec}, is determined replacing ε_c by ε_{cf}^{rec} on the envelope curve.

Finally, Eq. (4.13) simulates the path $\overline{FG}$, i.e. the returning to the envelope curve, where

$$E_{c,env}^{rec} = \left.\frac{d\sigma_c}{d\varepsilon_c}\right|_{\varepsilon = \varepsilon_{cf}^{rec}}^{env} \qquad [4.19]$$

is the tangent to the envelope curve, evaluated at the strain ε_{cf}^{rec}, and the b factor is determined from:

$$b = \frac{\sigma_{cf}^{rel} - \sigma_{cf}^{rec} - E_{c,env}^{rec}\left(\varepsilon_{cons}^{unl} - \varepsilon_{cf}^{rec}\right)}{\left(\varepsilon_{cons}^{unl} - \varepsilon_{cf}^{rec}\right)^2} \qquad [4.20]$$

This model was applied to the simulation of the cyclic compression tests. The comparison is presented in Fig. 4.24, from which it can be concluded that the model simulates with high accuracy the compression cyclic behaviour of SFRSCC specimens.

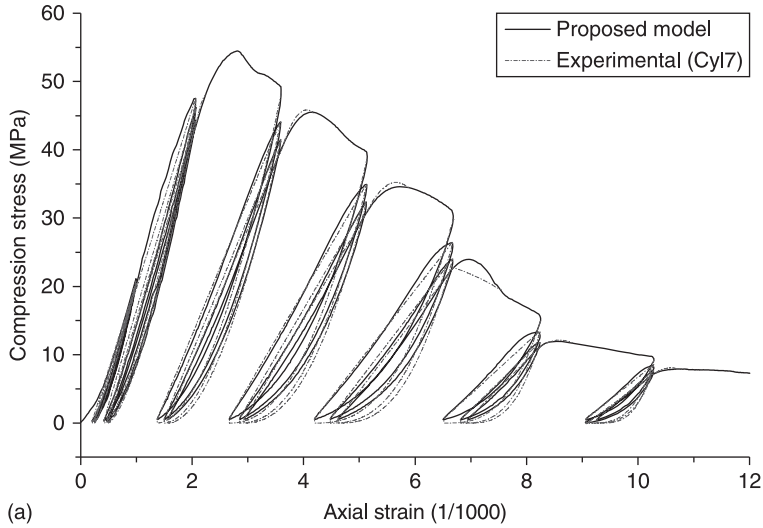

4.24 Experimental and analytical stress–strain curves cyclic compression tests: (a) Cyl7; (b) Cyl8 specimens.

4.5.4 Flexural behaviour

Test setup and design parameters

The composition number 1 (Table 4.1) was used to assess the influence of the SFRSCC age on its flexural behaviour. In the tests carried out, the recommendations of RILEM TC 162-TDF (Vandewalle *et al*. 2002) were adopted in terms of curing procedures, position and dimensions of the notch sawn into the specimen, load

and specimen support conditions, characteristics for both the equipment and measuring devices, and test procedures. The method for casting the beam specimens proposed by RILEM TC 162-TDF was adapted for SFRSCC, since they were cast without any external compaction energy. From the obtained force-deflection relationship, the equivalent ($f_{eq,2}$ and $f_{eq,3}$) and the residual ($f_{R,1}$ and $f_{R,4}$) flexural tensile strength parameters can be evaluated. The parameters $f_{eq,2}$ and $f_{eq,3}$ are related to the material energy absorption capacity up to a deflection of δ_2 and δ_3 ($\delta_2 = \delta_L + 0.65$ mm and $\delta_3 = \delta_L + 2.65$ mm, where δ_L is the deflection corresponding to the highest load recorded up to a deflection of 0.05 mm) provided by fibre reinforcement mechanisms ($D^f_{BZ,2}$ and $D^f_{BZ,3}$), as seen in Fig. 4.25. The parcel of the energy due to matrix cracking (D^b_{BZ}) is not considered in the f_{eq} evaluation. The parameters $f_{R,1}$ and $f_{R,4}$ are the stresses for the forces $F_{R,1}$ and

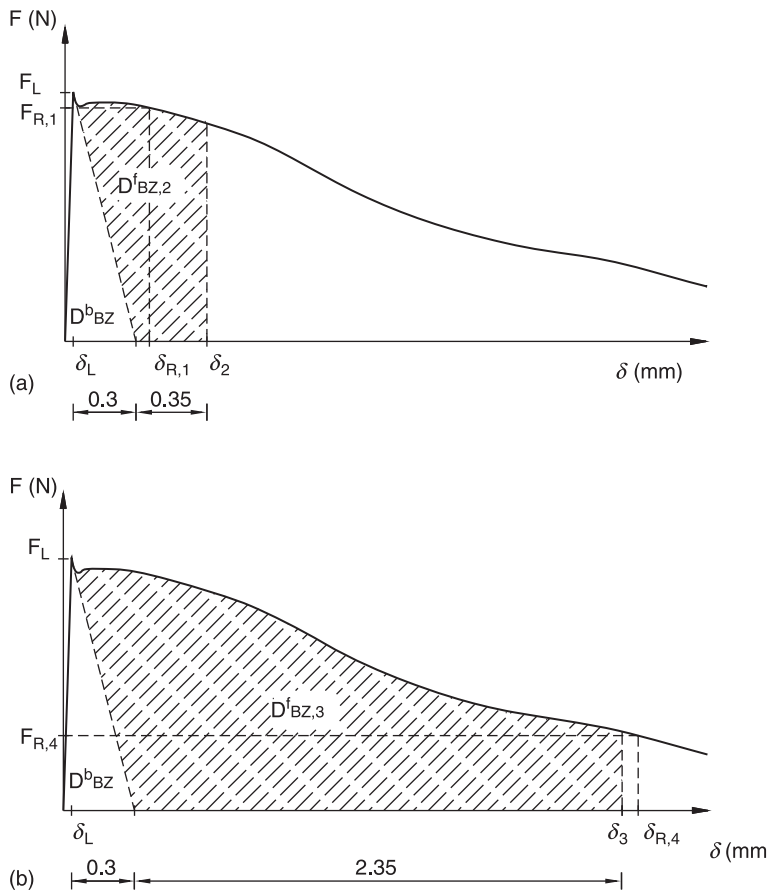

4.25 Evaluation of: (a) $f_{eq,2}$ and $f_{R,1}$; and (b) $f_{eq,3}$ and $f_{R,4}$ flexural tensile strength parameters according to RILEM TC 162-TDF (adapted from Vandewalle *et al.* 2000; 2002).

$F_{R,4}$, respectively, at deflections of $\delta_{R,1} = 0.46$ mm and $\delta_{R,4} = 3.0$ mm. According to RILEM TC 162-TDF, the equivalent (Vandewalle *et al*. 2000) and the residual (Vandewalle *et al*. 2002) flexural tensile strength parameters are obtained from the following equations:

$$f_{eq,2} = \frac{3}{2}\frac{D^f_{BZ,2}}{0.50}\frac{L}{bh^2_{sp}};\ f_{eq,3} = \frac{3}{2}\frac{D^f_{BZ,3}}{2.50}\frac{L}{bh^2_{sp}}\ (\text{N/mm}^2) \quad [4.21]$$

$$f_{R,1} = \frac{3}{2}\frac{F_{R,1}L}{bh^2_{sp}};\ f_{R,4} = \frac{3}{2}\frac{F_{R,4}L}{bh^2_{sp}}\ (\text{N/mm}^2) \quad [4.22]$$

where b (= 150 mm) and L (= 500 mm) are the width and the span of the specimen, and h_{sp} (= 125 mm) is the distance between the tip of the notch and the top of the cross-section.

Relevant results

The force–deflection curves, F–δ, obtained in the tested series (with specimens of distinct age) are depicted in Fig. 4.26. Each curve represents the average of the F–δ relationship values recorded in three specimens. This figure shows that, just after the deflection δ_L, a load decay occurred with an amplitude that also increased with the SFRSCC age, since a higher load had to be sustained by the fibres bridging the specimen fracture surface. This load decay was followed by a hardening phase up to a deflection level that decreased with the SFRSCC age. With the exception

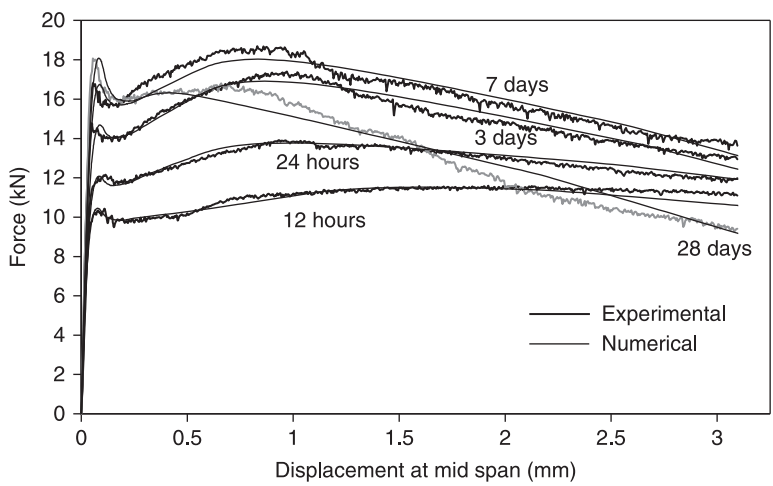

4.26 Experimental and numerical force-deflection curves of SFRSCC beam specimens for distinct age at testing.

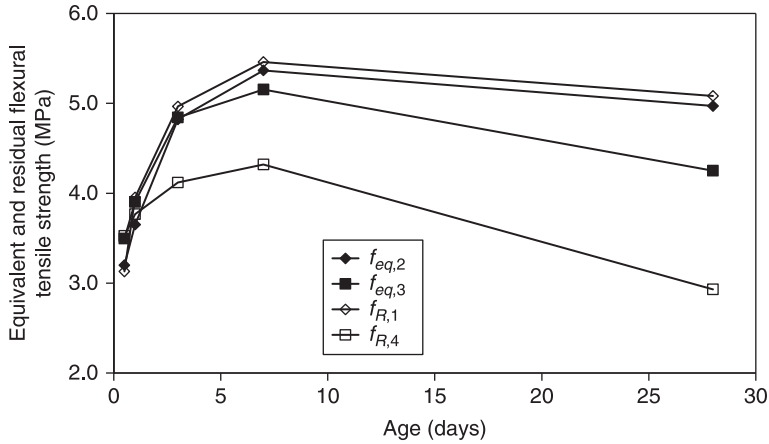

4.27 Influence of the SFRSCC age on the equivalent and residual flexural tensile strength parameters.

of the 12-hours series, all series exhibited a post-crack hardening phase followed by a softening branch. The decrease of residual strength in the softening branch was much more pronounced in the series of specimens of 28 days. The larger amplitude of load decay, just after δ_L, observed in the 28-days series would have adversely affected the fibre–concrete bond properties and the fibre anchorage effectiveness, leading to a decrease in the force necessary to pull out the fibres bridging the specimen's fracture surface. This fact may be the reason of the lower equivalent (f_{eq}) and residual (f_R) flexural tensile strength parameters at 28 days, as compared to 7 days, as shown in Fig. 4.27. This decrease was more pronounced in the $f_{R,4}$ curve, since this parameter is directly dependent on the shape of the force–deflection curve, and is evaluated for the largest measured deflection. As $f_{eq,2}$ and $f_{R,1}$ had similar variation with age, it may be concluded that, for low values of deflection (δ_2 and $\delta_{R,1}$), the energy and the force-based concepts provide identical results in this case.

4.5.5 Shear behaviour

Introduction

The application of stirrups in concrete elements, especially in those of hollow section or composed of thin-walled components, mobilizes significant labour time, resulting in important financial charges. In structural concrete elements of buildings in seismic risk zones, the density of steel stirrups and hoops may be difficult to obtain the desired concrete quality. Due to these types of reasons, the substitution of stirrups *per* steel fibres has been studied for several researchers (Casanova 1995; Casanova *et al*. 2000; Barragan 2002; Gettu *et al*. 2004). The

percentage of this replacement, however, depends on the type of element, support and loading conditions. In the present section, the results of an experimental research are presented in order to assess the steel-fibre reinforcement effectiveness for the shallow structural elements failing in shear. The analytical approach recommended by RILEM TC-162 TDF (Vandewalle *et al*. 2002) for the prediction of the fibre-reinforcement contribution in terms of shear resistance is presented, and its predictive performance is assessed.

Test series, specimens, mix compositions, test setup and monitoring system

The six series of high-strength concrete (HSC) indicated in Table 4.4 were developed, varying the dosage of steel fibres (0, 60 and 75 kg/m^3). Table 4.4 includes the six designed mix compositions. The acronym f_{cmx}_ FCY means a composition with Y kg/m^3 of fibres of a concrete of X MPa of average compressive strength. The steel fibres already presented in Section 4.3 were also used in this experimental program. For each mix composition, three cylinders (150 mm diameter and 300 mm height), three cubes of 150 mm edge, and four prismatic specimens ($600 \times 150 \times 150$ mm^3) were cast and tested to assess the compression and bending behaviour of the developed concrete compositions. To evaluate the influence of the percentage of fibres in shear resistance of HSC elements, three-point bending tests with shallow beams of $800 \times 170 \times 150$ mm^3 dimensions were carried out (distance between supports equal to 720 mm).

The experimental program was composed of 24 shallow beams, four beams for each series: two of plain concrete and two with two steel bars of 20 mm diameter as the tensile longitudinal reinforcement, which is a relatively high reinforcement ratio in order to force the occurrence of shear failure in these two beams. The geometry of the beams and the arrangement of the reinforcement are represented in Fig. 4.28.

Table 4.4 HSC mix compositions designed for the experimental program (per m^3 of concrete)

Series	Cement (kg)	Water (dm^3)	SP (kg)	LF (kg)	Coarse agg. 2 (kg)	Coarse Agg. 1 (kg)	Fine agg. (kg)	Fine sand (kg)	Steel fibres (kg)
f_{cm50}_ NoFibres	300.00	120.46	5.36	114.00	308.98	309.19	503.35	586.99	0.00
f_{cm50}_FC60	300.00	120.46	7.01	228.00	294.27	294.46	457.59	533.63	60.00
f_{cm50}_FC75	300.00	120.46	7.01	228.00	286.14	286.51	448.93	560.56	75.00
f_{cm70}_ NoFibres	400.00	114.00	7.84	200.00	303.10	303.30	471.32	549.63	0.00
f_{cm70}_FC60	400.00	114.00	10.65	342.00	282.50	282.69	439.29	512.28	60.00
f_{cm70}_FC75	400.00	114.00	10.65	342.00	266.11	266.45	417.50	521.32	75.00

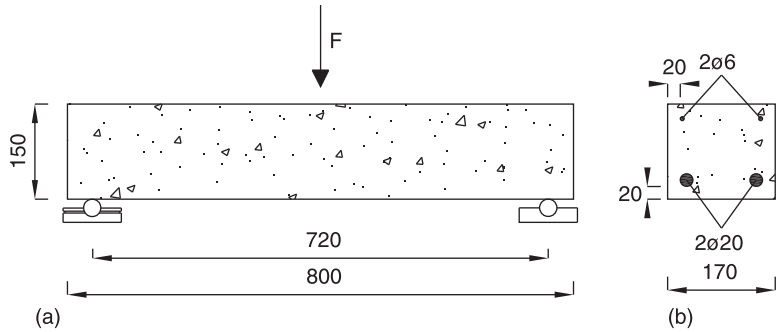

4.28 Ordinary reinforcement: (a) transversal view; (b) longitudinal view (dimensions in mm).

The tests were executed with servo-controlled equipment with a maximum load capacity of 300 kN. The tests were controlled by the displacement transducer of the actuator, at a displacement rate of 3 μm/s.

Results and analysis

At 7 days, the average compressive strength of the f_{cm50}*_Nofibres*, f_{cm50}*_FC60* and f_{cm50}*_FC75* was 41.7 MPa, 46.6 MPa, 48.1 MPa, respectively, while for the f_{cm70}*_Nofibres*, f_{cm70}*_FC60*, and f_{cm70}*_FC75* the compressive strength was 66.4 MPa, 65.7 MPa and 66.1 MPa, respectively. Each result is the average of three tests.

The load *vs* midspan deflection curves obtained from the three-point loading tests carried out with the shallow beams are presented in Fig. 4.29. Table 4.5 includes the force at a deflection corresponding to the serviceability limit state (L/400 with L being the beam span length in mm), F_{SLS}, and to the ultimate limit state (maximum force), F_{ULS}, registered in the tests. From these values it can be concluded that fibre reinforcement provided a contribution for the load-carrying capacity of the shallow beams, at deflection SLS analysis, ranging from 43% to 72%, while for the ULS analysis the fibre-reinforcement effectiveness varied from 80% to 118%.

As Fig. 4.30 shows, all tested RC beams failed in shear. However, the number of flexural cracks formed up to the ocurrence of the shear failure crack increased with steel fibres. Furthermore, it is visible that the inclination of the shear failure crack (angle of the shear crack plan with the beam longitudinal axis) decreased with the increase of the content of fibres, which justifies the resulting benefits of fibre reinforcement, since a larger area of crack bridged by fibres is available, and more favourable inclination of the fibre resisting tensile force is mobilized for the shear resistance. Moreover, due to the crack opening arrestment offered by fibres bridging the shear crack plans, a diffuse crack pattern occurred in the vicinity of the shear failure crack, contributing to the increase of energy dissipation and for the more ductile failure mode observed in HSSFRC beams, in comparison to HSC beams (Fig. 4.30).

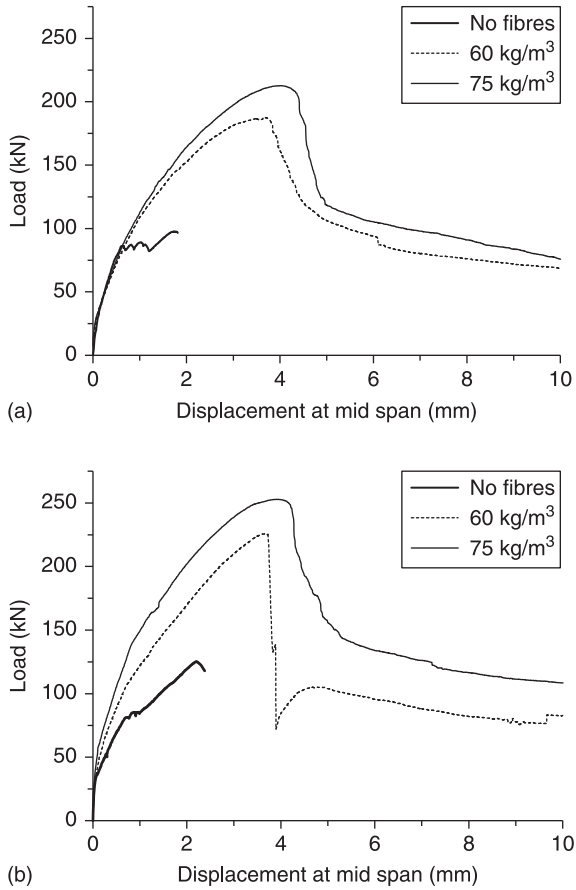

4.29 Load–displacement curves for the (a) f_{cm50} and (b) f_{cm70} series.

Table 4.5 Values (in kN) for the F_{SLS} and F_{ULS}

Series	F_{SLS}			F_{ULS}		
	F^{ref} (FC = 0)	F^{FRC} (FC = 60)	F^{FRC} (FC = 75)	F^{ref} (FC = 0)	F^{FRC} (FC = 60)	F^{FRC} (FC = 75)
f_{cm50}	97.35	146.06	154.83	97.66	187.50	212.73
f_{cm70}	112.10	160.29	192.36	125.23	225.82	252.90

FC: fibre content in kg/m^3

Predictive performance of the RILEM TC 162-TDF model

As a result of the 'Brite-Euram Project 97–4163, BRPR-CT98-0813' (2002), where numerical and experimental research were developed, RILEM TC 162-TDF (Vandewalle *et al*. 2003) proposed a formulation in a close format of CEB-FIP

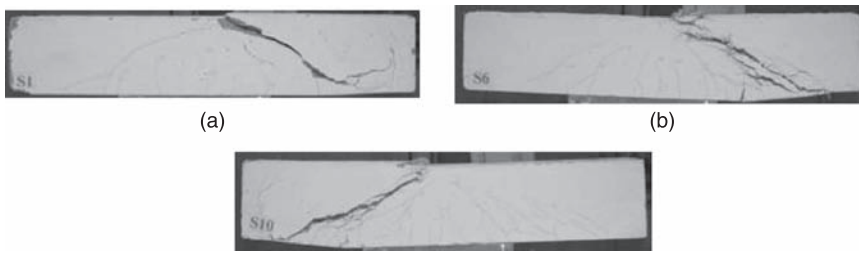

(a) (b) (c)

4.30 Crack pattern in f_{cm50} series: (a) without fibres; (b) with 60 kg/m^3; (c) with 75 kg/m^3 of fibres.

Model Code (1993). According to this formulation, the shear resistance of a concrete element reinforced with steel stirrups, steel fibres and ordinary longitudinal reinforcement is given by:

$$V_{Rd3} = V_{cd} + V_{fd} + V_{wd} \quad [4.23]$$

where V_{cd} and V_{wd} represent the contribution of concrete and steel stirrups, respectively, for the shear resistance, determined according to the CEB-FIP Model Code (1993), and V_{fd} is the contribution of fibre reinforcement:

$$V_{fd} = 0.7\, k_f\, k_l\, \tau_{fd}\, b_w\, d \text{ (N)} \quad [4.24]$$

where k_f and k_l are factors that for the cross-sections of the tested shallow beams assume a unitary value, b_w, and d is the width and the depth of the cross-section, and,

$$\tau_{fd} = 0.12\, f_{eqk,3} \text{ (N/mm}^2\text{)} \quad [4.25a]$$

or

$$\tau_{fd} = 0.12\, f_{Rk,4} \text{ (N/mm}^2\text{)} \quad [4.25b]$$

where $f_{eqk,3}$ and $f_{Rk,4}$ are the characteristic values of the equivalent and residual flexural tensile-strength parameters determined under the recommendations of RILEM TC 162-TDF (Vandewalle *et al.* 2003) (see Section 4.5.4).

Applying this formulation to the experimental program carried out in the present work, the contribution of steel fibres for the concrete shear resistance was evaluated. The obtained values included in Table 4.5 show that the smaller safety factor in series reinforced with fibres was 1.88. It should be mentioned that in the calculations of Table 4.6 average values were used for the equivalent and residual flexural strengthening parameters, since the use of characteristic values led to too-high safety factors due to the relatively high coefficient of variation (COV) that was obtained for these parameters. To help to decrease the COV of these parameters is the use of experimental programs composed of 10 to 12 bending specimens (in the present experimental program the series of notched beam tests were composed of three specimens).

Table 4.6 Contribution of steel fibres to the concrete shear resistance according to the RILEM TC 162-TDF formulation

Series	f_{cm} (kN)	f_{ck} (kN)	V_{cd} (kN)	$\tau_{fd,1}$ [(1)] (MPa)	$\tau_{fd,2}$ [(2)] (MPa)	V_{fd} [(1)] (kN)	V_{fd} [(2)] (kN)	V_{Rd} [(1)] (kN)	V_{Rd} [(2)] (kN)	SF,1 [(3)]	SF,2 [(3)]
f_{cm50}_NoFibres	41.74	33.74	30.36	–	–	–	–	30.36	–	1.61	–
f_{cm50}_FC60	46.58	38.58	31.65	0.97	0.91	18.23	17.15	49.88	48.80	1.88	1.92
f_{cm50}_FC75	48.10	40.10	32.16	0.87	0.82	16.29	15.34	48.45	47.50	2.20	2.24
f_{cm70}_NoFibres	66.39	58.39	36.45	–	–	–	–	36.45	–	1.72	–
f_{cm70}_FC60	65.73	57.73	36.31	1.13	0.82	21.15	15.45	57.46	51.76	1.95	2.17
f_{cm70}_FC75	66.08	58.08	36.38	0.90	0.49	16.95	9.19	53.33	45.57	2.36	2.72

[(1)] Considering $\tau_{fd} = 0.12 f_{eqk,3}$ (N/mm^2); [(2)] Considering $\tau_{fd} = 0.12\ f_{Rk,4}$ (N/mm^2); [(3)] Ratio between V_{exp} and V_{Rd} [(1)] (or V_{Rd} [(2)]).

4.6 Structural behaviour

4.6.1 Introduction

This section reviews the main achievements obtained in the research programs dedicated to the assessment of the potentialities of the developed SFRSCC for structural applications (for RC slab strips failed in bending, consult Barros *et al.* 2008).

4.6.2 Representative modules of the panel

In the scope of an applied research project involving a precasting company, SFRSCC panel prototypes were built and tested under punching and bending test setup conditions, allowing the evaluation of the SFRSCC behaviour under the two most demanding load conditions for the facade panels. The panel prototypes were fabricated by the SFRSCC composition number 1, indicated in Table 4.1. The punching tests were executed in panel prototypes of 600×600 mm^2 and 110 mm thick, and the flexural tests were carried out in panel prototypes of 1000×1000 mm^2 and the same thickness, both at an age of 7 days.

Modules failing in punching

As represented in Fig. 4.31(a), the lightweight central region of the panel prototypes subjected to punching load is composed of a concrete layer 30 mm thick. The procedure followed to assess the load–deflection behaviour of the lightweight SFRSCC panel prototype consisted of applying a load at the centre of the panel, by means of a square steel plate of 100 mm edge and 10 mm thick. The loading sequence was executed using the vertical displacement as a control variable, measured by the displacement transducer attached to the actuator. A vertical displacement rate of 25 μm/s was prescribed, and the test procedure was

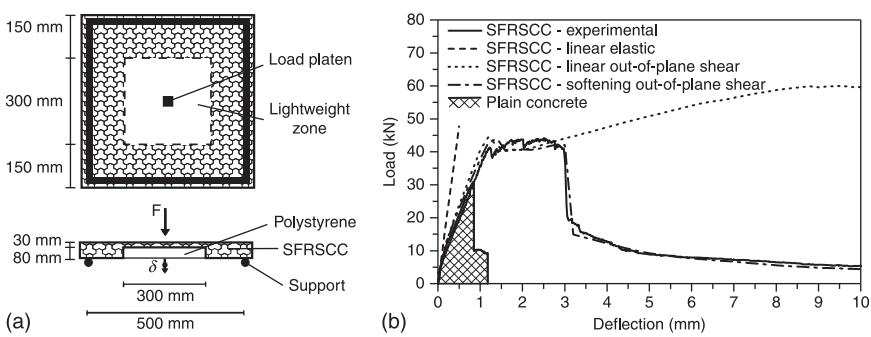

4.31 Punching test on panel prototype: (a) test setup, and (b) load-deflection experimental and numerical results (Pereira *et al.* 2008).

stopped when punching failure was observed. The results obtained in terms of the load–deflection curve are represented in Fig. 4.31(b). After a short linear elastic phase, the panel entered into an elastic-cracked phase and supported an increasing load up to 40 kN. This load level was then maintained practically constant from a deflection of 1.4 mm up to a deflection of about 3 mm, representing 1% of the lightweight zone span. Then, the load suddenly fell from the 40 kN to approximately 20 kN, suggesting the occurrence of failure by punching. Fibres bridging the surfaces of the punching failure crack offered some resistance to the opening of this crack, delaying the loss of contribution of the aggregate interlock for the punching resistance. This justifies the relatively high level of residual strength that decreases very slowly with the deflection increase. The estimation of the steel fibres contribution for punching strength increase is further discussed in the section dedicated to the numerical simulation of these tests.

Modules failing in bending

The panel prototypes destined for the evaluation of flexural behaviour were conceived using the same lightweight concept as in punching. As represented in Fig. 4.32(a), lightweight zones also had a concrete upper layer 30 mm thick, and the thicker zones of the panel constituted a grid system of two-per-two orthogonal ribs. The panel also has a contour rib of 100 mm width. The test procedure consisted of applying a constant displacement rate (25 μm/s) at the centre of a main, loading steel beam, connected to two other transversal secondary beams by means of two rollers. Load was transmitted to the four loading points at rib intersections by means of four square steel plates ($100 \times 100 \times 20$ mm^3) and four steel spheres of 20 mm diameter, in contact with the ends of the secondary loading beams (Pereira 2006). This entire loading mechanism was idealized with the intention of assuring that, independently of the observed deflection beneath each of the four loading points, the applied load was the same in each loaded area. To obtain the vertical deflection beneath each of these four loaded areas, four displacement transducers were there installed. The supports system consisted of eight elements placed at the ends of the grid ribs, each one consisted of a steel plate ($100 \times 100 \times 10$ mm^3) in contact with the bottom surface of the panel, and a steel sphere of 20 mm diameter, placed between the steel plate and the ground, guaranteeing that only the vertical displacement was constrained (lifting was not prevented). The results obtained in terms of load–deflection curve are represented in Fig. 4.32(b), showing that the load-retaining capacity of the structure assumes relevance similar to the results observed at punching tests. To simplify the analysis, only the average results were considered. A detailed analysis can be found elsewhere (Barros *et al*. 2005a). After reaching a peak load of approximately 55 kN, the panel demonstrates the ability to almost retain the maximum load-carrying capacity up to an average deflection of around 5 mm. Above this deflection, the load carrying capacity decreases very slowly with the increase of the average deflection. The test sequence was stopped

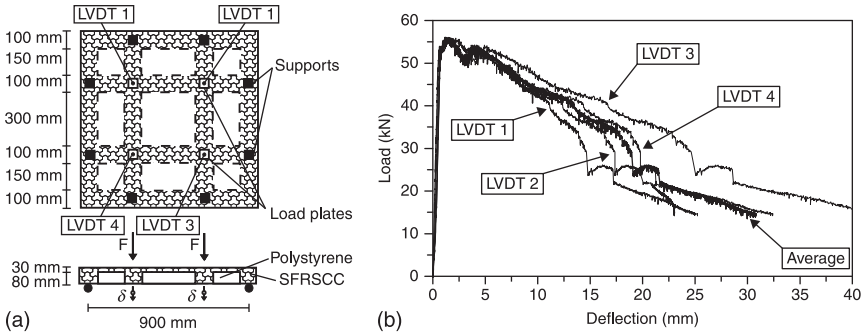

4.32 Flexural tests on panel prototypes: (a) test setup; (b) typical load-deflection experimental results.

for a load of 15 kN (27% of the peak load) due to an excess of deformation and incompatibility with the supports and the loading apparatus.

4.6.3 Test with full-size panel

With the aim of verifying if the procedures adopted in the laboratory, during the development of a SFRSCC, can be directly applicable in an industrial environment, the full-scale SFRSCC panel, represented in Fig. 4.33, was fabricated and tested in a precasting company. The test also had the purpose of evaluating the behaviour of a real panel when submitted to its dead weight and to an increased live load, up to its rupture.

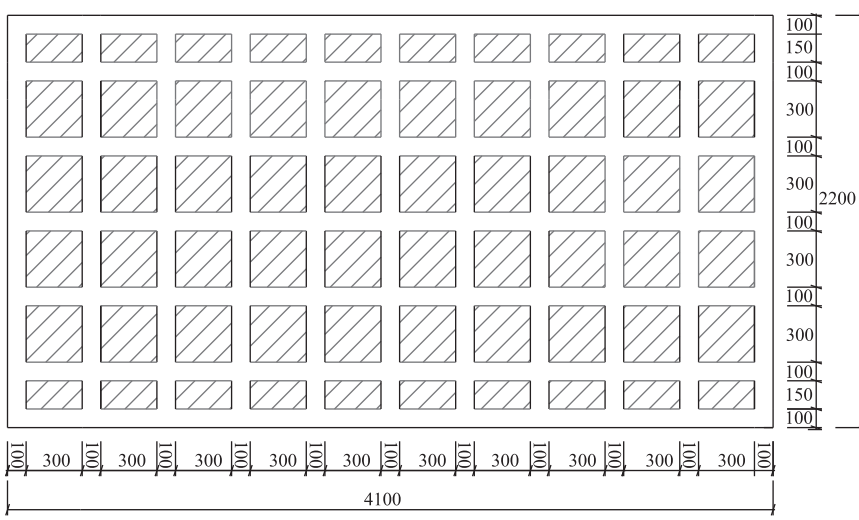

4.33 Panel geometry (dimensions in mm): thickness = 110 mm, total vol. = 0.882 m^3, vol. to cast = 0.522 m^3, approximate weight = 1305 kg.

Two concrete mixtures of 400 dm^3 were made to fabricate the panel, and both were stable without any indication of segregation. The spread was 600 mm and 630 mm in mixtures 1 and 2, respectively, while the H2/H1 parameter of the L-Box test was 0.80 (the test was carried out for the second mixture only). The demolding of the panel was done on the day after it has been cast, when the SFRSCC had an age of 24 hours. The panel was demolded in an almost vertical position. After that, the panel was placed on a support until the test, which occurred at 7 days of panel age. Fig. 4.34 represents the panel support conditions and the

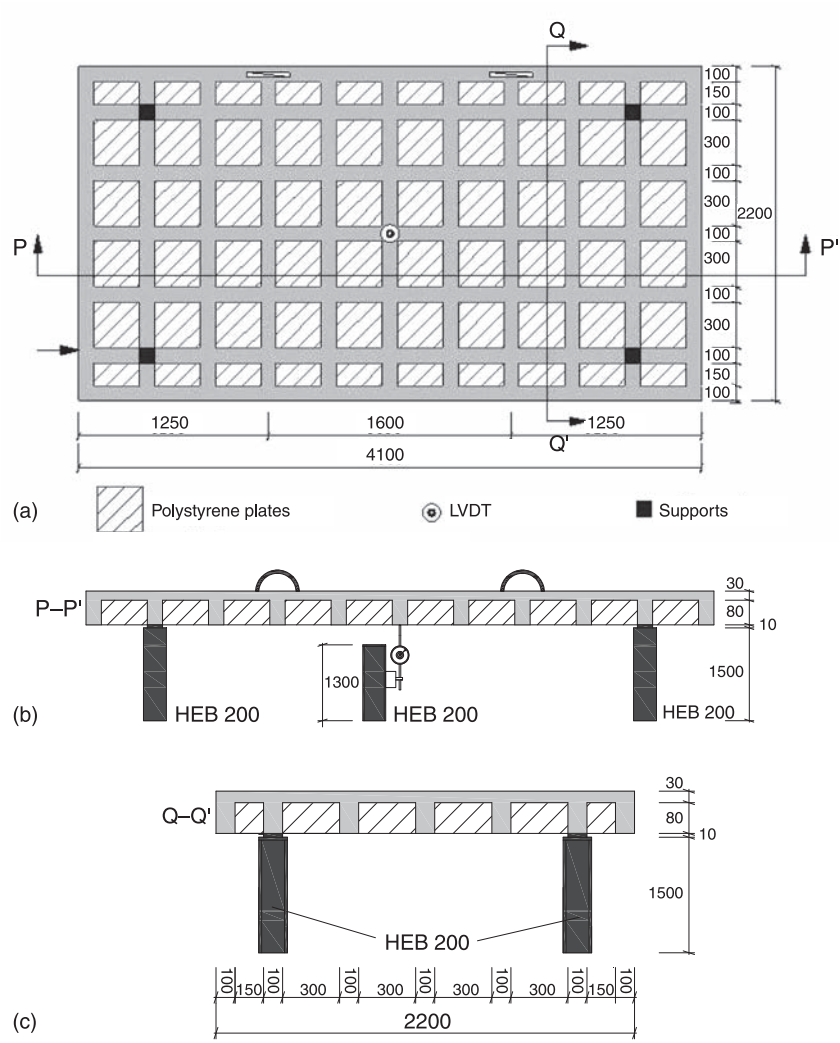

4.34 Setup of the loading test: (a) plant view; (b) cross section P–P′; (c) cross section Q–Q′ (dimensions in mm).

4.35 Final view of the panel, loaded with 33 concrete plates.

location where the deflection was measured (centre of the panel). The panel was supported on four points. To simulate a uniform, distributed live load, concrete plates of 500×500 mm^2, each one of 25 kg, were uniformly distributed in the area interior to the panel supports (Fig. 4.35). The panel supported 33 concrete plates, corresponding to a uniform distributed load of $8.25/(3.1 \times 1.5) = 1.77$ kN/m^2, plus its dead weight (1.47 kN/m^2). When placing the 33rd concrete plate, an abrupt increase of deflection occurred, and the test was interrupted due to safety reasons (Fig. 4.35). When the 18th concrete plate was placed, a deflection of 24 mm was measured. The test was interrupted when the deflection was about 44 mm and the maximum crack opening of the critical crack was around 3 mm. The live load of 1.77 kN/m^2 is higher than the characteristic value of the wind-dynamic pressure recommended by Eurocode 1–Wind actions (EN 1991-1-4 2005) for the buildings' design.

4.7 FEM models for the analysis of laminar SFRC structures

4.7.1 Introduction

The structural behaviour of laminar elements, the highly material nonlinear behaviour of hardened SFRC, and the determination of the fracture parameters that characterizes the SFRC post-peak behaviour constitute the three main challenges to be resolved. In the present chapter, the simulation of the behaviour of laminar structures is treated by employing the theory of plane shells, based on

the 'Reissner-Mindlin' formulation (Barros 1995). The SFRC post-cracking behaviour was simulated by a multi-fixed smeared-crack model. Details of this smeared-crack constitutive model can be found elsewhere (Gouveia *et al*. 2007). Since previous works have given indications that inverse analysis is an appropriate numerical strategy to determine the material fracture parameters (Barros *et al*. 2005b), it was applied to the results obtained in the flexural tests with specimens of 7 days, in order to determine the fracture parameters of the SFRSCC at this age (see Section 4.5.4). These numerical simulations were carried out with the FEMIX 4.0 computer program, which is a software whose architecture was conceived to allow for an easy implementation of new types of finite elements and new constitutive models (Sena *et al*. 2007).

4.7.2 Inverse analysis

The fracture mode I of the post-cracking behaviour of SFRC is described by the tri-linear, stress–strain softening diagram represented in Fig. 4.36(b). The shape of this function is defined by a group of fracture parameters ($\sigma_{n,i}^{cr}$, $\varepsilon_{n,i}^{cr}$, G_f^I, f_{ct}

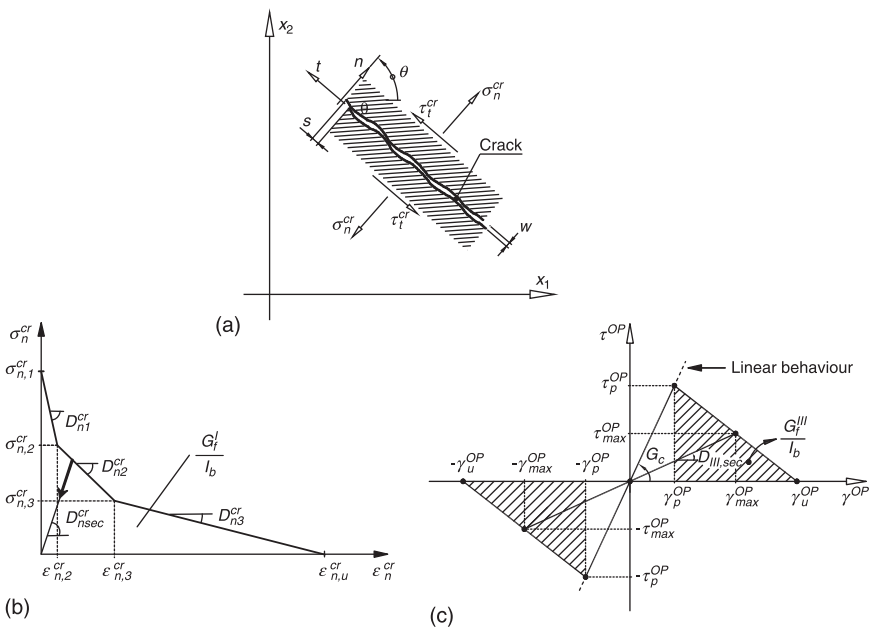

4.36 (a) Crack stress components, relative displacements and local coordinate system of the crack; (b) tri-linear stress–strain diagram to simulate the fracture mode I crack propagation of SFRSCC; (c) generic out-of-plane (OP) shear stress–strain diagram to simulate fracture mode III.

and l_b) and the accuracy of the FEM modelling largely depends on the values of these parameters, where G_f^i is the mode I fracture energy (RILEM 50-FMC 1985) and l_b is the crack bandwidth (Rots 1988). In this context, the experimental results of punching and flexural tests obtained may be predicted by a FEM model, if the correct values of the material fracture parameters are found and introduced into the constitutive model. The question is, though, what is the best strategy to obtain the accurate values for these parameters? In this work, it is suggested that the fracture parameters may be assessed by means of an inverse analysis of the flexural test results, in agreement with previous studies (Barros *et al*. 2005b). The procedure consists of the evaluation of the, $\sigma_{n,i}^{cr}$, $\varepsilon_{n,i}^{cr}$ and G_f^I parameters, the ones that define the shape of the tri-linear $\sigma_n^{cr}-\varepsilon_n^{cr}$ constitutive law, leading to the minimization of the $|A^{Num} - A^{Exp}|/A^{Exp}$ ratio, where A^{Num} and A^{Exp} are the areas underneath the force-deflection curve predicted numerically and recorded in the experimental test, respectively. The experimental curve corresponds to the average results observed in prismatic SFRSCC notched specimens, tested according to the RILEM TC 162-TDF recommendations, at the age of 7 days (see Section 4.5.4). The numerical curve consists of the results obtained by means of a FEM analysis (see Fig. 4.37(a)), where the specimen, the loading and the support conditions were simulated in agreement with the experimental flexural test setup. In this context, the specimen was discretized by a mesh of 8-nodes serendipity plane-stress finite elements. The Gauss–Legendre quadrature integration scheme with 2×2 integration points (IP) was used in all elements, with the exception of the elements at the specimen symmetry axis, where only 1×2 IP were used. This has the purpose of producing a trend for the development of a crack surface through the specimen symmetry plane, over the aligned integration points, in agreement with what was observed in the experimental tests. Linear elastic material behaviour was assigned to all elements, with the exception of the elements above the notch, where elastic-cracked behaviour in tension was assumed. The crack bandwidth, l_b, was assumed to be 5 mm, equal to the width of the notch and of the elements above the notch. In Fig. 4.37(b), the results obtained experimentally for flexural tests are compared with the ones resulting from the numerical model (see also Fig. 4.26). A very good agreement between the experimental and the numerical curve exists. The values assumed for the fracture parameters, $\sigma_{n,i}^{cr}$, $\varepsilon_{n,i}^{cr}$ and G_f^I, that resulted in the obtained numerical curve represented in Fig. 4.37(b), are presented in Table 4.7.

Table 4.7 Values of the fracture parameters defining the stress–strain softening laws.

Material	$\sigma_{n,1}^{cr}$ (MPa)	$\sigma_{n,2}^{cr}$ (MPa)	$\sigma_{n,3}^{cr}$ (MPa)	$\varepsilon_{n,2}^{cr}/\varepsilon_{n,ult}^{cr}$	$\varepsilon_{n,3}^{cr}/\varepsilon_{n,ult}^{cr}$	G_f^I (N/mm)
SFRSCC	3.50	1.750	2.065	0.009	0.150	4.3
PC	3.50	0.525	–	0.072	–	0.08732

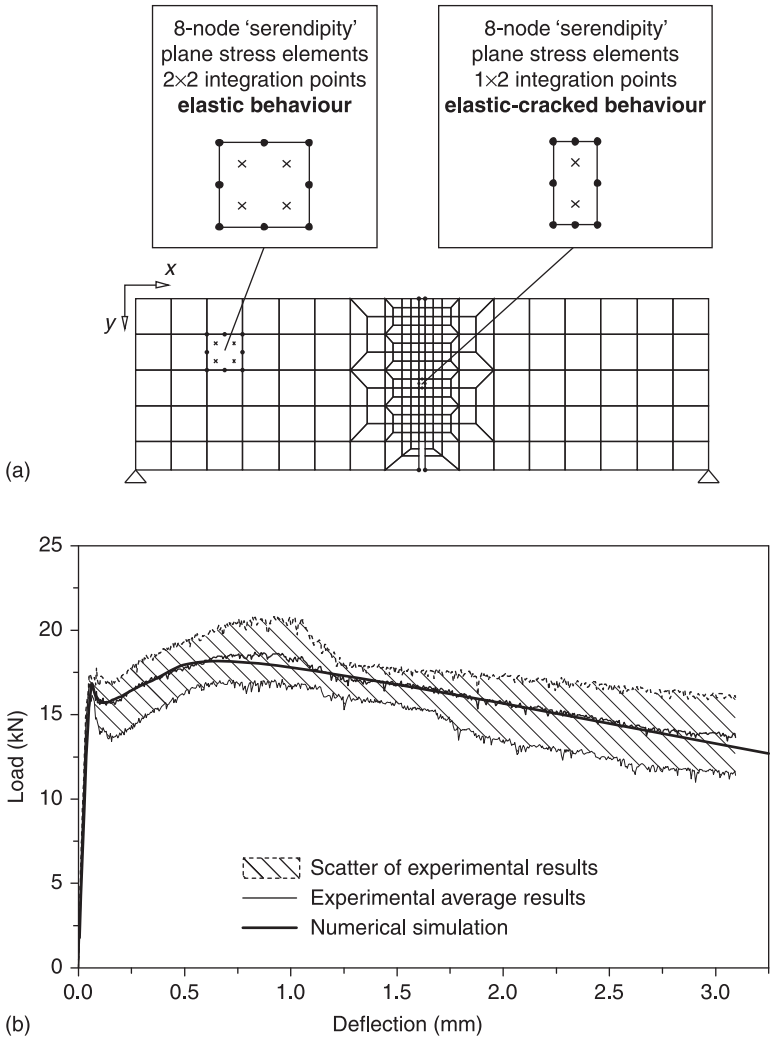

4.37 Three-pointed notched bending tests at 7 days: (a) FEM mesh used in the numerical simulation; (b) obtained results.

4.7.3 Simulation of the tests with panel prototypes failing in punching

The experimental results recorded from punching tests with panel prototypes are compared with the ones obtained from the numerical simulation. For this purpose, a FEM mesh was prepared, composed of 12-per-12 8-node serendipity plane shell elements, each one divided in 11 layers of 10 mm thick. Recognizing

that the panel had lightweight zones, materialized by the suppression of 80 mm of concrete at a $300 \times 300\,mm^2$ square central area (see Fig. 4.31(a)), the 8 lower layers of the finite elements at the lightweight central square zone were constituted by a fictitious material with numerically null stiffness. The remaining three upper layers, and all layers of the elements located outside the lightweight zone, were constituted by the SFRSCC, whose values for the fracture parameters are those indicated in Table 4.7, obtained from inverse analysis, as described in the previous section.

The out-of plane component of the elastic-cracked constitutive matrix was defined on the basis of a trial-and-error procedure (Gouveia *et al*. 2007). The out-of-plane shear fracture energy value that best fitted the punching failure experimental results ($G_f^{III} = 3.0$ N/mm) was determined in this fashion, since no other laboratory test was carried out to allow its assessment by inverse analysis. The results obtained from the numerical simulation are compared with the experimental ones in Fig. 4.31(b). A quite good simulation was obtained up to a deflection of 2.5 mm. For greater deflections, it is clearly an overestimation of the load-carrying capacity of the panel prototype, if a linear elastic behaviour is assumed for the out-of-plane shear components. At an approximate deflection of 3 mm, the load at the experimental curve suddenly fell, indicating the failure of the panel by punching, as visually found during experimental testing. This load decay, not possible to be simulated by assuming linear elastic behaviour for the out-of-plane shear components, however, was well captured by the numerical simulation when the bilinear function represented in Fig. 4.36(c) was used to model the softening behaviour of out-of-plane shear components, with $G_f^{III} = 3.0$ N/mm, and assuming a crack bandwidth l_b equal to the square root of the area of the corresponding integration point. The abrupt load decay from approximately 42 kN to 25 kN, observed experimentally, was almost perfectly followed by the numerical model, as well as the observed subsequent stage of smooth load decay.

The strategy here proposed to estimate the contribution of steel fibres for punching behaviour is based on the establishment of a softening stress–strain diagram for plain concrete (PC) in tension. The remaining characteristics of the numerical simulation were the same ones used in the previous SFRSCC material nonlinear analysis. The softening stress–strain law for PC in tension was established in accordance with (CEB-FIP 1993) recommendations. Assuming that the tensile strength is the same for SFRSCC and for the equivalent PC, the fracture parameters defining a bilinear stress–strain diagram ($D_{n2}^{cr} = D_{n3}^{cr}$ in Fig. 4.36(b)) were determined, and are indicated in Table 4.7. Figure 4.31(b) represents the predicted deformational behaviour of a PC panel prototype, from which it can be observed that PC has a punching strength that is around 70% of the punching strength of SFRSCC, and the energy absorbed up to the failure of plain concrete panel represents only around 15% of the energy absorbed by SFRSCC panel.

4.8 Possibilities of steel-fibre reinforced concrete (SFRC) for underground structures

4.8.1 Introduction

The crack opening arrestment provided by the reinforcement mechanisms of fibres bridging the crack surfaces of cement-based materials leads to significant increase in terms of load-carrying capacity and the energy dissipation capability of concrete structures, mainly those of high redundant support conditions, such is the case of structures surrounded by soil. In fact, as the degree of static indeterminacy is higher, the replacement of conventional steel bars by discrete steel fibres is more advantageous, since stress redistribution provided by fibre reinforcement allows an ultimate load much higher than the cracking load (see also section 4.2). In several underground reinforced-concrete (RC) structures, crack width limit is the governing design condition, since a crack width higher than a certain value can compromise the durability and the functionality of theses structures, with economical and technically harmful consequences.

Box culvert is one of this type of underground concrete structures, formed by a bottom and a top U-shaped RC laminar element connected by a concrete–concrete hinge. Box culverts are used for several purposes, such as underground passages for people, vehicles or animals (Fig. 4.38). These RC structures are subject to the soil dead weight, which in certain cases can attain a cover layer of 20 m thick. Other constructions can also transfer loads to the box culverts. On the soil surface, a live load (LL) can also actuate due to the action of vehicles or other non-permanent loads.

Since the construction of this infrastructure is made by phases, the numerical simulation of this construction process is mandatory for a realistic prediction of the behaviour of the intervening materials and structures. Figure 4.39 represents the current construction phase process used in this type of infrastructure. In general, the construction process is composed of 6 phases. In this figure $[P_i–P_j]$ means a material or structural component pertaining to phases P_i up to P_j.

4.38 Examples of application of a box culvert.

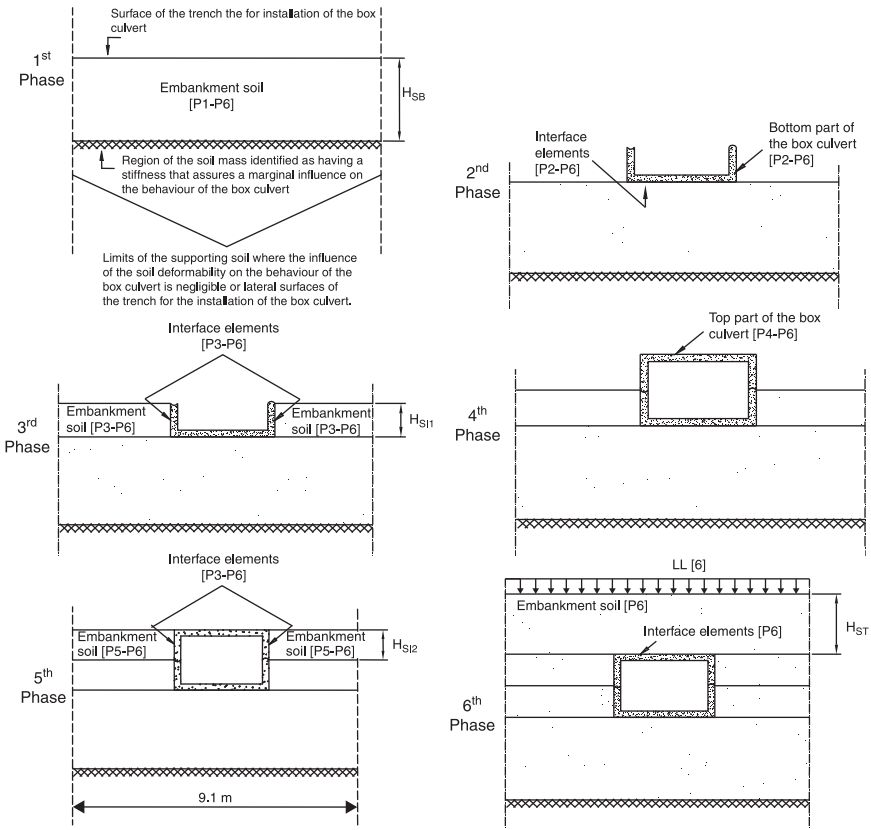

4.39 Phased construction process.

Figure 4.40(a) represents the reinforcement detailing for the box culvert, whose geometry of the top part is shown in Fig. 4.40(b). According to the information provided by a precast company, this reinforcement (118.5 kg/m^3) was designed for an embankment soil-layer thickness (H_{ST}) of 4 m (Fig. 4.39). In the present work, the use of a self-compacting concrete reinforced with 45 kg/m^3 of hooked-end steel fibres (SFRSCC), developed within the ambit of an applied research project (Barros *et al*. 2005a), was explored with the purpose of verifying the possibility of replacing the reinforcement applied in the box culvert of Fig. 4.40. In this example H_{SB} = 3.64 m, H_{ST} = 4.0 m and the width of the trench is 9.1 m.

Furthermore, the live load (LL in Fig. 4.39) that can be applied up to introduce a maximum crack width of 0.3 mm in the box culvert will be evaluated, since below this crack width the durability performance of SFRSCC is not affected by the action of the aggressiveness of environmental agents (Schupack 1986).

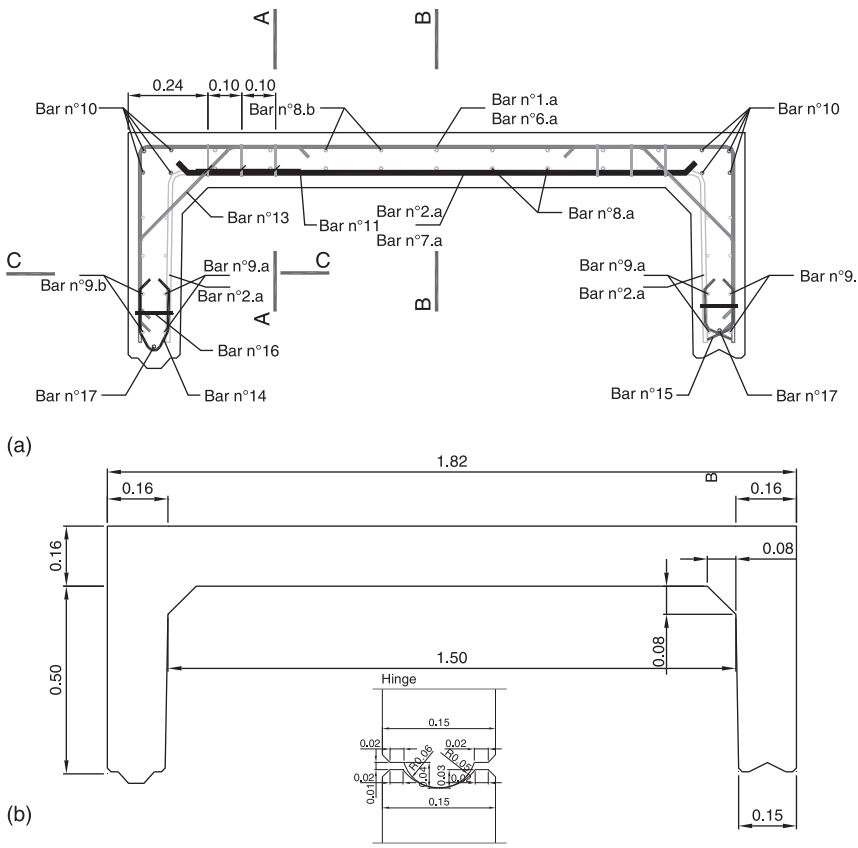

4.40 (a) Geometry; (b) reinforcement (dimensions in m).

4.8.2 Numerical model

For the analysis of FRC infrastructures taking into account the soil-structure interaction, the following new facilities were implemented into the FEMIX FEM-based computer program (Sena *et al*. 2007): (i) the simulation of phasing construction; (ii) constitutive models for soil, one based on the elasto-plasticity Mohr-Coulomb criterion and the other on the Ottosen failure criterion; the smeared crack model to simulate the crack initiation and propagation in the box culvert, already existing for plane-stress state problems, was adapted for modelling the behaviour of structures considered in plane-strain state conditions, such is the case of the present study; (iii) an opening-sliding constitutive model for interface finite elements to simulate the soil–concrete interaction. The post-cracking behaviour of the concrete box culvert was simulated by a multi-directional fixed smeared-crack model, while the soil was modelled by a Mohr-Coulomb criterion.

The details of these constitutive models can be found elsewhere (Barros *et al*. 2009; Pereira and Barros 2009).

Based on previous research on the development of SFRSCC for laminar structures (Barros *et al*. 2005a), the values for the properties indicated in Table 4.8 were taken for the simulation of the box culvert, assuming this structure will be precast with this material, in order to verify the possibility of replacing totally or partially the conventional reinforcement used in the type of box culvert. The values of the fracture parameters were obtained from inverse analysis (Pereira *et al*. 2008). The other values for the concrete constitutive model can be found in (Barros *et al*. 2009).

For the numerical simulations, the values of the parameters included in Table 4.9 were adopted, E_s, v_s, γ_s, c and, ϕ, being the Young's modulus, the Poisson coefficient, the specific weight, the cohesion and the frictional angle of the soil.

To simulate the soil–box culvert interaction, a 6-node 2D line interface element was used, whose formulation is described in Sena-Cruz (2004). For modelling the soil–concrete sliding behaviour, the law schematically represented in Fig. 4.41 was implemented, where:

$$\tau(s) = \begin{cases} \dfrac{\tau_o}{s_o} & \text{if} \quad 0 \le |s| \le s_o \\ \tau_m \left(\dfrac{s}{s_m} \right)^{\alpha_1} & \text{if} \quad s_o < |s| \le s_m \\ -\tau_m \left(\dfrac{s}{s_m} \right)^{-\alpha_2} & \text{if} \quad |s| > s_m \end{cases} \qquad [4.26]$$

Table 4.8 Values of the properties for the SFRSCC crack constitutive model (Fig. 4.36 (b))

γ_c (kN/m³)	E_c (GPa)	υ_c (–)	f_c (MPa)	$f_{ct} = \sigma^{cr}_{n,l}$ (MPa)	G_f (N/mm)	$\varepsilon^{cr}_{n,2} / \varepsilon^{cr}_{n,u}$	$\sigma^{cr}_{n,2} / \sigma^{cr}_{n,1}$	$\varepsilon^{cr}_{n,3} / \varepsilon^{cr}_{n,u}$	$\sigma^{cr}_{n,3} / \sigma^{cr}_{n,1}$
24.0	39.0	0.2	45.0	2.90	4.0	0.05	0.60	0.20	0.20

Table 4.9 Values of the properties for the Mohr-Coulomb soil constitutive model

E_s (MPa)	v_s (–)	γ_s (kN/m³)	c (kPa)	ϕ (°)
20.0	0.3	18.0	5.0	30.0

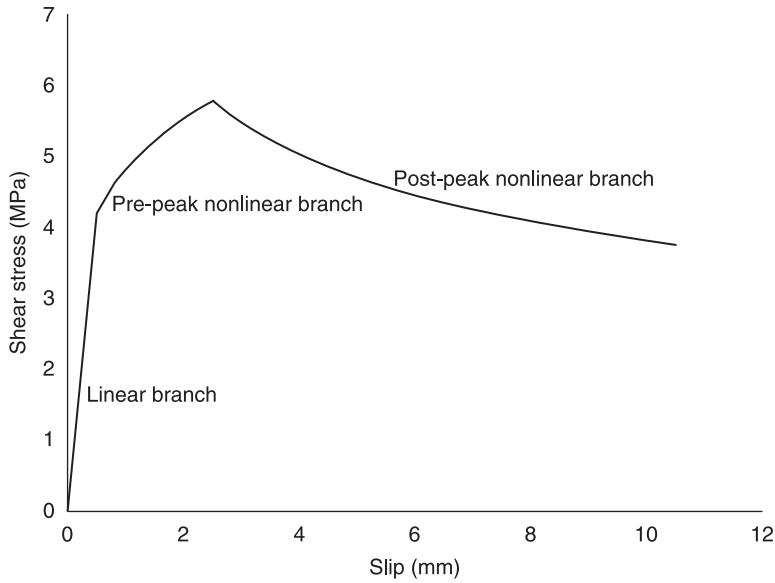

4.41 Diagram to simulate the soil–concrete sliding behaviour.

Table 4.10 Values of the properties to simulate the soil–concrete sliding behaviour

s_o (mm)	s_m (mm)	α_1 (–)	α_2 (–)	$\bar{c}$ (kPa)	δ (°)	D_n (kN/m)
0.5	2.5	0.2	0.3	5.0	30.0	1.0e + 05

$$D_t = \begin{cases} \dfrac{\tau_o}{s_o} & \text{if} \quad 0 \le |s| \le s_o \\ \alpha_1 \dfrac{\tau_m}{s_m}\left(\dfrac{s}{s_m}\right)^{\alpha_1 - 1} & \text{if} \quad s_o < |s| \le s_m \\ -\alpha_2 \dfrac{\tau_m}{s_m}\left(\dfrac{s}{s_m}\right)^{-\alpha_2 - 1} & \text{if} \quad |s| > s_m \end{cases} \qquad [4.27]$$

$$\tau_m = \bar{c} - \sigma_n \tan \delta \qquad [4.28]$$

with $\bar{c}$ and δ being the cohesion and the frictional angle of the soil–concrete interface, and σ_n is negative when in compression.

For the present study, the values indicated in Table 4.10 were considered.

4.8.3 Construction phases and finite element meshes

The simulation of the construction phases was implemented into FEMIX, being possible to have in distinct phases finite elements of different types and constitutive models, as well as distinct support conditions and load cases. For the present study the phases and the corresponding finite element meshes are represented in Fig. 4.42. The soil and the box culvert were discretized by 8-nodes finite elements, with a 2×2 Gauss–Legendre integration scheme, while the soil–concrete interface was simulated by 6-nodes interface elements with a 2 Gauss integration rule. In the analysis, a force convergence criterion with a tolerance of 0.001 was used with a Newton-Raphson technique based on the evaluation of the stiffness matrix in each iteration of the incremental-iterative loading process.

4.8.4 Load cases

In each phase the self-weight of the intervening materials (not affected by any factor) is the load case. In the last phase, after having applied the self-weight of the soil mobilized in this phase, an edge load applied on the surface of the embankment

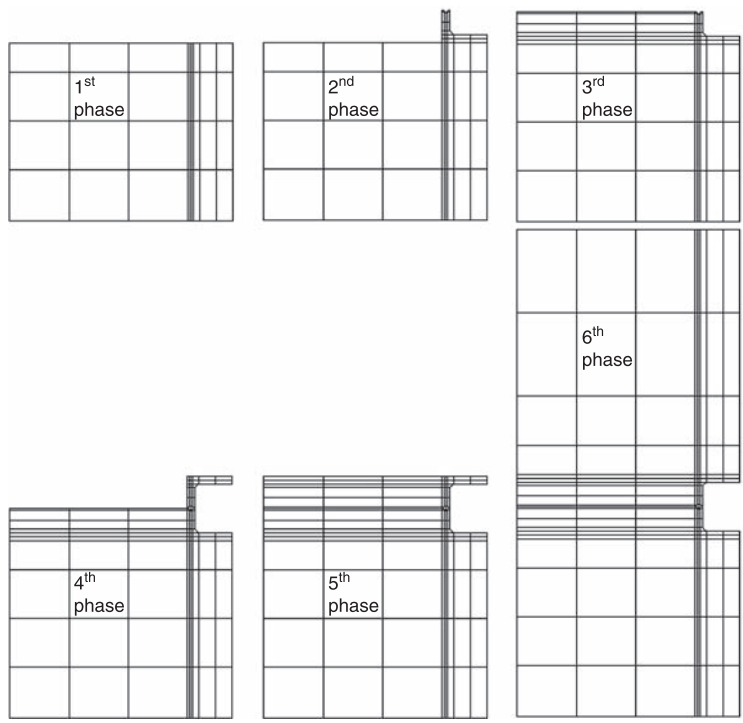

4.42 Finite element meshes of the sixth construction phase of the present study.

was increased monotonically in order to simulate a live load up to the attainment of a maximum crack width on the box culvert of about 0.3 mm (Fig. 4.39).

4.8.5 Results and analysis

Only the results corresponding to the occurrence of a maximum crack width of 0.27 mm are presented. This crack width was evaluated multiplying the maximum normal crack strain by the corresponding crack bandwidth. This crack width occurred for a live load (LL, see Fig. 4.39) of 30 kPa. Plate I (see colour section between pages 142 and 143) represents the displacement fields, while Fig. 4.43 shows the undeformed and the deformed meshes (for an amplifier factor of 11 for the displacements).

The crack pattern is illustrated in Fig. 4.44, showing that only flexural cracks formed on the top and bottom slabs of the two components composing the box culvert. As Plate II reveals, in the concrete in contact with the soil, at the symmetry axis of the problem, the σ_y compression stresses attained a maximum value of about 14 MPa, which is lower than the design value of the compressive strength of the SFRSCC considered for the box culvert. In terms of the σ_z stress field, the maximum tensile stresses attained a value of about 1 MPa in the exterior top part

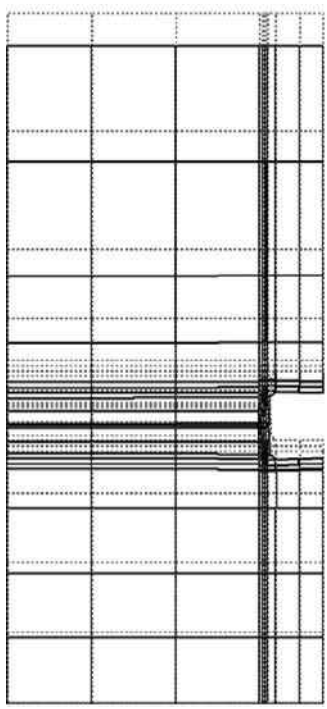

4.43 Deformed mesh.

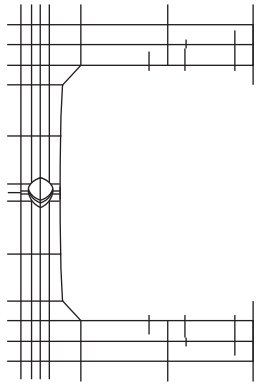

4.44 Crack pattern.

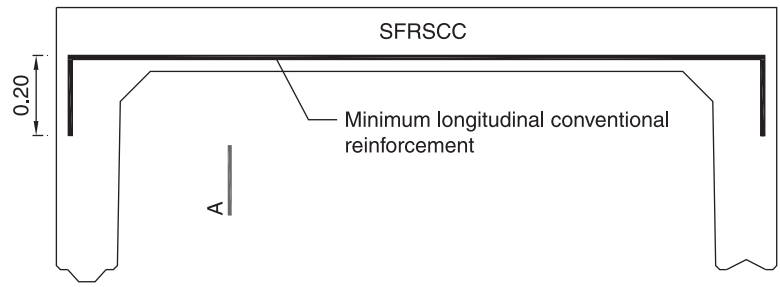

4.45 Proposed reinforcement.

of the arms of the two components of the box culvert, near the connection to the slab. The maximum compressive stresses in z direction occurred in the hinge connection, but is limited to 4.6 MPa. It is also notable that no cracks formed in the hinge region, revealing that the connection was well designed.

The shear stress field in the box culvert is represented in Plate III. The maximum τ_{yz} at the integration points in the shear critical zones is 650 kPa. According to the formulation proposed by the RILEM TC 162-TDF committee (Section 4.5.5), if only fibres are used for the reinforcement of the box culvert, the $f_{eqk,3}$ needs to be higher than 7.7 MPa ($V_{fd}/(b_w\ d) = 0.7\ \tau_{fd} = 0.7 \times 0.12\ f_{eqk,3} \geq 650$ kPa, in the case of assuming the maximum shear stress as the average one in the shear critical zone. This value is higher than the values registered experimentally for the developed cost-competitive SFRSCC for this type of application. Therefore, it is recommended to apply the minimum percentage of longitudinal conventional reinforcement, $\rho_{sl,min}$, as represented in Fig. 4.45. According to EC2 of 2002, $A_{s,min} = 0.0003$ m^2/m, $\rho_{sl,min} = 0.23\%$, which corresponds to 6 ϕ 8/m, that is 5.1 kg/m^3 of steel. For this percentage $\tau_{cd} = V_{cd}/(b_w\ d) = 503$ kPa, which requires a $f_{eqk,3}$ of about 1.75 MPa. The $f_{eqk,3}$ of the developed SFRSCC exceeds this value.

4.9 Acknowledgements

The content of this chapter is derived mainly from the research carried out in the ambit of PABERPRO, PONTALUMIS (QREN, n° 3456) and LEGOUSE (QREN, n° 5387) projects. The author wishes to acknowledge the materials generously supplied by: SECIL (cement), BASF and SIKA (superplasticizers), Bekaert (steel fibres) and Comital (limestone filler), as well as the collaboration of CASAIS company in the production of molds and steel-reinforcement arrangements for specimens. Special acknowledgement is given to the researchers who collaborated in the projects, namely: José Sena Cruz, Vitor Cunha, Eduardo Pereira, Simão Santos, Lúcio Lourenço, Delfina Gonçalves, and Ventura Gouveia. The author also wishes to acknowledge the grants SFRH/BSAB/818/2008 and SFRH/BSAB/913/2009 provided by FCT.

4.10 References

Banthia, N. and Trottier, J. (1994) 'Concrete reinforced with deformed steel fibres, Part I: Bond slip mechanisms', *ACI Materials Journal*, 91(5): 435–446.

Barragán, B.E. (2002) 'Failure and toughness of steel fiber reinforced concrete under tension and shear', PhD Thesis, UPC, Barcelona, March.

Barros, J.A.O., di Prisco, M. and di Prisco, C. (2009) 'Modelling FRC infrastructures taking into account the soil-structure interaction', Conference in Numerical Methods in Engineering 2009, Barcelona, 29 June–2 July.

Barros, J.A.O., Santos, S.P.F. and Lourenço, L.A.P. (2008) 'Flexural behaviour of steel fibre reinforced self-compacting concrete laminar structures', HAC2008, 1st Spanish Congress on Self-Compacting Concrete, Valencia, Spain, 18–19 February.

Barros, J.A.O., Cunha, V.M.C.F., Ribeiro, A.F. and Antunes, J.A.B. (2005b) 'Post-Cracking Behaviour of Steel Fibre Reinforced Concrete', *RILEM Materials and Structures Journal*, 38(275): 47–56.

Barros, J.A.O., Pereira, E.B., Cunha, V.M.C.F., Ribeiro, A.F., Santos S.P.F., Queirós, P.A.A.A.V., (2005a) 'PABERFIA – Lightweight sandwich panels in steel fiber reinforced self compacting concrete.' *Technical Report 05-DEC/E-29*, Dep. Civil Eng., School Eng. University of Minho, 63 pp.

Barros, J.A.O. and Figueiras, J.A., 'Nonlinear analysis of steel fibre reinforced concrete slabs on grade', Computers & Structures Journal, 79(1), 97–106, January 2001.

Barros, J.A.O. and Figueiras, J.A. (1998) 'Experimental behaviour of fiber concrete slabs on soil', *Journal Mechanics of Cohesive-frictional Materials*, 3: 277–290.

Barros, J.A.O. and Figueiras, J.A. (1999) 'Flexural behavior of steel fiber reinforced concrete: testing and modelling', *Journal of Materials in Civil Engineering, ASCE*, 11(4): 331–339.

Barros, J.A.O. (1995) 'Behaviour of fibre reinforced concrete – experimental analysis and numerical simulation', PhD Thesis, Dep. Civil Eng., Faculty of Eng. of Oporto University, 502 pp, December (in Portuguese).

Barros, J.A.O., Figueiras, J.A. and Veen, C.V.D. (1994) 'Tensile behaviour of glass fibre reinforced concrete', in J.F. Silva Gomes *et al*. (eds) *Recent Advances in Experimental Mechanics*, Vol. 2, 1073–1080.

Bartos, P.J.M. and Duris, M. (1994) 'Inclined tensile strength of steel fibres in a cement-based composite', *Composites*, 25(19): 945–952.

Bazant, Z.P. and Oh, B.H. (1983) 'Crack band theory for fracture of concrete', *RILEM Materials and Structures Journal*, 16(93): 155–177.

Brite-Euram (2002) 'Rational Production and Improved Working Environment through using Self Compacting Concrete', Brite-Euram project BRPR-CT96-0366. Technical report, Brite Euram/Swedish Cement and Concrete Research Institute.

Casanova, P. (1995) 'Bétons de fibres métalliques: du materiaux à la structure', PhD Thesis, École Nationale des Ponts et Chaussées (in French).

Casanova, P., Rossi, P. and Schaller. I. (2000) 'Can steel fibres replace transverse reinforcement in reinforced concrete beams?', *ACI Material Journal*, 94: 341–354.

CEB-FIP Model Code (1993) Comite Euro-International du Beton, Bulletin d'Information n° 213/214.

Cunha, V.M.C.F., Barros, J.A.O. and Sena-Cruz, J.M. (2006) 'Compression behaviour of steel fibre reinforced concrete (age influence and modelling)', Technical report no. 06-DEC/E-04, Department of Civil Engineering, University of Minho, 49 pp.

Cunha, V.M.C.F., Barros, J.A.O. and Sena-Cruz, J.M. 'Pullout behaviour of hooked-end steel fibers in self-compacting concrete', (2007) Technical report 07-DEC/E-06, Dep. Civil Eng., School Eng. University of Minho, 90 pp., April.

Cunha, V.M.C.F., Barros, J.A.O. and Sena-Cruz, J.M. (2008) 'Modelling the influence of age of steel fibre reinforced self-compacting concrete on its compressive behaviour', *RILEM Materials and Structures Journal*, 41(3): 465–478.

De Borst, R. (1986) 'Non-linear analysis of frictional materials', Dissertation, Delft Univ. of Technology.

di Prisco, M., Felicetti, R. and Plizzari, G.A. (2004) 'Precast SFRC Elements: from Material Properties to Structural Applications'. 6th RILEM Symposium on Fibre-Reinforced Concretes (FRC) – BEFIB, 20–22 September, Varenna, Italy.

EFNARC (2002) *Specification and Guidelines for Self-Compacting Concrete*, ISBN 0 9539733 4 4, 32 pp.

EN197-1:2000 (2000) *Cement. Composition, specifications and conformity criteria for low heat common cements*, ISBN: 058036456 9, 52 pp.

EN 1991-1-4 (2005) 'Europe 1: Actions on structures – Part 1-4: General actions – Wind actions', European Standard.

Falkner, H. and Teutsch, M. (1993) 'Comparative investigations of plain and steel fibre reinforced industrial ground slabs', Institut fur Baustoffe, Massivbau und brandschutz, n° 102.

Gettu, R., Barragán, B., García, T., Ramos, G., Fernández, C. and Oliver, R. (2004) 'Steel Fiber Reinforced Concrete for the Barcelona Metro Line 9 Tunnel Lining', 6th RILEM Symposium on Fibre-Reinforced Concretes (FRC) – BEFIB, 20–22 September, Varenna, Italy (Invited lecturer).

Gomes, P.C.C. (2002) 'Optimization and characterisation of high-strength self-compacting concrete', PhD Thesis, Universitat Plitècnica de Catalunya, Escola Técnica Superior D'Enginyers de Camins, Canals i Ports de Barcelona.

Gonçalves, D.M.F. and Barros, J.A.O. (2007) 'Cyclic compression behaviour of steel fibre reinforced self-compacting concrete – experimental and analytical research', Technical report CT_I&D/1107, November (in Portuguese).

Gouveia, A.V. Barros, J.A.O., Azevedo, A.F.M. and Sena-Cruz, J.M. (2007) 'Crack Constitutive Model to Simulate the Behavior of Fiber Reinforced Concrete Structures Failing in Punching', CMNE 2007 – Congress on Numerical Methods in Engineering and XXVIII CILAMCE – Iberian Latin American Congress on Computational Methods

in Engineering, Abstract pp. 287, Paper n° 232 published in CD – FEUP, 13 pp., Porto, 13–15 June.

Groth P. (2000) 'Fibre reinforced concrete – Fracture mechanics methods applied on self-compacting concrete and energetically modified binders', PhD Thesis, Department of Civil and Mining Engineering, Lulea University of Technology, Sweden.

Hillerborg, A. Modeer, M. and Petersson, P.E. (1976) 'Analysis of crack formation and crack growth in concrete by means of fracture mechanics and finite elements', *Cement and Concrete Research* 6: 773–782.

Hordijk, D.A. (1991) 'Local approach to fatigue of concrete', PhD thesis, Delft University of Tech.

Leung, C.K.Y. and Geng, Y.P. (1998) 'Micromechanical modeling of softening behaviour in steel fibre reinforced cementicious composites', *Int. Journal Solids Structures*, 25(32): 4205–4222.

Li, V.C. and Chan, Y.-W. (1994) 'Determination of interfacial debond mode for fibre-reinforced cementitious composites', *ASCE Journal of Engineering Mechanics*, 120(4): 707–719.

MC90 (1993) *CEB-FIP Model Code 1990: Design Code*. Lausanne: Thomas Telford.

Naaman, A.E. and Najm, H. (1991) 'Bond-slip mechanisms of steel fibres in concrete', *ACI Materials Journal*, 88(2): 135–145.

Okamura, H. and Maekawa, K. (1991) *Nonlinear analysis and constitutive models of reinforced concrete*. Tokyo: Gihodo-Shuppan Press.

Oliver, J. (1990) 'Modelado de la fissuracion en estructuras de hormigón', Centro de Métodos Numéricos en Ingenieria, Barcelona, 99 pp, (in Spanish).

Pereira, E.N.B. and Barros, J.A.O. (2009) '3D behaviour of a 4-parameter isotropic nonlinear hardening plasticity model for concrete', Conference in Numerical Methods in Engineering 2009, Barcelona, 29 June–2 Jul.

Pereira, E.N.B., Barros, J.A.O. and Camões, A.F.F.L. (2008) 'Steel fiber reinforced self-compacting concrete – experimental research and numerical simulation', *Journal of Structural Engineering*, 134(8): 1310–1321, August.

Pereira, E.N.B. (2006) 'Steel Fibre Reinforced Self-compacting Concrete: From material to mechanical behaviour', Dissertation for Pedagogical and Scientific Aptitude Proofs, Department Civil Engineering, University of Minho, 188 pp <http://www.civil.uminho.pt/composites>.

RILEM 50-FMC (1985) 'Determination of the fracture energy of mortar and concrete by means of three-point bending tests on notched beams', *Materials and Structures*, 85 (85): 285–290.

Robins, P., Austin, S. and Jones, P. (2002) 'Pull-out behaviour of hooked steel fibres', *RILEM Journal of Engineering Mechanics*, 35(251): 434–442.

Rots, J.G. (1988) 'Computational modeling of concrete fracture', Dissertation, Delft University of Technology.

Roshani, D. (1996) 'Shear Capacity of Steel Fiber Reinforced Concrete Beams', MSc Thesis, Göteborg University.

Schupack, M. (1986) 'Durability of SFRC exposed to severe environments', *Steel Fiber Concrete*, Elsevier, pp. 479–496.

Sena-Cruz, J.M., Barros, J.A.O., Azevedo, A.F.M. and Gouveia, A.V., (2007) 'Numerical Simulation of the Nonlinear Behaviour of RC Beams Strengthened with NSM CFRP Laminate Strips', CMNE 2007 – Congress on Numerical Methods in Engineering and XXVIII CILAMCE – Iberian Latin American Congress on Computational Methods in Engineering, Abstract pp. 289, Paper n° 485 published in CD – FEUP, 20 pp., Porto.

Sena-Cruz, J.M. (2004) 'Strengthening of concrete structures with near-surface mounted CFRP laminate strips.' PhD Thesis, Department of Civil Engineering, University of Minho.

Shah, S.P., Swartz, S.E. and Ouyang, C. (1995) *Fracture Mechanics of Concrete: Applications of Fracture Mechanics to Concrete, Rock and Other Quasi-Brittle Materials*. Chichester: John Wiley & Sons, Inc.

Taha, M.M.R. and Shrive, N.G. (2002) 'Fracture mechanics of concrete', *Fracture of Civil Engineering Materials*, ENCI 617.

Vandewalle, L. *et al*. (2000) 'Test and design methods for steel fibre reinforced concrete. Recommendations for bending test', *RILEM Materials and Structures*, 33(225): 3–5.

Vandewalle, L. *et al*. (2002) 'Test and design methods for steel fibre reinforced concrete – Final Recommendation', *RILEM Materials and Structures*, 35(253): 579–582.

Vandewalle, L. *et al*. (2003) 'Test and design methods for steel fibre reinforced concrete – σ–ε design method – Final Recommendation', *RILEM Materials and Structures*, 36: 560–567.

van Gysel, A.V. (1999) 'A pullout model for hooked-end steel fibres', *RILEM HPFRCC3 – High performance fibre reinforced cement composites*, Mainz, Germany, pp. 351–359.

van Mier, J.G.M., Schlangen, E., and Vervuurt, A. (1996) 'Tensile cracking in concrete and sandstone: part 2 – effect of boundary conditions', *RILEM Materials and Structures*, 29: 87–96.

van Vliet, M.R.A. (2000) 'Size effect In Tensile Fracture of Concrete and Rock', PhD Thesis, Delft University of Technology, ISBN 90–407–1994–2.

Wang, C.Z., Guo, Z.H. and Zhang X.Q. (1981) 'Experimental investigation of the complete stress–strain curves of concrete under cyclic loading', US/PRC Workshop on Seismic Analysis and Design of Reinforced Structures, Ann Arbor, Michigan, USA.

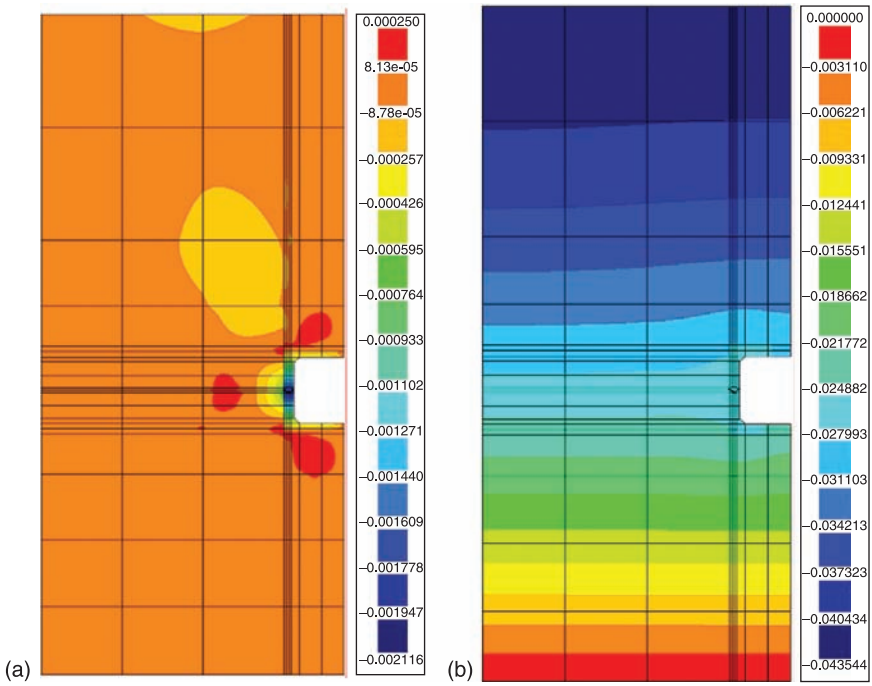

Plate I Displacement field: (a) in *y* direction (m); (b) in *z* direction (m).

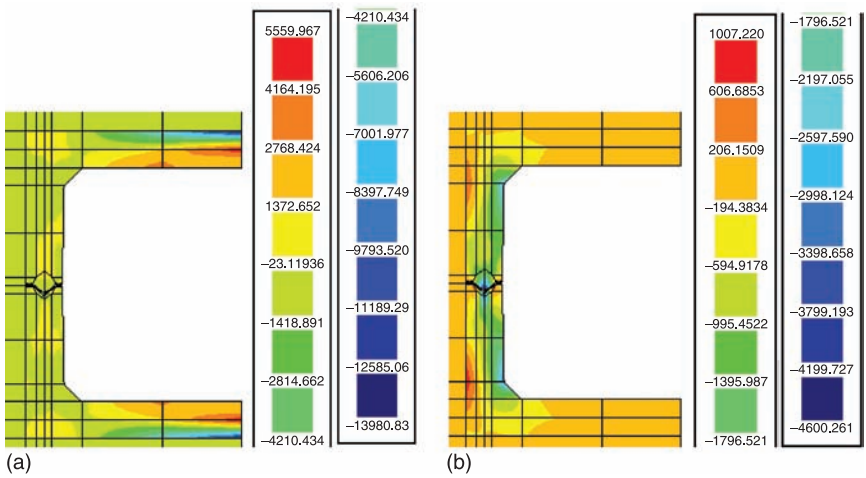

Plate II (a) σ_y and (b) σ_2 fields in the box-culvert (kPa).

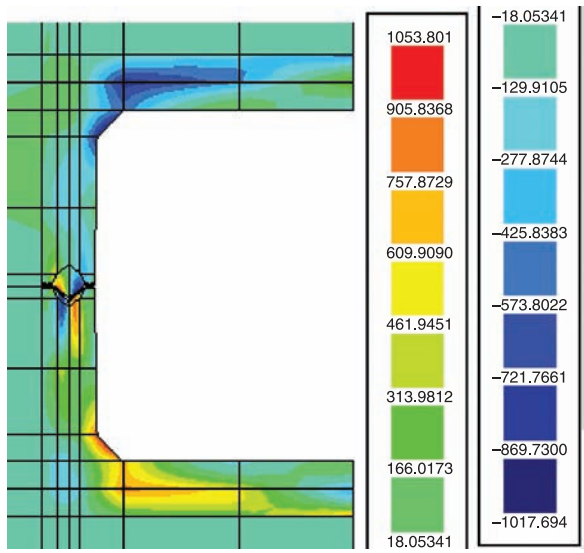

Plate III τ_{yz} field in the box-culvert (kPa).

5

Natural fiber reinforced concrete

F. P. TORGAL and S. JALALI, University of Minho, Portugal

Abstract: The construction industry is responsible for the depletion of large amounts of non-renewable resources. This activity generates not only millions of tons of mineral wastes but also carbon dioxide gas emissions. More building materials based on renewable resources such as vegetable fibers are needed. This chapter discusses the utilization of natural fibers for concrete reinforcement. It includes fiber characteristics, properties and the description of the treatments that improve their performance; it covers the compatibility between the fibers and the cement matrix and also how the fibers influence cement properties. It also includes the properties and durability performance of concrete reinforced with natural fibers.

Key words: reinforced concrete, natural fibers, properties, durability.

5.1 Introduction

The construction industry is one of the major and most active sectors in Europe. It represents 28% and 7% of the employment, respectively, in the industry and in all the European economy. Unfortunately, this industry is also responsible for the depletion of large amounts of non-renewable resources and for 30% of carbon dioxide gas emissions. This is particularly serious in the current context of climate change caused by carbon dioxide emissions worldwide, causing a rise in sea level (IPCC, 2007), and being responsible for a meltdown in the world economy (Stern, 2006). In order to achieve a more sustainable construction, the European Union recently established that, in the medium term, raw materials consumption must be reduced by 30% and also that waste production in this sector must be cut by 40%. The use of renewable resources by the construction industry will help to achieve a more sustainable pattern of consumption of building materials. Concrete is the most-used material on Earth and it is known for a high compressive strength and a low tensile strength. The combined use of regular concrete and steel-reinforcing bars is needed to overcome that disadvantage, leading to a material with good compressive and tensile strengths but also with a long post-crack deformation (strain softening). Unfortunately reinforced concrete has a high permeability that allows water and other aggressive elements to enter, leading to carbonation and chloride ion attack resulting in corrosion problems (Glasser *et al*., 2008; Bentur, 2008). Steel rebar corrosion is in fact the main reason for infrastructure deterioration. Gjorv (1994) mentioned a study of Norway OPC bridges indicating that 25% of those built after 1970 presented corrosion problems. Another author mentioned that 40% of the 600 000 bridges in the U.S. were affected by corrosion problems, resulting in an estimated US$50 billion for repair operations (Ferreira,

2009). Since world population is expected to grow more than 2000 million by the year 2030, more reinforced-concrete structures will be built and many more deterioration problems are expected to take place. Concrete durability is environment related, because if we were able to increase the life time of a concrete from 50 to 500 years, its environmental impact decreases 10 times (Mora, 2007). Since an average of 200 kg of steel rebar are used for each cubic metre of concrete structure, it is clear that the replacement of reinforced steel rebar by vegetable fibers is a major step to achieving a more sustainable construction. On the other hand, reinforced steel is a high-cost material, has high energy consumption and comes from non-renewable resources. As for synthetic fibers like polyvinyl alcohol (PVA) and polypropylene, their production requires phenol compounds as antioxidants and amines as ultraviolet stabilizers and flame retardants, which is not the path to more sustainable materials (Berge, 2007). Therefore, to promote the use of concrete reinforced with vegetable fibers could be a way to improve concrete durability and also sustainable construction. This chapter is divided into six sections: 5.1 Introduction, 5.2 Fiber characteristics and properties, 5.3 Matrix characteristics, 5.4 Properties, 5.5 Durability and 5.6 Future trends.

5.2 Fiber characteristics and properties

Vegetable fibers are natural composites with a cellular structure. Different proportions of cellulose, hemicellulose and lignin constitute the different layers. Cellulose is a polymer containing glucose units, and hemicellulose is a polymer made of various polysaccharides. As for lignin, it is an amorphous and heterogeneous mixture of aromatic polymers and phenyl propane monomers (John *et al*., 2005). Different fibers possess different compositions (Table 5.1), therefore it is expected that their behavior inside a cement matrix could differ.

Natural fibers possess a high tensile strength and they have a low modulus of elasticity (Table 5.2). Even so, their tensile performance compares favourably to synthetic fibers.

Table 5.1 Composition of vegetable fibers

Fiber	Lignin (%)	Cellulose (%)	Hemicellulose (%)	Extractives (%)	Ash (%)
Bagasse	21.8	41.7	28.00	4.00	3.50
Banana leaf	24.84	25.65	17.04	9.84	7.02
Banana trunk	15.07	31.48	14.98	4.46	8.65
Coconut coir	46.48	21.46	12.36	8.77	1.05
Coconut tissue	29.7	31.05	19.22	1.74	8.39
Eucalyptus	25.4	41.57	32.56	8.20	0.22
Sisal	11.00	73.11	13.33	1.33	0.33

Source: Arsene *et al.,* 2003

Table 5.2 Properties of natural and synthetic fibers

Properties	Specific gravity (kg/m^3)	Water absorption (%)	Tensile strength (MPa)	Modulus of elasticity (GPa)
Sisal	1370	110	347–378	15.2
Coconut	1177	93.8	95–118	2.8
Bamboo	1158	145	73–505	10–40
Hemp	1500	85–105	900	34
Caesar weed	1409	182	300–500	10–40
Banana	1031	407	384	20–51
Piassava palm	1054	34–108	143	5.6
Date palm (Kriker *et al.*, 2005)	1300–1450	60–84	70–170	2.5–4
Polypropylene	913	–	250	2.0
PVA F45 (Passuello *et al.*, 2009)	1300	–	900	23

Source: Arsene *et al.*, 2003

One of the disadvantages of using natural fibers is that they have a high variation in their properties that could lead to unpredictable concrete properties (Swamy, 1990; Li *et al.*, 2006). Pre-treatment of natural fibers was found to increase concrete performance. Pulping is one of the fiber treatments that improves fiber adhesion to the cement matrix and also resistance to alkaline attack (Savastano *et al.*, 2003). It can be obtained either chemically (kraft) or mechanically. The latter has a lower cost (around half) and does not require effluent treatments (Savastano *et al.*, 2001a). Table 5.3 presents some pulping conditions for sisal and banana fibers.

Some chemical treatments lead to a higher mechanical performance than others (Peanich, 2004). Some authors suggest the use of organofunctional silane coupling agents to reduce the hydrophilic of vegetable fibers (Castellano *et al.*, 2004; Abdelmouleh, 2004). But recently, Joaquim *et al.* (2009) compared the performance of cementitious composites reinforced by kraft pulp sisal fibers, and by sisal fibers modified by the organosolv process. They found that the best mechanical performance was achieved by the composites with kraft pulp fibers.

Table 5.3 Sisal and banana kraft pulping conditions

Parameter	Sisal	Banana
Active alkali (as Na_2O) (%)	9	10
Sulphidity (as Na_2O) (%)	25	25
Liquor/fiber ratio	5:1	7:1
Temperature (°C)	170	170
Digestion time	~75 minutes to temperature 120 minutes cook	~85 minutes to temperature 120 minutes cook
Total yield (%w/w)	55.4	45.9
Screened yield (%w/w)	45.5	45.3

Source: Savastano *et al.*, 2003

Arsene *et al*. (2007) suggest that using a pyrolisis process can increase the fiber strength by a factor of three.

5.3 Matrix characteristics

Savastano (2000) mentioned that acid compounds released from natural fibers reduce the setting time of cement matrices. Some authors reported that fiber sugar components, hemicellulose and lignin can contribute to preventing cement hydration (Bilba *et al*. 2003; Stancato *et al*., 2005). According to Sedan *et al*. (2008), fiber inclusion can reduce the delay of setting by 45 minutes. The explanation relies on the fact that pectin (a fiber component) can fix calcium, thus preventing the formation of calcium silicate hydrate (CSH) structures. According to Savastano and Agopyan (1999), the interfacial transition zone between concrete and natural fibers is porous, cracked and rich in calcium hydroxide crystals. Those authors reported a 200 µm thickness at 180 days. On the contrary, Savastano *et al*. (2005) reported that using vacuum dewatering and high pressure applied after molding led to a dense ITZ (Fig. 5.1(a)), also reporting fibers without hydration products (Fig. 5.1(b)).

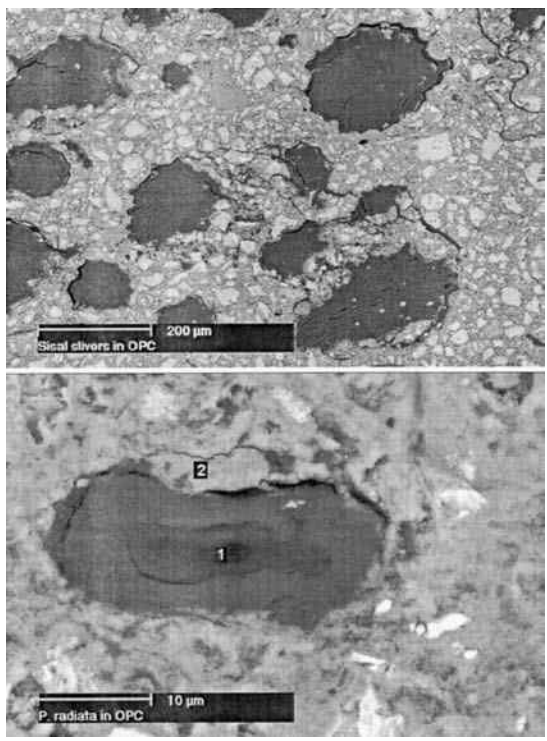

5.1 BSE image of sisal fibers in cement matrix: (a) fibers with ITZ; (b) EDS analysis on fiber lumen (spot 1) revealed that no mineralization due to the presence of hydration products has detected (Savastano *et al.,* 2005).

The use of water-repellents leads to a good bond between natural fibers and concrete (Ghavami, 1995). The mechanical treatment of the fibers also improves the bonding between the fiber and the cement (Coutts, 2005). According to some authors, alkaline treatment of fibers improves their strength and also fiber-matrix adhesion (Sedan *et al*., 2008). Tonoli *et al*. (2009) compared cement composites with vegetable fibers previously submitted to surface modification with Methacryloxypropyltri-methoxysilane (MPTS) and Aminopropyltri-ethoxysilane (APTS). The results of composites with fibers modified by MPTS show fibers free from cement hydration products, while APTS-based fibers presented accelerated mineralization that leads to a higher embrittlement behavior of cement composites.

5.4 Properties

5.4.1 Using small vegetable fibers

Some authors found out that the use of a 0.2% volume fraction of 25 mm sisal fibers leads to free plastic shrinkage reduction. The combined use of coconut and sisal short fibers seem to have delayed restrained plastic shrinkage and controlling crack development at early ages (Filho *et al*., 2005). As for the mechanical performance of natural fiber concrete, Al-Oraimi and Seibi (1995) reported that using a low percentage of natural fibers improved the mechanical properties and the impact resistance of concrete, and had similar performance when compared to synthetic fiber concrete. Other authors reported that fiber inclusion increases impact resistance by 3–18 times higher than when no fibers were used (Ramakrishna and Sundararajan, 2005). The use of small volumes (0.6–0.8%) of *Arenga Pinata* fibers shows that the capacity increases the toughness characteristics of cement-based composites (Raza *et al*., 2005). As for Reis (2006), studies showed that the mechanical performance of fiber concrete depends on the type of fiber. He found that coconut and sugar cane bagasse fiber increases concrete fracture toughness, but banana pseudostem fiber does not. The use of coconut fibers shows even better flexural than does synthetic fiber (glass and carbon) concrete. Silva *et al*. (2007) studied the addition of sisal fibers to concrete and reported that the compressive strength was lower than concrete samples without the fibers. The explanation for that behavior seems to be related to concrete workability. Savastano *et al*. (2009) compared the mechanical performance of cement composites reinforced with sisal, banana and eucalyptus fibers. Sisal and banana fibers with higher lengths (1.65 mm and 1.95 mm) than eucalyptus (0.66 mm) showed a more stable fracture behavior, which confirms that fiber length influences the process by which load transfers from the matrix to the fibers. Silva *et al*. (2010) tested cement composites reinforced by long sisal fibers placed at the full length of a steel mold in 5 layers (mortar/fibers/mortar). These composites reach ultimate strengths of 12 and 25 MPa under tension and bending loads. The vegetable type also influences the performance of cement composites (Tonoli *et al*., 2010), being that eucalyptus-

based ones present improved mechanical performance after 200 ageing cycles than pinus based. The explanation related to a better distribution of vegetable particles in the cement matrix.

5.4.2 Using long bamboo rebars

Khare (2005) tested several concrete beams made with stirrups and rebar bamboo and reported that this material has the potential to be used as a substitute for steel reinforcement (Fig. 5.2).

This author reported that the ultimate load capacity of bamboo was about 35% of the equivalent reinforced-steel concrete beams. Fig. 5.3 shows a concrete sample where fiber imprints are visible as an example for low adhesion between cement matrix and bamboo.

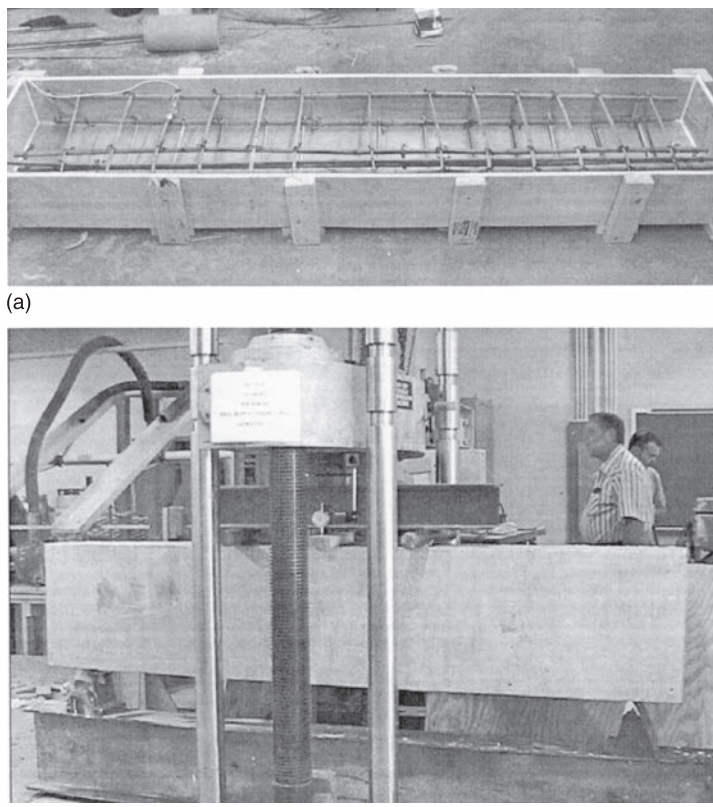

5.2 Concrete beam reinforced with bamboo rebars: (a) finished bamboo reinforcement; (b) test set-up (Khare, 2005).

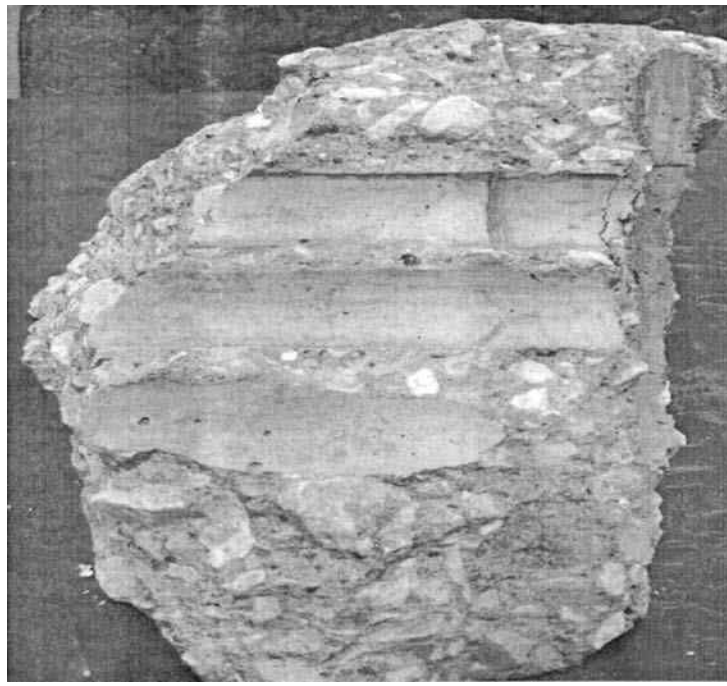

5.3 Imprints of fiber reinforcement (Khare, 2005)

Junior *et al*. (2005) mentioned just 25% of the equivalent reinforced-steel concrete beams' ultimate load capacity. Analysis of adhesion between cement and bamboo by pull-off tests (Fig. 5.4) shows that bamboo/cement have much lower adhesion than steel rebar/cement and that adhesion results are influence by node presence (Jung, 2006).

These authors suggest that bamboo rebar should previously be submitted to thermal treatment to improve bond strength. According to Mesquita *et al*. (2006), the bond strength of bamboo is 70% of smooth steel bond strength when a 35 MPa concrete is used. However, the bond strength of bamboo is almost 90% of smooth steel bond strength when a 15 MPa concrete is used. These authors analyzed the effect of artificial 2 pins (2 of bamboo and 2 of steel) studding in bamboo splints, noticing they led to a bond strength of bamboo higher than smooth steel. Ferreira (2007) also studied the effect of artificial pins (Fig. 5.5) in the bond strength of bamboo rebar using pull-out tests.

The results show that the use of just 1 pin is insufficient to increase bamboo bond strength (Table 5.4). In the same work this author studied several 20 MPa concrete beams reinforced with bamboo rebars ($2 \times 1\,cm^2$) and steel stirrups, which exhibited an acceptable structural behavior.

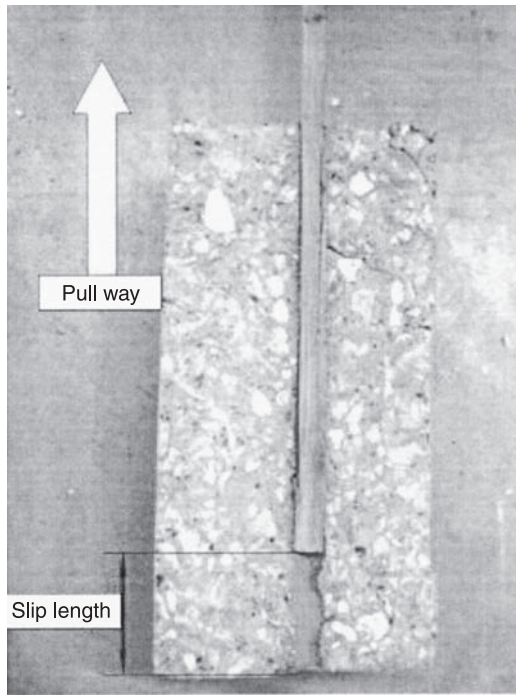

5.4 Pull-out test of concrete with bamboo reinforcement (Jung, 2006).

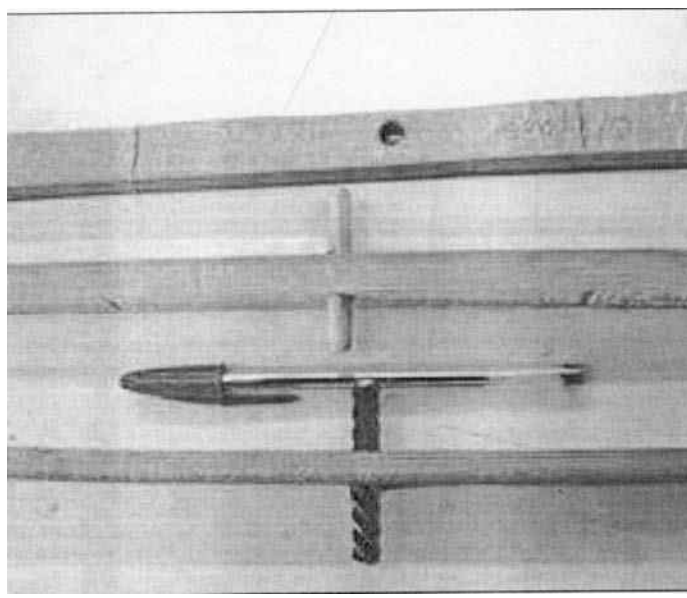

5.5 Bamboo rebars bamboo and steel pins (Ferreira, 2007).

Table 5.4 Bond strength using pull-out tests

Rebar type	Bond strength (MPa)
Bamboo	0.81
Bamboo with epoxy resin	0.32
Bamboo with 1 bamboo pin	0.82
Bamboo with 1 steel pin	0.69
Bamboo with hole	1.10
Rough steel	6.87
Smooth steel	1.33

Source: Ferreira, 2007

5.5 Durability

Durability of natural fiber reinforced concrete is related to the ability to resist both external (temperature and humidity variations, sulfate or chloride attack, etc.) and internal damage (compatibility between fibers and cement matrix, volumetric changes, etc). The degradation of natural fibers immersed in Portland cement is due to the high alkaline environment that dissolves the lignin and hemicellulose phases, thus weakening the fiber structure (Gram, 1983). Gram was the first author to study the durability of sisal and coir fiber reinforced concrete. The fiber degradation was evaluated by exposing them to alkaline solutions and then measuring the variations in tensile strength. This author reported a deleterious effect of Ca^{2+} elements on fiber degradation. He also stated that fibers were able to preserve their flexibility and strength in areas with carbonated concrete with a pH of 9 or less. Filho *et al.* (2000) also investigated the durability of sisal and coconut fibers when immersed in alkaline solutions. Sisal and coconut fibers conditioned in a sodium hydroxide solution retained, respectively, 72.7% and 60.9% of their initial strength after 420 days. As for the immersion of the fibers in a calcium hydroxide solution, it was noticed that the original strength was completely lost after 300 days. According to those authors, the explanation for the higher attack by $Ca(OH)_2$ can be related to a crystallization of lime in the fibers' pores. Ramakrishna and Sundararajan (2005a) also reported degradation of natural fiber when exposed to alkaline media. Other authors studied date palm reinforced concrete, reporting low durability performance that is related to fiber degradation when immersed in alkaline solutions (Kriker *et al*., 2008). Ghavami (2005) reported the case of a bamboo-reinforced concrete beam which was 15 years old and without deterioration signs. Lima *et al*. (2008) studied the variations of tensile strength and Young's modulus of bamboo fiber reinforced concrete exposed to wetting and drying cycles, reporting insignificant changes, thus confirming its durability. The capacity of natural fibers to absorb water is another path to decreasing the durability of fiber reinforced concrete. Water absorption leads to volume changes that can induce concrete cracks (Ghavami, 2005; Agopyan *et al*., 2005). In order to improve the durability of fiber reinforced concrete, the two following paths could be used:

5.5.1 Matrix modification

Using low alkaline concrete and adding pozzolanic by-products such as rice husk ash, blast furnace slag, or fly ashes to Portland cement (Gutiérrez *et al*., 2005; Agopyan *et al*., 2005; Savastano *et al*., 2005a). Results show that the use of ternary blends containing slag/metakaolin and silica fume are effective in preventing degradation (Mohr *et al*., 2007). But in some cases the low alkalinity is not enough to prevent lignin from being decomposed (John *et al*., 2005). Other authors reported that fast carbonation can induce lower alkalinity (Agopyan *et al*., 2005). These results are confirmed by others that used artificial carbonation in order to obtain $CaCO_3$ from $Ca(OH)_2$ leading to increased strength and reduced water absorption (Tonoli, 2010a). The use of cement-based polymers can contribute to increased durability (Pimentel, 2006). D'Almeida (2009) used blends where 50% of Portland cement was replaced by metakaolin to produce a matrix totally free of calcium hydroxide in order to prevent migration of calcium hydroxide to the fiber lumen, middle lamella and cell walls and thus avoid embrittlement behavior.

5.5.2 Fiber modification

Coating natural fibers to avoid water absorption and free alkalis. Use water-repellent agents or fiber impregnation with sodium silicate, sodium sulphite, or magnesium sulphate. Ghavami (1995) reported that using a water-repellent in bamboo fibers allowed only 4% water absorption. The use of organic compounds such as vegetable oils reduced the embrittlement process, but not completely (Filho *et al*., 2003). Recent findings report that silane coating of fibers is a good way to improve the durability of natural-fiber reinforced concrete (Bilba and Arsene, 2008). Other authors mentioned that using pulped fibers may improve durability performance (Savastano *et al*., 2001). Some even reported that a fiber extraction process can prevent durability reductions (Juárez *et al*., 2007). The use of compression and temperature (120, 160 and 200°C) leads to an increase of fiber stiffness and a decrease of fiber moisture absorption (Motta, 2009).

5.6 Future trends

Further investigations about natural reinforced concrete are needed in order to clarify several aspects that current knowledge does not. The available literature data is mostly related to the mechanical behavior of natural-fiber reinforced concrete. For instance, only recently has the delaying effect of fiber inclusion received the proper attention. Since the main reason for fiber degradation relates to alkaline degradation, much more research is needed about the chemical interactions between the cement matrix and the natural fibers. The right treatments to improve fiber- and cement-matrix compatibility are still to be found. The same

could be said about the variation on fiber properties, thus control quality methods are needed in order to ensure minimal variations on the properties of natural fibers. Durability related issues also deserve more research efforts.

5.7 References

Abdelmouleh, M., Boufi, S., Belgacem, M., Duarte, A., Salah, A. and Gandini, A. (2004) 'Modification of cellulosic fibers with funcionalised silanes: development of surface properties'. *International Journal of Adhesives & Adhesives* 24: 43–54. http://inderscience.metapress.com/link.asp?id=u1757l77k8135645

Al-Oraimi, S. and Seibi, A. (1995) 'Mechanical characterization and impact behavior of concrete reinforced with natural fibers'. *Composite Structures* 32: 165–171. doi:10.1016/0263–8223(95)00043–7

Agopyan, V., Savastano, H., John, V. and Cincotto, M. (2005) 'Developments on vegetable fiber-cement based materials in São Paulo, Brazil: an overview'. *Cement & Concrete Composites* 27: 527–536. doi:10.1016/j.cemconcomp.2004.09.004

Arsène, M-A., Savastano Jr, H., Allameh, S.M., Ghavami, K. and Soboyejo, W. (2003) 'Cementitious composites reinforced with vegetable fibers', in *Proceedings of the First Interamerican Conference on Non-Conventional Materials and Technologies in the Eco-Construction and Infrastructure*, 13–16 November, Joao-Pessoa Brazil, IAC-NO CMAT 2003 Proceedings (ISBN 85–98073–02–4).

Arsene, M., Okwo, A., Bilba, K., Soboyejo, A. and Soboyejo, W. (2007) 'Chemically and thermally treated vegetable fibers for reinforcement of cement-based composites'. *Materials and Manufacturing Processes*, 22: 214–227. http://www.informaworld.com/10.1080/10426910601063386

Bentur, A. and Mitchell, D. (2008) 'Material performance lessons'. *Cement and Concrete Research* 38: 259–272. doi:10.1016/j.cemconres.2007.09.009

Berge, B. (2007) *The Ecology of Building Materials*, 2nd edn. Princeton, NJ: Architectural Press (ISBN 978–1–85617–537–1).

Bilba, K. and Arsene, M. (2008) 'Silane treatment of bagasse fiber for reinforcement of cementitious composites'. *Composites: Part A,* 39: 1488–1495. doi:10.1016/j.compositesa.2008.05.013

Bilba, K., Arsene, M. and Ouensanga, A. (2003) 'Sugar cane bagasse fiber reinforced cement composites. Part I. Influence of the botanical components of bagasse on the setting of bagasse/cement composite. *Cement & Concrete Composites*, 25: 91–96. doi:10.1016/S0958–9465(02)00003–3

Brandt, A. (2008) 'Fiber reinforced cement-based (FRC) composites after over 40 years of development in building and civil engineering'. *Composite Structures*, 86: 3–9. doi:10.1016/j.compstruct.2008.03.006

Castellano, M., Gandini, A., Fabbri, P. and Belgacem, M. (2004) 'Modification of cellulose fibers with organosilanes: Under what conditions does coupling occur?' *Journal of Colloid and Interface Science*, 273: 505–511. doi:10.1016/j.jcis.2003.09.044

Coutts, R. (2005) 'A review of Australian research into natural fiber cement composites'. *Cement & Concrete Composites*, 27: 518–526. doi:10.1016/j.cemconcomp.2004.09.003

D'Almeida, A., Filho, J. and Filho, R. (2009) 'Use of curaua fibers as reinforcement in cement composites'. *Chemical Engineering Transactions*, 17: 1717–1722. DOI: 10.3303/CET0917287

Filho, R., Scrivener, K., England, G. and Ghavami, K. (2000) 'Durability of alkali-sensitive sisal and coconuts fibers in cement mortar composites'. *Cement & Concrete Composites*, 22: 127–143. doi:10.1016/S0958–9465(99)00039–6

Filho, R., Ghavami, K., England, G. and Scrivener, K. (2003) 'Development of vegetable fiber-mortar composites of improved durability'. *Cement & Concrete Composites*, 25: 185–196. doi:10.1016–S0958/9465(02)00018–5

Filho, R., Ghavami, K., Sanjuán, M. and England, G (2005) 'Free, restrained and drying shrinkage of cement mortar composites reinforced with vegetable fibers'. *Cement & Concrete Composites*, 27: 537–546. doi:10.1016/j.cemconcomp.2004.09.005

Ferreira, G. (2007), 'Vigas de concreto armadas com taliscas de bamboo *Dendrocalamus Giganteus*'. PhD Thesis, UNICAMP, Brazil (only in Portuguese).

Ferreira, R.M. (2009) *Service-life Design of Concrete Structures in Marine Environments: A probabilistic based approach*. Saarbrucken. Germany: VDM Verlag Dr. Muller Aktiengesellschaft & Co. KG (ISBN–13: 978–3639167108).

Gram, H. (1983), *Durability of Natural Fibers in Concrete*. Stockolm: Swedish Cement and Concrete Research Institute.

Glasser, F., Marchand, J. and Samson, E. (2008) 'Durability of concrete. Degradation phenomena involving detrimental chemical reactions'. *Cement and Concrete Research*, 38: 226–246. doi:10.1016/j.cemconres.2007.09.015

Gjorv, O. (1994) 'Steel corrosion in concrete structures exposed to Norwegian marine environment'. *ACI Concrete International*, 35–39

Ghavami, K. (1995) 'Ultimate load behavior of bamboo-reinforced lightweight concrete beams'. *Cement & Concrete Composites*, 17: 281–288. doi:10.1016/0958–9465(95)00018–8

Ghavami, K. (2005) 'Bamboo as reinforcement in structure concrete elements'. *Cement & Concrete Composites*, 27: 637–649. doi:10.1016/j.cemconcomp.2004.06.002

Gutiérrez, R., Díaz, L. and Delvasto, S. (2005) 'Effect of pozzolans on the performance of fiber reinforced mortars'. *Cement & Concrete Composites*, 27: 593–598. doi:10.1016/j.cemconcomp.2004.09.010

IPCC (2007) Intergovernmental Panel on Climate Change, *Climate Change 4th Assesment Report*.

Joaquim, A., Tonoli, G., Santos, S. and Savastano, H. (2009) 'Sisal organosolv pulp as reinforcement for cement based composites'. *Materials Research*, 12: 305–314. doi: 10.1590/S1516–14392009000300010

John, V., Cincotto, M., Sjotrom, C., Agopyan, V. and Oliveira, C. (2005) 'Durability of slag mortar reinforced with coconut fiber'. *Cement & Concrete Composites*, 27: 565–574. doi:10.1016/j.cemconcomp.2004.09.007

Juárez, C., Durán, A., Valdez, P. and Fajardo, G. (2007) 'Performance of *Agave lechuguilla* natural fiber in Portland cement composites exposed to severe environment conditions'. *Building and Environment*, 42: 1151–1157. doi:10.1016/j.buildenv.2005.12.005

Jung, Y. (2006) 'Investigation of bamboo as reinforcement in concrete'. Master of Science in Civil and Environment Engineering, University of Texas.

Júnior, H., Mesquita, L., Fabro, G., Willrich, F. and Czarnieski, C. (2005) 'Vigas de concreto reforçadas com bambu *Dendrocalamus giganteus*. I: Analise experimental'. *Revista Brasileira de Engenharia Agrícola e Ambiental* 9: 642–651 (only in Portuguese).

Khare, L. (2005) 'Performance evaluation of bamboo reinforced concrete beams'. Master of Science in Civil Engineering, University of Texas.

Kriker, A., Debicki, G., Bali, A., Khenfer, M. and Chabannet, M. (2005) 'Mechanical properties of date palm fibers and concrete reinforced with date palm fibers in hot dry climates'. *Cement & Concrete Composites*, 27: 554–648. doi:10.1016/j.cemconcomp.2004.09.015

Kriker, A., Bali, A., Debicki, G., Bouziane, M. and Chabannet, M. (2008) 'Durability of date palm fibers and their use as reinforcement in hot dry climates'. *Cement & Concrete Composites*, 30: 639–648. doi:10.1016/j.cemconcomp.2007.11.006

Li, Z., Wang, X. and Wang, L. (2006) 'Properties of hemp fiber reinforced concrete composites'. *Composites: Part A*, 37: 497–505. doi:10.1016/j.compositesa.2005.01.032

Lima, H., Willrich, F., Barbosa, N., Rosa, M. and Cunha, B. (2008) 'Durability analysis of bamboo as concrete reinforcement'. *Materials and Structures*, 41: 981–989. doi:10.1617/s11527–007–9299–9

Mesquita, L., Czarnieski, C., Filho, A., Willrich, F., Júnior, H. and Barbosa, N. (2006) 'Determinação da tensão de aderência do bambu-concreto'. *Revista Brasileira de Engenharia Agrícola e Ambiental*, 10: 505–516 (only in Portuguese). doi: 10.1590/S1415–43662006000200036

Mohr, B., Biernacki, J. and Kurtis, K. (2007) 'Supplementary cementitious materials for mitigating degradation of kraft pulp fiber cement-composites'. *Cement And Concrete Research*, 37: 1531–1543. doi:10.1016/j.cemconres.2007.08.001

Mora, E. (2007) 'Life cycle, sustainability and the transcendent quality of building materials'. *Building and Environment*, 42: 1329–1334. doi:10.1016/j.buildenv.2005.11.004

Motta, L., John, V. and Agopyan, V. (2009) 'Thermo-mechanical treatment to improve properties of sisal fibers for composites'. *5th International Materials Symposium MATERIALS 2009*. 14th meeting of SPM (Sociedade Portuguesa de Materiais), Lisbon.

Passuello, A., Moriconi, G. and Shah, S. (2009) 'Cracking behavior of concrete with shrinkage reducing admixtures and PVA fibers'. *Cement and Concrete Composites*, 31: 699–704. doi:10.1016/j.cemconcomp.2009.08.004

Pehanich, J., Blankenhorn, P. and Silsbee, M. (2004) 'Wood fiber surface treatment level effects on selected mechanical properties of wood fiber-cement composites'. *Cement and Concrete Research*, 34: 59–65. doi:10.1016/S0008–8846(03)00193–5

Pimentel, L., Beraldo, A. and Savastano, H. (2006) 'Durability of cellulose-cement composites modified by polymer'. *Engenharia Agricola*, 26: 344–353. doi: 10.1590/S0100–69162006000200002

Ramakrishna, G. and Sundararajan, T. (2005) 'Impact strength of a few natural fiber reinforced cement mortar slabs: a comparative study'. *Cement & Concrete Composites*, 27: 547–553. doi:10.1016/j.cemconcomp.2004.09.006

Ramakrishna, G. and Sundararajan, T. (2005a) 'Studies on the durability of natural fibers and the effect of corroded fibers on the strength of mortar'. *Cement & Concrete Composites*, 27: 575–582. doi:10.1016/j.cemconcomp.2004.09.008

Reis, J. (2006) 'Fracture and flexural characterization of natural fiber reinforced polymer concrete'. *Construction and Building Materials*, 20: 673–678. doi:10.1016/j.conbuildmat.2005.02.008

Razak, A. and Ferdiansyah, T. (2005) 'Toughness characteristics of Arenga pinnata fiber concrete'. *Journal of Natural Fibers*, 2: 89–103. doi:10.1016/j.matdes.2010.01.043

Savastano, H. and Agopyan, V. (1999) 'Transition zone studies of vegetable fiber-cement paste composites'. *Cement & Concrete Composites*, 21 : 49–57. doi:10.1016/S0958–9465(98)00038–9

Savastano, H., Warden, P. and Coutts, R. (2000) 'Brazilian waste fibers as reinforcement for cement-based composites'. *Cement & Concrete Composites*, 22: 379–384. doi:10.1016/S0958–9465(00)00034–2

Savastano, H., Warden, P. and Coutts, R. (2001) 'Ground iron blast furnace slag as a matrix for cellulose-cement materials'. *Cement & Concrete Composites*, 23: 389–397. doi:10.1016/S0958–9465(00)00083–4

Savastano, H., Warden, P. and Coutts, R. (2001a) *Performance of low-cost vegetable fiber-cement composites under weathering*. CIB World Building Congress, Wellington, New Zealand, 11 pp.

Savastano, H. Warden, P. and Coutts, R. (2003), 'Mechanically pulped sisal as reinforcement in cementitious matrices'. *Cement & Concrete Composites*, 25: 311–319. doi:10.1016/S0958–9465(02)00055–0

Savastano, H., Warden, P. and Coutts, R. (2005) 'Microstruture and mechanical properties of waste fiber-cement composites'. *Construction and Building Materials*, 27: 583–592. doi:10.1016/j.cemconcomp.2004.09.009

Savastano, H., Warden, P. and Coutts, R. (2005a) 'Potential of alternative fiber cements as building materials for developing areas'. *Cement & Concrete Composites*, 25: 585–592. doi:10.1016/S0958–9465(02)00071–9

Savastano, H., Santos, S., Radonjic, M. and Soboyejo, W. (2009) 'Fracture and fatigue of natural fiber reinforced cementitious composites'. *Cement & Concrete Composites*. 31: 232–243. doi:10.1016/j.cemconcomp.2009.02.006

Silva, J., Rodrigues, D. and Dias (2007) *Compressive strength of low resistance concrete manufactured with sisal fiber*. 51° Brazilian Congress of Ceramics. Salvador, Brazil.

Silva, F., Filho, R., Filho, J. and Fairbairn, E. (2010) 'Physical and mechanical properties of durable sisal fiber-cement composites'. *Construction and Building Materials*, 24: 777–785. doi:10.1016/j.conbuildmat.2009.10.030

Sedan, D., Pagnoux, C., Smith, A. and Chotard, T. (2008) 'Mechanical properties of hemp fiber reinforced cement: Influence of the fiber/matriz interaction'. *Journal of the European Ceramic*, 28: 183–192. doi:10.1016/j.jeurceramsoc.2007.05.019

Stancato, A., Burke, A. and Beraldo, A. (2005) 'Mechanism of a vegetable waste composite with polymer-modified cement (VWCPMC)'. *Cement & Concrete Composites*, 27: 599–603. doi:10.1016/j.cemconcomp.2004.09.011

Stern, N. (2006) *Stern Review on Economics of Climate Change*. Cambridge: Cambridge University Press.

Swamy, R. (1990) 'Vegetable fiber reinforced cement composites – a false dream or a potential reality?' *Proceedings of the 2nd International Symposium on Vegetable Plants and their Fibers as Building Materials, RILEM Proceedings 7*. London: Chapman and Hall, 3–8.

Tonoli, G., Filho, U., Savastano, H., Bras, J., Belgacem, M. and Lahr, F. (2009) 'Cellulose modified fibers in cement based composites'. *Composites Part A*, 2046–2053. doi:10.1016/j.compositesa.2009.09.016

Tonoli, G., Savastano, H., Fuente, E., Negro, C., Blanco, A. and Lahr, F. (2010) 'Eucalyptus pulp fibers as alternative reinforcement to engineered cement-based composites'. *Industrial Crops and Products*, 31: 225–232.doi:10.1016/j.indcrop.2009.10.009

Tonoli, G., Santos, S., Joaquim, A. and Savastano, H. (2010a) 'Effect of accelerated carbonation on cementitious roofing tiles reinforced with lignocellulosic fiber'. *ConstructionandBuildingMaterialsI*,24:193–201.doi:10.1016/j.conbuildmat.2007.11.018

6

The role of fiber reinforcement in mitigating shrinkage cracks in concrete

K. RAOUFI and J. WEISS, Purdue University, USA

Abstract: Tensile stresses are generated in concrete when volume changes caused by moisture loss, temperature reductions, and chemical reactions are restrained. If these tensile stresses are high enough, they may result in cracking. Short-fiber reinforcement can be added to concrete in low volumes (less than 2–3%) to increase the fracture toughness of the concrete, which will help to control the width of cracks that form. The shrinkage cracking performance of fiber reinforced concrete (FRC) is generally assessed using small-scale laboratory specimens. A need exists to link the results of laboratory experiments to the cracking behavior of full-scale concrete elements.

Key words: shrinkage cracking, fibers, size effect, fracture, cohesive zone model, crack width, and concrete slabs.

6.1 Introduction

Short, randomly distributed fibers are frequently added to concrete to enhance the restrained shrinkage cracking performance of concrete slabs. Shrinkage cracks are unsightly and can accelerate durability related problems such as corrosion of reinforcement (Østergaard, 2003; Sanjuan *et al*., 1997; Shah *et al*., 1997; Weiss and Shah, 1997). The use of fiber reinforcement as a method to mitigate shrinkage cracking of concrete has attained more attention recently as high-performance concrete materials have a higher potential to develop early-age shrinkage cracks (Bentz and Jensen, 2004; Weiss, 1999). Many studies have illustrated the beneficial effects of adding fibers to reduce the width of cracks that form, as well as delaying the age of visible cracking in concrete specimens (ACI-544.1R-96, 1996; Grzybowski and Shah, 1990; Shah and Weiss, 2006; Swamy and Stavrides, 1979). While several theoretical models and experimental techniques have been proposed to describe the cracking behavior of fiber reinforced concrete elements, further work is still needed to link the cracking behavior of laboratory specimens to field performance.

The main aim of this chapter is to present an overview of how fiber reinforcement mitigates shrinkage cracking of field concrete slabs. This chapter uses the fracture mechanics concept to examine factors influencing the cracking performance of concrete slabs. Both analytical and numerical techniques are used to estimate cracking performance of fiber reinforced concrete slabs. Furthermore, this chapter explores how the length of slab, type and volume of fibers and degree of restraint influence the cracking behavior of concrete slabs. Specifically, implications of

using small laboratory specimens in estimating the shrinkage cracking performance of larger field members are discussed.

6.2 Restrained shrinkage cracking of fiber reinforced concrete

Restrained shrinkage cracking can impact the durability of concrete infrastructures as cracks can increase the penetration of water and ions resulting in the acceleration of the corrosion of steel reinforcement (Østergaard, 2003; Sanjuan *et al*., 1997; Shah *et al*., 1997). Concrete shrinks due to moisture loss, thermal cooling, or hydration reactions. When these volume changes are restrained, tensile stress develops in concrete and cracking may occur. It is well known that restrained shrinkage cracking of concrete depends on combinations of a variety of factors, some of which include: the degree of restraint, creep and stress relaxation, rate and magnitude of shrinkage, mechanical property development, and fracture resistance of the concrete (Weiss, 1999).

One of most common techniques to mitigate restrained shrinkage cracking of concrete is to add low volumes of short, randomly distributed fibers to concrete mixtures (ACI-231R-10, 2010; ACI-544.1R-96, 1996). While a plain concrete is typically characterized by a low tensile strength and a low fracture resistance, fiber reinforcement can be added to increase fracture resistance (i.e. toughness) of concrete mixtures. When concrete cracks, fibers help to bridge a crack and transfer load across the crack. As such, fiber reinforcement will limit the extent of restrained shrinkage cracking by limiting the width of the crack that forms in concrete elements (Shah *et al*., 1995; Shah and Weiss, 2006).

The effectiveness of fiber reinforcement in enhancing the cracking performance of concrete is influenced by the volume of fibers, properties of fiber itself, properties of the matrix, quality of the bonding between the matrix and fibers, and aspect ratio (length-to-diameter ratio) of fibers (Bentur and Mindess, 2006). The volume of fibers in concrete is frequently limited to 1–3% in most field applications. When used in low volumes (i.e. less than about 3%), fibers primarily act to improve the fracture toughness (as determined by the area under the stress–crack opening curve) of concrete, and the shrinkage cracking of concrete is characterized by a gradual opening of a single crack. It should be noted that fibers (at these low volumes) do not increase the strength of concrete, rather the use of fiber reinforcement results only in an improvement in the fracture toughness and ductility of concrete elements in most practical cases (Shah, 2004). If higher volumes of fibers are used, the strength of concrete can be increased and several shrinkage cracks can form (Bentur and Mindess, 2006). These higher volumes of fibers are generally not used for ready-mixed concrete and rather are limited to specialty products (Balaguru and Shah, 1985).

Many efforts have been made to determine the beneficial effects of fibers in reducing the shrinkage cracking of concrete. Laboratory tests, such as flexural

toughness testing of fiber reinforced concrete beams with third-point loading (ASTM-C1018-97, 1997), uniaxial tensile testing of beams (RILEM-TC-162-TDF, 2002), flexural testing of round determinate panels (ASTM-C1550-08, 2008), or wedge splitting tests (Østergaard, 2003) have been used to assess the fracture resistance properties of fiber reinforced concrete mixtures. Although these tests may show an improvement in the toughness of FRC mixtures, they do not necessarily show the beneficial effects of fibers in improving the shrinkage-cracking performance of FRC elements. Similarly, shrinkage tests such as ASTM C157-08 have been performed to provide information on the free shrinkage of concrete mixtures while fibers (in conventional volumes) generally do not alter the shrinkage of mortar or concrete (Shah and Weiss, 2006). The shrinkage cracking performance of FRC mixtures can be evaluated using tests that provide restraint while the concrete is changing volume.

Several test geometries have been used to evaluate the restrained shrinkage-cracking performance of concrete mixtures. Some of these testing geometries include: a linear specimen with anchored ends (Banthia *et al*., 1993; Weiss *et al*., 1998), a linear specimen held between a fixed grip and a movable end to adjust the degree of restraint (Altoubat and Lange, 2001; Bloom and Bentur, 1995), a rectangular specimen where restraint provided along its base (Raoufi *et al*., 2011; Banthia *et al*., 1996), a concrete specimen cast along a steel rebar (Mihashi and Leite, 2004), and a restrained concrete ring specimen (Carlson and Reading, 1988; Grzybowski and Shah, 1990; Shah and Weiss, 2006; Swamy and Stavrides, 1979).

The restrained ring test consists of a concrete ring cast around a restraining steel ring and provides a simple way to assess the restrained shrinkage cracking potential of concrete mixtures. While different ring geometries have been used to evaluate the influence of new admixtures (Weiss, 1999), mixture proportions (Krauss and Rogalla, 1996), and fiber reinforcement (Banthia *et al*., 1993; Shah and Weiss, 2006; Swamy and Stavrides, 1979) on the shrinkage cracking potential of concrete mixtures, a geometry has been standardized as ASTM C1581-09a (2009). While earlier studies generally utilized the restrained ring test as a qualitative test to assess the shrinkage cracking potential of concrete mixtures, later efforts mainly focused on quantifying cracking and stress development using the strains that develop in the ring (Hossain *et al*., 2003; Moon and Weiss, 2006; Weiss and Furgeson, 2001). While this test has been widely used to demonstrate the benefits of fiber reinforcement on mitigating the shrinkage cracking (Rapoport and Shah, 2005; Shah and Weiss, 2006; Swamy and Stavrides, 1979; Voigt *et al*., 2004), the majority of information obtained from the restrained ring test on FRC mixtures has been limited to a pure comparison of the cracking behavior (mostly the width of cracks and age of cracking) of fiber reinforced concrete mixtures to that of a reference plain-concrete mixture (Fig. 6.1). In general it has been shown that fiber reinforcement generally reduces the width of shrinkage-induced cracks (Bentur and Mindess, 2006; Grzybowski and Shah, 1990; Krenchel and Shah,

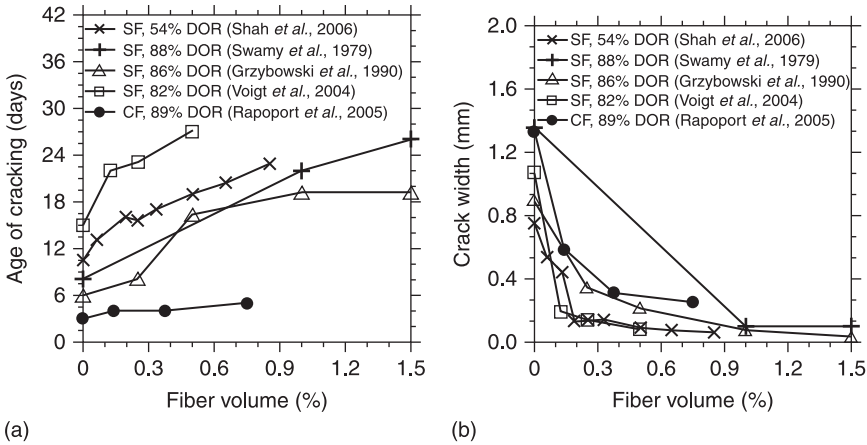

6.1 (a) Influence of fiber volume on the age of cracking; (b) influence of fiber volume on the width of crack in the restrained ring tests (after Raoufi *et al.,* 2010). (SF stands for steel fibers while CF stands for cellulose fibers.)

1987; Rapoport and Shah, 2005; Sarigaphuti *et al*., 1993; Shah and Weiss, 2006; Shah *et al*., 1994; Swamy and Stavrides, 1979; Voigt *et al*., 2004; Weiss, 1999; Weiss *et al*., 2000), delay the age of visible cracking (Altoubat and Lange, 2001; Bentur and Mindess, 2006; Grzybowski and Shah, 1990; Kim and Weiss, 2003; Rapoport and Shah, 2005; Sarigaphuti *et al*., 1993; Shah and Weiss, 2006; Voigt *et al*., 2004), promote multiple cracking (Banthia *et al*., 1995; Grzybowski and Shah, 1990; Sanjuan *et al*., 1997; Shah *et al*., 1995; Shah and Weiss, 2006), and increase the failure stress (Shah and Weiss, 2006).

6.3 Cracking and damage development in concrete

In order to improve existing models and testing geometries, it is essential to have a better understanding of how damage develops in a restrained concrete and how fiber reinforcement influences cracking of concrete. Cracking of concrete has been extensively studied by numerous researchers (Bazant and Planas, 1998; Jansen, 1996; Shah *et al*., 1995; van Mier and van Vilet, 2002). As a concrete specimen is restrained from shrinking, tensile stress develops. Once the tensile stress reaches 40–50% of the tensile strength, internal micro-cracks start to initiate. These micro-cracks are mostly isolated and randomly distributed in the specimen at this stage. As the concrete shrinks further, a greater number of internal cracks initiate and propagate. Once tensile stress increases to about 80% of the strength, micro-cracks begin to coalesce and localize in a small zone, called the damage or localization zone (Hillerborg *et al*., 1976; Kim and Weiss, 2003). Once the stress reaches the tensile strength of concrete, a single crack forms in the localization zone and

begins to grow in a stable manner. Upon further increase in restrained shrinkage deformations of concrete, the crack in the localization zone grows in size while the remaining portion of the specimen (bulk part) begins to unload. It should be noted that if fibers are present in the concrete, they bridge across the crack to transfer the shrinkage load, thereby limiting the size of the crack.

As a result, the shrinkage-induced crack opening of a concrete specimen can be approximated as the sum of the displacement of the bulk portion of the specimen (due to unloading) and the opening of the localization zone (due to an increase in the width of the crack) (Fig. 6.2). In a plain concrete, the stress that is transferred in the localization zone is due to aggregate interlock and friction between aggregates and cement paste. When fibers are added to concrete, the fibers can also bridge across the crack and provide additional toughening mechanisms to transfer the load and to limit crack opening in concrete. The efficiency of fibers in transferring forces across the crack depends on the length of fiber, the type of fiber, the orientation of fibers and the strength of the fiber-matrix shear bond (Balaguru and Shah, 1985; Bentur and Mindess, 2006).

As shown schematically in Fig. 6.3, as the length of a concrete specimen increases, the size of the localization zone remains relatively constant while the bulk portion of specimens increases in size (Bazant and Planas, 1998; Borges *et al*., 2004; Gopalaratnam and Shah, 1985; Jansen and Shah, 1997; Weiss *et al*., 2001). Consequently, the post-peak stress–strain behavior and shrinkage crack opening of concrete specimens is dependent on the length of specimens. As a result, a typical slab in the field, which is generally 3–6 meters long, can be

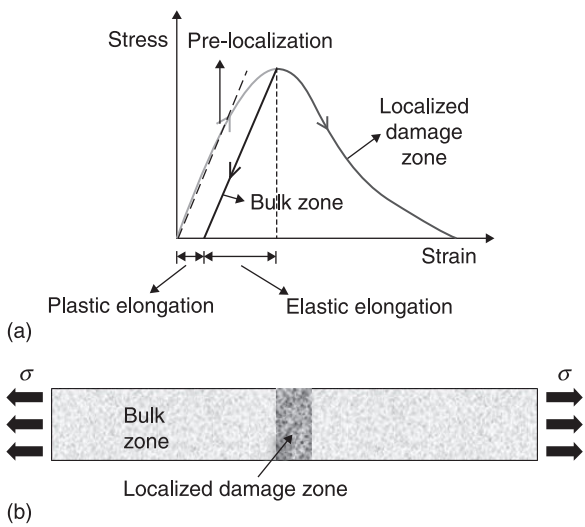

6.2 Crack localization in concrete specimens (after Jansen and Shah, 1997).

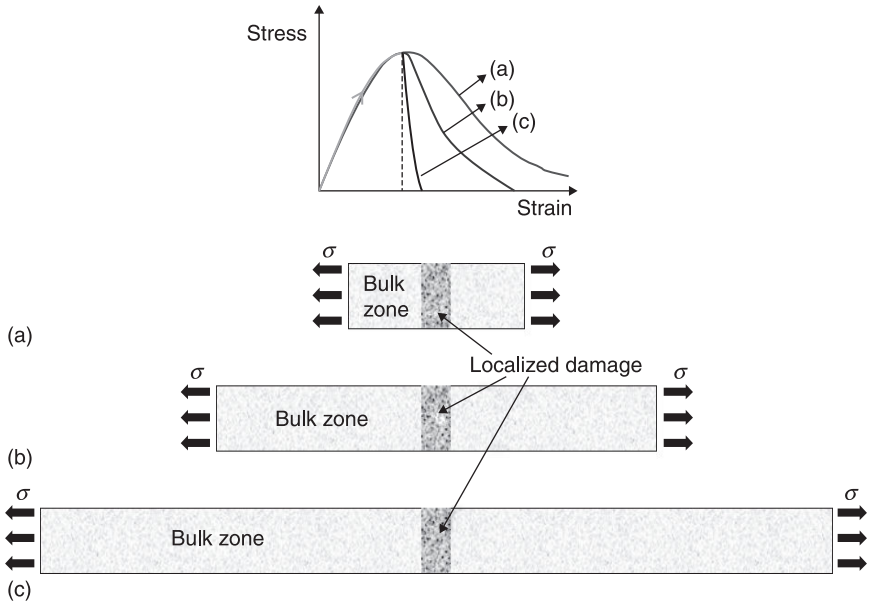

6.3 Influence of specimen length on post-peak response of concrete (after Weiss *et al.,* 1985).

expected to undergo a different post-peak softening behavior compared to the smaller geometries like the ASTM C1581-09 concrete ring, which corresponds to a slab of about one meter long.

6.4 Influence of the length of slabs on shrinkage cracking

To illustrate the influence of localization on the cracking behavior of concrete, a fracture mechanics approach is used. First, a simple model is used to calculate the crack opening in a slab based on linear elastic fracture mechanics (LEFM). Second, principles of non-linear fracture mechanics (NLFM) are used to analyze the fracture behavior of fiber reinforced concrete slabs. In addition to the analytical investigations, a finite element model is also used to simulate the fracture behavior of fiber reinforced concrete elements using the cohesive zone model.

6.4.1 Crack opening using linear elastic fracture mechanics (LEFM) approach

The LEFM approach divides a concrete specimen into two parts: a fracture zone (where cracking occurs); and a bulk portion, which behaves elastically. The elastic deformation of the bulk portion of the specimen can be calculated as:

$$\Delta_{bulk} = \varepsilon_{sh} L \quad [6.1]$$

where, L is the length of concrete and ε_{sh} is the shrinkage of concrete.

Figure 6.4 shows a single edge notch (SEN) test specimen subjected to uniform loading. This geometry resembles a concrete slab specimen subjected to uniform shrinkage if any shear force along the base is not considered. Using principles of LEFM, Eq. 6.2 can be used to calculate crack-opening displacement of the fracture zone (Tada *et al*., 1985).

$$\delta_{crack} = \frac{4a\sigma}{E} V_1(a/b) \quad [6.2a]$$

$$V_1(a/b) = \left[\frac{1.46 + 3.42\left[1 - Cos\left(\frac{a\pi}{2b}\right)\right]}{\left[Cos\left(\frac{a\pi}{2b}\right)\right]^2} \right] \quad [6.2b]$$

where, δ_{crack} is the crack-opening displacement of the fracture zone, σ is the applied stress, a is the initial crack length, E is the elastic modulus of the solid, and V_1 (a/b) is a geometry factor.

The total deformation of the concrete specimen subjected to shrinkage deformation can be calculated as the sum of the opening of the crack and the elastic deformation of the slab as:

$$\Delta_{total} = \delta_{crack} + \Delta_{bulk} \quad [6.3]$$

The influence of the magnitude of shrinkage on the crack opening of a one-meter-long concrete slab specimen is presented graphically in Fig. 6.5a. It can be seen that the crack opening in the localization zone (δ_{crack}) and the deformation of the bulk region (Δ_{bulk}) are both dependent on the shrinkage deformations of concrete. Consequently, the total deformation in the concrete slab (Δ_{total}) increase with increasing the magnitude of shrinkage. Figure 6.5b however shows the influence of the length of concrete on the deformations in the crack region and

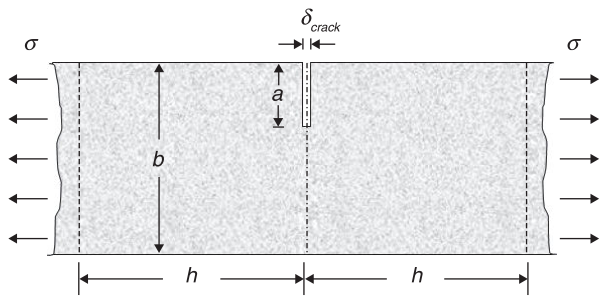

6.4 Single edge notch test specimen subjected to uniform loading (after Tada *et al.,* 1985).

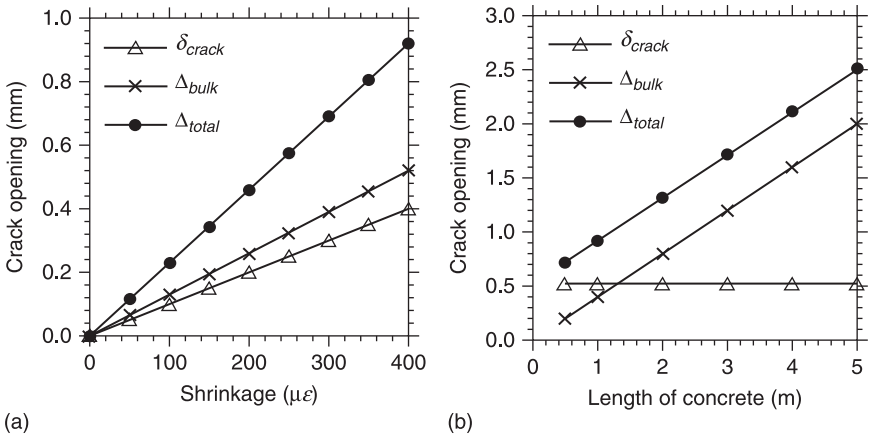

6.5 Influence of: (a) the magnitude of shrinkage; (b) the length of concrete on crack opening of concrete slabs (elastic modulus of 25 GPa and *a/b* of 0.33 was assumed in the calculation).

bulk region, provided sufficient shrinkage has occurred to result in cracking. Since the cracking resistance in the localization zone is only dependent on the loading configuration and geometry of the crack, similar crack opening in the localization zone is observed in concrete slabs, irrespective of the length of slabs. In contrast to the crack opening of the localization zone, the deformation of the bulk part increases with an increase in the length of a concrete slab. Consequently, the total deformation of a concrete slab is dependent on the length of the slab and increases with increasing the length of the slab as shown in Fig. 6.5b.

While LEFM provides a simple approach to describe the fracture behavior of a plain concrete element, it does not capture complexities of fracture processes that occur in a plain concrete or a fiber reinforced concrete material. Consequently, NLFM principles are widely used in modeling the fracture behavior of fiber reinforced concrete specimens as they provide more details on extensive amount of fracture works that occur in a fiber reinforced concrete specimen.

6.4.2 Crack opening based on non-linear fracture mechanics (NLFM) concept

The cohesive-zone model (CZM) is a widely used NLFM model for concrete materials. This model, also known as the fictitious crack or Dugdale–Barenblatt model (Barenblatt, 1962; Dugdale, 1960), was first proposed by Dugdale (1960) and Barenblatt (1962) to describe non-linear fracture processes and stress transfer across cracks in metals, polymers, ceramics and geo-materials. Hillerborg *et al.* (1976) and Bazant (1976) modified this model to describe the cracking behavior of concrete materials. This model assumes that the concrete behaves in a

linear-elastic manner until the stress reaches the strength of concrete. Cracking initiates wherever the maximum principal stress reaches the tensile strength of the material. This model assumes that the stress transfer through the cohesive crack is gradual in concrete and is a function of crack opening. One of the main advantages of the CZM is that it can be used in a finite element code to model the fracture behavior of concrete materials that are characterized with a different post-peak behavior (Bazant, 1976; Hillerborg *et al*., 1976).

Numerous attempts have been made to characterize the softening shape of the cementitious materials. It has been shown that the choice of the softening function greatly influences the material response (Roelfstra and Wittmann, 1986). Hillerborg *et al*. (1976) used a simple linear-softening curve to describe the post-peak behavior of concrete. Other researchers have used bilinear (Roelfstra and Wittmann, 1986), trilinear (Cho *et al*., 1984; Liaw *et al*., 1990), tetralinear, exponential (Gopalaratnam and Shah, 1985) and power expressions (Du *et al*., 1992) functions to characterize the softening shape of concrete. For the purpose of illustration, only linear and bilinear functions are discussed here.

The linear stress–crack opening relationship, which was initially introduced by Hillerborg *et al*. (1976), is the simplest softening function to describe the post-cracking behavior of concrete systems. This function (Eq. 6.4) requires the knowledge of the tensile strength and a critical crack width, beyond which no stress is transferred across a crack, to relate decreasing stress with the increasing crack width.

$$\sigma = f_t\left(1 - \frac{w}{w_c}\right) \qquad [6.4]$$

where, w_c is the critical crack width, f_t is the tensile strength, and w is the width of crack.

Many researchers have used a bilinear stress–crack opening function to model post-peak cracking behavior of concrete. A bilinear function provides a better fit to the softening relationship of most concrete materials, and it is still simple enough to be used in hand calculations. As shown in Fig. 6.6 and Eq. 6.5, this softening function is uniquely characterized by the tensile strength of concrete, a knee point (the $\sigma_1 - w_1$ point in Fig. 6.6), and the critical crack width.

$$\text{for} \quad w \le w_1 \qquad \sigma = f_t - (f_t - \sigma_1)\frac{w}{w_1} \qquad [6.5a]$$

$$\text{for} \quad w_1 \le w \le w_c \qquad \sigma = \sigma_1 - \sigma_1\frac{(w - w_1)}{(w_c - w_1)} \qquad [6.5b]$$

As soon as the maximum principal stress reaches the strength of a concrete at any point, cracking initiates. Once the concrete cracks, total shrinkage-driven displacement in a restrained concrete slab specimen can be summarized as:

$$\Delta L_{sh} = w + \Delta L_{\Psi} + \Delta L_{bulk} + \Delta L_{cr} \qquad [6.6]$$

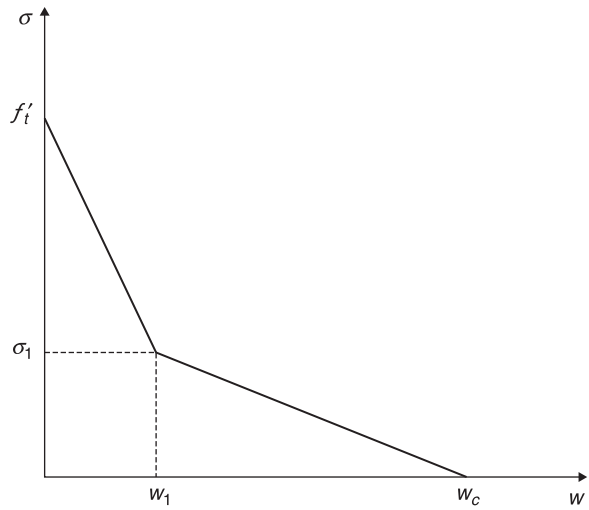

6.6 A schematic illustration of a bilinear softening function.

where, ΔL_{cr} is deformation due to creep, ΔL_{ψ} is deformation due to less than perfect degree of restraint, w is the width of crack and ΔL_{bulk} is the deformation of bulk part.

Using linear elasticity and a linear $\sigma - w$ relationship, the width of crack in concrete can be determined as:

$$w = \frac{L\left(\varepsilon_{sh}\Psi - \varepsilon_{cr} - \frac{f_t}{E}\right)}{\left(1 - \frac{f_t}{w_C E}L\right)} \qquad [6.7]$$

where, ε_{cr} is creep strain, ε_{sh} is shrinkage strain, ψ is the degree of restraint, and L is the original length of the concrete slab.

Similarly, assuming a bilinear softening model, the width of crack can be calculated as:

for $w \le w_1$ $$w = \frac{L\left(\varepsilon_{sh}\Psi - \varepsilon_{cr} - \frac{f_t}{E}\right)}{\left(1 - \frac{L(f_t - \sigma_1)}{E w_1}\right)} \qquad [6.8a]$$

for $w_1 \le w \le w_c$ $$w = \frac{L\left(\varepsilon_{sh}\Psi - \varepsilon_{cr} - \frac{\sigma_1}{E}\left(1 + \frac{w_1}{w_c - w_1}\right)\right)}{1 - \frac{L\sigma_1}{E(w_c - w_1)}} \qquad [6.8b]$$

Equation 6.8 provides a simple and easy way to assess the shrinkage cracking performance of concrete materials. It is noted that the approach used here assumes the formation of a single crack and is not valid when multiple cracking occurs. Therefore, this approach cannot be used in case of high-volume fiber reinforced concrete slabs, where several cracks can form. It should also be noted that Eq. 6.7 and 6.8 are only valid when the crack width is smaller than the critical crack width, w_c. Once the crack width exceeds the critical crack width, the concrete specimen breaks into two pieces, and stress can no longer be transferred across the crack.

Fracture behavior of concrete materials can be categorized as brittle, strain softening, and plastic and strain hardening materials. Brittle materials would correspond to plain cement paste or mortar and are characterized by low fracture toughness. Strain softening materials, such as concrete with large aggregate or light fiber reinforced concretes (when the fiber volume is smaller than about 2–3%), are characterized by a gradual reduction in post-peak stress as a crack advances. Plastic or strain-hardening materials, such as ECC and fabric reinforced concrete materials, are characterized by multiple cracking and strain hardening, post-peak behavior. These behaviors can be modeled by assuming proper $\sigma - w$ relationships using the CZM. Figure 6.7 illustrates typical $\sigma - w$ curves representing the aforementioned types of concrete materials.

Using the curves shown in Fig. 6.7, the width of crack for a brittle material a plain concrete, and a fiber reinforced concrete slab specimens can be calculated by substituting typical values for a concrete (E of 25 GPa, f_t of 4 MPa, and a degree of restraint of 1.0) into Eq. 6.8. The results of the calculations are illustrated

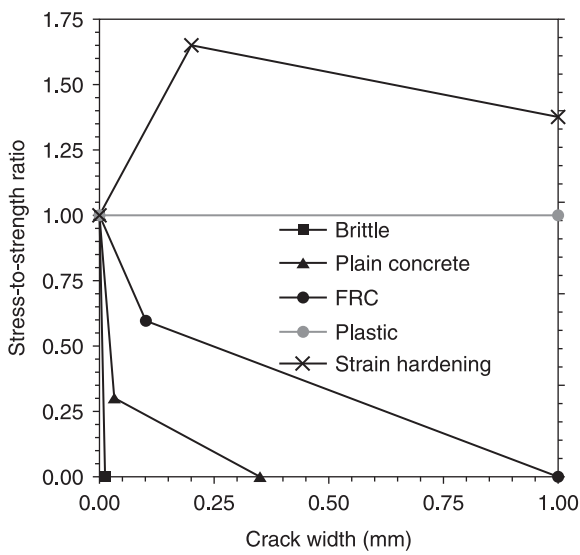

6.7 Typical fracture behaviors of brittle, plain, and concrete with various amounts of fiber reinforcement.

in Fig. 6.8, showing the influence of fracture toughness on crack opening of concrete materials. It should be noted that the creep of concrete was not considered in these calculations. In a brittle concrete slab specimen, failure occurs soon after residual stress reaches the strength of material and concrete becomes stress-free. Consequently, concrete fully unloads upon cracking and begins to deform freely. Cracking in a plain concrete is also characterized by a small fracture resistance from aggregate interlock and friction in the fracture zone, and the cracking behavior would be similar to that of the brittle concrete slab. In contrast, shrinkage cracking of the FRC slab is characterized by a gradual reduction in stress and a smaller width of crack.

The effect of sample size on the cracking performance of different types of concrete slabs can also be determined using Eq. 6.8, as shown in Fig. 6.9. In a

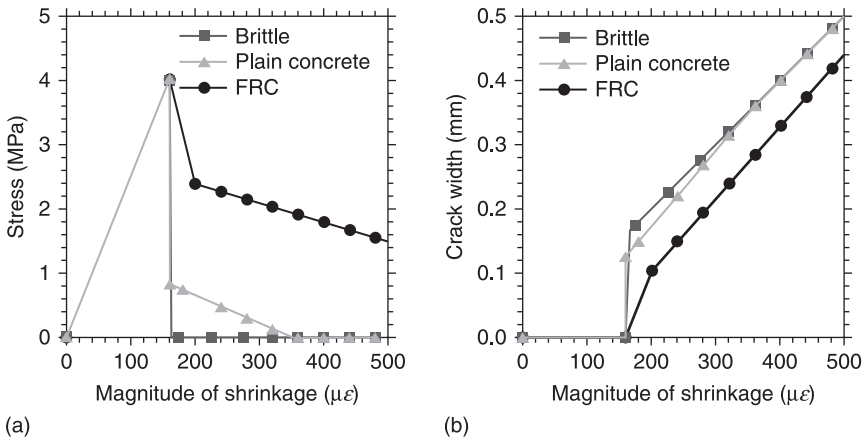

6.8 (a) Stress development; and (b) cracking behavior in one-meter-long concrete specimens assuming typical $\sigma - w$ relationships for brittle, plain, and fiber reinforced concretes.

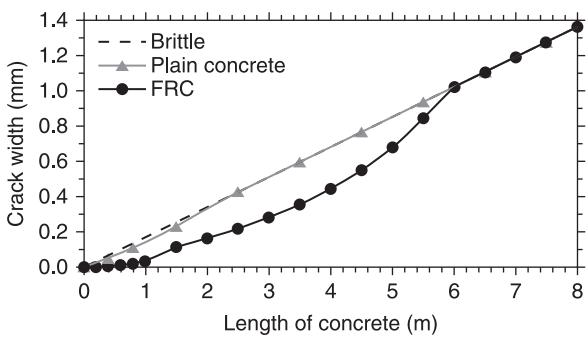

6.9 Influence of length on crack opening of brittle, plain, and fiber reinforced concrete materials. Results are calculated for a ε_{sh} of 170 με.

brittle concrete material, a crack becomes traction-free shortly after it forms and the width of crack increases freely as the concrete shrinks. As shown in Fig. 6.9, crack width in brittle concrete materials is directly proportional to the length of a concrete slab. A limited amount of toughening occurs in a plain concrete material that would result in a slight reduction in the width of crack only when the concrete member is relatively short (i.e. shorter than two meters in this case for the assumed strain softening curve). The crack opening in FRC slabs, however, is highly dependent on the length of a concrete specimen. In FRC specimens that are shorter than six meters (in this case), fiber reinforcement is effective in reducing the width of crack. However, once the crack width exceeds the critical crack width (assumed to be one millimeter for the example here, however this is less than the critical crack width that many commercial fibers would exhibit), the crack becomes traction-free and the slab behaves similar to a brittle slab. It can be seen that while a one-meter-long slab specimen in the lab can be used to estimate the cracking performance of a plain concrete slab in the field, small laboratory specimens such as the restrained ring geometry (about one meter long) may not be suitable in assessing the *in situ* cracking performance of longer, fiber reinforced concrete slabs.

6.4.3 Finite element approach

The earlier approach (i.e. Eq. 6.8) assumes the formation of only one crack and is not valid when several cracks form. The finite element method is used here to illustrate the multiple cracking behavior of materials that are characterized with plastic or strain hardening fracture behaviors using the cohesive zone model. The finite element model consists of a concrete slab which is restrained at its ends (Fig. 6.10). Typical concrete properties, such as those discussed earlier, are used in this analysis. The slab model is subjected to a uniform shrinkage increasing at a rate of 3 $\mu\varepsilon$/hr. The cohesive zone model is used to model the post-peak behavior of the concrete slabs. The concrete behaves as a linear elastic material until the maximum principal stress reaches the tensile strength of concrete (Mode I fracture behavior). Once a crack forms, the stress is reduced in the slab following the defined $\sigma - w$ curves (as illustrated in Fig. 6.7).

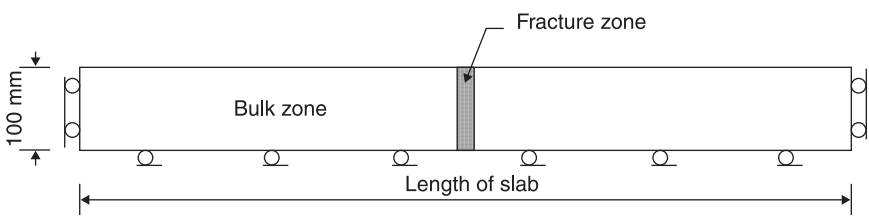

6.10 Finite element model of a concrete slab.

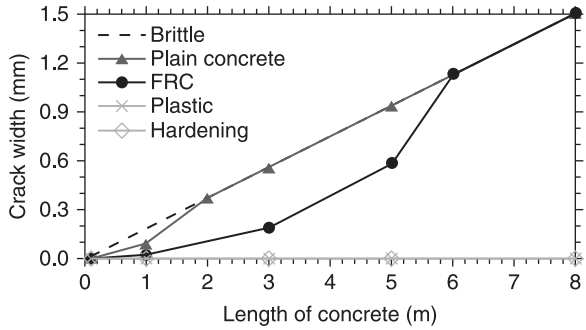

6.11 Influence of slab length on crack opening of concrete. Results are calculated for ε_{sh} of 189 $\mu\varepsilon$.

The result of the finite element analysis is summarized in Fig. 6.11, showing the influence of the length of a concrete slab on crack opening. For brittle, plain and fiber reinforced concretes, finite element analysis illustrates similar cracking behaviors to those predicted by Eq. 6.8 (Fig. 6.10). Unlike the plain and fiber reinforced concrete slabs, many fine cracks form in the plastic and strain hardening concrete slabs. As shown in Fig. 6.11, the width of crack is minimal (i.e. the maximum crack width for eight-meters-long slabs with plastic and strain hardening fracture behaviors are 0.007 mm and 0.003 mm, respectively). It should be noted that at a higher magnitude of shrinkage, and once the ultimate strength of these slabs is reached, one of these fine cracks would eventually grow in size and the slab would fail.

6.5 Influence of the degree of restraint on shrinkage cracking

The degree of restraint greatly affects the stress development and cracking behavior in concrete elements. Depending on the degree of restraint, residual stresses may or may not be high enough to lead to shrinkage cracking (Moon and Weiss, 2006; Weiss, 1999; Weiss *et al.*, 2000). As the degree of restraint decreases, a concrete specimen is allowed to move more freely, and a smaller stress level is developed in the concrete specimen. The width of crack is also reduced at lower degrees of restraint. Figure 6.12 shows the influence of the degree of restraint on the crack opening of typical FRC slabs using Eq. 6.8. For a similar length of slab, as the degree of restraint increases, the width of crack decreases. It is seen that concrete with a 100% degree of restraint has the greatest width of crack while the concrete specimens with 25% degree of restraint do not crack in this case. As shown by the arrows in Fig. 6.12, the length of a slab at which the final width of crack exceeds the critical crack width increases as the degree of restraint decreases. This implies that the cracking performance of a concrete slab may look better when tested at a lower degree of restraint than *in situ* restraint conditions.

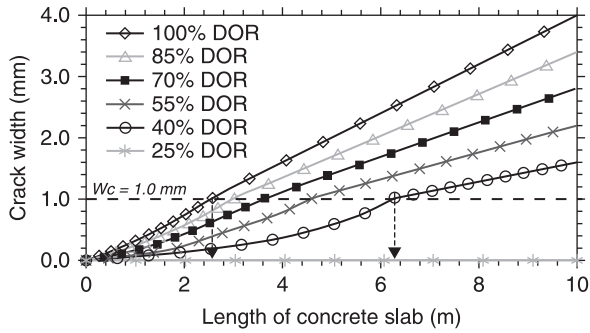

6.12 Influence of degree of restraint (DOR) on crack opening of FRC specimens.

6.6 Examples of shrinkage cracking in fiber reinforced concrete slabs

This section illustrates the shrinkage-cracking performance that may be expected in typical fiber reinforced concrete slabs. The shrinkage cracking performance of concrete slabs with two different types of fibers is discussed with each type of fiber added at different volumes. Measured $\sigma - w$ relationships are used in this analysis.

6.6.1 Measured stress–crack opening relationship of fiber reinforced concrete

Currently, there is no universally accepted testing technique to determine the tensile stress–crack opening response of concrete materials (commonly abbreviated as the $\sigma - w$ relationship). The $\sigma - w$ relationship can be obtained directly by a uniaxial tension test (Gopalaratnam and Shah, 1985) or indirectly by performing an inverse analysis on the results of three-point bending testing (Shah *et al*., 1995) or wedge splitting testing (Østergaard, 2003). The uniaxial tension test (UTT) is difficult to perform while the three-point bending geometry may not always be stable due to its substantial self-weight. In contrast, the wedge splitting testing (WST) can be performed using simple testing apparatus in a stable fashion. Consequently, researchers have started using this technique in determining the $\sigma - w$ relationship of both plain and fiber reinforced concrete materials (Elser *et al*., 1996; Kim and Kim, 1999; Lofgren *et al*., 2008; Østergaard, 2003). Inverse analysis is performed to determine the $\sigma - w$ relationship from the results of WST.

Li *et al*. (1993) determined the $\sigma - w$ relationships for two sets of fiber reinforced concrete mixtures: polypropylene fibers in normal-strength concrete and steel fibers in high-strength concrete. The steel fibers had an elastic modulus of 210 GPa, a length of 25 mm, and a diameter of 0.4 mm. The polypropylene fibers had an elastic

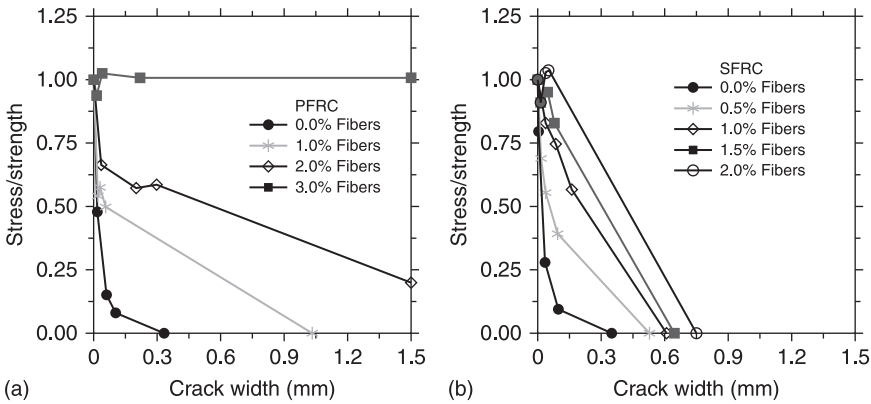

6.13 Measured $\sigma - w$ curves for (a) normal-strength polypropylene fiber reinforced concrete and (b) high-strength steel fiber reinforced concrete (after Li *et al.,* 1993).

modulus of 11.9 GPa, a length of 12 mm, and a diameter of 0.048 mm. Both concrete types were characterized with a maximum aggregate size of 8 mm. Figure 6.13 shows the $\sigma - w$ curves for these mixtures. Four different polypropylene fiber volumes of 0.5%, 1.0%, 1.5% and 2.0% were considered. Figure 6.13a compares $\sigma - w$ curves of these four mixtures with that of a similar plain concrete mixture. The addition of fibers causes an increase in fracture energy (as determined by the area under the $\sigma - w$ curves) as well as an increase in the critical crack width as shown in Fig. 6.13a. Similar behavior is seen in Fig. 6.13b, in which $\sigma - w$ curves for concrete mixtures with different volumes of steel fiber are shown.

6.6.2 Finite element analysis of concrete slabs

To show the influence of the type and volume, two series of finite element simulations were performed. Each series was characterized with one type of fiber. A finite element model similar to the one discussed earlier was adopted in this analysis. All concrete mixtures had a constant elastic modulus of 30 GPa while they were subjected to a uniform shrinkage at a rate of 3 $\mu\varepsilon$/hr. Cohesive zone model was used to model the post-peak behavior of each concrete element. Polypropylene fiber reinforced concrete mixtures had a tensile strength of 3.4 MPa while the tensile strength of the steel fiber reinforced concrete series was 5.0 MPa (Li *et al*., 1993).

According to the results presented in Fig. 6.14, the shrinkage cracking performance of polypropylene fiber reinforced concrete (PFRC) slabs are greatly influenced by the shape of the $\sigma - w$ curves and the critical crack width. The plain concrete slabs behave in a brittle fashion as expected. The plain concrete slabs that are longer than one meter are failed at the shrinkage level of 180 $\mu\varepsilon$, as their crack width is greater than the critical crack width of 0.35 mm. In the case of FRC slabs, as the fiber content increases, the critical crack width increases as well. As such,

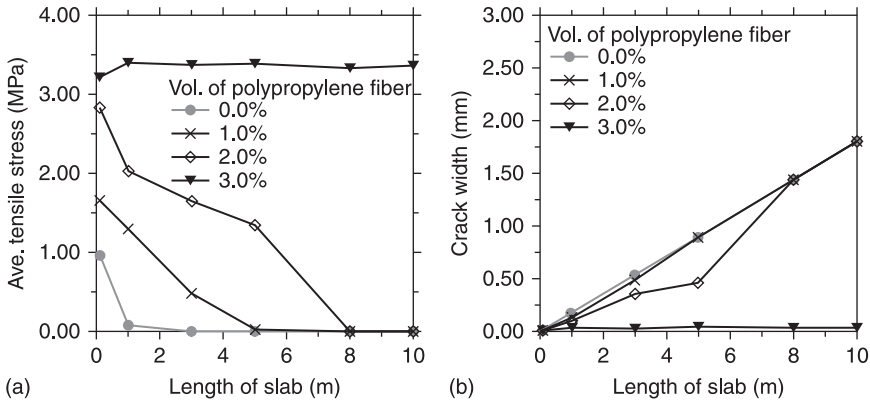

6.14 Influence of fiber volume on (a) stress development and (b) cracking performance of PFRC slabs. Results are illustrated for a shrinkage level of 180 $\mu\varepsilon$.

the length of a slab at which a slab becomes traction-free (the width of crack exceeds the critical crack width of concrete) increases. It can also be seen that as the fracture toughness of concrete (as determined by the area under the $\sigma - w$ curve) increases, the width of crack decreases. At a fiber content of 3% polypropylene fiber, multiple cracking occurs and many fine cracks continue to form at a constant stress in all slabs, irrespective of their lengths.

The shrinkage cracking performance of steel-fiber reinforced concrete (SFRC) slabs is shown in Fig. 6.15. Similar to the cracking behavior observed in the PFRC slabs, the width of crack in SFRC slabs is reduced as the volume of fibers increases. However, SFRC mixtures show more benefit of the fibers than what is shown in Fig. 6.14.

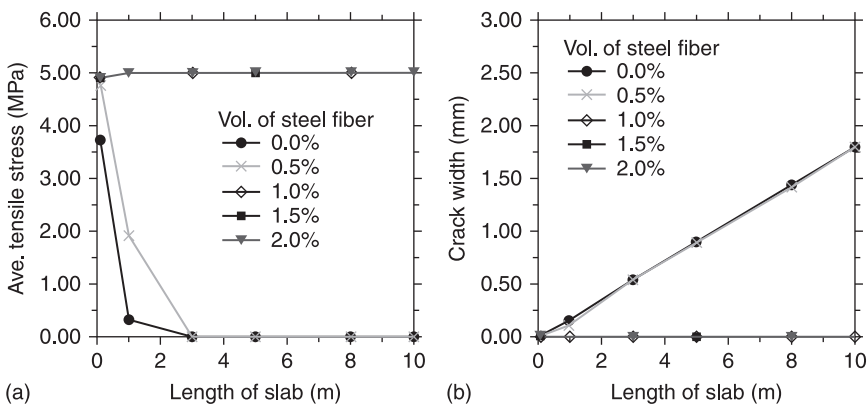

6.15 Simulated (a) stress development and (b) cracking performance of SFRC slabs. Results are illustrated for ε_{sh} of 180 $\mu\varepsilon$.

6.7 Conclusions

Conventional concrete exhibits a relatively brittle behavior. Fiber reinforcement is generally used in low volume (i.e. less than 2–3% by volume of concrete) in conventional concrete to enhance the toughness of the material. This is most frequently evident in the ability of fibers to transfer the shrinkage stress across the crack and to limit the width of cracks that form.

The restrained shrinkage cracking behavior of concrete is generally known to be a function of shrinkage strain, creep, elastic modulus, and fracture toughness (Weiss, 1999). However, this work has also shown that the length of the concrete specimen is an important factor as it relates to the width of the crack that forms. The width of crack is smaller in shorter concrete slabs. As the length of concrete slabs increases, smaller stress is transferred across the crack, and the width of crack increases. Models demonstrated the influence of slab length on the width of crack that develops.

It was shown that the width of crack in plain concrete slabs is directly related to the length of slab. Similarly, the width of crack in fiber reinforced concrete slabs is highly dependent on the length of concrete, and the crack width of small-scale lab specimens cannot directly be used to estimate the cracking performance of larger field concrete slabs. It was further shown that the cracking performance of the fiber reinforced concrete slabs is influenced by the volume and type of fibers.

Although small-scale laboratory specimens such as ASTM C1581–09 restrained ring geometry are easy to perform to evaluate the restrained shrinkage performance of plain-concrete mixtures, they do not directly relate to the crack-width performance of the fiber reinforced concrete that can be expected in the field. The length of a slab needs to be accounted for when determining the width of the crack that forms in the field.

6.8 References

ACI-231R-10, 2010. *Report on Early-Age Cracking: Causes, Measurement, and Mitigation*. Farmington Hills, MI: American Concrete Institute.

ACI-544.1R-96, 1996. *Report on Fiber Reinforced Concrete*. Farmington Hills, MI: American Concrete Institute.

Altoubat, S.A. and Lange, D.A., 2001. Creep, shrinkage, and cracking of restrained concrete at early age. *ACI Materials Journal*, 98(4): 323–331.

ASTM-C1018-97, 1997. *ASTM C1018-97 Standard Test Method for Flexural Toughness and First-Crack Strength of Fiber reinforced Concrete* (*Using Beam With Third-Point Loading*). West Conshohocken, PA: ASTM International.

ASTM-C1550-08, 2008. *ASTM C1550-08 Standard Test Method for Flexural Toughness of Fiber Reinforced Concrete* (*Using Centrally Loaded Round Panel*). West Conshohocken, PA: ASTM International.

Balaguru, P. and Shah, S.P., 1985. Alternative Reinforcing materials for developing countries. *International Journal for Development Technology*, 3: 87–105.

Banthia, N., Azzabi, M. and Pigeon, M., 1993. Restrained shrinkage cracking in fiber reinforced cementitious composites. *Materials and Structures*, 26(161): 405–413.

Banthia, N., Azzabi, M. and Pigeon, M., 1995. Restrained shrinkage tests on fiber reinforced cementitious composites. *Testing of Fiber Reinforced Concrete*, 155: 137–151.

Banthia, N., Yan, C. and Mindess, S., 1996. Restrained shrinkage cracking in fiber reinforced concrete: A novel test technique. *Cement and Concrete Research*, 26 (1): 9–14.

Barenblatt, G.I., 1962. The mathematical theory of equilibrium of cracks in brittle fracture. *Advance Applied Mechanics*, 7: 55–129.

Bazant, Z. and Planas, J., 1998. *Fracture and Size Effect in Concrete and Other Quasibrittle Materials*. Boca Raton, FL: CRC Press, 640 pp.

Bazant, Z.P., 1976. Instability, ductility, and size effect in strain-softening concrete. *Journal of the Engineering Mechanics Division-ASCE*, 102(2): 331–344.

Bentur, A. and Mindess, S., 2006. *Fiber Reinforced Cementitious Composites* (*Modern Concrete Technology*). London: Taylor & Francis, 624 pp.

Bentz, D.P. and Jensen, O.M., 2004. Mitigation strategies for autogenous shrinkage cracking. *Cement & Concrete Composites*, 26(6): 677–685.

Bloom, R. and Bentur, A., 1995. Free and restrained shrinkage of normal and high-strength concretes. *ACI Materials Journal*, 92(2): 211–217.

Borges, J.U.A., Subramaniam, K.V., Weiss, W.J., Shah, S.P. and Bittencourt, T.N., 2004. Length effect on ductility of concrete in uniaxial and flexural compression. *ACI Structural Journal*, 101(6): 765–772.

Carlson, R.W. and Reading, T.J., 1988. Model study of shrinkage cracking in concrete building walls. *ACI Structural Journal*, 85(4): 395–404.

Cho, K.Z., Kobayashi, A.S., Hawkins, N.M., Barker, D.B. and Jeang, F.L., 1984. Fracture process zone of concrete cracks. *ASCE Journal of Engineering Mechanics*, 110(8): 1174–1184.

Du, J., Yon, J.H., Hawkins, N.M., Arakawa, K. and Kobayashi, A.S., 1992. Fracture process zone for concrete for dynamic loading. *ACI Materials Journal*, 89(3): 252–258.

Dugdale, D.S., 1960. Yielding of steel sheets containing slits. *J Mech Phys Solids*, 8: 100–104.

Elser, M., Tschegg, E.K. and StanzlTschegg, S.E., 1996. Fracture behaviour of polypropylene-fiber reinforced concrete under biaxial loading: An experimental investigation. *Composites Science and Technology*, 56(8): 933–945.

Gopalaratnam, V.S. and Shah, S.P., 1985. Softening response of plain concrete in direct tension. *Journal of the American Concrete Institute*, 82(3): 310–323.

Grzybowski, M. and Shah, S.P., 1990. Shrinkage cracking of fiber reinforced concrete. *ACI Materials Journal*, 87(2): 138–148.

Hillerborg, A., Modéer, M. and Petersson, P.-E., 1976. Analysis of crack formation and crack growth in concrete by means of fracture mechanics and finite elements. *Cement and Concrete Research*, 6(6): 779–781.

Hossain, A.B., Pease, B. and Weiss, J., 2003. Quantifying early-age stress development and cracking in low water-to-cement concrete – Restrained-ring test with acoustic emission. *Concrete* 2003(1834): 24–32.

Jansen, D.C., 1996. Post-peak properties of high strength concrete cylinders in compression and reinforced beams in shear. Evanston, IL: Northwestern University.

Jansen, D.C. and Shah, S.P., 1997. Effect of length on compressive strain softening of concrete. *ASCE Journal of Engineering Mechanics*, 123(1): 25–35.

Kim, B. and Weiss, W.J., 2003. Using acoustic emission to quantify damage in restrained fiber reinforced cement mortars. *Cement and Concrete Research*, 33(2): 207–214.

Kim, J.K. and Kim, Y.Y., 1999. Fatigue crack growth of high-strength concrete in wedge-splitting test. *Cement and Concrete Research*, 29(5): 705–712.

Krauss, P.D. and Rogalla, E A., 1996. *Transverse Cracking in Newly Constructed Bridge Decks*. Washington, DC: NCHRP Report, Issue 380, 132 pp.

Krenchel, H. and Shah, S.P., 1987. Surface Reinforcement of Concrete Structures with Fibers. *Materials Science to Construction Materials Engineering*, 1–3: 422–429.

Li, V.C., Stang, H. and Krenchel, H., 1993. Micromechanics of Crack Bridging in Fiber reinforced Concrete. *Materials and Structures*, 26(162): 486–494.

Liaw, B.M., Jeang, F.L., Du, J.J., Hawkins, N.M. and Kobayashi, A.S., 1990. Improved Nonlinear Model for Concrete Fracture. *ASCE Journal of Engineering Mechanics*, 116(2): 429–445.

Lofgren, I., Stang, H. and Olesen, J.F., 2008. The WST method: A fracture mechanics test method for FRC. *Materials and Structures*, 41(1): 197–211.

Mihashi, H. and Leite, J., 2004. State-of-the-Art Report on Control of Cracking in Early Age Concrete. *Journal of Advanced Concrete Technology*, 2(2): 141–154.

Moon, J.H. and Weiss, J., 2006. Estimating residual stress in the restrained ring test under circumferential drying. *Cement & Concrete Composites*>, 28(5): 486–496.

Østergaard, L., 2003. *Early-Age Fracture Mechanics and Cracking of Concrete Experiments and Modelling*. Copenhagen: Technical University of Denmark, 286 pp.

Raoufi, K., Bernard, E.S. and Weiss, J., 2010. Shrinkage Cracking Behavior of Fiber Reinforced Concrete: As Assessed Using the Restrained Ring Test. *Journal of ASTM International*, 7(7): 1–15.

Raoufi, K., Pour-Ghaz, M., Poursaee A. and Weiss, J., 2011. Restrained shrinkage cracking in concrete slab elements: the role of substrate bond on cracking development and opening. *ASCE Journal of Materials in Civil Engineering* (accepted for publication).

Rapoport, J.R. and Shah, S.R., 2005. Cast-in-place cellulose fiber reinforced cement paste, mortar, and concrete. *ACI Materials Journal*, 102(5): 299–306.

RILEM-TC-162-TDF, 2002. *Recommendations of RILEM TC 162-TDF: Test and Design Methods for Steel Fiber Reinforced Concrete: Bending test*. Bagneux, France: RILEM Publications SARL.

Roelfstra, R.E. and Wittmann, F.H., 1986. A numerical method to link strain softening with fracture in concrete, fracture toughness and fracture energy in concrete, in F.H. Wittmann (ed.), *Fracture Toughness and Fracture Energy in Concrete*. Amsterdam: Elsevier Science, pp. 163–175.

Sanjuan, M.A., Andrade, C. and Bentur, A., 1997. Effect of crack control in mortars containing polypropylene fibers on the corrosion of steel in a cementitious matrix. *ACI Materials Journal*, 94(2): 134–141.

Sarigaphuti, M., Shah, S.P. and Vinson, K.D., 1993. Shrinkage cracking and durability characteristics of cellulose fiber reinforced concrete. *ACI Materials Journal*, 90(4): 309–318.

Shah, H.R., 2004. *Quantifying the Performance of Steel Fiber Reinforcement in Mitigating Restrained Shrinkage Cracking in Concrete*. West Lafayette, IN: Purdue University.

Shah, H.R., Swartz, S.E. and Ouyang, C., 1995. *Fracture Mechanics of Concrete*. Chichester: John Wiley & Sons Inc.

Shah, H.R. and Weiss, J., 2006. Quantifying shrinkage cracking in fiber reinforced concrete using the ring test. *Materials and Structures*, 39(9): 887–899.

Shah, S.P., Marikunte, S., Yang, W. and Aldea, C., 1997. Control of cracking with shrinkage-reducing admixtures. *Advances in Concrete and Concrete Pavement Construction*, 1574: 25–36.

Shah, S.P., Sarigaphuti, M. and Karaguler, M.E., 1994. Comparison of shrinkage cracking performance of different types of fibers and wiremesh. *ACI Special Publication*, 142: 1–18.

Swamy, R.N. and Stavrides, H., 1979. Influence of fiber reinforcement on restrained shrinkage and cracking. *Journal of the American Concrete Institute*, 76(3): 443–460.

Tada, H., Paris, P.C. and Irwin, G.R., 1985. *The Stress Analysis of Cracks Handbook*. St Louis, MI: Paris Productions Inc., 538 pp.

van Mier, J.G.M. and van Vilet, M.R.A., 2002. Uniaxial tension test for the determination of fracture parameters of concrete: state of the art. *Engineering Fracture Mechanics*, 69(2): 235–247.

Voigt, T., Bui, V.K. and Shah, S.P., 2004. Drying shrinkage of concrete reinforced with fibers and welded-wire fabric. *ACI Materials Journal*, 101(3): 233–241.

Weiss, W. and Furgeson, S., 2001. Restrained shrinkage testing: The impact of specimen geometry on quality control testing for material performance assessment, in F.J. Ulm, Z.P. Bazant and F.H. Wittman (eds), *Concreep 6: Creep, Shrinkage, and Curability Mechanic of Concrete and Other Quasi-Brittle Materials*, Cambridge MA, Elsevier, pp. 645–651.

Weiss, W.J., 1999. *Prediction of Early-age Shrinkage Cracking in Concrete*, Evanston, IL: Northwestern University.

Weiss, W.J., Guler, K. and Shah, S.P., 2001. Localization and size-dependent response of reinforced concrete beams. *ACI Structural Journal*, 98(5): 686–695.

Weiss, W.J. and Shah, S.P., 1997. Recent trends to reduce shrinkage cracking in concrete pavements. *Aircraft/Pavement Technology*: 217–228.

Weiss, W.J., Yang, W. and Shah, S.P., 1998. Shrinkage cracking of restrained concrete slabs. *ASCE Journal of Engineering Mechanics*, 124(7): 765–774.

Weiss, W.J., Yang, W. and Shah, S.P., 2000. Influence of specimen size/geometry on shrinkage cracking of rings. *ASCE Journal of Engineering Mechanics*, 126(1): 93–101.

7

Fibrous materials reinforced composites production techniques

A. T. MARQUES, University of Porto, Portugal

Abstract: This chapter presents the main processing techniques used with organic matrices fibrous materials reinforced composites, for civil engineering applications. After a brief introduction, followed by the characterization of the main matrices, thermosets and thermoplastics used in these composites, the different techniques applied in various civil engineering applications are presented and discussed: pultrusion, braiding, RTM, filament winding, hot plate press and, finally, hand lay-up.

Key words: organic matrices, processing techniques, preforms, sandwich conception.

7.1 Introduction

The use of fibrous composite materials for civil engineering applications started very much with decorative purposes in mind, for example façade panels made by hand lay-up or continuous laminating processes. Due to the freedom of design afforded by these materials, it has been possible to develop specific constructions with different purposes: one-off types of architectural demonstration, made by hand lay-up or the assembling of different components; rescue housing and, more recently, student housing (such as the Technical University of Delft Students' Accommodations), where hand lay-up, resin transfer moulding (RTM) or even filament winding can be used.

Almost simultaneously, the development of pedestrian bridges and the strengthening of concrete structures appeared. In these examples, as well as in the case of vehicle bridges, pultrusion and sandwich construction techniques are the dominant methods used.

The use of fibrous materials reinforced composites is gradually being introduced to the concrete reinforcement itself, with the aim of replacing the conventional steel. Hence, we may use pultrusion, braiding or braiding pultrusion, either directly or to produce preforms for subsequent processing. It may be said that another type of cement-based fibrous reinforced composite material is winning certain market niches. Here, the spray-up of fibres with cement is a possible production route.

In the construction of piping for water supplies and sewage networks, the following techniques may be considered: filament winding, centrifugal casting or continuous filament winding (e.g. the DROLSTHOM process).

After a brief introduction, followed by the characterization of the main matrices, thermosets and thermoplastics used in these composites, this chapter discusses the different techniques applied when civil engineering applications are considered: pultrusion, braiding, RTM, filament winding, hot plate press, continuous laminating and, even, hand lay-up.

7.2 Organic matrices

Although the fibrous materials reinforced composites used for civil engineering applications are produced with thermosetting resins, there has recently been increasing interest in using thermoplastics as an alternative group of construction materials. The primary motivation for this has been environmental. The selection of the matrix will be a decision based upon an evaluation of different aspects:

- life cycle and cost analysis;
- fibre/matrix interface;
- wettability of fibres by the matrix – an advantage for thermosetting matrices;
- processability;
- mechanical, thermal and chemical properties for a given application;
- durability;
- reaction to fire and smoke toxicity;
- recyclability – an advantage for thermoplastic matrices.

In a fibrous reinforced composite, fibres are mainly responsible for the on-axis strength and stiffness properties. On the other hand, the matrices normally provide the off-axis and out-of-plane properties, as well as the chemical resistance.

The role of the matrix in a composite can be given as follows:

(i) Design

- damage tolerance;
- off-axis property;
- shear strength;
- compressive longitudinal strength;
- transverse strength;
- specific weight (also in relation to fibre specific weight);
- rupture strain (also depending upon the rupture strain of the fibre);
- minor Poisson's ratio;
- linear expansion coefficient (off axis and in relation to the fibre);
- impact.

(ii) Processing

- viscosity;
- adhesion property;
- processing temperature;

- cycle time;
- cost;
- exothermal cure (thermosetting);
- shrinkage after cure (thermosetting);
- shrinkage after moulding (thermoplastic).

(iii) Service

- fire and smoke behavior (also in combination with the fiber);
- chemical resistance;
- glass transition temperature or, as is applicable in the case of semi-crystalline thermoplastics, glass transitions and melting temperatures;
- linear expansion coefficient.

It is important to note that the fibre/matrix interface may play the following roles:

- load transfer and inhibition of crack propagation, for design purposes;
- welding and adhesion during processing;
- chemical protection and resistance to humidity in service.

7.2.1 Thermosetting matrices

Thermosets are polymers in which a crosslinking reaction occurs promoting chemical bonding between macromolecular chains and creating a three-dimensional (3D) network. This process, normally named cure, is irreversible unless treated by chemical action, i.e. thermosets cannot be recycled by thermal action. Table 7.1 presents the most common thermosets resins used in civil engineering applications. Unsaturated polyester resins are considered to be of general application, whilst epoxy or vinyl-ester resins are normally used with carbon fibres for concrete strengthening and seismic protection applications. Vinyl-ester resins are also used in the production of profiles by pultrusion. Phenolic resins are mainly used when good fire performance is required, i.e. fire reaction and low smoke toxicity.

7.2.2 Thermoplastic matrices

Although the use of thermoplastic matrix composites is not common in civil engineering applications, the development of new impregnation techniques using either polymer melting, solvents or low viscosity precursors and the intimate fibre/matrix contact will overcome impregnation difficulties, which are the main barriers to entering this market.

Recyclability, together with specific properties such as higher toughness, can be a competitive advantage for fibre reinforced thermoplastic matrix composites.

Table 7.2 presents the thermoplastic matrices most likely to be used in civil engineering, both for non-structural and for structural applications.

Table 7.1 Thermosetting resins

Property / Material	Specific weight (Mg/m^3)	Young's modulus (GPa)	Tensile strength (MPa)	Notched impact strength kJ/m^2	Fracture toughness K^1_c ($MPa.m^{-1/2}$)	Coef. of thermal expansion ($10^{-6}.°C^{-1}$)	Tmax service (°C)	Rupture strain (%)	Post-cure shrinkage (%)	Relative cost per kg*
Unsaturated polyester	1.1–1.5	2–4.5	40–90	1–2.5	0.5–1.7	100–180	90–130	2–2.5	5–15	1
Vinylester	1.1–1.2	3.5–4	65–85			40–70	100–150	3–6	8–9	2–4
Epoxy	1.1–1.4	2–5	50–100	1–8	0.5–2	50–120	120–180	2–8	0.1–2.5	3–20
Phenolic	1.2–1.5	2.5–4.5	30–60	1–2	0.8–1.5	115–130	140–200	1–3	0.1–1.5	1–2

* Reference cost 1 has been allocated to unsaturated polyester

Table 7.2 Thermoplastic matrices

Property / Material	Specific weight (Mg/m3)	Young's modulus (GPa)	Tensile strength (MPa)	Rupture strain (%)	Notched impact strength kJ/m^2	Fracture toughness K^1_c ($MPa.m^{-1/2}$)	Tmax service (°C)	α (10^{-6}/°C)	*Relative cost per kg
PP	0.9–0.93	0.9–1.8	20–50	50–900	2–5	1.5–4.5	90–120	35–100	1
PEAD	0.95–0.97	0.9–1.1	20–30	100–1300	5–20	1.5–2	100–120	100–200	0.96–1.06
PC	1.15–1.2	2–2.5	60–70	90–150	50–100	2–4.5	100–145	120–130	2.5–4
PA 66	1.05–1.4	1–4	50–100	10–300	3–90	1.5–5	60–110	80–150	2.5–4
PET	1.3–1.4	2.8–4	50–75	60–300	2.5–7	4.5–5.5	55–120	70–120	1.1–1.3
PVC	1.3–1.6	2.25–4	40–65	10–100	4–140	1.5–5	50–100	60–180	0.7–1.6
POM	1.39–1.41	1.5–4.5	45–90	20–75	7–25	2–5	75–120	90–200	2.5–4
ABS	1.04–1.2	1–3	30–55	1.5–100	5–50	1–4	80–120	100–250	1.5–2
PEEK	1.3	3.7–4	70–100	30–150	6–7	2.5–4	240–280	70–200	70–90

* Reference cost 1 has been allocated to polypropylene PP; α – coefficient of linear expansion

7.3 Fibres

The properties of the most common fibres used in civil engineering are presented in Table 7.3. As can be seen in this book, textile technologies are increasingly being used to produce preforms of near net structural shape. Hence, it is possible to obtain structural-like shapes in 2D fabrics, 3D braiding, 3D non-woven fabrics, knitted and stitched layers and 3D interlacing tissues.

It is important to note the increased use of natural fibres in civil engineering applications, particularly in countries such as Brazil, Argentina, India and China where different types of natural fibres are available. Although there is a great need for research to improve the specific properties of the fibrous composite materials produced, the use of locally available fibres, together with the development of appropriate technologies, will be a possible way towards a more sustainable world.

7.4 Production techniques: general characteristics

The main characteristics of the processing techniques used with fibrous materials reinforced composites applied in civil engineering are presented in Table 7.4. The table refers specifically to thermosetting (currently the most-used matrices for civil engineering applications) and thermoplastic matrices.

Although the borders between artisanal (handicraft) and industrial processes are not clear, the distinction can be made as follows. Artisanal processes are those which are very much dependent on human skills, with low production rates and high levels of personnel working hours. At the other end of the spectrum, industrial processes are those which involve less human intervention, are very much dependent upon machine parameters, and are to be considered for medium to high production rates.

Some considerations have to be made regarding wet and dry processing. The first production techniques for polymeric matrix composite materials began with thermosetting resins because they are, generally, liquid at room temperature and can easily wet the fibres. Later on, with the advent of prepregs and moulding compounds, processes were developed in which the fibres are already impregnated with resin. Hence, this is called the dry process. The thermoplastic-based composite materials are processed, in general, in a dry state, which means there is no need to impregnate the fibres as the process will transform a semi-product like LFT (Long Fibre Thermoplastic), CFTP (Continuous Fibre Thermoplastic) e.g. Towpregs, commingled yarns, etc.

The definition of process efficiency can be given as:

$$\text{Efficiency} = \frac{\text{Value of production rate per hour}}{\text{(equipment depreciation rate + man power) per hour}}$$

In the following points, descriptions of the processing techniques outlined in Table 7.4 will be presented.

Table 7.3 Fibre properties

Property / Fibre	Specific weight (Mg/m^3)	Young's modulus (GPa)	Tensile strength (MPa)	Specific modulus	Specific strength	Rupture strain (%)	Coefficient of thermal expansion ($10^{-6}/°C$)	*Relative cost per kg
Glass								
E	2.54	70	2200	27.6	866	3–3.5	3–5	1
R	2.5	86	3200	34.4	1280	3.5–4	4	4–6
S	2.53	86	3500	33.9	1383	4.1		6–8
A	2.7	75	1700	27.7	666			0.75
Aramidic								
Kevlar® 29	1.44	59	2640	41	1833	3–5	–3 to –3.5	25–40
Kevlar® 49	1.45	130	2900	89.7	2000	1.5–3	–2 to –5	60–75
Kevlar® 149	1.47	146	2410	99.3	1639	1–2	–4 to –2	70–180
Carbon								
HS	1.80	230	4500	128	2500	2.0	–0.1	65–80
IM	1.76	290	3100	165	1761	1.1	–0.5	120–150
HM	1.86	380	2700	204.3	1452	0.7	–1.2	
UHM	1.94	588	3920	303	2021	0.7	–0.9	
Natural fibres								
Jute	1.4–1.6	6.0–6.5	120–145	3.75–4.3	75–100	1.5–2.5	20–30	0.3–1.5
Sisal	1.4–1.6	15–30	400–800	9.5–21	250–570	1.5–4.0	18–30	0.5–0.6
Flax	1.45– 1.5	9.0–20	450–550	6–14	300–380	0.5–3	16–30	1.5–4
Hemp	1.4–1.5	5–20	500–900	3.33–14	333–640	0.5–2.5	15–25	0.6–2

* Reference cost 1 has been allocated to E glass fibre

Table 7.4 Characteristics of production techniques

Characteristic process	Matrix		Production rate		Transformation process		Moulding pressure				Process type		Process efficiency
	Thermosetting	Thermoplastic	Artisanal (2)	Industrial	Wet	Dry	0	Up to 10 daN/cm^2	Up to 100 daN/cm^2	500 daN/cm^2	Open mould	Closed mould	
Hand lay-up	X		X		X		X				X		1–3
Spray up	X		X	X	X		X				X		1–4
Centrifugal casting	X			X	X		X				X		3–10
Continuous lamination	X			X	X		X				X		4–8
Pultrusion	X	X		X	X	X		X				X	5–15
Filament winding													
– In situ	X	X (CFT)[1]		X	X	X		X			X		4–12
– Factory	X			X	X	X		X			X		
Cold press	X			X	X			X				X	5–10
Hot plate press													
BMC[(1)], MC[(1)]	X			X		X		X	X			X	10–20
LFT[(1)]		X		X		X			X			X	12–25
RTM[1]	X	X	X	X	X			X			X	X	5–10
Injection moulding	X	X		X		X				X		X	10–30

[1] RTM, Resin Transfer Moulding; BMC, Bulk Moulding Compound; SMC, Sheet Moulding Compound; LFT, Long Fibre Thermoplastic; CFT, Continuous Fibre Thermoplastic.
[2] Artisanal: the word is associated to a slow rate process, where personnel time is considerable.

7.5 Processing: materials and parameters

7.5.1 Hand lay-up

Although the hand lay-up process requires very little investment, it is used only when a reduced number of pieces are needed, i.e. for low series production. It is a slow process and depends very much upon the skill of the workforce. However, this technique is often employed for large and complex parts, when a good surface finish is required on one side only. In Fig. 7.1, the materials and tools needed, as well as the production technique, can be seen.

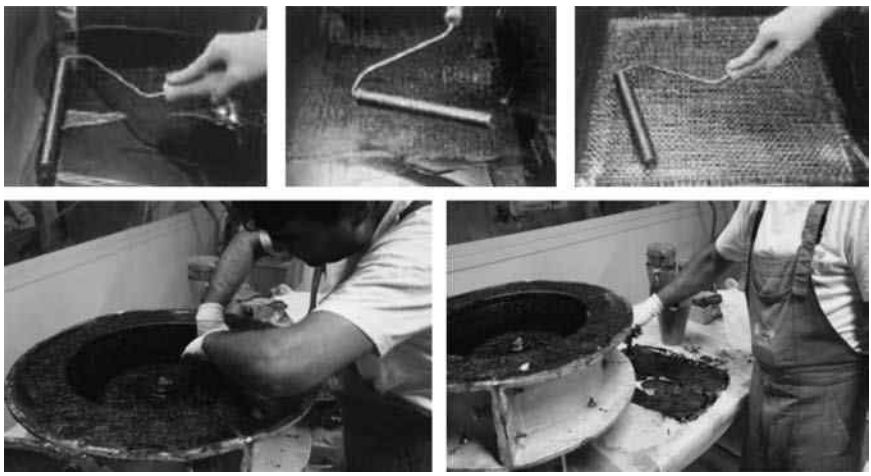

7.1 Hand lay-up process (Composite Materials Laboratory, INEGI, Porto, Portugal).

Typically, one uses the following materials, tools and moulds:

Fibres

Fibres are used in the form of chopped strand CSM or continuous filament mat (CFM) (300 to 600 g/m^2), woven–roving (450 to 900 g/m^2) or 'COMBI' (a combination of CSM and woven) roving. It is also possible to use a 'COREMAT', in order to increase specific stiffness.

Resins

The most-used resin is unsaturated polyester. The selection of the type of polyester resin (orthophthalic, isophthalic and bisphenolic) depends upon the application; for example, the orthophthalic type is used only when the required performance level is low. The cure of the resin implies the use of an initiator (a catalyst such as

peroxide methylethylketone) and, eventually, an accelerator (such as cobalt octoate) and an inhibitor (such as hydroquinone), following the specifications set out by the suppliers of the raw materials.

Vinyl ester and epoxy resins are also used, although less commonly. When fire/smoke properties are too strict, the use of phenolic resins may be required.

Pigments and fillers

Fillers can be used, for instance, to reduce the cost or to enhance a specific property of a product. On the other hand, pigments are used to give a specified colour to the product.

Core materials

If the product has a sandwich construction, core materials (such as foams and honeycombs) are used. The idea is to create a product with high specific stiffness and high specific strength. The sandwich construction can be applied with other processing techniques.

Table 7.5 shows the properties of some typical core materials.

Release systems

The surface quality of the final product can be enhanced if an adequate release system is used. This can be made with the following:

- release film (e.g. MELYNEX®)
- PVA – polyvinyl alcohol
- wax

Table 7.5 Structural core materials properties

Property / Core	Specific weight (Mg/m^3)	Young's modulus (GPa)	Compressive strength (MPa)	Tensile strength (MPa)	Rupture strain (%)	Coefficient of thermal expansion (10^{-6}/°C)	*Relative cost per kg
PU foam	0.03–0.08	0.02–0.07	2–3	3–5			1
PVC foam	0.04–0.4	0.03–0.5		1–13	3–5	20–45	9–20
PS foam-closed cell	0.045–0.055	0.025–0.03	0.25–1.5	1–1.5	3.5–.5	50–80	2–2.5
Cork	0.1–0.25	0.001–0.05	0.5–2	0.5–2.5	20–100	100–250	2–12
Honeycomb NOMEX®	0.02–0.06		0.25–3		6–20		3–30

PU, polyurethane; PVC, polyvinyl chloride; PS, polystyrene; NOMEX® from Du Pont de Nemours.

Tools

The tools needed are, essentially, a brush and a roller. Specific rollers exist for different purposes (e.g. a roller to help remove trapped air) and may be used. One also needs scissors or a knife to cut the fibres to size. A balance is used to carefully weigh the different components.

Moulds

The moulds are made from wood or a composite material. As no pressure is involved in the process, the moulds are generally light structures.

Having collected all the requisite materials, this technique requires the following steps:

- mould preparation;
- application of release systems (please note that, with some release systems, it may be necessary to apply several layers of a release agent);
- application of a gel-coat (this is a rich-resin layer, or resin only, normally pigmented);
- mix the cure system with the resin;
- lay and impregnate individual fibre layers, sequentially;
- cure and, eventually, post-cure according to resin supplier's instructions;
- demoulding.

7.5.2 Spray-up

Although the spray-up process requires both cutting and spray equipment (Fig. 7.2), it is also a relatively slow process, to be used for a small/medium series

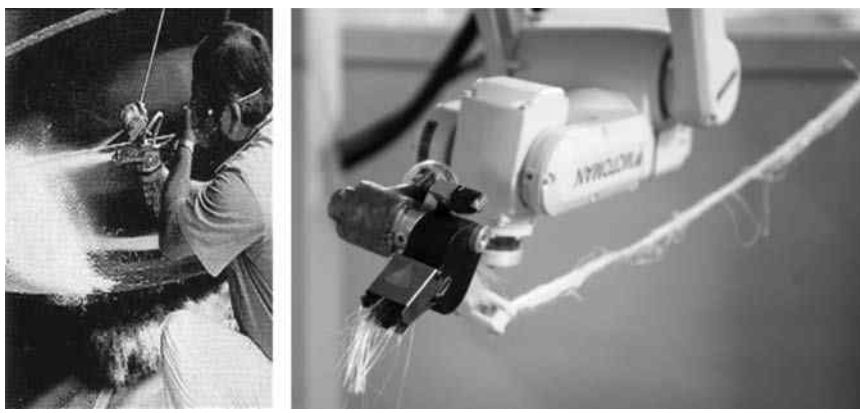

7.2 Spray-up process (Composite Materials Laboratory, INEGI, Porto, Portugal).

production size. In terms of materials, the main difference in comparison with hand lay-up is the fact that the fibres are cut and projected in the mould, whilst the resin is sprayed. For better impregnation, a roller may be used at the end of the spray-up process. The moulds are similar to those used with hand lay-up.

This process can be 'robotized' if the products to be made are of a regular shape (e.g. a parabolic antenna).

7.5.3 Centrifugal casting

Centrifugal casting is essentially used to produce pipes for sewage and water supplies. The technique consists of a cut/spray unit that goes through the interior of a cylindrical metallic mould in rotation, and distributes the fibre and resin along the length of the mould. The centrifugal effect of the rotation projects the fibre and resin against the mould wall, creating the impregnation effect.

The raw materials used can be similar to those used with the spray-up technique. However, a high content of sand is normally used, particularly for sewage applications.

7.5.4 Continuous lamination

Continuous lamination is used to produce flat panels (sheet) or corrugated channel sheets (1–2 m wide), continuously. The latter are used as a type of large roof tile, which can be either translucent or opaque.

The materials used are the following:

(i) Fibre: CSM (chopped strand mat); roving
(ii) Resin: unsaturated polyester
(iii) Fillers and pigments
(iv) Release film

The CSMs are continuously extended over the release film (or the roving are cut and sprayed) that transports the resin. Then a cover release film is placed over the materials, and the full set goes through a type of mould, slightly heated, where the impregnation and curing takes place. Finally, the sheets are cut to specific dimensions.

7.5.5 Pultrusion

The pultrusion process (Fig. 7.3) is used to produce specific profiles (i.e. I, U, L, etc.).

Moreover, it can be used to produce reinforcing profiles for concrete structures, replacing the equivalent steel profiles (Fig. 7.4).

This technique may be considered to be a wet transformation process if liquid thermosetting resin is used, or a dry process in the case of prepreg thermosetting systems or thermoplastic towpregs or commingled yarns. Bearing in mind the

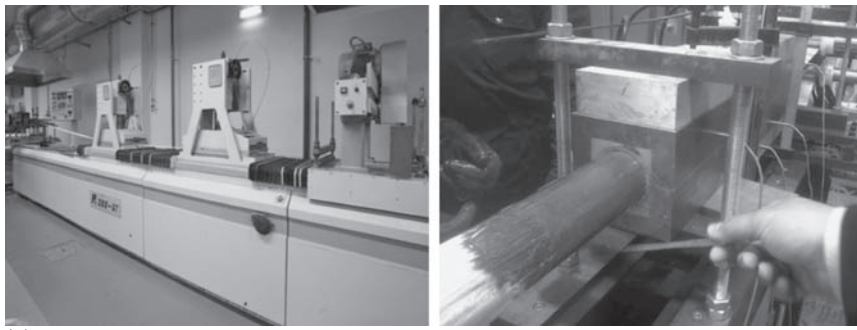
(a) (b)

7.3 Pultrusion process: (a) Composite Materials Laboratory, INEGI, Porto, Portugal; (b) POLIGHT S.A., Viana do Castelo, Portugal.

7.4 Reinforcing profiles (www.strongell.com).

different situations, the die has to be designed according to the shape and dimensions of the profile, as well as with the type of matrix system. Basically, in the case of the wet process, the different steps in this technique are the following:

- Roving only (or combined with CSM) are continuously pulled through a resin bath with all necessary curing elements, as well as release agents and fillers.
- The impregnated fibre goes through a die with three main areas: preheating, heating and cooling.
- The profile is cut to the required dimensions.

In the case of prepreg thermosetting systems or thermoplastic towpregs/commingled yarns, the semi-product (prepreg or thermoplastic towpreg or commingled yarn) goes through the heated die of which the first part has been sufficiently heated to allow the matrix to reduce viscosity and fully impregnate the fibre, being subsequently cooled and cut to size.

The materials used are the following:

- fibres: glass or carbon fibre roving; continuous filament mat or chopped strand mat;
- matrix: unsaturated polyester, vinyl-ester, epoxy or phenolic; different thermoplastic matrices (pa, pp, pom, etc.);
- fillers and pigments;
- Release agent.

The release agents are normally mixed internally with the matrix, or are applied externally.

The dies are made with steel. However, care must be taken with the specific finishing depending upon the type of matrix.

An example of a profile produced with this technique is shown in Fig. 7.5.

(a) (b)

7.5 Pultruded profile application: (a) www.strongell.com; (b) POLIGHT S.A.

Recently, a radius pultrusion production technique has been presented by Thomas GmbH. This process can be applied for bridge beams, pipes and other profiles.

7.5.6 Filament winding

Filament winding (Fig. 7.6) is a technique where fibres passing through a resin bath with all the curing agents or pre-impregnated fibres (prepregs-thermosets, or towpregs-thermoplastic) are wound in a rotational mandrel, allowing for a specific orientation according to the loading requirements. This technique can be used for pillar strengthening or in the production of water and sewage pipes, with given specifications. Pressure vessels for water and gas storage can also be produced using this technique. The ratio between rotational and translational speeds gives the winding angle.

The materials used with this technique are similar to those of pultrusion and adequate to the specific processing conditions. The size of the products made by filament winding can vary from 100 mm to 5000 mm (or even more), the latter being more frequently used in civil engineering when *in situ* techniques are required. Please note that before any mould takes place, a MELINEX® film is wound, and a gel-coat with a surface mat may be applied (a chemical-resistant layer with CSM may also be applied after the gel-coat, if necessary).

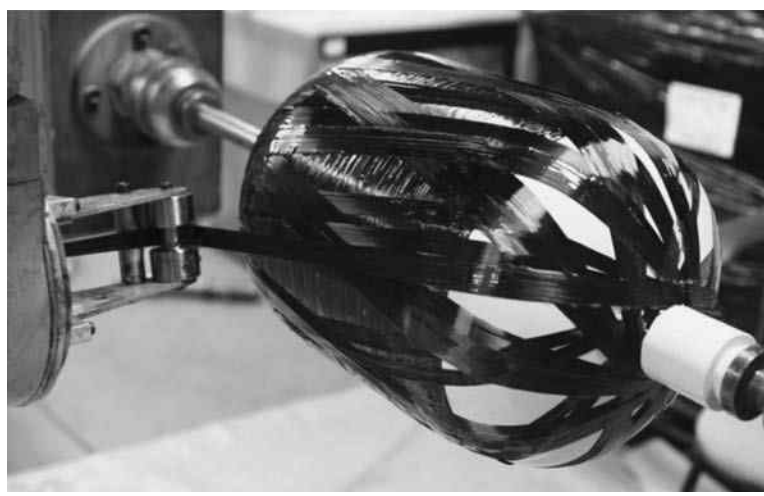

7.6 Filament winding process.

7.5.7 Cold press

In the cold press technique, a set of layers (chopped strand mat, woven-roving or preforms) is placed inside the mould, under pressure, to be impregnated with resin and cured. Alternatively, fibre preforms can be used. The type of materials used is similar to those used in hand lay-up, bearing in mind the specificity of the resin system to allow a faster cure.

7.5.8 Hot plate press

With hot plate press technology (Fig. 7.7), it is possible to process different semi-products, either thermosetting moulding compounds (BMC, bulk moulding compound; DMC, dough moulding compound; SMC, sheet moulding compound), thermosetting prepregs (glass or carbon fibre epoxy) or thermoplastic semi-products (LFT, long fibre thermoplastics and towpregs). The technique implies the placement of the semi-products inside the mould, after which a release system is applied, followed by the application of pressure and temperature, according to a specific set of conditions relating to pressure, temperature and time of application.

Some typical products for civil engineering applications obtained with this manufacturing technique are presented in Fig. 7.8.

7.7 Hot plate press (Composite Materials Laboratory, INEGI, Porto, Portugal).

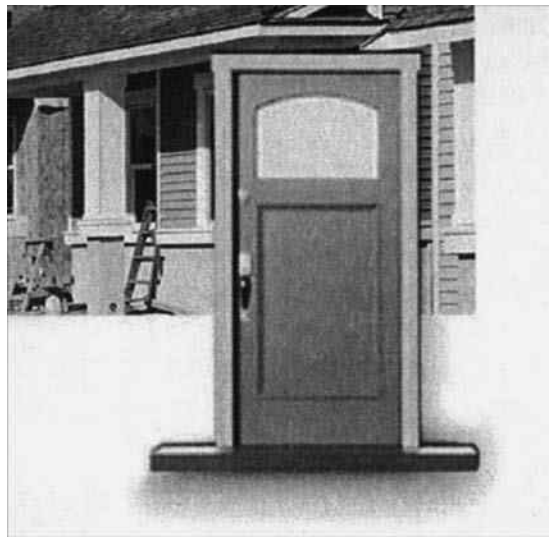

7.8 Products made with BMC or DMC.

7.5.9 Resin transfer moulding

Resin transfer moulding (RTM) is the designation for a technology where, in general, a fibre preform is placed in a female mould, the male mould closes leaving a gap to allow the resin to be injected and to impregnate the fibres (Fig. 7.9). For processes that are similar but which have only a female mould and a 'bag' that may allow for the application of pressure and/or vacuum (VARI, vacuum assisted resin injection; SCRIMP, SEAMANS Corporation resin injection moulding process, normally used for large boats or structures), the name used to describe this is an 'umbrella'.

The application of injection or vacuum pressure needs to be adequate in order to avoid voids and/or dry parts being formed. Typically, the following materials, equipment and moulds are used:

Fibres

The fibres used are in the form of chopped strand mat (CSM) or continuous filament mat (CFM) (300 to 600 g/m^2), woven-roving (450 to 900 g/m^2) or 'COMBI' (a combination of CSM and woven-roving). It is also possible to use a 'COREMAT', in order to increase specific stiffness.

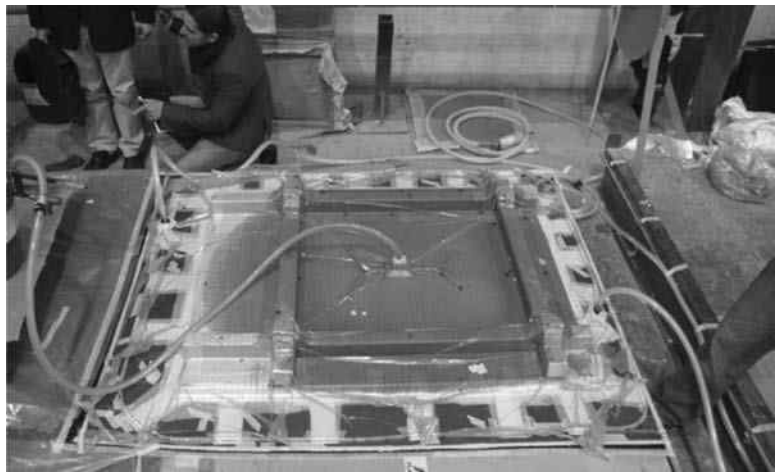

7.9 Resin Transfer Moulding process – VARTM (Estaleiros Navais de Peniche, Portugal).

It is quite common to use preforms made by braiding, weft knitting, warp knitting and embroidery, as well as 3D weaving or multidirectional fabrics.

Resins

The most-used resin is unsaturated polyester. The selection of the type of polyester resin (orthophthalic, isophthalic and bisphenolic) depends upon the application, for example the orthophthalic type used only when the required performance level is low. The cure of the resin implies the use of an initiator (a catalyst, such as peroxide methylethylketone) and, eventually, an accelerator (such as cobalt octoate) and an inhibitor (such as hydroquinone), following the raw materials suppliers' specifications.

Although less commonly, vinyl ester and epoxy resins are also used. When fire/smoke properties are too strict, the use of phenolic resins may be required.

Pigments and fillers

Fillers can be used, for instance, to reduce the cost or to enhance a specific property of a product. On the other hand, pigments are used to give a specified colour to the product.

Core materials

If the product has a sandwich construction, core materials (such as polyurethane, polyvinyl chloride, polypropylene or polystyrene foams, honeycombs and cork)

are used. The idea is to create a product with high specific stiffness and high specific strength.

Release systems

The surface quality of the final product can be enhanced if an adequate release system is used. This can be made with the following:

- release film (e.g. MELYNEX®)
- PVA – polyvinyl alcohol
- wax

Equipment

Depending upon the type of RTM, the following equipment may be used:

- vacuum pump
- pressure equipment
- pot
- valves, pipes and nozzles

Moulds

In the case of an RTM with resin injection and vacuum applied, when high quality products (with tight tolerances) are required, a male and female metallic mould is used. However, a composite mould may also be used.

For SCRIMP or VARTM techniques, a female mould made with composite or metallic materials, can be used, together with a vacuum bag. This technique, although of relatively low investment, can manufacture products with higher fibre volume content than the hand lay-up process, as well as producing fewer voids, a better surface finish and tighter tolerances. Moreover, the technique requires less manpower.

Considering the size of products normally required for civil engineering applications, SCRIMP can be an interesting alternative.

7.5.10 Injection moulding

Injection moulding is particularly suitable for high volume productions. Basically, the composite material is carried by a screw through a heated barrel and is injected, under a given pressure, into a metallic mould. The shape and size of the screw depends upon the type of matrix – thermoplastic or thermosetting.

In the case of a composite compound with a thermoset matrix, care must be taken to avoid premature curing inside the barrel.

The most common compounds and moulding parameters are presented in Tables 7.6 and 7.7 for thermoplastic and thermoset matrices respectively.

Some typical products for civil engineering applications obtained with this manufacturing technique are presented in Fig. 7.10.

Table 7.6 Thermoset moulding compounds for compression moulding

Type	Description	Matrix	Fibre	V_f (%)	Processing parameters
BMC	Bulk Moulding Compound	Unsaturated polyester	Glass plus fillers	15–25	Pressure (MPa): 1–15 Temperature (°C): 130–170
DMC	Dough Moulding Compound	Unsaturated polyester	Glass plus fillers	10–25	

Table 7.7 Thermoplastic composite for injection moulding

Type	Description	Matrix
SFRTP	Short (up to 2 mm) Fibre (glass or carbon) Reinforced Thermoplastic, with V_f up to 50%	PP, PEAD, PC, PA, PET, PEEK, PVC, POM, ABS
LFT	Long (10m) Fibre (glass or carbon) Reinforced Thermoplastic, with V_f up to 30%	PP, PEAD, PC, PA, PET, PEEK, PVC, POM, ABS

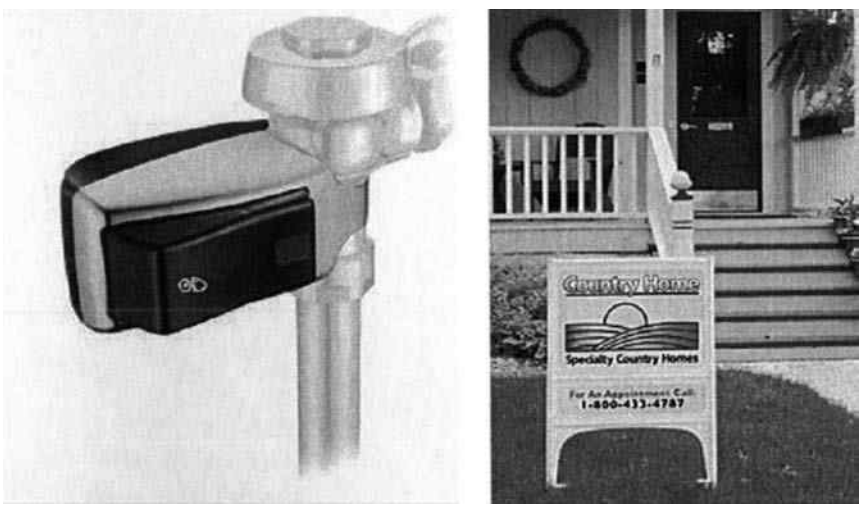

7.10 Injection moulding products made with SFRTP or LFT.

7.6 Strengthening of structures

7.6.1 Adhesive bonding

Fibrous materials reinforced composites can be used to strengthen concrete structures (Fig. 7.11).

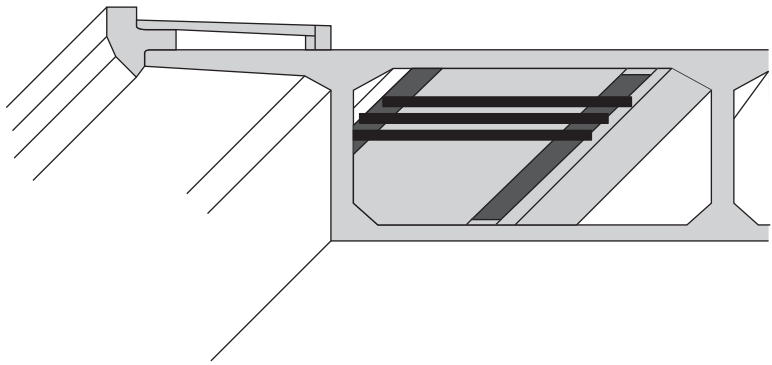

7.11 Strengthening of concrete using CFRP thin profiles.

The technology is used either to increase the load-carrying capacity of current concrete structures (e.g. bridges) or to cater for degradation problems (such as cracking, or the corrosion of metal reinforcement). Normally, a continuous band of carbon fibre reinforced epoxy or vinyl ester resin (CFRP) is produced by pultrusion, being subsequently bonded to the concrete structure. The bonding technology can be applied using either room temperature or high-temperature adhesives. With high-temperature curing adhesives, the strengthened structure can withstand working conditions with higher temperatures.

Besides the strengthening application, the adhesive technology can also be used to join different products (such as pipes and profiles).

7.6.2 *In situ* technology

The strengthening technology can be applied in the *in situ* manufacturing and curing of strengthening bands. Different materials and application technologies are available but, basically, they imply the use of dry or slightly impregnated fabrics, which are applied to the concrete structure using a liquid thermoset resin (Fig. 7.12).

The typical application procedure is as follows:

- Surface defects are removed mechanically, alternatively we can fill the defects using an adhesive paste.
- Cleaning of the surfaces to be strengthened using acetone.
- Mix the cure system with the resin.

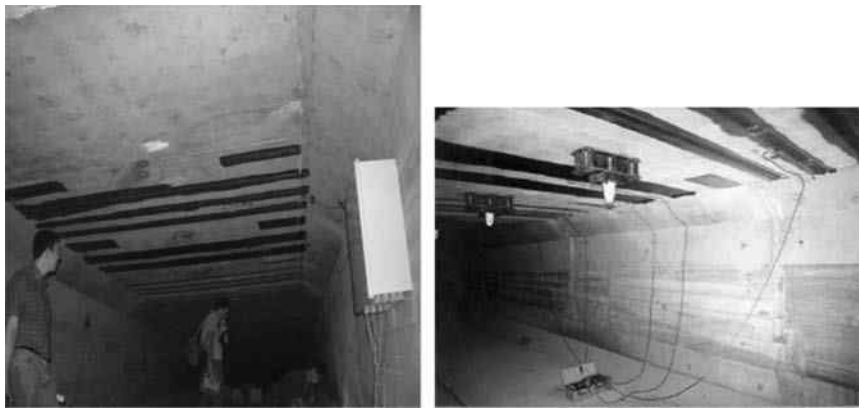

7.12 Strengthening of concrete structures – bridge (Bridge Nª S.ª da Guia = Ponte de Lima, Portugal).

- Lay and impregnate individual fibre layers (e.g. carbon fabrics), sequentially.
- Cure and, eventually, post-cure according to resin supplier's instructions.

A completely different situation can be described for the reinforcement of concrete pillars and columns. Here, the intention can also be the design of a structure with much better performance in terms of its anti-seismic behaviour. The most common situation can be seen in Fig. 7.13. The filament winding technique is used, but the 'mandrel' (i.e. the column to be reinforced) does not rotate. However, the moving carriage, in addition to its longitudinal movement, rotates around the column to be reinforced. In general, carbon fibres impregnated with an epoxy resin are used, and the final product has high-volume fibre content.

7.7 Properties of composite material laminates

Using different processing techniques, it is possible to produce composite materials laminates within a large range of values. The final properties depend upon the type of fibre, the type of resin, the type of fillers, the fibre-volume content V_f (related to the process and type of fibre construction), the orientation of the fibres, the stacking sequency and the void content (an indication of the quality of the laminate). Table 7.8 show the mechanical, physical and thermal properties of some typical laminates.

7.8 Conclusions

The production techniques for fibrous materials reinforced composites can be used in the manufacture of a large range of products for civil engineering applications. They may vary from low load carrying products to highly demanding

Table 7.8 Properties of typical composite materials laminates

Laminate \ Property	Specific weight (Mg/m^3)	Young's modulus (GPa)	Tensile strength (MPa)	Fracture toughness K^1_C ($MPa.m^{-1/2}$)	ε_r (%)	Tmax Service (°C)	α (10^{-6}/°K)	V_f (%)	*Relative cost/kg
GFRP									
Epoxy/UD glass:				3–20	1–4	120–200	8–10	70	10–15
Longitudinal	1.90	42	750						
Transverse	1.90	12	50						
GFRP									
Polyester/glass UD:						90–130	8–10	50	3–10
Longitudinal	1.93	38	750		1.8				
Transverse	1.93	10	22		02				
GFRP									
Polyester/CSM	1.4–1.6	7–9	75–95		1–3	90–130		30	1
GFRP									
Polyester/glass						90–140	10–12	50	
Woven:									2–6
Longitudinal	1.7–1.8	20	600						
Transverse	1.7–1.8	19	550						
AFRP									
Epoxy/Aramide UD:					~2	120–200	–0.3–0.5	50	
Longitudinal	1.3–1.5	60	1100						
Transverse	1.3–1.5	8	35						
AFRP									
Epoxy/Aramide Woven:						120–200	–4.0–5.5	50	
Longitudinal	1.3–1.4	30	500						
Transverse	1.3–1.4	30	450						

CFRP – High-strength carbon fibre									
Epoxy/UD:						120–200	–0.1	60	20–30
Longitudinal	1.5–1.7	130–200	1750–2000	10–100					
Transverse	1.5–1.7	8–10	25–40	2–80					
CFRP – High-strength carbon fibre									
Epoxy/Woven:						120–200	–0.5	60	20–30
Longitudinal	1.5–1.7	70	800						
Transverse	1.5–1.7	65	750						
CFRP – Intermediate modulus carbon fibre									
Epoxy/UD:						120–200		60	20–30
Longitudinal	1.5–1.7	170	2400						
Transverse	1.5–1.7	9	80						
CFRP – Intermediate modulus carbon fibre									
Epoxy/Woven:					~1	120–200		60	20–30
Longitudinal	1.5–1.7	90	900						
Transverse	1.5–1.7	90	850						
DMC/BMC	1.8–2	10–14	30–70	3–6	1–2	120–190	20–30*	10–25	2–3
SMC	1.75–2	10–14	50–100	4–12	2–3.5	150–200	15–30*	10–40	3–4

7.13 In situ strengthening of columns (The ROBO Wrapper I™).

ones, with requirements ranging from merely aesthetics to strengthening or increasing the performance of concrete structures. Depending upon the specific requirements, the technology selection will be made regarding the possibility of creating a product with low- or high-volume content, adequate specific strength and stiffness, adequate chemical resistance and adequate size and shape. For similar applications, a procedure is needed to adequately select materials and evaluate the technologies.

Bearing in mind that civil engineers are now more open to the use of fibrous materials reinforced composites, and considering the possibilities provided by the textile technology in terms of producing different fabrics and preforms, it is likely that different types of composite materials and related technologies will be used in the future for civil engineering applications. Moreover, the ease with which fibrous materials reinforced composites can be processed, may be exploited in remote areas and in developing countries using the so-called appropriate technologies. In other words, use local resources (such as natural fibres and resins) and/or recovered materials (e.g. convert plastic bags into composite matrices) to produce corrugate or flat sheets, or other products, with an adapted technology. This can help to give people a better life and contribute to a more sustainable world.

7.9 Bibliography

1. F. L. Mathew and R. D. Rawlings, *Composite Materials: Engineering and Science*. London: Chapman & Hall, 1995.
2. P. C. Powell, *Engineering with Fibre-Polymer Laminates*. London: Chapman & Hall, 1994.
3. C. A. Dostal, *Engineering Materials Handbook – Vol. 1: Composites*. Boca Raton, FL: CRC Press (ASM International), 1987
4. Technomic, *The Composite Materials Handbook (MIL-17)*, 3 volumes. Boca Raton, FL: CRC Press, 1999
5. J. A. Quinn, *Composites Design Manual*. Liverpool: James Quinn Associates, 2007
6. J. L. Clarke (ed.), *Structural Design of Polymer Composites. EUROCOMP Design Code and Handbook*. London: E&FN Spon, 1996
7. G. Akovali, *Handbook of Composite Fabrication*, Shrewsbury: RAPRA Technology, 2001
8. R. M. Christensen, *Mechanics of Composite Materials*. New York: Dover Publications, 2005 (ISBN: 0–486–44239-X).
9. A. Kelly (and C. Zweben (eds)), *Comprehensive Composite Materials*. Amsterdam: Elsevier, 2000 (ISBN: 0–08–042993–9).
10. S. W. Tsai (ed.), *Strength and Life of Composites*. Stanford: JEC Composites, 2008 (ISBN: 978–0–9819143–0–5).
11. D. Gay and S. V. Hoa, *Composites Materials: Design and Applications* (2nd edn), Baton Rouge, FL: CRC Press, 2007 (ISBN: 978–1–4200–4519–2).
12. M. Ashby, H. Shercliff and D. Cebon, Materials: Engineering, Science, Processing and Design (1st edn). Amsterdam: Elsevier, 2007 (ISBN 978–0–7506–8391–3)
13. M. Ashby, *Materials Selection in Mechanical Design* (3rd edn). Oxford: Butterworth-Heinemann, 2005 (ISBN 0–7506–6168–2).
14. M. Ashby and K. Johnson, *Materials and Design: The Art and Science of Material Selection in Product Design*. Oxford: Butterworth-Heinemann, 2002 (ISBN 0–7506–5554–2).
15. *Granta's CES EduPack 2009*. Cambridge: Granta Design, 2009.

8

Fibrous materials reinforced composite for internal reinforcement of concrete structures

R. FANGUEIRO, University of Minho, Portugal and
C. GONIGHO-PEREIRA, The Polytechnic
University of Setubal, Portugal

Abstract: The concrete construction industry deals with the deterioration of concrete structures mainly caused by the corrosion of reinforcing steel in concrete. Several techniques have been developed to reduce corrosion in steel-reinforced concrete elements, but the use of composite rods as concrete reinforcement material seems to be an effective solution to overcome durability problems of traditional steel-reinforced concrete structures. This chapter presents the composite rods raw materials and manufacturing processes and discusses mechanical and durability performance, and bond behaviour between rod and surrounding concrete and self-monitoring capabilities. Applications of composite rods are also presented.

Key words: composite rods, rods mechanical performance, rods durability performance, bond behaviour, self-monitoring rods.

8.1 Introduction

The concrete construction industry deals every day with the deterioration of concrete structures. Nowadays, a large number of bridges, buildings and other structural elements require rehabilitation and repair and their maintenance has become an increasingly serious problem. Concrete structures, when subjected to repeated loading and to aggressive environmental agents, present a decrease in terms of mechanical properties and durability performance. Corrosion of steel is one of the most serious problems of concrete structures.

Corrosion of reinforcing steel in concrete is the most significant process affecting reinforced concrete structures. The two most important causes of corrosion of the reinforcing steel are the carbonation and chloride contamination of concrete. Carbonation is a problem that mainly affects buildings. Chloride contamination affects structures that are exposed to de-icing salts or marine environments. Other less-common cause of corrosion are acidic gases such as sulphur dioxide, aggressive ions such as sulphates, fluorides and bromides, and stray electrical currents.

Corrosion is accompanied by a loss of rebar cross-section and a build-up of corrosion products. The corrosion products occupy a larger volume than the original metal from which they were derived. This generates the tensile stresses causing cracking and spalling of the concrete cover. Very often the first indication of a problem is the appearance of a crack following the line of reinforcement.

Several techniques have been developed to reduce corrosion of steel but none seems to be a suitable solution for the corrosion problem. Therefore, the use of composite rods as concrete reinforcement material seems to be an effective solution to overcome durability problems of traditional steel-reinforced concrete structures. The main advantages of composite materials over steel include the excellent corrosive resistance, mechanical properties similar to steel, high strength-to-weight ratio and excellent fatigue resistance, among others. Thus, the replacement of steel rebars with fibre-reinforced composite rods is gaining popularity worldwide.

Typically, fibre-reinforced composite rods are produced by pultrusion, although, besides this technique, fibre-reinforced composite rods can also be produced using braiding techniques (Kadioglu *et al*., 2005; Saikia *et al*., 2005). Braiding is a conventional textile technique known as the technique used to produce ropes. It is a low-cost technique that allows in-plane multiaxial orientation, conformability, excellent damage tolerance and core reinforcement. Moreover, braiding allows the production of ribbed structures and a wide range of mechanical properties may be improved when the core-braided fabrics are reinforced with the appropriate type of fibres (Fangueiro *et al*., 2004).

8.2 Raw materials for composite rods

Composite materials are a macroscopic combination of two or more distinct materials having a finite interface between them. One of the constituents is the reinforcement, while the other is the matrix.

Composite materials are generically classified into two different categories. The first one is related to the matrix phase, and the second one is based on the form of the reinforcement used.

The matrix provides environmental and damage protection to the reinforcing phase, acts as a binder of the reinforcement, and enables the material to be formed into shapes. The common types of composite are ceramic matrix composites, metal matrix composites and polymer matrix composites.

A minimum fibre volume fraction, generally not lower than 10%, is required for the reinforcement phase to provide a useful enhancement in the properties provided by the matrix phase alone. This can be in a variety of forms set in two categories: particulate reinforcements and fibre reinforcements.

Particulate reinforcements present roughly equal dimensions, are used for non-structural applications and are often named as ‘fillers’. Fillers are used to enhance fire resistance, electro-magnetic shielding, thermal conductivity and fracture toughness, among others. Fibre reinforcements present one dimension substantially larger than the other and are used for structural purposes. They can be classified into discontinuous or continuous reinforcements, presenting low aspect ratio in the first case, and lengths much greater than the cross-sectional dimensions in the second case. The continuous fibre reinforcements are usually used as bundles

called rovings or tows, and in the form of fabrics wherein a number of bundles are woven, knitted or braided in specific patterns. In some cases the reinforcement is specially formed using textile techniques into three-dimensional formwork.

Composite materials are not homogeneous. Their properties are dependent on many factors including the type of fibre, the quantity of fibre (volume fraction) and the fibre orientation.

In the production of composite materials for concrete elements reinforcement, the most commonly used fibres are glass, carbon or aramid. The use of other fibres, such as basalt or flax, is relatively insignificant.

The most important property of fibres is their elastic modulus, because it must be significantly stiffer than the matrix in order to pick up the stress applied to the composite. Therefore, fibres must have sufficient strength available to avoid failure. Fibres present a linear elastic response up to the ultimate load, with no significant yielding. Typical values for the properties of the different fibres are given in Table 8.1.

Glass fibres are the most commonly used as reinforcing fibres. They present good processing characteristics and are inexpensive. The processing characteristics of particular types of glass fibre have been modified and optimized over many years to achieve the required performance, such as chopability, low static build-up, conformability to complex shape, etc., and resin compatibility requirements such as fast wet-out, good fibre/matrix adhesion, among others. There are significant differences between the various types of glass fibres available to manufacture composite materials, each presenting benefits and drawbacks, and it is necessary to select the most appropriate for the particular specifications (Quinn, 2003).

As a broad generalization, glass fibres can be categorized into two sets: those with a modulus around 70 GPa and with low to medium strength (i.e. E, A, C, ECR), and those with a modulus around 85 GPa with higher strength (i.e. R and S2 glass).

Table 8.1 Typical fibre properties

Fibre	Tensile strength (N/mm^2)	Modulus of elasticity (kN/mm^2)	Elongation (%)	Specific density
Carbon – high strength	3430–4900	230–240	1.5–2.1	1.8
Carbon – high modulus	2940–4600	390–640	0.45–1.2	1.8–2.1
Aramid – high strength and high modulus	3200–3600	124–130	2.4	1.44
Glass – E	3300–3400	60–70	2.5	2.57
Glass – ECR	3300–3400	60–70	2.5	2.71
Glass – S2	4500–4700	75–90	3.0	2.47
Glass – R	4200–4600	75–90	3	2.55
Glass – C	2300–2400	75–90	2.5	2.46
Glass – A	2700–2800	70–90	2.5	2.46

Source: Clarke, 2003; Quinn, 2002

Carbon fibres are the predominant reinforcement used to achieve high stiffness and high strength. The primary characteristic of carbon fibre composites is definitely their very high specific stiffness (i.e. the ratio of modulus of elasticity to density) (Quinn, 2003).

Aromatic ether amide or aramid fibres are organic, man-made fibres, generally characterized as having reasonably high strength, medium modulus and a very low density. Their composites fit well into a gap in the range of stress–strain curves left by the family of carbon fibres at one extreme and of glass fibres at the other. Aramid fibres are fire resistant and perform well at high temperatures. They are insulators of both electricity and heat, and are resistant to organic solvents, fuels and lubricants. A major distinction of aramid fibres is that they are highly tenacious in the non-composite form and do not behave in a brittle manner as do both carbon and glass fibres. The typical tensile stress–strain curve of aramid fibres is essentially linear to failure. They can be set into two distinct categories: those in which their modulus of elasticity is similar to that presented by glass fibres, typically 70 GPa, and those with a modulus of elasticity at about twice this level. It should be noted that some aramids have a relatively very low compressive strength. Thus, when used in compression or flexural, special attention should be paid (Quin, 2003).

There is a wide choice of resins available, many of which, though not all, are suitable for forming composites (Table 8.2). Some restrictions are placed upon the uses of polyester resins for embedded composite materials. Nevertheless, the choice depends on the required durability, the manufacturing process and the cost. Thermosetting resins are generally used. However, once fully cured, the composites cannot be bent to form hooks, bends or similar shapes. The available alternative is the correct use of suitable thermoplastic resins that are nowadays being developed. When produced with these resins, the composites can be warmed and bent into the required shapes, guaranteeing that the full properties are restored after cooling. Attention must be paid to the fibres' distortion in the bend region, which reduces the composite strength locally. These composite materials are unlikely to find a significant application in civil infrastructure due to cost and processing-specific aspects; civil applications are more likely to use resin systems such as polyesters, vinylesters and phenolics and lower temperature epoxies rather than the higher-temperature curable epoxies and thermoplastics.

Table 8.2 Typical resin properties

Resin	Tensile strength (N/mm^2)	Modulus of elasticity (kN/mm^2)	Elongation (%)
Polyester	55–70	3.6–4.1	1.5–3.0
Vinylester	68–80	3.5	3.5–6.0
Epoxy	65–120	3.0–4.1	2.0–8.0

Source: Quinn, 2003

8.3 Composite manufacturing processes

The successful integration of fibre reinforcement and matrix materials to produce a composite is largely dependent on the choice of manufacturing process. There are a large number of manufacturing processes available and each process has specific attributes. Nevertheless an eight-step generic program may be outlined (Fig. 8.1).

The tailorability of composites for specific applications is one of the biggest advantages of the material. The wide choice of material combinations, manufacturing processes and shapes possible, presents bewildering problems of selection.

In the isotropic world of traditional materials it is possible to use tables, charts and simple formulae to check the validity of a concept, thereby relegating the need for specialists to produce the final stage before prototyping. This is not possible in composites, where every decision is unique in that it includes both shape and microstructure, either of which could be varied to attain a specific attribute.

The manufacturing of composites has limitations based on shape, microstructure and materials. Theoretically, any combination of the three aspects should be possible, although the development is a complex process and requires the simultaneous consideration of parameters such as:

- geometry;
- production volume;
- reinforcement type;
- matrix type;
- reinforcement and matrix relative volumes;
- tooling requirements;
- process and market economics.

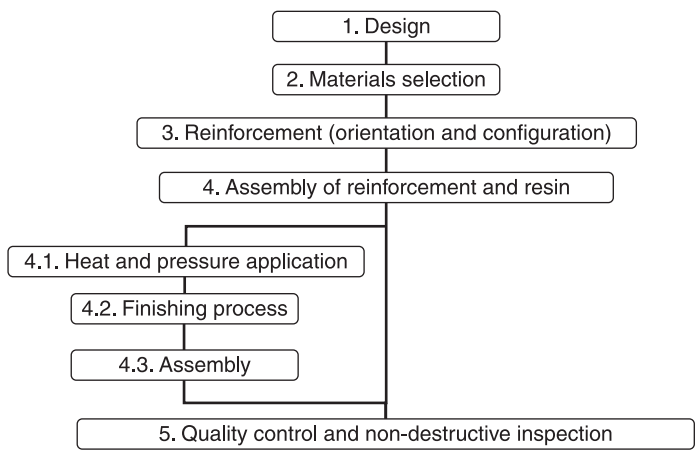

8.1 Manufacturing process outlined (adapted from Karhari, 2007).

In the composites manufacturing process, eight parameters may be outlined as fundamentals:

- fibre placement, the means by which the fibre is placed in or onto the mold in the position and orientation required;
- matrix application, the method of applying the resin to the reinforcement;
- wet through, means the penetration of the reinforcement by the resin;
- consolidation, removal of air from the laminate and the compaction of the laminate;
- conformation, the method of ensuring that the laminate conforms to the mold surface;
- cure, the chemical change in the resin from liquid to solid;
- release, the removal of the composite from the mold.

Usually, fibre-reinforced composite rods are produced by pultrusion. The pultrusion process is similar to extrusion in that continuous lengths of constant cross-section can be formed, although the reinforcement and resin is pulled through a die rather than being pushed through it as in the extrusion process. The reinforcement is pulled through a heated die (about 150°C) that not only provides the final shape but also causes the composite to reach an adequate level of cure (Fig. 8.2). The reinforcement is impregnated in a wet bath prior to being pulled through the heated die. Final compaction is conducted within the die that also controls dimensional tolerance. Because the reinforcement has to be pulled through the die, a high percentage of it has to be in the axial direction. Since the process is highly automated it provides a very high level of uniformity and can lead to the highest level of materials efficiency. Nevertheless, the major drawback of the manufacturing process is the constraint for constant cross-sections. The process uses a high filler content both to reduce material cost and, more importantly, to control shrinkage and to reduce frictional resistance in the die.

The precise positioning of the reinforcement materials prior to the die entrance is of paramount importance. It is achieved by a carefully engineered feed system.

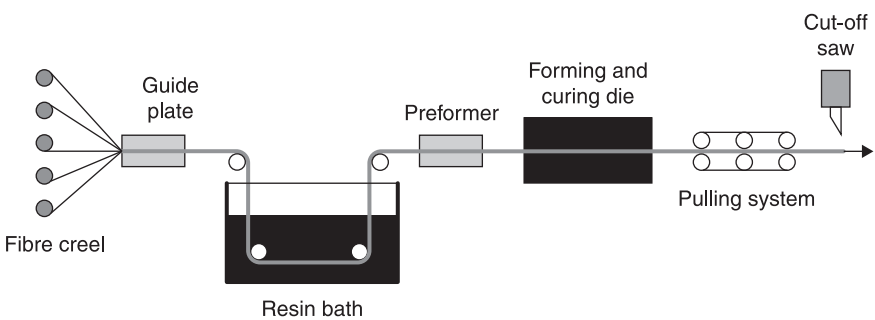

8.2 Pultrusion manufacturing process (http://www.substech.com).

This guides, locates, folds and tensions the various layers of reinforcing fibres. It also wipes any excess of resin from the reinforcement.

The resin is applied to the reinforcement either by the use of a dip tank or by injection. The dip tank approach is the most common and consists of a tank containing the resin through which the reinforcement is pulled. The tank is replenished as necessary to ensure that the process is continuous. The injection method is a cleaner option.

The time available for resin penetration and wet-out of the fibre is dependent on the speed of the profile and the length of the resin tank or injection cavity. The process is aided by the physical working of the reinforcement by the use of bars that break the reinforcement strands into their individual filaments.

The action of pulling the impregnated fibres into the die creates a hydraulic pressure which forces out any air that is present. For this to be effective the fibres must have been impregnated with a slight excess of resin.

The shape of the die determines the profile shape, but the quantities of reinforcement and resin mix are critical to ensure that the die is filled properly.

Resins systems must be highly reactive to cure in the available time. Machine speed, die temperature and resin reactivity are parameters that interact and must be balanced. As the process is 'hot cure', an accelerator is not required. It is normal with polyesters to use more than one catalyst, each initiating at a different temperature. This spreads the reaction and thus reduces the exothermic temperature to a manageable level.

Release agents applied to the mold surface cannot be relied on as they would be very quickly worn away, and therefore become inoperative. Hence, it is necessary to include internal release agents in the resin matrix.

Glass, carbon and aramid fibres can be pultruded but the most common is glass fibre. This is a reflection of the applications rather than an intrinsic problem with the process. The basic reinforcement geometry is unidirectional, i.e. glass-fibre roving or carbon-fibre tow. This defines the longitudinal properties and allows the reinforcement to be pulled through the die. In order to achieve transverse performance, either bi-directional or random reinforcement is needed, e. g. woven roving.

Polyester (isophthalic) is the most common matrix material, and vinylester is finding an important role in corrosion-resistance applications. Urethane methacrylate has very good fire, smoke and toxicity performance. Epoxy is used in the higher performance applications and almost always with carbon fibre. Phenolic resins are being developed to make them suitable for pultrusion. The driving force is their excellent fire resistance.

The major drawback of the pultrusion manufacturing process lies in the smooth surface of the pultruded composites. Pultruded composite materials present a smooth surface and, when used as internal reinforcement for concrete, the bond between rod and concrete is of paramount importance, as will be mentioned in forthcoming topics. The bond behaviour will have a direct influence on both the serviceability and ultimate limit. To improve bond behaviour of composite rod–concrete, a surface treatment is required to introduce deformations on the rod surface, and two different

approaches can be considered: deformation of the surface caused by the presence of ribs or indents or providing deformations in the outer resin layer, or surface treatments such as sand blasting or epoxy-coated sand (Lees, 2001). To guarantee that pultruded composite rods present the adequate adherence to surrounding concrete, a second manufacturing process needs to be added to the pultrusion (Fig. 8.3).

Pultruded composite rods are available in the market, some of which are presented in Table 8.3.

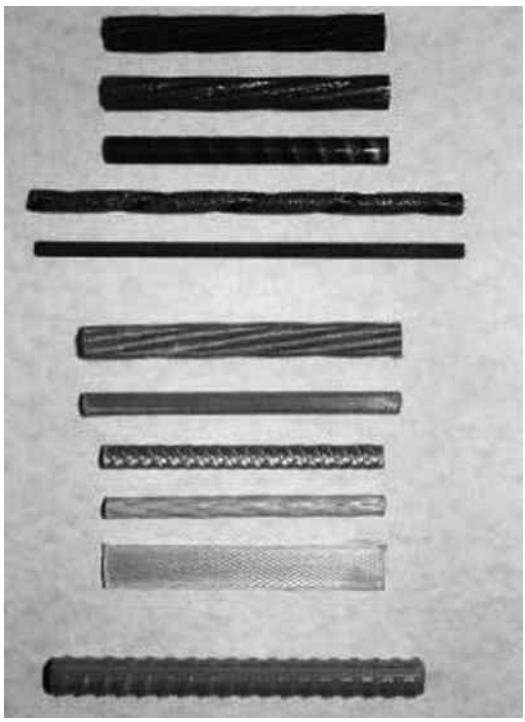

8.3 Surface configuration of FRP reinforcing bars (Balázs, 2000) (http;//fib.bme.hu).

Table 8.3 Commercial pultruded composite rods

Rod trade name	Manufacturer	Country	Fibre type
Aslan	Hughes Brothers	USA	Glass
Kodiak	International Grating	USA	Glass
V-ROD	Concrete Protection Products Inc	USA	Glass or carbon
ComBAR	Schöck	Germany	Glass
Carbopree	Sireg	Italy	Carbon
C-Bar	Marshall Composite Technologies LLC	USA	Glass

As mentioned, typically composite rods are produced by pultrusion, which is a well-known manufacturing method in fabricating fibre-reinforced composites with a constant cross-section. Besides pultrusion, composite rods can also be produced using braiding techniques.

Braiding is a low-cost technique allowing in-plane multiaxial orientation, conformability, excellent damage tolerance, and it allows core reinforcement. Moreover, braiding allows the production of ribbed structures and a wide range of mechanical properties may be improved when the core-braided structures are reinforced with the appropriate type of fibres (Fangueiro, 2004). The basic principle of braiding is the mutual intertwining of yarns (Figure 8.4). Braids are fibrous structures resulting from the yarns crossing in diagonal directions and can be tubular or flat, namely if they have round/oval cross-section or not.

Core-reinforced braided structures are braided tubular structures presenting, beside two systems of yarns moving helically, a third one that introduces yarns on the braid axial direction (Fig. 8.5). This third system of yarns may be composed of different types of fibres, namely natural or man-made. Moreover the use of a combination of different types of fibres to reinforce braided structures is also a possibility. The axial reinforcement fibres are responsible for the mechanical performance of core-reinforced braided structures. The influence of the braided structure itself is rather poor.

Braided composites rods are produced in a conventional braiding machine with minor modifications, developed by the Fibrous Materials Research Group, at University of Minho (Fangueiro *et al*., 2006).

The braiding machine has an integrated impregnation device that allows the impregnation of the axial reinforcement fibres in a polymeric matrix, in the instant immediately before the braiding process (Fig. 8.6). Therefore, it is a guarantee

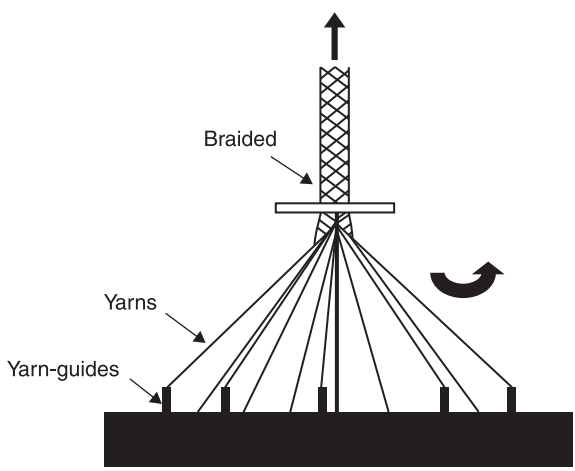

8.4 Braiding manufacturing process.

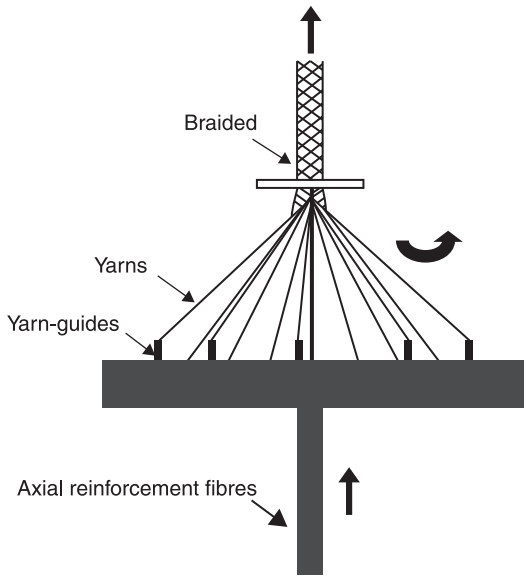

8.5 Braiding manufacturing process – core reinforcement.

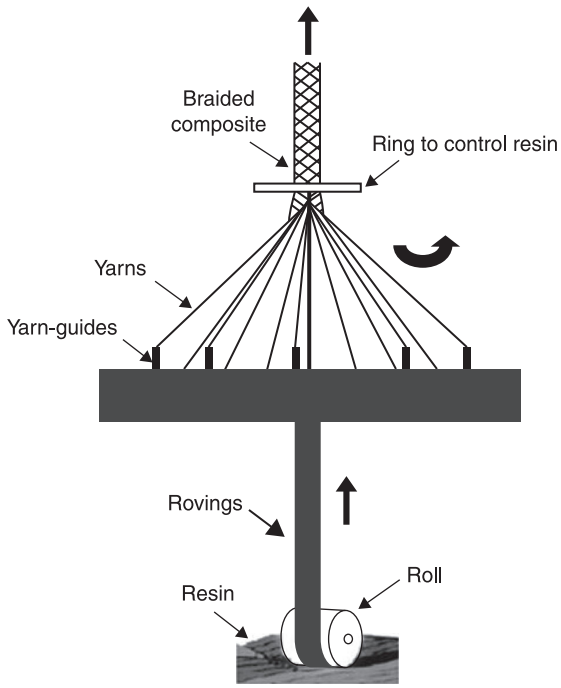

8.6 Braided composite rod manufacturing process.

that the impregnation of the axial-reinforced braided structure occurs from the inside to the outside of the structure. Moreover, the ribbed braided structure is obtained when yarns with significantly different linear densities are used in the production of the braided structure.

Hence, using braiding technology with minor adaptations, ribbed composite rods may be produced in a single step (Fangueiro, 2006; Gonilho Pereira, 2008).

Thanks to braiding technology capabilities, braided composite rods may be produced from different types of fibres. Varying the type of fibres used and their quantity, and varying the type of polymeric matrix used, different composite rods may be obtained with specific mechanical, physical and chemical properties for different applications.

8.4 Mechanical performance of composite rods

As mentioned, a number of manufacturers produce fibre-reinforced composite rods for concrete internal reinforcement. Carbon and glass are the most common fibres, though aramid is also used. Composite rods are usually made by pultrusion, as described in a previous section, with a secondary process to form a surface with adequate bond properties. Special attention to the importance of bond properties will be given in the following sections.

The composite rods are produced with thermosetting resins, and hence cannot be bent once the resin has fully cured. Some attempts have been made to bend partly cured elements, though this is not generally satisfactory as it leads to displacement of the fibres around the bend. Thus, various techniques are being considered for forming shapes such as shear links and hooks. These include filament winding, to form a cylinder or box, and can be cut to form appropriate closed shapes. An alternative approach is filament placing, in which the resin-impregnated fibres are wound around pins to give the required shape.

Composite rods are usually made of a single type of fibre such as carbon, glass or aramid. From the cost perspective, glass-fibre reinforcement rods are the most promising, since they are the least expensive and widely available. However, from the design and serviceability perspective, glass-fibre reinforcement rods do not have the stiffness and ductility requirements of conventional steel reinforcement bars. In many cases, concrete elements using glass-fibre reinforcement rods underutilize the material strength properties and thereby increase the cost of the overall project. On the other hand, carbon-fibre reinforcement rods present high stiffness and strength, comparable to those of steel reinforcement bars. However, their cost is high, making them not commercially viable for conventional reinforced concrete structures.

Composite reinforcing rods made of a single type of fibre, such as glass or carbon, behave linearly elastic until they rupture (Fig. 8.7), in contrast to steel reinforcement bars which have a definite yielding plateau.

In reinforced concrete structures, ductility is provided by the yielding of the longitudinal steel reinforcement (Fig. 8.8). The yielding of reinforcement is then

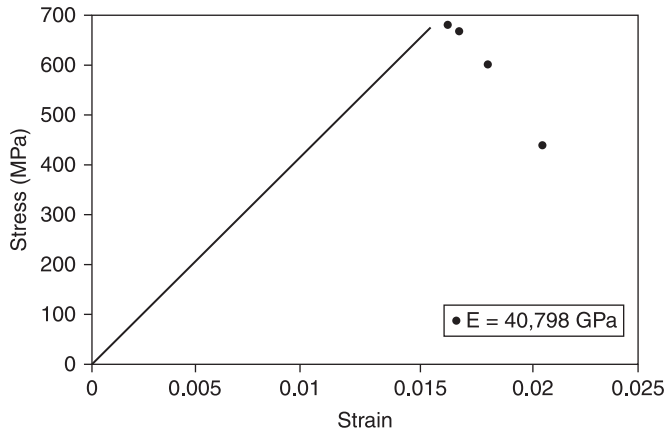

8.7 Glass-fibre reinforced composite rod stress–strain curve (http://www.hughesbros.com).

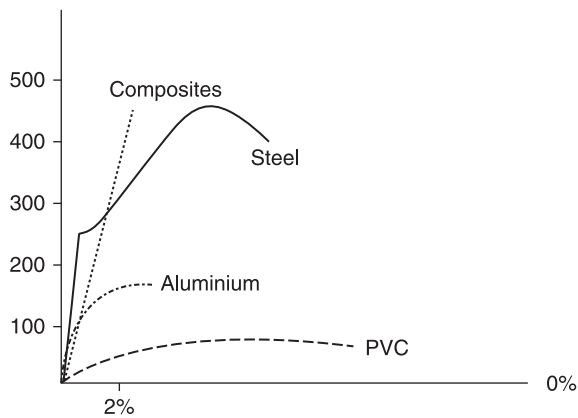

8.8 Glass-fibre reinforced composite rod stress–strain curve (http://www.frpindia.com).

translated into excessive deformation in the concrete element, providing a warning to the occupants that failure of the structure is imminent. With composite rods there is no yield point, since most fibres behave linearly elastic until failure (Gonilho Pereira, 2008). This brittle behaviour would give no early warning of structural failure.

To overcome this major drawback of composite rods, ductile hybrid reinforcement rods were developed. The material ductility is obtained due to the selection of different fibres that would fail at different strains, causing gradual failure of the hybrid composite rod – the so-called pseudo-ductility.

It is possible to obtain pseudo-ductility through a combination of different types of fibres together with the adoption of appropriate manufacturing processes. However, low modulus and the relatively high cost of hybrid-fibre reinforcement rods are still the main problems faced by the construction industry. The modulus of current composite rods, whether made of single-type fibres or hybrid ones is around 70 GPa; i.e. about one-third of the steel reinforcement bar modulus. Therefore, the development of cost-effective, high modulus and ductile reinforcement rods is needed for reinforced concrete structures.

The properties of some single-fibre pultruded composite rods available in the market are presented in Table 8.4.

Fangueiro (2004; 2006) and Gonilho Pereira (2008) performed research on the development of pseudo-ductile braided composite rods based on a conventional braiding machine with minor modifications, developed by the Fibrous Materials Research Group, at University of Minho.

Seven different braided composite rods were produced using polyester fibres for the braided structure production, E-glass, carbon and HT polyethylene fibres as braided structure core reinforcement, and a polyester resin was used for the core-reinforced braided structure impregnation.

Braided composite rods were produced maintaining the braided structure geometry and linear density and varying the type of core-reinforcement fibre, according to Table 8.5.

Braided composite rods were reinforced with a single type of reinforcement fibre, as well as with two and three types of fibres, varying the percentage of each one. The objective was to evaluate the influence of the type of fibre and its quantity on the mechanical behaviour of the braided composite rods. Table 8.5 presents the percentage of each type of fibre used as core reinforcement over the total linear density of the core reinforcement.

Table 8.4 Commercial pultruded composite rods

Rod trade name		Manufacturer	Ultimate tensile strength (MPa)	Ultimate strain in tension (%)	Modulus of elasticity (GPa)
Aslan	Glass	Hughes Brothers	480–825	–	40.8
	Carbon		2068	–	124
V-ROD		Concrete Protection Products Inc	550–874	1.20–1.90	52.7–76.9
ComBAR		Schöck	1000	0.725	60
C-Bar		Marshall Composite Technologies LLC	720–840	1.80–2.00	40–42

Table 8.5 Braided composite rods composition

Rod type	Type of core reinforcement fibre		
	E-glass fibre (%)	Carbon fibre (%)	HT polyethylene fibre (%)
1	100	–	–
2	77	23	–
3	53	47	–
4	–	100	–
5	50	45	5
6	52	45	3
7	75	22	3

Source: Gonilho Pereira, 2008

Table 8.6 Physical properties of braided reinforced rods

Rod type	Rod diameter (mm)	Mass fraction (reinforcement fibres) (%)
1	5.50	40.6
2	5.27	35.3
3	5.75	31.8
4	6.40	33.3
5	6.00	35.6
6	5.98	32.7
7	5.78	33.7

Source: Gonilho Pereira, 2008

Table 8.6 presents the rod diameter and the fibre mass fraction of the reinforcement fibres of each rod produced. In order to evaluate the mass fraction of the different braided composite rods produced, tests were conducted according to the Portuguese Standard NP 2216/1988 (determination of mass loss by calcinations of glass-fibre reinforced plastics). It was concluded that there is no relationship between the rod diameter variation and the volume fraction of the core reinforcement fibres. Therefore, the resin content varies from rod to rod.

During the curing period of the polyester resin, the core-reinforcement fibres were subjected to a pre-load of 100 N. In order to evaluate the mechanical performance of the different braided reinforced composite rods produced, tensile tests were carried out according to ASTM D 3916–94 standard, with a crosshead speed of 5 mm/min. A post-load of 50 KN was applied to the rods prior to performing the tensile tests. Table 8.7 presents the average values of the tensile test results obtained for each rod type and Fig. 8.9 presents the stress–extension curve for composite rod types 2, 3 and 4.

Table 8.7 Tensile test results obtained for the different braided reinforced composite rods

Rod type	Tensile strength (MPa)	Extension at failure	Tensile strength at 0.2% (MPa)	Modulus of elasticity (GPa)
1	485.35	0.01701	110.73	55.36
2	766.70	0.01416	157.05	78.52
3	740.41	0.01178	148.96	74.48
4	747.77	0.01183	192.58	96.29
5	679.45	0.01105	167.84	83.92
6	652.77	0.01098	162.17	81.09
7	690.99	0.01438	146.40	73.20

Source: Gonilho Pereira, 2008

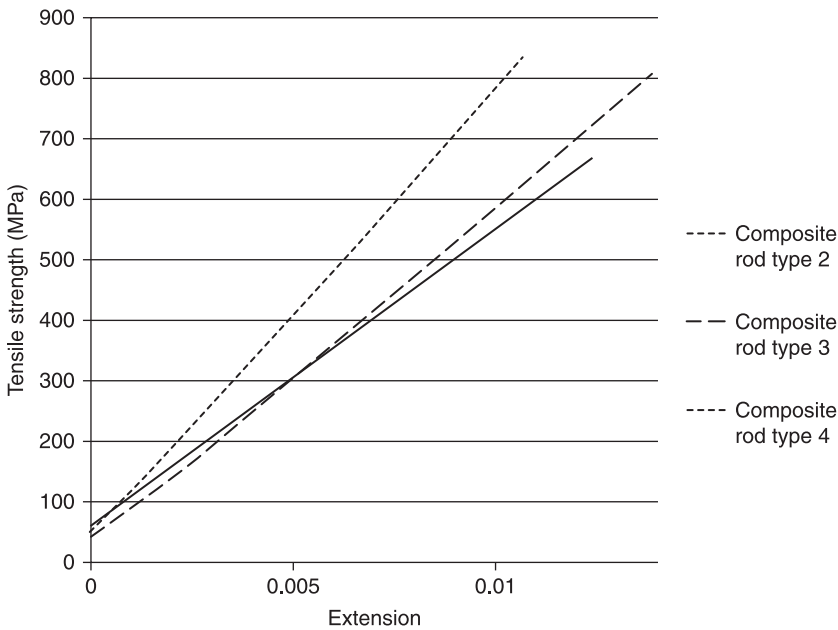

8.9 Braided fibre reinforced composite rod stress–extension curve.

Analysing the tensile strength, it can be concluded that hybrid braided composite rods type 2 (77% E-glass fibre, 23% carbon fibre) presented the highest tensile strength. Composite rod type 1 (100% E-glass fibre) presented the lowest tensile strength.

Considering the different composite rods' tensile strengths, extension at failure, tensile strength at 0.2% strain and modulus of elasticity, some conclusions can be withdrawn.

Braided composite rod 4 (100% carbon fibre) presented the most interesting tensile performance, while braided composite rod 1 (100% E-glass fibre) presented the least interesting one, although rod 1 presented the highest reinforcement fibre mass fraction.

Composite rods 2 and 7, presenting the same amount of E-glass and carbon fibres, presented significantly different tensile behaviour, mainly due to the reinforcement fibre mass fraction. Although rod 7 presented also HT polyethylene fibres, its fibre mass fraction was lower than in rod 2.

For composite rods 3, 5 and 6, with the same quantity of E-glass and carbon fibres, the presence and increasing amount of HT polyethylene fibre, as well as the increase of the fibre mass fraction, promotes an increase of the rods' tensile performance.

Although the tensile performance of the braided composite rods is influenced by the reinforcement-fibre mass fraction, one can conclude that the type of reinforcement fibre has a significantly higher influence.

When compared to the steel rebars currently used in the construction industry, composite rods reinforced by carbon, glass and polyethylene fibres present higher tensile strength. Current Portuguese steel rebars (A235NL, A400NR/ER and A500NR/ER) have values of tensile strength of 360 MPa, 460 MPa, and 550 MPa, respectively.

Braided composite rod 1 (100% glass fibre) was the only composite rod that presented tensile strength lower than 550 MPa, even though the tensile strength of E-glass, carbon and HT polyethylene-braided composite rods was higher than that of steel rebars.

However, composite rods have a lower modulus of elasticity when compared to that of steel rebars, 210 GPa.

Concrete beams reinforced with steel, composite rod types 2 and 4, were produced and tested under bending. Maintaining the reinforcement distribution and concrete beam dimensions, concrete beams produced with C30/37 concrete and reinforced with 6 mm composite rods and steel rebars were produced for mechanical performance comparison purposes. When compared to the steel-reinforced element, composite rod type 4 (100% carbon) reinforced concrete beam presented significant deflection at early stages of load, while composite rod type 2 (77% E-glass fibre, 23% carbon fibre) presented significantly lower load-bearing capability (Fig. 8.10).

8.5 Durability performance of composite rods

A very important aspect of the use of fibre-reinforced composite rods embedded in concrete is their durability. Unfortunately, the downside of composites is their inherent viscoelastic behaviour. Microstructural changes, time-dependent deformation and degradation in mechanical properties have been identified in fibre-reinforced composites when exposed to environmental

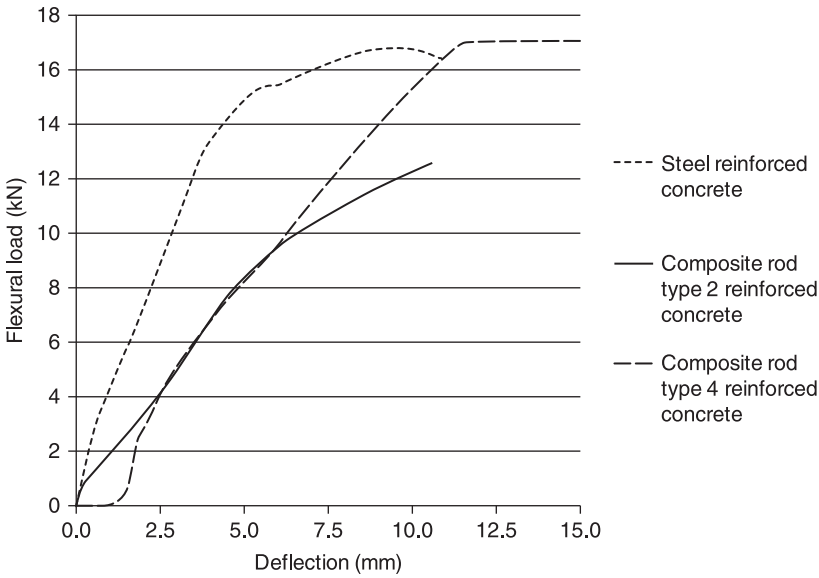

8.10 Concrete beam load–deflection curve.

conditions such as heat and moisture. The first form of damage in composite is usually matrix microcracking. These microcracks cause degradation in composite properties and also act as precursors to other forms of damage leading to failure. Nevertheless, fibre-reinforced composite rods are being increasingly used in concrete structures due to their high stiffness-to-weight ratio, good fatigue properties, ease of handling and, primarily, resistance to corrosion. But, due to the versatile applications of concrete in different construction fields, composite-reinforced concrete structures may often be exposed to wetting and drying cycles, sea-salts in hot/humid climates, freezing and thawing conditions, de-icing salts in cold climates, and many other severe environments. In addition to the above external attack, composite rods also readily attacked by concrete pore solutions having pH values of 12.4–13.7 (Ravindran, 2006). Therefore, the evaluations of long-term durability of composite rods are of primary importance in order to establish the life-cycle performance of composite-reinforced structures.

It is important to note that carbons and aramids are inherently more durable in an alkaline environment than the standard E-glass fibre. AR-glass (Alkali Resistant glass) has been used for some time for glass-reinforced cement and is used in some composite rods. The degradation mechanisms of glass fibres in water or alkaline solution can be classified into two categories: leaching and etching. The diffusion of the alkali ions out of the glass structure, known as 'leaching', is the most important reaction in the dissolution of glass in water. The second important reaction is called 'etching', in which the hydroxyl ions break the Si–O–Si

structure. The dissolution of glass fibres in water would eventually evolve into an alkali attack. All three mentioned degradation processes are aggravated in the presence of alkaline solutions (hydroxyl ions). As a consequence of chemical attack, the resulting formation of hydration products may cause notching and embrittling of the fibres. As with most organic polymeric fibres, aramid fibres are particularly susceptible to moisture absorption. Carbon fibres are known to be inert to chemical environments and do not absorb water. The degradation of interphase between fibres and matrix is complicated. The interphase is an inhomogeneous region with a thickness of about one micrometer. It is usually the primary weakest link and can degrade easily.

However, many resins degrade in the highly alkaline concrete environment. The Draft Canadian Highways Bridge Design Code specifically prohibits the use of polyester resins for composite rods for concrete internal reinforcement.

Currently, trials are being carried out on the resins and fibres in isolation and in the form of the composite, both in a range of artificial aggressive environments and embedded in concrete, with a view to developing the necessary confidence in the long-term properties of the materials.

Up until now, fibre-reinforced composite rods have been used mainly in nonstructural or secondary structural elements, such as ladders, handrails, and pavement grids. Their use in load-carrying structural elements, except for a few demonstration projects, is still limited to the fields of application with specific requirements of lightness or corrosion resistance, such as the oil, chemical, and water-treatment industries. Paradoxically, one of the factors delaying the widespread acceptance of fibre-reinforced composite rods as load-carrying structural elements is the lack of comprehensive and validated data on their durability, because the service life of construction infrastructures is generally expected to exceed 50 years. Furthermore, several authors have recently identified this factor as the most critical gap between the needed and available information regarding the future research.

The degradation in fibre-reinforced composite rods starts when free hydroxyl ions (OH^-) and water molecules diffuse through the matrix of fibre-reinforced composite rods (Chen, 2007). Polyester, vinyl ester, and epoxy are the most commonly used resins in fibre-reinforced composite rods in civil engineering. The ester group, the weakest bond in polyester and vinyl ester matrices, is prone to degradation by hydrolysis. The vinyl ester matrix with fewer esters groups is less susceptible to hydrolysis than the polyester matrix. The epoxy matrix is usually not affected by hydrolysis since there is no ester group in its molecular structure. The deterioration of matrices can also occur due to plasticization and swelling (Chen, 2007; Kim, 2006).

Once the durability of fibre-reinforced composite rods is affected by the alkaline environment of concrete, the environmental attacks begin at the bar surface, and the composite rod–concrete bond will be particularly affected by composite rod degradation. The resin matrix has a major role in transferring forces from the

surrounding concrete to the composite rod, while the matrix is also the first constituent material subject to environmental attack. Bond development is a critical issue for the successful application of composite rods as reinforcement in concrete structures. Bond characteristics affect the anchorage of bars, strength of lap splices, required concrete cover, and serviceability and ultimate states. The continued integrity of the bond is also a critical issue for the long-lasting performance of concrete structures reinforced with fibre-reinforced composite rods.

8.6 Composite rod/concrete bond behaviour

Most of the early design guidelines, as well as the design-oriented research studies, have extended the methodologies developed for steel-reinforced concrete structures to those reinforced with composite rods. However, several experimental studies have demonstrated that some key properties of the physical and mechanical behaviour of composite rods are qualitatively and quantitatively different from the well-known properties of steel bars. Such differences arise both from significant variations in the material properties and from remarkable changes in the interaction mechanisms between the reinforcement and the concrete matrix (Katz, 2000; Cosenza, 1997).

As mentioned, the bond behaviour is a critical aspect of the structural behaviour for any type of reinforcement. The performance of both reinforced and pre-stressed concrete elements depends on the properties of concrete and of the reinforcement, as well as on the bond behaviour between the two components (Tepfers, 2003). In the case of reinforced concrete structures, both at serviceability and at the ultimate state, the resisting mechanisms under bending, shear, and torsion are related to the development of an adequate bond. Moreover, several verifications at the serviceability limit state, such as the control of crack amplitude and structure deformations, involve evaluation of the effects of the tension stiffening that directly arises from bond.

In the past years, experimental studies have been conducted in order to investigate the bonds between composite rods and concrete. Such studies have been aimed either at understanding the resisting mechanisms activated in pullout tests and at determining the bond-slip constitutive laws. Moreover, comparisons of bond strength and deformability between steel and composite rods have also been carried out.

The bond of fibre-reinforced composite rods performs differently from that of conventional steel reinforcements because of the different manufacturing of the outer surfaces and of substantial material differences in both longitudinal and transverse directions. The bond of composite rods to concrete is controlled by several factors, as follows (Cosenza, 1997; Tepfers, 2003):

- chemical bond;
- friction due to surface roughness of the composite rod;
- mechanical interlock of the composite rod against concrete;

- hydrostatic pressure against the composite rod due to shrinkage of hardened concrete;
- swelling of the composite rod due to temperature change and moisture absorption.

During the initial pullout, the chemical bond is the main resisting mechanism. Afterwards it is replaced by friction and/or mechanical interlock. Since the chemical bond between concrete and composite rod is generally extremely low, friction and mechanical interlock really become the primary mean of stress transfer. Hence, two types of bond-resistant mechanisms may be outlined: one is the friction-resistant type, while the other one is the bearing-resistant type (Cosenza, 1997). For example, smooth surface bars exhibit a friction-resistant bond while ribbed composite rods develop a bearing-resistant bond. Moreover, the bond behaviour may be categorized into two categories according to the adopted surface process. A straight grain-covered bar presents very small slip, while braided rods are characterized by much larger values of the slip.

The anisotropic nature of composite rods cannot be forgotten and needs to be taken into consideration. Anisotropy is a result of the fact that the shear and transverse properties of composite rods are dominated by resin while the longitudinal properties are influenced by fibres. Resin-dependent strength may be lower than the compressive strength, thus resulting in a different bond interaction from that of steel reinforcements with failure due to damage of the ribs instead of cracking of the concrete. Therefore, failure stresses and strains in the longitudinal and transverse directions are very influential on bond behaviour. Such properties are especially important to determine the pullout strength and the earlier failure modes of composite rods.

Although bond behaviour is dependent on various effects, it seems convenient to separate the straight rebars (i.e. smooth, grain-covered, sandblasted-type rods) from the deformed ones (ribbed, indented, twisted, braided) and then to understand, within each of the groups, differences in the bond mechanisms and the influence of some significant parameters on bond strength (Cosenza, 1997).

The bond stress of commercial single-fibre pultruded composite rods is presented in Table 8.8.

Table 8.8 Commercial pultruded composite rods

Rod trade name		Manufacturer	Maximum bond stress (Mpa)	Observations
Aslan	Glass	Hughes Brothers	11.6	ACI 440.3R-04 Method B.3.
	Carbon		8.45	ACI 440.3R-04 Method B.3.
V-ROD		Concrete Protection Products Inc	13.7–20.5	–
ComBAR		Schöck	2.3–3.7	–

8.7 Self-monitoring composite rods

The interest in the safety of concrete structures has increased and monitoring and maintaining their safety has become a main goal. To achieve this main goal, monitoring systems that can be applied to the reinforced concrete elements are required. The damage sensing is conventionally performed by attached or embedded damage sensors, such as optical fibres, acoustic sensors, etc. However, these sensors have limited application because of high cost, low durability and limited sensing volume and spatial resolution. One solution is that the materials themselves can possess a self-diagnosing function for fracture; thus, strong and heavy design, complex and expensive equipment, and numerous sensors become unnecessary for the so-called self-diagnosing structural materials (Muto, 2001; Chung, 1997).

Structural materials have evolved from materials that are mechanically strong (such as steel) to materials that are both strong and lightweight (such as composite materials), and most recently to materials that are both strong and self-monitoring (Muto, 2001). By definition, a self-monitoring material is one that can sense its own strain and damage; and it can be considered a smart material. However, in contrast to smart materials such as optical fibres, piezoelectric sensors, etc., the self-monitoring materials are themselves structural materials. Thus, in contrast to structures rendered smart by embedded or attached sensors, self-diagnosing structural materials are intrinsically smart, so there is no need for embedded or attached sensors. For example, the basic principle of the carbonaceous, smart structural material to detect strain or damage lies in the electrical conductivity of the carbon fibres, as already known from the literature (Chung, 1997). As the carbon fibres are electrically conductive, the composite itself can exhibit electrical properties, which will depend upon strain, damage and temperature. The self-diagnosing structural material will, in this way, provide determination of the strain or damage by measuring the change in the electrical resistance during real-time loading (Bakis, 2001).

Hybrid, carbon-fibre (CF) and glass-fibre (GF) reinforced composite rods were tested for sensing performance (Okuhara, 2005). It was reported that the memorizing ability of the material resulted from the increased residual resistance of the composites after loading-unloading cycles, which was in dependence with the previously applied maximum strain. Under pre-stressed conditions, the composite gave remarkable memorizing ability with lower detectable strains. A main drawback raised by this study is related to damage detection: damage cannot be detected in the early stages, unless the carbon fibres are replaced with carbon particles (Okuhara, 2005). In the latter case, on the other hand, mass production is more expensive and demanding.

Another study using a glass-fibre reinforced composite rod, incorporating carbon particles dispersed in the resin, reported that the material can be used as an autonomous sensor, as it can monitor strain without external pre-stress conditions (Okuhara, 2007).

In a hybrid composite, the carbon fibre type and the relative percentage of carbon fibre and glass fibre are factors that determine the variations of the electrical resistance upon stress and/or strain. As mentioned before, the main drawback of hybrid CF–GF reinforced polymer composites is the lack of sensitivity at lower strains, which can be improved by pre-stressing (Nanni, 2007).

Nevertheless, by modifying the fibre reinforced composites' concentration formulations and geometry (e.g. carbon fibres at the core, and glass fibres insulating outer layer components), the electrical response of the composites can be tailored to a desired value (Nanni, 2006).

Fangueiro *et al*. (2006) and Zdraveva (2010) performed research on the development of self-monitoring pseudo-ductile braided composite rods based on a conventional braiding machine with minor modifications, developed by the Fibrous Materials Research Group at University of Minho.

Three types of braided composite rods with different carbon fibre content (23%, 77% and 100%) were produced by the single-step process of braiding and simultaneous resin impregnation. Table 8.9 shows the braided composite rods composition while Fig. 8.11 shows the corresponding composite cross-sections. A total number of 14 samples were prepared and evaluated. The mean value of the composite rod diameter is presented in Table 8.10.

The testing procedure carried on the braided composite rods was based on the electrical resistance measurement during the simultaneous application of a deformation in a cyclic three-point bending test (Fig. 8.12), and the testing

Table 8.9 Braided composite rod compositions

Rod type	Fibre composition	Fibre (%)	N° of rovings	Linear mass (tex)
2	E-glass/Carbon	77/23	18/3	1600/900
3	E-glass/Carbon	53/47	53/47	900
4	Carbon	100	12	900

Source: Zdraveva, 2010

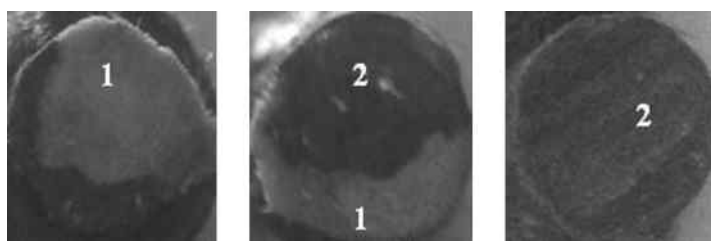

8.11 Braided composite rod cross-sections for rod types 2, 3 and 4: (1) glass fibre; (2) carbon fibre.

Table 8.10 Dimensional characteristics of the braided composite rods

Rod type	Diameter (mm)	Linear mass (g/m)
2	5.66	36.16
3	5.80	39.89
4	6.40	40.47

Source: Zdraveva, 2010

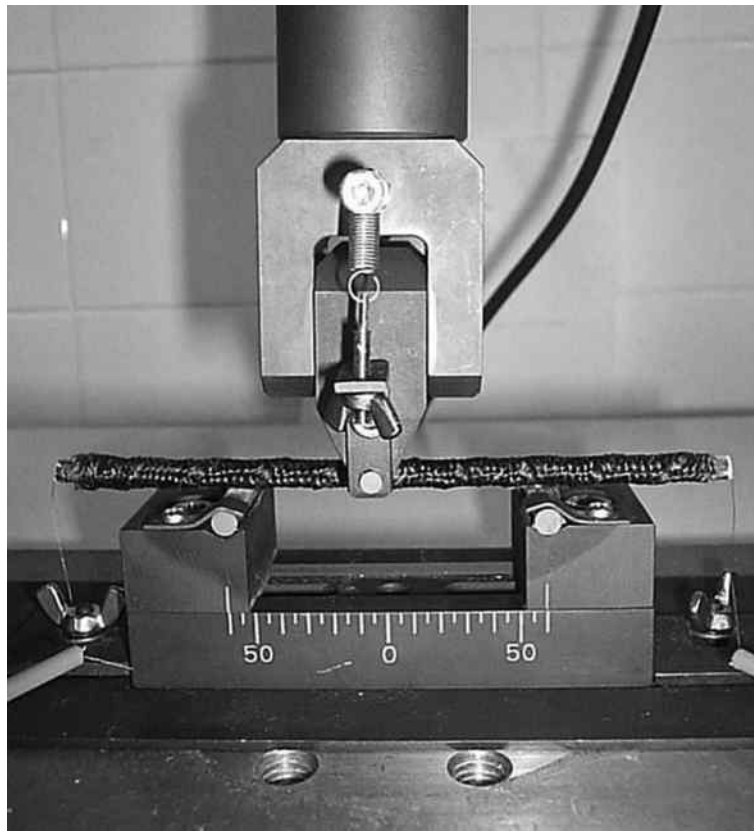

8.12 Sample set-up during three-point bending test (Zdraveva, 2010).

parameters are shown in Table 8.11. Cyclic three-point bending tests were carried out on a Universal Testing Machine – Autograph IS (Shimadzu) 500 N. The electrical resistance measurement was carried on a digital multi-meter (Agilent, 84401A). The electrical signal was acquired through golden wires attached to the cross-section of the samples with silver paint.

Table 8.11 Testing parameters

Parameter	Settings
No. of cycles	4
Load cell	500 N
Span	6 cm
Displacement limit	0.5 mm
Cross-head speed	0.3 mm/min
Sampling interval	500 ms

Source: Zdraveva, 2010

Representative examples of the two types of behaviour obtained for the mechanical and electrical results from the cyclic loading three-point bending tests and the simultaneous electrical resistance measurements are presented in Fig. 8.15 and 8.16 for the braided composite-rod samples tested. Figure 8.13 presents the increase in the electrical resistance with increasing displacement. Figure 8.14 presents the decrease of the electrical resistance with increasing deformation. In general, the electrical resistance during loading and unloading increases linearly at lower displacement values and nonlinearly at higher ones. In the case of the inverse response, during decrease of the electrical resistance and deformation increase, the nonlinearity is less evident. Whether it was a reverse or inverse response, in both cases the tested sample showed the change of the electrical resistance in proper compliance with the change of its deformation. The main factor influencing the type of response of each sample was the relative position of the fibres or, more precisely, the carbon fibre placement along the length of the rods.

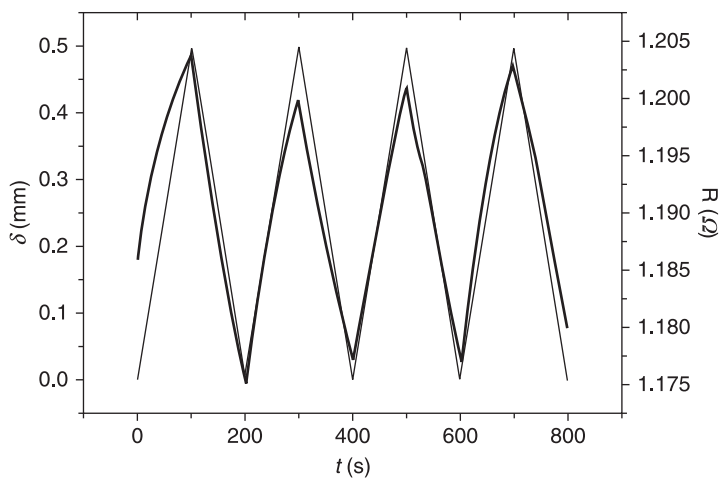

8.13 Displacement, resistance change and time dependence for braided-composite rod type 4 (100% carbon); positive response of tested samples (Zdraveva, 2010).

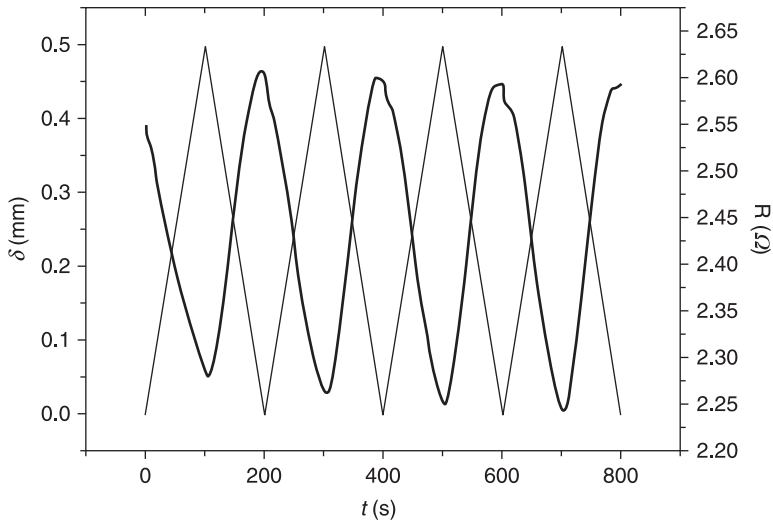

8.14 Displacement, resistance change and time dependence for braided-composite rod type 2 (77% glass, 23% carbon); negative response of tested samples (Zdraveva, 2010).

As shown in Fig. 8.11, from the images of the samples cross-sections, there were variations in the carbon-fibre placement. The fibres were not placed uniformly on one side of the cross-section and, more importantly, the distribution was not the same on both cross-sections of a rod sample. In this situation, increasing resistance with increasing deformation occurred when the carbon fibres are placed on the tensile side; and the opposite behaviour when their placement is on the compression side of the bending rod. This fact indicates the relevance of controlling carbon placement uniformly along the length of the composite rod. This is a difficult step in the production process, which sometimes results in non-uniformity along the length of the rods as the braiding process rotates the fibres.

On the other hand, for each rod, the cycles are reproducible, confirming the reliable sensing property of the rods. The difference between the peak values in each of the cycles is around 0.01 Ω to 0.02 Ω.

The range of the initial electrical resistance for the braided composite rod type 2 (77% glass, 23% carbon), varied from 1.46 Ω to 3.92 Ω, for the braided composite rod type 3 (53% glass, 47% carbon) from 1.11 Ω to 1.50 Ω and for the braided composite rod type 4 (100% carbon) from 0.80 Ω to 1.37 Ω.

Furthermore, for the comparison of the sensing behaviour differentiation due to carbon fibre content, the strain ε ($\times 10^{-2}$) and the fractional resistance change $\Delta R/R_0$ of the three types of braided composite rods are presented in Table 8.12. The strain is calculated from the displacement, and the fractional resistance change is calculated from the electrical resistance change. The values from the two parameters are presented over times of 100, 300, 500 and 700 seconds.

Table 8.12 Strain and fractional resistance change of the braided composite rods

	Cycle No.	1		2		3		4	
	t (s)	100		300		500		700	
Rod type	Sample No.	ε ($\times10^{-2}$)	$\Delta R/R_0$	ε ($\times10^{-2}$)	$\Delta R/R_0$	ε ($\times10^{-2}$)	$\Delta R/R_0$	ε ($\times10^{-2}$)	$\Delta R/R_0$
2	Xm 1, 2, 3	0.48	–0.10	0.48	–0.11	0.48	–0.12	0.48	–0.12
	12, 13, 14	0.47	0.08	0.47	0.07	0.47	0.07	0.47	0.06
3	3, 7, 12	0.48	0.04	0.48	0.02	0.48	0.01	0.48	0.01
	6, 10, 13	0.48	–0.06	0.48	–0.07	0.48	–0.07	0.48	–0.07
4	5, 7, 12	0.55	0.02	0.55	0.01	0.55	0.01	0.55	0.01

Source: Zdraveva, 2010

Figure 8.15 presents the correlation between the fractional resistance change ($\Delta R/R_0$) and the flexural deformation (ε) for all three: braided composite rod type 2 (77% glass, 23% carbon), braided composite rod type 3 (53% glass, 47% carbon), and braided composite rod type 4 (100% carbon) in the time range (0–100 s; 200–300 s; 400–500 s; 600–700 s) for the first half of the cycle (loading

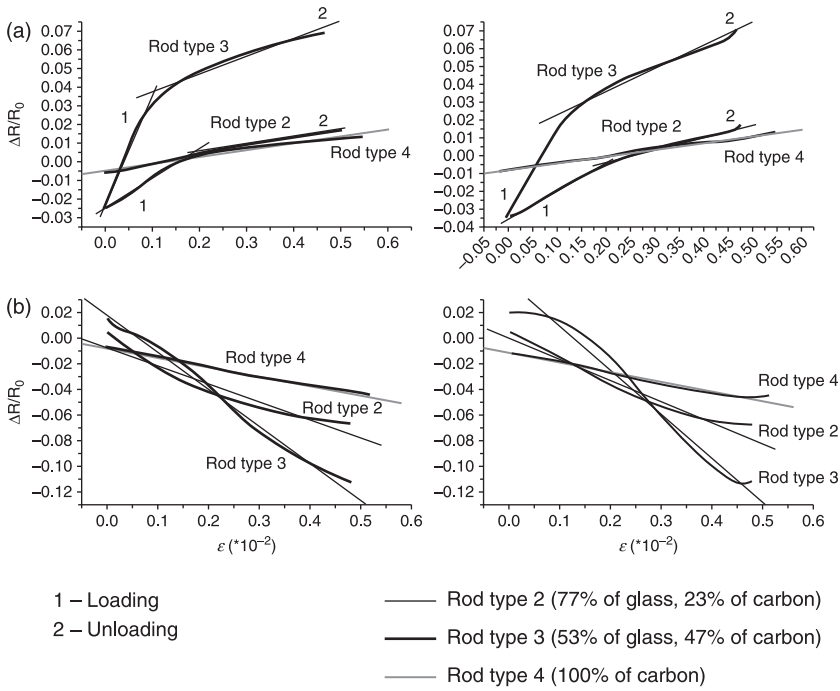

8.15 Fractional resistance change dependence on deformation. Comparison between the three types of composite rods 2, 3 and 4 in positive response (a) and negative response (b) (Zdraveva, 2010).

sequence); or (100–200 s; 300–400 s; 500–600 s; 700–800 s) for the second half of the cycle (unloading sequence). Figures 8.15(A1) and 8.15(A2) represent the positive type of response. Figures 8.15(B1) and 8.15(B2) represent the negative type of response. The numbers 1 and 2, respectively, represent the loading and unloading sequence of the cycles. Furthermore, the trend lines are presented for each of the plotted curves showing the linear accordance between the fractional resistance change and the deformation.

In the case of the positive response of composite rod type 2 (77% glass, 23% carbon) and composite rod type 3 (53% glass, 47% carbon), the plotted curves were divided into two parts presented by two trend lines (1 and 2) for each curve. The reason for this division is the sharp slope of the curves in the interval from 0 to 0.1 for composite rod type 2 (77% glass, 23% carbon) and 0 to 0.2 for composite rod type 3 (53% glass, 47% carbon) as a function of the strain (ε). The corresponding trend equations established in this study, as well as the resulting squared regression values and gauge factors, are presented in Table 8.13.

The fractional resistance change was expressed from the linear trend equations as a function of the strain for each of the three types of the composite rods, for the loading and unloading part of the cycle (1 and 2) for both types of responses.

The overall linear relationships of the two parameters obtained in the work showed a high satisfactory level of composite rods' sensing capability.

As can be seen in Table 8.13, the gauge factor for composite rod type 2 (77% glass, 23% carbon) is almost five times higher than that for both the composite rod type 3 (53% glass, 47% carbon) and composite rod type 4 (100% carbon). The gauge factor of composite rod type 3 (53% glass, 47% carbon) is slightly higher.

The gauge factor, known as the strain-sensing factor, shows the sensing behaviour of the composite rod samples. It increases with the decreasing of the carbon fibre percentage. This means that composite rod type 2 (77% glass, 23% carbon) has the most reliable monitoring behaviour.

Table 8.13 Gauge factors (GF) and squared regression values (R^2) of established trend equations

Rod type	GF		Xm	R^2		Response
	1*	2*		1	2	
	0.58100	0.46312	0.52206	0.98965	0.99602	Positive
2	0.09554	0.12951	0.11253	0.95651	0.97279	Positive
	–0.28869	–0.34058	–0.31464	0.99218	0.97288	Negative
	0.16095	0.15806	0.15951	0.98918	0.99668	Positive
3	0.03847	0.07018	0.05433	0.98339	0.98172	Positive
	–0.14084	–0.16380	–0.15232	0.93925	0.96892	Negative
4	0.03581	0.03702	0.03415	0.97118	0.99305	Positive
	–0.07451	–0.07684	–0.07568	0.99448	0.98699	Negative

Source: Zdraveva, 2010

* The number shows the first (1) or the second (2) half of the cycle, loading or unloading, respectively.

It is interesting to compare the resulting gauge factors of the braided composite rods with other materials for the same applications. For example, in a study of a carbon nanotube strain sensor, it was found that the range of the gauge factor was between 1 and 5, depending on the percentage of the single-walled carbon nanotube (SWCNT) polymer composites, and better sensitivity was established in the range of 3 to 10% of the SWCNT in the polymer (Kang, 2006).

Another study, investigating multi-walled carbon nanotube (MWCNT) films used as strain-sensing material, reported that the calculated gauge factors were 2, 3.09 and 3.76, respectively, for three types of samples (Li, 2008).

Comparing these examples with the samples investigated in this study, it is evident that the gauge factors calculated for the braided composite rods are all less than 1, much smaller than the sample studies set forth above. The reason for these small values of gauge factors would be, as mentioned, the higher percentage of the carbon component. On the other hand, the main advantage of the present materials is the superior reinforcing capabilities, and therefore the combination of reinforcing and sensing capabilities.

8.8 Applications of composite rods

Fibre-reinforced composite rods have been used to reinforce structures subjected to highly aggressive environments, mainly marine and coastal, due to the chloride ingress that is the prime cause of corrosion of reinforcing steel.

Several examples can be identified, mostly in the USA:

- Dry dock rehabilitation – Pearl Harbor, Hawaii (Fig. 8.16)
- Saudi Arabia ARAMCO Pier (Fig. 8.17)

8.16 Pearl Harbor, dock rehabilitation (http://www.hughesbros.com).

8.17 Saudi Arabia, ARAMCO pier (http://www.hughesbros.com).

- Seawall restoration – Estee Lauder estate, Palm Beach, Florida (Fig. 8.18)
- School buildings in very close proximity to waterfront – JaLuit High School and others in Republic of Marshall Islands (Fig. 8.19)
- Buffalo Creek Bridge, Brooks County, West Virginia
- Kennedy Mansion Seawall, West Palm Beach, Florida

8.18 Estee Lauder estate seawall (http://www.hughesbros.com).

8.19 JaLuit High School (http://www.hughesbros.com).

- Roger's Creek Bridge, Bourbon County, Kentucky
- Two-Mile Creek Bridge, Clark County, Kentucky
- Taylor Bridge, Headingly, Manitoba, Canada
- Joffre Bridge, Sherbrooke City, Quebec, Canada
- Walters Street Bridge, St. James, Missouri
- I-225 and Parker St. Interchange, Denver, Colorado
- Salem Ave. Bridge, Dayton, Ohio
- Pierce St. Bridge, Lima, Ohio
- Hydroelectric chambers for Hydro-Quebec, Montreal, Quebec
- Bayonne Bridge, New York
- Martha Queen's Bridge, Lewis County, West Virginia

8.9 Design and application recommendations

It is of paramount importance to determine the optimum combination of resin matrix and fibre, sizing chemistry and the manufacturing process for maximum durability of composite rods. For design purposes, it is clear that the design engineer must take into consideration the durability parameter. Therefore, civil engineers, contractors and designers must take care about the long-term behaviour of composite rods in different environmental conditions and then design structures with this behaviour in mind. (Benmokrane, 2007).

Composite rods with modified fibre architecture have to be evaluated for long-term serviceability. Design codes in North America and Japan (Japan Society of Civil Engineers, 1997; CAN/CSA-S6–00, 2000; ISIS-M03–01, 2001; CAN/CSA-S806–02, 2002; ACI 440–1R-03, 2003; ACI 440.3R-04, 2004; ACI 440–4R-04, 2004) provide factors for the reduction of resistance to account for the effects of environmental conditions, creep from sustained loads and fatigue from repeated loads.

Modified design rules for the use of composite rods reinforcement have been developed for BS 8110: Structural Use of Concrete, Part 1; Code of Practice for Design and Construction, 1997, Part 2; Code of Practice for Special Circumstances (1985) for buildings – and BS 5400: Steel, Concrete and Composite Bridges, Part 4; Code of Practice for Design of Concrete Bridges (1990) for bridges (Institute of Structural Engineers, 1999). The proposals are broadly in line with the codes being developed in Japan (Japan Ministry of Construction, 1995; Japan Society of Civil Engineers, 1997) and in North America (Canadian Standards Association, 1996).

The following significant differences when designing with composite reinforcement are summarized as follows (Clarke, 2003):

- Once composite materials have a straight-line response to ultimate, with no yielding, it is appropriate to use only elastic methods of analysis. For design purposes it should be assumed that no redistribution of the elastic bending moments and shear forces shall take place.

- The effective strength and the effective stiffness of embedded reinforcement may change with time, due to alkali attack, depending on the types of resin and fibre used in the composite. Appropriate factors of safety applied to the short-term values will be required to take account of the changes.
- The quality of the concrete will be governed mainly by strength considerations, and the cover by the aggregate size and the size of the reinforcing bar. Design-crack widths will be controlled by aesthetic considerations and, possibly, watertightness of the structure.
- The design equations and the design charts given in the Codes are not appropriate as they assume yielding of the reinforcement at ultimate. Because of the relatively low stiffness of composite rods, it is likely that failure will occur by compression of concrete and not by reaching the ultimate capacity of the tensile reinforcement.
- The shear capacity of the concrete cross-section should be calculated on the basis of an equivalent area of steel, transformed on the basis of the modular ratio. The strain in composites shear reinforcement should be limited.
- Because of the lower stiffness, deflections and crack widths may become dominant design criteria. However, as indicated above, with no limitation on crack width required from the point of view of durability, aesthetics will be the only criterion.
- Because there are no agreed standards, it will be necessary to determine the ultimate bond stress for the particular materials, and then use this in design with an appropriate partial safety factor.
- Reinforcement cages should be assembled with non-metallic ties and there should be no significant problems during the assembly of the reinforcement cages. Any cut ends of bars, or damaged areas, should be sealed with a suitable resin. During the casting of concrete the reinforcement will have the tendency to float because of its low density, and allowance must be made for this during fixing.

Care must be taken with the storage of composite materials prior to use, to avoid damage to the resin matrix. In particular, reinforcement should be protected from the effects of prolonged exposure to UV light, which can lead to the degradation of some resins.

8.10 References

ACI (American Concrete Institute) (2003) *ACI 440.IR-03, Guide for the Design and Construction of Concrete Reinforced with FRP Bars*. Farmington Hills, MI: American Concrete Institute.

ACI (American Concrete Institute) (2003) *ACI 440.IR-04, Prestressing Concrete Structures with FRP Tendons*. Farmington Hills, MI: American Concrete Institute.

ACI (American Concrete Institute) (2004) *ACI 440.3R-04, Guide Test Methods for Fibre reinforced Polymers (FRP) for Reinforcing or Strengthening Concrete Structures*. Farmington Hills, MI: American Concrete Institute.

Alsayed, S.H., Al-Salloum, Y.A. and Almusallam, T.H. (2000) Performance of glass-fibre reinforced plastic bars as a reinforcing material for concrete structures, *Composites, Part B: Engineering*, 31: 555–567.

Bakis C., Nanni, A. and Terosky, J. (2001) Self-monitoring, pseudo-ductile, hybrid FRP reinforcement rods for concrete applications, *Composite Science and Technology*, 61: 815–823.

Belarbi, A., Watkins, S. and Chandrashekhara, K. (2001) Smart fibre reinforced polymer rods featuring improved ductility and health monitoring capabilities, *Smart Materials and Structures*, 10: 427–431.

Balázs, G.L. and Borosnyói, A. (2000) Non-metallic (FRP) reinforcements in bridge engineering, *Vasbetonépítés*, 2000/1: 45–52.

Benmokrane, B., Rahman, H., Ton-That, M.T. and Robert, J.F. (1998) 'Improvement of the durability performance of FRP reinforcement for concrete structures', *Proceedings of the 1st International Conference on Durability of FRP Composites for Construction*, CDCC'98 Sherbrooke, Quebec, Canada, pp. 571–586.

Benmokrane, B. and Wang, P. (2001) *Durability of FRP Composites for Civil Infrastructure Applications*, Quebec: Civil Engineering Department, University of Sherbrooke.

Benmokrane, B. Robert, M. and Youssef, T. (2007) Reinforcement of concrete using fibre reinforced polymer composites, in V.M. Karbhari (ed.) *Durability of Composites for Civil Structural Applications – Part II: Applications and Monitoring of Composites in Civil Engineering*. Cambridge: Woodhead Publishing Limited

Burgoyne, C. (2001) *Fibre Reinforced Plastics for Reinforced Concrete Structures*. London: Thomas Telford.

CAN/CSA (Canadian Standards Association) (2000) *CAN/CSA-S6–00, Canadian Highway Bridge Design Code*. Rexdale, Ontario, Canada: CSA International.

CAN/CSA (Canadian Standards Association) (2002) *CAN/CSA-S806–02, Design and Construction of Building Components with Fibre reinforced Polymers*. Rexdale, Ontario, Canada: Canadian Standards Association.

Chaallal, O. and Benmokrane, B. (1996) Fibre reinforced plastic rebars for concrete applications, *Composites: Part B*, 27B: 245–252.

Chen, Y., Davalos, J., Ray, I. and Kim, H. (2007) Accelerated aging tests for evaluations of durability performance of FRP reinforcing bars for concrete structures, *Composite Structures*, 78: 101–111.

Chung, D.D.L. (1997) *Self-monitoring Structural Materials*. Composite Materials Research Laboratory, State University of New York at Buffalo, Buffalo, NY 14260–4400, USA.

Clarke, J. (2003) Alternative reinforcement for concrete, in J. Newman and B. S. Choo (eds) *Advanced Concrete Technology – Part 11 – Alternative Reinforcement for Concrete*. Oxford: Butterrworth-Heinemann.

Cosenza, E., Manfredi, G. and Realfonzo, R. (1997) Behavior and modelling of bond of FRP rebars to concrete, *Journal of Composites for Construction*, 40–51.

Dejke, V. (1998) *Durability of Fibre reinforced Polymers (FRP) as Reinforcements in Concrete Structures – An Update of Knowledge and an Overview of Current Research Activities*, Technical Report. Gothenburg: Department of Building Materials, Chalmers University of Technology, pp. 98–108.

Fangueiro, R., Sousa, G., Araújo, M., Gonilho Pereira, C. and Jalali, S., (2006) Core reinforced composite armour as a substitute to steel in concrete reinforcement, *International Symposium Polymers in Concrete*. ISPIC2006, 2–4 April, Universidade do Minho, Guimarães, Portugal.

Fangueiro, R., Soutinho, F., Jalali, S. and Araújo, M. (2004) *Development of Braided Fabrics for Concrete Reinforcements*, 4th World Textile Conference Autex 2004, Czech Republic.

Gonilho Pereira, C., Fangueiro, R., Jalali, S., Araújo, M. and Pina Marques, P. (2008) *Tensile Performance of Braided Composite Rods for Concrete Reinforcement*. Porto: University of Minho. http://hdl.handle.net/1822/8915

Harries, K., Porter, L. and Busel, J. (2003) FRP materials and concrete-research needs, *ACI Concrete International*, 25(10): 69–74.

Japanese Ministry of Construction (1995) *Guidelines for Structural Design of FRP Reinforced Concrete Building Structures*. Tokyo: Japanese Ministry of Construction.

Japanese Society of Civil Engineers (1997) *Recommendations for Design and Construction of Concrete Structures using Continuous Fibre reinforced Materials*. Tokyo: Japanese Society of Civil Engineering.

Kadioglu, F. and Pidaparti, R.M., (2005) Composite rebars shape efect in reinforced structures, *Composite Structures*, 67: 19–26.

Kang, I., Heung, Y.Y., Kim, J.H., Lee, J.W., Gollapudi, R., Subramaniam, S. *et al*. (2006) Introduction to carbon nanotube and nanofibre smart materials, *Composites: Part B*, 37: 382–394 (March).

Karbhari, V.M. (2007) Fabrication, quality and service-life issues for composites in civil engineering, in V.M. Karbhari (ed.) *Durability of Composites for Civil Structural Applications – Part I: Aspects of Composites Durability*. Cambridge: Woodhead Publishing Limited.

Katz, A. (1998) Effect of helical wrapping on fatigue resistance of GFRP, *Journal of Composites for Construction*, 2(3): 121–125.

Katz, A. (2000) Bond to concrete of FRP rebars after cyclic loading, *Journal of Composites for Construction*, 4(3): 137–144.

Katz, A. and Berman, N. (2000) Modeling the effect of high temperature on the bond of FRP reinforcing bars to concrete, *Cement & Concrete Composites* (22): 433–443.

Kym, H., Park, H., You, Y. and Moon, C. (2006) Durability of GFRP composite exposed to various environmental conditions, *Journal of Civil Engineering*, 10(4), 291–295 (July).

Lees, J.M. (2001) Fibre.reinforced polymers in reinforced and prestressed concrete applications: moving forward, *Prog Struct Engng Mater*, 3: 122–131.

Li, X., Levy, C. and Elaadil, L. 2008, Multiwalled carbon nanotube film for strain sensing. *Nanotechnology*, 19: 045501 (7 pp).

Liao, K. Schultheisz, C., Hunston, D. and Brinson, L. (1998) Long-term durability of fibre reinforced polymer-matrix composite materials for infrastructure application: a review, *Journal of Advanced Materials*, 30(4): 3–40.

Micelli, F. and Nanni, A. (2004) Durability of FRP rods for concrete structures, *Construction and Building Materials*, 18: 491–503

Muto, N., Arai, Y., Shin, S. G., Matsubara, H., Yanagida, H., Sugita, M. and Nakatsuji, T. (2001) Hybrid composites with self-diagnosing function for preventing fatal fracture. *Comp Sci and Tech* 61: 875–883.

Nanni, F., Auricchio, F., Sarchi, F., Forte, G. and Gusmano, G. (2006) Self-sensing CF-GFRP rods as mechanical reinforcement and sensors of concrete beams, *Smart Mater Struct*, 15: 182–186.

Nanni, F., Ruscito, G., Forte, G. and Gusmano, G (2007) Design, manufacture and testing of self-sensing carbon fibre glass-fibre reinforced polymer rods, *Smart Mater Struct*, 16, 2368–2374.

Okuhara, Y. and Matsubara, H. (2005) Memorizing maximum strain in carbon-fibre reinforced plastic composites by measuring electrical resistance under pre-tensile stress, *Comp Sci and TechI,* 65: 2148–2155.

Okuhara, Y. and Matsubara, H. (2007) Carbon-matrix composites with continuous glass fibre and carbon black for maximum strain sensing, *Carbon*, 45: 1152–1159.

Quinn, J.A. (2003) *Composites-Design Manual*, 3rd edn. Liverpool: James Quinn Associates Ltd.

Ravindran, N. and Cho, E. (2006) Durability of glass-fibre reinforced polymer nanocomposites in an alkaline environment, *Journal of Vinyl and Additive Technology*, 25–32

Saikia, B., Thomas, J., Ramaswamy, A. and Nanjunda Rao, K.S. (2005) Performance of hybrid rebars as longitudinal reinforcement in normal strength concrete, *Materials and Structures*, 38: 857–864.

Soebroto, H.B., Pastore, C.M. and Ko, F.K. (1990) *Engineering Design of Braided Structural Fibreglass Composite*. Structural Composites: Design and Processing Technology, 6th Annual Conference, Advanced Composites, Detroit.

Tepfers, R. and De Lorenzis, L. (2003) Bond FRP reinforcement in concrete – a challenge, *Mechanics of Composite Materials*, 39(4): 315–328.

Zdraveva, E., Gonilho Pereira, C., Fangueiro, R., Ferreira, A. and Lanceros-Mendez, S. (2010) Self-diagnosing braided composite rod, *1st International Conference on Structures & Architecture*. ICSA2010, 21–23 July, University of Minho, Guimarães, Portugal.

Zdraveva, E., Gonilho Pereira, C., Fangueiro, R., Lanceros-Mendez. S., Jalali, S. and Araújo, M. (2010) Self-diagnosing braided composite rod, *Advanced Materials Research*, Vols 123–125, pp 149–152.

9

Fibrous materials reinforced composites for structural health monitoring

A. GUEMES, Technical University of Madrid, Spain and
J. R. CASAS, Technical University of Catalonia, Spain

Abstract: Structural health monitoring (SHM) is becoming more and more used in civil engineering infrastructure. The technology for implementing SHM applications is presented in this chapter. Details on instrumented civil constructions are then discussed, together with the most innovative future trends.

Key words: strain sensors, damage detection, smart structures.

9.1 Introduction

Structural health monitoring (SHM) is becoming more and more used in civil engineering infrastructure. One of the fields where SHM has been widely applied recently is bridges. SHM systems have been implemented on bridges in Europe, North America, Japan, Korea and China (Ko and Ni, 2005). This is due to the important benefits that SHM provides for evaluation, assessment and monitoring of existing or newly built bridges. As reported by Ko and Ni (2005), they include:

- validation of innovative design assumptions and parameters;
- detection of anomalies in loading and response and possible damage/deterioration at an early stage;
- real-time information for safety assessment immediately after disasters and extreme events;
- instruction for planning and prioritizing bridge inspection, rehabilitation, maintenance and repair;
- monitoring of repairs;
- appraisal of massive amounts of *in situ* data for leading-edge research in bridge engineering, such as wind- and earthquake-resistant designs, new structural types and smart-material applications.

Additionally, one could also mention the monitoring of the correct performance of structures built with new materials (composites for new structures or strengthening of existing ones), and/or new construction techniques (launching, rotation, heavy-lifting, etc.).

The longest bridges in the world have been provided with SHM systems. The challenging bridge spans reached nowadays need a deep understanding of their behavior, not only during construction but also during the operation phase. In this way, many SHM applications start during the construction process to monitor the

behavior of the bridge according to the expected response predicted by the designer. However, after completion of the construction, the monitoring remains operative and/or more sensors are installed. In this way, some specific types of sensors can be embedded into the structure during certain bridge erection stages. The Akashi-Kaikyo Bridge in Japan (Fig. 9.1), the longest suspension bridge in the world, and the Sutong Bridge in China (Fig. 9.2), the longest cable-stayed bridge, have been both provided with SHM systems. The SHM systems were planned during the design stage and installed during construction and before opening to the traffic. In other cases, SHM had to be installed in existing bridges in order to check the correct performance. This is the case of the Europabrücke, or Europe's Bridge. The longest span of this bridge is 198 m and supported by piers with a height of 190 m. The bridge was opened in 1963 and at that time no monitoring system was designed. However, over the years, the bridge exhibited a large loading impact causing vibration intensities that could lead to fatigue-related problems. For this reason, in 2003, a permanent measuring system was installed. The system is composed of two displacement transducers at both abutments, three one-dimensional accelerometers at the cross-section's cantilevers, three

9.1 The Akashi-Kaikyo Bridge (Kobe, Japan).

9.2 The Sutong bridge (China).

tri-dimensional accelerometers at the orthotropic bottom plate, one wind sensor 5 m above the road surface and seven temperature sensors inside and outside the box girder; and the main objective is to determine the relation between the randomly induced traffic loads and the fatigue-relevant dynamic response of the structure. In this way, based on the recorded data, the remaining fatigue lifetime of the bridge can be accurately assessed and updated as more actual data is available. This assessment is of outstanding relevance for the Administration operating the bridge.

Also, the tallest towers recently built are equipped with SHM systems to check safety during construction and operation. The Guangzhou new TV tower (GNTVT) is the world's tallest TV tower with a total height of 610 m. The tower comprises a reinforced concrete interior tube and a steel external tube. A sophisticated long-term SHM system consisting of more than 600 sensors has been designed and implemented to monitor the GNTVT during both construction and service stages. The in-construction monitoring consists of 527 sensors, and the in-service monitoring of 280 sensors. The objectives of instrumentation include: (1) ensure structural conditions meet the design requirements, (2) evaluate structural safety during service stage, and (3) detect the existence and extent of damage that occurs during the tower's lifecycle period. The monitoring consists of a weather station (measuring air temperature, relative humidity, barometric pressure, and rainfall), anemometers (measuring wind direction and speed), wind pressure sensors and a seismograph (measuring the ground motion). These sensors are intended to monitor environmental conditions and to quantify external loads. To monitor the response of the tower to these conditions and loads, vibrating-wire temperature sensors, fiber-optic temperature gauges, vibrating-wire strain gauges, fiber-optic strain gauges, accelerometers, GPS, digital video cameras, and tiltmeters are installed. For durability assessment, a suite of corrosion

sensors was installed to monitor the corrosion condition of the reinforced-concrete tower. In the long-term service stage, the signals from the fiber-optic sensors are accessed by an interrogator situated in a local optical-fiber network. Signals from the other sensors are acquired by five substations through five optical-fiber networks.

9.2 Materials and systems: hardware and software

9.2.1 Sensors and sensor characteristics

Essential for the monitoring of structures are sensors which are robust and operate stably and reliable. It has to be assured that the characteristic qualities are not modified by environmental influences, such as temperature, humidity and mechanical influences, as well as electrical and magnetic fields. Sensors can monitor local properties or observe structures from a global point of view. Some are embedded within the structure and others are only placed on the surface. The variables normally measured are dimensions, deformation, strain, force, pressure, weight, velocity, acceleration, temperature and durability parameters (humidity and wind velocity). The most important sensors currently used within SHM of civil engineering structures are defined by SAMCO (2006).

Strain gauges

The type and length, depending on the structural material (concrete, steel, etc.), are the most important parameters to define. Depending on the measuring amplifier, a frequency range from 0 Hz to some kHz can be covered. Constrained to the measuring chain, a strain with a resolution up to 0.1 μm/m can be measured. They are attached to the exterior concrete or steel surface or attached to reinforcing bars and embedded into the concrete. The reference book from HBM, *An Introduction to Measurements using Strain Gages* which contains every practical aspect, can be obtained free from his website.

Fiber-optic (Bragg gratings)

These sensors are suited for strain measurements up to 10 000 μm/m and for a temperature range from −50 to 200°C. The sensors can be applied in the structural material as well as on its surface. The sensors' length can be adjusted to the measuring task. They have a very good linearity and a small hysteresis and they are non-sensitive to electromagnetic perturbation. Because of the sensors' thermal sensitivity, temperature compensation needs to be installed during strain measurements. Full details on the use and characteristics of fiber-optic sensors, and their application to textiles for buildings, are given in a book recently published by Güemes and Messervey (2010).

Piezofilm sensors for strain measuring

Piezofilm sensors have high pass characteristics, i.e. they measure dynamic strain beyond a limiting frequency. This threshold frequency can be established by an adaptation of the charge amplifier directly at the sensor. With copper-coated synthetic film, a threshold frequency of 0.2 Hz can be provided. The size of the sensor is variable and generally has dimensions of approximately 12×90 mm including the charge amplifier and the voltage amplifier. Piezofilm sensors, including integrated amplifiers, are applied with epoxy resin.

Displacement transducers

The main types of those sensors, which measure the relative displacement between two points based on the inductive principle, are the different types of linear variable displacement transducer (LVDT) with measuring ranges between ±1 mm and ±50 mm and a quasi-infinite resolution within a temperature range between −20°C and +120°C.

GPS-based displacement sensors

The determination of deflection in general requires a stable, accessible reference location for each measurement. In cases in which this is not practical, satellite-based sensors are available which measure the movement of structures. Sensor nodes mounted on the structure at sites of interest are able to observe the settlements of foundations as well as long-time-period movements of bridges and high-rise buildings. Each sensor node consists of a GPS receiver, micro-controller and data radio. Precisions less than 10 mm are achievable with the evaluation of the phase information of the satellite signals and use of DGPS.

Hydrostatic leveling systems (HLS)

This sensor system, applicable for displacement measurements, is based on the classical physical law of connected vessels. It consists of two ore more interconnected fluid cells mounted on a structure at selected locations in which one cell is designated to be the datum reference. HLS only can be used for static or quasi-static events. Within a measuring range, a resolution of 0.02 mm can be reached.

Displacement sensors for relative vibration measuring

Displacement sensors are usually applied for measuring crack widths. According to the measuring principle, one can distinguish between conductive, inductive and capacitive sensors. Depending on those principles, displacements from 0.1 to 10 000 µm in a frequency range of 0 Hz to some kHz can be measured.

Vibrating wire strain gauges

These sensors encased in sealed steel tubes can be used for measuring strain, strength, pressure and temperature; they are fixed on the surface of a structure or produced for embedding in concrete for static and dynamic measurements. The long-time stability is very good. The resolution is about 0.025% of the measuring range.

Vibration velocity sensors

For measurement of absolute motion values, these sensors are applied directly on the vibrating object. They do not need a reference point, and they can be used in a limited frequency range of approximately 2 Hz to 1000 Hz. In the lower-frequency range, deviances in amplitude and phase could occur. Depending on the integrated mechanic–electric conversion element, the sensors can be classified into absolute displacement sensor (inductive, capacitive or strain gauge converter) and vibration velocity sensor (electrodynamic converter).

Vibration acceleration sensors (accelerometers)

They are also applied directly on the vibrating object. Depending on the integrated mechanic–electric conversion element they can be used from 0 Hz (strain gauge or inductive converter as well as servo-acceleration sensors) or above a low-threshold frequency (piezoelectric sensors). The upper threshold frequency in both cases is at some kHz.

Laser detector for vibration measurements

With these sensors, non-contact measurements over relatively wide distances can be carried out. Usually so-called position sensitive detectors (PSD-sensors) are applied. The source is mostly a semi-conductive laser with low intensity. The measurable frequency range reaches from 0 Hz to 300 kHz, depending on the measuring system. The resolution goes up to 10 µm depending on the size of the PSD, the light intensity and the measuring system.

Inclinometers for angular displacement measurements

For frequencies up to 5 Hz, sensors can be applied using the capacitive principle. For higher-frequency applications, servo-acceleration sensors are more adequate. The resolution of those sensors lies usually within the range of 0.1 to 0.001 degrees.

Fiber-optic sensors

Depending on the applied measuring equipment, these sensors are suitable for crack width measurement, for crack detection and localization. Crack width measurement

and crack detection use the physical law that, with weakening the fiber cross-section, the uncoupled light is more absorbed. The weakened light measured at the end of an optical fiber is then a measure for the existence of a crack or for the changed width of the crack. It needs to be noted that upon reaching a certain crack width the sensor can be destroyed. To localize cracks, one needs to measure the reflection runtime within the optical fiber. This, however, results in a large procedural investment in equipment and data analysis technique. Different types of fiber-optic sensor are applied to monitor civil engineering structures (Casas and Cruz 2003).

Temperature, humidity and corrosion sensors

For permanent acquisition of these variables, commercially obtained sensors are suitable. The basic criteria for selection of sensors are minimal change of the variable to monitor (resolution, linearity, accuracy), measuring range, type of measurement (static, dynamic, etc.), test duration (long-term stability), test environment, installation environment and financial resources.

As an example, monitoring the penetration of threshold chloride concentration at various depths of concrete cover is used to update the time-to-corrosion initiation at rebar level (initiation phase). A series of corrosion macro-cells may be installed at various depths thorough the cover thickness in the structure to be monitored. Raupach and Schiessl (1995) and Schiessl and Raupach (1992) proposed two alternatives (Fig. 9.3). The first is the corrosion ladder, which is installed before placement of concrete. The second is the expansion-ring anode. In both systems, around 4–6 anodes are set up at equal spacing through the cover thickness, and are connected to a separated cathode. The limiting values to model corrosion initiation for the expansion ring system are 400 mV and 10 µA. With these monitoring systems, a plot of time to initiation of corrosion with depth can be obtained. From the plot, a prediction of the time until depassivation of the reinforcement (depth equal to concrete cover) can be extrapolated. But more importantly, the plot may be very useful in the updating of the input parameters that control the depassivation process. In this way the accuracy of existing deterioration models for the inititation phase of corrosion can be improved (Rafiq, 2005).

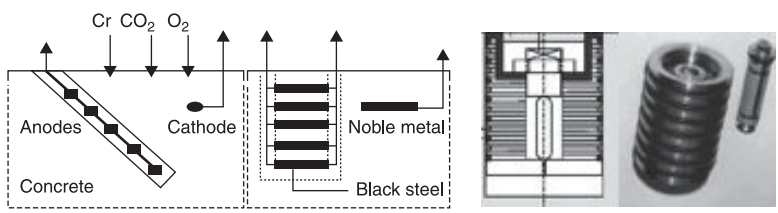

9.3 (a) Ladder arrangement; (b) expansion ring system.

Zimmermann developed an electrochemical sensor for chloride and resistivity measurements based on a solid silver chloride electrode for use in cement paste, mortar and concrete. The sensor element is placed at the same level as the steel rebar and oriented parallel to it. The potential of the chloride sensors and the rebars are measured versus an MnO_2 reference electrode embedded in the surrounding concrete.

In addition to the work developed for the initiation phase of the corrosion process, McKenzie (2005) has studied a monitoring technique for the propagation phase (corrosion rate). The idea is to embed linear polarization resistance (LPR) corrosion monitoring probes into reinforced concrete. The probes measure corrosion currents that are used to estimate corrosion rates. From the tests results reported by McKenzie, it seems that there are still a number of unresolved issues related to the variability of probe response as environmental conditions change (temperature and moisture conditions) and the interpretation of probe response in terms of corrosion activity. This is something easily attained as the embedded probes provide a continuous monitoring.

An important variable to monitor in prestressed concrete structures is the corrosion in prestressing wires, mainly in post-tensioned structures where, if the injection of the ducts is not done properly, corrosion may develop quickly and result in the failure of the prestressed elements. Casas and Villalba (Casas and Villalba, 2004; Villalba and Casas, 2004; 2005) have developed a monitoring technique that has been proven to work efficiently to monitor the corrosion progress as it occurs in the breakage of the different wires that form the prestressing strand and the tendon.

Acoustic emission sensors

The use of this type of sensor is still incipient in civil engineering structures. However, their suitability in the detection of progressive failure of materials (concrete, steel, composites) or of interfaces between different materials (bonding between steel and concrete, bonding between composites and concrete, etc.) gives them the potential for wider application, mainly for the detection of fatigue cracks in prestressing tendons and steel cables. The method has been widely used in the non-destructive inspection of metallic elements in civil engineering structures (offshore platforms, shear studs, orthotropic steel bridge decks, suspension bridges, bridge bearings). Although less used in concrete structures, laboratory experiments have shown their feasibility in identifying crack location, type and orientation (Ohtsu, 1996; Ohtsu *et al*., 1998; Colombo *et al*., 2004). One of the fields for application of this method is in the detection of corrosion, loss of prestressing, or progressive failure of wires in cables of internal/external prestressing or cable-stayed and suspended structures. As an example, in the USA six long-span bridges use this method, including the Bronx Whitestone Bridge. In Europe, it has been used in one suspension bridge and 10 post-tensioned concrete bridges. As an example, the Huntingdon Bridge is a post-tensioned concrete structure with a main span of 64.3 m. The inspection of the bridge detected the presence of voids, water

and chlorides in the prestressing tendon ducts. An SHM consisting of 36 acoustic emission sensors was installed in 1998 to monitor the tendon wire-break activity because of the corrosion likely to occur due to inappropriate tendon grouting. If more and more cables break over time, the bridge must eventually be closed to traffic. The objective of the monitoring was to see how many cables may break in the future years. The viaduct has not experienced any naturally ocurring wire breaks during monitoring, although the conditions for corrosion are present.

9.2.2 Measurement equipment

In general, long-term monitoring measurement equipment consists of the following components (SAMCO 2006):

- signal amplifier (voltage amplifier, charge amplifier, carrier frequency measuring amplifier, bridge amplifier);
- analogue anti-aliasing filter (tuned to the necessary cut-off frequency);
- measurement data acquisition system with analogue–digital conversion (16–24 bit conversion depth);
- data analysis computer for managing and processing data reduction and storing;
- data storage (semi-conductor, flashcard, disc, floppy, streamer tape, etc.);
- uninterruptible power supply;
- unit for remote data transmission with telecommunication devices (phone line for data or fax machine, mobile phone or transceiver for satellite communication) or data channels for traffic management systems.

Extensive information on existing testing and monitoring techniques, the measurement techniques and the available sensors can be found in ISIS (2001) and FIB (2003). Specific information in the case of bridge systems is available in Aktan *et al*. (2002).

9.3 Applications

Application of SHM systems to civil engineering structures is strongly indicated in the following cases:

9.3.1 Very large structures

In this section, structures that represent an important step forward in their main dimensions, or in the actions that they have to support (strong winds, earthquakes, etc.), are discussed.

Around 50 long-span bridges worldwide, with spans longer than 100 m, have been equipped with SHM systems. Some examples are shown below.

The Humber Bridge in the UK is one of the longest-span bridges in Europe. Its central span is 1.41 km long, total length is *ca*. 2 km. One concern regarding this

bridge, which was opened in 1981, is corrosion of the suspension cables (Hoult *et al*., 2008). There is the risk of corrosion, especially in the area of anchorage chambers, where the wire strands do not have protective wrapping. A wireless sensor network has been installed in the anchorage, consisting of 11 wireless sensors of the type 'MICAz motes'. The sensors do not monitor corrosion itself, but environmental conditions in the chamber: relative humidity and temperature. The data of relative humidity is used to trigger the operation of dehumidifying units, which must manage to keep the relative humidity below 60%.

Beside this monitoring system, a test with kinematic GPS sensors was carried out on this bridge. The GPS sensors measured deflection of the bridge. Measurement accuracy of several millimeters in horizontal and 1 cm in vertical direction was achieved. The maximum sampling frequency was 5 Hz. While these sensor specifications are not suitable for most bridges, the results at the Humber Bridge were satisfying. The bridge has a fundamental eigenfrequency of 0.116 Hz and showed deflections up to 70 cm.

The monitoring project at the Confederation Bridge project was originally aimed at demonstrating that fiber-optic sensors, in an early stage of development at that time, would be robust enough to withstand concrete construction on a large-scale project. A total of 22 sensors were installed on several sections of reinforcing steel and eventually embedded within a large prestressed concrete main girder component. Periodic monitoring of the sensors demonstrated their ability to withstand the construction process. During construction, 22 fiber-optic sensors were installed in the bridge at locations coinciding with conventional sensors. The project investigates the long-term durability of these sensors as well as testing new Bragg sensor instrumentation systems.

The city of Hong Kong has a vast experience in the field of SHM. Several of the most important bridge projects present a long-term monitoring system for the surveillance of the bridge performance (Wong, 2004; 2007). Health monitoring of cable-supported bridges in Hong Kong involves the integration of instrumentation, analytical and information technologies with knowledge and experiences in design and construction, operation and maintenance of cable-supported bridges for continuous monitoring of performance throughout their lifespan. A bridge health monitoring system called the WASHMS (Wind and Structural Health Monitoring System) has been devised and operated by the Highways Department to monitor the structural conditions of various long-span bridges. Five major bridges in Hong Kong are equipped with SHM systems. The main objective of instrumentation and health monitoring is to detect and evaluate any symptoms of operational anomalies and/or deterioration or damage that may induce adverse effects on service or safety reliability through the processing and analysis of data collected from transducers and sensors. This WASHMS is composed of six modules, namely the sensory system, the data acquisition and transmission system, the data processing and control system, the bridge health evaluation system, the portable data acquisition system, and the portable inspection and

maintenance system. The monitoring items are in general classified into three categories, namely the loading sources (or input parameters), which include wind, temperature, traffic (highway and railway) and seismic loadings; system characteristics (or system parameters), which include, static influence coefficients and global dynamic characteristics; and bridge responses (or output parameters), which include variation in geometric configuration (or displacements of the bridges), stress/strain distribution, cable forces and fatigue stress estimation.

The system comprises nine types of sensor: anemometers, temperature sensors, servo-type accelerometers, dynamic weigh-in-motion sensors, GPS, level sensing stations, displacement transducers, weldable strain gauges and CCTV video cameras. Strain is also measured in some bridges by FBG strain sensors. These sensors collect the signals and deliver them to the PC-based data acquisition units through category 5 unshielded twisted-pair (UTP) cables.

In China (not including the Hong Kong Special Administrative Region), more than 20 long-span bridges with a main span between 160 m and 1385 m have been instrumented with SHM systems (Ko and Ni, 2005). The most challenging one is the Sutong Bridge, which is the longest cable-stayed span (1088 m) in the world. The SHM deployed in the bridge is shown in Fig. 9.4.

The Jiangyin Suspension Bridge, with a main span of 1385 m and tower height of 190 m, is one of the bridges in the Chinese mainland that had long-term structural health monitoring systems installed at the end of last century.

After completion in 1998, the bridge was instrumented with a long-term SHM system, which consisted of 72 accelerometers to measure bridge dynamic response, 14 elastomagnetic sensors to measure the stress of main cables, 12 load pins to measure the tension force of hangers, one total station to measure global deflection of the deck, eight on-structure data acquisition units (DAUs) to collect and digitize signals, and an ethernet using 1 Mb-speed multi-mode fiber-optic cables for data transmission between the DAUs and the control room outside the bridge.

In 2004 an upgrade of the system was carried out (Zhou *et al*., 2006). The upgraded sensory system includes more than 170 sensors. Two tri-axial ultrasonic anemometers were installed on the tower top and the deck in the middle of main span for wind speed and direction measurement; eight GPS receivers were deployed to capture the bridge configuration, of which two GPS receivers were installed at the tops of the towers and the other six were installed at two edges of the deck at the locations of 1/4, 1/2, and 3/4 main span; 4 displacement transducers were installed to measure the longitudinal movement of two expansion joints (two for each expansion joint); 116 fiber-optic sensors were attached to the deck for strain and temperature measurement, including 72 fiber-optic sensors on nine equidistant cross-sections in the main span for longitudinal strain measurement, eight on the cross-section in the middle of main span for transverse strain measurement, and 36 on nine equidistant cross-sections for temperature measurement. 35 uniaxial accelerometers were installed for measurement of dynamic response, of which 15 accelerometers were installed on the deck, eight on main cables, and 12 on hangers. The instrumentation

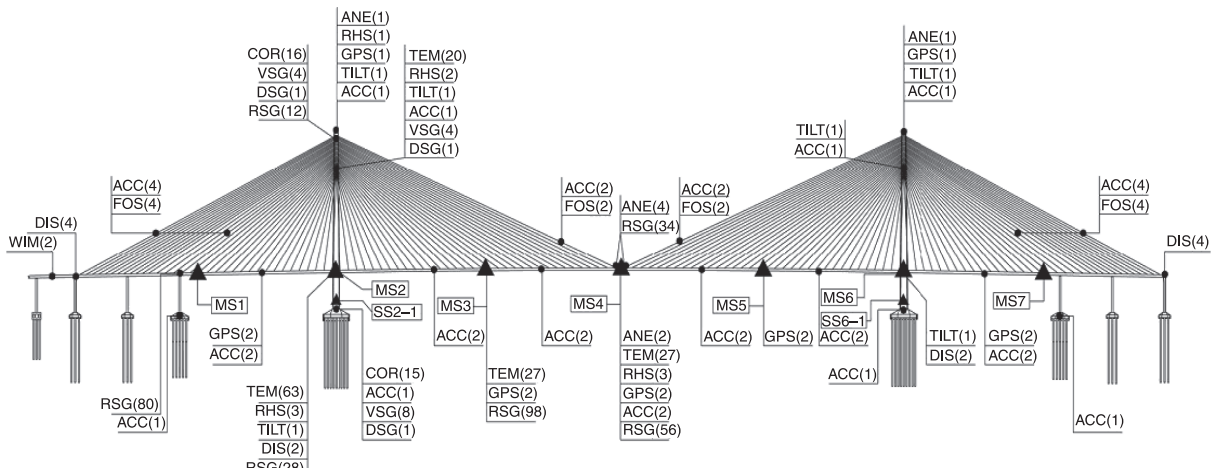

9.4 SHM system in the Sutong Bridge (Ko and Ni, 2005).

was used to analyze the wind conditions, defining the main directions and wind velocities, the intensity of the turbulence, the gust factor and the wind spectra.

The results show how actual wind loading is lower than predicted in the design. The SHM system has also been used to predict the time for the removal and change of deck joints and to obtain the global condition of the bridge after a ship collision. The experience in this bridge is a good example showing how the monitoring system has to be regularly inspected and maintained in order to obtain reliable and accurate data.

9.3.2 Innovative designs

In this section, structures that despite their common dimensions are innovative designs that have not been yet fully proved in their behavior, are discussed.

Within this category the following examples may be found:

In Port of Venice, Italy, a cable-stayed bridge has been constructed. Because of its rather complex structural behavior, a monitoring system has been implemented in order to verify design assumptions and to monitor its performance during service (ARCHES, 2009; Del Grosso *et al*., 2005).

The bridge deck construction is a composite steel and reinforced-concrete beam with two continuous spans of 105 m and 126 m length. The bridge axis is horizontally curved; it has a circular shape with a radius of 175 m in the plan view, which leads to the complex static and dynamic structural behavior. The deck is supported by nine cables in each span; the cable anchors are located in the middle of the cross-section. The reinforced-concrete pylon is nearly 80 m high.

The sensors have been installed and put into operation already during construction in order to acquire information about structural performance in significant construction phases. Static deformation values were of primary interest in this project, but the system also allows for performing periodic dynamic measurements.

The following sensors were implemented in the monitoring system:

Bridge deck:

- 48 linear fiber-optic strain sensors in four cross-sections
- four fiber optic inclinometers at bridge ends
- 24 temperature sensors.

Cables:

- one fiber-optic strain sensor at each cable.

Pylon:

- 12 linear fiber-optic strain sensors in four cross-sections
- two fiber-optic inclinometers at the top
- six thermocouples
- one anemometer.

The linear fiber-optic strain sensors feature a long base (1.5 m and 7.5 m) and an accuracy of 2 $\mu\varepsilon$.

The measured data has been used for curvature analysis of the bridge. The deformation shape of the structure was reconstructed from the data using the algorithm described by Inaudi *et al*. (1997). Future applications of the system will be in providing data during proof-load testing and the long-time service of the bridge.

A pedestrian bridge in Torino, Italy, has been equipped with a permanent monitoring system (Giacosa and De Stefano, 2008). The bridge is 380 m long and its arch-shaped pylon is 69 m high. The bridge deck is a box girder with triangular cross-section.

The following sensors were implemented in the monitoring system:

- 19 FBG strain sensors
- 12 accelerometer sensors
- 12 inclinometers
- 24 temperature sensors
- one LVDT relative displacement sensor.

The monitoring data was used as information about structural movements during service, especially due to temperature effects in various seasons.

In Taiwan, the Taichung Bridge has been monitored since its opening in 2003 due to the requirement to assess the cable forces, the global state of the structure and the dynamic behavior of the pylon.

The bridge has 44 cables that support the deck composed of steel girders and an orthotropic deck. The system consists of the following sensors:

- eight acceleration transducers in eight selected cables (out of 44)
- three velocity transducers at the main girders
- one tri-dimensional acceleration transducer at the pylon base
- one wind sensor 5 m above the road surface
- two temperature sensors inside and outside the box girder.

The bridge 'Herrenbrücke' in Lübeck, Germany, was built in 1964 and during inspection it showed signs of corrosion. It was assumed that up to 45% of the tendons were corroded. The bridge had to remain in service until the construction of a new bridge is finished, which meant an additional six years of service. Since an estimation of structural condition development was not possible from the knowledge of current condition only, a monitoring system was installed in the bridge. It was expected that failures of additional tendons would be observable as long-term gradual increase of strain.

The bridge has 18 spans of prestressed concrete orthotropic deck, each 19.4 m long. In the middle of the river is a steel bascule bridge with an 86 m span.

The following sensors were implemented in the monitoring system:

- five fiber-optic strain sensors
- 29 LDVT relative displacement sensors
- 15 temperature sensors.

The purpose of the monitoring system was to establish the serviceability of the bridge. Threshold values of strain have been determined from the long-term measurements. Due to temperature fluctuations, the threshold values were determined for different seasons. This approach proved to be insufficient due to temperature fluctuations within a season. Therefore, a neural network has been trained to separate temperature and load effects.

9.3.3 Other applications

In many cases, civil engineering structures adopt cables or stays to equilibrate the external actions. The correct performance of such stabilizing cables is of vital importance to the safety of the structure, as their failure will represent the collapse of the structure. Therefore, SHM of cable forces in cable-stayed structures is of maximum interest. Long-term monitoring of cables can be carried out using elastomagnetic or vibrating methods (Ladysz and Casas, 2009; Casas, 1995; Casas and Aparicio, 1998; Casas and Aparicio, 2009).

As examples, in the Tabor Bridge, in the Czech Republic, the elastomagnetic method is used to long-term monitor the force of the cables in the cable stays. In the Podturen Bridge, in Slovakia, the sensors are deployed to monitor the remaining force in the cables of the external prestressing. In the Alamillo bridge (Fig. 9.5), in Spain, the acceleration records are used to monitor the cable forces periodically.

In Slovenia, two corrosion monitoring systems have been implemented. Two larger highway viaducts were instrumented in years 2003 and 2004: viaduct Škedenj (Ljubljana–Maribor highway) and in viaduct Črni kal (Ljubljana–Koper highway). Corrosion sensors have been installed in critical bridge sections (Fig. 9.6 and Fig. 9.7). Electrical resistance probes (ERP) were used for

(a) (b)

9.5 (a) Alamillo Bridge (Sevilla, Spain); (b) view of accelerometer attached to the stay.

9.6 The ER probes installation on-site on a bottom side of bridge tendon before concreting (Črni kal viaduct).

9.7 The ER probes installation on existing structure elements (Škedenj viaduct).

measurement of corrosion rates of steel in concrete, and the measurement of corrosion rates was performed periodically.

The results of the measurements on probes installed in the viaduct Škedenj revealed that the ERP method can be efficiently used in combination with

conventional testing techniques (visual inspection, electrochemical potential mapping, galvanostatic pulse technique (GP)). The results of the visual inspection and the potential-mapping indicated eventual corrosion areas, whereas the installed probes showed the actual corrosion rates and their evolution in time.

Another long-term monitoring experience has been developed with the use of electrically isolated post-tensioning tendons with plastic ducts. Besides the corrosion protection provided, it is also possible to monitor the corrosion protection by non-destructive measurement of the electrical impedance. The experience gained from the monitoring of two bridges with electrically isolated tendons in Switzerland after some years in service shows the potential of the monitoring technique (Elsener, 2005).

9.4 Future trends

With the rapid development of information and sensing technologies, SHM has received extensive research in various disciplines such as civil, mechanical, and aerospace engineering. In civil engineering, SHM has been mainly applied to essential infrastructure systems such as highway bridges due to their immediate importance to the society. SHM is used to automatically detect, locate, quantify, and assess the level of structural damages and/or deterioration based on changes in salient response features, as measured by deployed sensor arrays, due to extreme loads and/or progressive long-term deterioration. The potentially successful civil application of SHM technologies, however, is contingent upon a thorough knowledge of their cost-effectiveness as opposed to traditional inspection methods in terms of unit cost, applicability, operation, resolution, capability, and long-term durability, among other relevant concerns. In particular, the ability of SHM to monitor corrosion and crack-induced debonding of steel reinforcement, which are among major causes for condition deterioration of reinforced-concrete bridges, is of special interest. Also, the monitoring of cable state in the overall length of the cable is of great interest in the case of cable-supported and cable-stayed bridges. The main problem related to localized cracking and corrosion is that the place where the damage will appear is not known *a priori*. Therefore, when using local-monitoring sensors such as strain gauges or FBG, it is almost impossible to detect the presence of cracking unless, luckily, the sensor has been attached to the damaged point. In this sense, the use of optical backscatter reflectometer (OBR) sensors is a promising measurement technology for SHM, as it offers the possibility of continuous monitoring of strain and temperature along the fiber. Several applications to materials used in aeronautical construction have demonstrated the feasibility of such technique (Güemes and Soller, 2009). These materials (composites, steel, aluminium), apart from having a smooth surface where the bonding of the sensor is easily carried out, also have a continuous strain field when subject to external loading, and therefore the bonding of the OBR on the material surface is not in danger for high levels of loading as the OBR can

easily follow the strain in the material. The application of such a type of sensor to concrete structures may present some difficulties due to: (1) the roughness of the concrete surface and the heterogeneity due to the presence of aggregates of several sizes, (2) the fact that reinforced concrete cracks at very low levels of load, appearing as a discontinuity in the surface and the strain field that may provoke a break or debonding of the optical fiber. However the feasibility of using OBR in the SHM of civil engineering constructions made of concrete is also of great interest, mainly because in this type of structure it is impossible to know where the crack may appear and therefore severe cracking (dangerous for the structure operation) can appear without warning from the monitoring if sensors are not placed in the particular location where the crack appears. Recent experimental tests with concrete elements in the laboratory have shown the potentiality of detecting cracks as they appear without failure or debonding, as well as the compatibility of the OBR bonding to the concrete surfaces (Villalba *et al*., 2009). The results obtained show how the OBR sensor is not only capable of detecting appearing cracks that are hardly visible, but also of performing correctly up to load levels producing a crack width in the range of 1 mm.

One of the fields with major prospective development in the next future is the use of information provided from SHM systems on the life-cycle management of structures to optimize future planning and budgeting. The main profit from a monitoring system is in the maintenance cost saving from optimized maintenance measures and/or in the extension of the structure lifetime. The maintenance measures can be optimized based on the information extracted from monitoring. Due to the cost of a monitoring system, the installation should be carefully chosen. Long-term monitoring should be used on structures that have either very high cost of failure, or high risk of failure, or both. Actually, research efforts are oriented to this end: how to use the gathered data in the maintenance policy. The life-cycle cost optimization should also take into account the cost of the monitoring system and the cost of its own maintenance (Ladysz and Casas, 2009).

When using SHM as a warning for damage detection, further research is needed on how to define warning thresholds that take into account the randomness in the variables that are measured and used for damage detection (Garcia *et al*., 2008; Campos *et al*., 2005).

Other future research trends include the use of diagnostic methodologies for a quick assessment of structures after unusual events (tornado, earthquake, etc.) and the monitoring of repaired/strengthened structures (Casas *et al*., 2002).

9.5 Sources of further information and advice

A comprehensive reference on SHM is the book edited by Balageas, Fritzen and Güemes (2006), which details the various sensing techniques used to achieve structural health monitoring. Its main focus is on sensors, signal and data reduction methods and inverse techniques that enable the identification of the physical

parameters affected by the presence of the damage on which a diagnostic is established. SHM is not oriented by the type of application or linked to special classes of problems, but rather presents broader families of techniques: vibration and modal analysis; optical-fiber sensing; acousto-ultrasonics using piezoelectric transducers; and electric and electromagnetic techniques. Specialists in the subject area who possess a broad range of practical experience have written each chapter. The book will be accessible to students and those new to the field, but the exhaustive overview of present research and development, as well as the numerous references provided, makes it required reading for experienced researchers and engineers.

Updated information on the forthcoming achievements in the field of SHM systems in civil engineering structures is available at the web pages of international organizations: ISHMII (International Society for Structural Health Monitoring of Intelligent Infrastructure, http://www.ishmii.org), SAMCO (European Association on Structural Assessment, Monitoring and Control, http://www.samco.org), and IABMAS (International Association for Bridge Maintenance and Safety, http://www.iabmas.org)

9.6 References

Aktan A E, Catbas F N, Grimmelsman K A and Pervizpour M (2002) 'Development of a Model Health Monitoring Guide for Major Bridges'. Drexel Intelligent Infrastructure and Transportation Safety Institute.

ARCHES (2009) Assessment and Rehabilitation of Central European Highway Structures. European Union – VI Framework Program. Available from: http://arches.fehrl.org [Accessed February 2009].

Balageas D, Fritzen C-P, Güemes A (eds) (2006) 'Structural Health Monitoring'. Hermes Science Publishing, London.

Campos J, Casas J R, Figueiras J (2005) 'A new methodology for damage assessment of bridges through instrumentation: Application to the Sorraia river bridge'. *Structure and Infrastructure Engineering*, 1(4): 239–252.

Casas J R (1995) 'Full-scale dynamic testing of the Alamillo cable-stayed bridge in Sevilla (Spain)'. *Earthquake Engineering and Structural Dynamics*, 24: 35–51.

Casas J R and Aparicio A C (1998) 'Monitoring of the Alamillo cable-stayed bridge during construction'. *Experimental Mechanics*, 38(1): 25–29.

Casas J R, Ramos G, Diaz S, Güemes J A (2002) 'Intelligent repair of existing concrete structures'. *Computer-Aided Civil and Infrastructure Engineering*, 17(1): 41–50.

Casas J R and Cruz P (2003) 'Fiber optic sensors for bridge monitoring'. *Journal of Bridge Engineering, ASCE*, 8(6): 362–373.

Casas J R and Villalba V (2004) 'Structural integrity of post-tensioned concrete bridges by tendon monitoring'. ICEM12,12th International Conference on Experimental Mechanics. Bari, Italy.

Casas J R and Aparicio A C (2009) 'Rain-wind induced cable vibrations in the Alamillo cable-stayed bridge (Sevilla, Spain). Assessment and remedial action'. *Structure and Infrastructure Engineering*, 6(5): 549–556.

Colombo S, Main I G, Shigeishi M, Forde M C (2004) 'NDT integrity and load carrying assessment of concrete bridges'. Proceedings of IABMAS '04, Kyoto, Taylor and Francis, pp. 803–805

Del Grosso A, Torre A, Inaudi D, Brunetti G, Pietrogrande A (2005) 'Monitoring system for a cable-stayed bridge using static and dynamic fiber optic sensors'. Second International Conference on Structural Health Monitoring of Intelligent Infrastructure, Shenzhen, China.

Elsener B (2005) 'Long-term monitoring of electrically isolated post-tensioning tendons'. *Structural Concrete*, 6 (3): 101–106

FIB (2003) 'Monitoring and safety evaluation of existing concrete structures'. Bulletin No. 22, Lausanne, Federation Internationale du Beton.

Garcia O, Vehi J, Campos J, Henriques A, Casas J R (2008) 'Structural assessment under uncertain parameters via interval analysis'. *Journal of Computational and Applied Mathematics*, 218(1): 43–52.

Giacosa L M, De Stefano A (2008) 'Long-term Structural Health Monitoring of the Torino's Pedestrian Cable-stayed Bridge'. Proceedings of 4th International Conference on Bridge Maintenance, Safety, and Management, Seoul, Korea.

Güemes A, Soller B (2009) 'Optical fiber distributed sensing: physical principles and applications'. 7th International Workshop on Structural Health Monitoring, Stanford University (USA).

Güemes A, and Messervey T B (2010) 'Smart textile and polymer fibers for structural health monitoring', in G Pohl (ed.) *Textiles, Polymers and Composites for Buildings*'. Woodhead Textiles Series No. 95, Cambridge.

Hoult N A, Fidler P R A, Middleton C R, Hill P G (2008) 'Turning the Humber Bridge into a Smart Structure'. Proceedings of IABMAS '08, 4th International Conference on Bridge Maintenance, Safety, and Management, Seoul, Korea (Taylor and Francis).

Inaudi D, Casanova N, Vurpillot S (1997) 'Fiber optic deformation sensors for bridge monitoring'. International Conference on New Technologies in Structural Engineering, Lisbon, Portugal.

ISIS (2001) 'Guidelines for structural health monitoring, Design Manual No. 2'. The Canadian Network of Centres of Excellence on Intelligent Sensing for Innovative Structures, Winnipeg, Canada (http://www.isiscanada.com).

Ko J M and Ni Y Q (2005) 'Technology developments in structural health monitoring of large-scale bridges', *Engineering Structures*, 27: 1715–1725.

Ladysz A, Casas J R (2009) 'Quantitative deployment of long-term force monitoring devices in cable-stayed bridges. A life-cycle cost (LCC) approach'. 10th International Conference on Structural Safety and Reliability (ICOSSAR2009), Osaka, Japan.

Mckenzie M (2005) 'The use of embedded probes for monitoring reinforcement corrosion rates', in G A R. Parke and P Disney (eds), *Bridge Management 5*, Thomas Telford, London, pp. 219–226

Ohtsu M (1996) 'The history and development of acoustic emission in concrete engineering'. *Magazine of Concrete Research, ACI*, 48(177): 321–330.

Ohtsu M, Okamoto T and Yuyama, S (1998) 'Moment tensor analysis of acoustic emission for cracking mechanisms in concrete'. *ACI Structural Journal*, 95(2): 87–95.

Rafiq M I (2005) Health monitoring in proactive reliability management of deteriorating concrete bridges. PhD Thesis, The University of Surrey, School of Civil Engineering.

Raupach M and Schiessl P (1995) 'Monitoring system for the penetration of chlorides, carbonation and the corrosion risk for the reinforcement', in M Forde (ed.), *Structural Faults and Repair 95*. Engineering Technics Press, London.

SAMCO (2006) 'Guideline for Structural Health Monitoring. Final Report'. European Thematic Network SAMCO, Structural Assessment, Monitoring and Control.

Schiessl P, Raupach M (1992) 'Monitoring system for the corrosion risk of steel in concrete structures'. *Concrete International*, (7): 52–55.

Villalba V and Casas J R (2004) 'Structural Health monitoring of post-tensioned bridges and structures based on fiber optics'. II European Workshop on Structural Health Monitoring. Munich, Germany.

Villalba V and Casas J R (2005) 'Long-term monitoring and up-dating of corrosion models in post-tensioned concrete structures'. IV International Workshop on Life-Cycle Cost Analysis and Design of Civil Infrastructure Systems. Cocoa Beach, Florida.

Villalba S, Fernandez A, Casas J R, Güemes A (2009) 'Feasibility of Structural Health Monitoring of Concrete Structures by Optical Backscatter Reflectometer'. 7th International Workshop on Structural Health Monitoring, Stanford University, Palo Alto, CA.

Wong K Y (2004) 'Instrumentation and health monitoring of cable-supported bridges'. *Structural Control and Health Monitoring*, 11: 91–124.

Wong K Y (2007) 'Design of a structural health monitoring system for long-span bridges'. *Journal of Structure and Infrastructure Engineering*, 3(2): 169–185.

Zhou H F, Ni Y Q, Ko J M (2006) 'Analysis of Structural Health Monitoring Data from the Suspension Jiangyin Bridge'. Proceedings of the Third European Workshop on Structural Health Monitoring, Granada, Spain.

10

Fibrous insulation materials in building engineering applications

X. LU and M. VILJANEN, Aalto University, Finland

Abstract: This chapter introduces basic material and mechanical characteristics of fibrous insulation materials in building engineering applications. Starting with the physical fundamentals of the raw material, the authors move to the issues of the manufacturing process that leads to certain common characteristics, thoroughly working out the physical and thermal properties of the fibrous insulation materials. Coupled heat and mass transfer through a fibrous insulation in buildings is studied, and a wide area of applications of fibrous materials in buildings are discussed. The fibrous insulation materials, various heat and mass transfer models in fibrous insulation, fibrous composites, properties of the composites, and their applications in buildings are reviewed also. The chapter provides a guide to the fundamentals and latest developments in building technology for fibrous materials.

Key words: fibrous material, building insulation material, fibrous composites, physical and thermal properties, raw material, manufacturing process, heat and mass transport, mathematical model, applications.

10.1 Introduction

Insulation has been used in pipes and roofs since the earliest recorded history of the ancient Egyptians, Greeks and Romans. The feature that all insulating materials have in common is their low thermal conductivity, in order to reduce the total coefficient of heat transmission. Dry stagnant gas is one of the best insulating materials with the lowest thermal conductivity over a wide range of temperatures, typically 0.024 W/mK (Karamanos *et al*., 2008). Cavity walls have a long history of use by the Greeks and Romans by filling in the air between the inner and outer walls to provide a degree of thermal insulation. Fibrous insulators function in the same way, by trapping air within and between their fibers. In addition to their high-efficiency adsorption capacity from gaseous media that makes them less conductive, fibrous materials exhibit other features that make their use advantageous as insulation materials for buildings compared to other materials: for example, they can be easily obtained in various convenient forms. These advantages allow cost-effective manufacture of fibrous insulation products.

In the early 1800s, Joseph Fourier formulated the law of heat conduction that has been considered as the theoretical basis for heat transfer. However, there was not a significant need or market for insulation until the late 1800s when companies started building steam power plants which required thermal insulators. After the

First World War, the insulation industry experienced massive demand for plaster and insulation with many fibrous products such as rock wool and silica fibers because of the post-war building boom (Lotz, 2006). Today, fibrous materials are still the most widely used categories of insulating materials in buildings.

This chapter presents an update of existing fibrous insulation materials and newly developed fibrous composites in building engineering applications. Starting with the physical fundamentals of the raw materials, the authors move to the issues of the manufacturing processes that lead to certain common characteristics, thoroughly working out the physical and thermal properties of the fibrous insulation materials. Coupled heat and mass transfer through fibrous insulations in buildings is studied. The fibrous insulation materials, heat and mass transfer models in fibrous insulation, fibrous composites, properties of the composites, their applications, and available studies on relevant themes are reviewed. The chapter provides a guide to the fundamentals and the latest developments in building technology for fibrous materials.

10.2 Raw materials and manufacturing process

10.2.1 Classification of fibrous insulation materials

Fibrous insulation materials can be classified in many ways; for example, by their physical structure. Figure 10.1 shows the most commonly used categorization of fibrous insulation materials (Papadopoulos, 2005).

Organic fibrous insulations have played an historically significant role for building engineering applications. Since ancient times, natural fibers, such as cotton, sheep's wool, straw, hemp, and asbestos fibers (see Fig. 10.2) have been

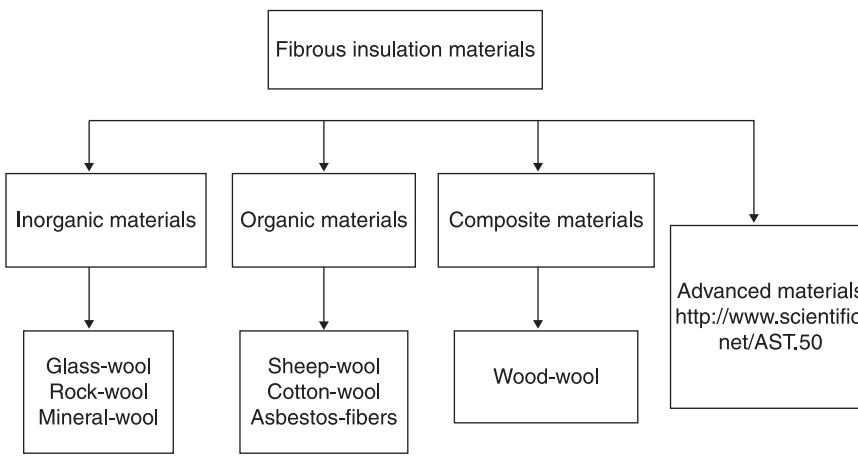

10.1 Classification of fibrous insulation materials (Papadopoulos, 2005).

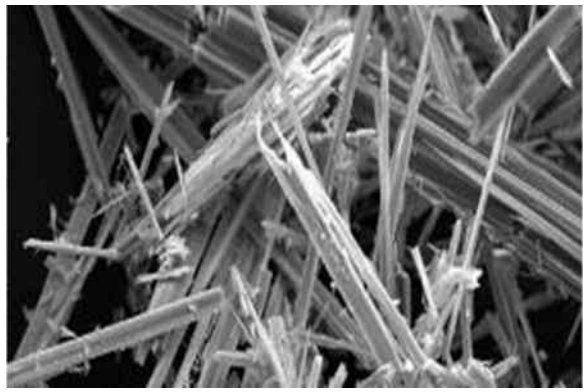

10.2 Asbestos fiber (extracted from *The Constructor of Modern World,* 2009).

used as insulators in buildings. These materials can be employed by themselves as roofing, wall, and mat materials, as well as combined with hydraulic-setting binders to make various types of building boards. However, organic fibrous materials have some shortcomings, which limit their applications. The low resistance to high temperatures and ultraviolet light constitutes one of their most serious defects as well as other environmental extremes (Rose, 1961).

Therefore, inorganic fibrous materials (see Fig. 10.3 as an example), such as high-performance glass wool and rock wool, have been widely used nowadays and are expected to play the main role, with growth rates of more than 5 per cent; whilst organic foamy materials are expected to show annual growth rates of some 2.5 per cent (Data from publications and the web-site of the Association of Plastics Manufacturers in Europe, 2004) even though the inorganic fibrous materials are comparatively new materials and were not commonly used before the Industrial Revolution (Hoskins, 2001). The high temperature resistance of inorganic fibrous materials is one of the most attractive properties when considering building fire protection. Throughout the twentieth century, chemists have become extremely successful at either synthesizing natural products or creating new products that are cheaper and/or better than natural products. In fact, a large variety of inorganic fibrous combinations of organic, inorganic and advanced materials has been developed, each designed with specific properties suitable for a particular use, and could not be replaced by organic materials. These materials can be engineered to provide superior characteristics to enhance their life and performance in extreme environments.

However, there have been many concerns associated with inorganic fibrous materials in buildings (Catherine *et al*., 1988). With the rapid increase in green building and sustainable-environment activities, engineers have responded by using organic instead of inorganic fibers, or combinations of different types of natural and synthetic fibers, to meet design requirements. Nevertheless, an

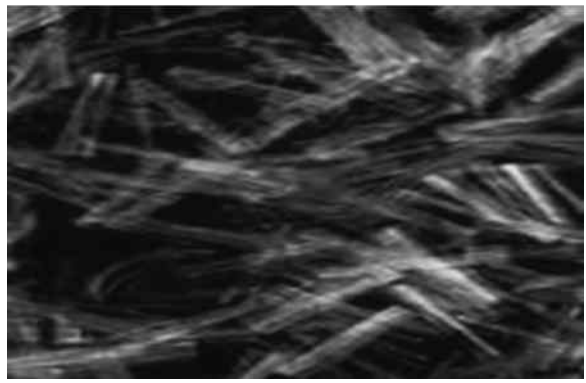

10.3 Glass fiber reinforced concrete (extracted from *The Constructor of Modern World*, 2009).

important common feature of the markets for most fibers is the balance between the increasing interest in natural products and the competition from cheaper, inorganic and synthetic fibers.

10.2.2 Raw materials

The raw materials of fibrous insulations can be categorized according to the fiber classification presented in Fig. 10.1 based on the specific types of insulation product. Among the organic materials that are regularly used as building insulators, cellulose is made from recycled newspaper and treated with chemicals. Cork is produced from natural cork oak. Sheep's wool is made from either new or recycled wool. Hemp fiber generally contains hemp fibers, cotton fibers and thermoplastic polyester binding fibers. Vermiculite consists of complex hydrated aluminium magnesium. Among the inorganic materials, mineral wool and mineral fibers are fibers made from natural or synthetic minerals or metal oxides. The metal oxides are generally used to refer to fiberglass, ceramic fibers and rock or stone wool. The basic raw materials for fiberglass are various natural minerals and manufactured chemicals. The major ingredients are silica sand, limestone, and soda ash. Ceramic fiber is made from high-purity alumina-silica materials and produced by melting these raw materials and blowing or spinning. Copper, gold or silver are extruded, or more brittle ones, such as nickel, aluminum or iron deposited, which are the major raw materials for metallic fibers.

10.2.3 Manufacturing process

Manufacturing involves processing raw materials into the products required to satisfy the needs of societies. Manufacturing enterprises use various raw materials

and operations organized according to a well-prepared plan or schedule. Nowadays, modern manufacturing can include all of the intermediate processes that are done by other people, which were disregarded before as part of manufacturing. The entire manufacturing process, beginning with the basic raw materials, is ecological. All the materials used in the manufacture of insulation can be recycled in the process. At the end of the lifecycle of a building, fibrous materials can be recycled back to the insulation material.

The uses and purposes of fibrous insulation products are mainly for cavity walls, solid walls, structural insulated panels, roof insulation, and insulation materials for heating systems as well as water services. Each product has its own role in different applications depending on its general properties. All products are likely to have both advantages and disadvantages for use in certain applications. Therefore, every property required for an application influences the material selection in varying degrees. When choosing a material, consideration needs to be given, for example, to the thickness requirement, fire resistance, acoustic performance, breathability, and reliability (BNIM01, 2008). Very often, a combination of different types of product would help to satisfy a wider range of requirements. Nevertheless, the very first step is to select the raw materials. The selection rules are the same as those applied to the products, according to many criteria including their physical and chemical properties, cost, and their human and environmental safety. Obviously, the basic criteria are the resources of the particular type of raw material, the cost, and the manufacturing progress.

Fundamentals of the fiber manufacturing process comprehensively cover the principles of transport phenomena and chemical reaction engineering. Figure 10.4 displays the four main areas of fiber manufacture: pumping, filtration, fiber forming, and fiber treatment; focusing on the fundamentals associated with the transport phenomena rather than the chemistry of fiber production (Weinberger, 1996).

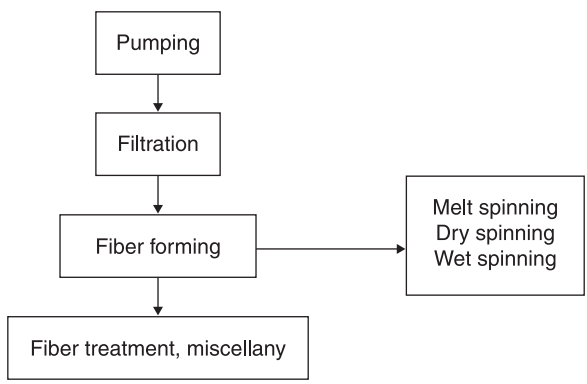

10.4 Synthetic fiber module – principle elements.

There are various fiber production processes depending on many different factors, including the quality and quantity of the final product. In some cases they are very specific. Take a mineral wool as an example: the most commonly used production process can be roughly divided into three different steps involving a jet of molten rock falling onto a series of rotating discs (Ohberg, 1987; Trdic *et al*., 1999; Angwafo *et al*., 1998; Westerlund & Hoikka, 1989). Figure 10.5 and Fig. 10.6 present these major steps with a more detailed flow chart and production line.

The raw material, rock for example, is melted to a molten material at a temperature of 1400–1600°C and formed as a highly viscous fluid that flows into a reservoir. The liquid rock then flows, under the action of gravity, to form the jet,

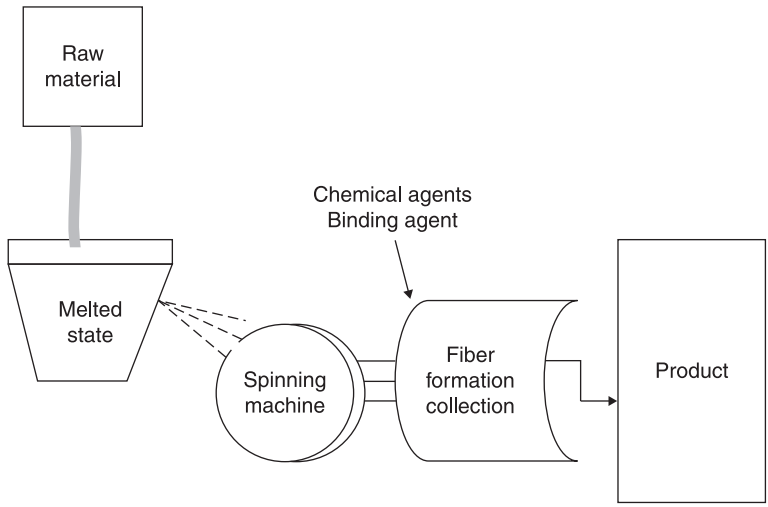

10.5 Major steps of a mineral wool production process.

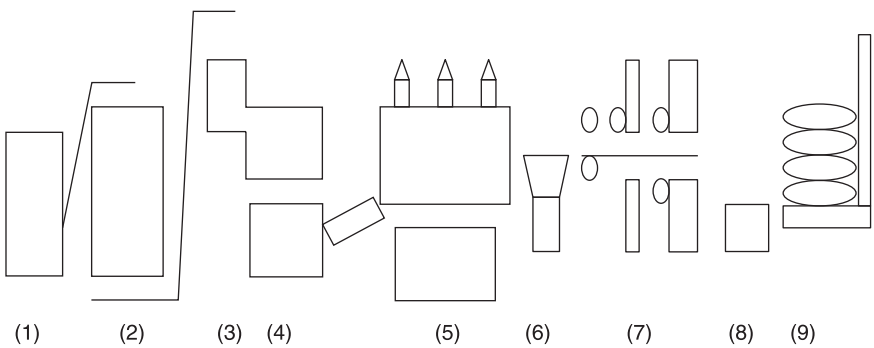

10.6 Schematic view of a mineral fiber production line: (1) raw material; (2) feeding; (3) melting; (4) dry binder addition; (5) condensation; (6) hardening; (7) cutting; (8) packaging; (9) product.

which flows onto the rotating disc of the spinning machine. Molten material is distributed over the surface of the machine and rotated to form the fibers. Air or steam is blown around the rotating machine to assist in fiberizing the fibers. Depending on the desired product, various chemical and binding agents may be applied to the newly formed fibers immediately following the rotation. After this the fibers enter the conveyor belt of the secondary mineral-wool layer where they are thermally treated and finalized to the desired density, thickness and size. Then they are collected in a chamber and mechanically formed, for example by compression, into the final product.

10.3 Fibrous materials: characteristics and properties

Thermal insulation is an important element of energy conservation. To maximize the energy efficiency of insulating materials, various factors that may affect the efficiency of heat insulation should be taken into account. The knowledge of simultaneous heat and mass transfer through the insulators is very important. Fibrous materials have a unique structure of complex geometry that belongs to a typical kind of porous material. Therefore, the study of porous media provides a fundamental understanding of the heat and mass performance of the fibrous materials.

10.3.1 Basic concepts

A porous medium is defined as a material characterized by the presence of a solid matrix, and a void phase that is presented by its porosity. Porosity ε describes the fraction of void space V_v in the material of volume V:

$$\varepsilon = \frac{V_v}{V}.$$

Porosity has been reported to be an important factor to the thermal insulating performance (Farnworth, 1983; Fan *et al*., 2004; Wu *et al*., 2007; Cheng & Fan, 2004).

Tortuosity is another important dimensionless parameter that describes the complex structure of the material and is defined as

$$\tau = \frac{L_{transverse}}{L},$$

where

$L_{transverse}$: length of the path transversed by fluid

L: body length of the path transversed by fluid.

In describing the properties of porous materials, pore shape factors are sometimes introduced, relating the behavior of real pore shapes to that which

would be obtained for circular pores. In the case of an oval shape with longer axis a and shorter axis b, the pore shape factor is defined as

$$\delta = \frac{b}{a}.$$

For a fibrous material, the fiber is often described by a convenient parameter called 'fiber aspect ratio' which is defined as a ratio of fiber length to diameter as

$$s = \frac{l_f}{D_f}.$$

For example, the aspect ratio of the dispersed fiber is about 75 (*The Constructor of Modern World*, 2009).

10.3.2 Heat and mass transfer models

It has been reported widely that moisture is one of the most serious factors in building and housing industry. Over the last decade, moisture failures in building systems have caused billions of Euros in damages in Europe, many of which involved the deterioration of sheathing panels. Additionally, excess moisture in envelopes can lead to the presence of moulds that results in poor indoor air. However, despite the vast research work on heat transfer in fibrous insulation, little has been done on coupled heat and moisture transfer until the 1980s. This subsection is devoted to modelling heat and moisture transfer in fibrous insulation materials.

The engineering analysis of the heat and moisture transfer in porous media can be dated as early as the 1920s in the field of drying science. The transport behavior of porous media is largely governed by the interactions between coexisting components, and these interactions occur through interfaces. Theoretically, transport processes in a porous medium domain may be described for a continuum at the microscopic level as taking into account the multi-phase nature of the material. However, this is impractical because of our inability to describe the complex geometry and to trace a large number of interfacial boundaries of the porous domain, although the lattice gas or lattice Boltzmann method did make such a description possible in some cases (Benzi *et al*., 1992; Rothman & Zaleski, 1994). Moreover, at this level we cannot measure physical quantities (Bachmat & Bear, 1986). Therefore, the porous media models are often constructed by averaging the governing equations in continua at the microscopic level over a representative elementary volume (*REV*). The statistical averaging method is another commonly used approach that treats the porous media as a random structure. The intrinsic medium properties are represented by statistical functions. The amounts of required data and statistical functions are large, which makes this approach impractical.

The terminology 'representative elementary volume' was first used by Bear (1972), and is defined as the minimum randomly selected volume that retains the porosity features of the entire volume of the site. In other words, if the volume is large enough it should account for the spatial heterogeneity of the parameter of interest within the scale of interest. A continuum approach attempts to describe mass, momentum and energy balance laws at macroscopic scale using *REV*. To summarize, the general macroscopic balance equation governing transport phenomena in porous media can be formulated as

$$\frac{\partial \rho \Psi}{\partial t} + \nabla \bullet (\rho v \Psi) - \nabla \bullet J - \rho F - \rho G = 0 \qquad [10.1]$$

where

ρ: mass density function

Ψ: intrinsic thermo-mechanical property

v: velocity

J: flux

F: external supply

G: rate of production.

The equation is volume averaged over *REV* as illustrated in Fig. 10.7. For example,

$$\rho_\alpha = \frac{1}{|REV|} \int_{REV^\alpha} \rho_{micro} d(REV^\alpha) \qquad [10.2]$$

where

ρ_α is the α-phase density function

ρ_{micro} is the microscopic density function

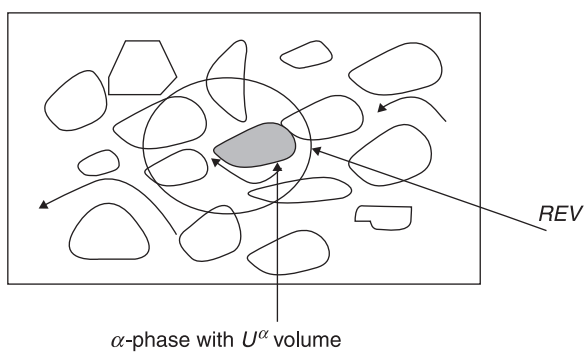

10.7 An illustrated representative elementary volume.

$|REV|$ denotes the volume of REV

REV^{α} is the subset of REV occupied by the α-phase.

At each spatial point within the porous medium, the transport properties such as density, conductivity, etc., are averaged, which reflects the corresponding microscopic properties. Details of the presentation of various averaging rules can be found in Bachmat (1972), Bachmat & Bear (1986), Bear (1972), Bear & Bachmat (1984), Bear & Bachmat (1986), Hassanizadeh & Gray (1979), and Whitaker (1966; 1967; 1969; 1985). In the following we present some of the commonly used fluid properties.

Energy transport

Over the decades, significant progress has been made in understanding the energy transport properties of fibrous materials (Daryabeigi, 2000; Lee & Cunnington, 2000; Verschoor, 1952; Hager & Steere, 1967; Larkin & Churchill, 1957). Heat transport through fibrous insulation involves the multiple heat transfer mechanisms of conduction, natural convection and radiation. The relative contributions of the various modes of heat transfer vary during re-entry. In high temperatures, radiation dominates, which is complicated because of the complex structures of the fibers and the inherent complexities associated with the transport mechanism itself (Zhang *et al*., 2008). Figure 10.8 illustrates the contributions from all three major heat transfer modes for mineral wool (RIL 155, 1984).

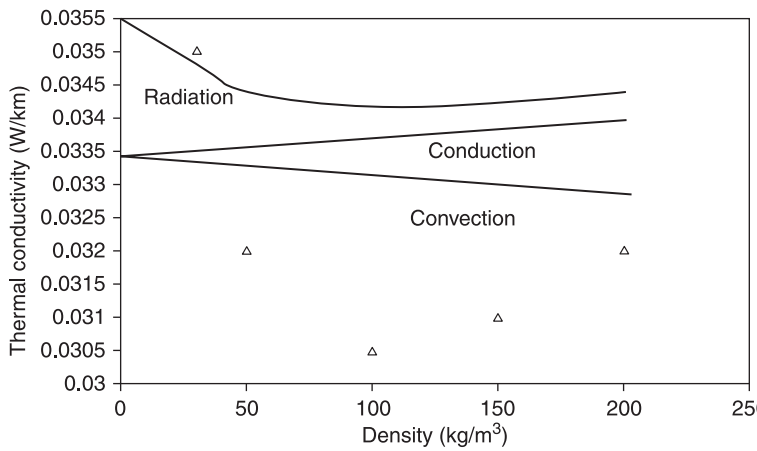

10.8 The contributions from all three major heat transfer modes for mineral wool.

Energy transport: conduction

Conduction is described by the first Fourier's Law which shows that the energy transport at the microscopic scale tends to flow from regions of high concentration of internal energy to regions of low internal energy. The macroscopic heat flux can be formulated as

$$Q_{conduction} = \lambda \nabla \bullet T \qquad [10.3]$$

where

T: temperature

λ: conductivity

subscript: heat transfer mode.

A simple heat balance equation can be expressed as

$$(\rho C_p)\frac{\partial T}{\partial t} = -\nabla \bullet (\lambda \nabla \bullet T) \qquad [10.4]$$

known as the second Fourier's law. For a fibrous material, if it has a low fiber volume fraction, heat conduction through its solid phase is often neglected. Therefore, only conduction through gaseous media is considered. The conductivity depends on the Prandtl number, Knudsen number, and the free path of the air's molecules, which is the function of temperature, the air's collision diameter and the pressure (Evseeva & Tanaeva, 2004). Karamanos *et al*. (2008) show a picture, Fig. 10.9, about how each transfer mode plays in the total heat transfer for stone wool fiber.

Energy transport: convection

By this mode, convection, heat is transferred via the movement of air. It can be classified according to its nature as natural convection and forced convection. Both forced and natural types of convection may exist together. Natural convection results from thermal buoyancy effects, whereas forced convection is typically driven by wind pressure and heating ventilating and air-conditioning (HVAC) equipment. The Rayleigh number is a dimensionless number that is associated with buoyancy-driven airflow and can be regarded as a measure of the driving forces of natural convection. The Nusselt number is another dimensionless number that is associated with forced convection and is a function of wind velocity and the shape of the fibrous insulation. In a fibrous material, convection exists due to the air movement in the pores between the fibers; but due to the small dimensions of the pores, convection is often neglected without loss of accuracy (Milandri *et al*., 2002; Karamanos *et al*., 2008).

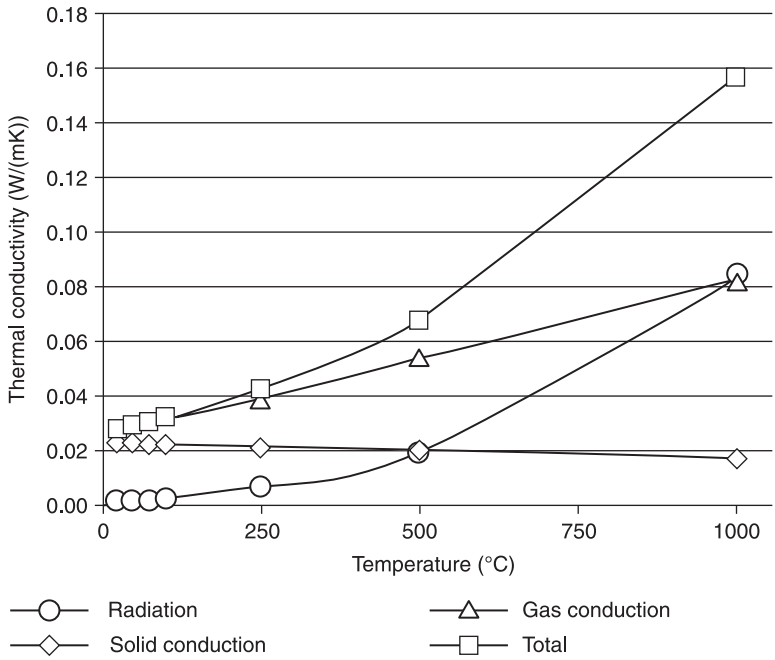

10.9 The contributions from major heat transfer modes for stone wool (extracted from Karamanos *et al.,* 2008).

Energy transport: radiation

Radiation is the transfer of energy by electromagnetic wave motion. It travels at the speed of light and does not require a medium to carry it. The radiative heat flux depends mainly on the absolute temperature of the emitting body based on the Stefan–Boltzmann law (Holman, 1997). For general porous media, the calculation of radiative heat transfer in porous media commonly requires solving the radiative transfer equation (Holman, 1997; Larkin & Churchill, 1959; Siegel & Howell, 1992; Webb, 1994; Lauriat & Ghafir, 2000; Lage & Narasimhan, 2000; Batycky & Brenner, 1997; Chen *et al*., 2002; Klements & Kim, 1985). But for fibrous materials, the prediction of radiative heat transfer means not only solving the radiative transfer equation but also requires knowledge of the radiative properties of the concerned material due to its absorbing, and scattering capabilities. Hence, the transport process of radiation in the fibrous insulation is complicated because of both its complex morphology and the inherent complexities associated with the transport mechanism itself. Such complexity of the heat transfer makes the analysis and the design of insulation quite difficult.

There has been extensive research on this theoretically, experimentally, and empirically (Tien, 1988; Hendricks & Howell, 1994; Singh & Kaviany, 1992; Tien & Drolen, 1987; Lee, 1990; Lee *et al*., 1994; Lee & Cunnington, 2000;

Verschoor *et al*., 1952; Hager & Steere, 1967; Tong & Tien, 1983). The refractive index, and the scattering and absorption coefficients are critical in determining the radiative properties. Viskanta and Mengüc (1989), and Baillis and Sacadura (2000), rigorously reviewed the methodology applied to the calculation of radiative transfer and its properties in dispersed media. Two basic methods are principally used: a theoretical model and identification approaches. Assuming that the media are composed of spherical particles, and starting from the properties of the basic components such as the optical indices, the theoretical model, based on Mie's theory, describes the interaction of an electromagnetic wave to predict the radiative properties of a fibrous material (Baillis & Sacadura, 2000). These models can provide the understanding of the physical side of the material. However, with the increasing complexity of, for example, the geometry of the fibrous material, theoretical models become sophisticated and are not very suitable. Therefore, on the experimental front an alternative way has been proposed to determine the radiative properties of a medium on which radiative behavior would not be easily modelled by a theoretical method (Baillis & Sacadura, 2000).

Radiative heat flux in a partially opaque medium is often expressed in the form of (Klemens & Kim, 1985)

$$Q_{radiation} = 4\sigma n^2 T^3 l \nabla \bullet T \qquad [10.5]$$

where

σ: Stefan–Boltzmann constant

n: average index of refraction

l: free path of photons.

The mean free path of photons are calculated by absorption and scattering inside the medium, as well as by the finite dimensions of the medium. Very often, the scattering and absorption coefficients are functions of frequency f. Mathematically, the mean free path is expressed as

$$l(f) = \frac{1}{\frac{1}{l_a(f)} + \frac{1}{l_s(f)} + \frac{1}{l_b}} \qquad [10.6]$$

where l_a is the absorption coefficient, l_s scattering coefficient and l_b the boundary mean free path (Klemens & Kim, 1985).

The transport process of radiation in the fibrous insulation is complicated by increasing temperature. Very often, to simplify the calculation, surface film coefficients are used to transpose the radiation into equivalent conduction through a fictitious surface layer. For example, the equivalent conductivity for radiation in fiber can be calculated as

$$\lambda_{radiation} = \frac{16\sigma}{3\beta} T^3 \qquad [10.7]$$

where β is the extinction coefficient depending on the material's density and the specific extinction coefficient (Yuen, 2003; Rice & Göransson, 1999; Karamanos *et al*., 2008).

Mass transport

Mass transport in fibrous materials can be due to several different modes. The three primary modes are: molecular diffusion for gases, capillary for liquids, and pressure-induced convection or Darcy flow.

Mass transport: molecular diffusion

Molecular diffusion is the transport of molecules from a region of higher concentration to one of lower concentration. Gases such as water vapour and air in fibrous media can move by molecular diffusion. Analogous to the heat conduction, the molucular diffusion is decibed mathematically by the second Fick's law. The macroscopic mass flux of gases is

$$J_{diffusion}^{gas} = - D_{gas} \nabla \bullet C_{gas} \qquad [10.8]$$

where

C: concentration

D: diffusivity

subscript: gas or liquid

superscript: gas or liquid.

The molecular diffusivity D can be related to the molecular diffusivity of gas in bulk in that

$$D_{gas} = \frac{D_{bulk}}{\tau} \varepsilon \qquad [10.9]$$

where D_{bulk} is diffusivity in bulk

So the mass conservation equation can be expressed as

$$\frac{\partial C_{gas}}{\partial t} = - \nabla \bullet (D_{gas} \nabla \bullet C_{gas}) \qquad [10.10]$$

which is the second Fick's law.

Mass transport: Darcy flow

In pressure-driven gas transport, Darcy's law is often used in calculating the mass flux in the form of

$$J_{pressure}^{gas} = -\rho_{gas}\frac{k_{gas}}{\mu_{gas}}\nabla \bullet P \qquad [10.11]$$

where

$k_{gas} = k.\, k_{relative}^{gas}$

k: intrinsic permeability

$k_{relative}$: relative permeability

μ: viscosity

Mass transport: capillary flow

Capillary flow is induced by a capillary attraction force that governs the action of a liquid against solid surfaces in small and confined areas. Darcy's law also describes the transport of liquid due to pressure. However, capillary attraction creates a negative pressure and therefore the mass flux of liquid is written as

$$J_{pressure}^{liquid} = -\rho_{liquid}\frac{k_{liquid}}{\mu_{liquid}}\nabla \bullet (P - p_c) \qquad [10.12]$$

where p_c is capillary pressure

The capillary pressure is defined as the pressure difference between the liquid and the gaseous phase.

Model equations

Mass and heat transfer through fibrous materials can be modelled based on the above-described mechanisms. In recent years, extensive research has been performed in this field. Depending on the level of detail desired, various macroscopic models have been proposed in the literature.

In the earlier literature, Bankvall (1973) conducted detailed experimental and theoretical research on the relative contributions of the three modes of heat transfer through fibrous insulation. He found that conduction in the gas phase was the most important heat transfer model in fibers. Radiation heat transfer was considerable at high porosities. The relative contribution of each type of heat transfer model with respect to critical porosities were proposed. Wijeysundera *et al*. (1989) set up an experiment to study thermal conductivity across a range of moisture contents using one-dimensional transient vapour diffusion and heat

conduction in an insulation slab. It was found that thermal conductivity had a linear relationship with the moisture content, and its magnitude increased with the increasing mean slab temperature and temperature difference.

Modi and Bennes (1985) studied spray-applied fiberglass and cellulose, and found that the rate of moisture gain and the total moisture gain increased with the relative humidity and the temperature difference. Moisture in the cellulose increased slightly more than that in the fiberglass under the same conditions. Hokoi and Kumaran (1993) studied heat and moisture transport through glass fiber insulation experimentally and analytically. They reported that for a medium density glass fiber insulation (about 50 kg/m^3), the value of the local moisture content at the fully saturated moisture state may reach 20 kg/kg of dry insulation material. Ogniewicz and Tien (1981) found a semi-analytical solution for solving a quasi-steady one-dimensional forced convective problem with convective boundary conditions. They found that the rate of condensation, though relative small, increased with external humidity, temperature levels and overall temperature differences. Motakef (1986) demonstrated the existence of a wet region sandwiched between two dry zones in a porous slab. Chen *et al*. (1997a; 1997b) investigated a transient two-dimensional forced convective case with a warm plate at the top and a cold plate, both experimentally and numerically. A total mass of moisture and frost accumulation on the insulation slab and cold surface of 0.0156 kg was found for one case, which was 50 per cent of the total vapour that flowed through the system in a 3.5-hour test. A 20 per cent decrease in the effective thermal conductivity was predicted to cause temperature, moisture and heat flux variations over 3–5 hours of up to 1.5 K, 0.5 per cent and 11 per cent, respectively.

Vafai and Whitaker (1986) conducted two-dimensional simultaneous heat and mass transfers in porous insulation. Gas pressure was assumed to be constant. They demonstrated that condensation occurred at any point in the insulation where the water vapour concentration became greater than the saturation concentration corresponding to the temperature at that point. Vafai and Sarkar (1986) studied condensation effects in a fibrous insulation slab and concluded that the condensation process was significantly affected by the thermophysical properties of the insulation, the infiltration velocity and the humidity levels. Condensation was a serious problem for large Peclet numbers. Tao *et al*. (1991a; 1991b) developed a frost model for studying the motion of the frozen boundary which started at a cold plate (sink) at subzero temperature on a fibrous insulation slab.

In recent literature, Fan *et al*. (2004) developed a coupled heat and moisture transfer model with phase change and mobile condensates in fibrous insulation. A super-saturation state in the condensing region, the dynamic moisture absorption of fibrous materials and the movement of liquid condensates were considered. Foss *et al*. (2003) presented a simultaneous heat and mass transfer model through a porous material for investigating transient moisture sorption by paper sheets from humid air. The model showed non-linearities of the moisture content isotherm and the heat of sorption. Charoenvai *et al*. (2005) reported the result on

heat and moisture transport in durian (*Durio zibethinus*) fiber-based lightweight construction materials composed of cement, sand and waste fiber from durian peel. The results showed that the weekly mean water content on the surface of the material was quite low. The effect of moisture on the apparent thermal performance of the composite was higher as water absorbed in the pore structure contributed to higher thermal conductivity than the air it replaced. However, the mean value of thermal conductivity in the material is still rather low as the mean value of water content in the material is low. An anisotropic three-dimensional geometric fiber model was used in studying two-dimensional transient heat and moisture transport behavior through fabric. The mass and energy conservation, as well as capillary phenomenon, was considered in the model (Luo & Xu, 2006).

Zhao *et al*. (2009) presented a numerical model of combined radiation and conduction heat transfer to predict the effective thermal conductivity of fibrous insulation at various temperatures and pressures. Effective thermal conductivities of the fibrous insulation were measured over a wide range of temperature and pressure. Using different mathematical models of heat flow, Roy *et al*. (2006) studied the porosity dependence of heat flux through glass fiber insulation. Karamanos *et al*. (2008) developed a model for evaluating the performance of stone wool under varying temperature and humidity conditions. Bao and Yee (2002) studied moisture absorption and hygrothermal aging in woven and woven/uni-weave composites. The short-term absorption curves of the uni-weave/woven/uni-weave and woven/uni-weave/woven composites were described by Fickian diffusion and the dual-diffusivity model, respectively.

In experimental literature, Fan *et al*. (2003) presented an experimental result on the temperature and water content distribution within the porous fibrous battings sandwiched by an inner and outer layer of thin covering fabrics using a novel sweating, guarded hot plate. It was found that most of the changes in temperature distribution took place within ½ hour of the tests and moisture absorption by the hygroscopic fibers affected the temperature distribution. Higher water content, a combined result of moisture absorption, condensation and liquid water movement, was found more at the outer regions than that at the inner regions of the battings.

For more general heat and moisture transfer model equations for hygroscopic fabrics or porous materials, please refer to Osanyintola & Simonson (2006), Abadie & Mendonca (2009), Kruger *et al*. (2009), Zhao *et al*. (2009), Wu (2009) and Lu (2002a; 2002b). Very often, the obtained model equations are complex, which does not permit simple analytical solutions. Therefore, different numerical approaches like the finite element method, finite difference method, and finite volume method are used to solve the equations (Pantaker, 1988; Zienkiewicz *et al*., 1991; Lewis & Schrefler, 1998). For more literature, refer to Pan and Gibson (2006) and Oduor (1999).

In this chapter, the macroscopic model configuration is presented in Fig. 10.10. The moisture transport is divided into liquid and vapour flow. The liquid transport is based on Darcy and capillary flow equations. The vapour flow is driven by

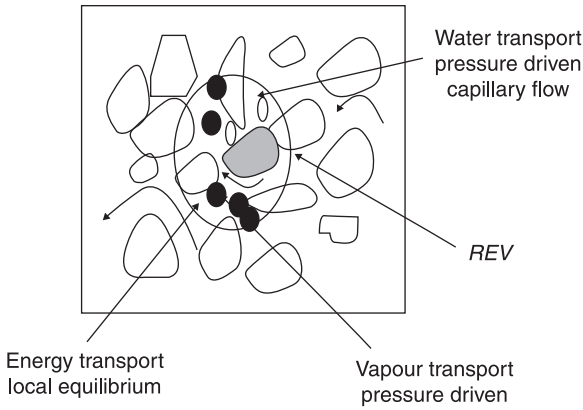

10.10 Macroscopic model configuration for heat and moisture transfer in fibrous materials.

vapour pressure gradient, and depends on the material's permeability coefficient. We assume that no air transfer occurs. The model is mainly based on one developed for fibrous material (Karamanos *et al*., 2008). Condensation is particularly studied based on both the building element's cross-section and in an area of the building element.

10.4 Applications

The building and construction industry constitutes one of the largest sectors to employ fibrous materials in a wide range of products, including light structural walls, insulation materials, wall and floor coverings, geotextiles and thatch roofing. We focus on building thermal insulation here, as the fibrous materials used in other applications do not differ significantly in composition, etc. The purpose of insulation is to provide a thermal barrier to minimize heat flow through the components of the buildings. Recently, increasing importance has been given to the acoustic, fire protection, and CO_2 reduction properties.

10.4.1 Thermal insulators

Fibrous materials have been extensively used as thermal insulators with a variety of applications ranging from interior or exterior walls, roofs, foundations, cavity walls, unheated garages, band joists, storm windows, seals around all windows, doors and heating systems, and hot and cold water services. Insulating the attic is a very important measure as the greatest heat loss occurs through the roof, which can be verified by noting the length of time required for snow on the roof to melt (Engineering Extension, 2001). Warm air goes up and the temperature in the upper air layers of heated rooms is always higher, which may cause a loss of heat

through the roof. Insulating the basement is also a very effective way to add energy efficiency. Insulating exposed ductwork that runs through unheated areas, such as crawl spaces and the attic, is equally important (Engineering Extension, 2001). Table 10.1 shows the thermal conductivity for some typical fibrous insulation materials (Release of Thermal Insulation Performance Value of Building Materials, 1999).

Youngquist *et al*. (1994) has made an extensive review of non-wood plant fibers for building materials and panels. The review covered a wide range of issues including the methods for efficiently producing building materials and panels from non-wood plant fibers, mechanical and physical properties of products made from non-wood plant materials, use of non-wood plant fibers as stiffening agents in cementitious materials and as refractory fillers, and the cost-effectiveness of using non-wood plant materials. Many different kinds of non-wood plant materials has been surveyed and grouped, by type of raw material, into five major sections: panel boards, including acoustical and thermal materials; cement/clay/gypsum/plaster materials; molded masses; miscellaneous; and materials used in their natural state.

In addition to the general thermal properties described above, the appropriate degree of insulation depends on local climate, building construction type, and many other factors. Soubdhan *et al*. (2005) studied the influence of radiant barriers on conductive and radiative heat transfers when they are integrated to a building envelope and compared their efficiency to traditional insulation materials (mineral wools, polystyrene) in a tropical climate. Different tests were performed to evaluate the influence of parameters such as roof absorptivity and roof air-layer ventilation on the heat flux reduction through the roof. Results demonstrated that the radiant barrier is comparable to polystyrene and fiberglass with no ventilation; when the airspace is ventilated the radiant barrier provides a better insulation. Pervaiz *et al*. (2003) reported the environmental performance of hemp-based natural fiber mat thermoplastic (NMT) by quantifying its carbon storage potential and CO_2 emissions, and comparing the results with commercially available glass fiber composites. Non-woven mats of hemp fiber and polypropylene matrix were used to make NMT samples by film-stacking method without using any binder aid. They showed that hemp-based NMTs have compatible or even better strength properties as compared to conventional flax-based thermoplastics, and their impact energy values are also promising. Hens *et al*. (1998) examined the performance of a self-drying roof in cool and cold climates. Three well-insulated roof sections, all covered with shingles and lined inside with a gypsum board, were tested in a hot box.

With regard to structural behavior, Wu (2009) reported the results of experimental and theoretical investigations into the structural behavior of glass fiber-reinforced gypsum walls, developed in the early 1990s, and offered a structural design methodology associated building system. Bojic *et al*. (2002) studied the insulation effects of including a thermal insulation layer in the fabric

Table 10.1 Thermal conductivity

Material	Density (kg/m^3)	Conductivty (W/mk)	Type	References
Glass wool insulation for dwellings	10	0.048		Release 1999*
Glass wool insulation for dwellings	16	0.040		Release 1999*
Glass wool insulation for dwellings	24	0.036		Release 1999*
Glass wool insulation for dwellings	32	0.035		Release 1999*
High-performance glass wool insulation	16	0.036		Release 1999*
High-performance glass wool insulation	24	0.034		Release 1999*
Loose fill glass wool insulation	13	0.050		Release 1999*
Loose fill glass wool insulation	18	0.049		Release 1999*
Loose fill glass wool insulation	30	0.038		Release 1999*
Loose fill glass wool insulation	35	0.038		Release 1999*
Rock wool insulation for dwellings	20–70	0.036	felt	Release 1999*
	40–100	0.034	board	Release 1999*
Cellulose fiber insulation	25–30	0.038	for dry loose fill (ceiling)	Release 1999*
	56–64	0.037	for dry loose fill (wall)	Release 1999*
	40–45	0.037	mat (wall)	Release 1999*
Fiber board	less than 270	0.045	tatami mat	Release 1999*
	less than 350	0.049	class A insulation board	Release 1999*
	less than 400	0.052	sheathing board	Release 1999*
Flax	5–50	0.038–0.075	mat	Kymäläinen & Sjöberg (2008)
Flax	20–100	0.035–0.045		Kymäläinen & Sjöberg (2008)

(Continued)

Flax and hemp	25–40	0.050		Kymäläinen & Sjöberg (2008)
Flax and hemp	39	0.033	mat	Kymäläinen & Sjöberg (2008)
Flax and hemp	19	0.060	mat	Kymäläinen & Sjöberg (2008)
Hemp, retted	5–50	0.040–0.082	mat	Kymäläinen & Sjöberg (2008)
Hemp, green	5–50	0.044–0.094	mat	Kymäläinen & Sjöberg (2008)
Hemp, frost-retted	25–100	0.040–0.049	loose-fill	Kymäläinen & Sjöberg (2008)
Hemp	20–45	0.040–0.060		Kymäläinen & Sjöberg (2008)
Glass wool	20–50	<0.040		Kymäläinen & Sjöberg (2008)
Glass wool	18–50	0.050		Kymäläinen & Sjöberg (2008)
Stone wool (mineral wool)	5–50	0.035–0.071	mat	Kymäläinen & Sjöberg (2008)
Stone wool (mineral wool)	25–300	0.037–0.050		Kymäläinen & Sjöberg (2008)
Stone wool	30–60	0.050		Kymäläinen & Sjöberg (2008)
Cellulose	30–45	0.041–0.050		Kymäläinen & Sjöberg (2008)
Cellulose (recycled paper)	30	0.041	loose-fill	Kymäläinen & Sjöberg (2008)
Cellulose (wood fiber)	30–60	0.050		Kymäläinen & Sjöberg (2008)
Expanded polystyrene EPS	8–58.7	0.025		Domínguez-Muñoz *et al.* (2009)
Polyester fiber	11.2–44.6	0.025		Domínguez-Muñoz *et al.* (2009)
Mineral wool (rock)	13.3–241	0.026	flow ⊥ fiber	Domínguez-Muñoz *et al.* (2009)
Mineral wool (glass)	8–150	0.026		Domínguez-Muñoz *et al.* (2009)
Cellular glass/foam glass	100–188	0.019		Domínguez-Muñoz *et al.* (2009)
Wood chip board	309–681	0.015		Domínguez-Muñoz *et al.* (2009)
Wood fiber board	100–298	0.030		Domínguez-Muñoz *et al.* (2009)
Wood wool board	260–719	0.019		Domínguez-Muñoz *et al.* (2009)
Sheep's wool	11–93.2	0.028		Domínguez-Muñoz *et al.* (2009)
Cotton	11–60	0.029		Domínguez-Muñoz *et al.* (2009)
Expanded cork	76–307	0.034		Domínguez-Muñoz *et al.* (2009)
Expanded perlite board	134–207	0.044		Domínguez-Muñoz *et al.* (2009)
Cellulose fiber (loose-fill)	17–115	0.026		Domínguez-Muñoz *et al.* (2009)
Sawdust		0.065–0.07		Hänninen *et al.* (1997)

Release 1999*: Release of Thermal Insulation Performance Value of Building Materials, 1999.

components that separate cooled spaces from the outdoors and from non-air conditioned spaces in high-rise residential buildings. The simulation results showed that the highest reduction in the yearly cooling load and in the maximum cooling demand would be achieved when a 50 mm thick thermal insulation layer was placed at the indoor side of the walls that enclose the cooled spaces. Fiber-based composite insulators have been very popular for decades due to their good mechanical and thermal properties. Abdou *et al.* (1996) investigated the thermal insulation characteristics of the prefabricated, interlocking fiberglass composite panel system in the construction of building envelope systems. The experiments showed that such envelope system could be a potential candidate for wider use in energy-conscious commercial buildings.

Besides the traditional application of these fabrics, randomly mixed palmyra fiber and glass fiber hybrid composites have been proposed as an eco-friendly composite and their mechanical properties and moisture absorption have been studied by Velmurugan and Manikandan (2007). It showed that the mechanical properties of the composites are improved due to the addition of glass fiber along with palmyra fiber in the matrix. The addition of glass fiber with palmyra fiber in the matrix decreases the moisture absorption of the composites. Furthermore, the mechanisms of fibrous insulation where the fiber of nanofiber technology (fiber diameter less than 1 micrometer) have been investigated (Gibson *et al.*, 2007). However, very little research has been done on this topic. It has been found that fibers below 1 μm in diameter are not thermally efficient at low fiber volume fractions, and performance gains in existing thermal insulation materials may be possible by incorporating a proportion of nanofibers into the structure, but large diameter fibers would still be necessary for durability and compression recovery.

10.4.2 Fire insulators

Because of their unique structure, based on quartz or basalt fibers in combination with non-decomposable binder for example, fibrous materials are capable of withstanding high heating temperatures for a long time (Zverev *et al.*, 2008). Therefore, fibrous heat-resistant materials, especially their composites (Bai & Keller, 2007), are widely used in practice in various high-temperature technologies such as fire insulators in buildings.

Bai *et al.* (2007) developed models for assembling the material properties of fibrous composites, thermo-chemical and thermo-mechanical models to predict the thermal and mechanical responses of the composites under elevated and high temperatures. The post-fire mechanical properties of fibrous materials have also been evaluated widely (e.g. Pering *et al.*, 1980; Springer, 1984). Haddad *et al.* (2008) evaluated the bond behavior between fiber-reinforced concrete and reinforcing steel rebars under elevated temperatures. Results showed that the use of fibers minimized the damage in the steel–concrete bond under elevated temperatures and hence the reduction in bond strength.

In high performance concrete, the addition of polypropylene fibers is widely used as an effective method to prevent explosive spalling and its efficiency was investigated by Liu *et al*. (2008).

Some experimental studies and results on the fire behavior of glass fiber-reinforced polymer load-carrying slabs for building applications were presented in a series of papers (Keller *et al*., 2005; 2006a; 2006b).

10.4.3 Sensors and actuators

Fiber-based sensors and actuators, for example optical fiber sensors, have been used widely to sense some qualities in buildings, typically temperature (Fernandez-Valdivielso *et al*., 2002), humidity (Arregui *et al*., 1999) and mechanical strain (Li *et al*., 2004), but sometimes also vibrations (Feng & Kim, 2006), pressure (Merzbacher *et al*., 1996), acceleration (Feng & Kim, 2006), concentrations of chemical species (Consales *et al*., 2006; Blumentritt *et al*., 2008), and many others (Canning, 2006).

Yilmaz and Karlik (2006) discussed the distributed temperature sensing method, detection system configuration, and required system parameters by using optical fiber sensors. Rajesh *et al*. (2006) described a simple, effective and inexpensive fiber-optic sensor for investigating the setting characteristics of various grades of cement and proposed the use of such sensors in a building during the construction process to monitor the deterioration process for the entire lifetime of the building. Consales *et al*. (2006) analysed the performances of silica-optic fiber (SOF) and quartz crystal microbalance (QCM) volatile organic compounds (VOCs) sensors, coated by single-walled carbon nanotubes (SWCNTs) multilayers, towards toluene and xylene vapors, at room temperature. Results demonstrated the possibility to use the data coming from carbon nanotubes SOF and QCM sensors to improve the VOC discrimination.

Blumentritt *et al*. (2008) introduced a new technique for producing a fiber-optical planar transmission sensor for monitoring pH in concrete structures. The current multicomponent fiber-forming technologies have also offered tremendous potential as a means to fabricate fiber actuators (Arora *et al*., 2007). Two types of prestrains (uniaxial and uniform) were applied to introduce and study anisotropy in the fiber behavior. The results demonstrate the significant influence of applied prestrain on actuation strains and blocking force (Arora *et al*., 2007).

10.4.4 Acoustic insulators

Fibrous materials have also been used to dampen acoustic resonances as proposed by Bradbury (1976). Voronina (1996) investigated the acoustic behavior of fibrous materials with a flexible frame experimentally. Characteristic impedance and propagation constants were measured for super-thin fiberglass with different fiber diameters and density. The empirical relations between the acoustic parameters

Table 10.2 Weighted sound reduction index

Wall	R_w (dB)
Plain brick wall	41
Covered brick wall	44
Plain concrete block	37
Covered concrete block	43
Dry wall without fiberglass	34
Dry wall with fiberglass	42

R_w is the weighted sound reduction index, conform ISO 140–3 and ISO 717–1.

and physical values characterizing an internal medium macrostructure were then derived. The model could predict values of the acoustic impedance and the sound absorption coefficient of material layers for different fiber diameter and density. Bradbury (1976) discussed a model of the interaction between sound waves and fibrous materials.

Zannin and Ferreira (2007) studied the acoustic performance of fibrous materials routinely used in Brazilian building construction, presented as the weighted sound reduction index and shown in Table 10.2. These walls, individually, displayed high levels of sound insulation index. As a thermal or acoustic insulation, a vegetal fiber extracted from the *Rhectophyllum camerunense* plant was proposed, and its mechanical properties were studied by Beakou *et al.* (2008).

10.4.5 Other applications

In addition to its performance in low and high temperatures, fibrous materials present interesting characteristics of mechanical strength and performance for moisture, wetness, etc. Binici *et al.* (2005) have investigated the mechanical properties of certain combinations of fibrous-waste materials and some stabilizers, and proposed that these materials can be used as earthquake-resistant materials due to their high compressive strength. They concluded that the interface layers of fibrous materials increased the compressive strength, and a certain geometrical shape of these layer materials gave the best results. Lignocellulosic agricultural by-products are a copious and cheap source for cellulose fibers. Agro-based biofibers have the composition properties and structure that make them suitable for uses such as composite. Reddy *et al.* (2005) reviewed the production processes, structure, properties and suitability of biofibers for various industrial applications. Ardente *et al.* (2008) presented a life-cycle assessment of a kenaf fiber insulation board following the international standards of the ISO 14040 series. Each life-cycle step has been checked, from kenaf production and board manufacture, to use and disposal. A comparison among various insulating materials was carried out.

Hyvarinen *et al.* (2002) investigated whether fungal genera and actinobacteria were associated with seven types of moisture-damaged building materials by systematically describing the mycobiota and enumerating fungi and bacteria in these materials. They found that the highest median concentrations of fungi were observed in wooden and paper materials, and the lowest in samples of mineral insulation, ceramic products, and paints and glues. Concentrations of viable bacteria in mineral insulation materials were significantly lower than in wood, paper, ceramic products and plastics. A rich variety of fungi was found in wooden materials.

Bioinspired fibrous materials that span the nano-to-meso scales have potentially broad applications. The review by Woolfson and Ryadnov (2006) focused on potential applications of bioinspired fibrous materials and centered on the developments in the design of peptide-based fibers and particularly those using the alpha-helix and the collagen triple-helix as building blocks for self-assembly. Seguchi (2000) presented new trends and potential applications for some fiber composites.

10.5 Sources of further information and advice

Building codes differ from country to country. This is partly because of the difference in climate in the countries, and also local building materials and methods. Building codes typically require the minimum requirements for insulation level. In most climates, it is both easy and cost-effective to increase these insulation levels beyond the minimum code requirements (see Table 10.3 below for recommended levels (Insulation Fact Sheet, 1997)). It is imperative, therefore, to insulate our buildings properly to reduce air leakage and improve energy efficiency.

However, it should be noted that bad airtightness may cause risk to building components and human health due to the cold bridging and trapped moisture.

Table 10.3 Recommended insulation levels

Climate	Heating system	Insulation levels			
		ceiling	wood frame walls	floor	basement/ crawl space walls
Warm	gas/oil heat pump	R-22 to R-38	R-11 to R-15	R-11 to R-13	R-11 to R-19
	electric resistance	R-38 to R-49	R-11 to R-22	R-13 to R-25	R-11 to R-19
Mixed	gas/oil heat pump	R-38	R-11 to R-22	R-25	R-11 to R-19
	electric resistance	R-49	R-11 to R-28	R-25	R-11 to R-19
Cold	gas/oil	R-38 to R-49	R11 to R-22	R-25	R-11 to R-19
	heat pump or electric	R-49	R-11 to R-28	R-25	R-11 to R-19

The use of good breathable insulation fibrous materials can help to prevent moisture. In addition, depending on other constructional details, the air barrier must have adequate water vapour resistance for ensuring the hygrothermal performance of the wall structure. Figure 10.11 shows a typical wall construction in Finland (Ulkoseinäratenteita, 2010).

These are now receiving increasing attention for building structures' relative humidity control since it is vital in the control of moulds, dust mites and VOC reactions which affect occupants' health and comfort or indoor air quality. Special attention should be paid to the temperature difference between exterior and interior temperatures for the exterior structure to avoid surface condensation of the structure.

Taylor *et al*. (1998) studied dynamic insulation in which cool fresh air is drawn into the building through air-permeable walls in naturally ventilated buildings to provide a viable and attractive alternative to mechanical air-conditioning in congested urban environments. In addition to thermal insulation, building regulations require that building components should perform with regard to integrity and load-bearing capacity. Evaluation of load-bearing capacity for horizontal insulation materials is then of great importance with regard to public safety. Asan (2000) investigated the optimum insulation position from a maximum time lag and a minimum decrement factor point of view. Four-centimeter thick insulation was placed in different positions of a 20-cm thick wall as a whole (one piece, 4 cm) or as two slices (2 + 2 cm). Six different insulation configurations were selected. Figure 10.12 shows the configurations. The analysis results demonstrated that placing half of the insulation in the mid-center plane of the wall and half of it in the outer surface of the wall gives very high time lags and low decrement factors (close to optimum values). Placing half of the insulation on the

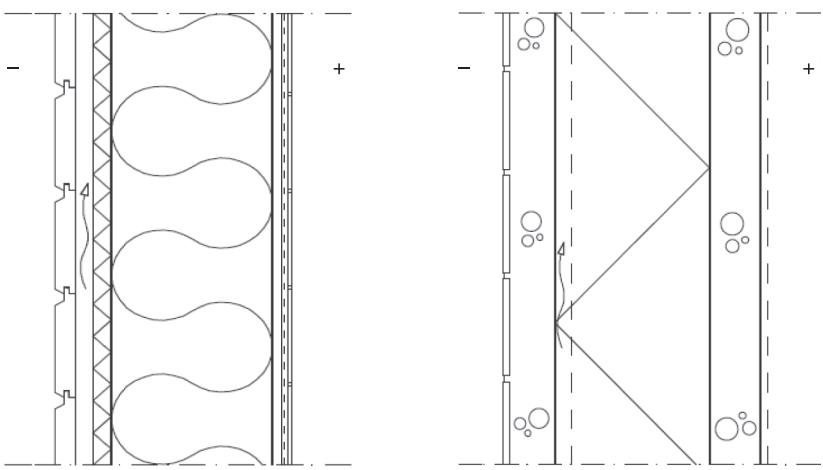

10.11 Typical wall structure.

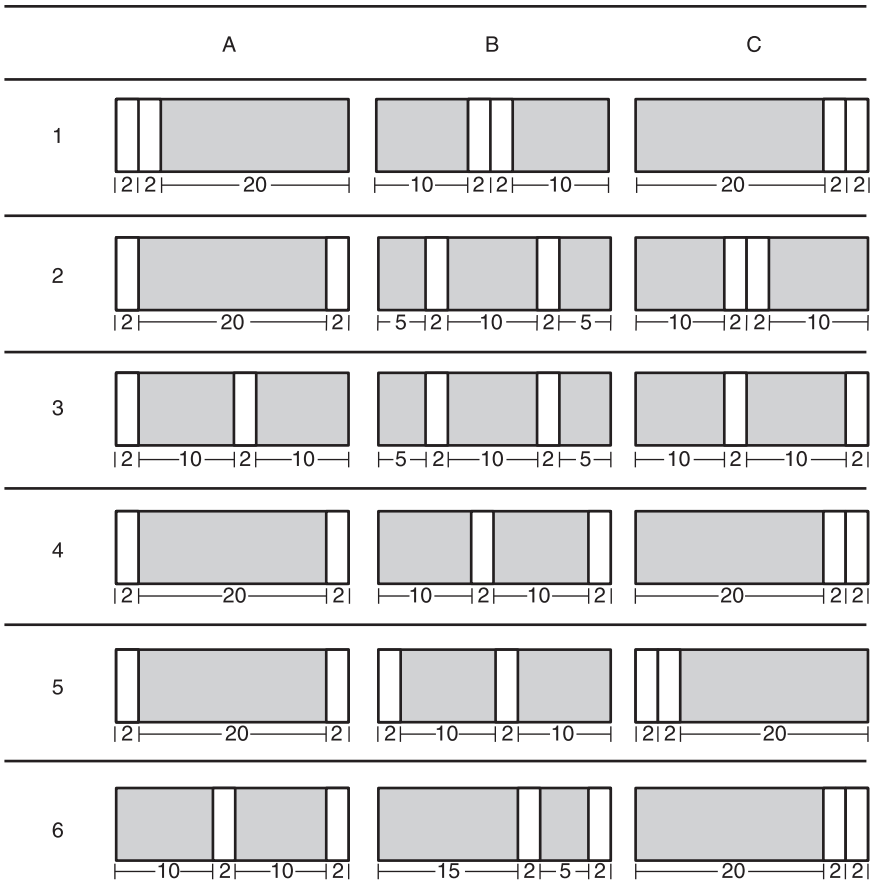

10.12 Six different configurations of insulation inside the wall.

inner surface and the other half on the outer surface of the wall gives minimum decrement factor. On the other hand, maximum time lag was obtained in the case of placing two slices of insulation a certain distance apart inside the wall. Placing half of the insulation in the mid-center plane of the wall and the half of it on the outer surface of the wall gives very high time lags and low decrement factors (close to optimum values). This configuration is very practical and can be done without any difficulty during construction.

Papadopoulos and Giama (2007) examined a building's environmental performance through the insulation material selection. Contemporary insulation materials with thermal conductivity values of less than 0.04 W/mK and a plethora of materials that fulfil specific requirements such as mechanical and physical features according to the object-specific specifications were selected. The results obtained

were used to set operating performance indicators and environmental condition indicators based on the ISO 14031 standard, and accomplish the Environmental Performance Evaluation for the two selected materials. Alturkistani *et al*. (2008) investigated the drying capacity of different envelope and fiber-insulation configurations.

Energy use in buildings covers a large share of the world's total end-use of energy. Due to the rapid increase of energy use in the building sector, the climate change driven by global warming, and rising energy shortage, there is no doubt that renewable energy is the way of the future. A challenging task of architects and other building professionals today is to design and promote low/zero-energy buildings in a cost-effective and environmentally responsive way.

New buildings will have to be designed to use less fossil fuel in a low- or zero-carbon world, maximize passive measures of more effective insulation, improve airtightness and greater thermal mass. Super-insulating materials have been suggested (BNIW01 2007). The choice of insulations to use in buildings is important.

Roberts (2008) reviewed the effect of climate change on the built environment with an emphasis on new build. As part of an effort to develop zero-energy building models, Kumar *et al*. (2007) studied the direct impact on energy consumption and the environment of different subsurface walls at varying depths for all building structures in which a significant area is in direct contact with the earth, and excludes indirect earth contact. Heat flux variations across the floor with varying insulation factor were presented.

10.6 References

Abadie, M.O. & Mendonca, K.C. (2009) Moisture performance of building materials: From material characterization to building simulation using the Moisture Buffer Value concept. *Building and Environment*, 44(2): 388–401.

Abdou, O.A., Murali, K. & Morsi, A. (1996) Thermal performance evaluation of a prefabricated fiber-reinforced plastic building envelope system. *Energy and Buildings*, 24(1): 77–83.

Alturkistani, A., Fazio, P., Rao, J. & Mao, Q. (2008) A new test method to determine the relative drying capacity of building envelope panels of various configurations. *Building and Environment*, 43(12): 2203–2215.

Angwafo, A.W., Bullen, P.R. & Philpott, D.R. (1998) Melt flow in the production of mineral wool by centrifugal spinning, *Proc. FEDSM'98*, 1998 ASME Fluids Eng. Div. Summer Meeting, Washington, USA, pp. 21–25.

Ardente, F., Beccali, M., Cellura, M. & Mistretta, M. (2008) Building energy performance: A LCA case study of kenaf-fibers insulation board. *Energy & Buildings*, 40(1): 1–10.

Arora, S., Ghosh, T. & Muth, J. (2007) Dielectric elastomer based prototype fiber actuators. *Sensors & Actuators: A. Physical.*, 136(1): 321–328.

Arregui, F.J., Liu, Y., Matías, I.R. & Claus, R.O. (1999) Optical fiber humidity sensor using a nano Fabry–Perot cavity formed by the ionic self-assembly method. *Sens. Actuators. B*, 59(1): 54–59.

Asan, H. (2000) Investigation of wall's optimum insulation position from maximum time lag and minimum decrement factor point of view. *Energy and Buildings*, 32(2): 197–203.

Association of Plastics Manufacturers in Europe (APME) (2004) Data from publications and the web-site <http://www.apme.org>.

Bachmat, Y. (1972) Spatial macroscopization of processes in heterogeneous systems. *Israel J. Tech.*, 10: 391–403.

Bachmat, Y. & Bear, J. (1986) Macroscopic modelling of transport phenomena in porous media, 1: The continuum approach. *Transport in Porous Media*, 1: 213–240.

Bai, Y. & Keller, T. (2007) Modeling of post-fire stiffness of *E*-glass fiber-reinforced polyester composites. *Composites Part A: Applied Science and Manufacturing*, 38(10): 2142–2153.

Bai, Y., Keller, T. & Vallée, T. (2007) Modelling of thermal responses for FRP composites under elevated and high temperatures. *Compos Sci Technol.*, 68: 47–56.

Baillis, D. & Sacadura, J-F. (2000) Thermal radiation properties of dispersed media: theoretical prediction and experimental characterization. *Journal of Quantitative Spectroscopy and Radiative Transfer*, 67(5): 327–363.

Bankvall, C.G. (1973) (Summary of) Heat Transfer in Fibrous materials. Document D4. *J. Testing Evaluation*, 1(3): 235–243.

Bao, L-R & Yee, A.F. (2002) Moisture diffusion and hygrothermal aging in bismaleimide matrix carbon fiber composites: Part II – Woven and hybrid composites, *Composites Science and Technology*, 62(16): 2111–2119.

Batycky, R.P. & Brenner, H. (1997) Thermal macrotransport processes in porous media. A review, Advances in water, *Advances in Water Resources*, 20(2): 95–110 (Apr).

Beakou, A., Ntenga, R., Lepetit, J., Ateba, J.A. & Ayina, L.O. (2008) Physico-chemical and microstructural characterization of 'Rhectophyllum camerunense' plant fiber. *Composites: Part A*, 39(1): 67–74.

Bear, J. (1972) *Dynamics of Fluids in Porous Media*. Elsevier, New York, 764 pp.

Bear, J. & Bachmat, Y. (1984) Transport phenomena in porous media – Basic equations, in J. Bear and M. Y. Corapcioglu (eds), *Fundamentals of Transport Phenomena in Porous Media*. Martinus Nijhoff, Dordrecht.

Bear, J. & Bachmat, Y. (1986) Macroscopic modelling of transport phenomena in porous media. 2: Applications to mass, momentum, and energy transport. *Transport in Porous Media* 1: 241–269.

Benzi, R., Succi, S. & Vergassola, M. (1992) The lattice Boltzmann equation: Theory and applications. *Phys. Rep.*, 222: 145–197.

Binici, H., Aksogan, O. & Shah, T. (2005) Investigation of fiber reinforced mud brick as a building material. *Construction and Building Materials*, 19(4): 313–318.

Blumentritt, M., Melhorn, K., Flachsbarth, J., Kroener, M., Kowalsky, W. & Johannes, H.H. (2008) A novel fabrication method of fiber-optical planar transmission sensors for monitoring pH in concrete structure. *Sensors & Actuators: B. Chemical*, 131(2): 504–508.

BNIW01 (2008) *Insulation Industry, Product and Market Overview*. Market Transformation Programme, http://www.mtprog.com.

Bojic, M., Yik, F. & Leung, W. (2002) Thermal insulation of cooled spaced in high residential buildings in Hong Kong. *Energy Conversion and Management*, 43(2): 165–183.

Bradbury, L.J.S. (1976) The use of fibrous materials in loudspeaker enclosures. *JAES*, 24(3): 162–170.

Canning, J. (2006) Fiber lasers and related technologies. *Optics and Lasers in Engineering*, 44(7): 647–676.

Catherine, H., Skinner, W., Ross, M. & Frondel, C. (1988) *Asbestos and Other Fibrous Minerals*, Oxford University Press, Oxford, 204 pp.

Charoenvai, S., Khedari, J., Hirunlabh, J., Asasutjarit, C., Zeghmati, B., Quenard, D. & Pratintong, N. (2005) Heat and moisture transport in durian fiber based lightweight construction materials. *Solar Energy*, 78(4): 543–553.

Chen, H., Besant, R.W. & Tao, Y. (1997a). Two-dimensional air exfiltration and heat transfer through fiberglass insulation. 1: Numerical mode 1 and experimental facility. *HVAC & R Research*, 3(3): 197–213,

Chen, H., Besant, R.W. and Tao, Y. (1997b). Two-dimensional air exfiltration and heat transfer through fiberglass insulation. 2: Comparisons between simulations and experiments. *HVAC & R Research*, 3(3): 215–232.

Chen, C-Y., Wang, L. & Kurosaki, Y. (2002) Numerical Simulations of Heat Transfer in Porous Media with Effect of Heterogeneities. *JSME International Journal Series B*, 45(2): 315–321.

Cheng, X. & Fan, J. (2004) Simulation of heat and moisture transfer with phase change and mobile condensates in fibrous insulation. *International Journal of Thermal Sciences*, 43(7): 665–676.

Consales, M., Campopiano, S., Cutolo, A., Penza, M., Aversa, P., Cassano, G., Giordano, M. & Cusano, A. (2006) Carbon nanotubes thin films fiber optic and acoustic VOCs sensors: Performances analysis. *Sensors & Actuators: B. Chemical*, 118(1): 232–242.

Daryabeigi, K. (2000) *Design of High-Temperature Multi-Layer Insulation for Reusable Launch Vehicles*, Ph.D. dissertation, University of Virginia, USA.

Data from publications and the web-site of the Association of Plastics Manufacturers in Europe (APME) (2004) <http://www.apme.org>.

Domínguez-Muñoz, F., Anderson, B., Cejudo-López, J.M. & Carrillo-Andrés (2009) An uncertainty in the thermal conductivity of insulation materials, *Eleventh International IBPSA Conference*, Glasgow, Scotland, July 27–30.

Engineering Extension (2001) http://www.engext.ksu.edu/ees/henergy/envelope/insulation.html.

Evseeva, L.E. & Tanaeva, S.A. (2004) Influence of impregnation on the thermal properties of heat-insulating fibrous materials. *Journal of Engineering Physics and Thermophysics*, 77(2): 99–102.

Fan, J., Cheng, X. & Chen, Y-S. (2003) An experimental investigation of moisture absorption and condensation in fibrous insulations under low temperature. *Experimental Thermal and Fluid Science*, 27(6): 723–729.

Fan, J. Cheng, J., Wen, X & Sun, W. (2004) An improved model of heat and moisture transfer with phase change and mobile condensates in fibrous insulation and comparison with experimental results. *International Journal of Heat and Mass Transfer*, 47(10&11): 2343–2352.

Farnworth, B. (1983) Mechanisms of heat flow through clothing insulation. *Textile Research Journal*, 53(12): 717–725.

Feng, M.Q. & Kim, D.H. (2006) Novel fiber optic accelerometer system using geometric moire fringe. *Sensors & Actuators: A. Physical*, 128(1): 37–42.

Fernandez-Valdivielso, C., Matas, I.R. & Arregui, F.J. (2002) Simultaneous measurement of strain and temperature using a fiber Bragg grating and a thermochromic material. *Sensors and Actuators A: Physical*, 101(1): 107–116.

Foss, W.R., Bronkhorst, C.A. & Bennett, K.A. (2003) Simultaneous heat and mass transport in paper sheets during moisture sorption from humid air. *International Journal of Heat and Mass Transfer*, 46(15): 2875–2886.

Gibson, P.W. Lee, C., Ko F. & Reneker, D. (2007) Application of Nanofiber Technology to Nonwoven Thermal Insulation. *Journal of Engineered Fibers and Fabrics*, 2(2): 32–40.

Haddad, R.H., Al-Saleh, R.J., Al-Akhras, N.M. (2008) Effect of elevated temperature on bond between steel reinforcement and fiber reinforced concrete. *Fire Safety Journal*, 43(5): 334–343.

Hadim, H.A. & Vafai, K. (eds) (2000) *Handbook of Porous Media*, Marcel Dekker, New York.

Hager, N.E. & Steere, R.C. (1967) Radiant heat transfer in fibrous thermal insulation. *J Appl Phys*., 38(12): 4663–4668.

Hassanizadeh, S.M. & Gray, W.G. (1979) General Conservation Equations for Multi-phase Systems. 1: Averaging Procedure. *Advances in Water Resources*, 2: 131–144.

Hens, H. & Janssens, A. (1998) Application of a new type of air and vapor retarder in a self-drying sloped roof with a cathedral ceiling, in *Thermal Performance of the Exterior Envelopes of Buildings VII*, Clearwater Beach, Florida.

Hendricks, T.J. & Howell, J.R. (1994) Absorption/scattering coefficients and scattering phase functions in reticulated porous ceramics, in *Radiation heat transfer: current research*, in Y. Bayazitoglu *et al*. (eds), *ASME HTD – Vol. 276*, ASME.

Holman, J.P. (1997) *Heat Transfer*, 8th edn, McGraw-Hill, Inc., New York, p. 430.

Hokoi, S. & Kumaran, M.K. (1993) Experimental and analytical investigations of simultaneous heat and moisture transport through glass fiber insulation. *J. Thermal Insul. and Bldg Envs*., 16: 263–292.

Hoskins, J. (2001) Review: mineral fibers and health. *Indoor and Built Environment*, 10(3–4): 244–251.

Hyvarinen, A., Meklin, T., Vepsalainen, A. & Nevalainen, A. (2002) Fungi and actinobacteria in moisture-damaged building materials — concentrations and diversity. *International Biodeterioration and Biodegradation*, 49(1): 27–37.

Hänninen, J., Rissanen, R. & Viljanen, M. (1997) *Sawmill industries by-products for using as building insulation material*, TKK-TRT-118, Laboratory of Structural Engineering and Building Physics, Helsinki University of Technology, Finland.

Insulation Fact Sheet 1997, U.S. Department of Energy.

Karamanos, A., Hadiarakou, S. & Papadopoulos, A.M. (2008) The impact of temperature and moisture on the thermal performance of stone wool. *Energy and Buildings*, 40: 1402–1411.

Keller, T., Tracy, C. & Zhou, A. (2006a) Structural response of liquid-cooled GFRP slabs subjected to fire – Part I: Material and post-fire modeling. *Composites Part A*, 37(9): 1286–1295.

Keller, T., Tracy, C. & Hugi, E. (2006b) Fire endurance of loaded and liquid-cooled GFRP slabs for construction. *Composites: Part A*, 37(7): 1055–1067.

Keller, T., Zhou, A., Tracy, C., Hugi E. & Schnewlin, P. (2005) Experimental study on the concept of liquid cooling for improving fire resistance of FRP structures for construction. *Composites: Part A*, 36(11): 1569–1580.

Klemens, P.G. & Kim, N. (1985) Radiative heat transfer in inhomogeneous media and insulations. *Thermal Conductivity*, 19: 453–458.

Kumar, R., Sachdeva, S. & Kaushik, S.C. (2007) Dynamic earth-contact building: A sustainable low-energy technology. *Building and Environment*, 42(6): 2450–2460.

Kruger, E.L., Adriazola, M., Matoski, A. & Iwakiri, S. (2009) Thermal analysis of wood-cement panels: Heat flux and indoor temperature measurements in test cells. *Construction and Building Materials*, 23(6): 2299–2305.

Kymäläinen, H-R. & Sjöberg, A-M. (2008) Flax and hemp fibers as raw materials for thermal insulations. *Building and Environment*, 43, 1261–1269.

Lage J.L. & Narasimhan, A. (2008) Porous media enhanced forced convection fundamentals and applications, in P. Vadasz, *Emerging Topics in Heat and Mass Transfer in Porous Media: From Bioengineering and Microelectronics to Nanotechnology* (*Series-Theory and Applications of Transport in Porous Media*), Springer Verlag, pp. 328.

Larkin B.K. & Churchill, S.W. (1959) Heat transfer by radiant through porous insulations. *AIChE J*., 4(5): 467–474.

Lauriat, G. & Ghafir, R. (2000) Forced convective transfer in porous media, in K. Vafai and H.A. Hadim (eds), *Handbook of Porous Media*, Marcel Dekker, New York.

Lee, S.C. (1990) Scattering Phase Function for Fibrous Media. *Int. J. Heat Mass Transfer*, 33: 2183–2190.

Lee, S.C. & Cunnington, G.R. (2000) Conduction and radiation heat transfer in high porosity fiber thermal insulation. *J. Thermophys. Heat Transfer*, 14(2): 121–136.

Lee, S.C., White, S. & Grzesik, J. (1994) Effective Radiative Properties of Fibrous Composites Containing Spherical Particles. *J. Thermoph. Heat Transfer*, 8: 400–405.

Lewis, R.W. & Schrefler, B. (1998) *The Finite Element Method in the Static and Dynamic Deformation and Consolidation of Porous Media*, 2nd edn, John Wiley & Sons, 508 pp.

Li, Q., Li, G. & Yuan, L. (2004) Calibration of embedded fiber optic sensor in concrete under biaxial compression. *Measurement*, 35(3): 303–310.

Liu, X., Ye, G., De Schutter, G., Yuan, Y. & Taerwe, L. (2008) On the mechanism of polypropylene fibers in preventing fire spalling in self-compacting and high-performance cement paste. *Cement and Concrete Research*, 38(4): 487–499.

Lotz, B. (2006) A brief history of thermal insulation, RSI report, 2006. http://www.rsimag.com/rsi/Insulation/A-brief-history-of-Thermal-Insulation/ArticleStandard/Article/detail/312975.

Lu, X. (2002) Modelling heat and moisture transfer in buildings: (I) Model program. *Energy and Buildings*, 34(10): 1033–1043.

Lu, X. (2002) Modelling heat and moisture transfer in buildings: (II) Application to indoor thermal and moisture control. *Energy and Buildings*, 34(10): 1045–1054.

Luo, X. & Xu, Q. (2006) A new numerical implementation on 2D heat and moisture transfer through fabric. *Applied Mathematics and Computation*, 174(2): 1135–1150.

Merzbacher, C.I., Kersey, A.D. & Friebele, E.J. (1996) Fiber optic sensors in concrete structures: a review. *Smart Materials and Structures*, 5(2): 196–208.

Milandri, A., Asllanj, F., Jeandel, G. & Roche, J.R. (2002) Heat transfer by radiation and conduction in fibrous media without axial symmetry. *Journal of Quantitative Spectroscopy & Radiative Transfer*, 74: 585–603.

Motakef, S. & El-Masri, M.A. (1986) Simultaneous heat and mass transfer with phase change in a porous slab. *Int. J. Heat Mass Transfer*, 29(10): 1503–1512.

Modi, D.B. & Bennes, S.M. (1985) Moisture gain of spray-applied insulations and its effect on effective thermal conductivity – Part 1. *J. Thermal Insulation*, 8: 259–277.

Oduor, S.O. (1999) *Simultaneous Air, Heat and Moisture Transfer in Fibrous Building Insulation*, PhD Thesis, University of Alberta, USA.

Ogniewicz, Y. & Tien, C.L. (1981). Analysis of condensation in porous insulation. *Int. J. Heat Mass Transfer*, 24: 421–429.

Ohberg, I. (1987) Technological development of the mineral wool industry in Europe. *Ann. Occup. Hyg.*, 31(4B): 529–545.

Osanyintola, O.F. & Simonson, C.J. (2006) Moisture buffering capacity of hygroscopic building materials: Experimental facilities and energy impact. *Energy & Buildings*, 38(10): 1270–1282.

Pan, N. & Gibson, P. (2006) *Thermal and Moisture Transport in Fibrous Materials*, Woodhead Publishing Ltd., Cambridge, UK.

Pantaker, S.V. (1988) A calculation procedure for two-dimensional elliptic problem. *Numerical Heat Transfer*, 4: 409–426.

Papadopoulos, A.M. (2005) State of the art in thermal insulation materials and aims for future developments. *Energy and Buildings*, 37(1): 77–86.

Papadopoulos, A.M. & Giama, E. (2007) Environmental performance evaluation of thermal insulation materials and its impact on the building. *Building and Environment*, 42(5): 2178–2187.

Pering, G.A., Farrell, P.V. & Springer, G.S. (1980) Degradation of tensile and shear properties of composites exposed to fire or high temperatures. *J Compos Mater*, 14: 54–68.

Pervaiz, M. & Sain, M.M. (2003) Carbon storage potential in natural fiber composites. *Resources, Conservation and Recycling*, 39(4): 325–340.

Rajesh, M., Geetha, K., Sheeba, M., Radhakrishnan, P., Vallabhan, C.P.G. & Nampoori, V.P.N. (2006) A fiber optic smart sensor for studying the setting characteristics of various grades of cement. *Optics and Lasers in Engineering*, 44(5): 486–493.

Reddy, N. & Yang, Y. (2005) Biofbersfrom agricultural byproducts for industrial applications. *Trends in Biotechnology*, 23(1): 22–27.

Release of Thermal Insulation Performance Value of Building Materials (1999) <http://www.eccj.or.jp/law/pdf_ken1_e/release_of_thermal_insulation_performance_value_of_building_materials.pdf>.

Rice H.J. & Göransson, P. (1999) A dynamical model of light fibrous materials. *International Journal of Mechanical Sciences*, 41: 561–579.

RIL 155 (1984) *Lämmön ja kosteudeneristys*, Suomen Rakennusinsinöörien Liitto, Finland (in Finnish).

Roberts, S. (2008) Effects of climate change on the built environment. *Energy Policy*, 36(12): 4552–4557.

Rose, J.H. (1961) Organic and Inorganic Fibrous Materials, ASD 711 <http://contrails.iit.edu/DigitalCollection/1961/ASDTR61–322article46.pdf>.

Rothman, D.H. & Zaleski, S. (1994) Lattice-gas models of phase separation: interfaces, phase transitions, and multiphase flow. *Rev. Modern Phys.*, 66: 1417–1479.

Roy, S., Junk, M. & Sundar, S. (2006) Understanding the porosity dependence of heat flux through glass fiber insulation. *Mathematical and Computer Modelling*, 43(5): 485–492.

Seguchi, T. (2000) New trend of radiation application to polymer modification — irradiation in oxygen free atmosphere and at elevated temperature. *Radiation Physics and Chemistry*, 57(3): 367–371.

Siegel, R. & Howell, J.R. (1992) *Thermal Radiation Heat Transfer*, 3rd edn, Hemisphere, Washington.

Singh, B.P. & Kaviany, M. (1992) Modeling Radiative Heat Transfer in Packed Beds. *Int. J. Heat Mass Transfer*, 35: 1397–1405.

Soubdhan, T., Feuillard, T. & Bade, F. (2005) Experimental evaluation of insulation material in roofing system under tropical climate. *Solar Energy*, 79(3): 311–320.

Springer, C.S. (1984) Model for predicting the mechanical properties of composites at elevated temperatures. *J Reinf Plast Compos*., 3(1): 85–95.

Tao, Y-X., Besant, R.W. & Rezkallah, K.S. (1991a) Unsteady heat and mass transfer with phase changes in an insulation slab: frosting effects. *Int. J. Heat Mass Transfer*, 34(7): 1593–1603.

Tao, Y-X., Besant, R.W. & Rezkallah, K.S. (1991b) Modelling of frost formation in a fibrous Insulation slab and on an adjacent cold plate. *Int. Comm. Heat Mass Transfer*, 18: 609–618.

Taylor, B.J., Webster R. & Imbabi, M.S. (1998) The building envelope as an air filter. *Building and Environment*, 34(3): 353–361.

The Constructor of Modern World (2009) *http://theconstructor.org/2009/11/fiber-reinforced-concrete*.

Tien, C-L. (1988) Thermal Radiation in Packed and Fluidized Beds. *ASME J. Heat Transfer*, 110: 1230–1242.

Tien, C.-L. & Drolen, B.L. (1987) Thermal Radiation in Particulate Media with Dependent and Independent Scattering. *Annual Review of Numerical Fluid Mechanics and Heat Transfer*, 1: 1–32.

Tong, T.W., Yang, S.Q. & Tien, C.L. (1983) Radiative heat transfer in fibrous insulations—Part II: experimental study. *J Heat Transfer*, 105(1): 70–75.

Tong, T.W. & Tien, C.L. (1983) Radiative heat transfer in fibrous insulations – Part I: analytical study. *J Heat Transfer*, 105(1): 70–75.

Trdic, F., Sirok, B., Bullen, P.R. & Philpott, D.R. (1999) Monitoring mineral wool production using real-time machine vision. *Real Time Imaging*, 5(2): 125–140.

Ulkoseinärakenteita (2010) Rakennustieto Rakennustieto, in Finnish.

Verschoor, J.D., Greebler, P. & Manville, N.J. (1952) Heat transfer by gas conduction and radiation in fibrous insulation. *J. Heat Transfer*, 74: 467–474.

Vafai, K. & Hadim, H.A. (eds) (2000) *Handbook of Porous Media*, Marcel Dekker, New York.

Vafai, K. & Sarkar, S. (1986) Condensation effects in a fibrous insulation slab. *J. Heat Transfer*, 108: 667–675.

Vafai, K. & Whitaker, S. (1986) Simultaneous heat and mass transfer accompanied by phase change in porous insulation. *Trans. ASME*, 108: 132–140.

Velmurugan, R. & Manikandan, V. (2007) Mechanical properties of palmyra/glass fiber hybrid composites. *Composites: Part A*, 38(10): 2216–2226.

Viskanta, R. & Mengüc, M.P. (1989) Radiative transfer in dispersed media, ASME, *Appl. Mech. Rev.*, 42(9): 241–259.

Voronina, N. (1996) Improved empirical model of sound propagation through a fibrous material. *Applied Acoustics*, 48(2): 121–132.

Webb, R.L. (1994) *Principles of Enhanced Heat Transfer*, Wiley, New York.

Weinberger, C.B. (1996) *Synthetic Fiber Manufacturing*, Dept. of Chemical Engineering, Drexel University. August 30.

Westerlund, T. & Hoikka, T. (1989) On the modeling of mineral fiber formation. *Comput. Chem. Eng*., 13(10): 1153–1163.

Wijeysundera, N.E., Zheng. B.F., Iqbal, M. & Hauptmann, E.G. (1996) Numerical simulation of the transient moisture transfer through porous insulation. *Int. J. Heat Mass Transfer*, 39(5): 995–1004.

Whitaker, S. (1966) The equation of motion in porous media. *Chem. Eng. Sci*., 21: 291–300.

Whitaker, S. (1967) Diffusion and dispersion in porous media. *AIChE J*., 13: 420–427.
Whitaker, S. (1969) Advances in theory of fluid Motion in porous media. *lndustr. Eng. Chem*., 61: 14–28.
Whitaker, S. (1973) The transport equations for multi-phase systems. *Chem. Eng. Sci*., 28: 139–147.
Whitaker, S. (1985) A simple geometrical derivation of the spatial averaging theorem. *Chemical Engineering Education*, 19: 18–52.
Wikipedia, the free encyclopedia, http://en.wikipedia.org/wiki/Cellulose_insulation. http://science.jrank.org/pages/532/Artificial-Fibers.html.
Woolfson, D.N. & Ryadnov, M.G. (2006) Peptide-based fibrous biomaterials: Some things old, new and borrowed. *Current Opinion in Chemical Biology*, 10(6): 559–567.
Wu, Y.F. (2009) The structural behavior and design methodology for a new building system consisting of glass fiber reinforced gypsum panels. *Construction and Building Materials*, 23(8): 2905–2913.
Wu, H., Fan, J. & Du, N. (2007) Thermal energy transport within porous polymer materials: effects of fiber parameters. *Journal of Applied Polymer Science*, 106(1): 576–583.
Yilmaz, G. & Karlik, S.E. (2006) A distributed optical fiber sensor for temperature detection in power cables. *Sensors & Actuators: A Physical*, 125(2): 148–155.
Youngquist, J.A., English, B.E., Scharmer, R.C., Chow, P. & Shook, S.R. (1994) *Literature Review on Use of Non-Wood Plant Fibers for Building Materials and Panels*, USDA Forest Service General Technical Report FPL-GTR-80.
Yuen, W.W. (2003) Combined conductive/radiative heat transfer in high porosity fibrous insulation materials: theory and experiment, *Proceedings of the 6th ASME-JSME Thermal Engineering Joint Conference*, March 16–20.
Zannin, P.H.T. & Ferreira, J.A.C. (2007) In situ acoustic performance of materials used in Brazilian building construction. *Construction and Building Materials*, 21(8): 1820–1824.
Zienkiewicz, O.C., Taylor, R.L. & Zhu, J.Z. (1991) *The Finite Element Method: Its Basis and Fundamentals*. 6th Edition, Elsevier; Butterworth-Heinemann, Oxford, 733 pp.
Zhang, B-M., Zhao S-Y. & He, X-D. (2008) Experimental and theoretical studies on high-temperature thermal properties of fibrous insulation. *Journal of Quantitative Spectroscopy and Radiative Transfer*, 109(7):1309–1324.
Zhao, S.Y., Zhang, B.M. & He, X.D. (2009) Temperature and pressure dependent effective thermal conductivity of fibrous insulation. *International Journal of Thermal Sciences*, 48(2): 440–448.
Zverev, V.G., Gol'din, V.D. & Nazarenko, V.A. (2008) Radiation-conduction heat transfer in fibrous heat-resistant insulation under thermal effect. *High Temperature*, 46(1): 108–114.

11

Acoustic behaviour of fibrous materials

J. ANTÓNIO, University of Coimbra, Portugal

Abstract: This chapter describes the behaviour of the fibrous materials with respect to sound attenuation applications. The chapter first describes sound absorbers and sound absorption parameters. Then the factors affecting sound absorption are discussed. Finally, the aspects related to airborne and impact sound insulation provided by fibrous materials are reviewed.

Key words: fibrous materials, acoustics, sound absorption, airborne sound insulation, impact sound insulation.

11.1 Introduction

Concerns for human well-being are the main reasons to control unwanted noise. Undesired sounds are potentially harmful to human health and can also compromise the effectiveness of some activities; they are likely to influence the aesthetic understanding of sound landscapes.

Sound transmission from one fluid medium to another can be inhibited by implementing systems and materials capable of dissipating sound energy. The energy of the propagating sound wave can be absorbed by materials contiguous to the fluid and capable of dissipating the sound energy into heat. Alternatively the sound wave can be partially reflected using a large change in impedance by changing cross-sections (expansion chambers) and applying partitions of solid materials. Fibrous materials are excellent sound absorbers and when used in conjunction with other materials they can increase airborne and impact sound insulation.

In this work, the acoustic applications of fibrous materials are discussed. The next sections describe sound absorbers and sound absorption parameters and the main factors affecting sound absorption. The use of fibrous materials in building partitions to increase airborne and impact sound insulation is then addressed.

11.2 Sound absorbers

Sound absorbers are used in many applications of noise control engineering. They can be used to control the sound field in theatres and concert halls, in walls or ceilings of buildings to increase sound insulation, to control reverberant noise in offices and canteens, as noise attenuators in ducts, in noise control enclosures to reduce reverberation, in vehicles' panels or engine compartments.

Sound-absorbing materials are generally resistive in nature, being fibrous, porous or, in rather special cases, reactive resonators (Bell and Bell, 1994). Porous

materials are available in the form of mats, boards, or preformed elements made of glass, mineral or organic fibres, wood chips, coconut fibres or felted textile or open-cell foam (Mechel and Ver, 1992). These materials can be divided into two groups in terms of the relation between their thickness and wavelength of the sound wave. They behave as bulk material if the wavelength of the sound wave is of the order of, or shorter than, the thickness of the material, or as a sheet if the sound wavelength is long compared with the thickness of the material (Bies, 1971). Viscous effects and area density control the behaviour of a sheet while the solid-material density, viscous and thermal effects manage the performance of a bulk material.

Sheet absorbers can be made of fibres (bonded, felted, woven, contained) or consist of perforated plates with small holes. The bulk materials are composed of fibres or foams and are available as unbounded fibres, blankets or boards.

During the process of sound absorption, the organized motion of sound is converted into the disorganized motion of heat (Fahy, 2001), and there is a transfer between aerodynamic and thermodynamic energy (Bell and Bell, 1994). The expansion and rarefaction of air inside the porous materials leads to adiabatic and thermal heat transfer. In fibrous materials, the action of the sound pressure forces the fibres to move, and the fibre bending and fibre-to-fibre friction induce a temperature increase (Bell and Bell, 1994). Most of the energy losses at high frequencies are due to friction caused by the oscillation of air molecules and their loss of momentum in the direction of wave propagation, owing to changes in flow direction and expansion and contraction of the flow through irregular pores (Mechel and Ver, 1992).

Several tests performed by Aso and Kinoshita (1965; 1966) showed that fibre assemblies that have no air space behind them exhibit different sound absorption characteristics. The viscosity resistance type has the absorption characteristics of porous materials with very slight sound absorption at low frequencies, but quite considerable absorption at higher ones. The fibrous resonance type is peculiar to fibres, and its absorption characteristics are resonance absorption at low frequencies (having a peak) while in the higher-frequency range the behaviour is similar to the viscosity resistance type. The intermediate or mixed type shows characteristics common to the other two types, presenting resonance absorption but no peak. When an air cavity is placed behind the sample, the material has the same resonance absorption as in the fibrous resonance type, but its absorption does not increase in the higher-frequency range.

11.3 Sound absorption coefficient

The parameter that best describes the sound absorption of materials is the absorption coefficient α. It is defined as the ratio of the sound energy absorbed by a surface to the sound energy incident on that surface, taking values between 0 and 1. The sound absorption coefficient depends on the angle of incidence. But

when there is a diffuse sound field incident on a surface it is assumed that there is an equal probability of sound waves impinging on the surface from all directions (Hopkins, 2007). This parameter also depends on the frequency of the sound wave and thus, in the literature, values are presented for standard frequency bands. Porous and fibrous absorbers are most efficient at the higher frequencies, but also perform well at the middle and low frequencies if sufficiently thick or if backed by an air space.

11.3.1 Noise reduction coefficient

Sound absorption can be described as a single number. The descriptor most often used is the noise reduction coefficient (NRC). This parameter is calculated by averaging the sound absorption coefficients at 250, 500, 1000 and 2000 Hz and rounding off the result to the nearest multiple of 0.05. However, the use of NRC has its limitations, since the same value of NRC for two different materials does not mean that they perform the same way. Thus it is advisable to use all the available frequency-based coefficients, especially for sound absorption at frequencies below 250 Hz or above 2000 Hz (Cavanaugh *et al*., 2009).

11.3.2 Measurement of sound absorption coefficients

The sound absorption of fibrous materials can be measured in two ways: in a reverberation chamber or in an impedance tube. The reverberation time method closely simulates the conditions encountered in buildings. According to EN ISO 354 (2003) the test should be performed in a reverberation chamber with a volume of 200 m^3, to create a sufficiently diffuse decaying sound field. The test specimen to be placed inside the chamber should have an area between 10 m^2 and 12 m^2. The mounting of the test specimen depends on the type/application of the material and a number of mountings are standardized in EN ISO 354 (2003). The sound absorption coefficient is calculated from reverberation time measurements, since reverberation time is inversely proportional to absorption. The reverberation time is measured with and without the test specimen to allow the calculation of absorption provided by the sample. The absorption is divided by the area of the sample to give a value per unit area, the absorption coefficient α.

Figure 11.1 illustrates the sound absorption coefficient measured in a reverberation chamber for a nonwoven sample made of polyester fibres (triangle marks) and for a sample of mineral wool (square marks). As can be observed, for these materials high absorption coefficients are obtained in the high frequency range.

Sometimes the reverberation chamber method yields coefficients in excess of 1, owing to diffraction effects along the sample's edges. The Sabine equation applied to small non-reverberant rooms may also yield coefficients higher than 1. As a rule, when working with larger spaces an α greater than 1 (as sometimes

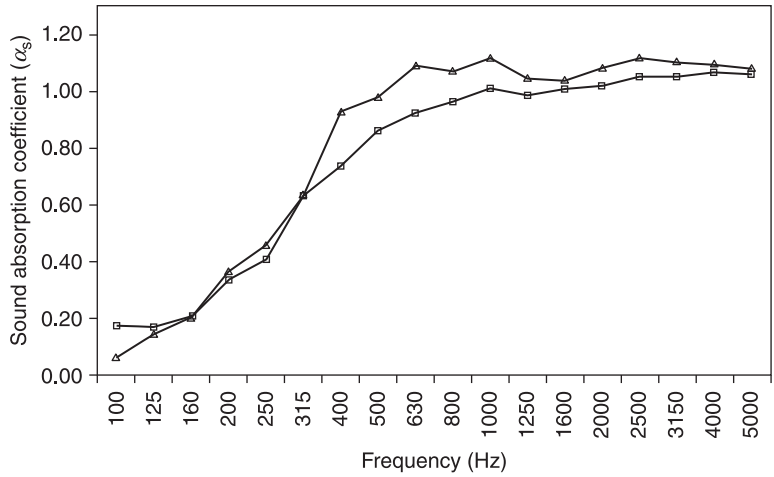

11.1 Sound absorption coefficients of a nonwoven polyester fibre (Δ) and of mineral wool (□).

reported in the manufacturer's literature) should be rounded down to no more than 0.99 (Cavanaugh *et al*., 2009).

The impedance tube yields normal-incidence absorption coefficients, from which random-incidence coefficients can be estimated.

The standing wave ratio (SWR) method is a traditional method in which a standing wave is generated in the impedance tube. The absorption coefficients are calculated from the sound pressure level difference between a pressure maximum and minimum. With this method it is only possible to measure one frequency at a time, as it employs pure tone excitation. The procedure for locating minima in the standing wave, which is needed to get phase information, is rather slow.

The steady state pressure in the tube is given by (Cox and D'Antonio, 2009)

$$p = A\left(e^{ikz} + R_r e^{-ikz}\right) \qquad [11.1]$$

where R_r is the reflection factor, k is the wavenumber, the sample is assumed to be at $z = 0$ (z is the distance measured along the impedance tube), and A is a complex constant. The first term represents the incident wave and the second term the reflected wave. The absorption coefficient is calculated from the reflection factor (Cox and D'Antonio, 2009; Allard and Atalla, 2009)

$$\alpha = 1 - \left|R_r^2\right| \qquad [11.2]$$

The reflection factor can be determined from the standing wave ratio $s = p_{max}/p_{min}$

$$\left|R\right| = \frac{s-1}{s+1} \qquad [11.3]$$

The maximum pressure p_{max} occurs when the first and second terms in equation [11.1] are in phase, and the minimum pressure p_{min} occurs when they are out of phase.

To find the pressure maximum and minimum, it is necessary to have a microphone probe mounted on a moving trolley.

The transfer function method uses two fixed microphones (at distances z_1 and z_2 from the sample) to acquire sound pressure near the sample. The complex acoustic transfer function of the two microphone signals is determined and then used to calculate the normal incidence absorption coefficient.

The complex pressure reflection coefficient is calculated as

$$R_r = \frac{H_{12}e^{ikz_1} - e^{ikz_2}}{e^{-ikz_2} - H_{12}e^{-ikz_1}} \qquad [11.4]$$

where $H_{12} = p(z_2)/p(z_1)$ is the transfer function between microphone positions.

The sound absorption coefficient is calculated as $\alpha = 1 - |R_r^2|$. There are restrictions in the microphone spacing, thus the frequency range where the method is valid is

$$\frac{0.05c}{|z_1 - z_2|} < f < \frac{0.45c}{|z_1 - z_2|} \qquad [11.5]$$

where c is the speed of sound.

The reverberation room and tube methods are essentially laboratory methods. Various authors consider that to predict and control acoustics in real environments it is important to measure material absorption characteristics *in situ*. Different reflection methods have been developed in order to achieve this goal (Garai, 1993; Allard *et al*., 1989; Allard and Champoux, 1989). These methods use two microphones and use pure tone signals or MLS (maximum length sequences) as a test signal. But there are some drawbacks, such as low-frequency limitation, inaccuracy with weakly absorbing materials, the need for complicated equipment and the practicality of the relative positioning of a sound source, microphones and sample (Takahashi *et al*., 2005). Further work has been done by Takahashi *et al*. (2005) in order to measure *in situ* normal surface impedance and the absorption coefficient of porous materials at frequencies below 500 Hz without a specific sound source. The method uses two microphones and ambient noise as excitation.

11.4 Factors affecting the sound absorption of fibrous materials

11.4.1 Fibre size

Studies performed with micro-fibre fabrics revealed that the sound absorption is superior to that of conventional fabric of the same thickness or weight (Na, 2007).

Nonwovens produced with recycled polyester fibres of different diameters and having the same length perform better in terms of sound absorption when the fine-fibre content increases (Lee and Joo, 2003). Jayaraman (2005) studied the influence of different parameters on the sound absorption of different nonwoven samples. He has concluded that the finer fibres present higher absorption coefficients. Ballagh (1996) studied the acoustic properties of wool and found that the absorption coefficients increase with decreasing fibre diameter. Similar results have been achieved by Nick (2002) when comparing the acoustic properties of standard material with Lyocell and with microfibre polyester felt. The variation in Lyocell fibre diameters shows higher noise absorption with smaller fibre diameters, whereas fibre length does not show any significant influence on absorption.

11.4.2 Fibre surface area

The influence of the surface area or the relation between mass/area in the sound absorption is reported in several works (Watanabe *et al*., 1999; Jayaraman, 2005). Sound absorption increases with the specific surface area of fibre, with an increase of relative density and friction of pore walls.

The surface area of a fabric is directly related to the denier and cross-section shape of the fibres in the fabric. Lower deniers yield more fibres per unit weight of the material, higher total fibre surface area, and greater possibilities for a sound wave to interact with the fibres in the fabric structure (Tascan and Vaughn, 2008).

11.4.3 Thickness

At lower frequencies, the effectiveness of absorption is directly related to the thickness of the material (Kosuge *et al*., 2005). Tea-leaf fibre (TLF) has been tested for its sound absorption properties using a two-microphone transfer function method (Ersoy and Küçük, 2009). It was found that the increase in the thickness of the sample resulted in an almost linear increase in the sound absorption coefficient.

Absorbers are most effective when their thickness is between one-quarter and one-half the wavelength of the sound, with the maximum performance where the thickness is one-quarter the wavelength (Hakamada *et al*., 2006). When absorption is desired at lower frequencies, and thickness and weight are limited, such as in an automotive application, materials with different specific air-flow resistances can be used to achieve desirable results. Both thickness and specific air-flow resistance must be taken into account when considering the performance of a material (Zent and Long, 2007).

11.4.4 Density

The density of a material influences its sound absorption, but density is not the best parameter for evaluating the optimum absorption, since different acoustic

properties may be achieved for the same density for different mean fibre diameters (Ballagh, 1996). Ballagh compared the normal incidence absorption coefficient of wool samples, varying the density and maintaining the thickness. For samples 25 mm thick, the sound absorption increases smoothly with the density. For samples 100 mm thick, increasing absorption with density can be seen for high frequencies only up to 47 kg/m^3, and tends to decrease for higher densities.

During the work developed by Na (2007) for the study of microfibre fabrics, fabric density was found to have more effect than its thickness or weight on sound absorption.

11.4.5 Porosity

Sound absorption mechanisms in porous materials depend on the number, size and type of pores. As the sound dissipation results from friction losses due to the sound wave entering the pores, there must be enough pores on the surface of the material to attenuate the sound.

The porosity (h) of a porous material is defined as the ratio between the volume of the voids and the total volume of the material (Bies, 1971),

$$h = \frac{V_a}{V_t} \qquad [11.6]$$

where V_a is the air volume in pores and V_t is the total volume of the material. The values of porosity range between 0 and 1 and, in general, for fibrous materials exceed 0.95.

The absorption characteristics of fibre assemblies change from viscosity resistance to, successively, the mixed and the resonance type as they decrease in porosity (Aso and Kinoshita, 1965).

Hakamada *et al*. (2006) compared the sound absorption of two samples with the same pore size but with different porosities. The sound absorption coefficient increased as porosity increased, indicating that highly porous materials are good sound absorbers. The relationship between pore size and sound absorption coefficient was investigated using samples having the same porosity but different pore sizes. The smallest pore size sample exhibited the highest sound absorption coefficient, but the largest pore size sample did not exhibit the lowest sound absorption. Thus, there was no apparent correlation between pore size and sound absorption coefficient.

The optimal functional relationship between porosity and distance along the propagation of the sound wave inside a nonwoven has been investigated by Shoshani and Yakubov (2001). Calculations clearly indicate that the functional variation of porosity of the fibreweb along the sound wave propagation plays a dominant role in the design of the web as a noise absorption element. They considered the linear, quadratic, exponential and logarithmic variations of porosity

in the sound propagation direction. For all the variations except the quadratic, an increase in absorption is observed when the porosity increases along the propagation of the sound wave.

11.4.6 Airflow resistivity

Sound absorption by, and sound insulation through, porous materials is partly described by their ability to resist airflow. The parameters that quantify this property are: airflow resistance, specific airflow resistance, and airflow resistivity (Hopkins, 2007).

Airflow resistance, R_f (Pa.s/m^3) is defined as

$$R_f = \frac{\Delta p}{q_v} \qquad [11.7]$$

where Δp is the air pressure difference (referred to as differential pressure) across the test specimen (a layer of porous material) with the respect to the atmosphere (Pa), and q_v is the volumetric airflow rating passing through the test specimen (m^3/s). The volumetric airflow rate is

$$q_v = uS \qquad [11.8]$$

where u is the linear air velocity (m/s) and S is the cross-section area of the porous material perpendicular to the direction of the flow (m^2).

Specific airflow resistance, R_s (Pa.s/m) applies to a specific thickness of a porous material. It is an appropriate specification parameter for both homogeneous and nonhomogeneous materials,

$$R_s = R_f S \qquad [11.9]$$

Airflow resistivity, r (Pa.s/m^2) is the specific airflow resistance per unit thickness, and is only appropriate as a specification parameter for homogeneous materials.

$$r = \frac{R_s}{d} = \frac{R_f S}{d} = \frac{S\Delta p}{dq_v} \qquad [11.10]$$

where d (m) is the thickness of the layer of porous material in the direction of airflow.

The airflow resistivity of common absorbent materials typically varies between 2×10^3 and 2×10^5 Pa.s/m^2.

For fibrous materials the airflow resistance depends on the direction of airflow through the material. Fibrous materials are generally anisotropic. Fibres in the material generally lie in planes parallel to its surface. The flow resistivity in the normal direction is different from that in the planar directions. In the first case, air flows perpendicular to the surface of the panel, while in the second case it flows parallel to the surface of the layer. Normal flow resistivity is greater than planar

flow resistivity (Allard and Atalla, 2009). There is a close relationship between flow resistivity, density and fibre diameter.

Results of flow resistivity as a function of density for various sound-absorbing materials, and of the approximate flow resistivity as a function of density with fibre diameter can be found in Mechel and Ver (1992).

Measurements in wool samples showed that optimum absorption is generally obtained when the product of thickness and flow resistivity is about 1000 Rayls (Pa.s/m) (Ballagh, 1996). At higher values there is some improvement in low-frequency performance, but at the expense of a reduction in high-frequency absorption. For wool fibre, flow resistivity is proportional to the material density and inversely proportional to the fibre diameter. For glass fibres it is inversely proportional to the square of the fibre diameter. Experiments conducted with samples of glass fibre and rock wool showed that the flow resistivity increases with a higher bulk density (Wang and Torng, 2001). Results obtained with nonwovens showed that higher flow resistances give better sound absorption values. However, there is an optimal value for an airflow resistance, beyond which sound starts reflecting from the material and so decreases absorption (Jayaraman, 2005).

11.4.7 Tortuosity

The structure shape factor, tortuosity, is the parameter that takes into account the irregular shape of the pore and the non-uniform distribution of pores per unit of section throughout the thickness of the porous material. The tortuosity, by increasing the path length of the sound which travels through the fibres, also increases the viscous losses which the air encounters as the sound waves try to find their way through the small passageways available for their propagation (Newell, 2008). The structure factor decreases with increasing frequency and ranges from high values of 6 down to 1 (Mechel and Ver, 1992). However, generally, it tends to lie between about 1.2 and 1.3 (Fahy, 2001).

Horoshenkov and Swift (2001) report that tortuosity is responsible for the behaviour of the real parts of the characteristic impedance and propagation constant of a porous medium, and for the positions of the interference maxima and minima in the absorption coefficient spectrum in a porous layer of finite thickness. In a fibrous mat the compression of the material slightly increases the tortuosity.

11.4.8 Surface impedance

The influence of surface impedance on sound absorption has been investigated by Jayaraman (2005), using airlaid samples of different configurations. An appreciable increase in the normal absorption coefficient was obtained by altering the surface impedance of the material. Surface impedance can significantly influence the sound absorption capacity of nonwovens by altering the porosity and tortuous path of the sample.

11.4.9 Compression of the fibre mat

As a porous or fibrous layer undergoes compression, the thickness decreases. Compressing the material affects the tortuosity, characteristic length, flow resistivity, porosity and density (Wang and Kuo, 2008).

Castagnède *et al*. (2000) investigated the effects of compression on the sound absorption of fibrous materials. Applying compression to a homogeneous porous layer reduces porosity and decreases the characteristic lengths, and at the same time increases tortuosity. Despite the variations of these physical parameters, it is mainly the smaller thickness that is responsible for the net reduction of the absorption coefficient. Similar conclusions have been arrived at by other authors (Jayaraman, 2005).

11.4.10 Back air space

When there is an air cavity behind a material, the material will act as a (frequency dependent) membrane of a certain mass. The air inside the cavity is analogous to a mechanical spring. The sound absorption of a sound-absorbing material is significantly improved by inserting an air gap between the sample and the rigid back surface (Hakamada *et al*., 2006). During their research into porous aluminium material, Hakamada *et al*. (2006) have found that the effect of the air gap increased with the decreasing thickness of the specimens.

In the work of Aso and Kinoshita (1965), it was concluded that the maximum absorption coefficient of a thin sample of large porosity decreases slightly as the depth of the air space increases. Furthermore, their investigation revealed that the maximum absorption coefficient of a thick sample of large porosity is almost constant, irrespective of the depth of its air space.

11.4.11 Temperature

Srivastava *et al*. (2006) investigated the influence of temperature on the sound absorption of mineral wool and the results indicated that sound absorption is independent of temperature in the range of 10–50°C. They have also established a theoretical relation between the noise reduction coefficient and the thermal conductivity using a least-squares regression method. These relations were established for different temperature conditions.

11.5 Modelling sound-absorbing materials

The acoustic properties of sound-absorbing material can be predicted by phenomenological and microstructural models. Their validity is constrained by certain conditions. In the formulation of empirical models, theoretical considerations are not usually taken into account, nor is the internal structure of the material considered (Ballagh, 1996).

Several models have been developed (Dunn and Davern, 1986; Qunli, 1988) once the principal had been established by Delany and Bazley (1970) with subsequent extensions by Mechel (Mechel and Ver, 1992). The characteristic impedance and propagation coefficients of the material can be predicted using the flow resistivity of the material, normalized by dividing it into the frequency of interest. From these two complex quantities other acoustic properties can be predicted. Although these methods have been extensively used, some materials, such as natural wool, are outside the limits of the available empirical models. In this case it is best to use microstructural models (Ballagh, 1996). These are based on a more-detailed knowledge of the internal structure of a material and consider fundamental physical properties to predict the acoustic performance. The models normally use the flow resistivity, tortuosity, porosity and shape factor(s) as model parameters. Different models have been developed over the years by authors such as Rayleigh (1896), Zwikker and Kosten (1949), Biot (1956) and Attenborough (1982). More complex structures using shape factors have been modelled by Johnson *et al*. (1987), and Allard and Champoux (1992).

11.6 Airborne sound insulation

Airborne sound is originated when a source radiates sound waves into the air and they then encounter the surfaces of obstacles, building elements, etc.

When a sound wave strikes an obstacle that is relatively large compared with the wavelength of the sound, some of the sound energy is reflected back while the rest is transferred into the obstacle's material where it is absorbed or transmitted through the obstacle. The amount of sound transmitted depends on the quantity of reflected and absorbed sound.

At a given frequency, the sound transmission coefficient τ is defined as the ratio between the sound power transmitted by the element W_2, to the sound power incident on the test element, W_1. The sound-reduction index or transmission loss, R, in decibels is defined as

$$R = 10 \lg\left(\frac{1}{\tau}\right) = 10 \lg \frac{W_1}{W_2} \qquad [11.11]$$

11.6.1 Measurement of airborne sound insulation

Measurements taken in laboratory conditions can be used to compare the performance of the different materials/elements in insulating airborne sound. The results obtained can also be used to predict the sound insulation of such elements in real building conditions.

The standard methods used to measure laboratory airborne sound insulation consider two contiguous reverberation rooms, the source room and the receiving room, divided by the element to be tested.

The rooms need to be mechanically and acoustically insulated in order to ensure that the flanking transmissions are negligible, which means that almost all the sound is transmitted via the element to be tested, and it is necessary to ensure diffuse fields in the source and receiving room.

Considering the condition of diffuse fields, it is possible to calculate the incident- and transmitted-sound power from sound pressure level measurements in each room (Hopkins, 2007). This leads to an expression for the sound reduction index, in decibels

$$R = L_{p1} - L_{p2} + 10\lg\left(\frac{S}{A}\right) \qquad [11.12]$$

where L_{p1} and L_{p2} are the temporal and spatial average sound pressure levels in the source and receiving room respectively, A is the absorption area of the receiving room and S is the area of the test element. The procedures necessary to carry out the laboratory measurements are stated in standards such as ISO 10140 series (Part 1 to Part 5) or their equivalents.

11.6.2 Influence of fibrous materials on airborne sound insulation

It is well known that placing a sound-absorption layer in the cavity of double-leaf constructions in buildings can improve the sound-reduction indices of such walls. Their principal function is to suppress acoustic resonances of the cavities by reducing the coupling between the leaf sheets (Fahy, 2001). The relation of the complex amplitudes of transmitted and incident pressures depends on the porosity, structure factor and flow resistivity of the materials, among other factors.

Figure 11.2 compares the sound reduction index obtained in a laboratory for a double-leaf plasterboard wall, with (triangle marks) and without (square marks) polyester fibres in the cavity. The plasterboard panels are 12.5 mm thick and are 48 mm apart. As can be observed, the sound insulation increases with the introduction of the fibrous material.

If the porous material is very close to, but not touching, the plate it can be treated as an equivalent fluid to calculate a radiation efficiency.

Several authors have treated the fibrous material as an equivalent fluid when modelling the sound insulation of the fibrous layer. António *et al.* (2003) used a multilayer model to simulate the airborne sound insulation of a double wall, where the fibrous material inside the cavity is modelled as an equivalent fluid.

Figure 11.3 shows the influence on the sound insulation of mineral wool with different densities and flow resistivities r, placed in the cavity of a double ceramic brick wall. The influence of the porous material is very evident in the attenuation of dips in the insulation curve controlled by the cavity resonances. This model is based on a discrete wavenumber representation. The pressures and displacements are written as a superposition of plane waves.

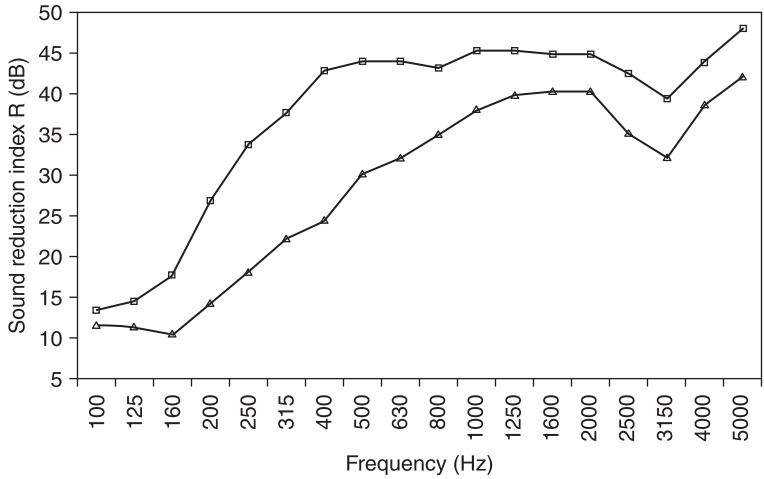

11.2 Sound reduction index of a double-leaf plasterboard wall with panels 12.5 mm thick and a cavity of 48 mm.

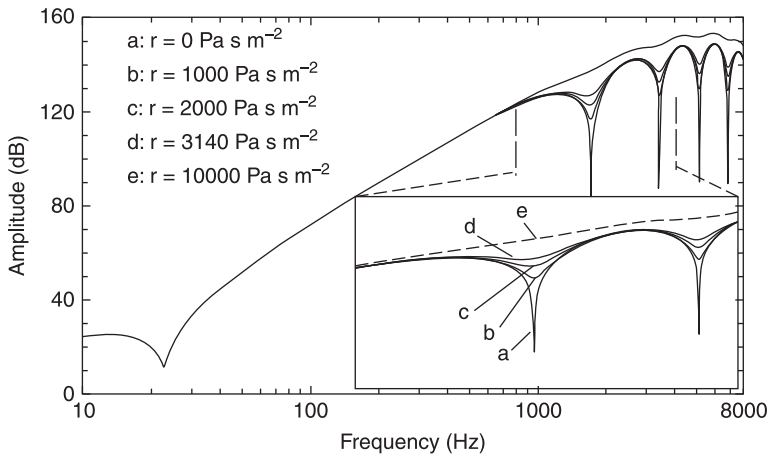

11.3 Average sound reduction provided by a double ceramic brick wall composed of panels 10.0 cm thick and an air layer 10.0 cm thick, filled with different absorbing materials, when subjected to normally incident plane waves.

The damping of the structure increases when the absorbent materials are in close proximity to (but not necessarily touching) structural elements (Tomlinson *et al*., 2004). This may be important in calculating the total loss factor of the plate because the efficiency of radiation into a porous material is usually greater than into air. For plates with low internal loss factors, such as in thin metal plates, and low coupling losses, this becomes an important loss mechanism. The damping

significantly increases as the porous material approaches the surface of the plate (Cummings *et al*., 1999). Plasterboard has higher internal losses than most metal plates and so the effect of radiation damping is less important (Hopkins, 2007). If the solid frame of the absorbent material is bonded to both lateral panels, then it can act as a vibration link between the panels and so decrease the transmission loss (Cummings *et al*., 1999).

To predict the direct-sound transmission when a porous material is touching or is fixed to the plate, the individual aspects of damping, radiation and sound propagation through the porous material, and vibration transmission into the frame of the porous material cannot be considered separately from each other (Hopkins, 2007). For this kind of sandwich plate, Biot's theory can be used to model wave propagation in the porous material and predict the sound radiation index.

Ballagh (1996) investigated the performance of wool in this application by measuring the transmission loss of two double-stud partitions with various grades of wool as cavity infill. The weighted sound reduction index increased by up to 6 dB when the thickest wool-bonded batt was placed in the cavity of the double-stud wall. The performance tends to improve less for thinner wool infill.

The use of polyester fibre blankets in plasterboard cavity walls affords an improvement of sound transmission loss over the whole frequency range when compared with a plasterboard wall system without added cavity absorption (Narang, 1995). It was found that the magnitude of improvement in sound transmission loss is comparable to the typical improvements given by installing fibreglass in the wall cavities.

The airborne sound insulation of the absorbing material itself was investigated by Tascan and Vaughn (2008) for nonwoven fabrics. The fabric air permeability, the density of the fabric, the fibre diameter and fibre shape all influence the sound insulation performance of the material.

11.7 Impact sound insulation

Impact noise or structure-borne sound originates in the solid elements of a building and is provoked by an impact on them. In buildings, these sounds occur mainly in floors with footsteps, dropping objects or moving furniture. Consider a slab floor subjected to impact noise. The induced vibrational energy is partially dissipated in the slab, partially radiated in the source room and the rest is transmitted through the slab to the structure.

The use of a resilient layer in the floor of a building reduces the transmission of structural vibrations. They can be incorporated in a system known as a floating floor, composed of a slab lying on the resilient material placed over a structural slab (preferably a concrete slab of some mass) (Cavanaugh *et al*., 2009). Lighter systems, such as those made of wood, provide considerably less insulation but may be useful where the structure cannot support the weight of the floating concrete slab.

11.7.1 Measurement of impact sound insulation

To measure the impact sound insulation it is necessary to use a structure-borne sound source. To avoid measuring the power input a standardized source is used. Laboratory measurements require two vertically adjacent rooms. The temporal and spatial average sound pressure level in the receiving room has to be measured L_p, while the floor in the source room is excited by an ISO tapping machine. The mean square pressure in the receiving room, L_n, for a given transmitted sound power, is proportional to the absorption area, A, of that room, and is given by

$$L_n = L_p + 10\lg\left(\frac{A}{A_0}\right) \qquad [11.13]$$

where A_0 is a reference absorption area of $10\,m^2$ for the receiving room.

The test method of measuring the normalized impact sound pressure level in laboratory conditions is specified in ISO 10140 series (2010) (Part 1 to Part 5).

The improvement of impact sound insulation, ΔL, provided by a floating floor can be assessed by means of the standard procedures described in ISO 10140 series (2010) (Part 1 to Part 5) or equivalent standards, and is expressed as

$$\Delta L = L_{n0} - L_n \qquad [11.14]$$

where L_{n0}, and L_n are the normalized impact sound pressure levels of the heavyweight standard floor without and with the floating floor, respectively.

11.7.2 Influence of fibrous materials on impact sound insulation

Fibrous materials can be used to attenuate impact noise if applied as an underlay of a floating floor acting as a resilient layer. Insulation materials suitable to be applied as a resilient layer under a floating floor need to have low dynamic stiffness. This is a parameter that describes the ability of a resilient material to transmit vibration. Materials suitable for use as resilient layers have a dynamic stiffness of less than $10\,MN/m^3$ (Cripps *et al*., 2004). However some countries have higher limits in their building regulations.

Standard EN 29052–1 (1992) (or equivalent standards) states the procedures to determine this quantity. Dynamic stiffness and compressibility are the main descriptors of resilient materials used in floating floors. The dynamic stiffness is always associated with the thickness of the material since the dynamic stiffness to some extent varies with the thickness.

Kim *et al*. (2009) tested different materials and found that dynamic stiffness decreased as the thickness of the resilient materials increased. As the dynamic stiffness of resilient materials decreased, the heavyweight impact sound reduction level tended to increase. They further tested multilayered elements and the results

show that if the resilient materials with low dynamic stiffness are laid on top of resilient materials with high dynamic stiffness, the dynamic stiffness of the layered structure is similar to that of the resilient materials with low dynamic stiffness.

Suitable fibres for this application are natural ones, such as coconut fibre, hemp and flax boards (Cripps *et al*., 2004), and synthetic ones, such as glass fibre, rock wool, polyester fibre, etc. The stiffness of natural fibres is not significantly influenced by the level of sorption moisture. Some fibres become limp with a higher level of sorption moisture. The combination of natural fibres and synthetic binder fibres is not disadvantageous if the synthetic binder fibre content guarantees a sufficiently elastic insulation material matrix (Mussig and Stevens, 2010).

The dynamic stiffness is dependent on the static load and this dependence is not the same for all materials. A resilient layer with high compressibility in a floating floor could suffer deflection under the floating slab weight, causing fibre breakage and thus reduce the thickness, which would increase the dynamic stiffness and impair the acoustic properties of the insulation layer (Schiavi *et al*., 2005).

11.8 Conclusions

The use of fibrous materials in civil engineering applications can contribute to acoustic comfort and noise control. Fibrous materials can be used as sound absorbers to control echoes and reverberation in rooms where speech needs to be intelligible, to control noise in rooms and equipment enclosures, and for noise attenuation in ducts. They can be applied in the form of suspended, spaced panels (covered with fabric) in ceilings in industrial plants with high ceilings, for example. In walls and ceilings they can also be used with protective open facings such as perforated or slotted panels (made of wood, metal or plasterboard) in lecture rooms, auditoriums, theatres, canteens and offices. The use of fibrous materials as internal lining in ducts or their application inside machinery enclosures are also quite common as noise control procedures.

Fibrous materials are also used to increase the sound insulation of building partitions. If they are encased in double-wall cavities this helps to increase the airborne sound insulation by diminishing the air-cavity resonances. Furthermore, these materials are very suitable for attenuating impact-noise transmission. Thus, the inclusion of fibrous materials as a resilient layer under a floating floor contributes to reducing the transmission of structural vibrations.

11.9 References

Allard J F and Champoux Y (1992) 'New empirical equations for sound propagation in rigid framed porous materials', *Journal of the Acoustical Society of America*, 91: 3346–3353.

Allard J F and Champoux Y (1989) 'In situ two-microphone technique for the measurement of the acoustic surface impedance of materials', *Noise Contr Eng J*, 32: 15–23.

Allard J F, Champoux Y and Nicolas J (1989) 'Pressure variation above a layer of absorbing material and impedance measurement at oblique incidence and low frequencies', *Journal of the Acoustical Society of America*, 86: 766–770.

Allard J F, Atalla N (2009) *Propagation of Sound in Porous Media: Modelling Sound Absorbing Materials*. Chichester: Wiley.

António J M P, Tadeu A and Godinho L (2003) 'Analytical evaluation of the acoustic insulation provided by double infinite walls', *Journal of Sound and Vibration*, 263: 113–129.

Aso S and Kinoshita R (1965) 'Maximum Sound Absorption Coefficient of a Fiber Assembly', *Journal of The Textile Machinery Society of Japan*, 11: 81–87.

Aso S and Kinoshita R (1966) 'Sound absorption coefficient of glass wool', *Journal of The Textile Machinery Society of Japan*, 12: 101–106.

Attenborough K (1982) 'Acoustical characteristics of porous materials', *Physics Reports*, 82(3): 179–227.

Ballagh K O (1996) 'Acoustical properties of wool', *Applied Acoustics*, 48: 101–120.

Bell L H and Bell D H (1994) *Industrial Noise Control: Fundamentals and Applications*. New York: Marcel Dekker Inc.

Bies D A (1971) 'Acoustical properties of porous materials', in Beranek L L, *Noise and Vibration Control*. New York: McGraw Hill Book Company, pp. 245–269.

Biot M A (1956) 'Theory of Propagation of elastic waves in a fluid-saturated porous solid. I: low-frequency range', *Journal of the Acoustical Society of America*, 28: 168–178.

Castagnède B, Aknine A and Brouard B (2000) 'Effects of compression on the sound absorption of fibrous materials', *Applied Acoustics*, 61: 173–182.

Cavanaugh W J, Tocci G C and Wilkes J A (2009) *Architectural Acoustics: Principles and Practice*. Chichester: Wiley & Sons.

Cox T J and D'Antonio P (2009) *Acoustic Absorbers and Diffusers: Theory, Design, and Application*. London: Taylor & Francis.

Cripps A, Handyside R and Dewar L (2004) *Crops in Construction Handbook*. London: CIRIA.

Cummings A, Rice H J and Wilson R (1999) 'Radiation damping in plates, induced by porous media', *Journal of Sound and Vibration*, 221: 143–167.

Delany M E and Bazley E N (1970) 'Acoustical properties of fibrous absorbent materials'. *Applied Acoustics*, 3: 105–116.

Dunn I P and Davern W A (1986) 'Calculation of acoustic impedance of multi-layer absorbers', *Applied Acoustics*, 19: 321–334.

EN 29052–1:1992 (1992) 'Acoustics – Method for the determination of dynamic stiffness – Part 1: Materials used under floating floors in dwellings'. Geneva: International Organization for Standardization.

EN ISO 354:2003 (2003) 'Acoustics – Measurement of sound absorption in a reverberation room'. Geneva: International Organization for Standardization.

Ersoy S and Küçük H (2009) 'Investigation of industrial tea-leaf-fibre waste material for its sound absorption properties', *Applied Acoustics*, 70: 215–220.

Fahy F (2001) *Foundations of Engineering Acoustics*. London and San Diego: Academic Press.

Garai M, (1993) 'Measurement of the sound-absorption coefficient in situ: the reflection method using periodic pseudo-random sequences of maximum length', *Applied Acoustics*, 39: 119–139.

Hakamada M, Kuromura T, Chen Y, Kusuda H and Mabuchi M (2006) 'Sound absorption characteristics of porous aluminum fabricated by spacer method', *Journal of Applied Physics*, 100: 114908–1.

Hopkins C (2007) *Sound Insulation*. Oxford: Butterworth-Heinemann.
Horoshenkov K V and Swift M J (2001) 'The effect of consolidation on the acoustic properties of loose rubber granulates' *Applied Acoustics*, 62: 665–690.
ISO 10140–1:2010 (2010) 'Acoustics – Laboratory measurement of sound insulation of building elements – Part 1: Application rules for specific products'. Geneva: International Organization for Standardization.
ISO 10140–2:2010 (2010) 'Acoustics – Laboratory measurement of sound insulation of building elements – Part 2: Measurement of airborne sound insulation'. Geneva: International Organization for Standardization.
ISO 10140–3:2010 (2010) 'Acoustics – Laboratory measurement of sound insulation of building elements – Part 3: Measurement of impact sound insulation'. Geneva: International Organization for Standardization.
ISO 10140–4:2010 (2010) 'Acoustics – Laboratory measurement of sound insulation of building elements – Part 4: Measurement procedures and requirements', Geneva: International Organization for Standardization.
ISO 10140–5:2010 (2010) 'Acoustics – Laboratory measurement of sound insulation of building elements – Part 5: Requirements for test facilities and equipment', Geneva: International Organization for Standardization.
Jayaraman K A (2005) 'Acoustical Absorptive Properties of Nonwovens'. MSc Thesis, North Carolina State University.
Johnson D L, Koplik J and Dashen R (1987) 'Theory of dynamic permeability and tortuosity in fluid-saturated porous media', *J Fluid Mech*., 176: 379.
Kim K-W, Jeong G-C, Yang K-S and Sohn J-Y (2009) 'Correlation between dynamic stiffness of resilient materials and heavyweight impact sound reduction level', *Building and Environment*, 44: 1589–1600.
Kosuge K, Takayasu A and Hori T (2005) 'Recyclable flame retardant nonwoven for sound absorption; RUBA®', *Journal of Materials Science*, 40: 5399–5405.
Lee Y and Joo C (2003) Sound absorption properties of recycled polyester fibrous assembly absorbers, *AUTEX Research Journal*, 3: 78–84.
Mechel F P and Ver I (1992) 'Sound absorbing materials and sound absorbers', in L Beranek and I Ber, *Noise and Vibration Control Engineering: Principles and Applications*: New York: John Wiley & Sons, pp. 203–243.
Müssig J and Stevens C (2010) *Industrial Applications of Natural Fibres: Structure, Properties and Technical Applications*. Chichester: John Wiley & Sons.
Na, Y J (2007) 'Sound absorption coefficients of micro-fiber fabrics by reverberation room method', *Textile Research Journal*, 77: 330–335.
Narang P P (1995) 'Material Parameter selection in polyester fibre insulation for sound transmission and absorption', *Applied Acoustics*, 45: 335–358.
Newell P (2008) *Recording Studio Design*. Oxford: Focal Press.
Nick A, Becker U and Thoma W (2002) 'Improved acoustic behavior of interior parts of renewable resources in the automotive industry', *Journal of Polymers and the Environment*, 10: 115–118.
Qunli, W (1988) 'Empirical relations between acoustical properties and flow resistivity of porous plastic open-cell foam', *Applied Acoustics*, 25: 141–148.
Rayleigh, J W S (1896) *Theory of Sound II*. London: Macmillan.
Schiavi A, Belli A P and Russo F (2005) 'Estimation of acoustical performance of floating floors from dynamic stiffness of resilient layers', *Building Acoustics*, 12: 99–113.
Shoshani Y and Yakubov Y (2001) 'Use of nonwovens of variable porosity as noise control elements', *International Nonwovens Journal*, 10: 23–28.

Srivastava R K, Dhabal R L, Suman B M, Saini A and Panchal P (2006) 'An estimation of correlation on thermo-acoustic properties of mineral wool', *Journal of Scientific & Industrial Research*, 65: 232–236.

Takahashi Y, Otsuru T and Tomiku R (2005) 'In situ measurements of surface impedance and absorption coefficients of porous materials using two microphones and ambient noise', A*pplied Acoustics*, 66: 845–865.

Tascan M and Vaughn E A (2008) 'Effects of fiber denier, fiber cross-sectional shape and fabric density on acoustical behavior of vertically lapped nonwoven fabrics', *Journal of Engineered Fibers and Fabrics*, 3: 32–38.

Tomlinson D, Craik R J M and Wilson R (2004) 'Acoustic radiation from a plate into a porous medium', *Journal of Sound and Vibration*, 273: 33–49.

Wang C-N and Kuo Y-M (2008) 'Effects of compression on the sound absorption of porous materials with an elastic frame', *Applied Acoustics*, 69: 31–39.

Wang C-N and Torng J-H (2001) 'Experimental study of the absorption characteristics of some porous fibrous materials', *Applied Acoustics*, 62: 447–459.

Watanabe K, Minemura Y, Nemoto K and Sugawara H (1999) 'Development of high-performance all-polyester sound absorbing materials', *JSAE Review*, 20: 357–362.

Zent A and Long J T (2007) 'Automotive sound absorbing material survey results', *Proceeding of the SAE Noise and Vibration Conference and Exhibition*, May 2007, St. Charles, IL., USA., p. 2186.

Zwikker, C and Kosten C W (1949) *Sound Absorbing Materials*. New York: Elsevier.

12

The use of textile materials for architectural membranes

J. MONJO-CARRIÓ, Polytechnic University of Madrid, Spain and
J. TEJERA, BAT (Buró Arquitectura Textil), Spain

Abstract: This chapter summarizes the main aspects of tensile structures made with specific fabric materials. The chapter first reviews the historical antecedents and the technical and formal typology for this type of structure in architecture. The chapter then discusses the construction conditions as well as the different materials and finishings necessary to build and maintain the textile structures and membrane covers.

Key words: textile architecture, form finding, coated fabric, membrane, synclastic, anticlastic.

12.1 Introduction

The term 'textile architecture' can be used to cover all architectural solutions (defining and encompassing habitable space) in which both structure and enclosure consist primarily of fabric. Indeed, 'textile technology' applied to building is acquiring growing importance. Paradoxically, the origin of the very modern type of architecture defined here is remote. And while it often draws from other fields of science or technology for its solutions, it is gaining acceptance in architectural design, where it has a promising future.

The idea that a 'mere piece of cloth' can constitute architecture in the traditional meaning of the word may be called into question, particularly since, to date, fabric has been chiefly used in building for protective or decorative purposes only. Nonetheless, when fabric is not an accessory, but comprises structure and enclosure and determines the shape of a building affording it the necessary functionality, it must be regarded not as an ancillary material but as a construction unit or even as a construction system. Consequently, the results obtained can ultimately be regarded to be architecture in the strictest sense. In today's world of high-technology building, then, 'fabric structures' are widely accepted solutions for large-scale, prominent international projects, such as the airports at Jeddah, Saudi Arabia and Denver, Colorado, USA (see Fig. 12.1(a)), the Millennium Dome in London (see Fig. 12.1(b)), any number of sports stadiums and so on. Horst Berger believes, in this regard, that in terms of spaciousness, natural lighting and even sculptural quality, a 'new architecture' has arisen, known as 'textile architecture'.

This new architecture is obviously identified by a number of traits that differentiate it from its more traditional sibling. Such features are not based exclusively on its

(a)

(b)

12.1 (a) Denver International Airport, Colorado; (b) Millennium Dome, London.

very specific (textile) technology. Rather, they affect the entire conceptual approach, beginning with the initial design and including compositional appearance and particularly functionality, inasmuch as the space enclosed is generally very distinctive. Indeed, the material and its mechanical capacity ensure a high efficiency – mass ratio while minimizing costs, all of which means that large spaces can be spanned with comparative constructional ease. Moreover, the shape of such surface structures constitutes a drastic change from conventional architectural canons (arch and lintel), with the appearance of the more 'organic' designs stemming from both the technology involved and the functional needs. Finally, the resulting spaces feature certain specific architectural characteristics, including more natural light and greater flexibility, although also certain limitations in terms of comfort. As a whole, they constitute what Horst Berger calls a 'megaspace' or 'improved

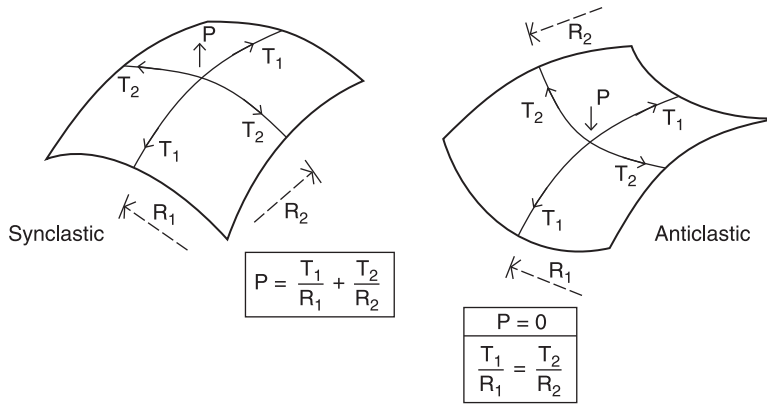

12.2 Two ways to keep tension in the membrane.

environment'. This pioneer in the field maintains that textile architecture stands at the bounds of nature itself and provides for habitable environments with a minimum amount of material and, therefore, low construction costs.

As discussed below, the fundamental basis for the constructional integrity and structural stability of enclosures built using textile technology lies in maintaining sufficient tensile stress at all points of the fabric in all directions for it to act optimally as a membrane. To this end, two types of solution can be applied that condition the appearance of the resulting structure (see Fig. 12.2):

(a) Application of a uniform, perpendicular force to the fabric in the form of air pressure that generates the necessary tangential tensile stress so that the overall form adopted by the perimetrically-anchored structure is synclastic. These are known as 'airhalls' or 'pneumatic structures'.
(b) Application of tensile stress at the perimeter, generating upward and downward forces until the fabric is stabilized throughout, giving rise to an anticlastic shape. This alternative, which has been more widely used in architecture and is the focus of the present discussion, gives rise to what are known as 'tensile membrane structures'.

12.1.1 Brief history

Tensile membranes have a much longer tradition, dating back to early history and the tents built by nomadic peoples. Their use has been ongoing through to the present whenever a need has arisen for provisional and portable shelters, such as those generated by travelling performers (circuses), hikers, armies and, of course, the nomad civilizations still existing today. Perhaps the oldest such structure of which we have written record is found in the Book of Exodus. According to Chapter 26, the first temple or tabernacle built by the Jewish people in their

journey to the Promised Land was made from 'ten curtains of fine twined linen', forming a rectangle 15.75 m long by 5.25 m wide. The tent still in use by Maghreb peoples has maintained its traditional structural conceit, which is much in keeping with what today is known as textile technology (see Fig. 12.3(a)).

The system has often been used throughout history for trade and public performances, from the canopies over outdoor market stands and streets in Mediterranean cities, which are still in use, to the 'Velarium' that covered Rome's

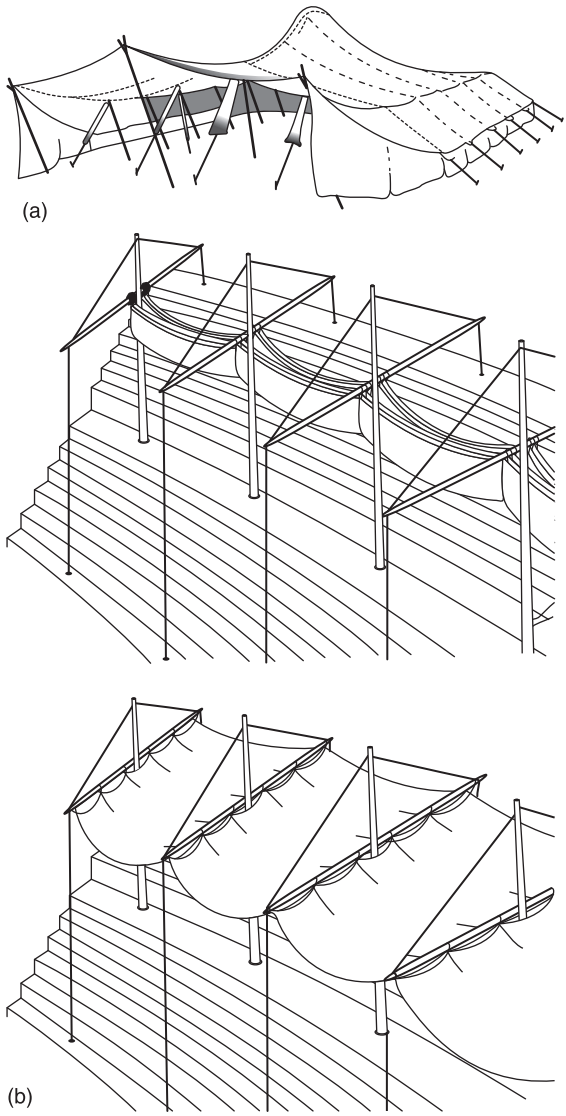

12.3 (a) Jaima; (b) Velarium.

Coliseum (see Fig. 12.3(b)), not to mention the structures roofing grandstands or even the entire area (Atlanta Dome, see Fig. 12.4) of today's sports stadiums or the nineteenth-century 'envelats' used for celebrations on the Catalonian coast. In any event, the use of cloth as an important component to define habitable space is deeply rooted in our history, although it has been primarily associated with temporary enclosures, a characteristic largely applicable to many of its uses today. Nonetheless, thanks to technological progress in textile engineering and the industry as well as in building itself, permanent textile architecture is now possible.

Architecture only accepted these materials and their technology on its turf beginning in the twentieth century, when the appearance of synthetic fibres and their treatment vested cloth with mechanical, physical and chemical properties better suited to permanently spanning large areas. The advent of these tensile membranes in European architecture dates from the 1960s, when they were pioneered primarily by Frei Otto in parallel with the evolution of large-scale cable-net roofing. They appeared in the United States somewhat later (1970) with the erection of the La Verne School 'tent' in California (see Fig. 12.5). All of this was preceded, in a way, by the development of huge airhalls for the U.S. Army, which Walter Bird designed and built from the same type of material. These advances in architecture have come about, however, thanks not only to improvements in textile technology, but also because the traditional use of these materials was kept alive to meet the needs of circuses, local Mediterranean cultural events and military facilities.

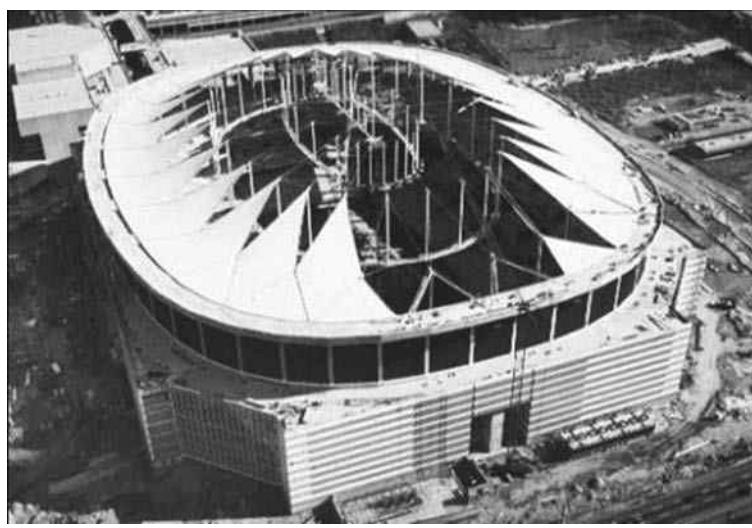

12.4 Atlanta Dome under construction.

12.5 La Verne tent.

12.1.2 Functional analysis

As noted, one of the most important characteristics of this new architecture is the type of indoor environment created, despite the weakness of the material as sole enclosure. Indeed, cloth is not an insulating material *per se*, but it does provide for more effective contact with the surrounding air. The abundance of natural light that penetrates spaces enclosed with textile membranes is one of their most highly esteemed features. While the amount of light depends on the translucency of the fabric used in each case, the market offers ranges from nearly total opacity to 80 to 90% translucency, with mean values on the order of 15%, as discussed below. Assuming the mean value, under a CIE (International Commission on Illumination) partly cloudy sky (2000 lux), the indoor light level would be around 300 lux, whereas under a clear sky (around 5000 lux), indoor illumination would be over 700 lux, which is highly satisfactory even for tasks calling for some precision (see Fig. 12.6).

As far as thermal comfort is concerned, the low insulating power of these structures should not be an obstacle to seeking architectural solutions for a suitable environment. In cold climates, for instance, the 'greenhouse effect' generated by their translucency can be used to control the inflow, and harness both direct and diffuse solar thermal energy by providing for still indoor air. This was done at the Eden Project, Cornwall, England. By contrast, in temperate and warm climates, the 'parasol effect' should be sought, using less translucent fabrics and generating drafts to lower the ambient temperature. By putting this principle into practice,

12.6 El Palenque, at Seville, 1992.

temperatures of 25 °C have been attained naturally in Haj Airport at Jeddah, Saudi Arabia, despite its location in the middle of the desert. In short, the use of textile solutions must go hand-in-hand with a suitable architectural (functional) design to ensure due habitability (comfort) in the resulting spaces. Adopting such an approach, moreover, enhances the possibility of global and permanent, rather than simply ancillary or temporary, textile solutions.

Finally, the functional advantage of this type of enclosure is that it is necessarily prefabricated, leading to more industrialized construction and more effective quality control. Indeed, cloth membranes for surface structures must be made in sufficiently specialized shops using specific industrial facilities for subsequent shipping and on-site assembly. Since achieving the geometry designed is important, the assembly site and the support structure must also be duly prepared to a very small dimensional tolerance. The highly skilled labour consequently required also reduces construction risk.

12.1.3 Form analysis

As noted earlier, one *sine qua non* of these textile solutions is ensuring the permanent tensile stress that is imperative to their stability and integrity. In stretched membranes, tension is maintained thanks to prestressing during erection and the anticlastic curvature of the dome, which provides for force equilibrium at all points of the membrane, for each is subjected to upward and downward tensile stress in all spatial directions. This tensional situation provides for the efficient use of materials, for tensile members (cables and membranes) reach higher

degrees of efficiency per unit of cross-section than compression (arches and vaults) or bending (beams) members. At the same time, it conditions the shape, resulting in a more organic-looking whole. A few words are in order here, then, on the conceptual basis underlying the force equilibrium required to reach structural stability.

Take the mechanics of a cable (see Fig. 12.7), for instance. It takes at least three outward forces to stabilize it on a given plane: two on each end and one in the middle. This actually stabilizes a point on a plane. Stabilizing the point in space calls for a fourth centrifugal force, forming two pairs of vectors on two perpendicular planes pulling away from one another, one upward and the other downward. To stabilize all the points on the cable, further pairs of opposing forces would have to be applied on planes perpendicular to the plane of the cable. The result can be likened to introducing a family of opposing cables perpendicular to the main cable. This ultimately leads to two families of cables crossing in opposite directions which, given the appropriate tensile stress on each end, ensure the force equilibrium of the whole and, with it, the necessary structural stability. The result is an anticlastic surface.

Stabilizing in this way, i.e. applying prestress at the membrane perimeter (which, as shown above, can also be applied at inner points) inevitably generates anticlastic surfaces defining high and low points on the dome. This conditions the final shape. The result is what are described above as organic forms whose curvature radii can be shortened or lengthened to design more or less 'dramatic' envelopes.

Prestressing is generally applied at around 50% of the maximum tension expected when the live loads are in place to reduce membrane deformation when

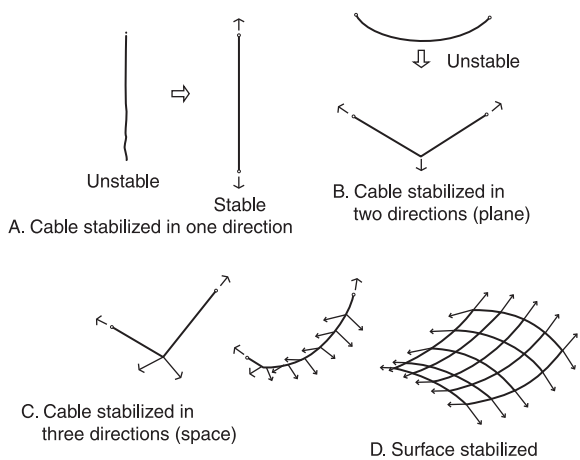

12.7 Mechanics of a cable.

such loads appear. Since fabric is, of course, a deformable material with a low modulus of elasticity, the tensile stress required to reach stability also causes elongation. If, as a result of external action, the tension at a given point drops or disappears, the cloth, which cannot withstand compression, becomes unstable and wrinkles appear due to the pre-deformation. In addition to detracting from the aesthetics of the structure, these wrinkles raise the risk of fabric flutter, which may lead to fatigue, tearing or even collapse.

Moreover, the curvature acquired at each point conditions the stress on that point. Providing tension is tangential, it is proportional to the radius of membrane curvature, and the basic equilibrium condition for these membranes can be expressed as $\sigma_1/R_1 = \sigma_2/R_2$ (see Fig. 12.2). Consequently, the greater the radius of curvature at a given point (the flatter the surface), the greater is the tension. By contrast, with smaller radii of curvature (more curved surfaces), the tension needed to stabilize the membrane is smaller. Briefly then, in more dramatic curves, i.e. with smaller radii, the amount of prestressing needed to obtain equilibrium is smaller, whereas for flatter surfaces, greater prestressing is needed to stabilize the fabric (see Fig. 12.8).

12.2 Typology

Tensile membrane typology[1] is conditioned by the aspects discussed above, i.e. aspects that affect either functionality or stability. Functionally speaking, the design must address questions such as protection for all necessary spaces, arrangements for rainwater drainage, ventilation (or otherwise) and so forth. From the standpoint of stability, in turn, it must make provision for anticlasticity, applied tension, curvature and uniformity, to control tension levels. On these grounds, the possible variations are discussed below, divided into two groups: typology defined (a) by the most widespread anticlastic forms, and (b) by the support structure.

12.2.1 Forms

As noted, in the enclosure surfaces characteristic of membrane architecture, anticlasticity is instrumental to stability and general integrity. An analysis of the

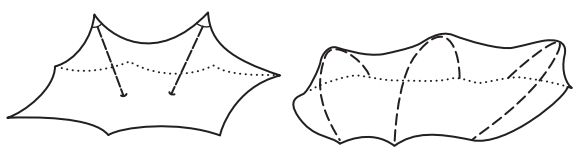

12.8 Different curvatures to stabilize the membrane.

types of geometric surfaces that accommodate such curvature follows. Note that each may be used either separately or in combination with others, to generate simple or compound forms. Surfaces may be generated using two possible methods, *geometric* or *tensional*.

The geometric approach is confined to surfaces with analytical formulas, whereas the tensional approach is compatible with all manner of surfaces, subject only to the condition that the curvature must be anticlastic at all points.

Within the geometric approach, in turn, three groups can be distinguished: *revolution, translation* and *fluted*, i.e. the types of surfaces to which designers were limited until the advent of computer software enabled them to perform equilibrium calculations speedily.

- Surfaces of revolution are obtained by rotating a curve around an axis located in its convex area (see Fig. 12.9). The anticlastic surface results from the fact that the two curves, the one that rotates and the circumference, have opposite concavities. This in turn generates different variations depending on the type of curve (circumference, parabola or hyperbole) and its position with respect to the axis, which may be simplified to be one of two:
  - Curves intersecting with the axis, resulting in *cone*-shaped surfaces with an inflection, whose uses are widespread because their symmetry is simple and they can be readily combined.
  - Curves that remain separate from the axis of rotation, and have an axis of symmetry essentially perpendicular to such axis of rotation. The result is a *saddle*-like surface.
- In surfaces of translation, one curve (*generatrix*) travels along another (*directrix*) with opposite concavity, likewise generating anticlastic surfaces. Both generatrices and directrices are usually circumferences, parabolas or hyperboles and generate saddle-like forms.

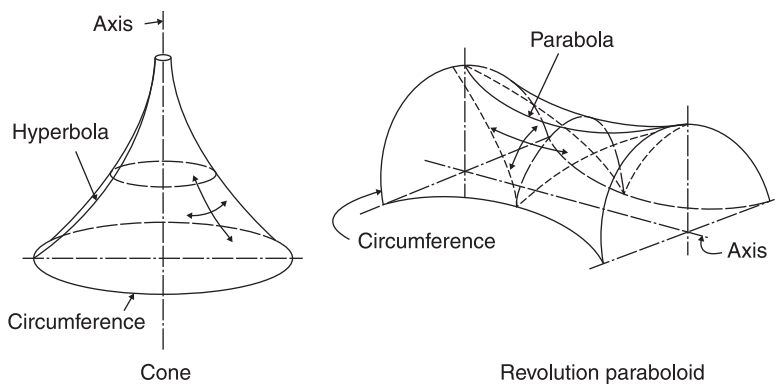

12.9 Surfaces of revolution.

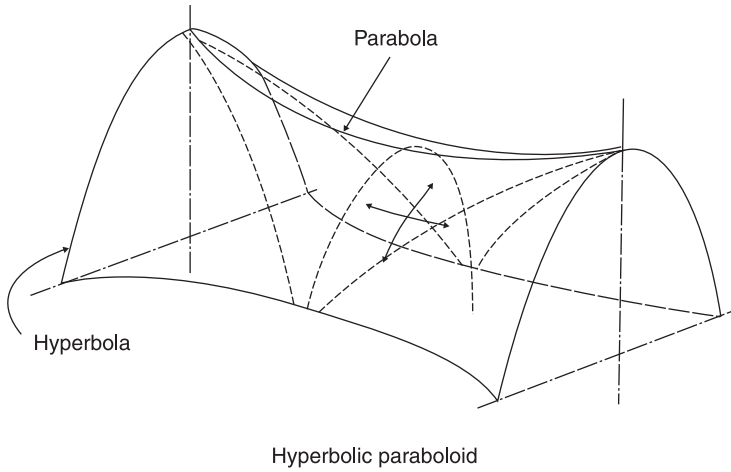

12.10 Fluted surfaces.

- Fluted surfaces, lastly, are ruled and can therefore be generated by the movement and rotation of a straight line that, depending on such movement, yields anticlastic surfaces (see Fig. 12.10). Two are particularly well known and widely used in textile membranes: the *conoid* and the *hyperbolic paraboloid*.
- *Conoids* are obtained by moving a straight line, a generatrix, along two parallel directrices, one straight and the other curved. Depending on the type of movement, the surface obtained is anticlastic.
- *Hyperbolic paraboloids* or *saddles* can be obtained by moving and rotating a straight line between a parabola and a hyperbole, which likewise results in an anticlastic surface.

Both whole and partial surfaces can be used in tensile membranes.

The tensional approach can be used to obtain any anticlastic surface from a very elastic membrane subjected to point or linear deformation at the edge or at any inner point, and which self-balances for each new geometric situation, adopting suitably shaped surfaces. This is in fact the procedure used in preliminary studies with both scale models and specific computer software. Elastic elements such as rubber mats, lycra fabric or soap bubbles are used in physical models. In 'form finding' computer software, a bar mesh is drawn in which the final geometry of the edge and fixed inner points are entered. A force density or dynamic relaxation system is used to attain equilibrium for the forces concurring at each point of the mesh with each new geometry, generating an anticlastic surface whose tensions are as uniform as possible and therefore exhibit a similar curvature at all points. The outcome is surfaces with geometries similar to the surfaces

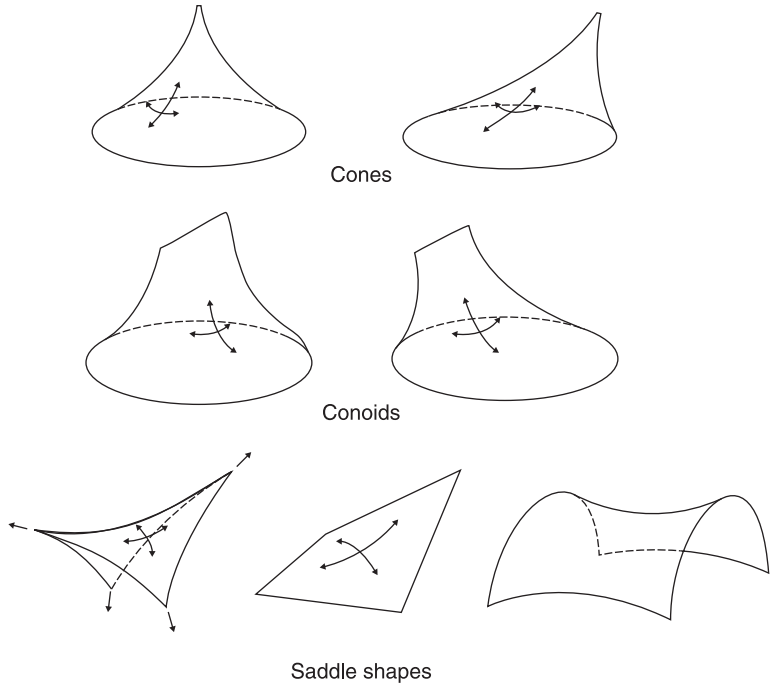

12.11 Tensional surfaces.

described in the preceding item, but better adapted to the specific conditions of the edges and fixed inner points (see Fig. 12.11).

All manner of anticlastic cones and saddles can be obtained with this approach, which can also be used to develop compound forms, since variations can be mixed with relative ease. The following classification lists some but by no means all of the most common solutions for tensile membranes.

Simple forms

- *Anticlastic cones and conoids*, equivalent to elastic surfaces with straight or curved, point or linear deformations (see Fig. 12.12).
- *Hyperbolic paraboloid*s (HP) with perimetric point deformations, equivalent to surfaces deformed at the perimeter with high and low points (see Fig. 12.13).
- HP with straight or curved linear perimetric deformations (see Fig. 12.14).

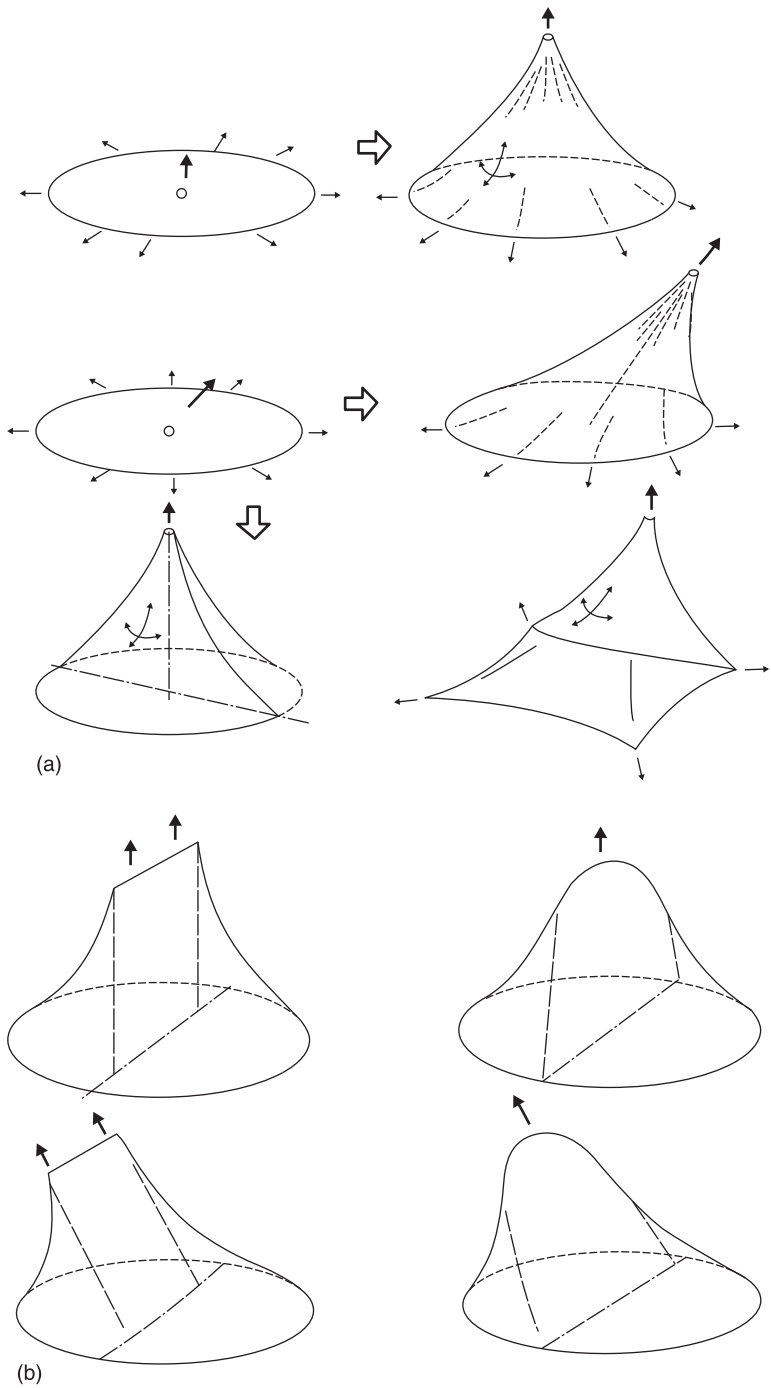

12.12 (a) Tensional cones; (b) Tensional conoids.

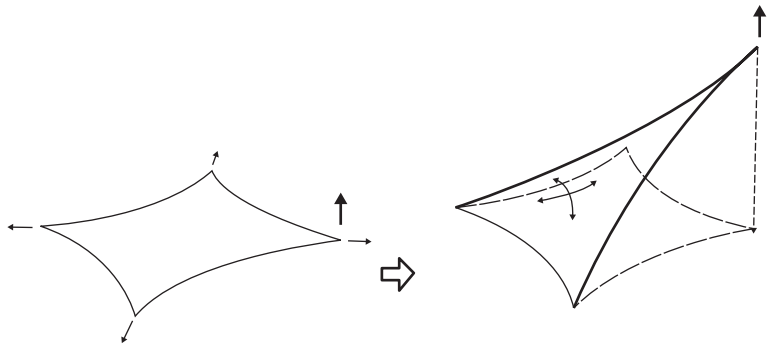

12.13 Tensional paraboloids with border points.

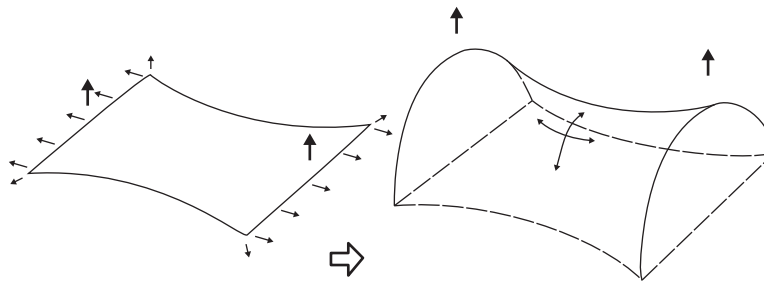

12.14 Tensional paraboloids with soft borders.

Compound forms

Compound forms occur where the joints between presumably simple forms may be either smooth or have a sharp edge:

- *Sum of anticlastic cones*: where there are more than two inverse cones are generally needed in the centre. The overall figure is equivalent to a surface with inner point deformations (see Fig. 12.15).
- *Sum of cones and paraboloids*, equivalent to a surface with inner point deformations combined with point and upward and downward linear deformations at the edge (see Fig. 12.16).
- *Sum of paraboloids*, perhaps the most widespread compound form, with straight or curved linear deformations; one especially popular variation is the so-called *ridge and valley* layout (see Fig. 12.17).

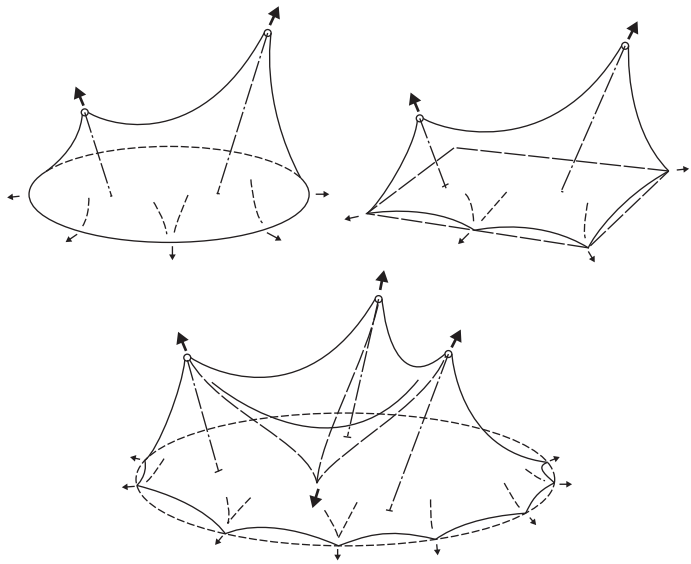

12.15 Combination of cones.

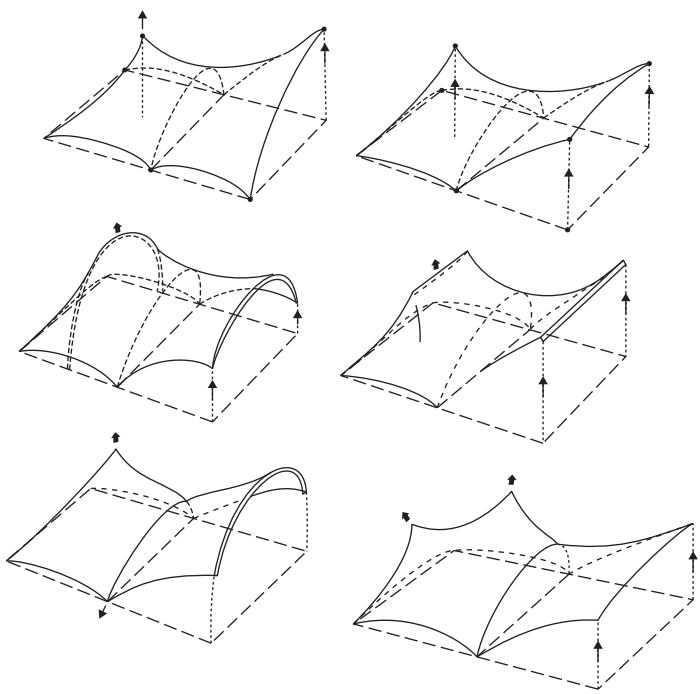

12.16 Sum of cones and paraboloids.

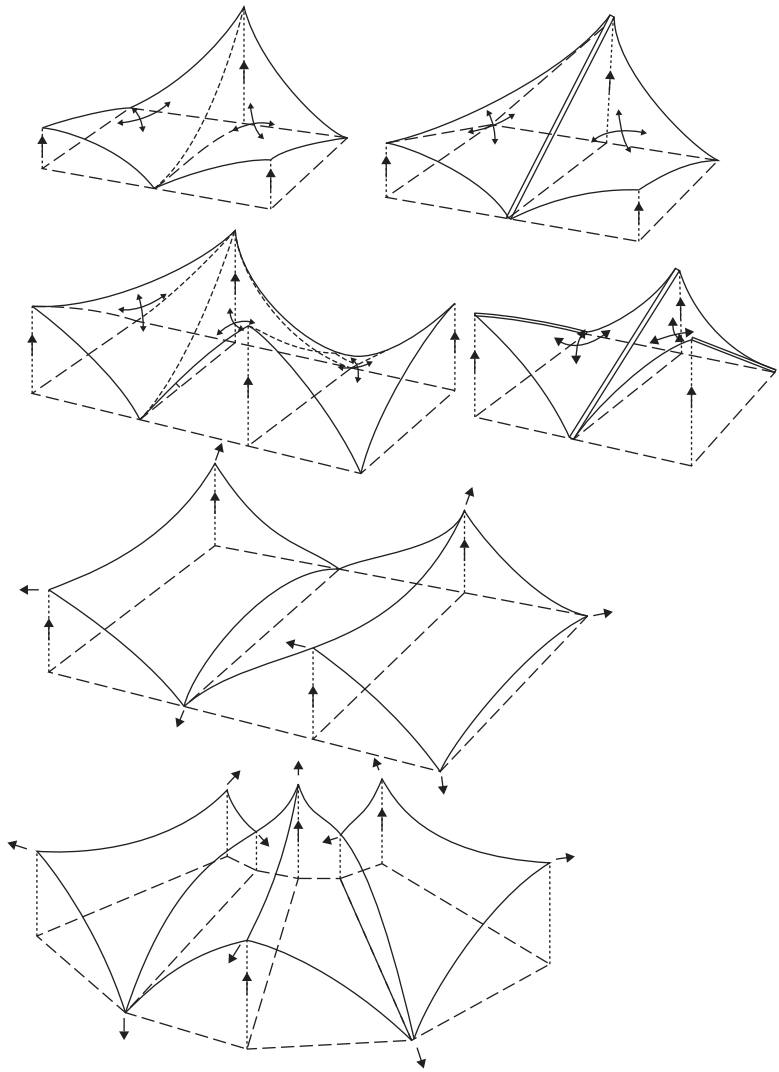

12.17 Sum of paraboloids.

12.2.2 Structure

Membranes, as structures necessarily subjected to tensile stress, must be secured at a series of points which may be either perimetric or central, but where anticlasticity is sought, they may not be in the same plane. Indeed, some of these points must be at a higher elevation than others (high and low points) to be able to readily apply pretension and attain anticlastic curvature. This condition likewise introduces a series of alternatives that can be grouped under two headings:

- *Internal structure* on which the cloth rests, in which case the structural members are in plain sight inside the enclosure, while the textile solution is more significant and dramatic from the outside. This may, however, forfeit the indoor aesthetics of textile solutions if the safety factors are not calculated accurately or are inordinately overdimensioned (see Fig. 12.18).
- *External structure*, from which the cloth suspends, providing for less-cluttered interiors but a less striking textile solution from the outside, where the supporting structure may come to prevail over the fabric (see Fig. 12.19).

Moreover, several formal and functional types of structural members may be used, which also condition overall appearance: *masts, portal frames, arches, tripods* and *buildings*. Combining the two preceding classification criteria yields the typology discussed below.

Where internal supports are used, the perimetric anchorage solution may differ in each case, involving either point anchors (attached directly to the ground, to perimetric masts used as struts, or to fixed points) or (straight or curved) linear attachments to maintain the anticlastic surface:

- *Internal masts* resting on the ground that yield very striking simple or combined cone-like shapes; this is one of the most widely used solutions, particularly for medium-span membranes (see Fig. 12.20).
- *Flying masts*, in what is known as the 'tensegrity' structural solution, with one or two struts usually arranged in circles or ellipses, and the entire assembly

12.18 Tennis court with internal structure.

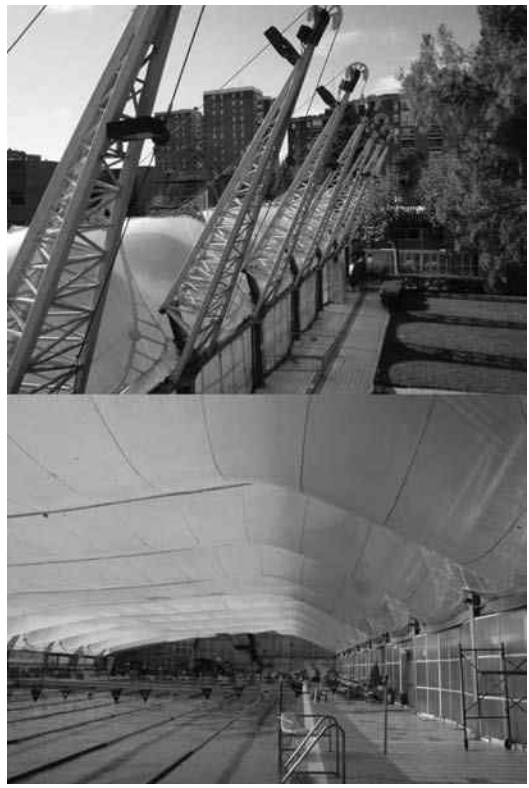

12.19 Swimming pool with external structure.

12.20 Internal masts.

anchored to a perimetric compression ring; this layout, comprising a series of successive cones resting on struts, is used to span large areas such as sports stadiums, bullrings and so on (see Fig. 12.21).

- *Internal portal frames* that generate intermediate (horizontal or double-pitched) support lines must be used in combination with some other type of attachment in another (inner or perimetric) plane to obtain anticlasticity at all points. This solution is used primarily for temporary rental tarps in which less importance is attached to structural stability (see Fig. 12.22).

12.21 Floating masts in the Zaragoza Arena.

12.22 Internal portal frames.

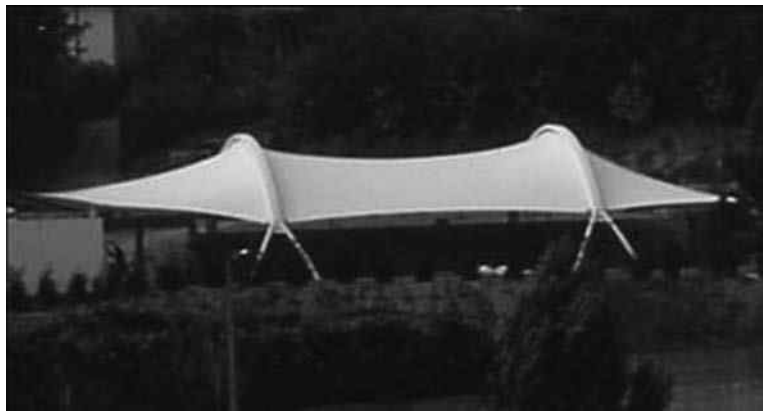

12.23 Internal arches.

- *Internal arches*, which define a generally curved, less angular shape. They provide for open-plan interiors with long spans. They may be arranged in parallel or crisscrossed to obviate the need for stretching cables because the arches themselves generate stable structures. These same arches may be positioned at the perimeter to together directly generate 'saddle'-type anticlastic surfaces. These are the types most commonly used to cover medium-scale sport facilities (tennis courts, swimming pools and similar (see Fig. 12.23)).

External supports usually also include a solution for perimetric anchorage:

- *External masts*, which come in several varieties:
  - masts that hold the edge of the membrane taut only at *alternating points*, while the intermediate points are anchored directly to the ground, generating simple or combined hyperbolic paraboloids, a frequent solution for short-span structures (see Fig. 12.24).
  - masts that hold the membrane taut with *alternating up and down cables*, forming the popular ridge and valley layout, which is widely used even in large spans (see Fig. 12.25).
  - masts that also hold *indoor points* of the membrane taut, generating successive small cones, also used to span large, spacious areas (see Fig. 12.26).
- *External portal frames* from which the membrane is suspended, normally at certain points, to generate a combination of cones. Since portal frames are bending members, the spans involved are not usually very large.
- *External arches*, which, like internal arches, are generally stable in themselves and from which the fabric is suspended either at specific points or linearly

12.24 Border mast.

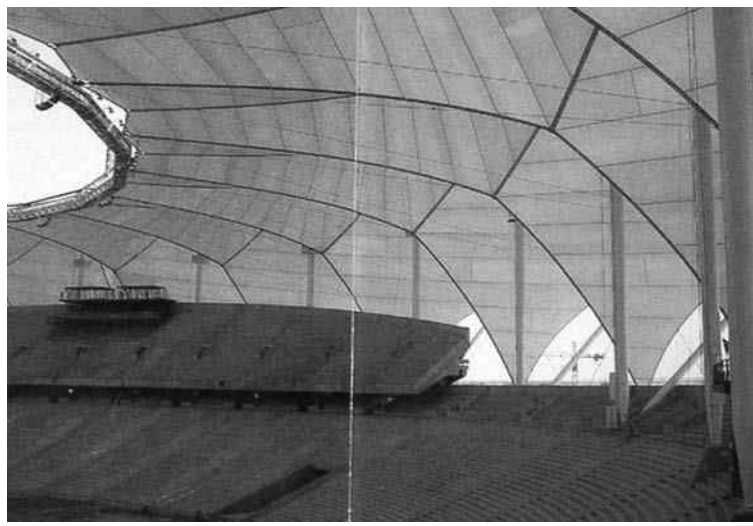

12.25 Suspending cables, up and down, to support the membrane.

along the arches. Here also, they may be arranged in parallel or crisscrossed; in either case, surface anticlasticity is practically ensured. They are seldom used, however, for they entail no material advantage over internal arches (see Fig. 12.27).

12.26 External masts to hang the fabric directly.

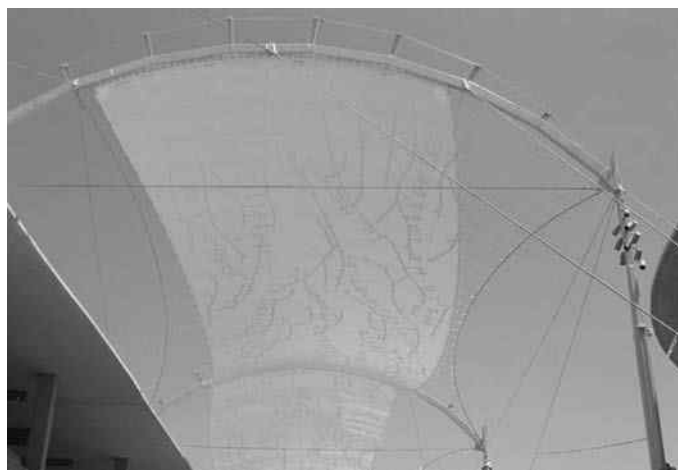

12.27 External arches to suspend the fabric.

- *External tripods*, which provide for high fixed points, obviating the need for stretching cables. The same variations as specified for masts can be used for tripods (see Fig. 12.28).
- *Buildings* to which the membrane edges are anchored. They are frequently used in small- and medium-span membranes. Two alternatives can be distinguished:
  - *point anchors*, which behave like external masts or tripods, with the same variations.
  - *linear anchorages*, consisting of shapes attached to buildings, which must be strong and are usually curved to ensure surface anticlasticity (see Fig. 12.29).

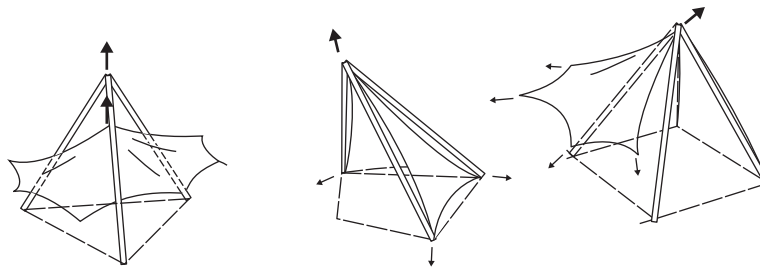

12.28 External tripods.

12.29 External linear anchorage.

12.3 Support systems

To hold the membrane in place, it must be attached to a series of members that can transfer the forces generated to the ground or to a stiff structure. The two types of such members are *external*, i.e. the support structure, and *reinforcements*, which are built into the cloth itself.[1,2]

12.3.1 Structural elements

Structural elements are needed to receive the tension loads exerted on the cloth either by stabilization prestressing or external actions, such as wind or snow. The type used depends on the loads and the position of the element, bearing in mind

that it may serve as a high or a low point in the membrane. *Masts, portal frames, arches* and *fixed structures* are the types discussed hereunder.

Masts, perhaps the most representative structural members in this type of architecture, can be positioned on the inside or around the perimeter of the membrane. Different types can be distinguished, depending on their *connection to the ground* (see Fig. 12.30):

- *Restrained*, which must withstand bending at the base and therefore call for sufficient mechanical inertia.
- *Hinged*, which receive compression loads only, whose joint may consist of a hinge that moves freely in a single plane, or of a ball and socket able to move in all directions, providing for better constructional operation.
- *Flying*, which are raised by tensed cables at the bottom and tied at the top by another family of cables or the fabric itself. They behave like struts in a tensegrity-type structure, and therefore are also subjected to compression.

Portal frames or arches, from which the cloth is often suspended, may be positioned inside or on the edge of the membrane. Arches provide for longer spans and generate safer anticlastic surfaces, in addition to constituting stable structures themselves. As separate elements, they can also be restrained or hinged at the base, which affects the type of forces absorbed. The lintel in linear portal frames is subjected to bending stress, and the legs subjected to compression or bending stress, whereas arches essentially withstand compression, although restrained arches also absorb bending stress (see Fig. 12.31).

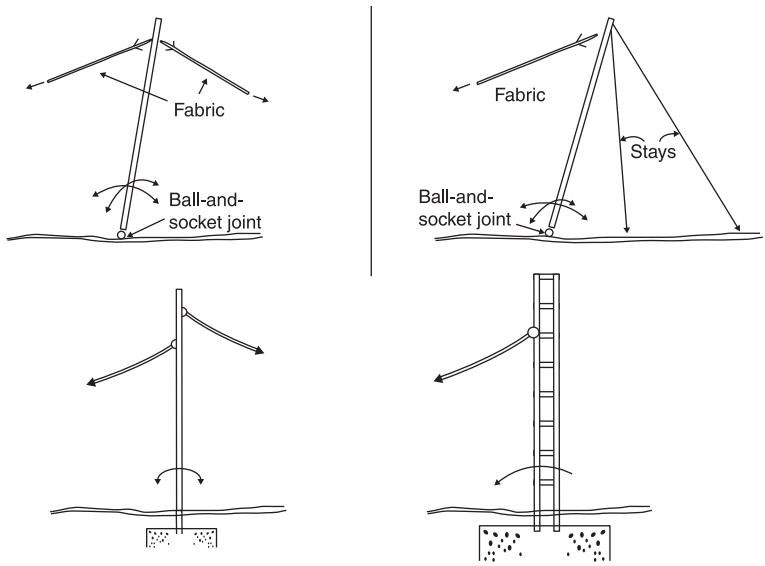

12.30 Masts: internal and external, hinged or restrained.

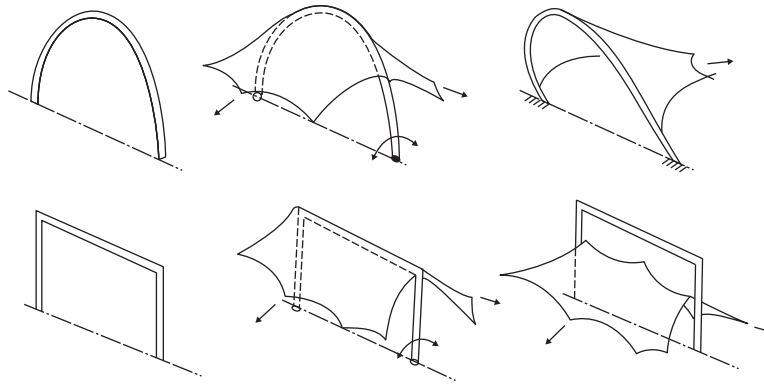

12.31 Arches and portal frames: internal and external, hinged or restrained.

Fixed structures are understood to mean any point in space able to withstand the tensile stress transferred to it by a textile membrane. The following are the most common types:

- Specific *tripods* to anchor high points (see Fig. 12.28).
- *Buildings* with anchorage attached to strong points, in turn connected to their bearing structure. This is generally the solution used for supplementary roofing.
- A *foundation member* designed to withstand tensile forces either as a counterweight or by friction with the ground (piles) (see Fig. 12.32).

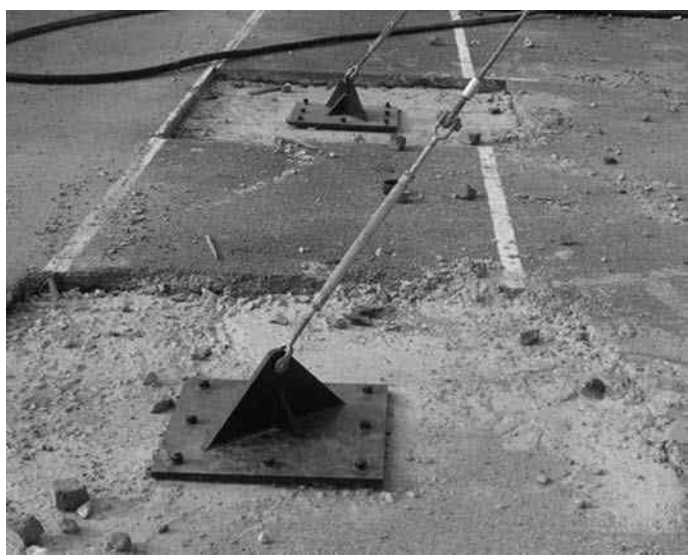

12.32 Anchorage to foundation.

12.3.2 Detailing and connections

These are the reinforcements that must be built into the fabric itself, normally around the perimeter, to attach the membrane to the support structure and transfer forces in a way that ensures the integrity of the cloth. The two major types are *linear* and *point* reinforcements, the former for the edges, where they may be likened to the 'leech ropes' on a sail, and the latter for the corners, similar to 'earrings', to resort to the same simile.

The forces generated when the membrane is prestressed or exposed to external actions are distributed across the cloth in all directions, although the vectors along the web of the fabric prevail. When these forces reach the edge, however, they are redirected, with a concomitant increase in stress levels, which calls for linear reinforcement. Moreover, membrane edges may be *flexible*, i.e. unattached, or *rigid* when joined to a fixed linear element. In both cases, reinforcement must be provided either to resist accumulated stress in flexible edges or to secure the membrane attachment in rigid edges. The options for such reinforcements are discussed below.

For flexible edges:

- A *fold* in the cloth itself (a *hem*) is the simplest form of reinforcement, where two or more layers of fabric are overlain, increasing tensile strength in the respective direction.
- For flexible edges with medium or long lengths, a *cable* with the cross-section needed for the design longitudinal stress may be run along the edge. This cable is instrumental in transferring the prestress from the support structure and edge of the membrane to the rest of the fabric: the larger the radius of curvature (the straighter the edge), the greater is the tension at the edge and the tension transferred to the cloth. Such cables may be positioned inside or outside the hem (see Fig. 12.33).
  - The *internal* position is most widely used for small and medium-span membranes, with cable diameters of up to 40 or 50 mm. This arrangement protects the cable from the elements, although since stress is transferred to the cloth by friction, care must be taken at the ends where the cable protrudes.
  - Cables must be positioned *externally* when the diameter of the cable is over 50 mm, as in large-scale membranes. In such cases, to be able to transfer loads, the cable is attached to the cloth by means of point anchors consisting either of lacing (for small-span membranes) or of separate rings or clasps, which can be used in any size membrane, but are imperative when large spans are involved. When external anchors are used, the eyelets in the fabric must be reinforced.
- A *polyester cord*, used in much the same way as cables for small and medium-span (especially folded) membranes and positioned inside the perimetric hem.

For rigid edges (see Fig. 12.34(a), (b), (c)):

- A *solid bar* or hollow tube positioned as if it were a flexible leech rope inside or outside the hem, which transfers perpendicular stress only to the cloth. The connecting systems and conditions between bar and membrane are the same as for flexible edges (a).
- A *PVC cord* positioned inside the hem, which prevents the edge from pulling out of the longitudinal track on an aluminium shape, while allowing it to move freely along the track ('keder'-type solution) (b).
- A *flatbar* to clamp and reinforce the edge. These elements, generally made of steel or aluminium, are designed for joints subjected to heavy or minor stress, or as internal reinforcements (c). Two variations can be distinguished:
  - *single* for clamping the cloth against a straight or curved stiff longitudinal shape;
  - *double*, when acting merely as reinforcement.

Some mention must also be made of intermediate cables or reinforcements used at membrane inflections, such as adjacent cones or ridge and valley arrangements. They may be placed above or below the fabric and call for an attachment pocket or other reinforcement in the cloth. They may also be *flexible* or *rigid*. The former, consisting of cables or reinforcement belts generally made from 'Trevira' fabric, are used in small- and medium-span membranes. The latter are portal frames or arches, discussed above in the section on support structure typology (see Fig. 12.35).

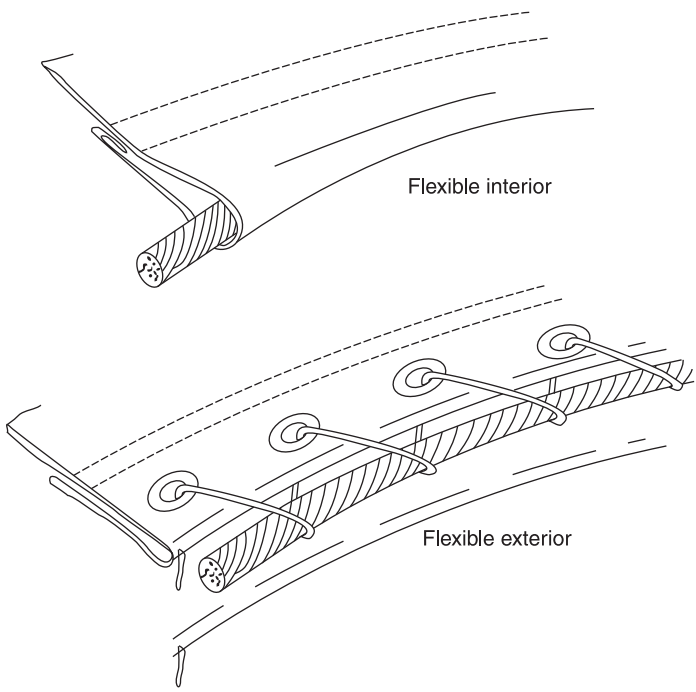

12.33 Cable in the edge.

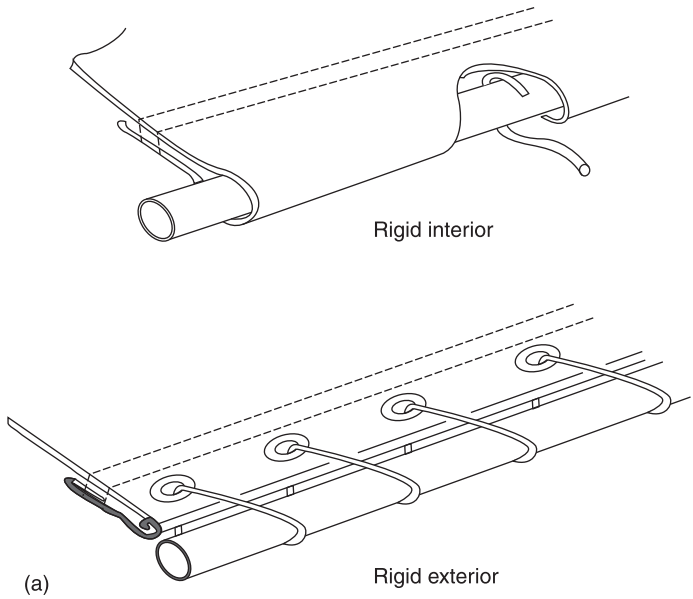


(b)

12.34 (a) rigid bar in the edge; (b) 'Keder'; (c) clamping system.

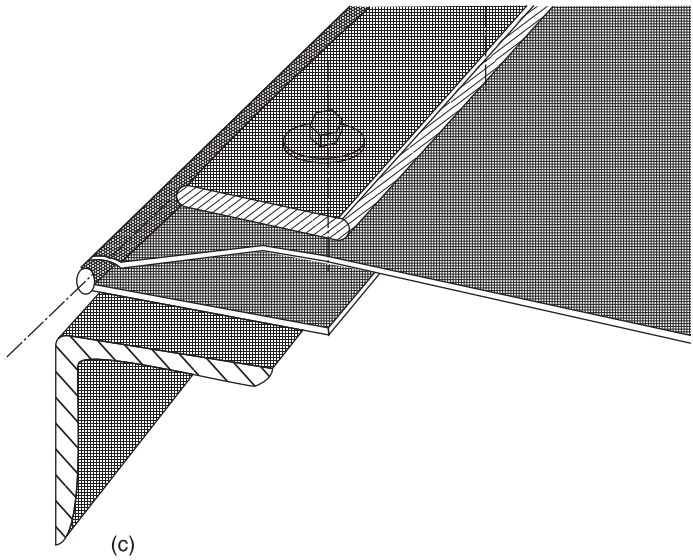

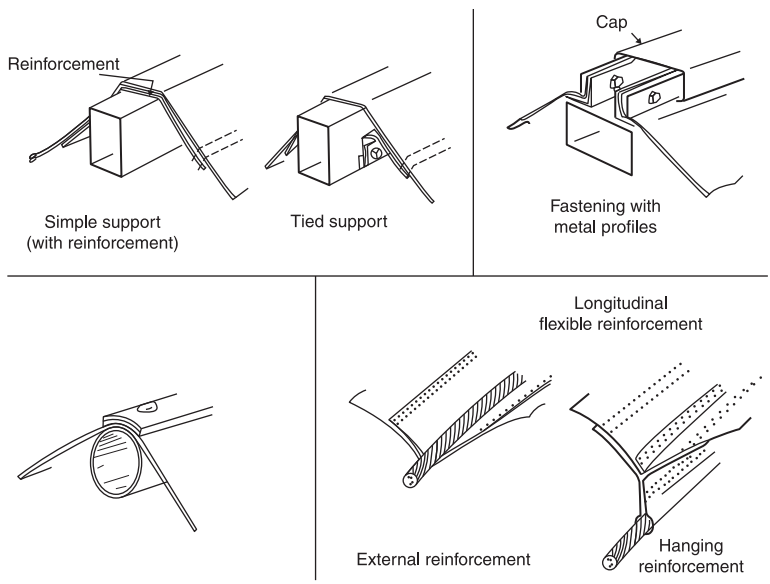

12.35 Internal linear reinforcements.

Point reinforcements, in turn, are indispensable, for forces are highly concentrated at the corners and vertices where the cloth is anchored, i.e. the points where stabilization prestress is applied and where membrane tension is regulated. These reinforcements may adopt different shapes, both for *internal* and *external* solutions. All of this must be supplemented with the anchorage and regulation systems *per se*.

Internal anchorages are needed for conical surfaces. Membrane prestress is applied across them by suspension. Two types can be defined, depending on the tensional intensity and the inflection angle of the cloth:

- For *small inflections*, the device is similar to a spherical cap from which the membrane can be pushed upward or downward to maintain cloth continuity. The radius of rotation depends on the size of the membrane and the tensions converging on the point in question, although the cloth must be reinforced in any event. Another solution is to pull on a previously installed linear belt reinforcement that runs across the suspension point (see Fig. 12.36(a), (b)).

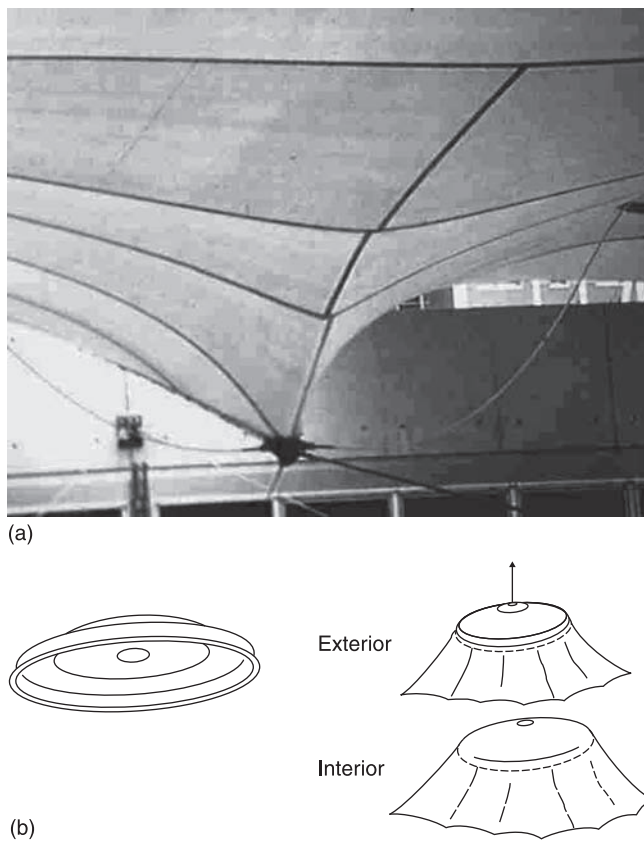

12.36 (a) Internal soft point with linear reinforcement; (b) Internal soft point with spherical reinforcement.

- *Large inflections* call for leech rope-type linear reinforcements in the cone formed. Either flexible or rigid reinforcements may be used.
- *Flexible* types consist of loops forming a 'rosette' with which the membrane can be uniformly stretched (see Fig. 12.37).
- The *rigid* types are usually hollow steel rings of a size in keeping with the size of the membrane and with the necessary clamping braces to secure the cloth. The solution for small membranes may consist of a steel cone at whose base the cloth is clamped and whose vertex is the suspension point (see Fig. 12.38).

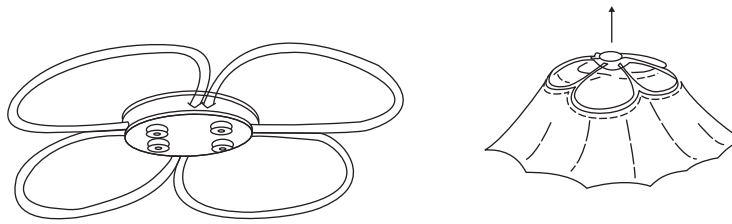

12.37 Internal sharp point with loops.

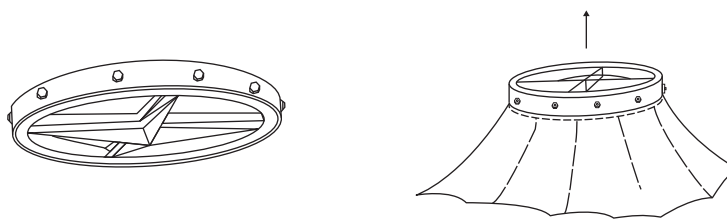

(a)

(b)

12.38 (a) Internal sharp point with rigid junction; (b) Internal sharp point with steel cone.

External or perimetric anchors (earrings) are needed in all flexible edge solutions to apply and regulate cloth tension. Two types can be defined, depending on the tensional intensity and the need to regulate the tension on the leech ropes:

- *Single earrings*, in which the tension on the leech ropes cannot be regulated separately. They are used in small membranes where the rope generally runs from side to side. They consist of cloth reinforcements on both sides to absorb the accumulated tension and they anchor the fabric to the support structure. The reinforcement may range from very simple systems, such as belts made of the cloth itself, to rigid arrangements consisting of steel flatbars bolted together to secure the fabric. In any event, the cloth must be secured at the anchor itself to prevent it from slipping away from the earring, with the concomitant risk of tearing. This is an error often committed, however, leading to radial wrinkles or ripping around the earring (see Fig. 12.39).
- *Compound earrings*, in which the tension on the leech ropes and the cloth can be controlled separately. Under standard design and implementation, they consist of steel devices to which the leech rope cables converging on the earring (including any intermediate reinforcements, as appropriate) are attached, with some manner of separate regulation for each, which may be an axial tie-rod or threaded bolt and nut. The cloth must also be secured to this device to prevent unexpected movement. Lastly, the device must be anchored to an external cable that joins it to the support structure, which must also be fitted with a tension regulating system for applying and regulating the tension on the membrane as a whole (see Fig. 12.40).

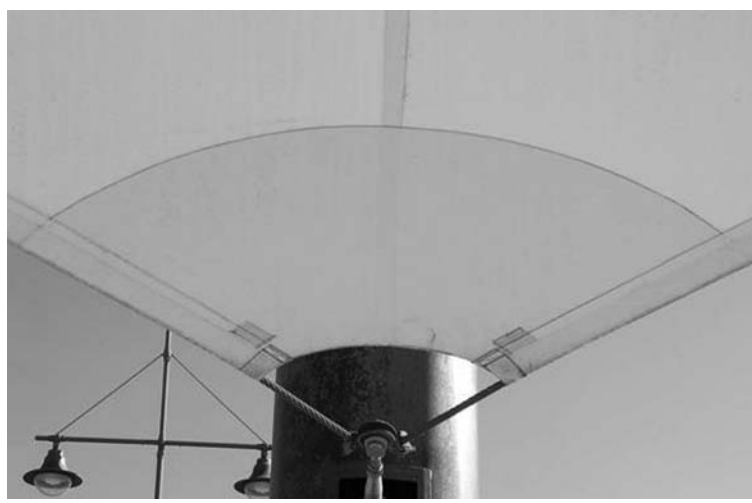

12.39 Simple corner.

12.40 Compound corner.

12.4 Textile materials

12.4.1 Coated fabrics vs. foils

Very few textile materials[2] are suitable for this type of architecture, and each has a specific use. They can be divided into two groups, coated fabrics and foils. The former are layered, while foils are made from a single sheet of the same material. Consequently, their intrinsic characteristics are radically different and that in turn strictly delimits their scope of application.

Since coated fabrics are composite materials, each layer fulfils a specific function:

- the cloth or fabric essentially provides mechanical strength;
- the coating vests the fabric with stability and cohesion, weatherproofing, protection against UV and abrasion, and fireproofing;
- the finish constitutes a seal against dirt and other agents and enhances durability.

These features make coated fabrics suitable for any type of textile construction. The use of foils, however, is more restricted, for they owe all their characteristics to the nature and thickness of the constituent material, which translates into lower mechanical strength values.

For this reason, as a rule, foils are used in indoor enclosures, for small stretched membranes or as cushions in airhalls, which may be somewhat larger. Even in this latter case, however, the maximum cushion size should not exceed certain limits, otherwise the foil may need to be reinforced with cable mesh. This, moreover, reduces the general radius of curvature and therefore the prestressing is required. (see Fig. 12.41).

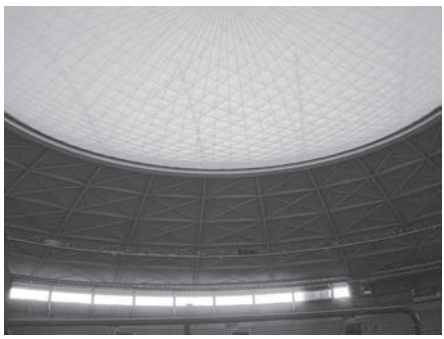

(a)

(b)

(c)

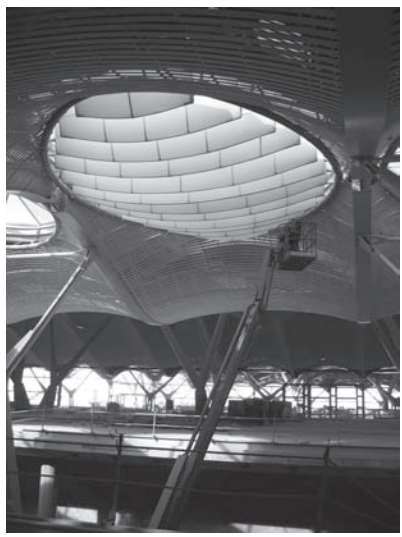

(d)

12.41 (a) ETFE foil pneumatic structure reinforced with cable net (Palacio de Vistalegre, Madrid. Schlaich); (b) PESPVC tensile surface structure (CC Almenara, Lorca. Javier Tejera, BAT, Spain); (c) PTFE tensile structure (Authorities Pavilion of Barajas Airport, Madrid. Lamela and Rogers); (d) Silicon/glass tensile light diffusers (Barajas Airport. Madrid. Lamela and Rogers).

The materials most commonly used at this time in coated fabrics include:

- polyester with a polyvinyl chloride (PVC) coating, the most widely used for the optimal cost–durability ratio.
- fibreglass with polytetrafluoroethylene (PTFE) coating.
- fibreglass with silicone coating
- others, such as PTFE fabric with PTFE coating or aramid fibre-based fabrics, which are less frequently used.

The most common foils, in turn, are:

- ETFE (ethylene tetrafluoroethylene) used, as noted above, primarily as cushions in airhalls.
- bulk PVC, highly elastic and readily installed when heated, for use exclusively in interiors (suspended, stretched ceilings and partitioning).

12.4.2. Woven fabrics

Coated fabrics, as noted, comprise a series of layers, each of which affords the composite material certain characteristics to enable it to respond more efficiently to the strength and durability demands increasingly required of this type of structure.

The cloth provides mechanical characteristics (stiffness, tensile strength, tear resistance) that enable the membrane to withstand prestressing plus external loads within a given range of safety factors.

The cloth comprises strands or twisted strands of yarn spun by extruding a molten prime material (polyester, glass or similar) and subsequently woven on looms.

This yarn is woven into the polyester and fibreglass cloth with which the most common type of coated fabrics are made, i.e. PVC- and PTFE-coated materials, respectively.

The characteristics of the yarn used to make the fabric (number of strands, diameter, density, number of spins per metre when the yarn is twisted to make stronger strands and treatment to improve the finish) crucially determine the mechanical properties of the woven cloth, and therefore of the coated fabric of which it forms a part.

Yarn properties are summarized in Table 12.1.

The strand or strands of yarn are woven on a loom in two perpendicular directions (lengthwise known as the warp, and crosswise as the weft). One of two types of weave may be used: plain, in which one weft yarn or group of yarns is interlaced alternately under and over the warp yarns one by one, or a 2×2 basket (or 'Panama') weave, in which two weft yarns are interlaced across the warp, two yarns at a time. The latter arrangement entails less crimp on the yarn and therefore less elongation (see Fig. 12.42).

Table 12.1 General properties of yarn

	High tenacity polyester	Fibreglass	High modulus aramid	LCP (liquid crystal polymer)
Density (g/cm^3)	1.38	2.6	1.45	1.40
Tensile strength (GPa)	0.97–1.17	2.4	3.32	3.28
(N/tex)	0.70–0.85	0.92	2.35	2.4
Elongation at failure (%)	11–15	4.5	1.5	2.5
Modulus of elasticity (GPa)	12–15	73	160	104
(N/tex)	9–11	28	109	74
Water uptake (%)	0.4	<0.1	1.2–3	<0.1

Source: adapted from Foster and Mollaert, 2004

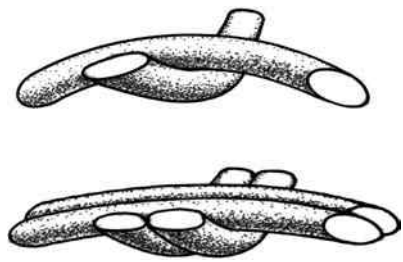

12.42 Woven material 1x1 and 2x2 (from Foster and Mollaert, 2004).

To enhance this effect and provide the fabric with more uniform stiffness and hence greater stability, certain coated fabrics are made from cloth that is prestressed in both directions prior to coating. This means that the yarns are loaded sooner than if they have first to flatten and deform. (see Fig. 12.43)

Before applying the resin coating, the fabric is treated with a finish that improves the compatibility between cloth and coating (impregnating the yarn for better bonding) and vests the inner membrane with additional desirable characteristics. Scant or nil capillary diffusion of moisture in the polyester, for instance, prevents inner membrane pollution due to the ingress of polluting agents contained in the moisture absorbed around the edges, where the fabric may be imperfectly welded to the outer layers. This effect may be visible from within where, due to the translucency of the membrane, stains can be seen around the seams.

Consequently, despite the finish described, fabric edges should always be 'sealed' by electrode (or whatever other type of welding system is used).

In fibreglass fabric, the finish aims to improve the bond to the PTFE coating, which is ideal precisely because of its anti-adhesive, slippery and dirt-repellent properties.

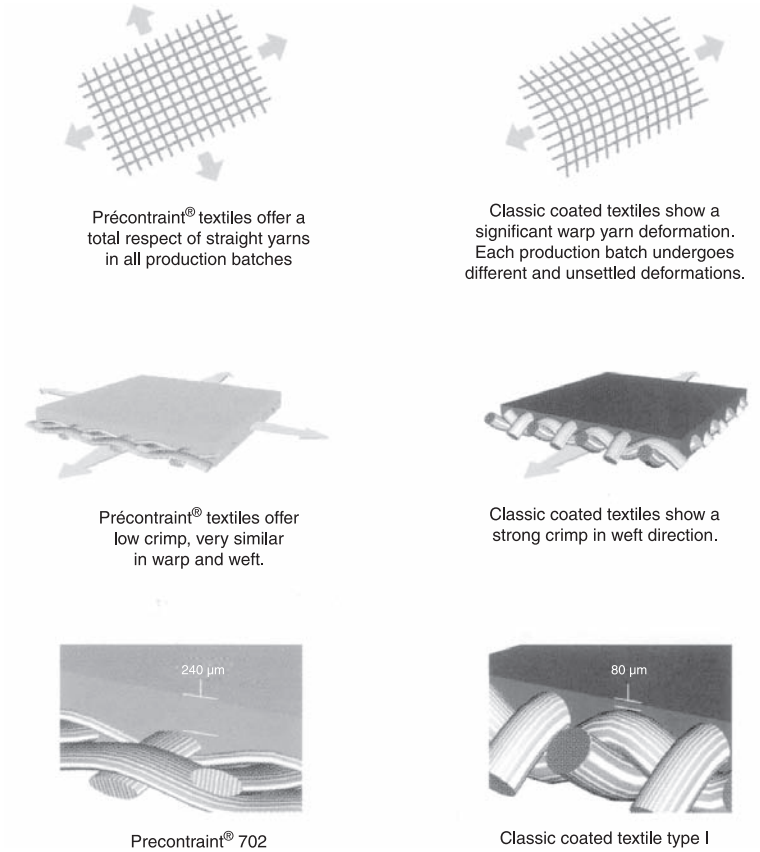

12.43 Pre-stress process for coated materials (Ferrari description).

12.4.3 Coating and finishes

Coated fabric has an outer layer consisting of a sticky resin whose components fulfil its various functions and a finishing film that acts as an additional protective barrier (see Fig. 12.44).

More specifically, the most relevant of the functions assigned to the coating supplement are the mechanical properties of the fabric, which in itself is neither stable nor able to withstand diagonal tension, due to its low cohesion in respect of such actions.

In addition, the coating provides protection against ultraviolet rays – because carbon-based yarn such as polyester and aramid deteriorate rapidly when exposed to such light. Other coating functions include mechanical (particularly anti-abrasive) protection, water-proofing for the porous fabric, flame-retardants to enhance membrane fire performance, fungus protection and colourfastness.

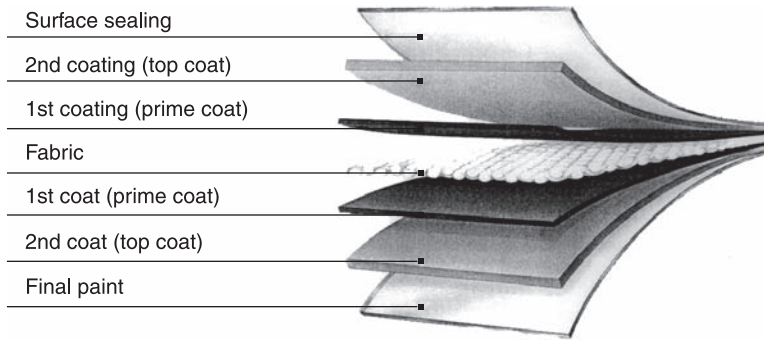

12.44 Multi-layered composition for woven and coated materials (from Foster and Mollaert, 2004).

The most widely used coatings and the respective finishes are as follows:

- PVC. A paste with a PVC emulsion or suspension base is used, mixed with plasticizers for subsequent treatment to convert the stiff base material (PVC pellets) into a thin elastic film.
- The plasticizer also accounts (in phosphate-based compounds, for instance) for some of the fireproofing properties, together with other retardants and the composition of the PVC itself, because the chloride released by fire extinguishes the flame. Plasticizer quality and manufacturer formulation hold the key to strong and durable membranes, for the proper choice prevents migration and the concomitant exposure to bacterial or fungal attack.
- Given the characteristics of the base coating material (PVC or PTFE), in fabric coated with PTFE (as discussed below) the 'brand' chosen is less important than in the case of PVC, where the information included in the manufacturer's specification sheets is of utmost importance.
- The finish on PVC-coated fabric is usually an acrylic substance mixed with PVDF (polyvinylidene fluoride), pure PVDF or PVF (polyvinyl fluoride). This finish protects the coating from polluting agents, rendering the membrane more slippery and curbing possible plasticizer migration (see Fig. 12.45).
- PTFE is used primarily as a coating on fibreglass fabrics. Its molecular structure (fluoride atoms wrapped around a helix chain nucleus that houses the carbon atoms) ensures very effective chemical protection. The membrane conservation afforded by its high resistance to polluting gases and low surface energy (and consequently high anti-adherence) has led to its growing use.

  The other characteristics in which it out-performs PVC are likewise intrinsic to the material, and therefore call for no additives (usability in a wider range of ambient temperatures, UVA and IR resistance, anti-ageing, water-repellence, insolubility in solvents and so forth).

  The finish used with PTFE is FEP (fluoroethylene propylene copolymer), which makes the whole easier to weld and more moisture- and fungus-proof.

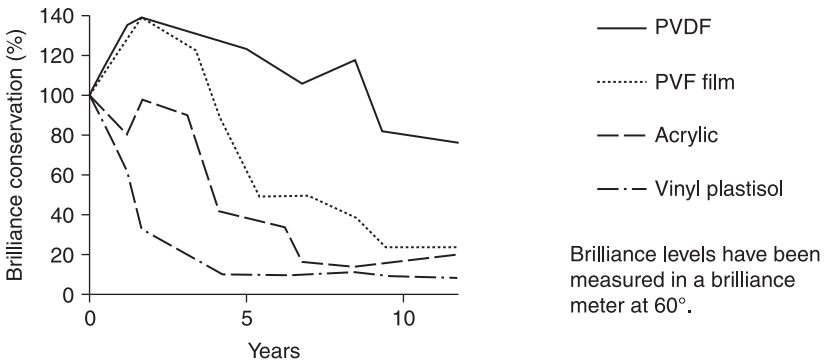

12.45 Comparison between different final coating along time (FERRARI).

- Silicone. The primary advantage to fabrics (usually fibreglass) coated with silicone is their much greater translucency than PVC- or PTFE-coated textiles. The drawbacks, however, are readier soiling (despite the improvements in the finishes of them all), which calls for more intensive maintenance, and more complex welding.

Finally, the titanium dioxide (TiO_2) finishes that have recently come to market can be applied to both PVC- and PTFE-coated fabric. The active oxygen generated in a photocatalytic reaction mediated by this compound, and its hydrophilic surface, protects the membrane from soiling while decomposing pollutant gas and purifying the air (NO_x removal is estimated in 2.6 vehicles emission per 1000 m^2) (see Fig. 12.46).

12.4.4 Characteristics and properties

Coated fabric manufacturers' advertising literature usually includes product specification sheets that contain information indispensable for material selection by textile architects:

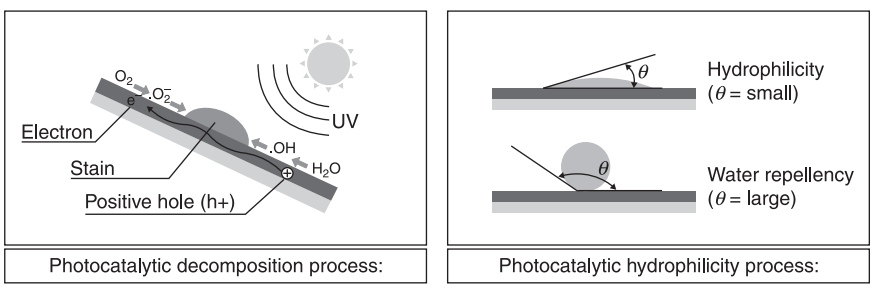

12.46 TiO_2 effect on coating (TAIYO).

- information on the yarn used: material, weight, weave, number of strands;
- characteristics of the protective and outer layers: material, weight, total thickness and coating thickness;
- characteristics of the fabric protected: weight, thickness, colour, width;
- fire performance and translucency;
- mechanical information on the fabric protected: weft and warp tensile strength, tear resistance, bonding to coating, and biaxial stress–strain curves (i.e. warp–weft relationship).

The number of coated fabric manufacturers is so large that both a French design guide and the Messe Frankfurt Working Group have established classification systems for PVC- and PTFE- coated materials, as shown in Table 12.2.

Table 12.3 shows the seven types of PTFE-coated fibreglass fabrics.

Lastly, ETFE foils can also be classified (see Table 12.4) but, as noted earlier, any variations in its characteristics depend on thickness only (for its behaviour is isotropic, since only one material is involved).

Mechanical behaviour (tensile strength, tear strength, bonding, biaxial tests)

The low deformation stiffness of coated fabrics, compared to the very high stiffness in the direction of the yarn, make them ideal for building tensostatic membranes with geometrically complex curves. In other words, a flat material,

Table 12.2 Coated fabric classification: PVC-coated polyester fabric

Type	1	2	3	4	5
Surface weight (g/m^2)					
French design guide	720	1000	1200	1400	2000
Messe Frankfurt WG	800	900	1050	1300	1450
Yarn linear density (dtex)					
French design guide					
Messe Frankfurt WG	1100	1100	1670	1670	2200
Weft/warp tensile strength (kN/m)					
French design guide	60/60	84/80	110/104	120/130	160/170
Messe Frankfurt WG	60/60	88/79	115/102	149/128	196/166
Weft/warp trapezoid tearing (N)					
French design guide					
Messe Frankfurt WG	310/350	520/580	800</950	1100/1400	1600/800
Number of yarns per cm in weft/warp					
French design guide					
Messe Frankfurt WG	9/9	12/12	10.5/10.5	14/14	14/14

Table 12.3 Coated fabric classification: PTFE-coated fibreglass

Type	G1	G2	G3	G4	G5	G6	G7
Weft/warp tensile strength (kN/m)	26/22	43/28	70/70	90/72	124/100	140/120	170/158
Yarn diameter (microns)	9	6	3	6	3	3 or 6	3
Surface weight (g/m^2)	500	420	800	1000	1200	1500	1600
Weft/warp trapezoid tearing (N)			300/300	300/300	400/400	500/500	450/450

Table 12.4 ETFE foil properties

Thickness (microns)	Weight (g/m^2)	Tensile strength L/C (N/mm^2) (DIN 53455)	Tensile deformation L/C (%)	Tear resistance L/C (N)
50	87.5	64/56	450/500	450/450
80	140	58/54	500/600	450/550
100	175	58/57	550/600	430/440
150	262.5	58/57	600/650	430/430
200	350	52/52	600/600	430/430
250	4376.5	>40/>40	>300/>300	>300/>300

L/C (lengthwise-crosswise)

deformable in its plane, can be adapted to a complex geometry with high tensile strength in the direction of the yarns.

Inasmuch as the material is anisotropic, stiffness can be found with a combination of biaxial tests and mathematical interpolations.

Biaxial tests (conducted by pulling a cross-shaped sample in both directions of the cloth) furnish information on coated fabric behaviour, relating stress to its respective strain. This relationship yields the modulus of elasticity for each stress state and with it the fabric stiffness values used to dimension the membrane.

Textile architects should use the coated fabric manufacturer's stress–strain curves to select the most suitable material. These results of these tests should also be used to establish the compensation values to be applied to the unstressed patterns, which are flat during the manufacturing stage and must be cut to a smaller size for subsequent prestressing and deformation to the design dimensions. Nonetheless, wherever possible, samples of the actual lot of material to be used for the membrane should be analyzed to obtain the most accurate data possible (see Fig. 12.47).

Other parameters that should be listed on fabric specification sheets are tensile strength and bonding (measured in daN/5 m or kN/m), and tear resistance (measured in daN or kN).

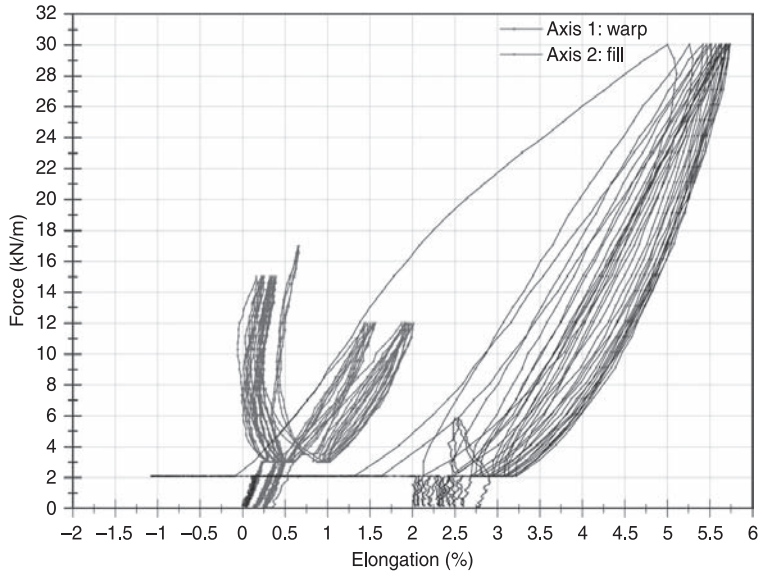

12.47 Biaxial curves for a PVC-coated polyester material (FERRARI, lab. BLUM).

Bonding impacts on the manufacturing method and seam width, while tear resistance is relevant for the intents and purposes of controlling the propagation of existing rips (the result of vandalism or installation-related or other accidents) when the stress on the membrane increases as a result of external actions (see Fig. 12.48).

Fire reaction

The first consideration to be taken into account in connection with coated fabric and foil fire behaviour is the site where the membrane is to be installed.[3] The applicable legislation, including statutory codes, recommendations and so on, depends on that circumstance. Moreover, the legislation must not be interpreted to require membranes to meet the same standards as conventional materials, for while fire reaction or behaviour may be applicable in both cases, criteria such as fire resistance (measured in time) may be less so. Structures, for instance, should logically be fire resistant for the amount of time needed to evacuate the building, whereas in membranes the important question is its behaviour when ignited: flammability and the characteristics of both the smoke generated and the burning droplets, if any.

This is the thrust of the classification most widely used today, the so-called Euroclass system[3] which defines new fire safety requirements. The system consists of a series of classes, from A to F, and subclasses, as well as the respective tests and classification requirements. Provision is also made for the correspondence

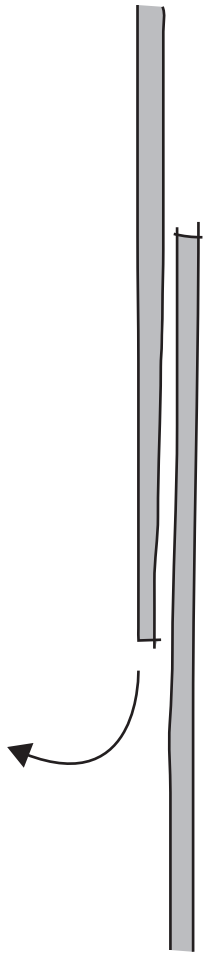

12.48 Tear resistance effect in composed fabrics (from Foster and Mollaert, 2004).

between preceding classes and the minimum requirements laid down in the new legislation (see Table 12.5).

Subclasses are likewise defined based on the smoke generated, assigned the letter S and a number, and the existence of droplets or otherwise, assigned the letter D and a number.

PVC-coated polyester fabrics are generally classified from B to non-fire repellent, whereas silicone- and PTFE-coated fibreglass materials and ETFE foils qualify for a number of class A ratings.

The safety afforded by low PTFE flammability compared to flame retardant PVC is controversial, however. Since the former cannot be perforated by fire, both

Table 12.5 Euroclass system for fire safety requirements

Euroclass	Test Method(s)	Test criteria	Additional information
A1	Non-combustibility	Temperature rise Mass loss Sustained flaming	none
	AND Calorific content	Total energy in product Energy per internal & external component	
A2	Non-combustibility	As Above	Smoke production & Flaming droplets or particles
	OR Calorific content	As above	
	AND Single Burning Item [SBI]	Fire growth rate Lateral flame spread & total heat release in 600s	
B	Single Burning Item [SBI]	As SBI above	Smoke production & Flaming droplets or particles
	AND Small flame test for 30s	Lateral flame spread in 60s	
C	Single Burning Item [SBI]	As SBI above	Smoke production & Flaming droplets or particles
	AND Small flame test for 30s	Lateral flame spread in 60s	
D	Single Burning Item [SBI]	As SBI above	Smoke production & Flaming droplets or particles
	AND Small flame test for 30s	Lateral flame spread in 60s	
E	Small flame test for 15s	Lateral flame spread in 20s	Flaming droplets etc
F	No performance	Determined	

smoke and heat (the two major causes of casualties in fires) are trapped inside the structure.

In PVC-coated fabrics, by contrast, the flames perforate the membrane, creating a natural 'draft' that evacuates smoke and heat. If the PVC-coated fabric also contains 'non-drip' flame retardants, this material is more fire safe than PTFE-protected fabrics, even though it tests to a lower classification (see Fig. 12.49).

Thermal and acoustical performance

The thermal or acoustic insulation afforded by coated fabrics and foils is not, initially, comparable to the levels attained by so-called 'traditional' materials. Indeed, in a horizontal position, 1500 g/m^2 PVC-coated polyester fabric, one of the heaviest on the market, has a global thermal conductivity of 6.4 W/m^2/°C,

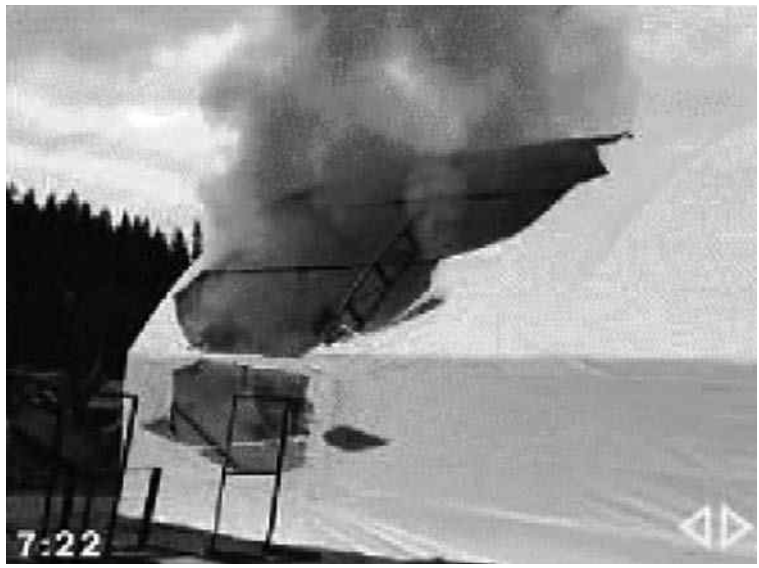

12.49 Fire behaviour during tests of PVC-coated polyester material, flames perforate the membrane, exacuating smoke and heat (FERRARI tests).

compared to the 0.5 to 3 $W/m^2/°C$ provided by extruded polystyrene insulation, in addition to the insulation provided by the other layers of conventional enclosures.

Comparisons in this regard can only be drawn between different combinations of textile materials or different membrane layouts in terms of the values that meet increasingly demanding acoustic and energy legislation.

Today, low emissivity or 'low-e' coated fabric can be found on the market that drastically reduces heat transfer across the membrane.

One good practice may consist of using double or triple layers that form either suspended textile ceilings under tensile roofs or cushion-type membranes. The effective combination of several layers of coated fabric (or foils in the event of ETFE) separated by air chambers and treated or even environmentally controlled air significantly improves thermal behaviour.

Coated fabric or foil translucency is largely responsible for heat transfer and consequently greenhouse effect, thereby overheating the inside surface structures made of these materials. In this regard, the authors believe that 'fashionable' solutions such as ETFE foil airhalls (that transfer 95% of the incident radiation) should only be used in certain climates. They should be avoided where solar-induced heating generates indoor environments that are uninhabitable or unsustainable because of the energy demand involved in lowering the temperature to comfortable levels. Paradoxically, membranes made of this material have sometimes had to be subsequently 'duplicated', i.e. shaded inside or out by

awnings, umbrellas or similar. This raises the question of whether ETFE should have been used in the first place or whether, given the climate and use, a less translucent material would have been preferable.[4]

Coated fabrics that aim to deliver satisfactory acoustical performance (the acoustic attenuation afforded by a single layer of the fabric mentioned above comes to a mere 17 dBA) should be designed as described in the foregoing, i.e. with several layers, to enhance indoor comfort. In this case, the innermost layer or suspended ceiling should preferably be made of microperforated materials in order to lower transmission and reverberation levels, and should be supplemented by an inert insulating material positioned between the two layers of fabric. The presence or otherwise of that insulation and its composition should be carefully studied, however, for it has a dramatic effect on the light transmitted across the membrane, unless highly transparent latest-generation (cellulose-based or aerogel) insulation is used.

Translucency

The translucency of a membrane depends on the fabric used, which in turn depends on the membrane type, design and size. Small membranes may be, as a rule, more translucent than larger ones, for structures with greater spans need to be stronger and hence heavier and more opaque. Conversely, a very translucent material such as ETFE cannot be used for all types of membranes because of its very low mechanical strength.

Membrane translucency depends on the fabric, the coating and, to a lesser extent, the finish.

The intermediate translucency of polyester fabrics can be increased with black polyester fabric, along with a sheet of black PVC to achieve greater opacity where needed. Since PVC coatings are also medially translucent as a rule, in PVC-coated polyester membranes translucency ranges from 10% for 1500 g/m^2 coated fabric to 45% for 400 g/m^2 material.

In silicone-coated fibreglass fabric, in turn, these values may reach up to 80%.

In PTFE-coated fibreglass, while the fibreglass exhibits medium values, PTFE is scantly translucent. Consequently, translucency in these membranes is very low (from 10–20%) but is altered over time due to the chromatic changes in PTFE when exposed to sunlight. When installed, PTFE-coated membranes are brown but after a few months they are bleached by the sun to a nearly perfect white (with a gradual increase in translucency). If used on suspended ceilings or two-layered roofs, however, the soffit whitens less than the side exposed to sunlight.

As noted, the static analysis of a membrane determines the strength of the material needed and therefore its type and weight. Membrane translucency, in turn, is directly related to weight.

Moreover, lighting should not be considered alone, but in conjunction with thermal questions. Membranes with high or ideal light transmission may generate excessive indoor radiation, creating an undesired greenhouse effect. Attention

Table 12.6 General comparison of properties of tensile membrane materials

	PVC-coated polyester	PTFE-coated fibreglass	Silicone-coated fibreglass	PTFE-coated PTFE
Weft/warp tensile strength (kN/m)	115/102	124/100	107/105	84/80
Weight (m/m^2)	1200 (type 3)	1200 (type G5)	1100	830
Weft/warp trapezoid tearing (N)	800/950	400/400	960/700	925/925
Light transmission (%)	10–15	10–20	< 80	19–38
Fold recovery/ flexibility	High	Low	High	High
Reaction to fire	M2 (NFP 92 503) B1 (DIN 4102)	M1 (NFP 92 503) B1/A2 (DIN 4102)	A (ASTM E-108) no toxicity or smoke	
Cleaning	Easier with upper layers	Self-cleaning	Self-cleaning	Self-cleaning
Seams	High frequency	Thermal	Vulcanization	Stitching
Service life (years)	>15–20	>25	>225	
Cost	Low	High	High	

should be drawn in this regard to the growing, albeit fashionable and indiscriminate, use of ETFE in climates ill-suited to this material, which ultimately leads to a lack of thermal comfort (or even visual comfort due to glare) and the concomitant need for air conditioning out of season.

Table 12.6 compares a number of types of coated fabrics.

Finally, the type of finish may also impact membrane translucency. Silicone tends to soil more readily than acrylic, PVDF, PTFE or FEP finishes, and membrane translucency varies dramatically with the thickness of the dirt cover, regardless of the fabric or coating used in its manufacture.

12.5 Membrane manufacture and installation

12.5.1 Cutting pattern

Since stretched membranes are most effectively functional when the right combination of shape and prestressing is applied, the radii of their double curvature geometry must be as small as possible to attain stability with minimum prestressing.

To produce the curvatures needed for a membrane from a flat piece of fabric coming off an industrial roll of a given width, the cloth must be cut into pieces (patterns)[5] with a curved geometry that are then joined to construct the three-dimensional membrane.

Consequently, before the patterns for cutting membranes can be defined, the directions of the main stresses (radial in cones, diagonal in paraboloids) must first

be established to arrange the patterns to accommodate those vectors. Suitable roll width is requisite to optimal use of the fabric and to ensuring a reasonable number of patterns per membrane, which must be commensurate with envelope curvature. In other words, it would make little sense to define only two patterns for a membrane with small curvature radii, even assuming a membrane twice as large as the width of the roll of fabric, for a single seam would have to support the entire curvature. Under these conditions, wrinkles would inevitably appear due to the lack of stress in certain areas (see Fig. 12.50).

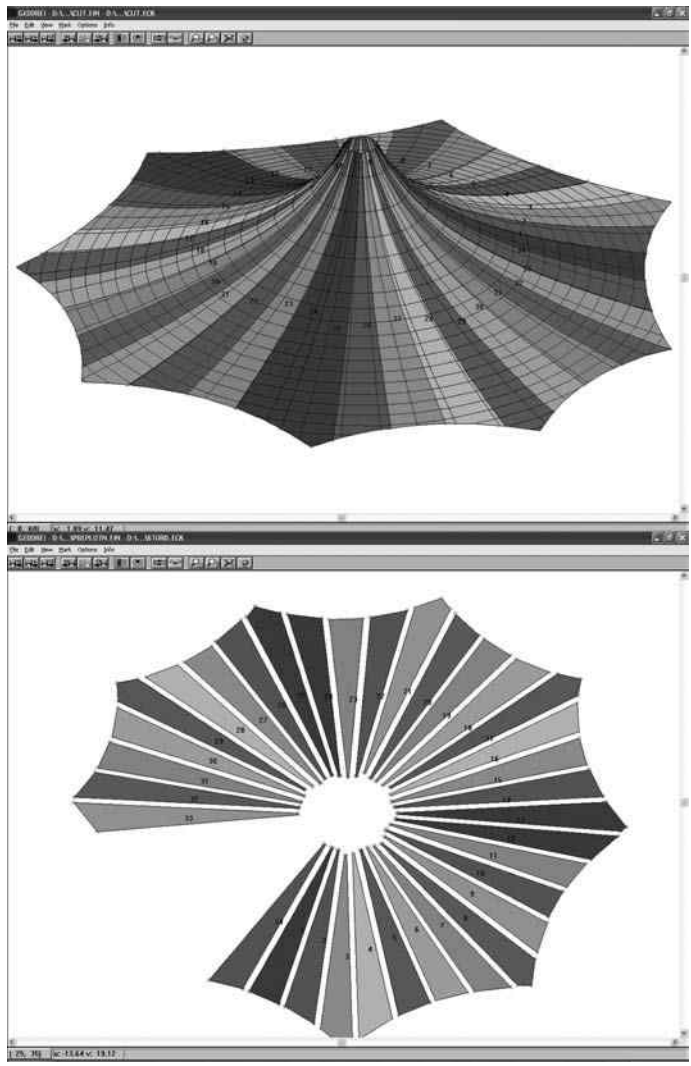

12.50 Flattening surfaces getting the patterns (from *Easy Software for Tensile Structures* technet-gmbh).

Traditionally, patterns were designed using stiffened scale models made of elastic materials, on which the cutting lines were drawn and then transferred to a drawing. Today textile membrane software includes cutting modules that provide for higher precision, allow designers to verify pattern widths and include fabric compensation values, welding width and pocket dimensions. The vectorial output can then be exported directly to the cutting plotter (see Fig. 12.51).

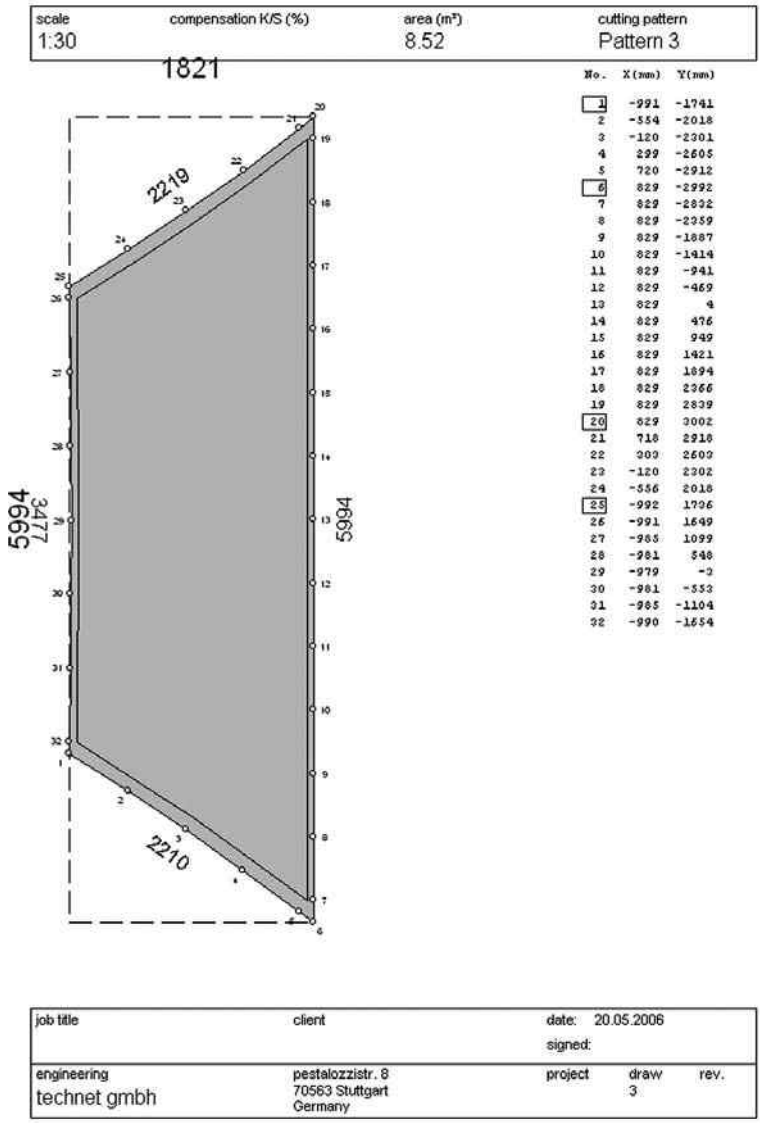

12.51 Result of a patterning by specialised software (from *Easy Software for Tensile Structures* technet-gmbh).

12.5.2 Seams

Seam types[2] and procedures depend on the membrane composition and type.

Once the membrane patterns have been designed and cut in the shop, the pieces are joined using different methods and procedures.

The traditional solution, associated not with membranes but with fabric in general, was to sew the parts together with a variety of types of seam overlaps and stitching (see Fig. 12.52(1), (2)).

In sewn seams the (usually polyester) thread, which deteriorates when exposed to UVA rays, has a much shorter durability than the fabric, while each stitch lowers mechanical strength and water resistance. The first problem can be mitigated by using UVA-resistant thread, but no reliable solution exists for the latter two.

Consequently, a more advanced procedure is used for today's coated fabrics: welding with different seam widths depending on the type of fabric. At the time of writing, high-frequency welding, which melts and welds the PVC coating, is universally recommended for PVC-polyester coated fabric and hot pressure welding for fibreglass PTFE-coated fabric and ETFE foils, with an intermediate layer of FEP or PFA (perfluroalkyl vinyl ether) to facilitate welding (see Fig. 12.53).

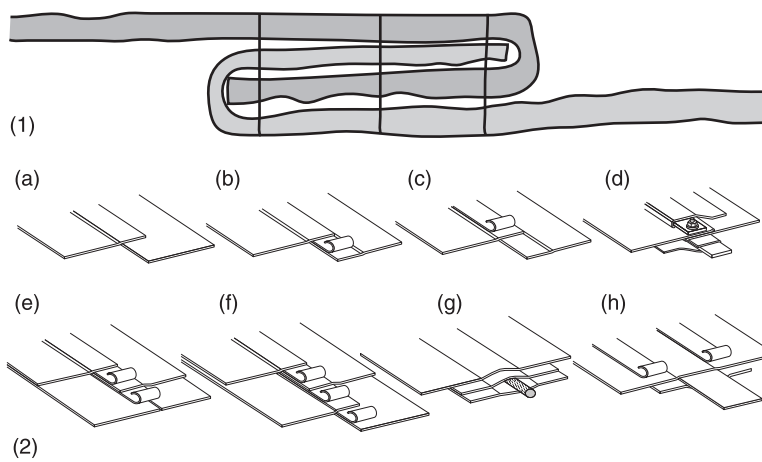

12.52 (1) Double overlapping for sewing unions. Foster and Mollaert, 2004. (2) Different types of overlapping for welding and sewing material. (a) High frecuency welding for PVC-polyester fabrics. (b) Welding for PTFE-glass fiber fabrics (c) Overlapping with reinforcement for PVC-polyester fabrics. (d) Union with rigid material. (e) Reinforcements with double layered material (f) Reinforcement with triple layered material and strands for high resistance unions. (g) Reinforcement with cable inside a pocket. (h) Reinforcement with a rigid material inside a pocket (from *Detail* (2000). 6. Membrane Construction).

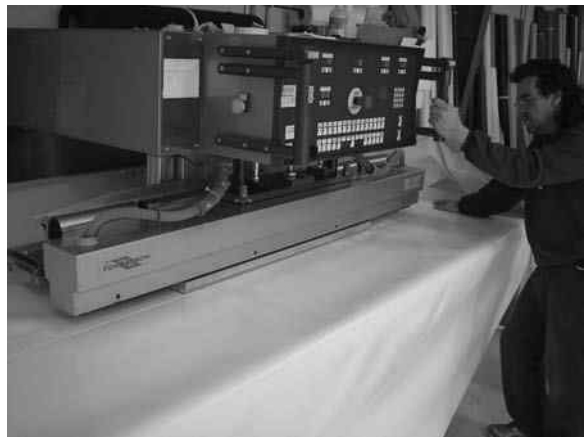

12.53 High-frequency electrode for welding.

Hot air or hot wedge welding should not be used in membrane manufacture, except for certain finishing touches or details inaccessible to the high-frequency welding machine or in works repairs where its use is not feasible.

Seam width recommendations for PVC-coated polyester range from 40 mm for Type I, 60 mm for Type II, 80 mm for Types III and IV and up to 100 mm for Type V, but in any event they should be determined on the grounds of strength tests conducted on the actual material to be used.

Welds must be periodically inspected and the inspection recorded during the manufacturing process at the beginning of each shift by *in situ* testing (which should be supervised by the textile architect). Such verification should consist:

- first, in pulling on a weld lengthwise until the bond is severed along one section, and checking to ensure that the coating on one of the two sides has adhered to the other, exposing the fabric on the former side;
- second, in making sample (50-mm strip) welds made at different stages in the process under the same conditions of intensity, time and pressure. These welds should be analyzed in the laboratory to ensure that the weld is at least 80% as strong as the fabric itself under a number of temperature conditions

12.5.3 Installation and maintenance

Planning for membrane installation should not be confined to on-site erection, but considered during all the preliminary work, including design, engineering, manufacture and shipping.

In fact, the decisions made in the design stage have an enormous impact on installation. In the characteristic case in which a membrane is to be retrofitted to an existing building, attention must be paid to the circumstances surrounding the installation to prevent the appearance of insurmountable obstacles. Specifically, the

items to be covered include verification that the existing structure can support the new element and that the membrane can be anchored to the building and duly staked out and unfolded *in situ*. Accessibility, particularly for heavy machinery building, working hour, etc., are other relevant questions to be borne in mind by the designer.

Consequently, textile membrane installation can and should be planned from the design stage. In other words, to avoid site- or erection timing-related inadequacies, installation should be regarded to be one of the major boundary conditions, determining anything from the size of the membrane and its structure to the material used.

To this end, the textile architect should have sufficient installation experience or be backed by a team with the necessary expertise to furnish advice on an erection plan, the elements involved, their stability during the works, the tools and machinery needed and on-site safety. In this final respect, the specifics of textile membrane installation should be borne in mind, in addition to standard health and safety criteria, for practices that are acceptable in traditional building construction may be less so in membrane erection.

The differences have to do with the fact that workers erect the membrane from the structure itself (wearing a harness attached to a lifeline). Whereas safety boots in traditional construction, for instance, have rippled, non-skid black rubber soles with steel reinforcements, in textile membranes the non-skid soles must be made of white rubber and may not be reinforced, for the steel could damage the material. Similarly, the standard hardhat differs widely from the type used in textile membranes (ventilated, with a chin strap and no visor) and certain fall protection elements (railings, nets and so on) may not be suitable (see Fig. 12.54).

Design and installation documentation must include specific, 'dense' drawings with all the necessary information. The underlying premise should be to streamline erection procedures by avoiding the need to check countless sets of drawings, for assembly time is limited and spur-of-the-moment decision-making may entail risks and the gain or loss of material and human resources.

An erection supervisor must be appointed, for such leadership is crucial to interpreting drawings and organizing work and crews (see Fig. 12.55).

Drawings must contain at least the following graphics:

- References to the structural centrelines on the membrane or the building where it is to be installed, numbered or coded to specify the membrane anchor points.
- All the structural members, with their respective references, for due identification with the labels on the parts themselves and the installation points.
- Membrane or membranes referenced at their vertices, with their names, constituent patterns, dimensions and areas to stake out the space needed on site for unfolding and preparation.
- Edge, tie, brace and safety cables, likewise coded to specify position, diameter and ends.
- Ancillary parts and fittings, plates, earrings, tie-rods, shackles and so on, specifying layout, number and codes.

12.54 Equipment for textile installation in high works.

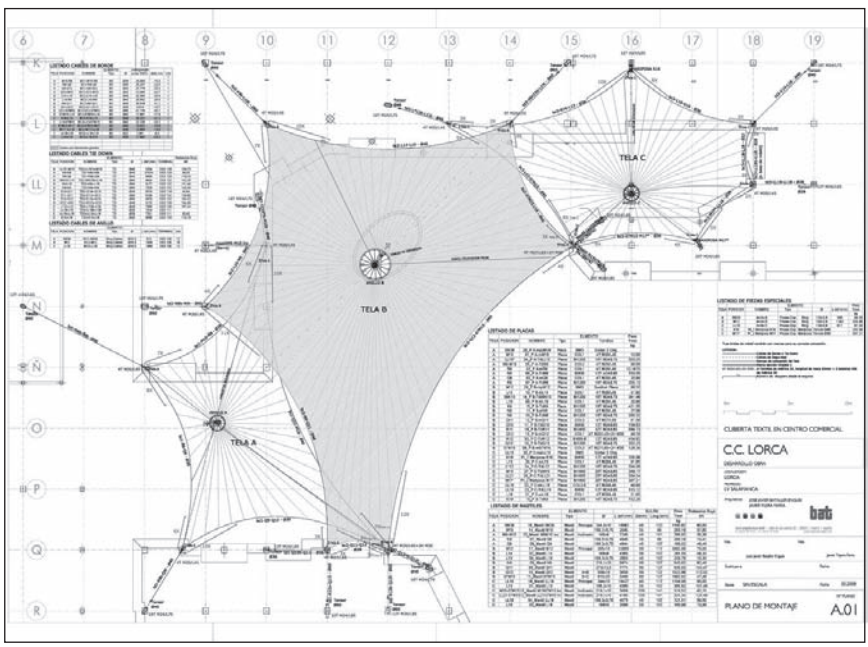

12.55 Installation drawing for three textile membranes (CC Almenara, Lorca. Javier Tejera, BAT, Spain).

- Standard construction details and details, preferably in 3D, of points with particularities, specifying the codes of all the component parts.

The drawings themselves or other documents should also contain checklists such as the example below which, in addition to the information described in the drawing, include data of crucial importance for installation (see Table 12.7).

Table 12.7 Checklists for a textile membrane (CC Almenara, Lorca. BAT, Spain)

BORDER CABLES CHECKLIST

Roof	Position	Name	Element Type	Element Ø	Cutting length under 50KN	Delta mm	Uds
							1
A	M10-N8	BC1-M10-N8	BC	Ø28	23.083	–15.3	1
A	N8-Q9	BC1-N8-Q9	BC	Ø36	25.247	–22.5	1
A	Q9-Q12	BC1-Q9-Q12	BC	Ø30	27.776	–25.3	1
A	Q12-M10	BC1-Q12-M10	BC	Ø40	43.085	–44.7	1
B	L14-L10	BC2-L14-L10	BC	Ø48	32.384	–33.6	1
B	L10-N9	BC2-L10-N9	BC	Ø40	25.952	–24.0	1
B	N9-Q11	BC2-N9-Q11	BC	Ø48	36.918	–31.1	1
B	Q11-Q12	BC2-Q11-Q12	BC	Ø28	8.616	–10.7	1
B	Q12-07M15	BC2-Q12-07M15	BC	Ø65	47.715	–35.7	1
B	07M15-L14	BC2-07M15-L14	BC	Ø40	17.861	–17.6	1
C	K16-L13	BC3-K16-L13	BC	Ø36	25.231	–31.2	1
C	L13-07M15	BC3-L13-07M15	BC	Ø40	22.235	–25.2	1
C	07M15-M17	BC3-07M15-M17	BC	Ø36	16.022	–20.9	1
C	M17-LL18	BC3-M17-LL18	BC	Ø36	10.864	–13.0	1
C	LL18-L18	BC3-LL18-L18	BC	Ø22	7.961	–8.3	1
C	L18-K16	BC3-L18-K16	BC	Ø36	17.842	–20.3	1

TIE DOWN CABLES CHECKLIST

Roof	Position	Name	Element Type	Element Ø	L def (mm)	Terminal	Prestress Rxyz kN
A	LL10-M10	TD1-LL10b-M10t	TD	Ø48	5304	OSS 128	159.75
A	N6-N8	TD1-N6b-N8t	TD	Ø40	17024	OSS 120	98.00
A	R8-Q9	TD1-R8b-Q9t	TD	Ø40	8699	OSS 120	119.10
B	06K15-L14	TD2-06K15b-L14t	TD	Ø60	9904	OSS 132	142.25
B	K9-L10	TD2-K9b-L10t	TD	Ø60	9177	OSS 132	151.49
B	N8-N9	TD2-N8b-N9t	TD	Ø60	7926	OSS 132	143.30
B	Q10-Q11	TD2-Q10b-Q11t	TD	Ø36	9379	OSS 118	40.64
B	R11-Q11	TD2-R11b-Q11t	TD	Ø60	9199	OSS 132	130.80
B	R12-Q12	TD2-R12b-Q12t	TD	Ø60	6676	OSS 132	183.22
B	Q13-Q12	TD2-Q13b-Q12t	TD	Ø48	5110	OSS 128	164.69
C	L12-L13	TD3-L12b-L13t	TD	Ø48	7689	OSS 128	187.22
C	LL18-L18	TD3-LL18b-L18t	TD	Ø28	7414	OSS 111	
C	LL19-LL18	TD3-LL19-LL18	TD	Ø28	7521	OSS 111	62.45
C	K19-L18	TD3-K19-L18	TD	Ø40	9988	OSS 120	115.79

RING CABLES CHECKLIST

Roof	Position	Name	Element Type	Ø	L def (mm)	Terminal	Uds
A	0609	RC1-0609	Ring cables	Ø16.5	913	OSS 100	12
B	M12	RC2-M12	Ring cables	Ø16.5	1936	OSS 100	16
C	LL16	RC3-LL16	Ring cables	Ø16.5	1069	OSS 100	12

MASTS CHECKLIST

Roof	Position	Name	Element Type	Ø	Bolt L def (mm)	Bolt Ø (mm)	Bolt Long (mm)	Total weight kg	Prestress Rxyz kN
A	06O9	16_Mast 06O9	Main mast	244.5×10	16562	45	132	1190.82	60.00
A	M10	14_Mast M10	Mast	139.7×3.75	2945	35	69	263.19	37.83
A	M9-M10	13_Mast M9M10 Inc	Sloped mast	168×6	7245	45	151	286.92	35.38
A	N8	07_Mast N8	Mast	139.7×3.75	4945	35	69	260.16	13.41
A	Q9	08_Mast Q9	Mast	168.3×3.75	4844	45	107	186.02	48.46
B	M12	17_Mast M12	Main mast	355×16	23955	60	117	3582.06	75.00
B	L14	02_Mast L14	Mast	168×6	4383	55	107	281.03	48.33
B	L10	06_Mast L10	Mast	168.3×3.75	2893	45	107	226.79	10.36
B	N9	05_Mast N9	Mast	219.1×10	5874	60	107	543.62	82.46
B	Q11	09_Mast Q11	Mast	273×12.5	7774	85	127	935.03	144.47
B	Q12	10_Mast Q12	Mast A+B	508×16	3650	60	127	1522.98	112.52
B	07M15	11_Mast 07M15	Mast B+C	610×20	3460	80	127	1982.62	47.38
C	LL16	18_Mast LL16	Main mast	244×10	16427	45	117	1194.09	95.00
C	L13	01_Mast L13	Mast	168.3×10	4360	55	107	365.82	101.46
C	M15-07M15	15_Mast M1507M15 Inc	Sloped mast	219.1×10	3956	100	141	319.52	62.15
C	LL21-07 M15	12_Mast LL2107M15 Inc	Sloped mast	219.1×10	4185	100	141	331.34	124.49
C	LL18	04_Mast LL18	Mast	168.3×3.75	4075	45	107	121.51	59.55
C	L18	03_Mast L18	Mast	168×6	3566	55	107	169.66	73.99

In addition to the data needed to distribute, position and install the membrane parts on site, other information is likewise important, such as the installation prestressing on cables, tie-rods, bolts or membranes, and the weight of component parts to determine the type of machinery needed for hoisting and installation.

The installation stage itself depends largely on membrane size and complexity, but in general involves preliminary logistics to coordinate shop manufacture, shipping and timely delivery of the materials needed.

Once all the parts are on site, they must be inspected against a checklist to detect any perceptible flaws or shortcomings in quality. The largest structural members (primary structure) are then distributed, assembled and anchored to the existing structure or foundations (see Fig. 12.56).

(a)

(b)

12.56 Preparing the structural members, (a) central mast, (b) corner mast (CC Almenara, Lorca. BAT, Spain).

Once the primary structure is prepared, a sufficiently large worksite area must be protected to roll out the membrane completely and prepare the edges, cable connections, reinforcement plates, rings, arches and so forth (see Fig. 12.57).

12.57 Preparing the membrane and connection with the structure (CC Almenara, Lorca. BAT, Spain).

When the membrane is fully prepared, a series of prior conditions must be met before proceeding to uplift:

- The day before erection, final review of the checklist of materials, tools and hoisting machinery that will be needed the following day. Conventional tools include all manner of wrenches, electric drills, cutting and welding equipment, tensioning tools such as tensioners, chain hoists, ratchet strap tensioners, polyester slings, tower or mobile cranes for hoisting loads, and cherry pickers for height workers (see Fig. 12.58).
- Verification of crane and cherry picker working height and bearing capacity to ensure both are sufficient for the work at hand.
- Weather forecast for the installation site on the uplift day, requested from the respective meteorological institute. In the event of adverse conditions (in the supervisor's judgement and obviously in proportion to the difficulty involved in installing the membrane), erection should be postponed. By way of indication, based on the authors' experience, installation should not be attempted in fog, dew, rain, snow or hail, no matter how slight, or in the event of electric storms even when dry, low temperatures (<5°C) or, of course, wind (>20 km/h). Where large membranes are to be erected, portable anemometers should be used to measure possible gusting during installation and to detain the work if necessary (and possible).
- Uplift start-up early in the morning (or even the night before if possible) when the wind is generally slacker, to use the rest of the day to complete the most

(a)

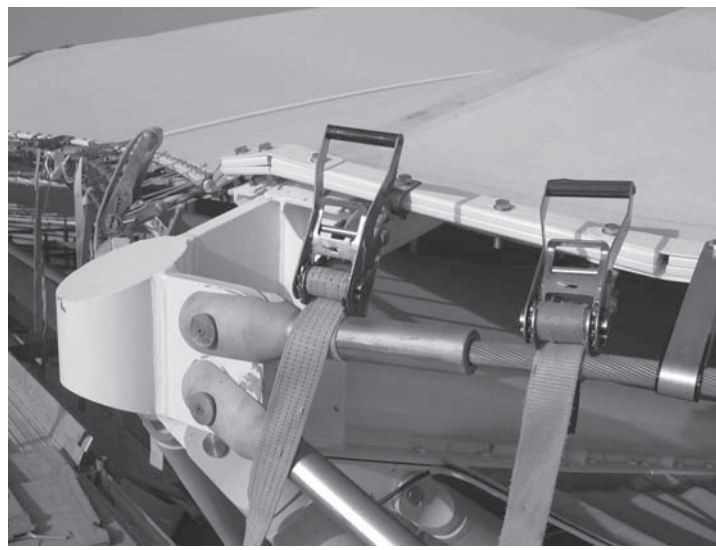

(b)

12.58 Special tools for tensioning the membrane, (a) hydraulic jacks prestressing from high point, (b) ratchets prestressing from borders.

sensitive process the same day, either finishing installation or at least securing the membrane.

- Provision and verification of the safety measures required for all workers, depending on their respective tasks.
- Provision of all workers with walkie-talkies for receiving instructions and advising the supervisor of possible incidents. These units must be separate from the walkie-talkie used by the supervisor to communicate with crane operators (see Fig. 12.59).
- Beaconing and roping off the installation area, prohibiting the presence of third parties or machines during the uplift and stabilization process (see Fig. 12.60).
- A site log must be kept to record installation progress daily, including operations performed, possible damage and any immediate repairs, as well as weather conditions.
- The service life of the membrane begins after installation is finished and all necessary rectifications have been made. The duration of manufacturers' guarantees depends on the material and is usually conservative compared to the actual length of time that membranes maintain their mechanical properties, within reasonable limits. The loss of such properties and aesthetic characteristics in particular depends largely on where the membrane is installed (climate, pollution and so on) (see Fig. 12.61).

Good practice, therefore, calls for establishing a maintenance plan beginning in the design phase which should be implemented by the textile contractor, engineering firm, manufacturer and membrane installer. Such plans should establish timing and operating procedures, which may include:

12.59 Lifting the membrane (CC Almenara, Lorca. BAT, Spain).

12.60 Stabilization of central mast during lifting process (CC Almenara, Lorca. BAT, Spain).

12.61 Repairing works needed after lifting process (CC Almenara, Lorca. BAT, Spain).

- Membrane inspection and, on the grounds of the findings, the operations listed below. Two types of inspections are envisaged: cursory (once a year or after every relevant meteorological event) performed by the maintenance staff,

and detailed (once every two years at most), performed by the outsourced maintenance company, preferably the contractor that erected the membrane.

- Re-tensioning materials where feasible (membranes, cables, tie-rods and other fittings). This operation should only be performed in the event of a decline in stress or relaxation, which should be verified with tensometers, dynamometers or strain gauges (although for experienced inspectors the 'feel' of the material may suffice).
- Membrane cleaning (at least once every three years, no more than once every two years) with pressurized water and detergent. The membrane manufacturer and textile contractor should be consulted to determine the most suitable procedure, water pressure and detergent (see Fig. 12.62).
- In the event of rust or corrosion only: structure, fitting and cable cleaning, repair, painting and lubrication.
- *In situ* welding and preferably patching to repair possible damage to the membrane.
- Inspection to detect water or snow ponding on the membrane (usually due to a combination of loss of stress and the existence of areas with low grade slopes or curvatures).
- Replacement of the membrane at the end of its service life. To this end, all possible documentation on the original membrane should be kept, for the initial engineering will very likely need to be revised with time. New tests will very likely be needed, for instance, to compare the compensation values in the new membrane, which may need to be reshaped. New patterns may also have to be designed if the roll width differs.

12.62 Results of cleaning membrane (CC Almenara, Lorca. BAT, Spain).

The membrane should be dismantled prior to replacement so that structural members, cables and fittings can be repaired, rectified or replaced as necessary.

12.6 Sources of further information and advice

Since this is only a brief description of the problem, containing the main aspects of tensile structures and its use in building, we would like to suggest some other references for textile architecture.

TensiNet association

TensiNet is a multi-disciplinary association for all parties interested in tensioned membrane construction. The website, www.tensinet.com, contains a Project Database as well as articles and links to manufacturers, fabricators, material producers, coaters, weavers, architecture and engineering offices, distributors of machinery, steelwork and ropes, software companies, academic and research institutes. The TensiNet partners are the editors of the European Design Guide on tensile surface structures, and will continue to publish reference documents on this and associated topics. Also, TensiNet publishes the TensiNews newsletter twice a year and supports teaching and training activities in the field of tensioned membrane construction. TensiNet members meet once a year for an Annual General Meeting.

There is an 'Iberia Branch' of TensiNet, formed by the Spanish and Portuguese members of the net.

Main publications related with Textile Architecture

Armijos, Samuel J. *Fabric Architecture: Creative Resources for Shade, Signage, and Shelter*

Berger, Horst *Light Structures, Structures of Light: The Art and Engineering of Tensile Architecture*

Bing, Wang Bin *Free-Standing Tension Structures: From Tensegrity Systems to Cable-Strut Systems*

Capasso, Aldo *Fabric Membrane Tension Structures in Architecture: Introduction to Design*

Detail Magazine, 6(2000). Published by Institut für internationale Architektur-Dokumentation GmbH, Munich

Deutscher Beton-Verein *Bauen mit Textilien*

Drew, Philip *New Tent Architecture*

Koch, Klaus-Michael *Membrane Structures: Innovative Building with Film and Fabric*

Kronenburg, Robert *Flexible: Une architecture pour répondre au changement*

Kuma, Kengo *Kengo Kuma: Breathing Architecture: The Teahouse of the Museum of Applied Arts*

Le Cuyer, Annette *ETFE: Technology and Design*

Mollaert, Marijke *The Design of Membrane and Lightweight Structures: From Concept to Execution*
Moncrieff, Erik & Gründig, Lothar *Architecture and Structural Engineering Design*
Motro, René *Form Finding of Tension Structures*
Nerdinger, Winifred, *Frei Otto Complete Works*
Otto, Frei *Tensile Structures Design, Structure and Calculation of Buildings of Cables, Nets and Membranes*
Schlaich, Jörg *Light Structures*
Schock, Hans-Joachim *Soft Shells: Design and Technology of Tensile Architecture*
Seidel, Michael *Tensile Surface Structures: A Practical Guide to Cable and Membrane Construction*
Technet-gmbh, Easy Software for Tensile Structures, www.technet-gmbh.de
Tejera Parra, Javier and Garcia Santos, Alfonso, *Tectónica Magazine, 19: Plastic Materials Used in Architecture*

12.7 References

1. Monjo-Carrió J (1991) Introducción a la arquitectura textil. Cubiertas colgadas. Madrid: COAM.
2. Foster B and Mollaert M (2004) European Design Guide for Tensile Surface Structures. Brussels, TensiNet.
3. The EU has established the fire safety requirements as Euroclass system, stemming from Directive 89/106/CEE of 21/12/1988 on construction products (see Appendix A3. 4).
4. Tejera J, Monjo-Carrió J and La Torre J (2010) Heritage preservation strategies through textiles. Tensinet Symposium 2010 Tensile Architecture. Sofia: Tensinet.
5. Tejera J (2002) Fifth material: approach to patterning process in textile architecture. poStboks magazine, number 4. Madrid: poStboks S. L.

Index